HIGHWAY RESEARCH BOARD
Special Report 61D

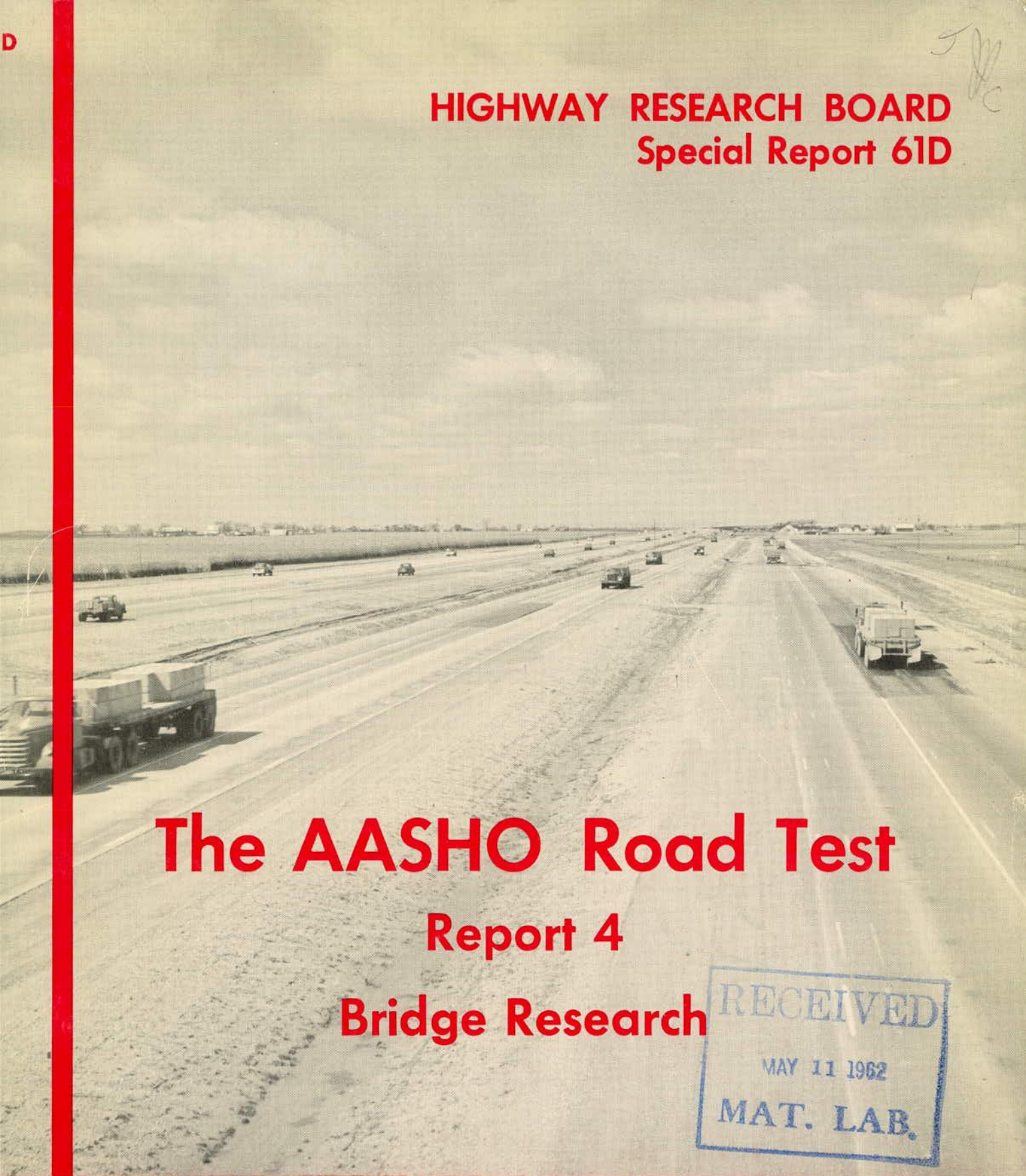

The AASHO Road Test

Report 4

Bridge Research

National Academy of Sciences—
National Research Council

publication 953

HIGHWAY RESEARCH BOARD

Officers and Members of the Executive Committee

1962

OFFICERS

R. R. BARTELSMEYER, *Chairman* C. D. CURTISS, *First Vice Chairman*

WILBUR S. SMITH, *Second Vice Chairman*

FRED BURGGRAF, *Director* WILLIAM N. CAREY, JR., *Assistant Director*

Executive Committee

REX M. WHITTON, *Federal Highway Administrator, Bureau of Public Roads* (ex officio)

A. E. JOHNSON, *Executive Secretary, American Association of State Highway Officials* (ex officio)

LOUIS JORDAN, *Executive Secretary, Division of Engineering and Industrial Research, National Research Council* (ex officio)

PYKE JOHNSON, *Retired* (ex officio, Past Chairman 1960)

W. A. BUGGE, *Director of Highways, Washington Department of Highways* (ex officio, Past Chairman 1961)

R. R. BARTELSMEYER, *Chief Highway Engineer, Illinois Division of Highways*

E. W. BAUMAN, *Director, National Slag Association, Washington, D. C.*

DONALD S. BERRY, *Professor of Civil Engineering, Northwestern University*

MASON A. BUTCHER, *County Manager, Montgomery County, Md.*

J. DOUGLAS CARROLL, JR., *Director, Chicago Area Transportation Study*

C. D. CURTISS, *Special Assistant to the Executive Vice President, American Road Builders' Association*

HARMER E. DAVIS, *Director, Institute of Transportation and Traffic Engineering, University of California*

DUKE W. DUNBAR, *Attorney General of Colorado*

MICHAEL FERENCE, JR., *Executive Director, Scientific Laboratory, Ford Motor Company*

D. C. GREER, *State Highway Engineer, Texas State Highway Department*

JOHN T. HOWARD, *Head, Department of City and Regional Planning, Massachusetts Institute of Technology*

BURTON W. MARSH, *Director, Traffic Engineering and Safety Department, American Automobile Association*

OSCAR T. MARZKE, *Vice President, Fundamental Research, U. S. Steel Corporation*

J. B. MCMORRAN, *Superintendent of Public Works, New York State Department of Public Works*

CLIFFORD F. RASSWEILER, *Vice President for Research and Development, Johns-Manville Corporation*

GLENN C. RICHARDS, *Commissioner, Detroit Department of Public Works*

C. H. SCHOLER, *Applied Mechanics Department, Kansas State University*

WILBUR S. SMITH, *Wilbur Smith and Associates, New Haven, Conn.*

K. B. WOODS, *Head, School of Civil Engineering, and Director, Joint Highway Research Project, Purdue University*

Editorial Staff

FRED BURGGRAF HERBERT P. ORLAND EARLE W. JACKSON

2101 Constitution Avenue Washington 25, D. C.

Tear along Perforation

KEY TO CHARACTERISTICS OF TEST BRIDGES

LOOP 5

STEEL BEAMS

Noncomposite 1A 27,000 psi Cover plate, bottom 18 WF 55	Noncomposite 1B 35,000 psi No cover plate 18 WF 50
Noncomposite 2A 35,000 psi No cover plate 18 WF 55	Composite 2B 35,000 psi Cover plate, bottom 18 WF 50

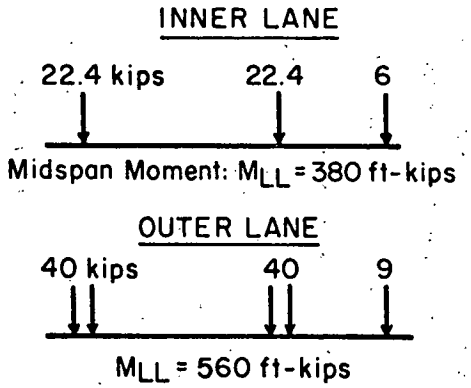

PRESTRESSED CONCRETE BEAMS

Pretensioned 6B 300 psi	Pretensioned 6A 800 psi
Post-tensioned 5B 300 psi	Post-tensioned 5A 800 psi

DIRECTION OF TRAFFIC

LOOP 6

STEEL BEAMS

Noncomposite 3A 27,000 psi No cover plate 21 WF 62	Composite 3B 27,000 psi Cover plate, bottom 18 WF 60
Noncomposite 4A 35,000 psi Cover plate, bottom 18 WF 60	Noncomposite 4B 35,000 psi Cover plate, bottom 18 WF 60
Noncomposite 9A 27,000 psi Cover plate, top and bottom 18 WF 96	Noncomposite 9B 27,000 psi Cover plate, top and bottom 18 WF 96

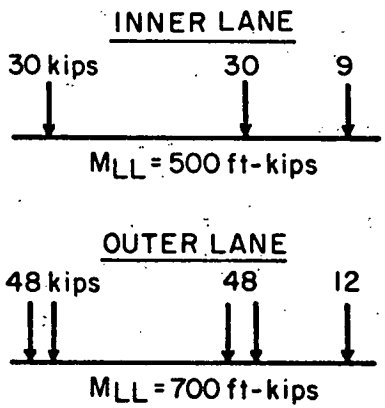

REINFORCED CONCRETE

30,000 psi 8B	30,000 psi 8A
40,000 psi 7B	40,000 psi 7A

The AASHO Road Test

Report 4

Bridge Research

By the

HIGHWAY RESEARCH BOARD
of the
NAS-NRC Division of Engineering and Industrial Research

Special Report 61D

Publication No. 953
National Academy of Sciences—National Research Council
Washington, D.C.
1962

This is one of a series of reports of work done under a fiscal agreement of June 10, 1955, between the National Academy of Sciences and the Bureau of Public Roads relating to AASHO Road Test Project; and under individual agreements covering Cooperative Highway Research Project (AASHO Road Test) made between the National Academy of Sciences and the several participating state highway departments, members of the American Association of State Highway Officials.

Included in the series are the following reports:

Report	*Subject*	*HRB Special Report No.*
1	History and Description of Project	61A
2	Materials and Construction	61B
3	Traffic Operations and Pavement Maintenance	61C
4	Bridge Research	61D
5	Pavement Research	61E
6	Special Studies	61F
7	Final Summary	61G

Available from the
Highway Research Board
National Academy of Sciences—
National Research Council
Washington 25, D. C.

Library of Congress Catalog Card No. 61-60063

NATIONAL ADVISORY COMMITTEE

This committee was appointed by the Highway Research Board to advise the Board and its project staff in relation to administrative and technical matters.

K. B. Woods, *Chairman*
Head, School of Civil Engineering, and
Director, Joint Highway Research Project, Purdue University

W. A. Bugge, *Vice-Chairman*
Director, Washington Department of Highways

W. F. Abercrombie,[1] Engineer of Materials and Tests, Georgia State Highway Department

R. R. Bartelsmeyer, Chairman, AASHO Committee on Highway Transport, and Chief Highway Engineer, Illinois Division of Highways; Chairman, Highway Research Board [2]

W. G. Burket, Tire Industry; Chairman, Technical Advisory Committee, Rubber Manufacturers Association;[3] Manager, Truck Tire Engineering, Goodyear Tire and Rubber Company

H. M. Straub,[4] Tire Industry; Manager, Tire Construction and Design, B. F. Goodrich Company

D. K. Chacey, Director of Transportation Engineering, Office of the Chief of Transportation, Department of the Army Transportation Corps

W. E. Chastain, Sr., Engineer of Physical Research, Illinois Division of Highways

R. E. Fadum, Head, Civil Engineering Department, North Carolina State College

E. A. Finney, Director, Research Laboratory, Michigan State Highway Department

C. E. Fritts, Vice-President for Engineering, Automotive Safety Foundation

R. H. Winslow,* Highway Engineer, Automotive Safety Foundation

Sidney Goldin, Petroleum Industry; General Manager, Head Office Marketing, Shell Oil Company

J. O. Izatt,* Petroleum Industry; Asphalt Paving Technologist, Products Application Department, Shell Oil Company

W. D. Hart,[5] Transportation Economist, National Highway Users Conference

E. H. Holmes, Assistant Commissioner for Research, Bureau of Public Roads

C. F. Rogers,* Special Assistant, Office of Research, Bureau of Public Roads

J. B. Hulse, Managing Director, Truck Trailer Manufacturers Association

F. N. Hveem, Materials and Research Engineer, California Division of Highways

A. E. Johnson, Executive Secretary, American Association of State Highway Officials

M. S. Kersten, Professor of Civil Engineering, University of Minnesota

George Langsner, Chairman, AASHO Committee on Design;[6] Assistant State Highway Engineer, California Division of Highways

R. A. Lill,[7] Chief, Highway Engineering, American Trucking Associations

George Egan,* Chief Engineer, Western Highway Institute

R. E. Livingston, Planning and Research Engineer, Colorado Department of Highways

L. C. Lundstrom, Former Chairman, Automobile Manufacturers Association Committee for Cooperation with AASHO Road Test; Director, General Motors Proving Ground

T. F. Creedon,*[8] Highway Engineering Adviser, Automobile Manufacturers Association

G. W. McAlpin,[9] Assistant Deputy Chief Engineer (Research), New York State Department of Public Works

B. W. Marsh, Director, Traffic Engineering and Safety Department, American Automobile Association

R. A. Moyer, Professor of Highway Transportation Engineering, and Research Engineer, Institute of Transportation and Traffic Engineering, University of California

R. L. Peyton, Assistant State Highway Engineer, Kansas State Highway Commission

K. M. Richards, Manager, Field Services Department, Automobile Manufacturers Association

John H. King,* Manager, Motor Truck Division, Automobile Manufacturers Association

T. E. Shelburne, Director, Highway Investigation and Research, Virginia Department of Highways

H. O. Thompson, Testing Engineer, Mississippi State Highway Department

J. C. Womack, President, American Association of State Highway Officials;[10] State Highway Engineer and Chief of Division of Highways, California Division of Highways

---

The following persons served on the National Advisory Committee during the years indicated in the same capacity as the current member bearing the same footnote indicator:

[1] J. L. Land, Chief Engineer, Bureau of Materials and Tests, Alabama State Highway Department (1956)

[2] C. H. Scholer (1958); H. E. Davis (1959); Pyke Johnson (1960); W. A. Bugge (1961)—Chairman, Highway Research Board

[3] G. M. Sprowls (1956); C. R. Case (1957); W. C. Johnson (1958); Louis Marick (1959); H. M. Straub (1960)

[4] Louis Marick (1960)

[5] R. E. Jorgensen, Engineering Counsel, National Highway Users Conference (1956-1961)

[6] J. C. Young (1956); C. A. Weber (1957-1959); J. C. Womack (1960)

[7] H. A. Mike Flanakin, Highway Engineer, American Trucking Associations (1956-1957)

[8] I. E. Johnson, Manager, Chrysler Corporation Proving Ground (1956-1960)

[9] L. K. Murphy, Construction Engineer, Primary Highways, Maine State Highway Commission (1956-1959)

[10] C. R. McMillan (1958); D. H. Stevens (1960); D. H. Bray (1961)

A. A. Anderson, Chief Highway Consultant, Portland Cement Association (1956-1960)

Hugh Barnes, Assistant Vice-President, Portland Cement Association (Resigned March, 1961)

Douglas McHenry,* Portland Cement Association (1956)

Earl J. Felt,* Portland Cement Association (1957-1960)

B. E. Colley,* Portland Cement Association (Resigned March, 1961)

H. F. Clemmer, Consultant, D. C. Department of Highways and Traffic (1956-1960)

W. C. Hopkins, Deputy Chief Engineer, Maryland State Roads Commission (1956-1961)

R. D. Johnson,* Assistant Engineering Counsel, National Highway Users Conference (1958-1961)

A. S. Wellborn, Chief Engineer, The Asphalt Institute (1956—Resigned March, 1961)

J. M. Griffith,* Engineer of Research, The Asphalt Institute (1956—Resigned March, 1961)

Rex M. Whitton, First Vice-Chairman (1956-1961); Chief Engineer, Missouri State Highway Department. Resigned March 1961 to become Federal Highway Administrator

W. C. Williams, State Highway Engineer, Oregon State Highway Commission (1956-1961)

* Alternate

Preface

The AASHO Road Test was conceived and sponsored by the American Association of State Highway Officials as a study of the performance of pavement and bridge structures of known characteristics under moving loads of known magnitude and frequency. It was administered and directed by the Highway Research Board of the National Academy of Sciences—National Research Council, and was considerably larger and more comprehensive than any previous highway research study.

This report is the fourth in a series of seven major reports on the AASHO Road Test and, except for special studies described in the sixth report, is a comprehensive description of all research related to bridge structures. Titles of the other major reports, and several associated publications, are listed in Section 1.3 of this report.

The report is presented in six chapters. The first describes the objectives, scope and background of the research and the organization necessary to carry out the research. The second chapter is a description of the test structures and the experiments; the third chapter contains results of tests with repeated stresses; and the fourth contains results of dynamic load tests. The fifth chapter discusses several supplementary tests and studies, and the sixth contains a summary of findings and conclusions.

Acknowledgments

Personnel from many organizations and industrial firms assisted in various phases of the bridge research activities at the AASHO Road Test. It is impractical to list in this report the names of all individuals who contributed to this endeavor. However, the efforts of the following organizations are particularly acknowledged:

The Bureau of Public Roads of the U. S. Department of Commerce, for technical advice, services, loan of personnel and loan of bridge instrument trailer.

The Illinois Division of Highways, for making available facilities for testing of materials and for services in preparing construction specifications and in providing construction control.

The University of Illinois, for loan of equipment, performance of tests of materials, advice and conduct of the cooperative investigation "Analysis and Interpretation of Dynamic Behavior of Test Bridges at the AASHO Road Test."

The Portland Cement Association, for loan of equipment, technical services and conduct of fatigue tests of reinforcing bars and other materials.

The Lehigh University, for conduct of fatigue tests of prestressing wire and strand.

The American Trucking Associations, the Canadian Good Roads Association, and the Portland Cement Association, for the services of resident observers and consultants.

The Association of American Railroads, for loan of the mechanical oscillator; the U. S. Army Transportation Corps, the U. S. Army Ordnance Corps, the Caterpillar Tractor Company, the White Motor Company, and Hutchens and Son Metal Products, for loan of special vehicles used in the post-traffic tests; and the U. S. Steel Corporation, for loan of billets used for loading the special vehicles.

Definitions of Terms

The following definitions apply to the terms as used in this report:

Exterior beam. The bridge beam closest to the bridge curb.

Interior beam. The bridge beam closest to the center of the roadway.

Center beam. The bridge beam between the interior and exterior beams of the same bridge.

Unloaded bridge. The state of loading in which the bridge is subjected only to its own weight and is at rest.

Loaded bridge. The state of loading in which a vehicle, either moving or stationary, is on the bridge.

Approach end of plate. The end of the partial-length cover plate nearest to the turnaround.

Exit end of plate. The end of the partial-length cover plate nearest to the test pavements.

Regular test vehicle. The vehicle assigned to the particular bridge during the regular test traffic.

Outside wheelpath. The wheelpath closest to the bridge curb.

Inside wheelpath. The wheelpath closest to the center of the roadway.

Original bridges. Test bridges completed prior to the beginning of regular test traffic (Bridges 1A, 1B, 2A, 2B, 3A, 3B, 4A, 4B, 5A, 5B, 6A, 6B, 7A, 7B, 8A and 8B).

Replacement bridges. Bridges 9A and 9B, which replaced Bridges 4A and 4B during the period of regular test traffic.

Crawl speed. Slow speeds of approximately 3 mph; sometimes referred to as creep speed.

Fatigue failure. A complete or very extensive fracture caused by repeated stressing.

Fatigue life. The number of cycles of stress to fatigue distress.

Fatigue cracking. Visible cracks caused by repeated stressing.

Fatigue distress. Both fatigue cracking and fatigue failure.

Endurance limit. The limiting value of stress range below which the material can presumably endure an infinite number of stress cycles.

Amplification factor. The ratio of the measured instantaneous dynamic response to the maximum crawl response.

Dynamic increment. The instantaneous difference between the dynamic response and the corresponding crawl ordinate, expressed in terms of the maximum crawl response.

Stress range. The sum of the maximum live load stress and the rebound stress.

Minimum stress. The difference between dead load stress and the rebound stress.

Rebound stress. The largest amplitude of the negative half-cycles of stress fluctuations after a vehicle crossed the bridge.

Rebound factor. The ratio of the sum of the maximum transient stress and the rebound stress to the maximum transient stress.

Transient stress (or deflection). Temporary stress (or deflection) caused by a moving vehicle.

Effective yield strength. The difference between the yield point and the average residual stress of the flange.

Static yield point. The maximum stress that the tension test coupon can support permanently without yielding. It was obtained by stopping and balancing the testing machine after yielding was reached.

Overstress. Stresses in excess of the allowable stresses given in the eighth edition of the Standard Specifications for Highway Bridges of the American Association of State Highway Officials. The following values of allowable stresses are of particular interest in this report:

Tension in extreme fibers of rolled shapes of structural carbon steel subject to bending ...	18,000 psi
Tension in precompressed tensile zone of prestressed concrete beams after losses have occurred	zero
Tension in steel reinforcement of intermediate grade in reinforced concrete flexural members	20,000 psi

Failure. A condition reached in a bridge when the concrete of the slab was crushed or the tension steel fractured, or when an already extreme permanent deformation at midspan continued to increase at an increasing rate with each passage of the vehicle.

Ultimate strength. The bridge moment resistance corresponding to failure in tests with increasing loads.

Ultimate capacity. The moment resistance or vehicle loads at failure in tests with increasing loads.

Note: The symbols (nomenclature) used throughout this report are listed in Appendix C.

Contents

THE AASHO ROAD TEST
Report 4
Bridge Research

Chapter 1

Introduction

This chapter describes the objectives, scope and limitations of the bridge research, and includes brief descriptions of the background of the project and the organization for the research. It also lists associated reports on various phases of the bridge research and other activities at the project site.

1.1 OBJECTIVES AND SCOPE

1.1.1 Objectives

The AASHO Road Test was conceived and sponsored by the American Association of State Highway Officials as a study of the performance and capabilities of highway pavement and bridge structures of known characteristics under moving loads of known magnitude and frequency. It was intended to develop engineering knowledge that could be used in the design and construction of new highway pavements and bridges, in the preservation and improvement of existing pavements and bridges, and in advancing toward the ultimate goal of determining the optimum balance between the cost of vehicle operation and the cost of the highway.

The bridge experiment was included in the AASHO Road Test to determine significant effects of specified axle loads and gross vehicle loads when applied at known frequency on bridges of known design and characteristics. The experiment was designed as a series of case studies of specific problems related to repeated load applications and to dynamic effects of moving vehicles.

In accord with the general aim and the scope of the experiment, detailed objectives of the bridge research were formulated by an Advisory Panel on Bridges and approved by the National Advisory Committee as follows:

1. To determine the behavior of certain short-span highway bridges under repeated applications of overstress;
2. To determine the dynamic effects of moving vehicles on these short-span highway bridges.

In connection with the first objective, the primary questions were concerned with the fatigue life of structures subjected to repeated high stresses and the manner in which distress is caused by repeated high stresses. This study was effected by observations of cumulative effects of the repeated overstress and correlation of the observed behavior with the available laboratory information.

The second detailed objective of the bridge research was concerned with the behavior of individual test bridges under a range of loads. It involved the correlation of observed dynamic effects with those predicted by theoretical computations.

1.1.2 Scope

The selection of the test bridges was based on the requirements of the first objective. Each bridge was designed for a particular vehicle approximating closely the regular test vehicles assigned to the bridge for repeated load tests.

Eighteen slab-and-beam bridges were included. Each bridge was a simple-span structure consisting of three beams and a reinforced concrete slab. The beams, spanning 50 ft, were wide-flange, rolled steel sections with or without cover plates, precast prestressed concrete

I-sections and reinforced concrete T-beams cast monolithically with the slab. The slabs, 15 ft wide, provided one 14-ft lane for the test traffic.

The specific factors included in the bridge research program are grouped under two headings, beam type and stress level, as in Table 1. There were six different beam types: three types of steel beams—noncomposite without cover plates, noncomposite with cover plates and composite with cover plates; two types of prestressed concrete beams — post-tensioned and pretensioned; and one type of reinforced concrete beams—cast-in-place.

Two levels of maximum tensile stress were chosen for the design of each beam type: 27,000 and 35,000 psi for the steel beams, 300 and 800 psi for the concrete of prestressed concrete beams, and 30,000 and 40,000 psi for the reinforcing bars of the reinforced concrete beams. The chosen stress levels were obtained by variations of the cross-section and of the design vehicles; thus the stress level encompassed two principal variables: the characteristics of the cross-section and the characteristics of design vehicle, axle loadings and configurations. Each variant of the stress level was accompanied by a change in the characteristics of the cross-section or of both the cross-section and the design vehicle, axle loadings and configurations.

The investigation included five types of tests:

1. Regular test traffic;
2. Dynamic tests;
3. Post-traffic tests;
4. Miscellaneous tests; and
5. Determination of properties of finished structures.

Items 1, 2 and 5 were connected directly with the major objectives of the test. Item 3, including accelerated fatigue tests, tests with special or specially-equipped vehicles and tests to failure with increasing loads were added to supplement the major objectives and to better utilize the test structures available. The miscellaneous tests listed as Item 4 were related to the over-all bridge behavior and were generally helpful in the interpretation of the test data, but were not essential to achieving the major objectives of the test.

1.1.3 Limitations

The findings of this report pertain to the specific structures included in this investigation. Because of the relative simplicity of the test bridges and the uniformity of the test traffic, the results are not directly applicable to bridges used as part of the highway system, except where such applications are made on the basis of theories proven elsewhere to be able to account for the effects of the differences between the test and practical structures.

Each "x" in Table 1 represents one bridge and each "y" represents a pair of duplicate bridges. There were fourteen different kinds of bridges and four replicates. Each pair of duplicate bridges was placed in the same lane of traffic in tandem, so that both were subjected to vehicles of the same characteristics. However, the dynamic effects of the vehicles could differ for the two structures because of changes in dynamic behavior of the moving vehicles induced by the first bridge. To this extent, no two bridges of replicate design received replicate treatment.

TABLE 1

PRINCIPAL DESIGN FEATURES OF TEST BRIDGES [1]

Beam		Design Stress Level, Maximum Tension (psi)		No. of Bridges
Material	Type			
Steel		*27,000*	*35,000*	
	Noncomposite, no coverplates	x	xx	3
	Noncomposite, coverplates	xy	y	5
	Composite, coverplates	x	x	2
Prestressed concrete		*300*	*800*	
	Post-tensioned	x	x	2
	Pretensioned	x	x	2
Reinforced concrete		*30,000*	*40,000*	
	Cast-in-place	y	y	4

[1] x represents one bridge; y, one pair of duplicate bridges.

The choice of the stress levels was dictated by the objective concerned with the effects of repeated overstress under test traffic. In steel bridges, the primary interest was in the fatigue strength of rolled beams with partial-length cover plates and in the progression of yielding. In prestressed bridges, attention was focused on the fatigue cracking of prestressed concrete subjected to tensile stresses and on the fatigue behavior of prestressing steel in cracked beams. In reinforced concrete bridges, studies were made of the width and spacing of tensile cracks and the fatigue behavior of deformed bars.

Thus, the designs of the steel, prestressed concrete and reinforced concrete beams were based on different criteria, each aimed at obtaining answers to problems peculiar to the type involved. Because of the differences in these design criteria, *there is no basis for direct comparisons between the steel, prestressed concrete and reinforced concrete test structures.*

1.2 DEVELOPMENT AND EXECUTION OF BRIDGE RESEARCH

1.2.1 Background

The test facility was located near Ottawa, Ill. The history of events and the primary factors considered in selecting the site and in designing the experiment are discussed in "The AASHO Road Test: History and Description of the Project" (HRB Special Report 61A).

The Road Test included facilities for both pavement research and bridge research. The principal design variables were those that specified pavement or bridge structures and test vehicles. The test facilities for pavement research included asphaltic concrete and portland cement concrete pavements of a wide range of design. The test vehicles were of single- and tandem-axle types with the axle load varying from 2,000 lb to 30,000 lb for single axles and from 24,000 lb to 48,000 lb for tandem axles. Ten different axle arrangement-axle load combinations were used. During regular test traffic, any particular pavement section or bridge was tested with only one of the ten combinations.

Early planning for the Road Test contemplated only pavement research. In December 1951, the scope of the project was expanded at the request of the AASHO Committee on Bridges and Structures by the inclusion in the test facility of several test bridge spans for case studies of the effect of repeated overstress on the life of highway bridge structures. The design variables for bridge research were selected and the criteria for the design of the test bridges were prepared by a special subcommittee of the AASHO Working Committee. Preliminary plans included only steel I-beam bridges. The special subcommittee expanded the program by the inclusion of reinforced and prestressed concrete structures.

The designs were carried out by the personnel of the Bridge Division of the Bureau of Public Roads, except that preliminary designs for the concrete test structures were made by the personnel of the Structural and Railways Bureau of the Portland Cement Association. Construction drawings and specifications were prepared by the personnel of the Illinois Division of Highways. The experiment outline and the bridge designs were reviewed by the Advisory Panel on Bridges and by the National Advisory Committee. Upon the recommendations of these groups the experiment was approved by the Highway Research Board.

1.2.2 Organization

The project was sponsored by the American Association of State Highway Officials. It was financed by 49 States, the District of Columbia, the Commonwealth of Puerto Rico, the Bureau of Public Roads of the U. S. Department of Commerce, the Automobile Manufacturers Association, the American Petroleum Institute and the American Institute of Steel Construction. The Department of Defense, through its Army Transportation Corps Road Test Support Activity, furnished the drivers for the test vehicles. Foreign countries and domestic materials and transportation associations furnished resident observers and staff consultants.

The Highway Research Board, with the approval of its parent organization, the National Academy of Sciences-National Research Council, accepted the responsibility for administration and direction of the project. The administrative organization established by the Highway Research Board for the supervision and direction of the project is discussed in "The AASHO Road Test: History and Description of the Project."

Bridge research was conducted by the staff of the Bridge Research Branch which was responsible for materials sampling during construction, instrumentation, testing (except for operation of vehicles), collection, reduction and analysis of the data, and preparation of reports on bridge research. The branch was guided by the Advisory Panel on Bridges, appointed by the Highway Research Board.

Studies of the dynamic effects of moving vehicles on the response of the test bridges were conducted in cooperation with the Civil Engineering Department of the University of Illinois under the guidance of the Special Committee on Dynamic Behavior of Test Bridges. The dynamic tests were planned jointly by the staffs of the Road Test and the University. The tests were conducted by the Road Test staff, and the data were analyzed and reported by the staff of the University.

The supervision of the construction of the test bridges was performed by the Illinois Division of Highways through a permanent task force assigned to the project. All superstructures were constructed by Valley Builders, Inc., of Spring Valley, Ill.

The personnel of the Bridge Research Branch included the bridge research engineer and his assistant, two to four junior engineers assigned to the project by the Bureau of Public Roads, and three to five technicians. Additional engineering services were provided by resident staff consultants and observers assigned to the branch for specific studies.

Several other branches of the project provided services to the Bridge Branch, particularly the Data Analysis Branch, the Materials Branch and the Special Assignments Branch.

1.3 ASSOCIATED REPORTS

A brief description of the bridge research may be found in AASHO Road Test Report 1, "History and Description of the Project," HRB Special Report 61A. Detailed data on bridge materials are contained in Chapter 7 of AASHO Road Test Report 2. Miscellaneous tests of bridges with special vehicles are described in AASHO Road Test Report 6.

The results of the cooperative investigation were reported to the Road Test by the University of Illinois in a report entitled "Dynamic Studies of Bridges on the AASHO Test Road," and issued as Structural Research Series No. 227 of the Civil Engineering Studies of the University of Illinois. Chapter 4 of this report is a condensation of the Illinois Report.

Further information on bridge research at the AASHO Road Test may be found in the following special reports of the Highway Research Board:

"Bridge Research at the AASHO Road Test," HRB Special Report 38, pp. 24-43 (1958).

"Creep and Shrinkage of Concrete in Outdoor Exposure and Relaxation of Prestressing Steel," HRB Special Report 66, pp. 103-131 (1961).

"Fatigue Tests of Bridge Materials of the AASHO Road Test," HRB Special Report 66, pp. 132-147 (1961).

All principal test data collected at the Road Test are stored on IBM punch cards. The titles of the data systems pertaining to bridge research are listed in Appendix A. The data are available from the Highway Research Board at the cost of reproduction.

Chapter 2

Description of Test Structures and Experiments

This chapter contains descriptions of the test structures and their properties, and the instrumentation necessary to measure and record the phenomena connected with their behavior. It also describes the various test programs and methods as well as the environmental conditions at the test site.

2.1 TEST BRIDGES

2.1.1 Layout of Project

The test facility was laid out in six loops shown in Figure 1; four major loops (3 through 6) which were tested under tractor-semitrailer truck traffic, one smaller loop (2) tested under light truck traffic, and one auxiliary loop (1) provided for study under static, creep speed and vibrating loads and for observations of the effects of time and weather with no traffic.

Each loop was a segment of a four-lane divided highway whose parallel roadways, or tangents, were connected by turnarounds at both ends. The four major loops were located along the line of Interstate Route 80 so that upon completion of the test and rehabilitation, the tangents could be used as a portion of the new highway.

The tangents of the major loops were 6,800 ft long. Each turnaround on the four major loops had 200-ft radius and was superelevated to permit vehicle operation on the outer lane at 25 mph with no side thrust. The north tangent of each loop was a flexible pavement with asphaltic concrete surfacing. The south tangent of each loop was a rigid pavement with portland cement concrete surfacing.

The test bridges were located in Loops 5 and 6 which were subjected to the traffic with the heaviest trucks. They were placed in groups of four at the beginning of the tangents containing the pavement test sections (Fig. 2). The bridges at the west ends of Loop 5 and Loop 6 were made with steel beams. At the east end of Loop 5 the bridges were made with prestressed concrete beams, and at the east end of Loop 6 with reinforced concrete beams. Early in the course of the tests two of the bridges at the west end of Loop 6 failed and were replaced. Thus, eighteen test bridges were included in the experiment.

Each bridge provided one traffic lane. At both ends of each bridge site there were heavily reinforced concrete pavement slabs 20 ft long supported by the bridge abutments. Beyond these slabs portland cement concrete pavements extended for at least 145 ft towards the turnarounds and for at least 35 ft towards the test pavements.

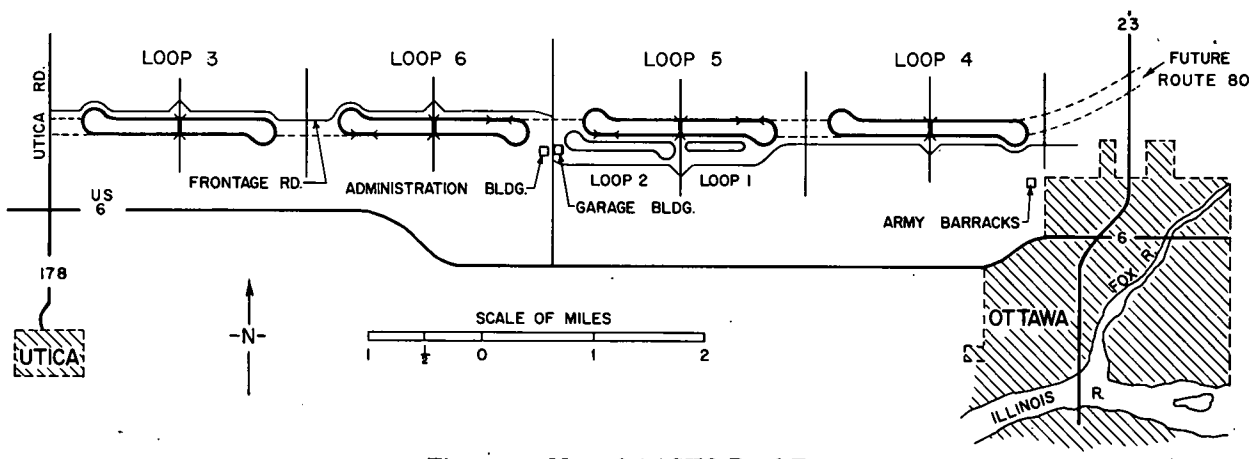

Figure 1. Map of AASHO Road Test.

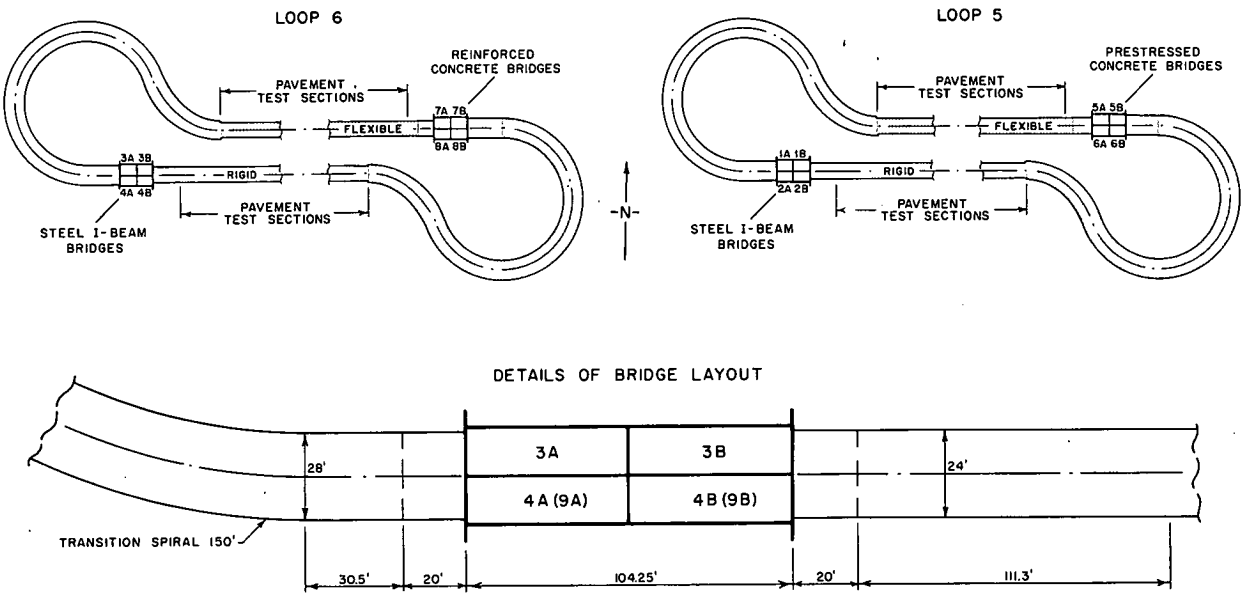

Figure 2. Locations of test bridges.

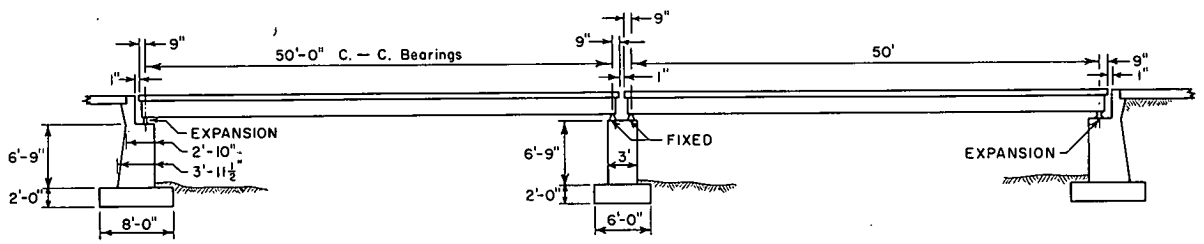

Typical Longitudinal Section

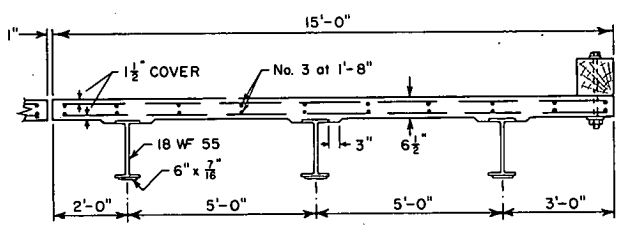

Section of Bridge 1A at Midspan

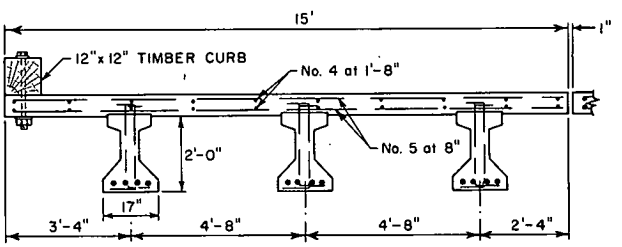

Section of Bridge 5A at Midspan

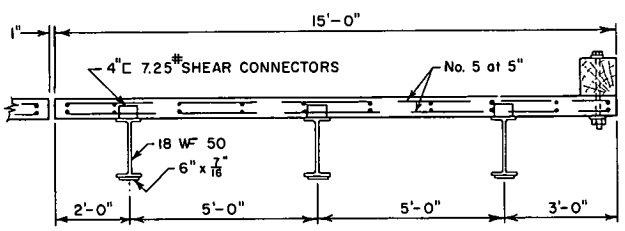

Section of Bridge 2B at Midspan

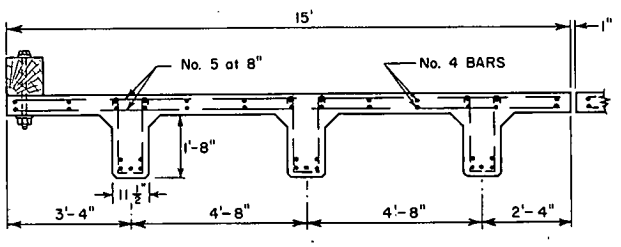

Section of Bridge 7A at Midspan

Figure 3. Typical bridge sections.

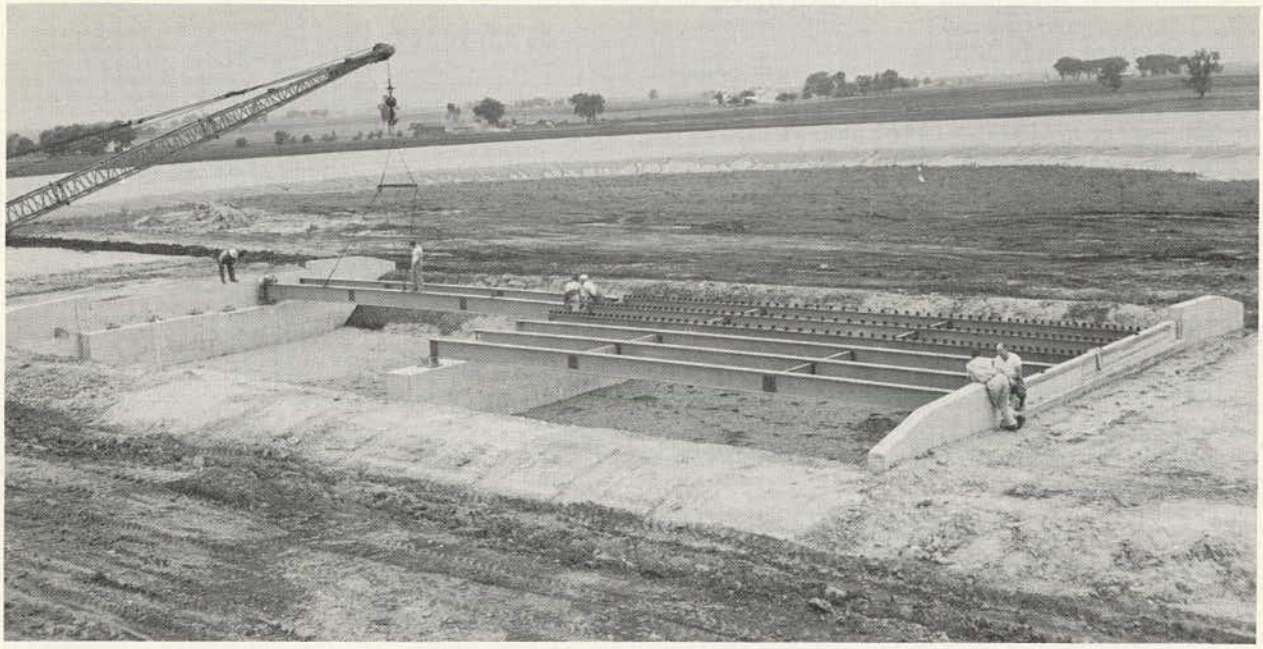

Figure 4. Erection of steel beams.

On each traffic lane the end of the tangent was located about 50 ft beyond the nearest bridge abutment towards the turnaround. The distance between the bridge abutment and the nearest pavement test section was in excess of 130 ft at all locations.

All test bridges were built on 0.2 percent grades. Bridges at the west end of Loop 5 sloped toward the pavement test sections; all other bridges sloped toward the nearest turnaround.

2.1.2 Description of Test Structures

Typical cross-sections of test bridges are shown in Figure 3. The four bridges at each location were supported on a common concrete substructure consisting of two abutments and one pier (Fig. 4). The piers and abutments for all bridges were identical in all major details. They were supported on spread footings located on a hard-clay till.

Steel bearings supported the superstructures. Fixed bearings were placed on the center piers and expansion rockers on the end abutments. A preformed bearing pad, ⅛ in. thick, was provided for distribution of the load from the bearing to the substructure. Both the fixed and the expansion bearings are shown schematically in Figure 7.

Each bridge superstructure consisted of three identical beams, an exterior beam near the outside edge of the roadway, a center beam, and an interior beam near the center of the roadway. The three beams were simply supported on a 50-ft span and carried a reinforced concrete slab 6½ in. thick and 15 ft wide. The slab was separated from the adjacent bridges and the backwall of the abutment by 1-in. clear space and was provided with a 12- by 12-in. timber curb bolted to the outside edge. The timber curb was made of two pieces spliced loosely at midspan.

Principal details of bridges are discussed; a more detailed description of the test bridges may be found in Section 7.1 of Report 2.

Steel Bridges.—The cross-sections of Bridges 1A and 2B (Fig. 3) are typical of all noncomposite and composite steel bridges. The steel bridges differed among themselves in the size of beams, in the length and presence or absence of cover plates, in the presence or absence of shear connectors and in the slab detail around the top flange of the steel beams.

The slabs of noncomposite bridges (those with no shear connectors) were built with 3-in. wide haunches flush with the bottom of the top flanges to provide lateral support for the beams. The slabs of composite bridges were built flush with the top surface of the beams. Along the transverse edges over the supports, the slabs of steel bridges were thickened and were in contact with the top surface of the end diaphragms (Fig. 5).

The slab reinforcement was the same for all ten steel bridges. It consisted of two layers of longitudinal and transverse deformed bars, placed at the top and at the bottom of the slab. The minimum concrete cover over the steel was

1½ in. Each layer was made of longitudinal No. 3 bars spaced at 1 ft 8 in. and transverse No. 5 bars spaced at 5 in.

The steel sections were rolled wide-flange beams with or without cover plates. The three beams in each bridge were spaced at 5 ft (Fig. 3). The nominal size of the rolled sections and the lengths of the cover plates are given for each bridge in Table 2.

Three noncomposite bridges had no cover plates, three had cover plates on the bottom flange only and two had cover plates of equal size on both flanges. The two composite bridges had cover plates on the bottom flange only. All plates were 7/16 by 6 in. in cross-section and were welded to the flange with 5/16-in. continuous fillet welds along the longitudinal edges. The ends of the plates were not welded to the rolled sections.

The top surface of the steel beams in noncomposite bridges was coated with a 1:4.43 mixture of graphite and linseed oil to inhibit formation of bond. In composite bridges, the interaction between the slab and the steel beams was obtained with mechanical shear connectors. The connectors were 4-in., 7.25-lb channels 5½ in. long attached to the top flanges with welds transverse to the beam axis. The spacing and positioning of connectors are shown in Figure 5.

TABLE 2

STEEL BRIDGES, BEAM SIZES AND LENGTHS OF COVER PLATES

Bridge		Nominal Beam Size	Length of Cover Plate	
Desig.	Type		Top	Bottom
1A	Noncomposite	18WF55	0	20 ft 6 in.
1B	Noncomposite	18WF50	0	0
2A	Noncomposite	18WF55	0	0
2B	Noncomposite	18WF50	0	14 ft 0 in.
3A	Noncomposite	21WF62	0	0
3B	Composite	18WF60	0	18 ft 6 in.
4A, 4B	Noncomposite	18WF60	0	19 ft 0 in.
9A, 9B	Noncomposite	18WF96	17 ft 0 in.	17 ft 0 in.

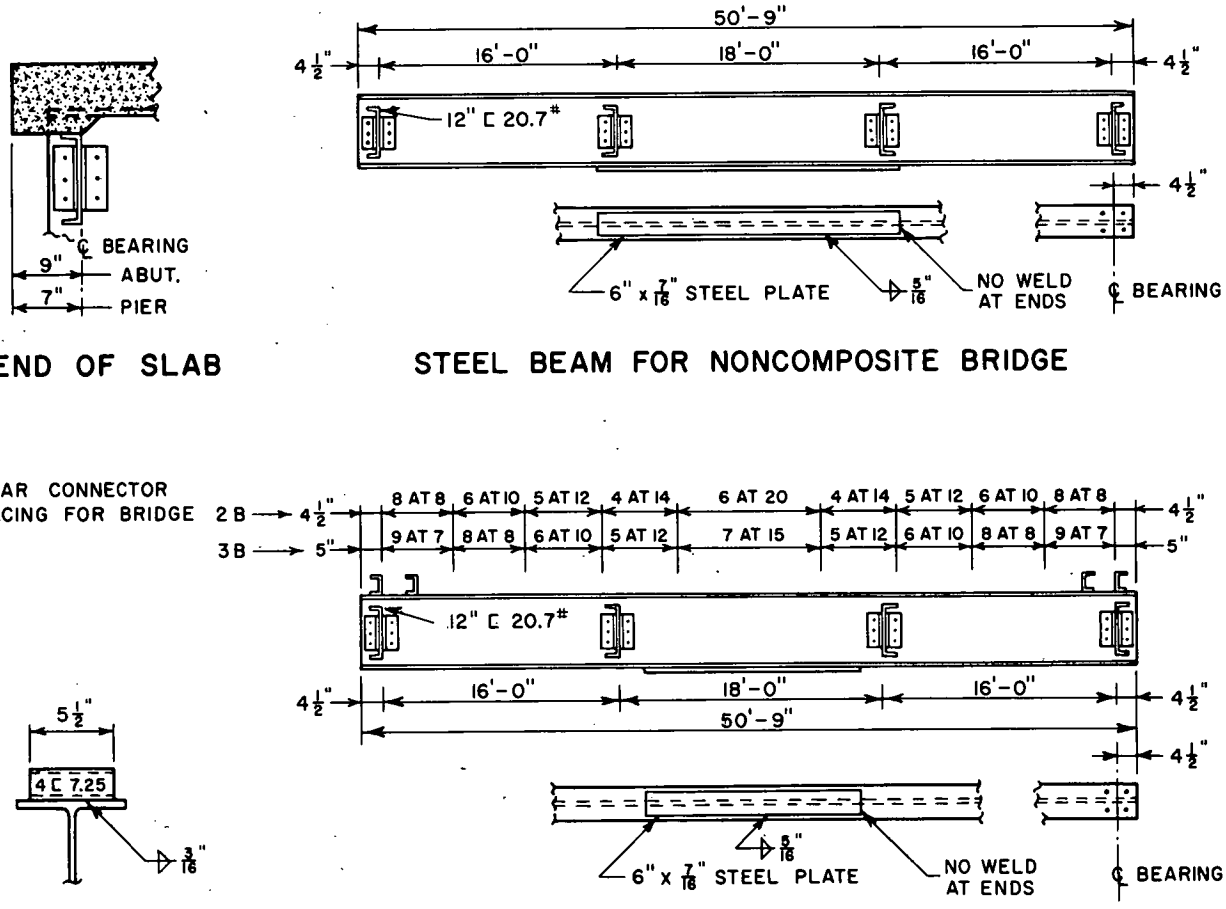

Figure 5. Details of steel bridges.

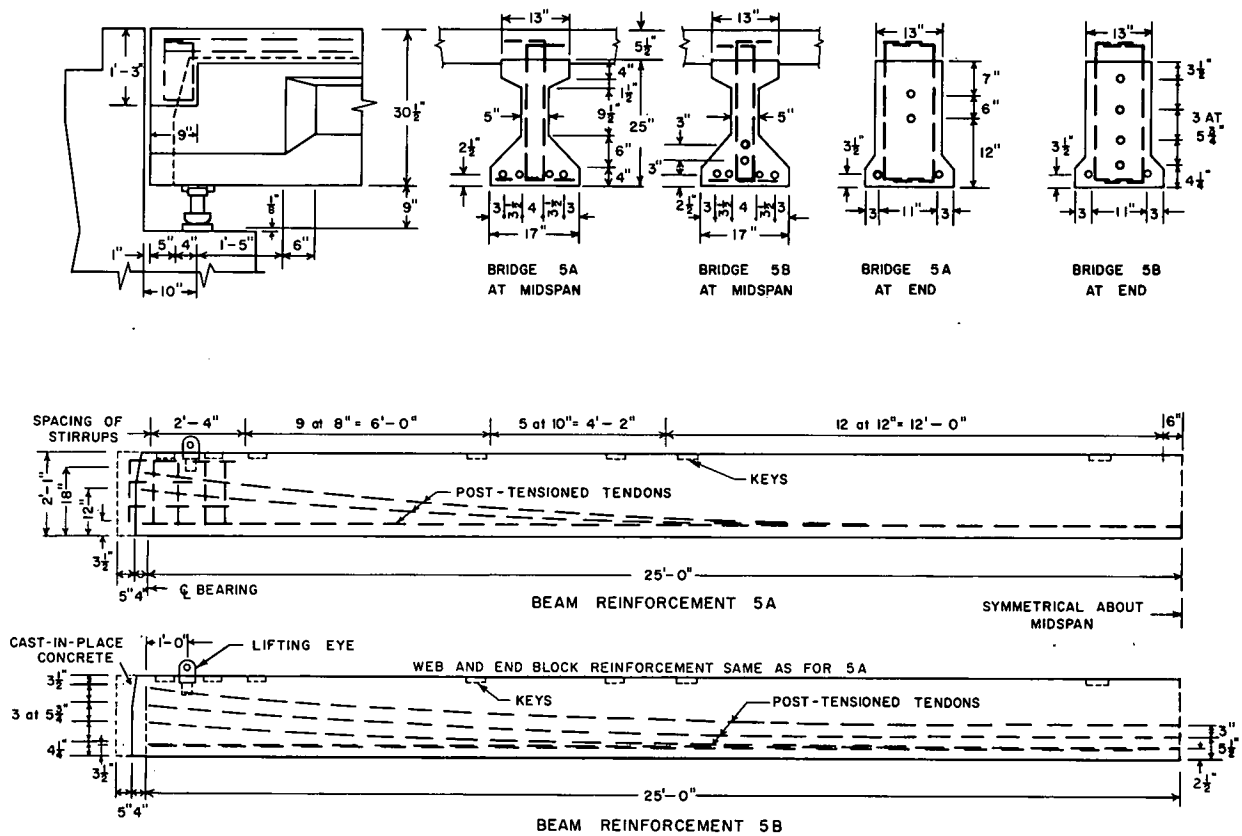

Figure 6. Details of Bridges 5A and 5B.

All ten bridges were provided with diaphragms near the third points and at the ends. The diaphragms (Fig. 5) were fastened to the beams by means of angles bolted to the beams and riveted to the diaphragms.

Prestressed Concrete Bridges.—The four bridges with prestressed concrete beams had the same cross-section except for the type and placement of prestressing steel, and details connected with end anchorages. A cross-section of Bridge 5A is shown in Figure 3.

The slab extended between ¼ in. and 1 in. below the top surface of the beams. It was reinforced with two layers of deformed bars placed in the top and bottom of the slab. Each layer consisted of transverse No. 5 bars on 8-in. centers and longitudinal No. 4 bars on 1-ft 8-in. centers. The minimum concrete cover over the reinforcement was 1½ in.

The beams, spaced at 4 ft. 8 in., were precast I-sections 25 in. deep and 17 in. wide at the bottom. Beams for Bridges 5A and 5B were post-tensioned and those for Bridges 6A and 6B were pretensioned. The details of the two types of bridges are shown in Figures 6 and 7, respectively.

The post-tensioned beams were reinforced with draped parallel-wire cables. Each tendon was made up of ten wires of 0.192-in. nominal diameter enclosed in a flexible metal conduit, anchored by Freyssinet cone anchorages and grouted. There were four such tendons in each beam of Bridge 5A and six in each beam of Bridge 5B.

The pretensioned beams were reinforced with straight ⅜-in., 7-wire strands anchored by bond. Sixteen strands were used in each beam of Bridge 6A and 20 in each beam of Bridge 6B.

The web reinforcement, the end blocks, the connection between the slab and the beams, and the diaphragms were the same in all prestressed concrete bridges. The web reinforcement was made of No. 3 bars extending above the precast beams. The end blocks (Figs. 6 and 7) were reinforced with No. 4 horizontal bars in addition to vertical stirrups. The connection between the slab and the beams was furnished

by extensions of the stirrups and by recessed keys (2 by 6 by 6 in.) located at alternate spaces between the stirrups. In addition, the top surfaces of the precast beams were left in a rough condition.

Concrete diaphragms were cast at each end of the beams. In bridges with post-tensioned beams they were cast monolithically with the end caps and the slab. In bridges with pretensioned beams they were cast monolithically with the slab and were connected to the beams with reinforcing bars passing through sleeves in the precast sections.

Reinforced Concrete Bridges.—The reinforced concrete bridges were of monolithic T-beam construction. The cross-section of all four reinforced concrete bridges was the same as that shown for Bridge 7A (Fig. 3) except for details of the tension reinforcement in the beams.

The slab reinforcement for the reinforced concrete bridges consisted of two layers of longitudinal and transverse bars placed within the slab so as to provide a minimum concrete cover over the steel of 1½ in. In each layer, the longitudinal reinforcement was made up of 13 No. 4 bars and the transverse reinforcement of No. 5 bars spaced at 8 in.

The stems of the T-beams were 11½ in. wide, 1 ft 8 in. deep below the bottom of the slab and were spaced at 4 ft 8 in. (Fig. 8). The beams were reinforced in tension with two layers of deformed bars. Three No. 11 bars were placed in the bottom layer and two No. 9 bars were placed in the top layer of all concrete beams. In addition, the top layer of each beam of Bridges 8A and 8B included one No. 8 bar.

The webs were reinforced with vertical stirrups made of No. 3 bars. The stirrups were omitted from the center portion of each beam (Fig. 8). Concrete diaphragms, cast monolithically with the beams and the slab, were provided at both ends of each bridge.

2.1.3 Design of Superstructures

The design of test bridges evolved from two basic requirements: (1) the experiment was to be limited primarily to the study of the behavior in flexure of the principal load-carrying members, that is, the beams; and (2) the beams were to be subjected to the selected stress level at each passage of the regular test vehicles.

To obtain the desired stresses in the tests, the designs of beams were based on moments computed by an elastic analysis rather than on moments obtained by conventional design methods. On the other hand, the slabs, web reinforcement and miscellaneous details were designed by conventional methods.

The bridges were designed for loadings approximating the spacing and weights of axles of the regular test vehicles. The design loadings are shown in Figure 9. Loadings 1 and 2 approximated trucks used on Loop 5, whereas loadings 3, 4 and 5 approximated trucks used on Loop 6. Loadings 4 and 5 represented the same vehicles. Loading 4 was used in the de-

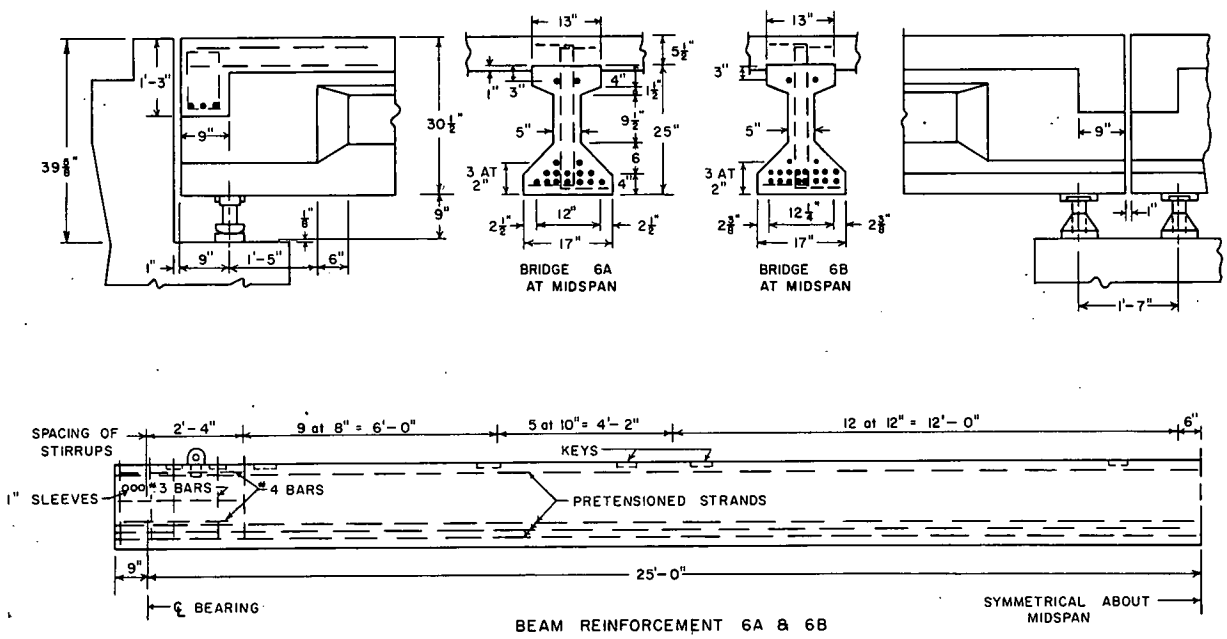

Figure 7. Details of Bridges 6A and 6B.

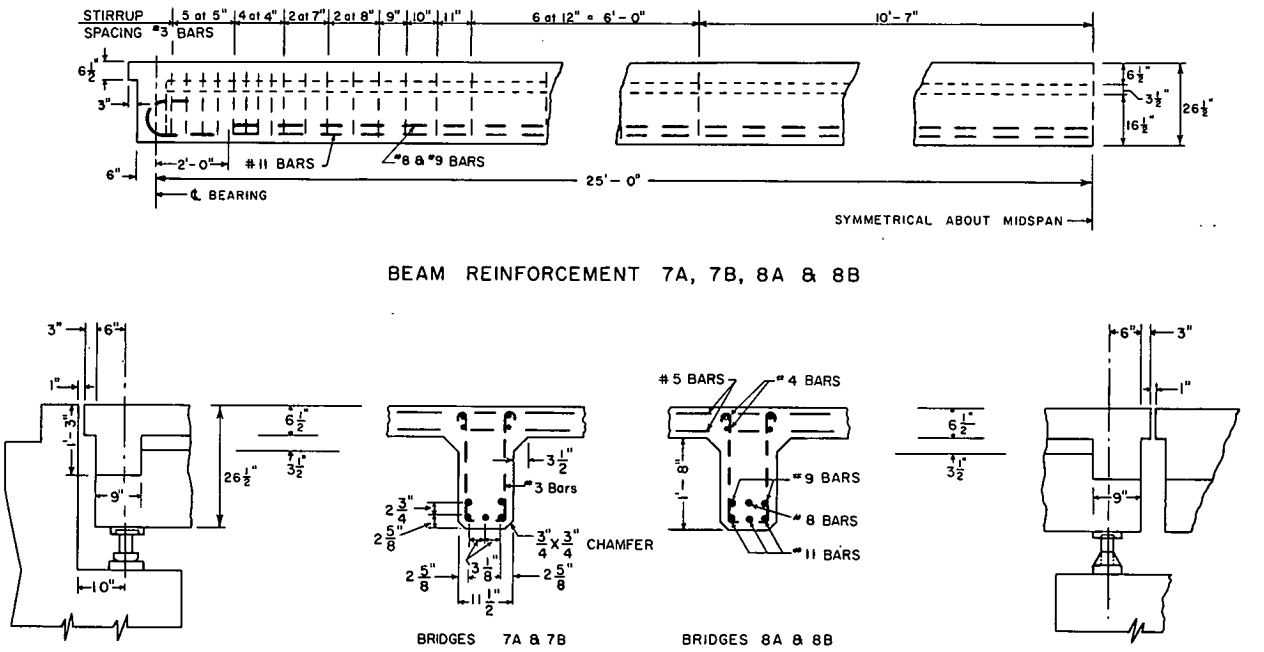

Figure 8. Details of reinforced concrete bridges.

sign of original bridges completed before the final axle weights had been established. Loading 5, used in the design of replacement bridges 9A and 9B, represented the average axle weights and dimensions of actual test vehicles.

Bridges 1 through 8 were designed before the work was started at the test road site; they are referred to in this report as the original bridges. Bridges 9A and 9B replaced original bridges 4A and 4B, and were designed after the test traffic began. The following discussion applies to the original bridges unless specifically noted otherwise.

Beams.—It was assumed in designing the beams that the trucks would straddle the center beam and that the dead loads would be distributed equally among the three beams. For these conditions, the stresses in the center beam governed. Accordingly, all data presented in this section for the original bridges refer to the center beam.

The major criteria and results of the design of beams are summarized in Table 3. The factors for the distribution of external moment to the slabs and the individual beams were obtained from an elastic analysis.* The impact factors were estimated on the basis of theoretical studies of the effect of smoothly rolling loads.

Two of the steel bridges and all concrete bridges were designed assuming complete interaction between the slab and the beams. In six steel bridges 10 percent composite action was assumed to account for the effects of friction between the slab and the beams. This assumption of partial interaction made it unnecessary to provide top cover plates in Bridges 1A, 4A and 4B.

The designs of Bridges 9A and 9B were made for the exterior beam (beam closest to the timber curb) since measurements on the original structures showed it to be the most highly stressed. No composite action was assumed to exist between the slab and the beams because none was found in the original bridges. The truck was again assumed to straddle the center beam, but the distribution of the dead load, the distribution factor for the live load and the impact factor were selected to conform to actual conditions that had been observed at the Road Test.

The designs of all steel beams were based on the moment of inertia method. The critical stress in beams with partial-length cover plates was the tensile stress in the bottom flange of the rolled section at the end of the plate (Table 3). The maximum stresses in the cover-plated

* Siess, C. P., "Moments in the Simple-Span Slab and Girder Bridges." MS thesis, Univ. of Illinois (1939).

Newmark, N. M., and Siess, C. P., "Moments in I-Beam Bridges." Univ. of Illinois Eng. Exp. Sta., Bull. No. 336 (1942).

TABLE 3
DESIGN OF BEAMS

Bridge		Design Loading [1]	Distribution Factor [2] (%)	Impact Factor (%)	Composite Action [3] (%)	Governing Design Stress	
Desig.	Type					Location	Max. Tension (psi)
			(a) STEEL BRIDGES				
1A	Noncomposite [4]	1	30.0	10	10	Bottom fiber, end plate	27,025
1B	Noncomposite	1	29.4	10	10	Bottom fiber, near midspan	34,800
2A	Noncomposite	2	29.3	10	10	Bottom fiber, near midspan	35,010
2B	Composite [4]	2	32.6	10	100	Bottom fiber, end plate	35,000
3A	Noncomposite	3	30.6	10	10	Bottom fiber, near midspan	27,330
3B	Composite [4]	3	33.0	10	100	Bottom fiber, end plate	26,940
4A, 4B	Noncomposite [4]	4	30.4	10	10	Bottom fiber, end plate	34,735
9A, 9B	Noncomposite [4]	5	29.5	20	0	Bottom fiber, end plate	26,970
			(b) PRESTRESSED CONCRETE BRIDGES				
5A	Post-tensioned	2	32.2	8	100	Bottom fiber, near midspan	820
5B	Post-tensioned	2	33.3	6	100	Bottom fiber, near midspan	346
6A	Pretensioned	1	33.3	2	100	Bottom fiber, near midspan	828
6B	Pretensioned	1	32.9	2	100	Bottom fiber, near midspan	310
			(c) REINFORCED CONCRETE BRIDGES				
7A, 7B	Cast-in-place	4	32.9	4	100	Re-bars, near midspan	40,000
8A, 8B	Cast-in-place	3	32.9	0	100	Re-bars, near midspan	30,900

[1] See Figure 9.
[2] Ratio of design beam moment to total static moment.
[3] Interaction between slab and beam; partial interaction accounted for by proportional decrease of effective slab width.
[4] With cover plate.

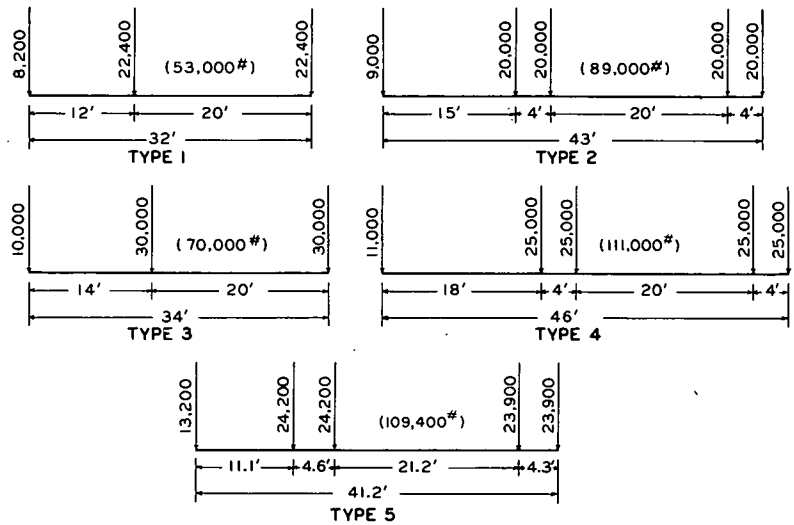

Figure 9. Design loadings.

portion were substantially lower. The critical stress in beams without cover plates was the tensile stress in the bottom flange near midspan. The computed maximum design stresses were very close to the specified values of 27,000 and 35,000 psi.

The prestressed concrete beams were designed on the basis of the moment of inertia of the uncracked section. Except for the governing tensile stresses, the design was made in accordance with the criteria for prestressed concrete bridges developed by the Bureau of Public Roads.* The governing tensile stresses on the bottom surface of concrete beams are given in the last column of Table 3. The stresses in excess of 800 psi were considered to be fictitious values because the concrete was expected to crack at lower stresses.

The reinforced concrete beams were designed by the straightline, cracked section theory. The governing design stresses (Table 3) were those in the bottom layer of the reinforcing bars.

Miscellaneous.—It is apparent from the preceding discussion that the beams of all sixteen test bridges were underdesigned. On the contrary, the slab, shear connectors, web reinforcement and miscellaneous details were designed for current allowable stresses.

The slabs for all bridges were of the same thickness. The reinforcement for each type of bridge (steel, prestressed concrete and reinforced concrete) was designed for its heaviest loading. The distribution factor, the impact factor and the allowable stresses were selected according to AASHO Specifications.**

The design of web reinforcement was based on the nominal shear strength. Conditions at both the ultimate and working load were considered. The design of shear connectors followed the 1956 revision of the AASHO Specifications,* but the procedure was modified to account for the higher design stresses in the steel beams. Additional information on the design of test bridges may be found in HRB Special Report 38.

2.1.4 Construction

The construction of the bridges began in October 1956 with the excavation for the substructures and the casting of the footings, piers and abutments. The substructures at all four locations were completed in the spring of 1957.

The superstructures of the original eight steel bridges, the four reinforced concrete bridges and prestressed concrete bridges 6A and 6B were completed during the 1957 construction season. The post-tensioned beams for Bridges 5A and 5B were in place and the forms for the slabs were substantially complete by the end of the 1957 construction season; the slabs for these two bridges were cast in April 1958. The bridges became accessible to vehicles during the summer of 1958 after the completion of the approach slabs and pavements.

The superstructures for Bridges 9A and 9B were erected adjacent to the existing bridges, moved in place and opened to traffic in the late spring of 1959. Four completed bridges at one

* "Criteria for Prestressed Concrete Bridges." U.S. Department of Commerce, Bureau of Public Roads, Washington, D.C. (1954).

** American Association of State Highway Officials, "Standard Specifications for Highway Bridges." 6th edition, Washington, D.C. (1953).

* American Association of State Highway Officials, "Standard Specifications for Highway Bridges." 7th edition, Washington, D.C. (1957).

Figure 10. Set of four completed bridges.

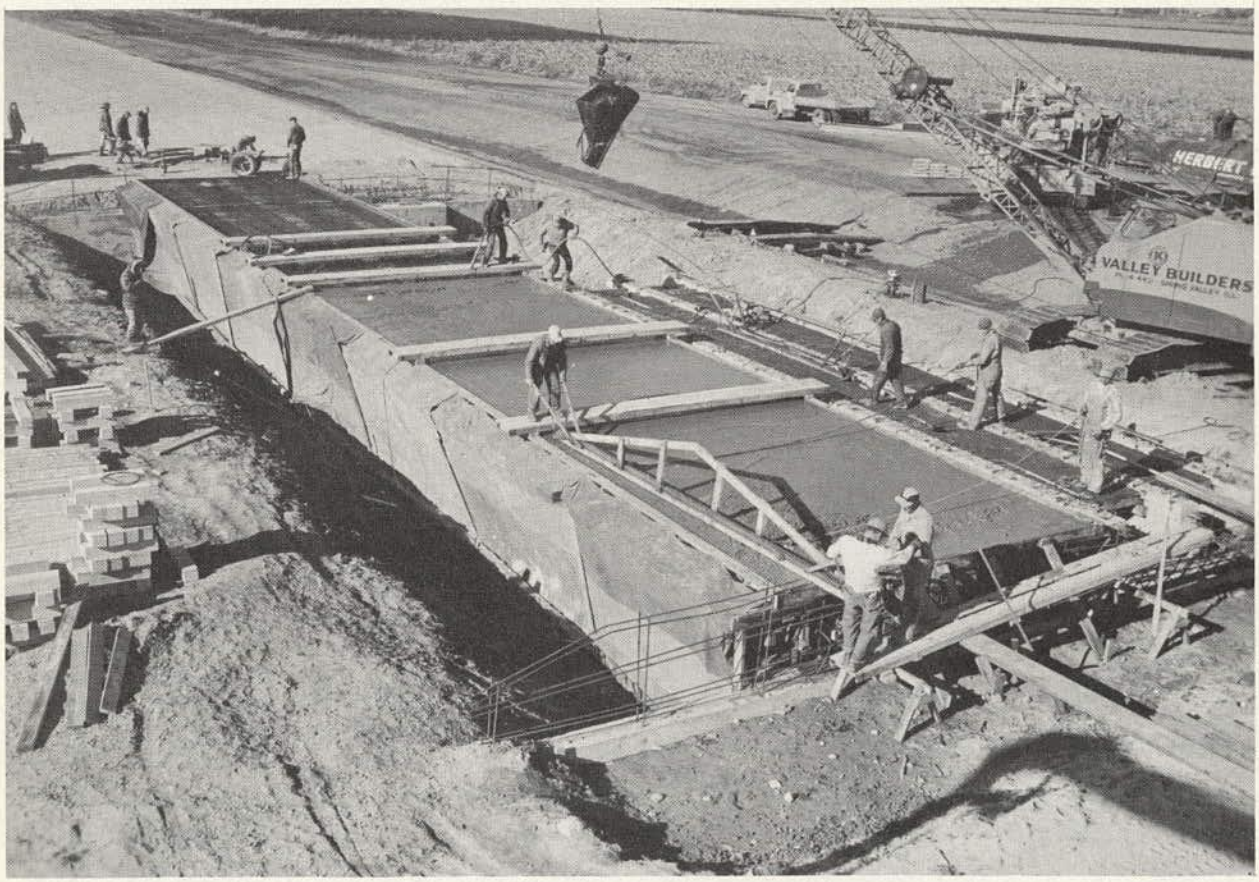

Figure 11. Casting a concrete slab.

location are shown in Figure 10. Other significant construction dates for the test bridges are listed in Appendix B and details concerning construction may be found in Road Test Report 2.

Off-Site Fabrication of Beams.—The steel beams and cover plates were rolled to a greater length than that required by the bridge dimensions. The excess lengths were cut off at the fabricating shop, marked and delivered to the road site to provide material for tension tests. All beams were cambered.

The precast prestressed concrete beams were manufactured at a prestressing plant. The two outside beams of each pretensioned bridge were cast simultaneously on one prestressing bed; the center beam was cast alone. The prestressing strands were stressed one at a time. The load on each strand was measured by a calibrated load cell. The stress was released three to five days after casting, after the strength of concrete had reached 4,000 psi.

Each post-tensioned beam was manufactured independently. The beams were stressed after the concrete had reached a strength of at least 4,000 psi. The tendons were pretensioned with two double-acting Freyssinet jacks, one placed at each end of the beam. The load was measured by a calibrated pressure gage. After the tensioning of all three beams of one bridge, the space between the steel conduit and the wires in each tendon was filled with a neat cement grout.

The concrete for the prestressed beams was mixed at the site of the prestressing beds. It was consolidated in the forms by internal vibration. The beams were steam-cured for 12 to 84 hr. Because the air temperature was low, the post-tensioned beams were steam-cured for an additional 24 hr after grouting.

Control tests of slump and air content were made on each batch of concrete. They averaged 1⅝ in. and 3.9 percent, respectively. Specimens taken for determination of the properties of materials included standard concrete cylinders, several sizes of concrete beams and several different lengths of prestressing steel and of reinforcing bars.

On-Site Construction.—The forms for the construction of the concrete deck slab were supported separately for each bridge. Those for the steel bridges and prestressed concrete bridges were supported from the beams. The forms for each reinforced concrete bridge were supported on bents placed near the abutment and pier, and at the quarter points and midspan.

The concrete for the slabs was mixed at the project site. The placement of concrete began at midspan and progressed simultaneously in both directions (Fig. 11). Consolidation was accomplished by internal vibration along the vertical edges of all slabs and within the beams of the reinforced concrete bridges, and by hand spading elsewhere. The final finish was obtained with two passes of burlap drag.

The concrete in the slabs of all bridges except 6A and 6B was moist-cured for 7 days under two layers of wet burlap blanket covered with waterproof paper. The slabs of prestressed bridges 6A and 6B were winter-cured for 12 days using a layer of insulating material over the top surface, a canvas enclosure along the edges of the forms (Fig. 11). and heating units beneath the structure. The forms and falsework were removed after the concrete had attained the specified strength but not before 14 days after casting the slab.

Control tests of slump and air content were made on each batch of concrete placed in the beams of the reinforced concrete bridges, and on the first three batches and every succeeding third batch placed in the slabs. The average slumps for all concrete cast on the site were 3⅝ in. for concrete bridges and 4⅛ in. for the slabs of the steel bridges. The average air contents were 4.3 and 3.5 percent. Standard concrete cylinders and samples of reinforcing bars were taken during construction for determination of the properties of the bridge materials.

The construction of the two replacement bridges 9A and 9B was essentially the same as that of the original steel bridges, but they were constructed on temporary supports adjacent to Bridges 4A and 4B. This was required to reduce to a minimum the interruption of the test traffic on the loop. The new superstructures were moved on steel rails over the existing substructures and lowered with jacks on the existing steel bearings (Fig. 12).

2.2 PROPERTIES OF FINISHED STRUCTURES

A comprehensive sampling and testing program was conducted to determine the physical characteristics of the materials used in the superstructures of the test bridges. The program included the determination of mechanical properties, fatigue strength, long-time characteristics and residual stresses.

The results of the static tests were subjected to variance analyses and significance tests at the 5 and 1 percent levels. Where no significant differences were found, the test data are presented as means for groups of bridges. Only data essential for understanding of this report are included. Other strength data and details of sampling and testing are given in Section 7.4 of Road Test Report 2.

The results of fatigue and long-time tests are presented as regression equations. The test data were correlated with the aid of several mathematical models containing empirical coefficients and the coefficients were evaluated by regression analysis.* The error term, included

at the end of each equation, delineated limits containing over 90 percent of the test data. (The error terms are equal to twice the standard error of estimate for the fatigue characteristics and 2.5 times the mean absolute residual for the long-time characteristics.) The tests and the analytical studies of the long-time characteristics and of the fatigue characteristics are described in HRB Special Report 66. Only the final equations, found to describe satisfactorily the test data, are reported here.

Actual dimensions of the test bridges were measured on completion of construction. Those dimensions that were different from the values given in Section 2.1.2 and were needed in the analyses are included in this section. A more detailed discussion of the measurements and dimensions is given in Section 7.5 of Road Test Report 2. Certain properties of cross-sections, computed from measured dimensions, are also given in this section.

2.2.1 Properties of Steel

Structural Steel.—The rolled beams and cover plates for the steel bridges were made of structural carbon steel meeting the requirements of ASTM Designation: A7-55T. The chemical composition was determined by separate ladle analyses for all heats of steel. The ranges of chemical elements are given in Table 4.

Mechanical properties of the structural steel were determined by tests of coupons of as-rolled thickness and 1 or 1½ in. wide. The coupons were tested in tension at a speed of 0.104 in. per min up to yielding and of 0.36 in. per min to fracture. The lower speed corresponded approximately to a srain rate of 0.00014 per sec. All specimens exhibited a distinct yield point. The mean values and standard deviations of the yield point and ultimate strength are given in Table 5 for groups of bridges; the mean value of the Young's modulus of elasticity for all structural steel is given in Table 6.

Additional tests of coupons were made to determine the relationship between the yield point (Table 5) and the so-called static yield point corresponding to zero strain rate. A statistical analysis of the results showed that the static yield points for all wide-flange beams and cover plates were equal to 92.5 percent of the yield points given in Table 5.

Laboratory fatigue tests* have indicated a fatigue life of about 2,000,000 cycles for rolled I-beams subjected to tensile stresses fluctuating between approximately 0.5 and 30 ksi. Tests reported by Wilson and those reported by Hall and Stallmeyer** have shown that welding of cover plates substantially decreased the fatigue life of a steel beam.

* For an explanation of regression analyses see, for example, Anderson, R. L., and Bancroft, T. A., "Statistical Theory in Research," McGraw-Hill (1952).

* Wilson, W. M., "Flexural Fatigue Strength of Steel Beams." Univ. of Illinois Eng. Exp. Sta., Bull. No. 377 (1948).

** Hall, L. R., and Stallmeyer, J. E., "The Fatigue Strength of Flexural Members." Univ. of Illinois, Dept. of Civil Eng. (1959); and Hall, L. R., "Fatigue Tests of Scale-Model AASHO Road Test Bridges." Univ. of Illinois, Dept. of Civil Eng. (1961).

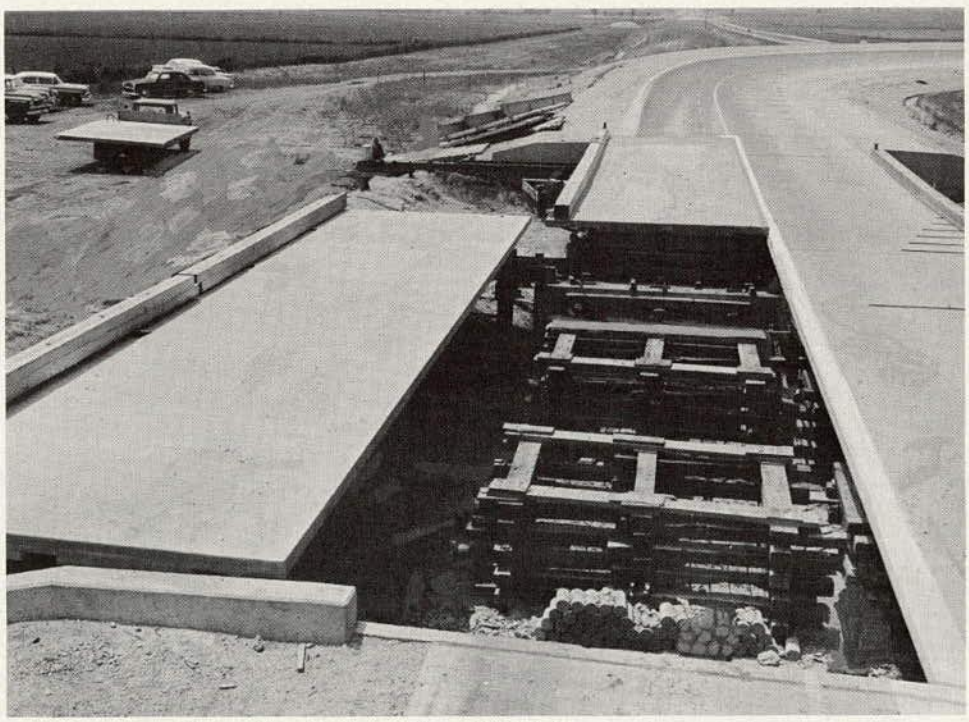

Figure 12. Bridges 9A and 9B during moving operation.

TABLE 4

CHEMICAL COMPOSITION OF STEEL

Type of Steel	Chemical Analysis (%)				
	Carbon	Manganese	Phosphorus	Sulfur	Silicon
Structural	0.20–0.24	0.41–0.71	0.007–0.014	0.023–0.040	
Prestressing wire	0.80	0.65	0.016	0.039	0.25
Prestressing strand	0.73	0.75	0.016	0.037	0.24
Reinforcing bars	0.37	0.60	0.023	0.030	

TABLE 5

YIELD POINT AND ULTIMATE STRENGTH OF STRUCTURAL STEEL

Bridge	No. Tests	Yield Point (ksi)		Ultimate Strength (ksi)	
		Mean	Std. Dev.	Mean	Std. Dev.
(*a*) WF BEAMS, FLANGE SPECIMENS					
1A, 2A	24	34.7	1.33	59.5	1.03
1B, 2B	24	37.9	1.52	63.7	0.87
3A	12	35.3	0.47	61.3	0.47
3B, 4A, 4B	36	35.1	1.53	64.9	2.40
9A, 9B	24	32.5	1.21	62.0	1.35
(*b*) WF BEAMS, WEB SPECIMENS					
1A, 2A	12	38.0	1.91	61.5	2.01
1B, 2B	12	41.4	1.48	65.9	1.86
3A	6	39.1	1.39	63.6	1.02
3B, 4A, 4B	18	39.9	2.18	66.6	3.10
9A, 9B	10	36.1	1.22	62.2	1.87
(*c*) COVER PLATES					
1A, 2B, 3B, 4A, 4B	30	38.4	0.95	60.2	1.65
9A, 9B	24	37.5	1.04	61.2	1.23

Hall and Stallmeyer tested ten beams with the same details of cover plates as those used in the Road Test bridges. The stress range and the level of minimum stress were the only variables, and for any one test both the stress range and the minimum stress were kept constant. The tests were made at two minimum stress levels, tension of 0.4 and 15.4 ksi. The stress range, also tension, was varied from 12.3 to 25.4 ksi.

The following equations, reported in HRB Special Report 66, were found to describe satisfactorily the test data discussed in the preceding paragraphs:

$$\log N_1 = 7.136 - 0.0742\,S_r - 0.0102\,S_{min} \pm 0.257 \quad (1)$$

$$\log N_2 = 7.216 - 0.0729\,S_r - 0.0129\,S_{min} \pm 0.188 \quad (2)$$

in which

N_1, N_2 = number of cycles to failure;
S_r = stress range, ksi; and
S_{min} = minimum stress, ksi.

Eq. 1 expresses the number of cycles N_1 at which the last inspection of the specimen was made prior to failure. Either no crack or one very short crack usually was found at such time.

Eq. 2 expresses the number of cycles N_2 at which the deflection of the cracked beams exceeded the static deflection of the uncracked beam by 0.05 in. At this stage, about one-quarter of the cross-sectional area of the tension flange usually was fractured.

Residual stresses caused by rolling the wide-flange sections were determined by the method of sectioning (Appendix D) on 9-ft sections cut from each beam of Bridges 9A and 9B and

on 2-ft sections cut from ten other bridge beams. The sections were cut prior to fabrication of the bridge beams. The tips of the flanges of all beams had compressive residual stresses; whereas the flange core had residual tension in all samples except those from 9A and 9B. The residual stresses in the web were tensile in beams from Bridges 9A and 9B, and compressive in the web of the beams of other bridges. Table 7 contains approximate values of residual stresses in the flanges of rolled sections caused by rolling alone. The values were obtained from the measured residual stresses by the method suggested in Appendix D.

Prestressing Steel.—Prestressing steel was made of cold-drawn, stress-relieved, high-carbon wire and strand. The chemical composition of both the wire and strand was determined by check analyses. The mean values of the results are given in Table 4.

The mechanical properties of the prestressing steel were determined by tension tests of wire samples 1½ to 2 ft long and by tension tests of 4-ft samples of strand. The stress-strain diagrams for both types of steel were typical of stress-relieved wire, showing a rapid change in the slope at the strain of approximately 1.2 percent. The cross-sectional area, the yield strength at 1 percent strain and the ultimate strength are given in Table 8. The initial modulus of elasticity is given in Table 6. The mean elongation after failure was 4.6 percent in 10 in. for the wire and 3.9 percent in 32 in. for the strand.

The fatigue strength of the prestressing wire and strand was determined by laboratory tests with stress fluctuating between a minimum and a maximum tension. The tests were carried out on samples of materials used in the test bridges.

The experiment for each material included two minimum stress levels between 128.8 and 162.2 ksi and four or more maximum stress levels between 174.1 and 226.6 ksi. For any one specimen, both the minimum stress level and the stress range were held constant throughout the test. Tests were conducted on 18 samples of strand and on 50 samples of wire. The following equations were found to describe satisfactorily the test data:

$$\log N_3 = 9.354 - 0.0423\,S_r - 0.0102\,S_{min} \pm 0.418 \quad (3)$$

$$\log N_4 = 8.722 - 0.0272\,S_r - 0.0074\,S_{min} \pm 0.460 \quad (4)$$

in which N_3, N_4 = number of cycles to failure.

Eq. 3 expresses the number of cycles to failure for the prestressing strand. The test results indicated an endurance limit of S_r = 35 ksi; therefore, the equation is not applicable to stress ranges smaller than 35 ksi.

Eq. 4 expresses the number of cycles to failure for the prestressing wire. The test results indicated an endurance limit of S_r = (124 ksi − 0.5 S_{min}); the equation does not apply to stress ranges smaller than this value.

The relaxation characteristics of the prestressing steel were determined by tests of ten samples of strand and ten samples of wire taken from the materials used in the construction of the test bridges. The initial stress ranged from 158.0 to 199.1 ksi. Analytical correlations of the observed relaxation losses resulted in separate equations for strand (Eq. 5), for wire used in the interior beam of Bridge 5A (Eq. 6) and for wire used in all other post-tensioned beams (Eq. 7):

$$\Delta_r = 0.0488\,f_i\,(f_i/f_s')^{5.04}\,t^{0.274} \pm 1.48 \text{ ksi} \quad (5)$$

$$\Delta_r = 0.0313\,f_i\,(f_i/f_s')^{4.28}\,t^{0.284} \pm 0.95 \text{ ksi} \quad (6)$$

$$\Delta_r = 0.1020\,f_i\,(f_i/f_s')^{6.08}\,t^{0.238} \pm 2.80 \text{ ksi} \quad (7)$$

in which

Δ_r = relaxation stress loss at time t, ksi;
f_i = initial stress, ksi;
f_s' = ultimate strength of steel, ksi; and
t = time from the application of initial stress in hours.

TABLE 6
MODULUS OF ELASTICITY

Type of Steel	No. Tests	Modulus of Elasticity (10^3 ksi)	
		Mean	Std. Dev.
Structural	104	30.0	0.98
Prestressing wire	34	28.6	0.71
Prestressing strand	33	27.6	0.88
Reinforcing bars	35	28.8	1.06

TABLE 7
RESIDUAL STRESSES DUE TO ROLLING

Beam Size	Estimated Residual Stress (ksi)		
	Tip of Flange	Center of Flange	Flange Mean [1]
18WF50	−14.3	21.6	8.0
18WF55	−10.2	24.3	11.3
18WF60	− 7.6	11.1	4.0
18WF96	−10.5	− 5.7	− 7.4
21WF62	−15.2	22.6	8.4

[1] Computed from stresses at tips and center, assuming parabolic distribution.

TABLE 8

AREA, YIELD AND ULTIMATE STRENGTH OF PRESTRESSING STEEL

Bridge	Type of Steel	Mean Area (sq in.)	Yield Strength[1] (ksi)			Ultimate Strength (ksi)		
			No. Tests	Mean	Standard Deviation	No. Tests	Mean	Standard Deviation
5A, 5B	Wire	0.0293	32	227.4	2.91	90	257.3	2.50
6A	Strand	0.0807	15	229.4	7.18	15	265.6	4.11
6B	Strand	0.0806	18	243.0	7.36	18	275.2	7.01

[1] Stress at 1 percent strain.

The relaxation equations were derived from tests of 1,000-hr duration. Tests of two strands and one wire were continued for additional 11,000 hr and the results were in agreement with the values predicted by corresponding Eqs. 5 and 7.

Reinforcing Bars.—All reinforcing bars used in construction of the test bridges were rolled from billet steel and had deformations conforming to ASTM Designation: A305–53T. The deformed bars Nos. 8, 9 and 11 which were the tension reinforcement of the reinforced concrete beams were of intermediate grade conforming to ASTM Designation: A15–54T and had diamond-shaped deformations (Fig. 59). Table 4 gives the chemical composition as determined by ladle analysis.

The mechanical properties of the reinforcing bars were determined by tension tests of 2-ft coupons. The stress-strain diagrams showed a distinct yield point. The areas, yield points and ultimate strengths are given in Table 9 for No. 3 and No. 4 bars, used for longitudinal reinforcement of the slabs, and for the three large sizes. The modulus of elasticity is given in Table 6.

The fatigue life of the No. 11 bars was determined by laboratory tests of 20 concrete beams, each reinforced with 1 bar. The bars were specimens cut from the reinforcement used in the test bridges. The bar in any one beam was subjected to a stress fluctuating between a minimum and maximum tension. The experiment included two minimum stress levels, 5.0 and 15.0 ksi, and four maximum stress levels ranging from 34.0 to 49.0 ksi. The following equation for the fatigue life of the bars represented satisfactorily the test results:

$$\log N_5 = 7.432 - 0.0515\, S_r \pm 0.182 \qquad (8)$$

in which N_5 = number of cycles to failure.

The test results indicated an endurance limit of $S_r = 24$ ksi. Eq. 8 is not applicable below this endurance limit.

2.2.2 *Properties of Concrete and Timber*

The concrete placed at the project site was made of Type I portland cement, crushed gravel and natural bank sand. The crushed gravel was predominantly limestone, consisting of approximately 30 percent crushed material; the sand was mainly siliceous.

Two mix designs were used for on-site construction: a 3,000-psi design for the reinforced concrete bridges and for the slabs of the prestressed concrete bridges, and a 4,000-psi design for the slabs of the steel bridges. Standard 6- by 12-in. cylinders made during casting of the bridge beams and slabs were tested at the age of 28 days, at the beginning of regular test traffic and at the end of regular test traffic.

The compressive strengths and moduli of elasticity are given in Table 10. The compressive strengths were obtained by tests of 6 cylinders per slab at each age for prestressed concrete and steel bridges, and a minimum of 15 cylinders at every age for reinforced concrete bridges. The modulus of elasticity was usually determined on one-half of the total number of cylinders tested.

The concrete for the prestressed concrete beams was made of Type I portland cement, crushed limestone and natural sand, mainly siliceous. The concrete mix was designed for a minimum 5,000-psi strength at 28 days.

Standard 6- by 12-in. cylinders and 6- by 6- by 30-in. beams made from each batch of concrete were tested at the time of application of the prestressing force to the bridge beams, at the age of 28 days, at the beginning of regular test traffic and at the end of regular test traffic. The mean values of strength were determined for each bridge by tests of 6 cylinders and 6 modulus of rupture beams at any one time (Table 10).

The unit weight of concrete determined at the age of 28 days, at the beginning of test traffic and at the end of test traffic was approximately 148 pcf except for concrete used in the slab of Bridge 1B, which had a portion of the coarse aggregate replaced by steel punchings and had a unit weight of approximately 161 pcf. (The unit weight of concrete for Bridge 1B was increased to accommodate certain changes in the test program without changing the sizes of the rolled sections.) The unit weight of

fresh concrete was approximately 1 pcf more than that of the hardened concrete.

The coefficient of thermal expansion of concrete was determined separately for the reinforced concrete bridges, for the slabs of steel bridges and prestressed concrete bridges, and for the beams of prestressed concrete bridges. Laboratory tests covered temperature changes between 37 and 73 F and between 73 and 100 F in both directions. The values of the coefficient of thermal expansion ranged from 0.0000048 to 0.0000075 per deg F.

The shrinkage and creep characteristics of the concrete used in the prestressed concrete beams were determined by outdoor tests of 6- by 12-in. cylinders. Eight cylinders were loaded to 2,000 psi, eight to 1,000 psi, and eight were left unloaded. Periodic strain measurements on all 24 cylinders were continued for 3½ yr. The strain data were described satisfactorily by the following equations for shrinkage (Eq. 9) and creep (Eq. 10):

$$\Delta_s = 0.000280\,(1 - e^{-t/166})^{0.5} - 0.000087\,(1 - e^{-t/10}) \sin \frac{\pi\,(t' + 60)}{182} \pm 0.000108 \qquad (9)$$

$$\Delta_c = 0.00356\,(f_c/f'_{ci})^{0.96}\,(1 - e^{-t/500})^{0.73} \pm 0.000155 \qquad (10)$$

TABLE 9

AREA, YIELD POINT AND ULTIMATE STRENGTH OF REINFORCING BARS

Bar Size	Mean Area (sq in.)	No. Tests	Yield Point (ksi)		Ult. Strength (ksi)	
			Mean	Std. Dev.	Mean	Std. Dev.
3	0.111	40	61.2	1.28	86.3	1.49
3 [1]	0.110	4	47.9	2.60	75.3	2.60
4	0.199	16	54.9	1.43	84.2	2.82
8	0.782	6	52.6	0.78	81.5	1.22
9	0.957	15	51.8	1.13	79.7	1.39
11	1.524	15	49.5	0.77	81.0	1.72

[1] Used only in slabs of Bridges 9A and 9B; chemical composition given in Table 4 does not pertain to these bars.

TABLE 10

COMPRESSIVE STRENGTH, MODULUS OF ELASTICITY, AND MODULUS OF RUPTURE OF CONCRETE

Bridge	Structural Element	Value							
		Prestressing		28 Days		Begin. Traffic		End Traffic	
		Mean	Std. Dev.	Mean	Std. Dev.	Mean	Std. Dev.	Mean	Std. Dev.
(a) COMPRESSIVE STRENGTH (PSI)									
1A,1B,2A, 4B	Slab			4,270	214	5,110	432	5,430	346
2B	Slab			4,060	157	4,760	203	5,200	337
3A,4A	Slab			4,470	255	5,460	313	5,770	199
3B	Slab			4,830	289	5,740	219	6,020	295
9A,9B	Slab			5,310	400	6,040 [1]	458 [1]	6,410	394
5A	Slab			4,950	203	6,440	237		
5B	Slab			4,490	343	5,700	315	5,530 [2]	572 [2]
6A	Slab			3,010	408	5,480	799		
6B	Slab			2,860	364	4,890	643		
5A,5B,6A,6B	Beams	5330	823	6,650	645	9,260	639	8,900	945
7A,8B	Bridge			3,750	324	4,560	411	4,950	374
7B	Bridge			3,470	293	4,390	331	4,800	415
8A	Bridge			4,020	342	4,960	476	5,290	409
(b) MODULUS OF ELASTICITY (1,000 KSI)									
1A to 4B,9A,9B	Slab			4.4	0.51	5.2	0.52	5.6	0.35
5A,5B,6A,6B	Slab			3.9	0.34	5.6	0.46	5.9	0.32
5A,5B,6A,6B	Beams	4.2	0.57	5.1	0.21	5.7	0.30	5.8	0.32
7A,7B,8A,8B	Bridge			4.0	0.34	5.0	0.52	5.5	0.59
(c) MODULUS OF RUPTURE (PSI)									
5A,5B,6A,6B	Beams	670	66	700	27	739	94	1,155	190

[1] At 117 days; traffic began at 28 days.
[2] Cylinders mixed up; could not distinguish between bridges.

in which

Δ_s = shrinkage strain at time t;

Δ_c = creep strain at time t;

e = base of natural logarithm;

t = time from casting the cylinder in days;

t' = time from January 1 in days*;

f_c = load per unit area of concrete, psi;

f'_{ci} = strength of concrete at time of loading, psi.

An additional characteristic needed in the interpretation of the bridge tests was the fatigue strength in flexural tension of the concrete used in prestressed concrete beams. The probability of fatigue fracture of plain concrete subjected to bending was studied by McCall** who proposed the following equation relating the stress, number of cycles and probability of survival.

$$\log p = -0.0957 f_r^{3.32} (\log n)^{3.17} \quad (11)$$

in which

p = probability of survival at n cycles of stress;

f_r = ratio of the applied stress to the modulus of rupture of concrete; and

n = number of cycles of applied stress.

Eq. 11 was derived from tests with complete reversal of stress. Earlier studies suggested that only the magnitude of the tensile stress is critical so that in the use of Eq. 11 for stress conditions other than full reversal it appears reasonable to compute f_r on the basis of the tensile stress alone.*

The only property of the timber guard of interest in the bridge tests was its unit weight. It was approximately 40 lb per lin ft, including the hardware.

2.2.3 Characteristics of Beams

Cross-section properties of wide-flange beams and of wide-flange beams with cover

* For example, t' for February 15 of any year would be 45 days.

** McCall, J. T., "Probability of Fatigue Failure of Concrete." *Jour. of the A.C.I.*, pp. 233-244 (August 1958).

* Murdock, J. W., and Kesler, C. E., "Effect of Range of Stress on Fatigue Strength of Plain Concrete Beams." *Jour. of the A.C.I., pp.* 221-231 (August 1958).

TABLE 11

PROPERTIES OF WIDE FLANGE BEAMS

Bridge	Nominal Beam Size	Weight (lb/ft)	Area (sq in.)	Depth (in.)	Flange		Web Thick. (in.)	Moment of Inertia (in.^{4})	Y_b [1] (in.)
					Width (in.)	Thick. (in.)			
1B, 2B	18WF50	51.9	15.25	18.10	7.58	0.578	0.371	837	9.06
1A, 2A	18WF55	56.8	16.71	18.22	7.64	0.641	0.396	932	9.11
3B, 4A, 4B	18WF60	59.3	17.42	18.29	7.54	0.666	0.416	972	9.13
9A, 9B	18WF96	93.7	27.53	18.22	11.78	0.617	0.487	1656	9.11
3A	21WF62	61.2	17.98	20.91	8.15	0.600	0.402	1292	10.46

[1] Distance from neutral axis to bottom face of beam.

TABLE 12

PROPERTIES OF WF BEAMS WITH COVER PLATES

Bridge	Nominal Beam Size	Weight (lb/ft)	Area (sq in.)	Depth (in.)	Plate Thick. [1] (in.)	Moment of Inertia (in.^{4})	Y_b [2] (in.)
2B	18WF50	61.3	18.02	18.57	0.452	1,040	8.11
1A	18WF55	65.9	19.37	18.68	0.441	1,132	8.29
3B, 4A, 4B	18WF60	68.4	20.07	18.76	0.444	1,176	8.37
9A,[3] 9B [3]	18WF96	111.7	32.84	19.10	0.443	2,118	9.55

[1] All cover plates 6 in. wide.
[2] Distance from neutral axis to bottom face of cover-plated section.
[3] Cover plates on both top and bottom flange; all other bridges had cover plates only on bottom flange.

TABLE 13
PROPERTIES OF PRESTRESSED CONCRETE BEAMS

Bridge	Weight (lb/ft)	Area [1] (sq in.)	Depth Below Slab (in.)	Area of Bottom Steel (sq in.)			Area of Top Steel (sq in.)	Moment of Inertia [1] ($in.^4$)	Y_b [2] (in.)
				Bottom Row	Middle Row	Top Row			
5A	275.0	267	24.76	1.173	0	0	0	17,600	10.77
5B	270.3	264	24.53	1.172	0.293	0.293	0	17,500	10.79
6A	275.4	268	24.28	0.565	0.404	0.161	0.161	17,800	10.99
6B	283.9	276	24.05	0.645	0.645	0.161	0.161	18,300	11.06

[1] Based on uncracked transformed section.
[2] Distance from neutral axis to bottom face of beam in uncracked transformed section.

plates are given in Tables 11 and 12. The properties are based on measured dimensions. Only one set of values is given for any one beam size, because the differences between the means for individual bridges were found to be always less than 1 percent.

Cross-section properties of prestressed concrete beams computed from measured dimensions are given in Table 13. The area, moment of inertia and the position of neutral axis are for uncracked transformed sections. They are applicable at any age, since only negligible variations in these quantities were caused by time variations in the modulus of elasticity of concrete.

TABLE 14
INITIAL STEEL STRESSES IN PRESTRESSED CONCRETE BEAMS

Bridge	Beam	Init. Tension at Mid-span [1] (ksi)	Bridge	Beam	Init. Tension at Mid-span [2] (ksi)
5A	Interior	154.1	6A	Interior	170.1
	Center	153.1		Center	166.5
	Exterior	152.9		Exterior	170.1
5B	Interior	160.7	6B	Interior	179.5
	Center	159.8		Center	178.4
	Exterior	161.1		Exterior	179.5

[1] Immediately after completion of post-tensioning.
[2] Immediately after release of strands.

TABLE 15
PROPERTIES OF THE STEMS OF REINFORCED CONCRETE T-BEAMS

Bridge	Weight (lb/ft)	Depth (in.)	Area of Bottom Steel (sq. in.)	
			Bottom Row	Top Row
7A	264.0	19.98	4.57	1.94
7B	262.8	20.03	4.58	1.92
8A	264.1	19.95	4.58	2.69
8B	264.9	19.97	4.57	2.66

The initial tension in the prestressing steel at midspan of the prestressed concrete beams was computed from the measurements made during stressing of the prestressing steel and is given for each beam (Table 14). For post-tensioned beams the computations involved corrections for friction losses and elastic shortening. Computations for pretensioned beams required corrections for temperature, relaxation and elastic shortening.

The properties of the stems of reinforced concrete T-beams, based on measured dimensions, are given in Table 15.

2.2.4 Characteristics of Slabs

The actual weights and thicknesses of the bridge slabs are given in Table 16. The weight per square foot is given to the nearest 0.5 lb and the thickness to the nearest 0.05 in. The thickness was obtained by measurements. The weight is based on the measured thickness of the slab, the measured unit weight of concrete, and the amount of reinforcing steel present.

The transverse and longitudinal profiles of

TABLE 16
WEIGHT AND THICKNESS OF BRIDGE SLABS

Bridge	Weight [1] (lb/sq ft)	Thickness (in.)
(*a*) STEEL BRIDGES		
1A, 2A, 3A, 4A	83.0	6.45
1B	91.0	6.55
2B	81.5	6.30
3B, 4B	83.5	6.45
9A	87.5	6.75
9B	85.0	6.55
(*b*) CONCRETE BRIDGES		
5A, 8A	84.0	6.60
5B	85.0	6.70
6A, 7B	83.0	6.55
6B, 8B	83.5	6.60
7A	82.5	6.50

[1] Reinforcement included.

all slabs of the original bridges were determined for the first time approximately three months after casting the slab. On Bridges 9A and 9B, they were determined one month after casting. Figure 13 shows the transverse slab profiles at midspan relative to the average profile of the slabs over the supports.

The slabs of steel bridges sloped toward the curb. In the construction of the original eight steel bridges no provision was made for the uneven distribution of the weight of the slab to the three beams, so that the exterior beam deflected more than the other two beams. In the construction of Bridges 9A and 9B form elevations were set to compensate for the expected additional deflection of the exterior beam. The resulting profile showed relatively little transverse slope.

The slabs for prestressed concrete Bridges 6A and 6B also were built without compensation for the uneven distribution of the dead load, and the resulting slabs had an appreciable transverse slope toward the curb. In Bridges 5A and 5B, compensation was made similar to that for Bridges 9A and 9B, and the slab at midspan was relatively flat.

The reinforced concrete bridges were built with a camber in excess of the expected immediate dead load deflections. An upward camber at midspan of 1 to 1¼ in. was present in all four reinforced concrete bridges (Fig. 13). Except for Bridge 7A, the camber was approximately uniform across the width of the bridge and was to compensate for creep deflections.

With few exceptions, the longitudinal profiles were essentially symmetrical about midspan with the maximum deviation from the plane connecting the abutments occurring at midspan. Thus, Figure 13 indicates that the decks of Bridges 5A, 5B, 9A and 9B were essentially flat; those of the original steel bridges and of prestressed concrete bridges 6A and 6B were mostly concave; and those of the reinforced concrete bridges were convex.

2.2.5 Characteristics of Combined Elements

In the preceding sections sufficient data are given on the properties of materials, beams and slabs to enable calculations of all bridge properties needed for the analyses of the results of the bridge tests. This section presents certain characteristics of combined slab and beams.

Composite Beams.—In composite steel bridges and in all concrete bridges the slab and the beams were tied together. The section properties of the composite section, made up of one beam and a portion of the slab, depended on the choice of the effective width of the slab and on the age of concrete. Throughout most of this report, the moment of inertia of the composite beams was computed on the following assumptions: (1) the effective width of the slab was equal to the beam spacing for the center beam and to the sum of the width of the overhang plus one-half of the beam spacing for the edge beams; and (2) the modulus of elasticity of concrete was equal to that determined at the beginning of test traffic.

Table 17 gives the moments of inertia and the distance of neutral axis from the bottom of the beam or from the bottom row of the tension reinforcement (for reinforced concrete beams) for each beam. The moments of inertia for steel bridges pertain to a section transformed to steel; those for the prestressed concrete bridges pertain to an uncracked section transformed to concrete of the beam; and those for reinforced concrete bridges pertain to a cracked section transformed to concrete.

Bridges.—Table 18 gives three properties of each bridge considered as a unit: the weight, the stiffness and the natural frequency. The bridge weights were computed from measured dimensions and unit weights of materials; and varied from 73 to 104 kips.

The stiffness at midspan is the flexural rigidity of the entire cross-section of the bridge. For the composite steel bridges and the concrete bridges, it was computed as the sum of the stiffnesses of the three composite

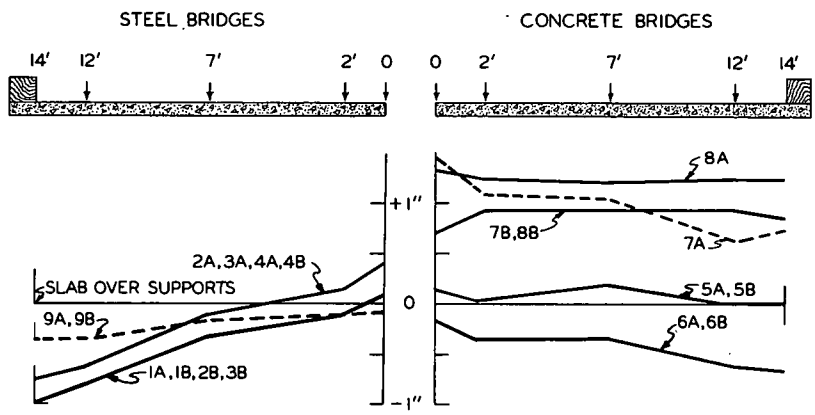

Figure 13. Transverse slab profiles at midspan.

beams; that is, the sum of the products of the moments of inertia from Table 17 and the appropriate modulus of elasticity. For the noncomposite steel bridges, the total stiffness was computed as the sum of the stiffnesses of the three steel beams and the slab. The stiffness of the slab was computed from

$$\frac{1}{12}\left(\frac{E_c t_s^3 b}{1-\mu^2}\right) \qquad (12)$$

in which

t_s = average thickness of the slab;
E_c = modulus of elasticity of slab concrete;
μ = Poisson's ratio (assumed equal to 0.1); and
b = total width of the slab.

The stiffness of bridges increased in the following order: noncomposite steel bridges, reinforced concrete bridges, composite steel bridges and prestressed concrete bridges. It should be noted, however, that the stiffness of the concrete bridges depends heavily on the degree of tensile cracking of the beams. Thus, if cracked, the prestressed concrete bridges could have been considerably less stiff than indicated (Table 18). Similarly, if the cracking of the reinforced concrete bridges was not fully developed, the stiffness of Bridges 7A, 7B and 8A and 8B could have been substantially higher than indicated.

The natural frequencies were computed on the assumption that the bridges responded as simply supported beams. With the exception of the steel bridges with cover plates, the frequencies were calculated from Eq. 13*:

$$f_b = \frac{\pi}{2L^2}\sqrt{\frac{EIg}{w_b}} \qquad (13)$$

in which

f_b = natural frequency of a bridge;
L = span length;
EI = stiffness of bridge cross-section;
g = acceleration due to gravity; and
w_b = weight of bridge per unit length.

The natural frequencies of steel bridges with cover plates were computed with Stodola's iterative procedure.**

The natural frequencies ranged from 2.31 cps for Bridge 1B to 7.00 cps for Bridge 5A. For

* Eq. 13 is dimensionally consistent and may be entered with any compatible units. Explanations of the terms of equations throughout this report contain no units whenever the corresponding equation is dimensionally consistent.

** Timoshenko, S., "Vibration Problems in Engineering." D. Van Nostrand (1955).

TABLE 17
MOMENTS OF INERTIA OF COMPOSITE BEAMS[1]

Bridge	Moment of Inertia (in.⁴)			Distance Y_b[2] (in.)		
	Interior Beam	Center Beam	Exterior Beam	Interior Beam	Center Beam	Exterior Beam
			(a) COMPOSITE STEEL BRIDGES			
2B[3]	3,810	3,840	3,960	18.53	18.79	19.00
	2,850	2,873	2,980	18.73	18.95	19.10
3B[3]	4,160	4,290	4,360	18.60	18.87	19.10
	3,240	3,320	3,385	18.76	18.99	19.18
			(b) PRESTRESSED CONCRETE BEAMS			
5A	64,200	64,500	70,300	20.80	20.68	21.54
5B	62,400	63,400	69,100	20.76	20.58	21.67
6A	61,400	61,500	64,800	20.53	20.51	21.27
6B	61,100	60,600	65,800	20.40	20.28	21.01
			(c) REINFORCED CONCRETE BEAMS[4]			
7A	14,630	14,510	14,960	18.94	18.83	19.34
7B	14,780	14,760	15,030	19.07	19.01	19.39
8A	15,900	15,760	16,360	18.85	18.81	19.19
8B	15,770	15,730	16,310	18.81	18.77	19.23

[1] Computed with properties at beginning of test traffic.
[2] Distance from neutral axis to bottom face of beam for steel and prestressed concrete bridges and to bottom layer of reinforcing bars for reinforced concrete bridges.
[3] Upper line pertains to coverplated sections, lower to sections without cover plates..
[4] Cracked section.

TABLE 18
PROPERTIES OF BRIDGES

Bridge	Total Weight (kips)	Stiffness at Midspan [1] (kip-in.^{2})	Natural Frequency [1] (cps)
	(*a*) NONCOMPOSITE STEEL BRIDGES		
1A	75.2	122.9×10^6	2.62
1B	80.5	97.2×10^6	2.31
2A	74.5	104.7×10^6	2.49
3A	75.5	137.2×10^6	2.86
4A	75.8	126.5×10^6	2.64
4B	76.0	127.9×10^6	2.66
9A	84.4	214.2×10^6	3.21
9B	82.4	213.0×10^6	3.23
	(*b*) COMPOSITE STEEL BRIDGES		
2B	72.9	348.2×10^6	4.26
3B	76.2	384.3×10^6	4.52
	(*c*) PRESTRESSED CONCRETE BRIDGES		
5A	102.7	$1{,}135 \times 10^6$	7.00
5B	102.8	$1{,}111 \times 10^6$	6.91
6A	102.4	$1{,}069 \times 10^6$	6.80
6B	103.8	$1{,}069 \times 10^6$	6.75
	(*d*) REINFORCED CONCRETE BRIDGES		
7A	102.2	220.5×10^6	3.08
7B	102.7	222.9×10^6	3.10
8A	103.4	235.1×10^6	3.16
8B	103.3	239.0×10^6	3.19

[1]Computed with properties at beginning of test traffic.

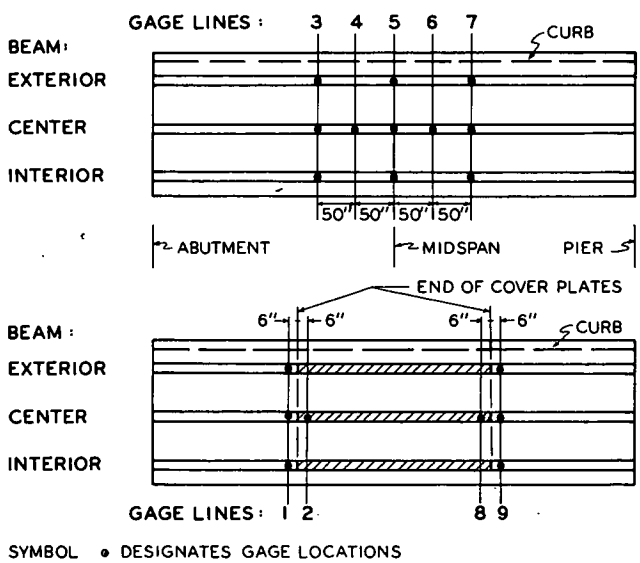

Figure 14. Gage lines on bridge beams.

prestressed concrete bridges with cracked beams the natural frequencies would be lower and for reinforced concrete bridges with incompletely cracked beams they would be higher than given in Table 18.

2.3. INSTRUMENTATION

2.3.1 Bridge Deformations Under Moving Loads

The bridge beams were instrumented for measurement of strains and deflections caused by vehicles. The transducers for determination of transient strains were electric resistance strain gages bonded to the bridge beams. The transient deflections were measured with demountable cantilever beams equipped with bonded electric resistance strain gages. When the range of the cantilever deflectometers was exceeded, the maximum deflections were determind with slip ring reflectometers.

The strain gages were located on beams. The gages were placed at midspan and at other cross-sections (Fig. 14). There were two or more gages at each location designated by a dot. The locations of the individual strain gages on typical cross-sections are shown in Figure 15.

The gages were bonded to the surface of steel beams, to the prestressing steel or the surface of the concrete on prestressed concrete beams, and to the reinforcing bars in the reinforced concrete beams. Gages were attached during construction on the strands of the pretensioned beams and on the top reinforcing bars of the reinforced concrete beams. They were waterproofed and embedded in the concrete. All other gage locations were accessible so that gages could be replaced when necessary. Access to the gages on the cables of post-tensioned beams and on the bottom reinforcing bars of the reinforced concrete beams was provided through holes formed at the desired locations.

The gages were placed on or near the bottom

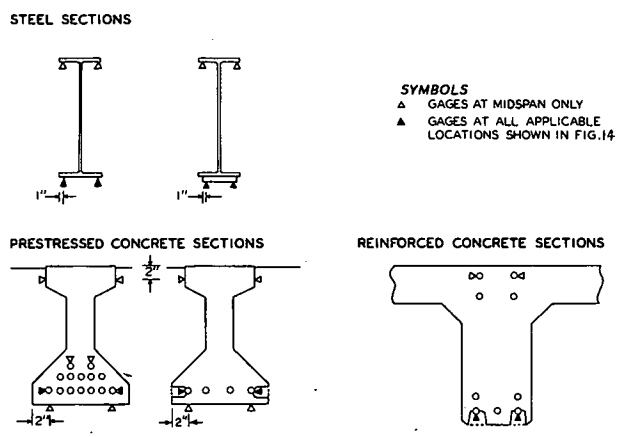

Figure 15. Locations of individual strain gages.

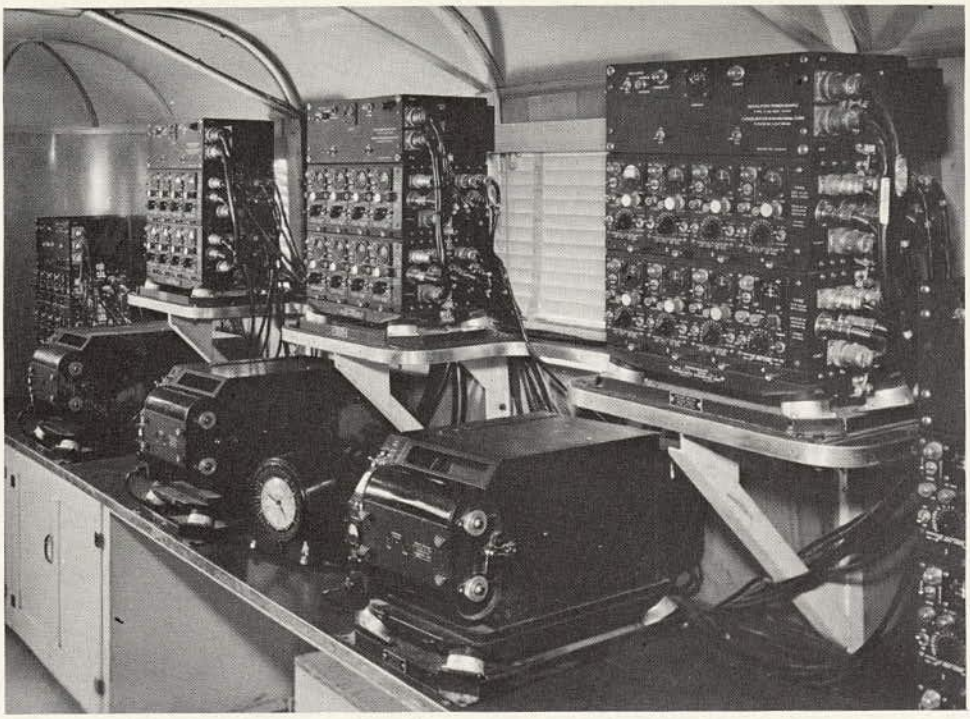

Figure 16. Amplifiers and recording oscillographs in bridge trailer.

of the beams, except that two gages at midspan were located near the top (Fig. 15).

The gages on the steel beams and on prestressing strand were 1 in. long, and those on the surface of the concrete were 6 in. long. Gages ¼ in. long were used at all other locations. The strain gages were protected against moisture by several types of waterproofing.

Each pair of gages placed at the same elevation on any one beam section formed one or two arms of an external Wheatstone bridge; the remaining arms were provided by dummy gages attached to a steel plate or to a small concrete block located close to the active gages. The Wheatstone bridge was connected through amplifiers to recording oscillographs. The oscillographs, equipped with galvanometers having a frequency range of 0 to 350 cps, recorded the deflections of each galvanometer in the form of a trace on a light-sensitive paper. The amplifiers provided a choice of several attenuations ranging from 1 to 1,000. For attenuation of 1, the galvanometer trace deflection of 1.0 in. corresponded approximately to a strain of 0.00002 or less. The amplifiers and the oscillographs were housed in a trailer (Fig. 16). Forty-eight channels were available for simultaneous recording of strains and deflections.

The cantilever deflectometers consisted of triangular cantilever beams attached rigidly to the underside of the bridge beam at one end and fastened with a chain to the ground at the other end (Fig. 17). The deflectometers were used mostly at midspan. The cantilever of each deflectometer was equipped with four bonded strain gages forming an external bridge connected to the amplifiers and recording oscillographs. For amplifier attenuation of 1, the galvanometer trace deflection of 1.0 in. corresponded approximately to 0.01 in. of bridge deflection. The deflectometers were calibrated with deflections of known magnitude; they had a range of 2½ in.

Large deflections were measured with the slip ring deflectometer, a device consisting of a fork attached to the underside of the beam, a rod supported on the ground and extending through the prongs of the fork and a ring sliding along the rod. Prior to the entrance of the test vehicle on the bridge, the slip ring was bearing against the underside of the fork. As the bridge deflected under the vehicle, the fork pushed the slip ring downward. The slip ring was then brought up manually to bear against the underside of the fork once again. Readings were made of the position of the slip ring before vehicle passage, after vehicle passage with the slip ring in the lower position, and after the slip ring was brought up against the fork, providing data on maximum live load deflection and on permanent set. The position of the slip ring was read with a ruler graduated to the nearest 0.02 in.

2.3.2 Deformations of Unloaded Bridges

Observations of changes with time in the deformations of unloaded bridges were made with instruments of demonstrated long-time stability. Strains were determined with a Whittemore mechanical strain gage, elevations with a precise level and widths of cracks in concrete with hand microscope gages.

A strain gage line for the Whittemore gage consisted of two small holes drilled 10 in. apart in the surface of the structural steel beams, in the reinforcing bars of the reinforced concrete beams, in brass plugs set in the surface of the prestressed concrete beams or in steel collars fastened to the prestressing strands. Every bridge beam had one or two gage lines at midspan (Fig. 18). In addition, gage lines were placed at the ends of cover plates of Bridges 9A and 9B.

The Whittemore gage, with each division on the dial equal to the strain of 0.00001, was used in conjunction with a standard bar for compensation of temperature effects. Additional standard bars were kept in a safe and used to check the Whittemore gage at 6-month intervals.

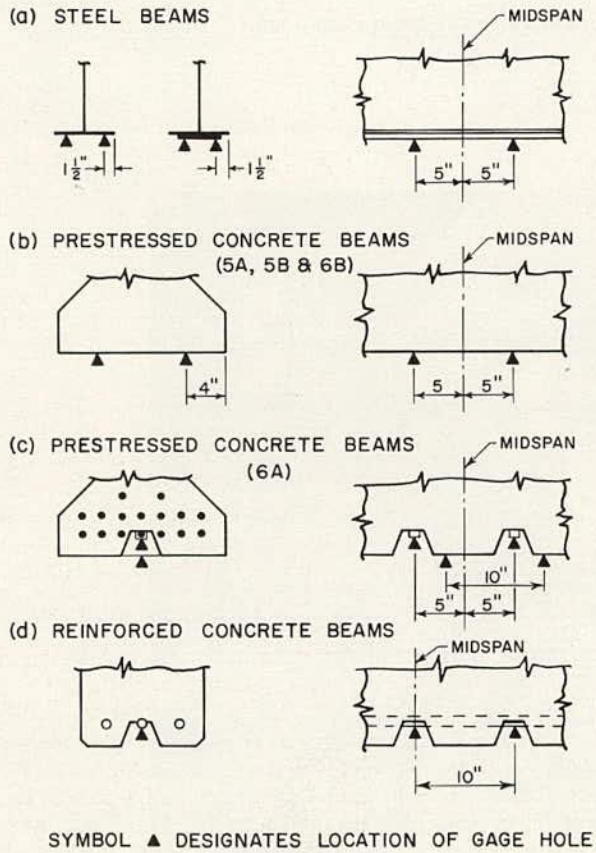

Figure 18. Locations of gage holes for Whittemore strain gage.

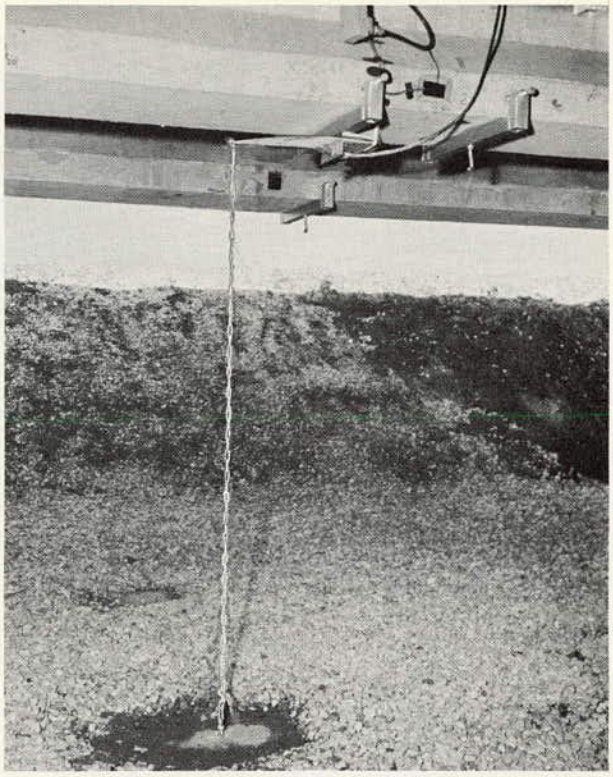

Figure 17. Cantilever deflectometer in place.

The elevations of the bridge beams as well as transverse and longitudinal profiles of the slabs were measured with a precise level graduated to 0.001 ft. For measurement of beam elevations, permanent brackets to support a removable 1-ft scale were installed on the underside of each beam at midspan and at the two quarter points (Fig. 19). A standard level rod placed on the surface of concrete was used for determination of the profiles of the slab. As all measurements of elevations were relative, there was no need for fixed points.

Two microscopes (20 and 40 power) were used for measurement of the width of cracks in reinforced concrete and prestressed concrete beams. They were portable, self-illuminated instruments with an internal scale graduated to 0.001 in. on the 40-power microscope and to 0.002 in. on the 20-power microscope. The readings were usually recorded on mark-sense cards.

2.3.3 Vehicle Characteristics and Placement

Instrumentation was provided for static and dynamic determination of axle weights and spring deflections, for static measurements of tire deflections, for recording of wheel load variations and frequency of vehicles in motion, and for determination of vehicle speed and position.

Figure 19. Brackets and scales for measurement of beam elevations.

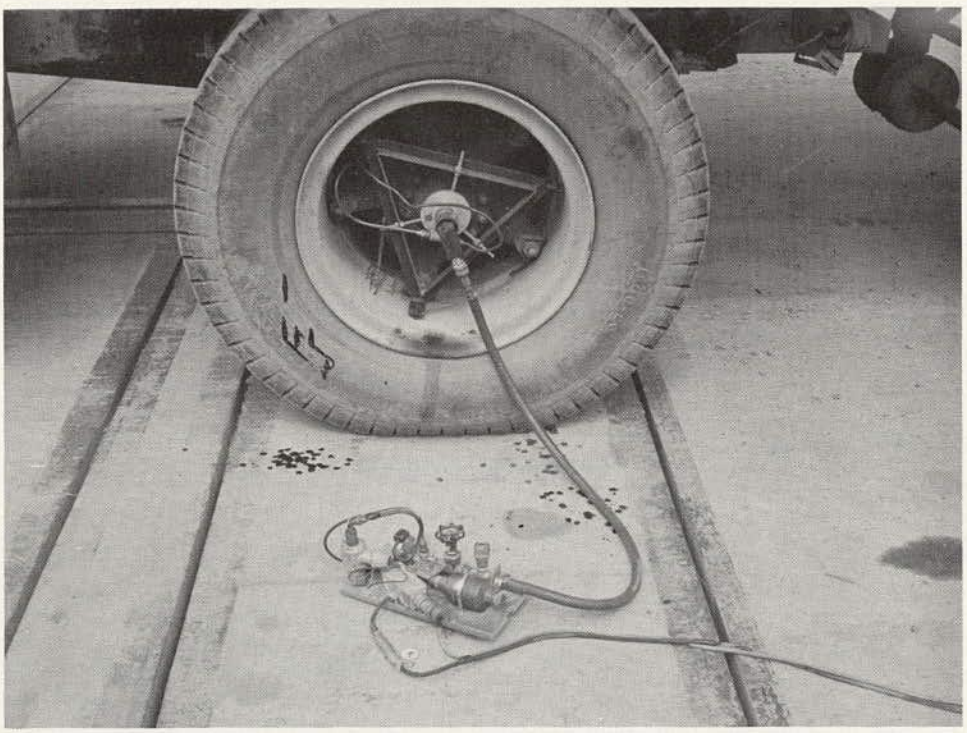

Figure 20. Equipment for determination of differential tire pressure.

The weights of the vehicles were determined on an electronic scale which weighed one axle at a time. The platform of the scale was supported on load cells equipped with bonded electric resistance strain gages. Static loads were indicated on a dial; dynamic loads were recorded in analog form on calibrated paper.

Static and dynamic spring deflections were measured with potentiometers attached to the underside of the truck or trailer bed. The potentiometers were actuated by a wire connected to the axle of the vehicle. The response of the potentiometer was fed through an amplifier to a direct-writing oscillograph. The spring deflections were measured to the nearest 1/16 in.

Deflections of tires caused by static loads were measured with 0.001-in. dial indicators.

To measure the fluctuation of a wheel load on a moving vehicle, an instrument was developed to record continuously changes in tire pressure (Fig. 20). The tire was connected to a pressure cell through a slip joint mounted on the wheel. The electrical signals from the pressure cell were fed through an amplifier to a direct-writing oscillograph. The equipment was capable of recording differential pressures up to $\pm$ 1½ psi. The linear range of the oscillograph was 0 to 60 cps.

The equipment was calibrated dynamically, in the frequency range of 0 to 10 cps, on the electronic scale to relate the pressure to the wheel load. Its accuracy in terms of changes in the wheel load was estimated as $\pm$ 500 lb.

Four complete units of the tire-pressure equipment were available. They were transferable from vehicle to vehicle.

The passage of the vehicle over a bridge was timed with the aid of two pressure hoses, one at each end of the bridge. The speed was determined to a resolution of 0.1 mph.

The longitudinal position of a moving vehicle on the bridge was marked on the oscillograph records of bridge deformations with pips produced by pressure switches connected to hoses placed at each end of the bridge. The longitudinal position was marked also on the spring-deflection records; the pip was produced with the aid of a microswitch activated by a trip stand placed on the roadway. The intermediate positions of the vehicle on the bridge and the variation in speed were determined with the aid of an auxiliary odometer wheel counter connected to a direct-writing oscillograph carried on the truck; the time base was provided by the oscillograph.

Hoses connected to pressure switches were used also for determination of the transverse position of the moving vehicles on the bridge (Figure 21). Each pressure switch was connected to a mechanical counter. The hoses were of varying lengths in 12-in. increments; the first hose crossed by a wheel actuated the corresponding counter.

Frequencies of moving vehicles were determined with a linear accelerometer mounted at the desired location on the truck and connected to a direct-writing oscillograph.

Figure 21. Pressure hoses of transverse placement device.

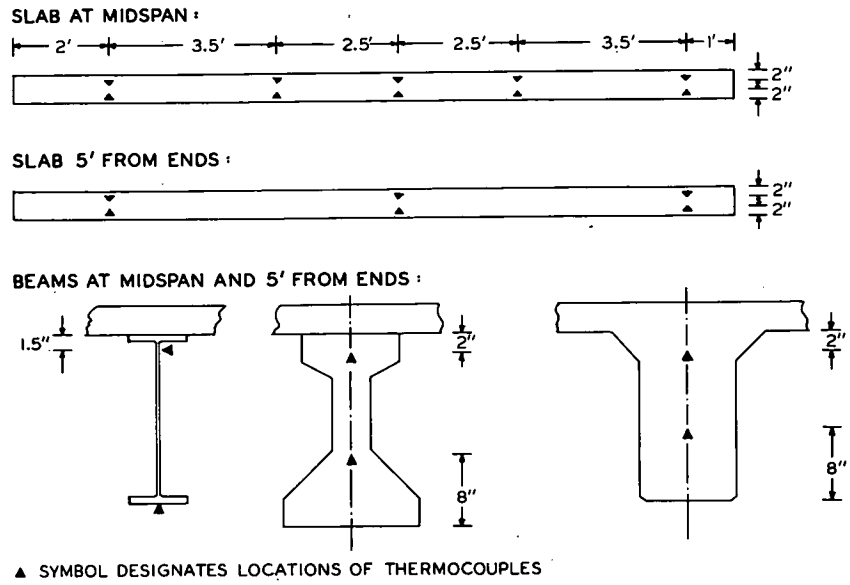

Figure 22. Locations of thermocouples.

2.3.4 Temperature

Temperature of the bridges was measured with bimetallic thermocouples embedded in the concrete or attached to the surface of the structural steel. The thermocouples were installed at midspan and 5 ft from both ends of the bridge. The locations of the thermocouples in the slab and beam cross-sections are shown in Figure 22. Forty thermocouples were installed on each of the following bridges: 2B, 3B, 4A, 4B, 5A, 6A, 7A, 8A, 9A and 9B.

One manually operated and two self-balancing potentiometers were available for measuring the output of the thermocouples. The manually operated potentiometer had to be connected to the leads of one thermocouple at a time. One portable self-balancing potentiometer contained six channels with an automatic switching circuit. The switching circuit had a capacity of 72 thermocouples. The output was fed to a point printout on a calibrated paper. The other self-balancing potentiometer was mounted in a trailer and was connected to the thermocouples through circuits capable of scanning 216 thermocouples at 5-min or longer intervals. The output of the potentiometer was fed to a digitizer and punched on a paper tape.

The air temperature was recorded every hour with a portable self-balancing potentiometer connected to a thermocouple located 5 ft above the ground at a central location on the project. Additional air temperature readings were taken with a thermometer in conjunction with other measurements on bridges. The accuracy of all temperature measuring systems was about ±1 deg F.

2.4 TEST PROGRAMS AND METHODS

2.4.1 Observations of Unloaded Bridges

To determine the combined cumulative effects of time and test traffic, a number of measurements and observations were made on bridges with no load other than their own weight. Strain and deflection measurements, determination of the degree of cracking of concrete beams, measurements of longitudinal and transverse slab profiles and condition surveys served this purpose. Additional measurements on unloaded structures included the strains caused by weight of the slab and those caused by variations in temperature.

Strains and Beam Elevations.—A program of strain measurements with a Whittemore gage was initiated before casting the slab on all bridges except 1A, 2B, 7A, 7B, 8A and 8B. Since the major contributor to dead load strain was the weight of the slab, a set of readings was taken on the morning before casting of concrete and another on the following morning. On Bridges 9A and 9B an additional set of readings was taken immediately after finishing the slab.

In reinforced concrete bridges the initial readings with a Whittemore gage were taken after removal of the formwork. On Bridges 7A and 8B electric resistance strain gages were bonded to the bottom layer of tension reinforcement and to the top layer of compression reinforcement near midspan to determine the strains caused by the weight of concrete. The gages were read just before and just after the removal of intermediate supports. No attempt was made to determine dead load strains on Bridges 7B and 8A.

On Bridges 1A, 2B, 7A, 7B, 8A and 8B the strain measurements with the Whittemore gage were initiated 1½ to 2 months after casting the slab. Further readings on all bridges were taken at least once every month. Strain readings were taken only when the temperature differences within the bridge were less than 5 F. The last set of Whittemore strain readings was taken after completion of the regular test traffic.

Initial readings of beam elevations at midspan and at quarter points were taken on each bridge before first crossing with the regular test vehicle. Readings of beam elevations were repeated at least once every month, and the last set was taken after the completion of test traffic.

Tension Cracking of Concrete Beams.—Beginning in May 1958, the number and width of tension cracks on the beams of all four reinforced concrete bridges were determined once every three months. Two sets of readings were taken before the beginning of regular test traffic, nine during the traffic period, and one after the completion of the test traffic. Approximately one day was required to make the crack observations on one bridge.

The crack width was determined by a sampling procedure developed on the basis of preliminary studies. The surface of each beam was divided into 30 sampling regions 10 ft long as shown in Figure 23. Sampling within each region required the following six steps:

1. Count of the number of cracks;
2. Visual selection of the point of maximum crack width for entire region;
3. Measurement of the maximum crack width at the selected point;
4. Random selection of three sample cracks from all cracks within the region;
5. Visual selection of the point of maximum width on each sample crack; and
6. Measurement of the crack width at the selected points.

The measurement in step 3 was designated as the "maximum crack width" and the average of the measurements in step 6 was designated as the "sample crack width." During the sampling period a record was kept of air temperature and other weather conditions.

On prestressed concrete beams the number of cracks was relatively small. Therefore, each crack was mapped and its width measured. A set of readings was taken soon after the cracks were found, one or more times during the remainder of the traffic period and once after completion of the test traffic.

The observations on Bridge 5A were made on the surface of the bottom flanges. The maximum width was determined for each crack by three measurements. Four sets of readings were made in addition to the initial and final set.

On Bridges 5B, 6A and 6B the lower half of the vertical surfaces of the bottom flanges was covered with a coat of epoxy resin to aid in finding the tension cracks. Where cracks were found on beams of Bridge 6A, the width was measured on the vertical surface immediately above the epoxy resin. In addition to the initial and final sets, readings were made once during the traffic period. The air temperature was recorded in conjunction with all crack measurements on the prestressed concrete beams.

Special studies were made in April and July 1960 to obtain data on variations in the crack width within a sampling region on reinforced concrete beams. These observations were limited to four sampling regions at the bottom

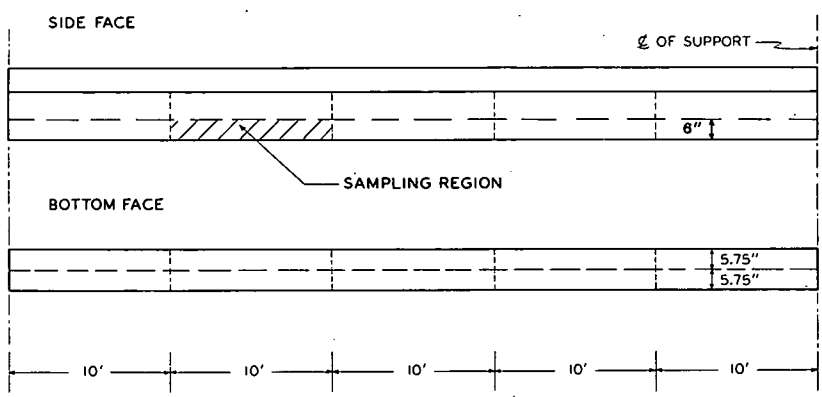

Figure 23. Sampling regions for crack measurements on reinforced concrete beams.

of each beam at midspan and differed slightly from those made at regular intervals. The sampling included ten cracks selected at random within any one region, and the crack width was measured at the level of the tension reinforcement and at three other locations along the crack in addition to the usual point of visually selected maximum width.

Miscellaneous.—Transverse profiles of all slabs were determined over the supports, at midspan and at quarter points of the span. All measurements were relative to the northeast corner of the bridge site. At least six sets of readings were taken on each bridge. The first set was taken approximately 3 months after casting the slab, additional sets usually were taken at 5- to 10-month intervals, and the last set was taken after completion of the regular test traffic.

Longitudinal profiles of the slabs were determined in the two wheelpaths and included a 100-ft length of pavement on the tangent end and a 20-ft length of pavement on the turnaround end of the bridge. Readings were taken at 1-ft intervals relative to the abutment on the tangent end. The first set was taken during the month preceding the beginning of the test traffic, two sets during the period of test traffic, and the last set after the completion of the test traffic.

A special study of the effect of differential temperature on beam strains at midspan was made on all bridges, except 1B, 2A, 4A and 4B, in the late spring and summer of 1960. Strains and bridge temperatures were recorded during 24-hr periods. Strains at midspan were measured with the Whittemore gage approximately every 4 hr; the temperature of 36 thermocouples was recorded every ½ hr. A record was kept of the air temperature and other weather conditions.

All bridges were inspected weekly starting immediately before the beginning and ending after the completion of the regular test traffic. Records were kept of yielding and fatigue cracking of the steel beams, cracking of the reinforced and prestressed concrete beams, cracking and movements of the slabs and abutments, and of the condition of rockers of the expansion bearings. In addition, comprehensive photographic records of the test structures were made as needed during all stages of the project.

2.4.2 Regular Test Traffic

Traffic.—The behavior of the test bridges under repeated application of overstress was studied from November 1958 to December 1960. During this period, test vehicles were operated counterclockwise around each loop (Fig. 2). On Loops 5 and 6, the vehicles crossed the test bridges after leaving the turnarounds and prior to reaching the test pavements (Fig. 24). Each lane was assigned one type of vehicle with specified axle weights and spacings. Except for a minor amount of miscellaneous traffic, no other than the assigned regular test vehicles were permitted to cross the bridges during the regular test traffic period. During other tests, except for post-traffic tests, only the assigned or lighter vehicles were used. (The limiting criterion for selection of vehicles for special tests on bridges was the static moment at midspan computed for the assigned regular test vehicles.)

Prior to the regular traffic phase, the loops were subjected to a brief period of traffic with light loads to condition the pavements, familiarize the vehicle operators with the test loops and permit field checks of measuring devices. A limited number of trips were made with regular test vehicles for collection of initial readings on all bridges.

From November 1958 to January 1960, regular test traffic consisted of six vehicles in each lane operating 15 hr, during an approximately 19-hr daily period, except on Sundays and holidays. Approximately 5 hr per day remained for special studies and maintenance of pavements and vehicles. In January 1960, the number of vehicles per lane was increased to ten, and the operating schedule was expanded to 7 days per week. The 6-day schedule was resumed in July 1960.

The original schedule theoretically provided for 870 daily trips over a bridge, and the increased schedule theoretically corresponded to 1,480 trips per day. However, pavement distress, truck breakdowns, bad weather and other causes made it impossible to attain the theoretical rate.

At the start of traffic operations, the drivers were instructed to maintain a constant speed of 30 mph. After experience had shown this to be excessive on turnarounds, the speed was set at 25 mph on the turnarounds and at 35 mph on the tangents.

Speed was controlled by several means. One vehicle in each loop, designated as the lead truck, was equipped with a recording speedometer. As no passing was permitted, the speed of the lead truck controlled the speed of all other vehicles. A general check on speed was made simply by observing the time required for a given number of trips around the loop. In addition, frequent speed checks were made by supervisory personnel as they moved about the project.

The vehicles were scheduled to operate over the test bridges in a single line centered on the 14-ft lane. Guide lines were painted on the left side of each traffic lane to assist drivers in maintaining proper transverse placement (Fig. 21). An additional 2-ft wide centerline between lanes aided drivers in keeping the test vehicles off the adjacent bridge.

Figure 24. Test vehicles in regular operation.

The count of the number of vehicle trips over any one bridge was determined from vehicle trip counts made by the driver crew chiefs on each loop, and from reports on special tests. The count was checked occasionally with mechanical counters.

Data on the trip count and transverse placement of vehicles on bridges is given in Section 3.3.1. More detailed descriptions of the traffic operations are given in Section 2.3 of Road Test Report 3.

Vehicles.—The regular test vehicles operating over the bridges are shown schematically in Figure 25 as Types 1 and 2. They were tractor-semitrailer combinations built to specifications developed around available commercial equipment.

The single-axle (Type 1) vehicles operated over the bridges located in inside lanes and the tandem-axle (Type 2) vehicles operated over bridges located in outside lanes of both loops. Thus, vehicles designated in Table 19 as 51 were assigned to Bridges 1A, 1B, 6A and 6B, vehicles 52 to Bridges 2A, 2B, 5A and 5B, vehicles 61 to Bridges 3A, 3B, 8A and 8B, and vehicles 62 to Bridges 4A, 4B, 9A, 9B, 7A and 7B.

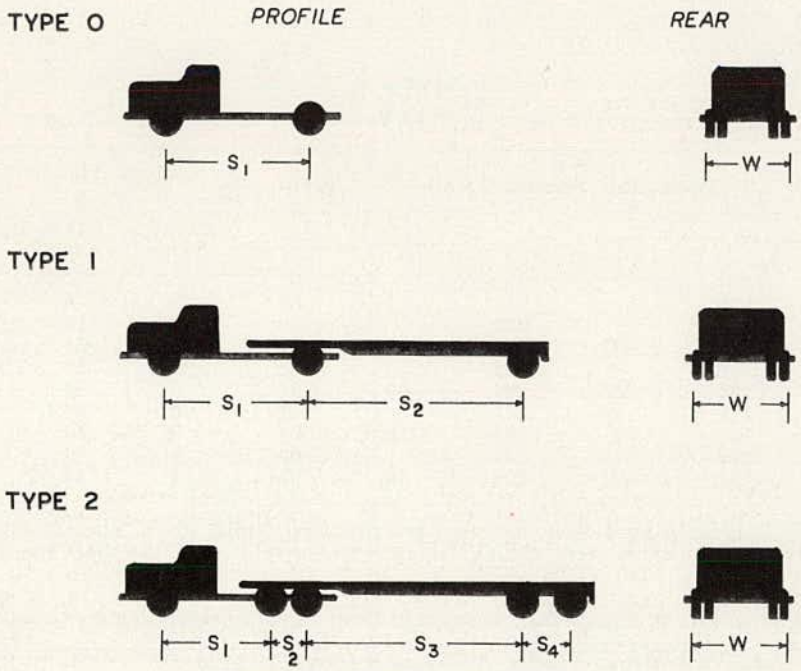

Figure 25. Regular test vehicles.

The dimensions and specified weights of the vehicles are given in Table 19. The actual axle weights were determined before the beginning and toward the end of the regular test traffic. Additional determinations were made as necessary during the period of the regular test traffic. The variations were generally within ±5 percent of the values given. The tandem axle weights were divided fairly evenly between the two component axles. However, in a few cases, differences of the order of 20 percent were noted. A detailed description of the test vehicles may be found in Section 2.2 of Road Test Report 3.

Data Collection.—The transient strains and deflections caused by the test vehicles were determined by a sampling procedure developed on the basis of a study made at the beginning of the regular test traffic. During the first three months, sampling of strains and deflections was in progress through the full duration of the traffic operations. Statistical analyses of the data showed that the mean values of the measured quantities varied significantly from day to day as compared with variations within a day. The variations within a day were small.

During the remainder of the test traffic, the sampling was carried out in 20 series each subdivided into three subseries. A subseries consisted of one 4-hr visit to every bridge during which transient deformations were recorded for six vehicle passages.

Strains at the bottom of beams at midspan or, for steel beams with cover plates, at the ends of cover plates were recorded for each beam. Deflections at midspan were recorded for at least one beam. In addition, strains on all operative strain gages at midspan and midspan deflections on all three beams were recorded during at least one subseries of each series. The longitudinal location of the vehicle was indicated on most of the deformation records taken during the regular test traffic.

One series of sampling required approximately one month. The order of visits to the bridge sites, the 4-hr period within the day and the times for recording of the bridge response within the 4-hr period were selected at random.

The transverse placement of vehicles during the regular test traffic was sampled from July 1959 through November 1960. This interval was divided into three periods. During each period every pair of tandem bridges was visited three times. On each visit, the transverse placement was recorded for all vehicle passages in two days. The order of visiting the pairs of bridges was randomized.

2.4.3 Dynamic Tests

The dynamic effects of moving vehicles on the response of test bridges were studied through special tests conducted at irregular intervals from September 1958 through February 1961. The study included the following 15 bridges: noncomposite steel bridges 2A, 4A, 4B, 9A and 9B; composite steel bridges 2B and 3B; prestressed concrete bridges 5A, 5B, 6A and 6B; and reinforced concrete bridges 7A, 7B, 8A and 8B. The tests were made with 14 vehicles. A detailed description of the dynamic tests may be found in the University of Illinois report, "Dynamic Tests of the Bridges on the AASHO Test Road." A condensation of the

TABLE 19
CHARACTERISTICS OF REGULAR TEST VEHICLES USED FOR BRIDGE TESTS

Vehicle [1]	Vehicle Type [2]	Mean Axle Spacing [2] (in.)				Width [2], W (in.)	Nominal Weight [3] (kips)			Type of Test [4]
		s_1	s_2	s_3	s_4		Front Axle	Other Axles	Gross Weight	
22	0	128				83	2	6	8	2,3
31	1	142		238		86	4	12	28	2,3
32	2	131	48	241	50	87	6	24	54	2,3
41	1	142		238		91	6	18	42	2,3
42	2	136	48	234	50	91	9	32	73	3
51	1	141		241		91	6	22.4	51	1,2,3
52	2	142	51	234	50	91	9	40	89	1,3
61	1	147		237		93	9	30	69	1,3
62	2	141	54	226	50	93	12	48	107	1,3,4

[1] Test vehicles were designated by 4-digit numbers; the first two digits, given here, designate loop and type of axle (single, 1; tandem, 2); the third digit, distinguishing between vehicles of the same type, is used in this report only where needed.
[2] See Figure 25.
[3] Front axle is first from left in Figure 25; second and third axles, whether single or tandem, had equal nominal weights.
[4] 1 = regular test traffic; 2 = dynamic tests; 3 = load deformation study; 4 = tests to failure with increasing loads.

Illinois report is included as Chapter 4 of this report.

Vehicles and Conduct of Tests.—Three types of vehicles were used for dynamic tests: trucks with two single axles (Type 0), tractor-semitrailer combinations with three single axles (Type 1) and tractor-semitrailer combinations with one single and two tandem axles (Type 2). The vehicle combinations are shown schematically in Figure 25 and the axle spacings and mean weights are listed in Table 20.

Vehicles 91 and 94 were dump trucks and vehicle A was the tractor of vehicle 511. Vehicles B and C were the tractor-semitrailer combination 511 loaded with different weights. All others were regular test vehicles loaded with weights used during the regular traffic operations.

The vehicles were usually weighed immediately before or after the dynamic test runs. The loads (Table 20) are means for all available weighings. The number of weighings per vehicle varied between 1 and 12.

Both the axle and the gross weights varied from day to day with the maximum observed variation from the mean for the heavy axles (single or total tandem) equal to 4 percent. (The distribution of the total load between the two individual axles of a tandem showed variations of up to 20 percent from the means in Table 20.) Variations in the amount of fuel and in the moisture content of concrete blocks, used for loading the trucks, are believed to have been the principal factors responsible for load variations.

The dynamic tests were conducted in 72 subseries mostly during the daily 5-hr break periods in the regular test traffic. All tests of one subseries were conducted at one time and were usually completed in 4 hr or less. With few exceptions, a subseries included only one pair of tandem bridges and one vehicle.

Static, crawl and dynamic tests were conducted. The static tests were conducted only during the initial phases of the investigation. They were discontinued after comprehensive studies showed an excellent correlation between the static and the more convenient crawl tests.

In the crawl tests, the vehicle moved across the bridge at approximately 3 mph. At least two crawl tests were made at the beginning and at the end of each subseries.

The dynamic tests covered a range of speeds varying from 20 to 50 mph in 2- to 10-mph increments. A tolerance of 1 mph was set with respect to the desired speed. Within each subseries, the order of dynamic runs was randomized with respect to speed.

In all dynamic tests, the vehicle operated in a direction opposite to that used in regular tests; that is, the vehicle approached the bridge from the tangent rather than from the turnaround. In the majority of tests the vehicle was centered on the bridge lane. Transverse placement was controlled visually with a tolerance of ± 4 in. When this tolerance or the tolerance on speed was exceeded, or when the recording equipment did not function properly the run was repeated.

The longitudinal position of the vehicle was recorded on both the bridge and vehicle deformation records. Except for a few initial tests, the trip across a bridge was timed and

TABLE 20
CHARACTERISTICS OF VEHICLES USED FOR DYNAMIC TESTS

Vehicle	Vehicle Type [1]	Axle Spacing (in.)				Mean Axle Load [2] (kips)			Gross Load (kips)
		s_1	s_2	s_3	s_4	Front Axle	Second Axle	Third Axle	
221	0	126				2.0	6.0	—	8.0
A [3]	0	144				5.1	15.1	—	20.2
91	0	132				6.3	15.0	—	21.3
94	0	132				6.6	15.0	—	21.6
315	1	142		241		4.2	12.3	12 2	28.7
415	1	143		235		5.8	18.3	18.6	42.7
417	1	137		260		6.3	18.7	18.8	43.8
B [4]	1	144		244		4.5	15.8	14.1	34.4
C [4]	1	144		244		4.6	20.2	20.6	45.4
513	1	144		244		4.8	22.5	23.0	50.3
517	1	137		237		6.2	23.6	22.9	52.7
324	2	130	48	242	50	5.8	12.6–12.4	14.0–12.6	56.4
325	2	132	48	236	49	5.6	12.6–12.4	12.1–13.1	55.8
327	2	132	48	241	49	5.7	12.2–12.2	12.0–13.3	55.4

[1] See Figure 25.
[2] Front axle is first from left in Figure 25.
[3] Tractor from vehicle 511.
[4] Vehicle 511 loaded with other than regular test loads.

the variations in speed were determined with the aid of an auxiliary odometer wheel. In the majority of tests, oscillographic records were made of strains and deflections at midspan of all three beams and of deflections of four vehicle springs. Usually strains were recorded only on the bottom of the beams. Tire pressure measurements were obtained in all tests of the third series and in tests on pavements described below.

Principal Tests.—The tests were divided into five series, each subdivided into several subseries. The speed of the vehicle was usually the only independent variable within one subseries.

The first series was exploratory. It was conducted on Bridges 2A, 2B, 4A, 4B, 5A, 6A, 7A and 7B using vehicles A, B and C. Most of the test runs were made with the vehicle following a concentric path over the center bridge beam. In a few tests, however, the vehicle was straddling the centerline of the roadway, thus loading the tested bridge with one line of wheels only.

The second, third, fourth and fifth series consisted of several parts, with each part formulated as a study of the effect of one major test condition on the dynamic behavior of the bridges. In addition to the speed, varied within each subseries, the bridge type was usually the major variable within any one part.

The following major test conditions were studied: regular tests—(a) variations in vehicle characteristics, (b) change of bridge characteristics with time; and special tests—(a) condition of the springs (acting or blocked), (b) initial oscillations of the vehicle, (c) simulation of continuous traffic, (d) lateral position of the vehicle on the bridge, and (e) sudden braking on the bridge.

The regular tests comprised a majority of all runs. In these tests, the bridge was at rest when the vehicle entered, there were no artificially induced initial oscillations in the vehicle, the vehicle suspension system was in its normal operating condition, the vehicle followed a path centered over the center beam of the bridge, and the speed of the vehicle remained the same throughout the passage over the bridge. In the special tests, the testing procedure was changed by modifying one or more of these conditions. Approximately 1,900 dynamic test runs were made.

Auxiliary Tests.—The properties of bridges and vehicles, indispensable to adequate understanding and analysis of the dynamic bridge response, were determined through several independent tests, including the following:

1. Crawl and static tests;
2. Bridge vibration measurements;
3. Loading tests of vehicles;
4. Dynamic tests on pavements;
5. Measurements of vehicle vibrations; and
6. Frequency-response tests of bridges.

Loading tests of bridges with stationary vehicles and with vehicles moving at crawl speed were made to determine the stiffness of the bridges at various stages of the test program, to determine to what extent the test bridges behaved as beams, and to provide data for a statistical correlation of the two types of tests.

On several dates special runs were made to excite the bridges and to record, with high amplification, the response of the bridge after the passage of the vehicle. Such records permitted studies of natural frequencies and of damping characteristics of the test bridges.

Static load-deflection characteristics of springs and tires were obtained for most vehicles by loading the vehicles in approximately 1,000-lb increments. Readings of deflections were taken during loading and unloading. In several tests loading and unloading were performed also at intermediate levels.

The response of vehicles to various pavement surfaces was studied by runs over smooth and rough pavements. In several runs over smooth pavements the vehicle was excited by passing over long ramps or narrow boards. Some of the runs were performed with blocked springs. Vehicle records included continuous recordings of spring deflections and of changes in tire pressures. In addition, the roadway profile was measured with the pavement profilometer described in Road Test Report 5.

The vibration characteristics of several vehicles were studied in runs over smooth pavements with various types of artificial obstructions. The vibrations of the vehicle were measured with an accelerometer placed on the bed and the axles of the vehicle.

After the completion of the regular test traffic and of the accelerated fatigue tests, frequency-response tests were conducted on Bridges 3B, 6A, 6B, 8A and 9A. The mechanical oscillator (Section 2.4.4) was bolted to the bridge slab at midspan and operated at successively higher speeds until the bridge was excited to its natural frequency. Following this, the vibrator was started at a frequency in excess of the natural frequency and was run at successively lower speeds until the bridge was excited again to its natural frequency.

2.4.4 Post-Traffic Tests

The bridges that survived the regular test traffic were subjected to one or more of the following tests: (1) accelerated fatigue tests, (2) tests with special or specially equipped vehicles, and (3) tests to failure with increasing loads. The special tests are described in Road Test Report 6; the others are included in this report. A summary of the special tests is included in Section 5.7 of this report.

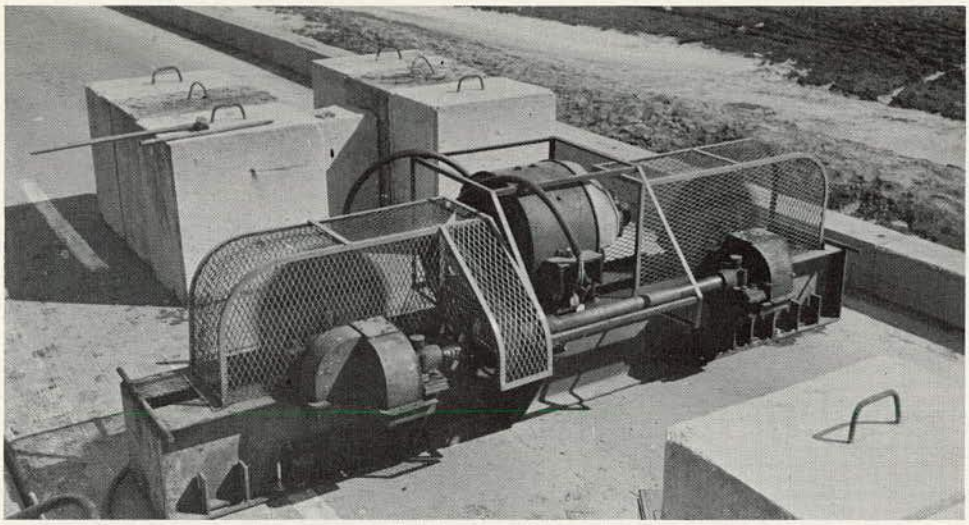

Figure 26. Mechanical oscillator on a bridge.

Accelerated Fatigue Tests.—The number of repetitions of maximum stress caused by the regular test traffic was augmented in Bridges 2B, 5B, 6A, 6B, 7A, 7B and 8A by accelerated fatigue tests either to failure or to a total of approximately 1,500,000.

The testing was done with the aid of a mechanical oscillator shown in Figure 26. The oscillator consisted basically of two identical rotors lying in the same vertical plane and turning at equal speeds in opposite directions. The rotors were geared in phase so that the vertical components of the centrifugal forces exerted by their revolving unbalanced masses were in conjunction while the horizonatal forces were in opposition. The rotor bearings were mounted on a stiff welded frame of wide-flange beams; thus, the horizontal forces were not transmitted externally. The resultant external force was then in the vertical direction and, ignoring the effect of small vertical movements of the oscillator, was a simple harmonic force.

The rotors were driven by a 15-hp variable dc motor with a gasoline driven generator as a power source. A rheostat control provided a speed range from 2 to 5.8 cps.

The frame of the oscillator was bolted to the floor of the test bridge at midspan. To compensate for the upward deflections caused by the upward component of the rotor forces, the slab was loaded with concrete blocks (Fig. 26).

At the beginning of the test, the speed of the oscillator was slowly increased until strains at midspan or, on Bridge 2B at the ends of the cover plates, reached the mean stress range observed during the regular test traffic. From then on the speed was kept constant except for occasional adjustments needed to keep the strains in the desired range. All bridges were tested at speeds close to their natural frequencies.

The strain gages at the critical section on the bottom of all three beams were connected to oscillographs and their response was observed visually on a ground glass. The desired deflection of the beam of light, monitoring the response of the gages, was marked on the glass. Permanent records of the output of the strain gages and of deflectometers placed at midspan of each beam were taken at least once per hour. The number of cycles was recorded with a mechanical counter attached to the oscillator.

The duration of the tests varied from bridge to bridge: the shortest was completed in three days; the longest required nine working days. Approximately 1,000,000 stress cycles were accumulated in the nine days. The tests were conducted during the winter of 1960-61.

Tests to Failure with Increasing Loads.—During spring 1961, bridges that survived the earlier tests were tested to failure with increasingly heavier loaded vehicles. The vehicles included a tandem-axle regular test truck 62, tractor-scraper unit designated as vehicle 96, the special-purpose vehicle 97 (Fig. 27) and special-purpose vehicles 98 and 99. Vehicles 96, 97, 98 and 99 are shown schematically in Figure 28.

Bridge 1A was tested with truck 62, the scraper (vehicle 96) and vehicle 97. Bridge 3B was tested with vehicles 97, 98 and 99. All other bridges, including 5A, 5B, 6A, 6B, 8A, 8B, 9A and 9B, were tested with the special-purpose vehicle 97.

The first load applied to a bridge was selected to produce a maximum static moment at the critical section equal to or slightly in excess of the maximum static moment produced by the assigned regular test vehicle. After 30 trips the load was increased and another 30 trips were made across the bridge. This procedure was repeated until the bridge was considered

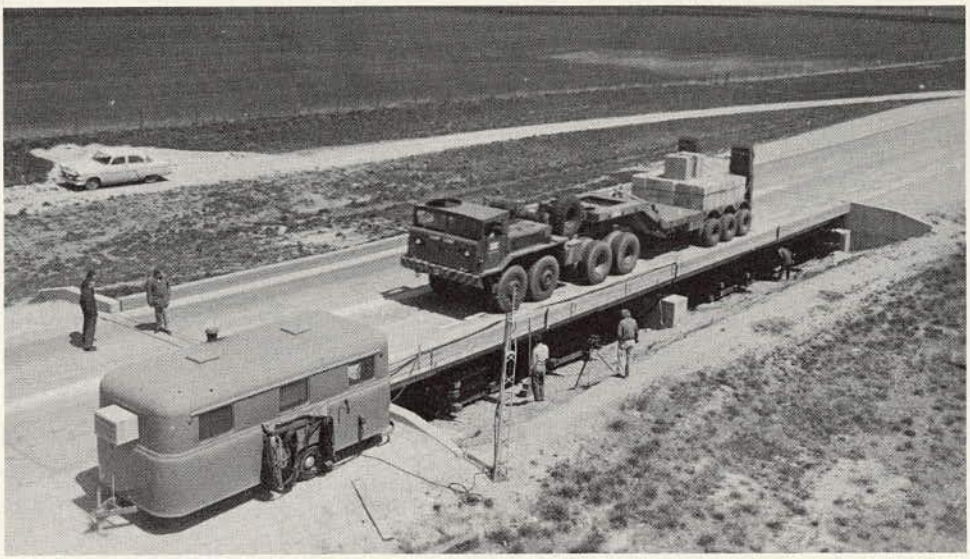

Figure 27. Special vehicle during test to failure with increasing loads.

failed or further loading of the test vehicle was considered undesirable.

The load increments were selected so that at least three loads were needed to failure. Depending upon the expected capacity of the bridge and other factors, the increments of the maximum static moment at midspan ranged up to 430 ft-kips.

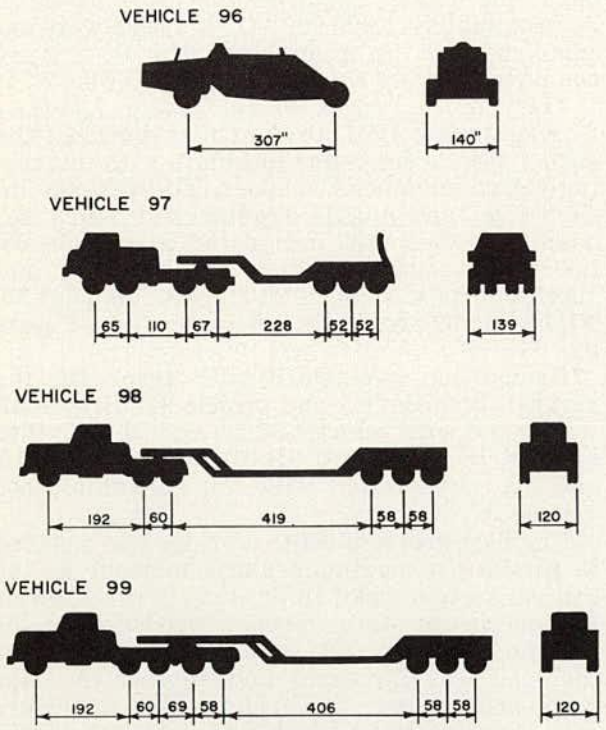

Figure 28. Special test vehicles.

In most tests the vehicle traveled in the same direction as during the regular test traffic. However, in the last phases of tests of Bridges 3B, 5B and 6B it was found necessary to move the vehicle across the bridge at creep speed alternately forward and backward, with the vehicle facing in the direction of regular test traffic. In all tests, the vehicle was centered on the bridge lane.

At the beginning of the tests the vehicle traveled across the bridge at about 30 mph. However, as the load and permanent deformations of the bridge increased, it was often necessary to decrease the speed. Several creep speed runs were made with most of the loads to provide data on the magnitude of impact.

Deflections at midspan of each bridge beam were measured with the slip ring deflectometers. In early stages of the tests, midspan deflections were measured also with the cantilever deflectometers. Strains were measured at midspan and at the ends of cover plates. When gages at these locations became inoperative, the oscillographs were connected to gages at the third points.

The completion of the tests with increasing loads on June 13, 1961, marked the end of the experiments on the test bridges.

2.4.5 Other Tests

Reference Data.—Before the beginning of the regular test traffic, initial strain and deflection data were obtained for every bridge. The tests, including static, crawl and 30-mph runs with regular test vehicles, were repeated approximately every six months.

In the static tests the vehicle was placed in the position for the maximum moment at midspan, at the third points and at the ends of the cover plates. In the crawl tests the vehicle was

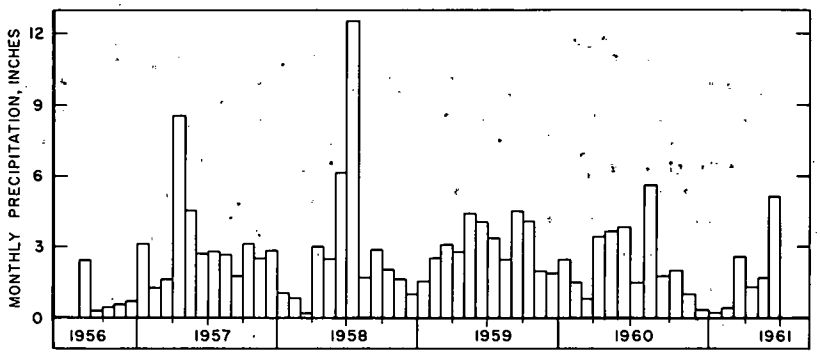

Figure 29. Monthly precipitation.

traveling at approximately 3 mph. In the 30-mph tests the speed varied between 28 and 32 mph.

The vehicle was centered on the 14-ft bridge lane within ± 4 in. Strains were recorded for all operative strain gages and for deflectometers placed at midspan of each beam. A minimum of 5 replica runs were made for each test.

Crack Width and Spacing in Loaded Bridges.—The effect of load on the width and spacing of cracks in reinforced and prestressed concrete beams was determined twice during the period of regular test traffic and on the completion of the traffic. A regular test vehicle was placed on the bridge in the position for maximum moment at midspan. The procedure used for crack measurements was the same as that described (Section 2.4.1) for unloaded structures.

Miscellaneous Tests.—In addition to the tests conducted to obtain information directly related to the two principal objectives of the bridge research, several minor studies were carried out providing information on the response of the test bridges to loading. Three of these studies, included in this report, are (a) transverse distribution of moments and deflections, (b) load-deformation study, and (c) stress at ends of cover plates.

To obtain data for a study of the transverse distribution of moments and deflections, every bridge was tested with the two-axle vehicle 91 or 94 (Table 20) placed in four or six transverse positions (Fig. 141). The vehicle was placed in positions for maximum static moment at midspan or at the third points, or was operated over the bridge at crawl speed. At least three replicate sets of data were collected for each vehicle position and speed, including deflections at midspan of all three beams and strains on the bottom steel at midspan of all three beams as well as at several other locations.

To determine the relationship between the external moment and the bridge deformations, standard vehicles from the outside lane of Loop 2 and from both lanes of Loops 3, 4, 5 and 6 were operated at crawl speed over Bridges 7A, 7B, 9A and 9B. The vehicles were arranged into a train traveling in the direction of regular test traffic. Strains at midspan, at the third

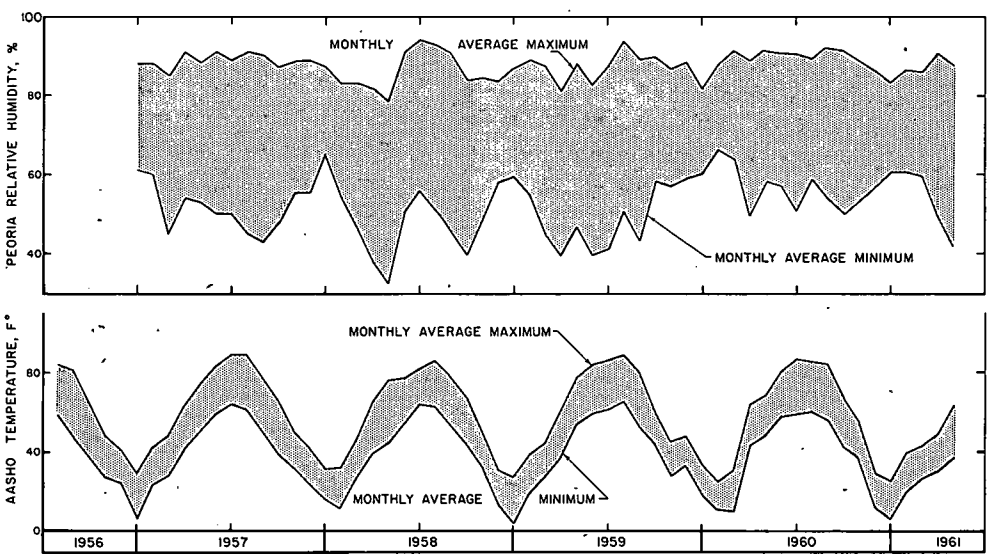

Figure 30. Average monthly relative humidity and temperature.

points of the span and at ends of cover plates, and deflections at midspan were measured during each passage of every vehicle.

A special test was carried out on Bridge 2B to obtain data on the magnitude of stress concentrations at the ends of cover plates. The test was made with a regular test truck placed in the position for maximum moment at the exit end of the cover plates. Bottom flange strains were recorded for the gages at the third points, on the cover plates near their end and on the rolled sections near the ends of the cover plates. The strains were recorded individually for each gage with a strain indicator.

2.5 ENVIRONMENTAL CONDITIONS

In addition to recording of temperature and other weather conditions in conjunction with the observations described in Section 2.4, the environmental conditions at the test road were observed at a centrally located weather station. The results of the precipitation and temperature measurements are summarized in Figures 29 and 30, respectively, which cover the period from August 1956 through June 1961. Total monthly precipitation and monthly average maximum and minimum temperatures are given.

The program for measurements at the weather station also included relative humidity. However, because of technical difficulties the measurements were discontinued in 1957. The monthly average maximum and minimum humidity data (Fig. 30) were compiled from the tables of local climatological data of the U. S. Weather Bureau in Peoria, Ill.

Chapter 3

Tests with Repeated Stresses

This chapter contains descriptions and summaries of data from the results of the major tests with repeated stresses. It includes sections on stresses and deformations before traffic, during reference tests, and during and after the period of regular test traffic. It also details the behavior of certain bridges under accelerated fatigue tests and tests to failure with increasing loads, and contains an analysis of the fatigue strength of beams.

3.1 STRESSES AND DEFORMATIONS BEFORE TRAFFIC

3.1.1 Variation of Dead Load Strains with Time

Time-Strain Curves.—All original superstructures were completed 6 to 13 months before the first trip of a vehicle over the bridges. During this period, the bridges were subjected only to the effects of their weight, of internal stresses, and of the environment. The major variation in the environment was in temperature. Only negligible variations in load were caused by changes in moisture conditions and by the presence of water or snow collected on bridges.

Changes in bottom strains at midspan of the center beams measured during the period prior to traffic are shown in Figure 31 for typical bridges. The strain change, corrected for the effects of changes in temperature, is plotted as a function of time. The corresponding curves for the exterior and interior beams of the same bridges had essentially the same shape and differed from those shown only in magnitude. Corresponding curves for bridges of the same types showed similar characteristics. Beam strain measurements were started on most bridges before the slabs were cast. Except for abrupt changes associated with the added weight of the slabs; all changes in the curves (Fig. 31) were gradual. Slabs were cast on the dates indicated by vertical dashed lines.

Except for prestressed concrete bridges, where appreciable drop in strain was noted, the strains showed little variation after casting the slab. The slopes of the time-strain curves during this period were significantly (at 5 percent level) different from zero only for Bridges 1A, 2B, 3B and 8B; but even for these bridges the magnitude of the changes with time was practically negligible.

The strains measured on prestressed concrete beams indicated a continuous decrease in the length of the bottom surface during the period between the beginning of March and the end of July 1958. The shortening was about the same on all four prestressed concrete bridges. This suggests that creep was not a major factor and that shrinkage and incorrect compensation for temperature changes (Section 5.5) were the possible causes. Comparisons of the measurements on beams with shrinkage measurements on cylinders* indicated that shrinkage was the primary cause of the time variations.

Methods for Determination of Dead Load Stresses.—The dead load stresses in steel beams were caused by the weight of the beams, the reinforced concrete slab, the timber curb and miscellaneous details. Of these, the weight of slab accounted for more than two-thirds of the total stress. The dead load stresses in prestressed concrete beams were caused by the prestressing force and by the weight of the beams, the reinforced concrete slab, the timber curb and miscellaneous details, and by time losses. The largest contributing factor was the prestressing force which caused compression on the bottom of the beams. The largest tensile stress was caused by the weight of the slab which amounted to somewhat less than two-thirds of the stress caused by the prestressing force. In reinforced concrete bridges almost all stresses were caused by the weight of the slab and the beams; only a minor portion of the stresses was caused by the timber curve and miscellaneous details.

Dead load strains were measured on most of the test bridges, but the data usually included only the effects of the weight of the slab and were generally contaminated by secondary effects of unknown magnitude such as temperature and shrinkage. It was considered necessary, therefore, to evaluate the dead load stresses by computations. Where available, the strain measurements were used as a guide in selection of the methods of analysis.

No data were obtained on the stresses in beams caused by the weight of the prefabricated beams. Strains caused by the weight of

* Kingham, R. I., Fisher, J. W., Viest, I. M., "Creep and Shrinkage of Concrete in Outdoor Exposure and Relaxation of Prestressing Steel." HRB Special Report 66, pp. 103-131 (1961).

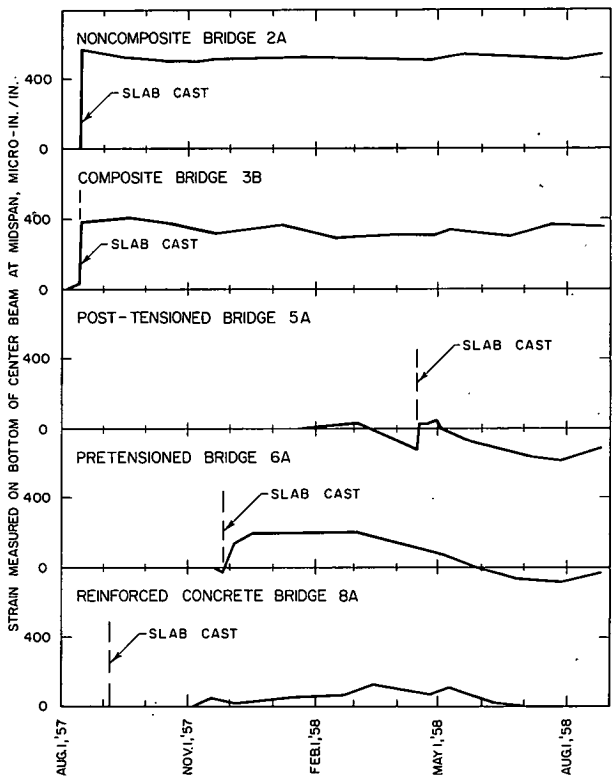

Figure 31. Typical strain histories before traffic.

concrete cast at the bridge sites were measured on most structures. Strain data were also obtained for time losses in prestressed concrete beams. Only a few measurements were taken of the effects of the timber curb on strain; they were too small to be considered reliable.

Test Data vs Analyses for Steel Bridges.—On steel bridges 1B, 2A, 3A, 3B, 4A, 4B, 9A and 9B one set of strain readings was taken on the morning before casting the slab and another on the morning following the placement of concrete. Static moments at midspan computed from the weight of concrete and wet burlap used for curing were consistently 10 to 20 percent lower than the moments computed from the strain measurements. No definite reason was established for the discrepancy. It seems probable, however, that it was caused by shrinkage and changes of temperature accompanying the hardening of the slab.

Measurements on Bridges 9A and 9B were made also on the day of casting shortly after finishing the slab. The strains are given in Table 21, which also includes calculated strains and ratios of measured strains to calculated strains. The calculated values include the effects of the weight of fresh concrete and of wet burlap. All strains are for the bottom flange at midspan.

The calculated values were obtained by two methods, both taking into account the system

TABLE 21

STRAINS DUE TO CASTING OF SLAB

Bridge	Beam	Strain[1] (10^{-6} in./in.)			Strain Ratios	
		Measured	Calculated		Meas. A	Meas. B
			Meth. A	Meth. B		
9A	Interior	214	203	215	1.05	1.00
	Center	241	239	215	1.01	1.12
	Exterior	315	275	287	1.15	1.10
	Mean				*1.07*	*1.07*
9B	Interior	198	189	200	1.05	0.99
	Center	232	223	201	1.04	1.15
	Exterior	266	256	267	1.04	1.00
	Mean				*1.04*	*1.05*
Mean	Interior				1.05	1.00
	Center				1.03	1.14
	Exterior				1.10	1.04
	Over-all				*1.06*	*1.06*

[1] Strain on bottom flange of steel beam at midspan caused by weight of fresh concrete and of wet burlap; measurements taken on morning before casting and shortly after finishing slab; method A considered cross-beams supporting forms as simple beams in contact with exterior and interior beams only; method B considered cross beams as 2-span continuous beams, on deflecting supports, in contact with all three bridge beams.

of forming (Road Test Report 2, Section 7.3.3). The forms between the bridge beams were assumed to act as simple beams. The forms for the overhangs were considered as simple beams supported on one end by the steel beam and on the other end by cross beams forming part of the falsework. The cross beams were connected by hangers to the exterior and interior bridge beams and were pulled up tight against the center bridge beam. Depending on the tightness of the fit at the center beam and on the magnitude of relative deflections of the three bridge beams, the cross beam may have exerted an upward reaction or no reaction on the center beam.

The two methods were designated (Table 21) as A and B. An absence of contact between the cross beams and the center bridge beam was assumed in method A; in method B the cross beams were considered as 2-span continuous beams in contact with all three bridge beams. The necessary conditions for computation of moments were obtained by assuming compatibility of deflections of the bridge beams and the cross beams at all points of contact.

The measured strains averaged 6 percent in excess of the computed strains. This excess is substantially less than that indicated by measurements made on the morning following the day of casting. As the first set had taken place by the time the strain readings were taken, it is possible that this excess also was caused by hardening of concrete.

The strain ratios for individual beams indicate that the distribution of strain to the individual beams was predicted better by

TABLE 22
STRAINS DUE TO WEIGHT OF CURED CONCRETE

Bridge	Beam	(Strain[1] 10^{-6}in./in.)			Strain Ratios	
		Measured	Calculated		Meas. / A	Meas. / B
			Meth. A	Meth. B		
1B	Interior	466	469	483	0.99	0.96
	Center	570	598	570	0.95	1.00
	Exterior	777	727	740	1.07	1.05
	Mean				*1.00*	*1.00*
2A	Interior	399	377	390	1.06	1.02
	Center	527	485	460	1.09	1.15
	Exterior	894[2]	579	592	—	—
	Mean				—	—
3A	Interior	370	314	327	1.18	1.13
	Center	398	404	377	0.99	1.06
	Exterior	547	493	506	1.11	1.08
	Mean				*1.09*	*1.09*
3B	Interior	308	279	290	1.10	1.06
	Center	345	358	337	0.96	1.02
	Exterior	364	438	449	0.83	0.81
	Mean				*0.96*	*0.96*
4A	Interior	281	277	288	1.01	0.98
	Center	382	357	335	1.07	1.14
	Exterior	475	436	446	1.09	1.07
	Mean				*1.06*	*1.06*
4B	Interior	313	281	292	1.11	1.07
	Center	299	361	339	0.83	0.88
	Exterior	406	440	451	0.92	0.90
	Mean				*0.95*	*0.95*
Mean[3]	Interior				1.08	1.04
	Center				0.96	1.02
	Exterior				1.00	0.98
	Over-all				*1.01*	*1.01*

[1] Strain on bottom flange of steel beam at midspan caused by weight of cured concrete and timber curb; measured values are averages of strains observed between finishing slab and beginning of test traffic; method A considered cross-beams supporting the forms as simple beams in contact with exterior and interior beams only; method B considered cross-beams as 2-span continuous beams, on deflecting supports, in contact with all three bridge beams.

[2] A few slip lines indicated that some yielding occurred in the exterior beam of Bridge 2A during casting of the slab.

[3] Data for Bridge 2A not included.

method A than by method B, particularly for Bridge 9B. Method B appeared to underestimate the strain in the center beam.

On steel bridges 1B, 2A, 3A, 3B, 4A and 4B the strain readings were taken initially before casting the slab and approximately every month thereafter. The differences between the initial reading and the monthly readings were averaged for the period before traffic. The averages are compared with strains calculated by the two methods (Table 22). The strains are those at midspan of the bottom flange of the steel beams caused by the weight of cured concrete and the weight of timber curb.

The over-all mean of the strain ratios for Bridges 1B, 3A, 3B, 4A and 4B shows an excellent agreement between the measured and calculated quantities. However, although the over-all mean was equal to 1.01, the means for individual bridges varied from a low value of 0.95 to a high value of 1.09. The ratios for individual beams varied from 0.81 to 1.18 with method B giving results usually a little closer to the measured strains than method A. The differences between the strains calculated by the two methods seldom exceeded 0.000020 which corresponded to a stress of only 600 psi in the steel. In view of this and in view of the large scatter in the strain ratios, the two methods appear equally suited for computation of dead load stresses.

Test Data vs Analyses for Prestressed Concrete Bridges.—On prestressed concrete bridges strain measurements were made prior to casting the slab and on the day after casting. Strains measured over a period of time after casting the slab showed considerable systematic variation (Fig. 31). Therefore, no direct evaluation of strains caused by dead load was possible on the basis of the strain measurements. However, the method of forming was the same for prestressed concrete bridges as that for steel bridges. Accordingly, it was considered sufficiently accurate to compute the stresses caused by the weight of the slab in prestressed concrete beams by either of the methods found satisfactory for steel bridges.

The creep and shrinkage of concrete and the relaxation of prestressing steel caused losses of prestress. The stress changes resulting from this loss were small in relation to the stresses caused by the slab weight, but were of sufficient magnitude to require their inclusion in the computation of dead load stresses. Strain measurements after the beams were placed on the bearings at the bridge sites permitted a direct evaluation of a portion of the stress changes caused by loss of prestress. However, no such data were available for losses in prestress that occurred before such time. Estimates have indicated that about two-thirds of the total stress changes caused by losses must have occurred during the early period. Thus, a major portion of the stress changes had to be evaluated by computations.

Beams for Bridges 5A and 5B were placed on their bearings approximately four months before casting the slab. Strain measurements taken during this period provided a check on the method of computation selected for evaluation of the stress losses. Table 23 gives both the measured and the computed strains for the six beams of the two bridges. The computed strains were obtained by the rate of creep method* using creep, shrinkage and relaxation characteristics determined by tests of materials used in the prestressed concrete beams (Section 2.2).

The computed strains compared favorably with the measured values for center and ex-

* Corley, W. G., Sozen, M. A., Siess, C. P., "Time Dependent Deflections of Prestressed Concrete Beams." HRB Bull. 307, pp. 1-25 (1962).

TABLE 23

STRAINS CAUSED BY TIME-DEPENDENT EFFECTS

Bridge	Beam	Data at Prestressing		Strain[1] (10^{-6}in./in.)		Ratio, Meas. Comp.
		Age (days)	f'_c (psi)	Meas.	Comp.	
5A	Interior	3	4,600	108	206	0.52
	Center	13	5,850	129	132	0.93
	Exterior	5	5,050	153	168	0.91
5B	Interior	97	8,100	97	87	1.11
	Center	4	4,950	172	193	0.89
	Exterior	3	4,600	94	220	0.43

[1] Strains on bottom surface of beams at midspan caused by shrinkage and creep of concrete and by relaxation of prestressing steel; strain differential over period 12-26-57 through 4-16-58 for Bridge 5A and 12-16-57 through 4-16-58 for Bridge 5B.

TABLE 24
STRAINS IN REINFORCING BARS DUE TO SHORE REMOVAL

Bridge	Beam	Strain (10^{-6}in./in.) Top Bars[1]		Bottom Bars	
		Meas.	Comp.	Meas.	Comp.
7B	Interior	−115	−127	—	596
	Center	−161	−127	392	612
	Exterior	—	−122	364	692
8A	Interior	−168	−126	460	567
	Center	−125	−127	373	571
	Exterior	−115	−122	466	634

[1] At midspan; negative values indicate compressive strains.

terior beams of Bridge 5A and for interior and center beams of Bridge 5B. On the other hand, the computed strains were about twice the measured strains for the interior beam of Bridge 5A and for the exterior beam of Bridge 5B. An examination of strains measured on these two beams, in light of the data on prestressing (Table 23) indicates that they were considerably out of line with the strain measurements on the other four beams.

Test Data vs Analyses for Reinforced Concrete Bridges.—On reinforced concrete bridges the presence of forms prevented measurements with Whittemore strain gages prior to casting the slab. To obtain some data on the magnitude of strains caused by the weight of concrete, electric resistance strain gages were mounted on the tension bars at midspan of Bridges 7B and 8A prior to casting of concrete. The response of these strain gages, as well as of the gages on the compression reinforcement, was recorded immediately before removal of the falsework supporting the forms and immediately after its removal. Table 24 gives the resulting strains compared with computed strains.

The computed values were obtained by assuming a straightline stress distribution and a cracked section. The weight of concrete was assumed to be distributed to the individual beams according to the effective slab width: 5 ft 8 in. for the exterior beam and 4 ft 8 in. for the center and interior beams. For the top bars the computed strains are in reasonable agreement with the measured quantities, but for bottom bars the computed values are 20 to 90 percent in excess of the measured quantities. It is believed that the discrepancy in the tension strains was caused by incomplete cracking of the stem of the beams. Considerable additional cracking was observed after the beginning of test traffic (Section 3.3.7) which was undoubtedly accompanied by an increase in dead load strains. It is believed, therefore, that stresses computed on the basis of the straightline, cracked-section theory represented reasonably well the conditions existing in the bridges after the beginning of the test traffic.

3.1.2 Dead Load Stresses

The evaluation of dead load stresses involved both calculations and field measurements, and included only flexural stresses on the bottom surface or in the bottom row of steel at midspan and just off the end of partial-length cover plates. Except for a portion of the time losses in prestressed concrete beams, the values given in this section were obtained by calculations. The observed strains were used for checking the accuracy of the chosen methods of computations and for checking the variation of dead load stresses with time (Section 3.1.1).

The computations were based on weights and dimensions of the various bridge components as determined by measurements. The measured values are listed in Section 2.2 and in Chapter 7 of Road Test Report 2. The following items were considered:

1. Beam weight, weight of shear connectors, diaphragms and end connections;
2. Prestress;
3. Loss of prestress before and after casting the slab;
4. Weight of concrete and of steel reinforcement;
5. Weight of timber curbs; and
6. Weights of concrete fillets and portions of structures placed outside the span length, and the residuals from the weight of the forms in composite steel bridges and in prestressed concrete bridges.

The weights listed as items 1 and 6 were considered to be distributed directly to the individual beams. For reinforced concrete bridges the weight in item 4 was also assumed to be

distributed directly to the individual beams; the dividing lines for the contributory areas of the slab were taken half way between the adjacent beams. The moments caused by these weights were computed by statics.

For steel and prestressed concrete bridges, the distribution of the weight of the concrete slab was influenced by the method of forming. The forms placed between the beams were considered as simple beams exerting equal reactions on the two adjacent bridge beams. The forms for the overhangs were considered as simple beams with one overhang; one of the reactions was applied directly to the bridge beams and the other to five cross beams spaced uniformly along the bridge span and suspended from the interior and exterior beams. It was assumed in computation of moments that the cross beams exerted reactions on the exterior and interior bridge beams but were independent of the center bridge beam (Method A, Section 3.1.1).

TABLE 25

DEAD LOAD STRESSES IN STEEL BEAMS

Bridge	Beam	Stress (ksi) at Midspan [1] Due to Weight of			Dead Load Stress [1] (ksi)	
		Beam, Diaphr. and Connectors	Slab	Misc. Items	At Midspan	Near End of Cover Plate
		(1)	(2)	(3)	(4)	(5)
1A	Interior	1.8	9.7	−0.4	11.1	12.3
	Center	1.9	11.4	0.5	13.8	15.3
	Exterior	1.8	13.1	1.3	16.2	18.0
	Mean				*13.7*	*15.2*
1B	Interior	2.3	15.7	−0.5	17.5	—
	Center	2.4	18.5	0.7	21.6	—
	Exterior	2.3	21.3	2.0	25.6	—
	Mean				*21.5*	—
2A	Interior	2.2	13.0	−0.4	14.8	—
	Center	2.4	15.2	0.7	18.3	—
	Exterior	2.2	17.5	1.8	21.5	—
	Mean				*18.2*	—
2B	Interior	1.8	10.1	−0.1	11.8	15.0
	Center	2.0	11.9	0.9	14.8	18.8
	Exterior	1.9	13.7	1.8	17.4	22.1
	Mean				*14.7*	*18.7*
3A	Interior	1.9	10.7	−0.4	12.2	—
	Center	2.1	12.6	0.5	15.2	—
	Exterior	2.0	14.5	1.4	17.9	—
	Mean				*15.1*	—
3B	Interior	1.8	9.5	0.1	11.4	13.1
	Center	1.9	11.2	0.9	14.0	16.0
	Exterior	1.8	12.9	1.8	16.5	18.9
	Mean				*13.9*	*15.9*
4A	Interior	1.8	9.4	−0.3	10.9	12.3
	Center	1.9	11.1	0.5	13.5	15.3
	Exterior	1.8	12.8	1.3	15.9	18.0
	Mean				*13.4*	*15.2*
4B	Interior	1.8	9.4	−0.3	10.9	12.3
	Center	1.9	11.1	0.5	13.5	15.3
	Exterior	1.8	12.8	1.3	15.9	18.0
	Mean				*13.4*	*15.2*
9A	Interior	1.9	6.3	−0.3	7.9	8.5
	Center	1.9	7.4	0.2	9.5	10.3
	Exterior	1.9	8.5	0.7	11.1	12.0
	Mean				*9.5*	*10.3*
9B	Interior	1.9	6.1	−0.3	7.7	8.3
	Center	1.9	7.1	0.2	8.8	9.5
	Exterior	1.9	8.2	0.7	10.8	11.7
	Mean				*8.8*	*9.5*

[1] In bottom fibers of steel section; negative sign indicates compressive stress.

TABLE 26

DEAD LOAD STRESSES IN PRESTRESSED CONCRETE BEAMS BEFORE BEGINNING OF TRAFFIC

Bridge	Beam	Concrete Stress[1] at Midspan (psi)					Steel Stress[2] at Midspan (ksi)
		Initial Prestress and Beam Weight	Slab Weight	Time Losses	Misc. Weights	Total	
		(1)	(2)	(3)	(4)	(5)	(6)
5A	Interior	−1,047	841	117	5	− 84	144.9
	Center	−1,044	900	119	47	22	144.8
	Exterior	−1,026	1,151	112	161	398	146.7
	Mean					*112*	*145.5*
5B	Interior	−1,868	855	157	− 3	−859	152.8
	Center	−1,791	915	194	39	−643	149.1
	Exterior	−1,822	1,170	178	153	−321	152.9
	Mean					*−608*	*151.6*
6A	Interior	− 922	841	97	− 11	5	164.6
	Center	− 879	899	79	30	129	163.3
	Exterior	− 924	1,150	104	143	473	165.9
	Mean					*202*	*164.6*
6B	Interior	−1,446	830	167	− 21	−470	170.1
	Center	−1,425	888	143	20	−374	171.1
	Exterior	−1,415	1,136	157	131	9	172.3
	Mean					*−278*	*171.2*

[1] On bottom surface of uncracked section; negative sign indicates compressive stress.
[2] In bottom layer of prestressing steel.

The moments caused by the weight of the timber curb were obtained from an analysis accounting for interdependence of deformations of the three beams and the slab. The slab was assumed to be concentrated into five equally spaced cross beams having the same deflections as the bridge beams at all points of contact. Each cross beam was subjected to a concentrated load representing the contributory weight of the timber curb.

The stresses were computed from the moments using the concepts of elastic bending. For noncomposite steel bridges, the moments were assigned to the beams alone. For the composite steel bridges, prestressed concrete bridges and reinforced concrete bridges, the section properties of the individual beams were based on composite sections with the dividing line for the effective slab width assumed to be half way between the adjacent beams. However, the moments caused by the beam, slab and form weights and by prestress in the composite steel and prestressed concrete bridges were assumed to be resisted by the beam sections alone.

Steel Beams.—Table 25 gives the computed dead load stresses on the bottom of the steel beams. The stresses are for the conditions existing before the beginning of traffic. Column 1 gives the stresses caused by the weight of beam, of connectors and of intermediate diaphragms including connections. The weight of the rolled section was assumed to be uniformly distributed throughout the span and the weight of the cover plates was assumed to be uniformly distributed throughout their length. The shear connectors were replaced by a series of concentrated loads placed at the center of the length over which they were uniformly spaced. The intermediate diaphragms were considered to have no end fixity and were replaced by concentrated loads.

Column 2 contains stresses caused by the weight of the slab. A uniform weight per square foot was assumed throughout the deck area using the unit weight of concrete determined at the beginning of test traffic, the mean slab thickness corrected for the area of reinforcing bars, and the weight of reinforcing bars.

Column 3 contains stresses caused by the weight of the timber curb, the weight of concrete fillets cast with the slab of the noncomposite bridges for lateral support of the compression flange, the weight of portions of concrete slab extending beyond the supports, and the stresses left in the beams of composite bridges as a result of the weight of the forms.

Stresses listed in Columns 1, 2 and 3 are for midspan; their sum is given in Column 4. The dead loads caused the largest bottom flange stresses in the exterior beam and the smallest in the interior beam.

Bridges 1A, 2B, 3B, 4A, 4B, 9A and 9B were designed so that the most highly stressed area was just off the ends of cover plates. The dead load stresses at these locations were computed assuming a parabolic distribution of the

total moment along the length of the beam (Col. 5). The stresses at the ends of cover plates exceed the stresses at midspan in every case.

Prestressed Concrete Beams.—Table 26 gives computed dead load stresses at midspan of prestressed concrete beams. The stresses are for the conditions existing just before the beginning of traffic.

The stresses in Column 1 include the effects of prestress and beam weight. The beam weight was assumed distributed uniformly throughout the span. The initial prestress in post-tensioned beams included the average initial tension determined by jack pressure, and the decrease in the initial tension caused by differential elastic shortening and friction between the cable and the cable sheathing. (The cables were stressed one at a time; the stressing of subsequent cables caused change in stress in the cables already anchored.) The prestressing force for the pretensioned beams included the average initial tension determined by a calibrated load cell; corrections for the change in temperature between the time of stressing the strands and the time of release; elastic shortening on release; and relaxation losses between the time of stressing the strand and release.

For post-tensioned beams, stresses (Col. 1) were computed on the basis of section properties of the concrete beam excluding the cross-sectional area of the ducts of prestressing cables; for pretensioned beams, stresses were computed using the transformed areas of the beam cross-section.

The moment caused by the slab weight was computed using the approach outlined for steel beams. The stresses were computed from the moments on the basis of a transformed uncracked section.

The stresses caused by time losses of prestress (Col. 3) were evaluated in two parts: those that occurred before the slab was cast and those that occurred between casting the slab and the beginning of traffic. The first part was computed as described in Section 3.1.1. The effective prestress, creep and shrinkage at various times were computed from the initial prestress and from Eqs. 5, 6, 7, 9 and 10. The second part was obtained from measured differential strains that occurred after casting of the slab and before beginning of the traffic. Uncracked transformed cross-sections and linear distribution of strains were assumed in all computations of stresses due to time losses.

The stresses in Column 4 include the effects of the weight of the timber curb, the embedment of the beams in the slab, the weight of the extension of slab beyond the supports, and the weight of the end diaphragms; and the stresses left in the beams as a result of the weight of the forms.

TABLE 27
DEAD LOAD STRESSES IN CRACKED REINFORCED CONCRETE BEAMS

Bridge	Beam	Stress[1] (ksi) Due to Weight of		Dead Load Stress[1] (ksi)
		Beam and Slab	Misc. Items	
		(1)	(2)	(3)
7A	Interior	18.1	−0.4	17.7
	Center	18.2	0.1	18.3
	Exterior	20.4	1.3	21.7
	Mean			*19.2*
7B	Interior	18.1	−0.4	17.7
	Center	18.1	0.1	18.2
	Exterior	20.5	1.3	21.8
	Mean			*19.2*
8A	Interior	16.8	−0.4	16.4
	Center	16.9	0.1	17.0
	Exterior	18.7	1.3	20.0
	Mean			*17.8*
8B	Interior	16.9	−0.4	16.5
	Center	16.9	0.1	17.0
	Exterior	18.8	1.2	20.0
	Mean			*17.8*

[1] In bottom layer of reinforcing bars at midspan; negative sign denotes compressive stress.

The sum (Col. 5) represents the dead load stress on the bottom surface of the concrete beam at midspan just before beginning of traffic. The largest compressive stress was always in the interior beam and the largest tensile stress was always in the exterior beam. Furthermore, the relative magnitude of the stresses reflected the fact that Bridges 5A and 5B were designed for larger live loads than Bridges 6A and 6B, and Bridges 5A and 6A were designed for a higher allowable tensile stress than Bridges 5B and 6B.

The steel stresses in the bottom layer of prestressing steel at midspan just before beginning of traffic are given (Col. 6) for uncracked sections.

Reinforced Concrete Beams.—Computed dead load stresses for the bottom layer of reinforcing bars at midspan of cracked reinforced concrete beams are given in Table 27.

Column 1 includes stresses caused by the weight of the beam and the contributory slab, using the unit weight of concrete determined at the beginning of test traffic and the mean slab thickness. The weight of concrete and of the reinforcing bars was assumed to be uniform throughout the span length. The stresses were computed for fully cracked transformed sections.

Column 2 gives the stresses caused by the weight of the timber curb, by the portion of the slab extending beyond the support and by the diaphragms.

The stresses in Columns 1 and 2 are for midspan; their sum is given in Column 3. The largest dead load stresses were present in the exterior beams and the smallest in the interior beams. As the fully cracked condition was attained only after the beginning of traffic, the stresses are larger than those present in the beams before the traffic started but are considered representative of the dead load stresses existing in the tension reinforcement shortly after the beginning of the regular test traffic.

3.1.3 Slab Profiles at Beginning of Test Traffic

The slabs for all bridges, except 9A and 9B, were completed several months before the beginning of traffic. During this period the bridges were subjected to their weight and to the changes in environmental conditions. Some changes were observed in the profiles of the slabs.

The transverse and longitudinal profiles of all slabs were measured for the first time approximately one to three months after casting the slab. Another set of readings was taken shortly before the beginning of traffic. The transverse slab profiles at midspan after casting the slab are shown in Figure 13, and those obtained shortly before the beginning of test traffic are shown in Figure 32. The average vertical displacements shown by the two sets of measurements are given in Table 28.

The slabs of steel, reinforced and post-tensioned prestressed concrete bridges showed downward displacements, whereas the slabs of the pretensioned concrete bridges moved up. The magnitude of the displacements for the steel and prestressed concrete bridges was well within that expected for daily and seasonal variations caused by changes in the environment. On the other hand, the magnitude of the displacements for reinforced concrete bridges indicated that the displacements were caused, at least in part, by creep of concrete.

TABLE 28
VERTICAL DISPLACEMENT OF SLAB SURFACE AT MIDSPAN BEFORE BEGINNING OF TRAFFIC

Type of Bridge	Period of Observation (months)	Vertical Displacement[1] (in.)
Noncomposite steel	10	0.05 to 0.26
Composite steel	10	0.18 to 0.30
Post-tensioned prestressed concrete	7	0.07 to 0.29
Pretensioned prestressed concrete	2	−0.09 to −0.08
Reinforced concrete	10	0.33 to 0.62

[1] Range of average values for individual bridges; negative sign denotes upward movement.

3.2 REFERENCE TESTS

During the period of regular test traffic the vehicles operated simultaneously on all loops. As only one set of equipment was available to measure the bridge deformations caused by test vehicles and the number of trips increased at a relatively rapid rate, special runs were made with regular test vehicles before the beginning of test traffic to collect initial data on stresses and deformations.

These initial reference tests, and reference tests made at 6-month intervals during the period of traffic, included strain readings at all gage locations for a standing vehicle, for a vehicle moving at crawl speed (3 mph) and for a vehicle moving at 30 mph. The results of the reference tests are discussed in this section.

3.2.1 Initial Live Load and Total Stresses

Records of Live Load Strain.—The recording of the response of a strain gage began before a vehicle entered a bridge and was completed several seconds after the vehicle left the bridge.

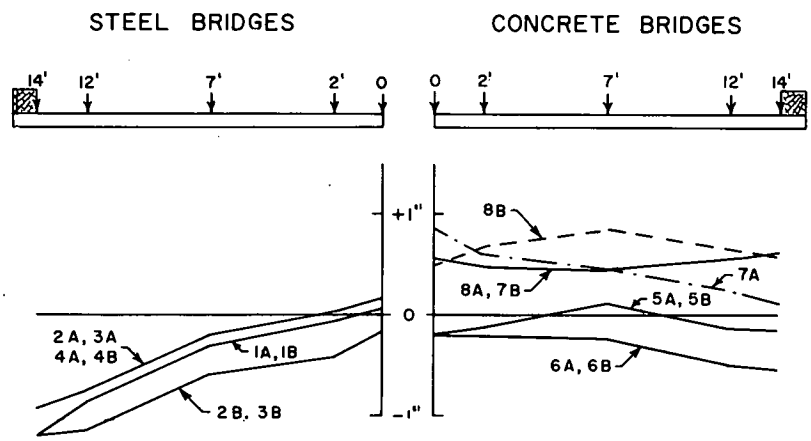

Figure 32. Transverse slab profiles at midspan at beginning of test traffic.

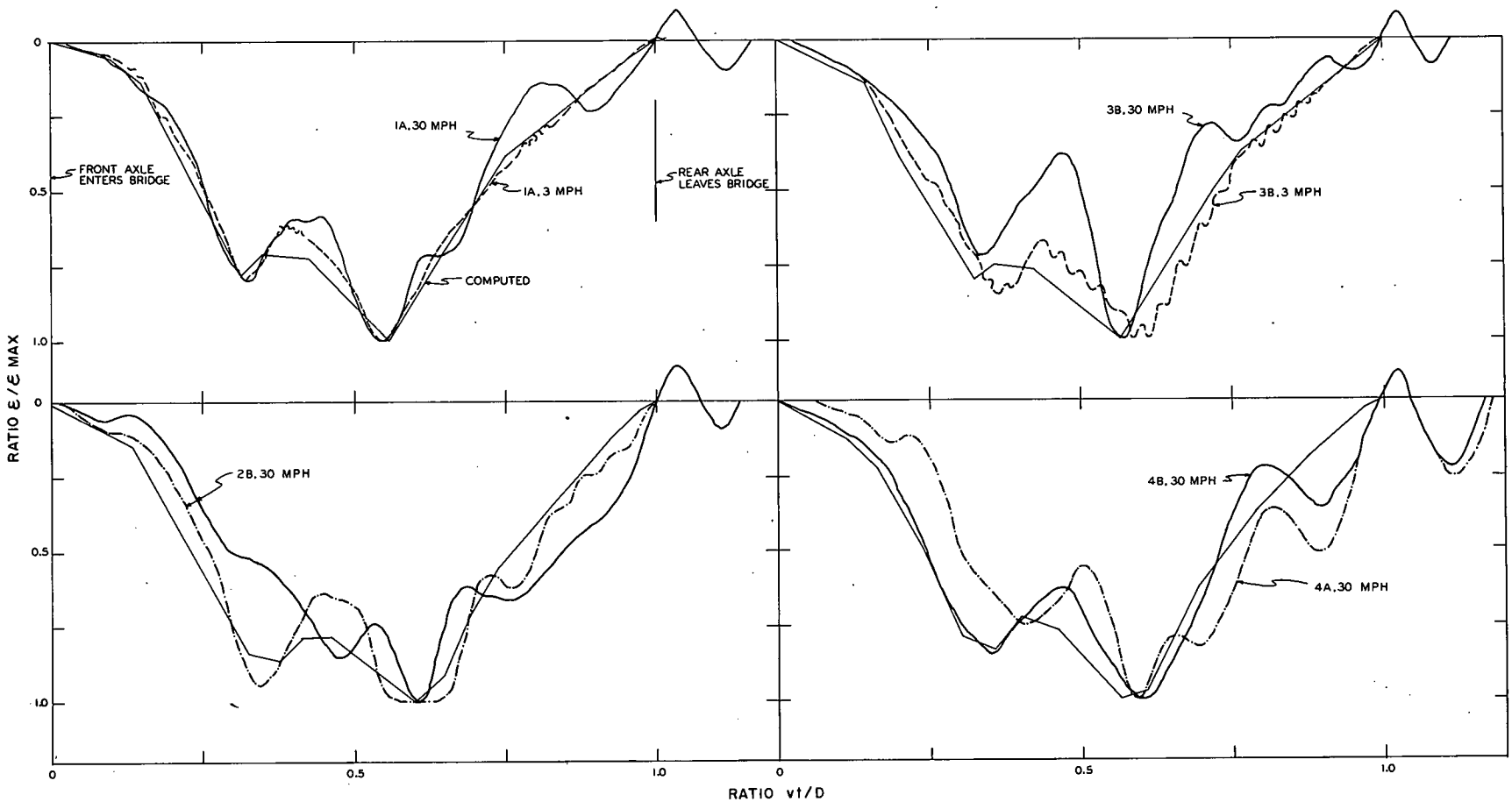

Figure 33. Variation of bottom strain on passage of vehicle, gages on center beam off cover plate at approach end.

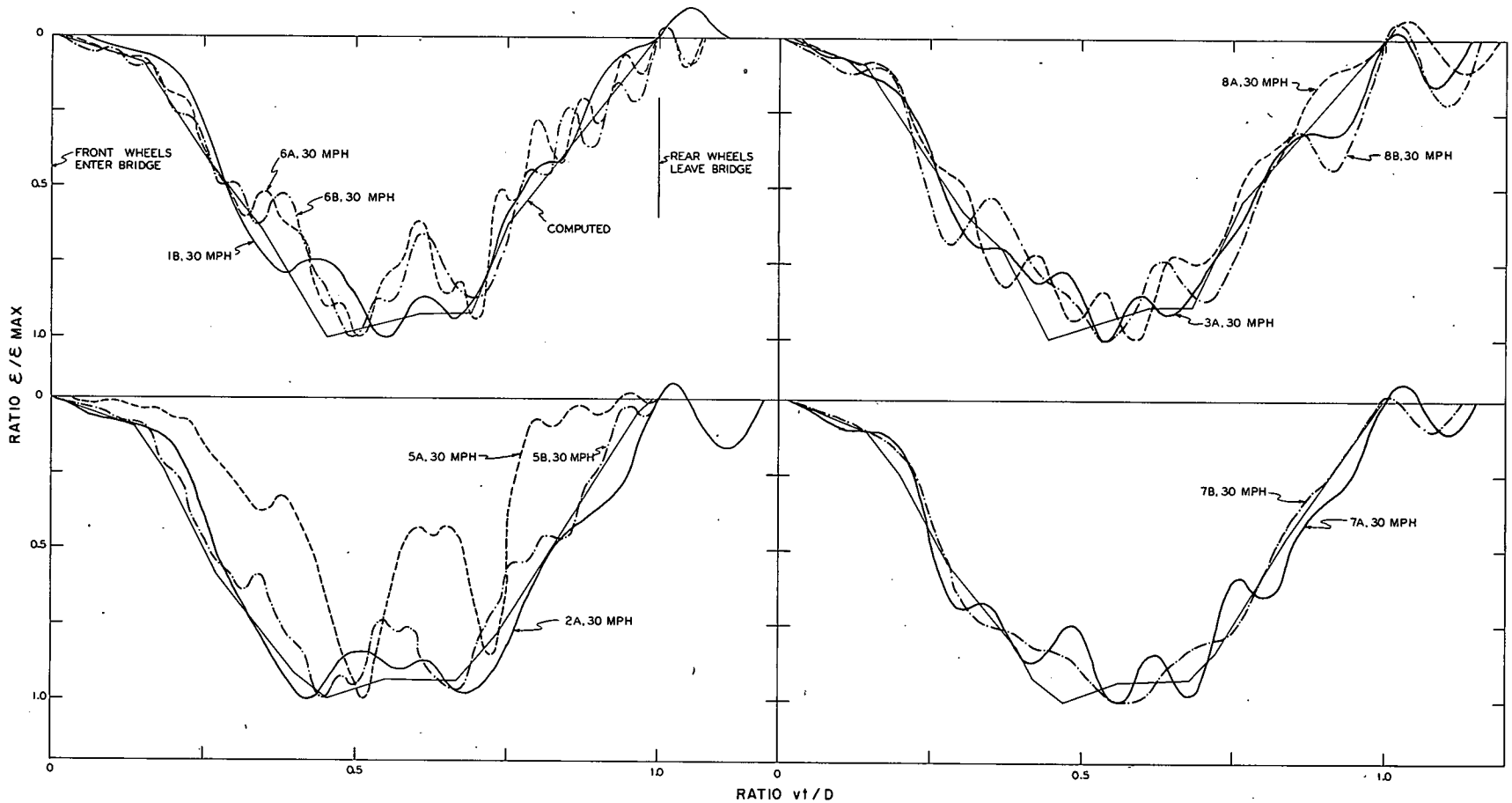

Figure 34. Variation of bottom strain on passage of vehicle, gages on center beam at midspan.

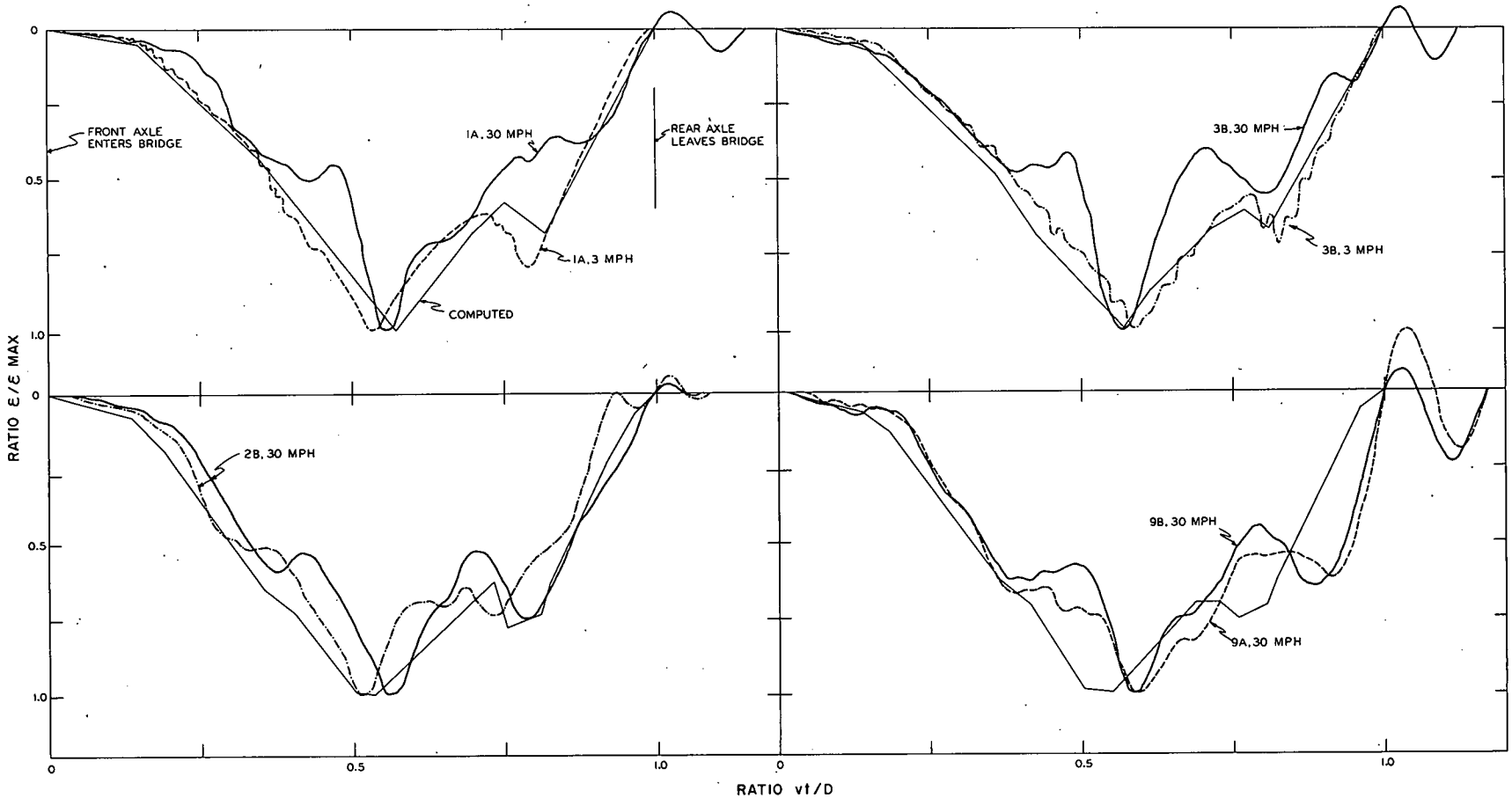

Figure 35. Variation of bottom strain on passage of vehicle, gages on center beam off cover plate at exit end.

The resulting curves for bottom flange strains are shown in a nondimensional form in Figures 33, 34 and 35. The curves represent the response of strain gages located 6 in. off the end of the cover plates at the approach side of the bridge, at midspan, and 6 in. off the ends of the cover plates at the exit side of the bridge. Each figure is divided into four parts; each part includes strains for bridges assigned the same test vehicles. A computed curve (neglecting impact), common to all bridges, is included in each part.

The abscissas are plotted as vt/D, in which v is speed of the vehicle, t is time elapsed after front axle entered the bridge, and D is span length plus the distance between front and rear axle. The ordinates are plotted as ratios of strain ε at time t to the maximum strain ε_{max} for the passage of the vehicle. The computed curves are shown as light lines. Experimental curves are given for 30-mph runs for every bridge and for 3-mph runs for Bridges 1A and 3B (Figs. 33 and 35).

The experimental curves for the 3-mph runs were in close agreement with the computed curves except for relatively minor differences probably caused by small vibrations and by variations in speed while the vehicle was on the bridge. On the other hand, the curves for the 30-mph runs exhibited considerable deviations from the computed curves, even though the general characteristics of the computed lines were reflected in the experimental curves. The most pronounced differences between the experimental and the computed curves were observed for cracked prestressed concrete beams, shown in Figure 34 with the curve for Bridge 5A.

The curves for different bridges varied considerably in detail. However, differences of similar order of magnitude were noted also between different runs on the same bridge (Bridge 2B in Figs. 33 and 35).

After the passage of a vehicle at 30 mph, the bridge continued to vibrate about its unloaded position as indicated by the curves beyond $(vt/D) = 1.0$. The vibrations continued at a slowly decreasing amplitude for several seconds. These free vibrations were usually not noticeable on the records of 3-mph runs.

Maximum Live Load Strains.—Figure 36 compares the maximum response of individual gages along the center beam of four bridges with the computed curve of maximum strains. The test data are the averages of all 3-mph runs made in reference tests. The strains, shown as ordinates, are plotted in a dimensionless form obtained by division with the maximum strain, ε_0, within the prismatic center portion of the beam. In selecting ε_0, strains off the cover plates were disregarded. For prismatic beams, the ratio $\varepsilon/\varepsilon_0$ cannot exceed 1.0.

The maximum strains for Bridges 2A and 5B, shown as solid symbols, were typical of

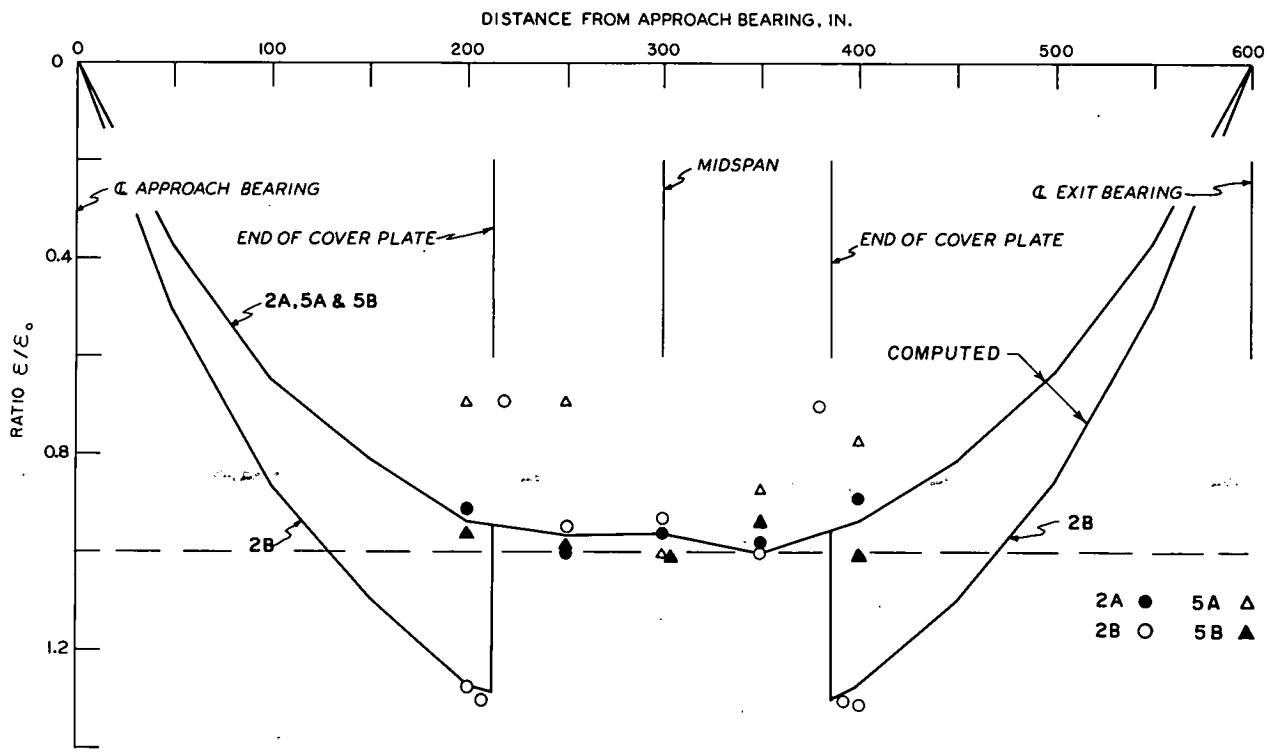

Figure 36. Maximum bottom strains on passage of vehicle, gages on center beam.

steel beams without cover plates, uncracked prestressed concrete beams and reinforced concrete beams. Although the points followed closely the computed curve, the experimental scatter in the data completely masked the minor theoretical variations in maximum strains between midspan and 50 in. on each side of midspan.

The maximum strains for Bridge 2B, shown as circles, were typical of steel beams with partial-length cover plates. Computations indicated a sudden increase of strain at the ends of the cover plates. Gages located 6 in. or more off the plate followed closely the computed line. On the other hand, gages located on the cover plate 6 in. from its end showed systematically strains lower than those obtained by computations, indicating that the plate was not fully developed at these locations (see Section 5.3). The gages placed on the cover-plated sections farther away from the ends of the plate were again in good agreement with the computations. In every case, the maximum bottom flange strains were observed off the cover plate.

Only for cracked prestressed concrete beams there was no agreement between the test data, shown as open triangles, and the computed line. In all such beams the maximum measured strain occurred at midspan.

TABLE 29
INITIAL STRESSES AT CRITICAL SECTIONS OF STEEL BEAMS

Bridge	Beam	Location of Critical Section	Bottom Flange Stress (ksi)			Design Stress (ksi)
			Dead Load	Live Load [1]	Total	
1A	Interior	End plate	12.3	13.0	25.3	—
	Center	End plate	15.3	12.4	27.7	27.0
	Exterior	End plate	18.0	12.1	30.1	—
	Mean				*27.7*	
1B	Interior	Midspan	17.5	15.0	32.5	—
	Center	Midspan	21.6	13.8	35.4	34.8
	Exterior	Midspan	25.6	14.9	40.5	—
	Mean				*36.1*	
2A	Interior	Midspan	14.8	20.2	35.0	—
	Center	Midspan	18.3	21.1	39.4	35.0
	Exterior	Midspan	21.5	19.6	41.1	—
	Mean				*38.5*	
2B	Interior	End plate	15.0	15.2	30.2	—
	Center	End plate	18.8	15.0	33.8	35.0
	Exterior	End plate	22.1	13.7	35.8	—
	Mean				*33.3*	
3A	Interior	Midspan	12.2	16.4	28.6	—
	Center	Midspan	15.2	15.7	30.9	27.3
	Exterior	Midspan	17.9	17.5	35.4	—
	Mean				*31.6*	
3B	Interior	End plate	13.1	12.9	26.0	—
	Center	End plate	16.0	12.8	28.8	26.9
	Exterior	End plate	18.9	12.1	31.0	—
	Mean				*28.6*	
4A	Interior	End plate	12.3	23.6	35.9	—
	Center	End plate	15.3	23.6	38.9	34.7
	Exterior	End plate	18.0	23.1	41.1	—
	Mean				*38.6*	
4B	Interior	End plate	12.3	26.8	39.1	—
	Center	End plate	15.3	26.8	42.1	34.7
	Exterior	End plate	18.0	24.3	42.3	—
	Mean				*41.2*	
9A	Interior	End plate	8.5	14.4	22.9	—
	Center	End plate	10.3	14.4	24.7	—
	Exterior	End plate	12.0	13.5	25.5	27.0
	Mean				*24.4*	
9B	Interior	End plate	8.3	15.7	24.0	—
	Center	End plate	9.5	15.1	24.6	—
	Exterior	End plate	11.7	14.3	26.0	27.0
	Mean				*24.9*	

[1] Stress caused by regular test vehicle moving at 30 mph.

TABLE 30
INITIAL STRESSES AT MIDSPAN OF PRESTRESSED CONCRETE BEAMS

Bridge	Beam	Concrete Stress on Bottom Surface (psi)			Stress in Bottom Layer of Prestressing Steel (ksi)			Design Stress on Bottom Surface (psi)
		Dead Load	Live Load [1]	Total	Dead Load	Live Load [1]	Total	
5A	Interior	− 84	—	—	144.9	23.4	168.3	—
	Center	22	—	—	145.0	18.4	163.4	820
	Exterior	398	—	—	150.5	26.1	176.6	—
	Mean						*169.4*	
5B	Interior	−859	1,019	160	152.8	4.5	157.3	—
	Center	−643	1,020	377	149.1	4.5	153.6	346
	Exterior	−321	968	647	152.9	4.3	157.2	—
	Mean			*395*			*156.0*	
6A	Interior	5	530	535	164.6	2.6	167.2	—
	Center	129	570	699	163.5	2.8	166.3	828
	Exterior	473	—	—	167.8	4.6	172.4	—
	Mean						*168.6*	
6B	Interior	−470	468	− 1	170.1	2.3	172.4	—
	Center	−374	489	115	171.1	2.4	173.5	310
	Exterior	9	549	558	172.3	2.7	175.0	—
	Mean			224			*173.6*	

[1] Stress caused by regular test vehicle moving at 30 mph.

In the portions of the report that follow, the sections located 6 in. off the cover plate, and for prismatic beams, the sections at midspan are referred to as critical sections for strain and stress. (There were two critical sections in beams with cover plates: at the approach and exit ends. They are referred to as the approach critical section and exit critical section.) The strains measured at the critical sections were the maximum or nearly the maximum tensile strains caused in the beam by the passage of a regular test vehicle.

Stresses at Critical Sections.—Initial stresses at the critical sections of all beams are given in Tables 29, 30 and 31. Included are dead load stresses from Section 3.1.2, mean live load stresses computed from strains measured for 30-mph runs in reference tests before and six months after the beginning of test traffic, the total dead load plus live load stress and the governing design stress from Table 3. As the live load stress was computed from strains measured under moving vehicles, the stresses include also the impact effects.

In general, the total actual stress in the beam compared favorably with the design stress. The principal exceptions were the noncomposite steel bridges 2A, 4A and 4B in which the actual stress exceeded the design stress by more than 10 percent. There was practically no interaction between the beams and the slab, whereas 10 percent interaction was assumed in the design; the effect of this difference was particularly large in these three bridges because of the high live load stresses. It is also possible that the measured strains included small inelastic strains. In all bridges the largest total stress was that in the exterior beam, and the smallest was usually that in the interior beam. Except for Bridges 9A and 9B, the design was made for the center beam. Therefore, in all original bridges the maximum total stress exceeded the design stress.

The bottom flange stresses at the critical sections of steel beams are given in Table 29. Comparing the total stresses with values in Table 30, in Bridges 2A, 4A, and 4B the yield point of the material was exceeded in every beam; in Bridges 1B and 3A the total stress exceeded the yield point in the exterior beam. Furthermore, in Bridge 1B the mean of the total stress for the three beams was close to the yield point. In computing the live load stress, strains indicating yielding were excluded from the mean. All values included were very close to the mean value, indicating that they were essentially elastic strains even though total stress exceeded the yield point of the material. However, large strains indicating yielding were recorded for most gage locations for at least one run; they were not included in the mean.

The stresses in Table 29 are the maximum tensile stresses in any one beam. At composite cross-sections and at symmetrical noncomposite cross-sections, the compressive stresses were always smaller or equal to the tensile stresses. At noncomposite cross-sections with tension cover plates only (Bridges 1A, 4A and 4B) the compressive stresses were in excess of the tensile stresses. However, measurements have shown that these compressive stresses were always smaller or, at the most, equal to the

TABLE 31

INITIAL STRESSES AT MIDSPAN OF REINFORCED CONCRETE BEAMS

Bridge	Beam	Stress in Bottom Layer of Reinforcing Bars (ksi)			Design Stress (ksi)
		Dead Load	Live Load [1]	Total	
7A	Interior	17.7	23.5	41.2	—
	Center	18.3	21.7	40.0	40.0
	Exterior	21.7	22.7	44.4	—
	Mean			*41.9*	
7B	Interior	17.7	22.4	40.1	—
	Center	18.2	21.8	40.0	40.0
	Exterior	21.8	22.6	44.4	—
	Mean			*41.5*	
8A	Interior	16.4	15.5	32.9	—
	Center	17.0	14.7	31.7	30.9
	Exterior	20.0	14.7	34.7	—
	Mean			*33.1*	
8B	Interior	16.5	13.5	30.0	—
	Center	17.0	14.9	31.9	30.9
	Exterior	20.0	15.4	35.4	—
	Mean			*32.4*	

[1] Stress caused by regular test vehicle moving at 30 mph.

maximum tensile stresses measured off the ends of the cover plates of the same beam.

Table 30 gives the initial stresses at midspan of prestressed concrete beams. The stresses on the bottom surface of concrete are for uncracked sections. Where no live load stresses are given, the strain measurements indicated that cracking of concrete occurred during the first trips of test vehicles. Steel stresses in the bottom layer of prestressing steel are given for all beams. Where applicable, dead load stresses for prestressing steel were computed both for the uncracked and cracked sections, and the larger of the two values is listed.

The strain measurements indicated early cracking in all beams of Bridge 5A and in the exterior beam of Bridge 6A. The total concrete stresses in these four beams exceeded the modulus of rupture of concrete which was 739 psi at the beginning of test traffic (Table 10). It is also noteworthy that the live load steel stress in the exterior beam of Bridge 6A was of the same order of magnitude as in the uncracked beams and substantially smaller than the live load steel stresses in Bridge 5A.

The initial stresses in the bottom layer of reinforcing bars at midspan of reinforced concrete beams are given in Table 31. The total stress for every beam was below the yield point of the reinforcing bars (Table 9).

Bridges 4A–4B, 9A–9B, 7A–7B and 8A–8B were replicates placed in tandem. Except for 4A–4B, the stresses for the two bridges of a pair were in a satisfactory agreement. The larger differences between Bridges 4A and 4B were probably caused by large permanent deformations of Bridge 4A, the first in line of travel. The impact on Bridge 4B was about twice that observed on Bridge 4A.

Good agreement was found also between live load stresses in Bridge 6B and those in the uncracked beams of Bridge 6A. The two bridges differed only in the amount of prestressing steel and the magnitude of prestressing force. They also were located in tandem.

3.2.2 Deflections in Initial Reference Tests

Live load deflections at midspan are given in Table 32 as means for the 30-mph runs of the initial reference tests. The variations from run to run were small, seldom exceeding 10 percent of the mean. Variations from bridge to bridge reflected differences in load, beam size, and degree of interaction between slab and beams, together with cracking in the concrete. The relative magnitude of deflections of the three beams of one bridge showed no consistent variations for steel bridges. On the other hand, for prestressed concrete and reinforced concrete bridges the maximum deflection was observed always in the interior or in the center beam.

Table 32 also gives the total set that occurred at midspan of each beam during the initial reference tests. Initial tests caused permanent set in all steel and reinforced concrete bridges.

Slip lines formed during the reference tests in the rolled steel sections indicating that the permanent set of the steel bridges was the result of yielding. Yielding was observed on the compression flanges of Bridges 9A and 9B, on the compression and tension flanges of all

original noncomposite bridges, and on the tension flanges of both composite bridges. In addition, a few scattered yield lines were noted at other locations (see Sections 3.2.5 and 3.3.3).

Studies of the extent of cracking (Section 3.3.7) suggested that the permanent set in reinforced concrete bridges was the result of the development of more extensive tension cracking.

For the replicate pairs of bridges (4A–4B, 9A–9B, 7A–7B, 8A–8B) and for Bridges 6A–6B, the live load deflections and permanent sets differed to some extent. These differences may have been the result of minor variations between the two replicates, such as differences in the crack patterns in the reinforced concrete beams, or they may have been the result of differences in treatment due to the variations in impact. However, the differences were inconsistent in that the higher stresses and permanent set were observed in some cases in the first and in other cases in the second bridge in the direction of traffic.

The largest permanent set was observed in Bridges 2A, 4A and 4B for which the mean of the total stresses exceeded the yield point in all three beams, followed by Bridges 1B and 3A in which the yield point was exceeded by the total stress in two beams. The permanent set in beams of all other bridges was less than 0.5 in.

3.2.3 Variation of Transient Stresses and Deflections with Time

Data on the variation of transient stresses and deflections obtained from reference tests at 30 mph are given in Table 33. Maximum stresses in the tension steel at the critical section and the deflections at midspan are given as means for the three beams of every bridge. Values for the beginning of traffic include measurements made before and six months after the beginning of test traffic; values for the end of traffic include measurements made six months before and immediately after the end of the test traffic.

In general, the reference tests indicated only small changes in stresses. The principal exceptions were the exterior and center beams of Bridge 6A, in which progressive cracking (Section 3.3.6) caused large increases, of the order of 75 percent, in the stresses in prestressing

TABLE 32
TRANSIENT AND PERMANENT DEFLECTIONS AT MIDSPAN IN INITIAL REFERENCE TESTS

Bridge	Live Load Deflection[1] (in.)			Permanent Set[2] (in.)		
	Interior Beam	Center Beam	Exterior Beam	Interior Beam	Center Beam	Exterior Beam
			(*a*) STEEL BRIDGES			
1A	1.89	1.71	1.59	0.42	0.45	0.45
1B	1.85	2.01	1.92	1.81	1.85	1.89
2A	2.49	2.49	2.21	3.19	3.15	3.19
2B	1.08	1.03	1.08	0.29	0.29	0.29
3A	1.61	1.65	1.72	1.19	1.16	1.19
3B	0.70	0.79	0.76	0.10	0.06	0.10
4A	2.48	2.37	—	3.50	3.36	3.26
4B	2.56	2.68	2.77	3.94	3.71	3.54
9A	1.60	1.69	1.80	0.31[3]	0.32[3]	0.32[3]
9B	1.51	1.44	1.42	0.25[3]	0.29[3]	0.29[3]
			(*b*) PRESTRESSED CONCRETE BRIDGES			
5A	0.31	0.30	0.26	0.00	−0.02	−0.01
5B	0.28	0.26	0.21	0.01	0.00	0.00
6A	0.18	0.19	0.16	−0.04	−0.04	−0.02
6B	0.18	0.17	0.16	−0.01	0.01	0.01
			(*c*) REINFORCED CONCRETE BRIDGES			
7A	1.16	1.11	1.13	0.08	0.07	0.08
7B	1.20	1.34	1.20	0.14	0.09	0.10
8A	0.61	0.60	0.61	0.06	0.07	0.06
8B	0.71	0.74	0.67	—	0.09	0.09

[1] Mean of 30 mph runs.
[2] Total set caused by initial reference tests.
[3] Permanent set includes reference tests and three days of regular test traffic.

steel at midspan. Stresses at midspan of all other concrete bridges showed a tendency to decrease and those at the critical sections of steel bridges showed a tendency to increase with time; however, these changes exceeded 10 percent only in Bridges 1A and 5B, and were always below 17 percent.

Deflections of all bridges increased with time. The largest increase occurred in cracked prestressed concrete bridge 5A—0.41 in. or 93 percent of the deflection at the beginning of test traffic. The smallest increase, 0.05 in. or 5 to 6 percent, occurred in composite steel bridges 2B and 3B. The decreases of stiffness, indicated by these increased transient deflections, are believed to have been the result of progressive development of cracks in concrete beams and slabs (Sections 3.3.6, 3.3.7 and 3.3.8).

The data for the pairs of bridges (9A–9B, 7A–7B and 8A–8B) were in good agreement both at the beginning and at the end of traffic. However, the data indicated that the second bridge in the direction of traffic (9B, 7A and 8A) tended to undergo higher stresses and deflections.

3.2.4 Neutral Axis, Moment Distribution and Impact

The static and crawl tests and the close control of speed and location of the vehicle made possible the use of strain data obtained in the reference tests for determination of the position of neutral axis and the distribution of moments, and for evaluation of the impact factor. These quantities were evaluated separately for each series of reference tests, and means for all series are given in Table 34.

Neutral Axis.—The actual location of the neutral axis was determined from strains measured on the bottom and top of beams at midspan assuming straightline strain distribution. Each value listed in Column 1 (Table 34) is the distance of the experimental location of the neutral axis from the theoretical one, and is a mean for all 30-mph runs. The location of the neutral axis for static and crawl tests did not differ appreciably from the values given.

In calculating the theoretical location of the neutral axis, steel bridges 2B and 3B and all concrete bridges were considered as fully composite; for the other steel bridges a complete absence of interaction between the slab and the beams was assumed. The calculations were made with cross-sectional properties based on tests of concrete at the end of test traffic, using a transformed uncracked beam section for prestressed concrete bridges and a transformed cracked section for reinforced concrete bridges.

The difference between the measured and the theoretical location of the neutral axis in steel

TABLE 33
TIME VARIATION OF TRANSIENT STRESSES AND DEFLECTIONS

Bridge	Mean Stress[1] (ksi)		Change in Stress (ksi)	Mean Deflection[2] (in.)		Increase in Deflection	
	Beginning of Traffic	End of Traffic		Beginning of Traffic	End of Traffic	(in.)	(%)
			(*a*) STEEL BRIDGES				
1A	12.5	14.6	+2.1	1.64	1.81	0.17	10
2B	14.6	15.8	+1.2	1.00	1.05	0.05	5
3A	16.5	17.5	+1.0	1.93	2.22	0.29	15
3B	12.6	12.8	+0.2	0.81	0.86	0.05	6
9A	14.1	14.4	+0.3	1.73	1.90	0.27	16
9B	15.0	15.1	+0.1	1.75	2.02	0.27	15
			(*b*) PRESTRESSED CONCRETE BRIDGES				
5A	22.6	21.3	−1.3	0.44	0.85	0.41	93
5B	4.4	3.8	−0.6	0.24	0.31	0.07	29
6A	3.3	5.2	+1.9	0.17	0.23	0.06	35
6B	2.5	2.4	−0.1	0.17	0.22	0.05	29
			(*c*) REINFORCED CONCRETE BRIDGES				
7A	22.6	21.8	−0.8	1.32	1.71	0.39	30
7B	22.3	20.7	−0.5	1.31	1.54	0.23	18
8A	15.0	14.5	−0.5	0.78	1.04	0.26	33
8B	14.6	14.4	−0.2	0.79	1.06	0.27	34

[1] Stress in tension steel at critical section.
[2] Live load deflection at midspan.

TABLE 34
NEUTRAL AXIS, MOMENT DISTRIBUTION AND IMPACT

Bridge	Location of Neutral Axis[1] (in.)	Σ Beam Mom.	Beam Mom./Σ Beam Mom. (%)			Average Impact at Critical Section (%)
		Truck Mom. (%)	Interior Beam	Center Beam	Exterior Beam	
	(1)	(2)	(3)	(4)	(5)	(6)
			(a) STEEL BRIDGES			
1A	0.0	85.1	32.3	33.3	34.4	26.8
1B	+0.2	77.7	32.6	32.6	34.8	12.9
2A	+0.1	79.1	33.1	32.9	34.0	11.0
2B	+0.2	89.3	34.0	32.0	34.0	14.5
3A	+0.2	85.1	33.3	33.1	33.6	18.9
3B	−0.1	92.1	33.8	33.4	32.8	29.2
4A	+0.2	90.7	33.7	33.8	32.5	12.8
4B	−0.1	86.7	35.6	33.4	31.0	27.3
9A	+0.1	88.0	31.5	33.7	34.8	13.8
9B	0.0	89.2	32.0	34.1	33.9	17.4
			(b) PRESTRESSED CONCRETE BRIDGES			
5A	+3.6[2]	102.8	37.4	34.1	28.5	7.5
5B	+0.4	101.9	34.6	31.4	34.0	9.7
6A	0.0[3]	76.7	39.1	41.6	19.3	11.9
6B	−1.1	93.5	30.8	33.8	35.4	10.7
			(c) REINFORCED CONCRETE BRIDGES			
7A	+0.2	95.4	34.6	32.6	32.8	6.5
7B	+1.0	94.4	32.6	33.3	34.1	7.3
8A	+1.2	97.8	34.8	33.4	31.8	5.1
8B	−0.4	86.8	33.2	31.8	35.0	13.7

[1] Distance from theoretical position assuming no interaction between beams and slab for steel beams without shear connectors, complete interaction for all other beams; plus sign indicates position above theoretical.

[2] Increased from +1.9 at beginning of test traffic to 4.0 at end of test traffic.

[3] At end of test traffic, center and exterior beams had neutral axis 1.3 and 1.7 in. above theoretical location for uncracked section.

bridges was small, indicating that the bridges with mechanical connectors were fully composite whereas the others had practically no composite action.

In prestressed concrete beams the neutral axis for Bridge 5A was consistently several inches above the theoretical location. Similarly, the last set of reference tests made on Bridge 6A indicated that the neutral axes of the exterior and center beams were more than 1 in. above the theoretical location. In both cases strain measurements and visual observations revealed the presence of tension cracking. The neutral axis in Bridge 5B was reasonably close to the theoretical location for uncracked sections, but in Bridge 6B it was more than 1 in. below. No explanation was found for this difference.

In reinforced concrete bridges the results were erratic. It is possible that the variations from the theoretical location were caused by inaccuracies in the strain gage readings on the top reinforcement. All strain gages on the top steel ceased to operate during the period of test traffic.

Moment Distribution.—The moments resisted by the individual bridge beams at midspan were computed from the bottom strains measured in static tests with the truck placed in the position for maximum moment at midspan. The computations utilized section properties based on the theoretical position of the neutral axis. The only exceptions were the cracked beams of Bridges 5A and 6A for which a cracked section was assumed. A method of successive approximations (based on the assumptions of linear strain distribution and no resistance of concrete to tension) was developed for this purpose.

Column 2 (Table 34) gives the sum of the moments for the three beams of each bridge as the percentage of the total static moment caused by the truck. With the exception of Bridges 5A and 5B, the calculations indicated that the beams resisted less than 100 percent of the external moment. Obviously, the balance was resisted by the slab.

Figure 37 plots the percentage of the applied moment resisted by the beams as a function of the relative stiffness, H, of the beams and the

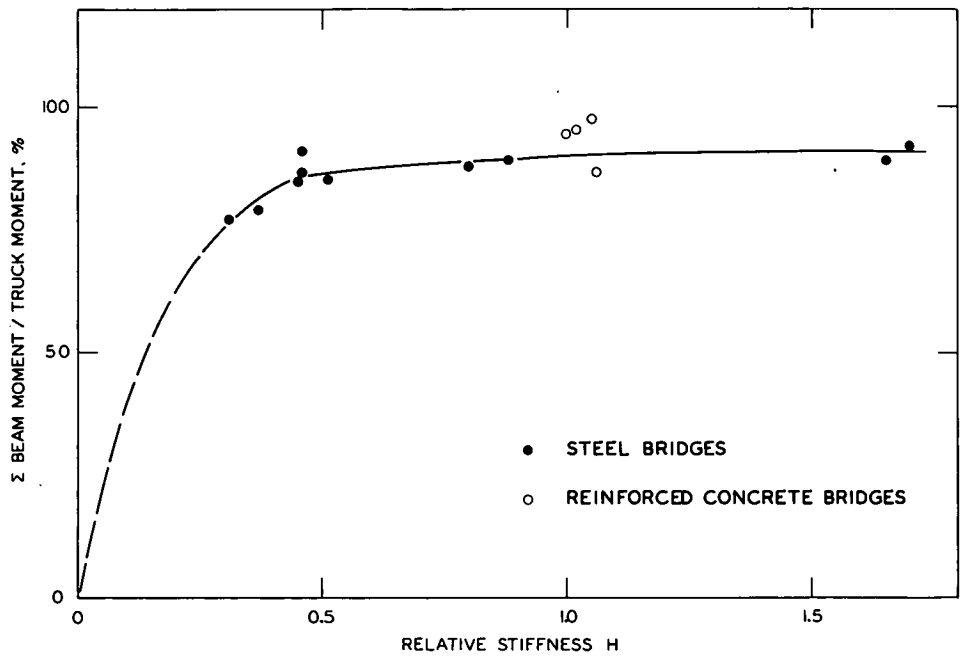

Figure 37. Effect of relative stiffness on total beam moment.

slab. Only steel beams (shown as dots) and reinforced concrete beams (shown as circles) are included. The relative stiffness H of the uncracked prestressed concrete beams was approximately 4.5, falling outside the range shown. The relative stiffness was computed from

$$H = \frac{(EI)_{\text{beam}}}{L(EI)_{\text{slab}}} \qquad (14)$$

in which

H = relative stiffness of beam to slab expressed as a dimensionless quantity;
$(EI)_{\text{beam}}$ = average beam stiffness at midspan;
$(EI)_{\text{slab}}$ = stiffness of a 1-ft wide strip of uncracked slab; and
L = span length.

It is apparent that the beam moment increased with increasing relative stiffness of the beams, but for H greater than about 0.5 the increase was very gradual. As the slab stiffness, the span length and the modulus of elasticity of the steel beams were essentially constant, the increase of H corresponds closely to the increase in the moment of inertia of the beams.

The moments resisted by individual beams are given in Columns 3, 4 and 5 (Table 34) as percentage of the total beam moment. Except for Bridges 5A and 6A, the variation of moment from beam to beam was small and unsystematic. For practical purposes, each beam carried one-third of the total beam moment.

The distribution of moment in prestressed concrete bridges 5A and 6A was apparently influenced by cracking of beams. In Bridge 6A the exterior beam was cracked during the entire traffic testing period. In both bridges the exterior beam was cracked more extensively than the other two beams. As cracking decreased stiffness, the exterior beams resisted a smaller proportion of the total moment than either of the other two beams. Section 5.1 gives a more detailed study of the distribution of moments.

Impact.—Moments were computed from the bottom strains measured at the critical sections during the 30-mph runs and the 3-mph runs. The difference between the two moments, expressed as percentage of the moment for the 3-mph runs, was designated as impact. The impact at the critical sections, averaged for all series of reference tests, are given in Column 6 (Table 34). For beams with two critical sections the larger of the two averages is listed.

There was a substantial variation in the magnitude of impact from one series of tests to another. For example, the impact varied from 10.5 to 38.2 percent in Bridge 3B, from —8.0 to 36.5 percent in Bridge 6A and from 7.1 to 24.2 percent in Bridge 8B.

Because of the wide variation in the impact factors and the complex nature of the phe-

nomena related to dynamic effects, no attempt was made to explain the variations in the values. Chapter 4 reports a comprehensive study of the impact characteristics of the test bridges.

3.2.5 Failure of Bridges 1B, 2A, 4A and 4B

Bridges 2A, 4A and 4B yielded heavily during the initial reference tests. In Bridge 2A yield lines visible on the bottom flanges spread to a distance of 14 ft from midspan toward both supports; the most severe yielding was observed in the exterior beam. In Bridges 4A and 4B severe yielding was observed in the tension flanges within 5 ft from each end of the cover plates toward the supports. Extensive yielding was also observed along the compression flanges, and a few yield lines were found on the cover plates of Bridge 4A. The testing was discontinued when the permanent set at midspan was substantially in excess of 3 in. in all three beams of any one bridge.

The initial reference tests of Bridge 1B caused an average permanent set at midspan of 1.85 in. During traffic with regular test vehicles on October 15, 1958, two vehicles from the adjacent lane, corresponding approximately to a 40 percent increase in the live load moment, accidentally crossed Bridge 1B. The additional traffic of regular test vehicles on that day and the two trips of heavier vehicles increased the permanent set of each beam to a total of more than 3 in. and further testing of the bridge was discontinued. At the conclusion of the test, the yielding in the bottom flanges of Bridge 1B extended 14 ft from midspan toward both supports.

Table 35 summarizes traffic and test data for Bridges 1B, 2A, 4A and 4B. The mean initial applied stress (from Table 29) was in excess of the static yield point of the flanges in every one of the four bridges and in beams of Bridges 2A, 4A and 4B it was also in excess of the estimated dynamic yield point for the tests with vehicles moving at 30 mph.* Furthermore, it was estimated that the two heavier loads increased the maximum stress in Bridge 1B to 41.9 ksi, also well in excess of the corresponding dynamic yield point of the bottom flange.

The test of Bridge 2A was discontinued after 26 trips of the regular test vehicles. The beams of this bridge had no cover plates, so that yielding occurred in the middle 28 ft of the bottom flange. The tests of Bridges 4A and 4B were discontinued after 106 trips of regular test vehicles. In these beams the yielding of the bottom flange was restricted by the cover plates. The test of Bridge 1B was discontinued after 235 trips of regular test vehicles. This bridge, having a higher yield point than Bridges 2A, 4A and 4B, failed in this early stage primarily because of the two trips of heavier vehicles.

In addition to the total number of trips of the regular test vehicles assigned to any particular bridge, Table 35 includes also the number of trips with heavier and lighter vehicles. The two heavier vehicles that crossed Bridge 1B were regular test vehicles, 52, from the adjacent lane (Table 19). The count of trips of vehicles lighter than regular includes all vehicles causing at midspan less than 100 percent but more than 50 percent of the moment caused by the regular test vehicles.

The last set of measurements of the transverse profile at midspan of Bridges 1B, 2A, 4A and 4B is shown in Figure 38. A comparison with the initial transverse profiles in Figure 32 indicates that the three beams of Bridges 1B and 2A assumed about the same permanent set, but in Bridges 4A and 4B the largest set occurred in the interior beam and the smallest in the exterior beam. The values of total permanent set (Table 35) show the same relationship.

* Based on the discussion in Appendix D of AASHO Road Test Report 4, on vehicle dimensions and gage locations, the ratio of the dynamic yield point to the static yield point was estimated at 1.10.

TABLE 35
SUMMARY OF TEST DATA FOR BRIDGES 1B, 2A, 4A AND 4B

Item	Bridge 1B	Bridge 2A	Bridge 4A	Bridge 4B
Date (1958) of initial vehicle crossing	11 Sept.	11 Sept.	29 Aug	29 Aug.
No. of trips of vehicles:				
Regular test vehicles	235	26	106	106
Heavier than reg. test vehicles	2	—	—	—
Lighter than reg. test vehicles	131	174	188	188
Static yield point for flanges of rolled beams (ksi)	35.1	32.1	32.5	32.5
Mean initial DL + LL stress on bottom surface of critical section, ksi	36.1	38.5	38.6	41.2
Total permanent set at midspan (in.):				
Interior beam	3.26	3.56	3.50	3.94
Center beam	3.32	3.56	3.36	3.71
Exterior beam	3.32	3.60	3.26	3.54

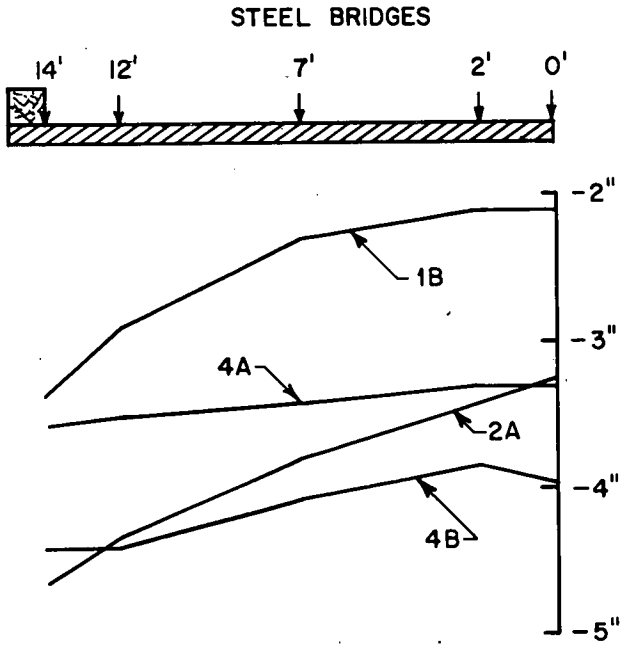

Figure 38. Transverse profiles at midspan before failure of Bridges 1B, 2A, 4A and 4B.

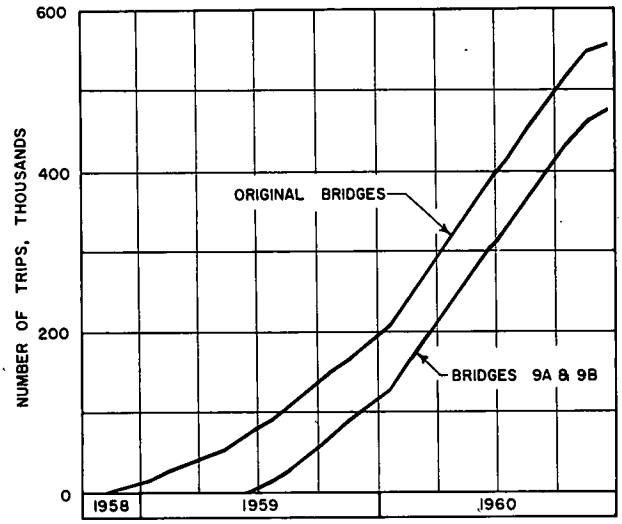

Figure 39. Cumulative trips of regular test vehicles.

3.3 BEHAVIOR DURING REGULAR TEST TRAFFIC

3.3.1 Traffic Data

The first trips of vehicles across the test bridges occurred on the dates given in Table 36. Until the beginning of October 1958, all vehicles crossing any one bridge were lighter than the assigned regular test vehicles. The first regular test vehicles made a few trips over the bridges in October. The regular test traffic began on November 5, 1958, and was continued through December 3, 1960.

Figure 39 shows the accumulation of trips of regular test vehicles as a function of time. The rate of increase of the number of trips showed an upward trend from the beginning of traffic until the end of the summer of 1959. During this period experience was gained with traffic operations and many light pavement sections were removed from the test. During the remainder of 1959 the rate of trip accumulation was essentially constant. In January 1960, the number of vehicles operating on any one lane was increased. The operation of regular traffic was shut down gradually during October and November 1960.

The total number of trips of regular test vehicles over any one bridge is given in Table 36. Original bridges that survived the regular test traffic were subjected to between 556,100 and 558,400 trips of regular test vehicles. Bridges

TABLE 36
TRAFFIC COUNT ON BRIDGES [1]

Bridge	Date of Initial Vehicle Crossing, 1958	Number of Trips of Vehicles [2]		
		Regular Test Vehicles	Lighter than Reg. Test Veh.	Heavier than Reg. Test Veh.
1A	11 Sept.	557,400	275	8
2B	11 Sept.	558,400	335	—
3A	3 Sept.	392,400	722	1
3B	3 Sept.	557,800	722	2
5A,5B	23 Sept.	556,700	210	—
6A,6B	23 Sept.	556,800	275	2 [3]
7A,7B	10 Sept.	556,100	346	—
8A,8B	10 Sept.	558,400	668	1
9A,9B	21 June	477,900	100	—

[1] Traffic count for Bridges 1B, 2A, 4A, and 4B given in Table 35.
[2] At the end of test on any particular bridge.
[3] Two additional trips, recorded on October 29, 1958, uncertain.

9A and 9B, which replaced original bridges 4A and 4B, had 477,900 vehicle trips at the conclusion of regular traffic. Bridge 3A was eliminated from further testing after 392,400 trips of vehicles.

The regular test vehicles were scheduled to operate in the center of the 14-ft wide traffic lane of each bridge, that is, the vehicle was centered over the center beam. An estimate of the actual transverse placement of vehicles during the regular test traffic was determined by sampling carried out from July 1959 to November 1960. Table 37 gives the mean position of the vehicles as the displacement from the desired position. At every bridge location the mean position was several inches closer to the center of the roadway than the desired position. Tandem axle vehicles on Loop 5 traveled closest (on the average 3.8 in.) to the desired position. The last column indicates the displacement toward the center of the roadway that was exceeded by 10 percent of the vehicles operating at any one bridge location.

Histograms (Fig. 40) show the distribution of traffic samples at each bridge location. On all bridges of Loop 5, more than 50 percent of the vehicles were within ± 6 in. of the desired transverse location. The distribution was skewed toward the center of the roadway. On Loop 6, the distribution on Bridges 3A and 3B was similar to the distribution on Loop 5. At all other locations on Loop 6, more than 40 percent of the placements fell between +6 and +18 in., and the distribution varied from normal on Bridges 8A and 8B to skewed toward the center of the roadway.

During miscellaneous special tests, vehicles lighter than the regular vehicles assigned to any particular bridge operated at all locations. A record was kept of those that produced static moments greater than 50 percent of that caused by the assigned regular test vehicles. The total number of such trips is given in Table 36; the largest number of such trips was the 722 recorded for Bridges 3A and 3B.

The tandem axle vehicles were always heavier than the single axle vehicles operating in the adjacent lane of the same loop. In a few instances the tandem axle vehicles accidentally crossed the bridges in the wrong lane, thus loading the bridges more than the assigned regular test vehicles. The recorded number of such accidental trips is listed in the last column of Table 36.

3.3.2 Stresses and Deformations in Steel Beams

Response curves of individual strain gages during the regular test traffic exhibited the characteristics discussed in Section 3.2.1 (Figs. 33-35).

The corresponding curves for the three beams of the same bridge were practically identical. There was also good correspondence among replicate runs, particularly among runs made within the same month.

TABLE 37
TRANSVERSE PLACEMENT OF VEHICLE ON TEST BRIDGES

Vehicle Type	Bridges	No. of Samples	Mean Displacement [1] (in.)	10% Over [2] (in.)
		(*a*) Loop 5		
Single axle	6A,6B	18,467	5.7	17.0
	1A,1B	17,843	4.7	17.1
Tandem axle	5A,5B	18,965	5.6	17.1
	2A,2B	18,627	3.8	15.3
		(*b*) Loop 6		
Single axle	8A,8B	18,704	6.4	18.0
	3A,3B	18,937	6.1	18.0
Tandem axle	7A,7B	18,599	8.9	22.8
	9A,9B	18,370	10.1	23.4

[1] Mean displacement of vehicles from desired transverse position toward center of roadway.
[2] Ten percent of vehicles operated this far or farther from desired transverse position.

The variation of stresses and deformations during the period of regular test traffic is shown in Figures 41 and 42. Figure 41 shows data for the center beam of noncomposite bridge 1A. The top sections show transient stresses in the bottom flange at the critical section and transient deflections at midspan. Each dot represents the mean for one sampling period. The dispersion of the individual readings is indicated by the shaded area the limits of which are equal to two standard deviations from the mean. Both transient stresses and transient deflections showed variation from one sampling period to another, but stress fluctuated essentially around a constant level whereas deflection fluctuated about a level slowly increasing with time.

The bottom sections of Figure 41 show the bottom flange strains and the permanent set, measured at midspan of the bridge subjected only to dead load. Data taken shortly before the first crossing with regular test vehicles were used as the base for both curves. Both the strains and the permanent set showed a rapid increase during the first few crossings with regular test vehicles, but after 235 trips the increase was very gradual until the middle of October 1960. On October 19, 1960, an accident on Bridge 1A resulted in a substantial increase of permanent deformations of all three beams.

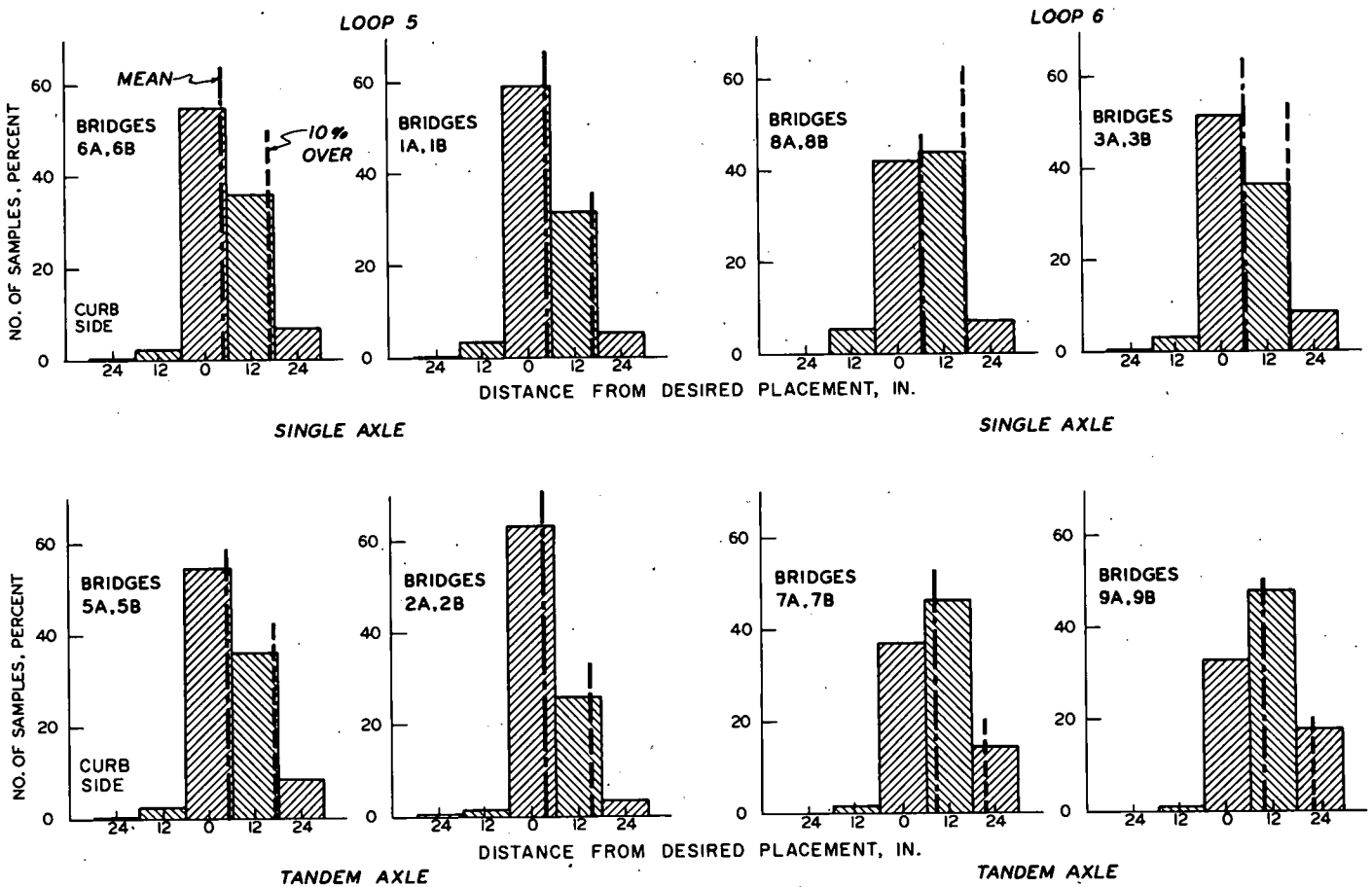

Figure 40. Transverse placement of vehicles on bridges.

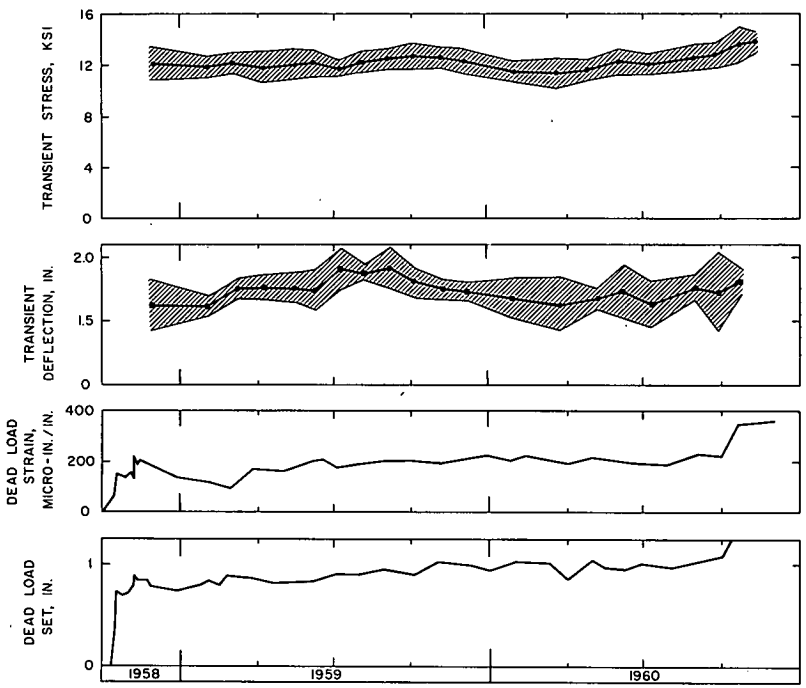

Figure 41. Time-stress and time-deformation relationships for center beam of noncomposite Bridge 1A.

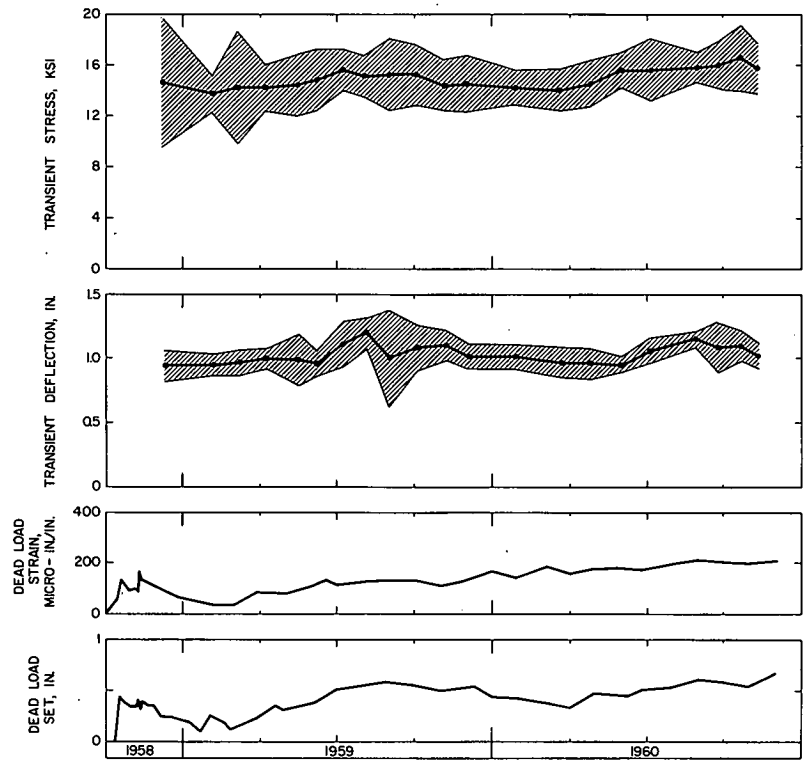

Figure 42. Time-stress and time-deformation relationships for center beam of composite steel Bridge 2B.

The time relationships for the center beam of composite bridge 2B are shown in Figure 42. The effects of regular test traffic were similar to those observed in noncomposite bridge 1A, except for smaller initial dead load strains and permanent set at midspan and for the shape of the curve of dead load set. The dead load set showed seasonal fluctuations about a steadily increasing level—during the winter months the midspan of the bridge moved up; during summer it moved down. These seasonal movements were probably caused by cyclic expansion and shrinkage of the slab.

The stresses and deformations (Figs. 41 and 42) were typical of all noncomposite and composite steel bridges, even though the magnitudes of the individual effects varied from bridge to bridge. The principal exception to this typical behavior was that of Bridge 3A in which three distinct phases were observed: a period of very rapid increase of permanent deformations, a period of rapid but slower increase of permanent deformations, and a period of a very slow increase of permanent deformations. The second period, not observed in other bridges, was ended after approximately 50,000 trips of regular vehicles. During this period the permanent set at midspan increased from 1.2 to 3.0 in. The very slow but steady increase of permanent deformations during the third period was ended by an accident (see Section 3.3.4).

The stresses and deformations caused in steel beams by regular test traffic are summarized in Table 38. Columns 1 and 4 give the means of the transient stresses computed from strains measured on the bottom flange at the critical section during the full period of test traffic. Individual values showed a normal distribution around the mean at all but three critical sections. The standard deviations (Cols. 2 and 5) varied from 0.64 ksi to 1.61 ksi; thus, about 90 percent of the stresses were within approximately 1.3 and 3.1 ksi of the mean.

After a vehicle crossed a bridge, the bridge continued to vibrate causing alternate upward and downward deflections of decreasing amplitude. The deflections were accompanied by strain fluctuations. The maximum amplitude of the first negative half-cycle of the strain fluctuation was designated as rebound strain. The rebound strain was of a sign opposite to that of the strain observed while the vehicle was on the bridge and thus increased the range of the fluctuating stress. The ratio of the sum of the maximum transient stress and the re-

TABLE 38

STRESSES AND DEFORMATIONS CAUSED IN STEEL BEAMS BY TEST TRAFFIC

Bridge	Beam	Transient Stress at Critical Section (ksi)						Mean Transient Deflection (in.)		End of Test	
		Approach End			Midspan or Exit End[1]						
		Mean	Std. Dev.	Rebound Factor	Stress	Std. Dev.	Rebound Factor	Beg. of Test	End of Test	Dead Load Strain (10^{-6} in./in.)	Dead Load Set (in.)
		(1)	(2)	(3)	(4)	(5)	(6)	(7)	(8)	(9)	(10)
					(a) NONCOMPOSITE						
1A	Int.	11.7	1.01	1.14	13.7	1.21	1.13	1.66	1.91	278	1.73
	Cen.	12.1	0.76	1.12	14.0	0.92	1.12	1.63	1.81	345	2.05
	Ext.	11.3	0.81	1.15	13.2	0.94	1.15	1.62	1.78	590	2.39
3A	Int.				16.9	1.02	1.13	1.87	2.02	1,575	3.94
	Cen.				16.7	0.70	1.13	2.00	2.09	1,929	4.22
	Ext.				18.2	1.14	1.15	1.95	2.06	2,759	4.53
9A	Int.	15.5	1.21	1.15	15.4	1.13	1.15	1.80	2.04	93	0.70
	Cen.	14.8	0.64	1.17	14.6	0.78	1.17	1.86	2.02	104	0.65
	Ext.	13.5	1.05	1.20	13.6	1.08	1.20	1.80	1.92	157	0.60
9B	Int.	15.1	1.12	1.17	15.4	1.09	1.16	1.82	1.98	160	0.68
	Cen.	14.8	0.79	1.19	14.7	0.83	1.20	1.89	2.00	114	0.70
	Ext.	14.0	0.94	1.22	13.7	1.06	1.23	1.92	2.05	115	0.50
					(b) COMPOSITE						
2B	Int.	14.9	1.56	1.07	15.4	1.32	1.03	0.93	1.12	131	0.80
	Cen.	15.0	1.56	1.06	14.6	1.24	1.06	0.94	1.02	198	0.68
	Ext.	14.2	1.61	1.07	14.2	1.35	1.07	0.83	0.92	176	0.52
3B	Int.	12.8	1.48	1.07	12.6	1.55	1.08	0.77	0.81	175	0.50
	Cen.	13.0	1.08	1.07	12.5	1.17	1.08	0.82	0.91	88	0.29
	Ext.	12.3	1.48	1.08	12.4	1.46	1.09	0.79	0.80	1	0.19

[1] At midspan for Bridge 3A, at exit end of plate for all other bridges.

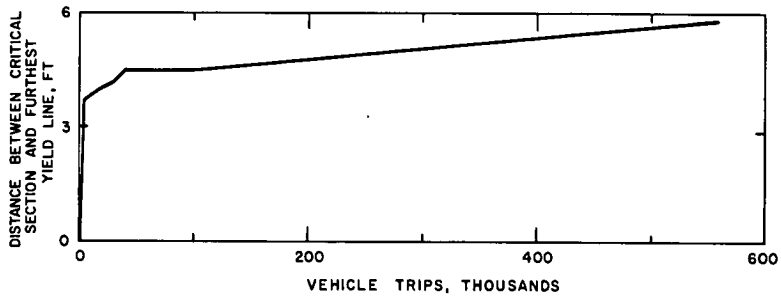

Figure 43. Progression of yielding in Bridge 3B.

bound stress to the maximum transient stress alone was designated as rebound factor (Table 38). The rebound factor was in excess of 1.1 for all noncomposite bridges but less than 1.1 for composite bridges. For any one bridge the rebound factor was essentially constant throughout the traffic period.

Table 38 also gives the means of the maximum transient deflections at midspan measured during the sampling periods at the beginning of the test and at the end of the test. The deflection at the end of the test was always larger than that observed at the beginning of the test. Similarly, as in the reference tests (Table 33), this increase of transient deflections was particularly small in composite bridges.

The values of dead load strain and set at midspan (Cols. 9 and 10) show that the test traffic caused permanent deformations in all steel bridges. The values for noncomposite bridges 1A and 3A include the deformations caused by accidents (Section 3.3.4); prior to the last accident, the dead load set at midspan averaged 1.06 in. in Bridge 1A and 3.44 in. in Bridge 3A. It is apparent that the regular test traffic caused very large permanent set only in Bridge 3A. In all other bridges the permanent set caused by regular test traffic was less than 1/500 of the span length and also less than the transient deflections of the same bridge. Composite bridge 3B had the smallest permanent set; in all three beams it was substantially less than 1/1,000 of the span length.

3.3.3 Yielding and Fatigue Cracking of Steel Beams

The regular test traffic caused yielding in all steel beams and fatigue cracking in several beams with partial-length cover plates. Yielding was observed immediately after the first few trips and most of it took place during the early period of test traffic. On the other hand, the first fatigue cracks were observed shortly before the end of the test traffic. In no case did the traffic with regular test vehicles result in a collapse of an entire bridge.

Yielding—After the first few trips of regular test vehicles, the paint on the steel beams was noticed to flake off along straight lines characteristic of yielding of steel. These yield lines formed primarily on the bottom flanges of rolled sections at an inclination of approximately 45 deg with the beam axis. They were first noticed near the critical sections; others formed along the beams toward the supports as the traffic continued. (For the discussion of yielding in Bridges 1B, 2A, 4A and 4B, which failed before the beginning of regular test traffic, see Section 3.2.5.)

Typical progression of yielding is shown in Figure 43. The distance between the critical section and the yield line closest to the nearest support is plotted as a function of the number of vehicle trips. Average values for the three beams of Bridge 3B are shown. The beams of Bridge 3B had cover plates 18½ ft long. Thus, at the end of the test traffic yield lines reached to within 10 ft of the supports.

The development of yielding in Bridges 1A, 2B and 3A was similar to that in Bridge 3B. At the end of the test traffic yield lines reached to within 8 ft of the supports in Bridge 1A, within 9 ft in Bridge 2B and within 7 ft in Bridge 3A. Of course, yielding was most extensive near the critical sections. The density of yield lines generally decreased with increasing distance from the critical section.

In addition to the yielding of the bottom flanges, yield lines were found also on the compression flanges of noncomposite bridges and in the webs. However, this yielding was limited to a few apparently random locations. No yielding was noted in the cover plates.

No tension yielding was observed in the beams of Bridges 9A and 9B. Light compression yielding was found on the edges of the top flanges in both bridges.

With the exception of the exterior beams of Bridges 2B and 3A, the total stresses caused by dead and live loads (Table 29) were always lower than the static yield point of the steel. However, the yield point determined from tension tests of coupons could not be a satisfactory indicator of the magnitude of applied stress that would cause yielding because it did not account for residual stresses in the rolled beams. The difference between the yield point and the residual stress, designated as the effec-

TABLE 39
EFFECT OF RESIDUAL STRESS ON YIELDING OF ROLLED STEEL BEAMS

Bridge	Effective Yield Strength,[1] f_e	Mean LL + DL Stress,[2] S (ksi)	S/f_e	Mean Permanent Set (in.)	
				Initial[3]	Final[4]
(a) NONCOMPOSITE BRIDGES					
1A	26.7	27.7	1.04	0.44	1.06[5]
3A	26.9	31.6	1.17	1.18	3.41[6]
9A	25.1	24.4	0.97	0.32	0.65
9B	25.1	24.9	0.99	0.29	0.63
(b) COMPOSITE BRIDGES					
2B	26.6	33.3	1.25	0.29	0.67
3B	31.1	28.6	0.92	0.09	0.33

[1] Difference between yield point (Table 5) and mean residual stress in flanges (Table 7).
[2] From Table 29.
[3] Mean of data for individual beams given in Table 32.
[4] Mean of data for individual beams given in Table 38 except when noted otherwise.
[5] Prior to accident on 19 October 1960.
[6] Prior to accident causing failure.

tive yield strength, was expected to be more significant than the yield point alone.

Tests discussed in Section 2.2.1 indicated the presence of residual stresses of considerable magnitude in all rolled steel sections. Furthermore, the residual stresses varied from one point on the cross-section to another with the largest tensile stresses in the flange at its center (Table 7).

The average residual stress in flanges of beams of Bridges 1A, 2B, 3A and 3B was tensile; yield lines were noted primarily on the bottom flange. On the other hand, the average residual stress in the flanges of beams of Bridges 9A and 9B was compressive; yield lines were found only on the top flanges.

For the purposes of quantitative comparisons, the effective yield strength was defined as the difference between the yield point and average residual stress of the flange. The effective yield strengths are compared in Table 39 with the mean ($LL + DL$) stresses and with the magnitude of permanent set. Although several other differences undoubtedly influenced the relative magnitudes of the permanent set, it is apparent that the permanent set increased with increasing ratio of the applied

TABLE 40
TRIP COUNT AT TIME OF FATIGUE CRACKING OF STEEL BEAMS

Bridge	Beam	End of Cover Plate	No. of Trips (1,000's)	
			North Weld	South Weld
1A	Interior	Approach	556.9	557.4
		Exit	557.4	557.4
	Center	Approach	—[1]	536.0
		Exit	549.9	536.0
	Exterior	Approach	536.0	557.4
		Exit	536.0	—[1]
2B	Interior	Approach	—[2]	531.5
		Exit	—	—
	Center	Approach	531.5	555.3
		Exit	558.4	531.5
	Exterior	Approach	—[2]	—[2]
		Exit	—	—
3B	Interior	Approach	—[1]	—[1]
		Exit	—[1]	—[1]
	Center	Approach	—[1]	535.5
		Exit	—[1]	—[1]
	Exterior	Approach	—[1]	557.8
		Exit	—[1]	—[1]
9A	Interior	Approach	—[1]	—[1]
		Exit	—[1]	—[1]
	Center	Approach	—[1]	—[1]
		Exit	—[1]	—[1]
	Exterior	Approach	—[1]	—[1]
		Exit	477.9	477.9
9B	Interior	Approach	—[1]	—[1]
		Exit	—[1]	—[1]
	Center	Approach	477.9	—[1]
		Exit	—[1]	—[1]
	Exterior	Approach	—[1]	—[1]
		Exit	—[1]	—[1]

[1] Fatigue cracks found during tests to failure with increasing loads; tests to failure with increasing load not performed on Bridge 2B.
[2] Fatigue crack found during accelerated repeated load test.

stress to the effective yield strength. Furthermore, the residual stresses apparently had smaller effect on permanent deformations of composite bridges than on those of noncomposite bridges. Because of the smaller distance between the neutral axis and the highly stressed flange of the beam, an equal inelastic elongation causes larger rotations in a noncomposite beam than in a composite beam.

Fatigue Cracking—During the weekly bridge inspections particular attention was given to examination of the ends of the welds of the cover plates for possible fatigue cracks. The presence of fatigue cracks was definitely established during the inspection on October 27, 1960. Four cracks were found on Bridge 1A, three on Bridge 2B and one on Bridge 3B. Additional fatigue cracks became visible during the last month of test traffic.

Figure 44 shows typical fatigue cracks. When the cracks were first discovered they were usually ¼ to ½ in. long and were confined to the toe of the bead of the weld (Fig. 44a and b); the ends of the cracks are indicated by arrows. The only exception was the crack shown in Figure 44c which was located on the interior beam of Bridge 2B at the south weld on the approach end of the cover plate. On further repetitions of load, some cracks spread in both directions along the toe of the weld, and later extended perpendicularly to the beam axis toward the web on one end and toward the edge on the other end. The crack then became visible on the vertical face and, subsequently, on the top face of the bottom flange, progressing slowly from the edge toward the web.

Table 40 gives the number of trips of regular test vehicles at the time the presence of the fatigue cracks was first established. Four locations are given for each beam. By the time the regular test traffic was concluded, fatigue cracks were known to exist at 10 of the 12 possible locations on Bridge 1A, at 5 on Bridge 2B, at 2 on Bridges 3B and 9A and at 1 on Bridge 9B.

The most extensive crack (Fig. 44d) was on the interior beam of Bridge 2B at the south weld on the approach end of the cover plate. At the end of the regular test traffic the crack extended from the edge of flange to the web so that the south half of the flange was completely broken.

The second largest crack was located on the center beam of Bridge 3B at the south weld on the approach end of the cover plate. It extended about ½ in. beyond the weld on the bottom face and about ¼ in. from the edge on the top face of the bottom flange (see Fig. 65).

Another crack on Bridge 2B extended to the edge of the flange; all others were confined to the region of the toe of the weld.

During the accelerated repeated load tests on Bridge 2B and the tests to failure with increasing loads on the other four bridges several additional fatigue cracks were found (Table 40). The tests to failure with increasing loads were not made on Bridge 2B, which may account for the fact that in Bridge 2B fatigue cracks were found only at eight locations.

3.3.4 Accidents on Test Bridges and Failure of Bridge 3A

Bridges 1A, 3A, 3B, 6A, 6B, 8A and 8B, located on the inside lanes of Loops 5 and 6, were assigned single-axle test vehicles. The heavier tandem-axle vehicles operated on the outside lanes. A few times during the regular test traffic the vehicles assigned to the outside lanes accidentally crossed the bridges in the inside lane. The recorded numbers of such trips are given in Table 36.

Whenever a trip of a tandem-axle vehicle over the bridges in the inside lane was reported, the elevations of the bridge beams and the dead load strains at midspan were checked to determine whether any measurable permanent deformations had been caused by the heavier vehicle.

Bridge 1A.—Bridge 1A was crossed eight times by tandem-axle vehicles 52 causing approximately 40 percent higher live load moment at midspan than the assigned regular test vehicles 51. The first two accidental trips were reported on October 15, 1958, after the bridge had been subjected to less than 200 trips of regular test vehicles. The two trips with vehicles 52 and the additional 117 trips with vehicles 51 resulted in a 0.29-in. permanent set at midspan.

Five more trips with vehicles 52, that were noted on later dates, caused no apparent permanent deformations.

The last recorded trip of a vehicle 52 over Bridge 1A occurred on October 19, 1960. In this case the truck went out of control after leaving the turnaround, veered into the single lane, hit the timber curb on Bridge 1A, and the trailer turned over on Bridge 1B (Bridge 1B was out of test before the accident). The accident caused substantial permanent deformations in all three beams of Bridge 1A. The largest increase in the set at midspan was greater than 1 in. and in dead load strain about 0.0003.

Bridge 3A.—Only one trip of tandem-axle vehicle 62 over Bridge 3A was recorded. It occurred on April 24, 1960, and corresponded to an increase of approximately 25 percent over the live load moment caused by the assigned test vehicle 61. Strain and deflection data disclosed no measurable permanent deformation which could be attributed to the accidental trip.

On June 20, 1960, a regular test vehicle 61 went out of control on leaving the turnaround. The outside set of wheels jumped the wingwall of the abutment on the approach end of the

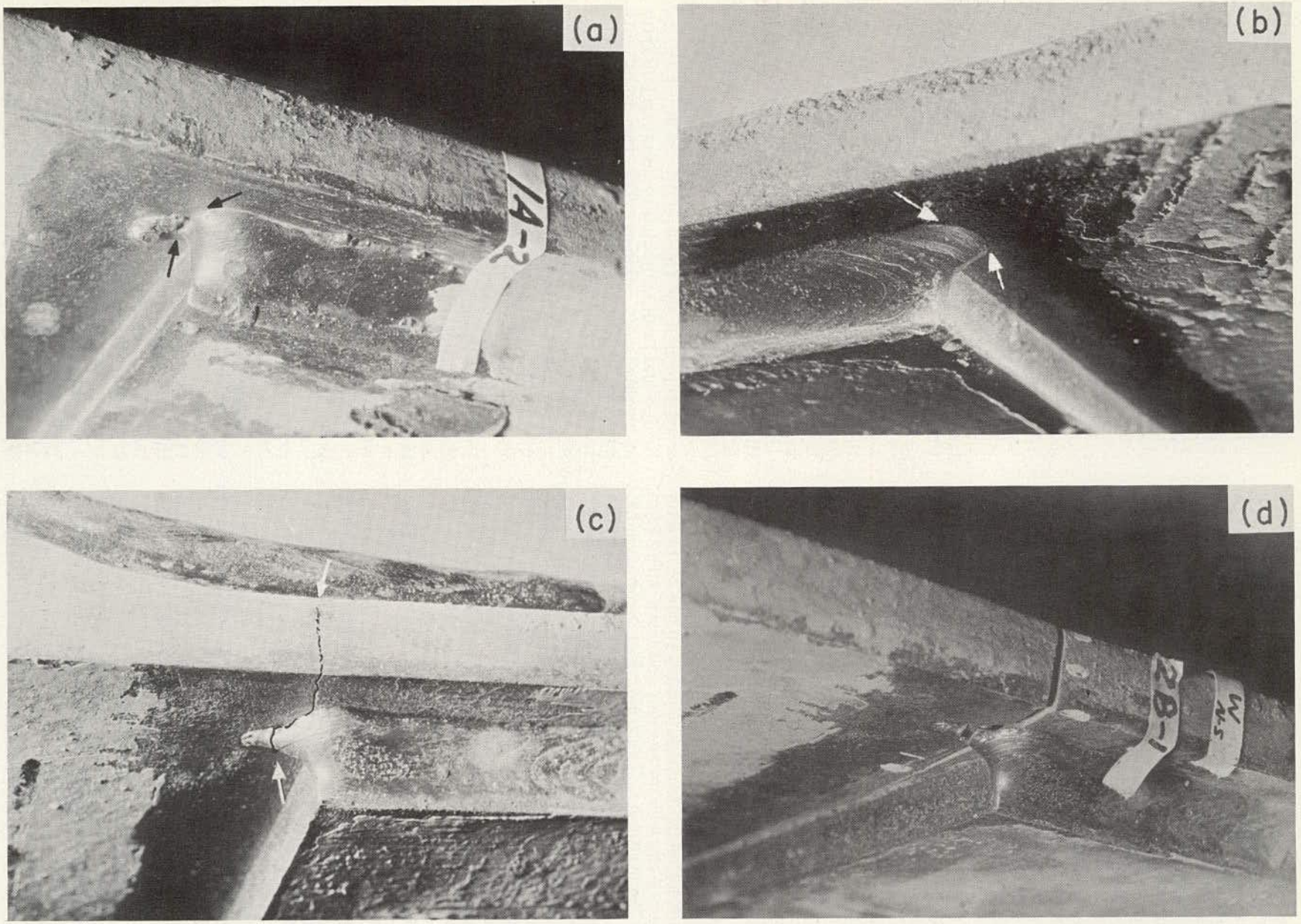

Figure 44. Typical fatigue cracks.

bridge, the wheels were carried over the timber curb and landed on Bridge 3A. The vehicle came to rest with the inside front wheel on Bridge 9A and all other wheels on Bridge 3A.

The permanent set increased substantially over that recorded before the accident. The increase at midspan was 0.42 in. for the interior beam, 0.78 in. for the center beam and 1.17 in. for the exterior beam. The maximum increase in dead load strain attributable to the accident was greater than 0.0002. After the accident, the total permanent set at midspan was substantially in excess of 3 in. (Table 38) and the bridge was declared out of test. Prior to the accident, the bridge had sustained 392,400 trips of regular test vehicles.

Other Bridges.—All recorded trips of vehicles 62 over Bridges 3B, 8A and 8B occurred in 1960. The increase (about 25 percent) over the live load moment corresponding to regular test vehicles 61 left no permanent deformations that could be detected by measurements of beam elevations or of dead load strains.

Bridges 6A and 6B were crossed by two tandem-axle vehicles 52 on November 2, 1960. Two vehicles 52 may have crossed the bridges also on October 15, 1958, but these trips were indicated as questionable. No permanent effects were detected on either date.

3.3.5 Stresses and Deformations in Concrete Beams

Response curves of individual strain gages from regular test traffic exhibited the same characteristics as those discussed in connection with initial tests (Fig. 34). The curves for three beams of the same bridge were practically identical for reinforced concrete bridges and for uncracked prestressed concrete bridges 5B and 6B. They were similar for prestressed concrete bridge 5A in which all three beams were cracked. However, the curves for the three beams differed for prestressed concrete bridge 6A, apparently because of the differences in the degree of cracking of the three beams. The agreement among individual runs was fair for reinforced concrete bridges, and for uncracked prestressed concrete bridges, particularly among runs made within the same month.

The variation of stresses and deformations with time is shown in Figures 45 and 46. Figure 45 contains data for the center beam of the cracked prestressed concrete bridge 5A and for the center beam of the uncracked bridge 5B. The top sections show the maximum transient stresses in the bottom layer of steel at midspan and the maximum deflections at midspan. Each dot represents the mean for one sampling

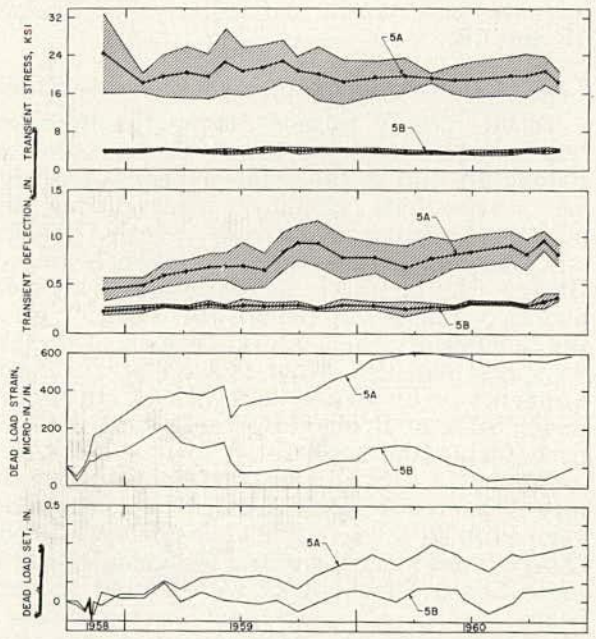

Figure 45. Time-stress and time-deformation relationships for center beam of prestressed concrete Bridges 5A and 5B.

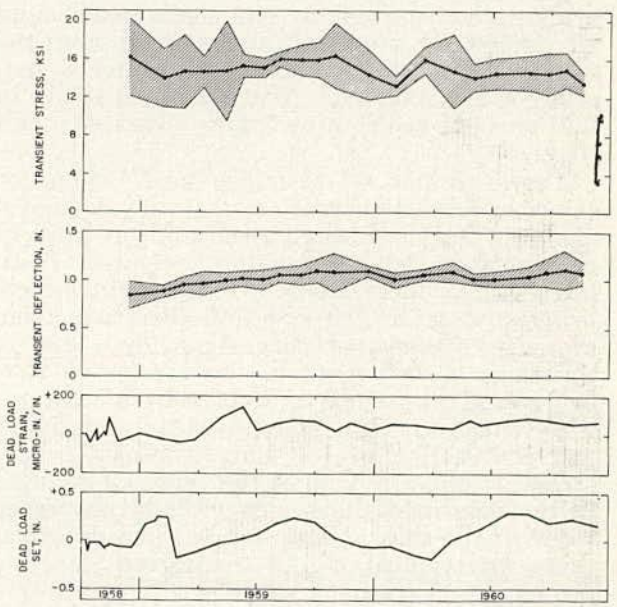

Figure 46. Time-stress and time-deformation relationships for center beam of reinforced concrete Bridge 8B.

period. The dispersion of the individual readings is indicated by the shaded areas, the limits of which are equal to two standard deviations from the mean.

In Bridge 5A the transient stress showed decrease from the first to the second sampling period. During the remainder of the test traffic, the transient stress fluctuated around an essentially constant stress level. A similar fluctuation around a constant stress level was observed in Bridge 5B throughout the entire period of test traffic. The transient deflections fluctuated around a gradually increasing level.

The bottom sections (Fig. 45) show changes in dead load strains on the bottom surface of the concrete beams and in the dead load set at midspan. Data taken shortly before the first crossings with regular test vehicles were used as the base for both curves. All four curves showed seasonal fluctuations. The strains indicated shortening of the bottom surface through March, April and June, and lengthening through October, November and December. The shortening of the bottom surface was accompanied by an upward movement and the lengthening by a downward movement of the bridge at midspan. The dead load strains in Bridge 5B fluctuated around an essentially constant level, but the strain in Bridge 5A and the set in both bridges showed an over-all increase with time.

The stresses and deformations of the center beam of Bridge 5A were typical of all cracked prestressed concrete beams, and those of the center beam of Bridge 5B were typical of all uncracked prestressed concrete beams.

The time relationships for the center beam of reinforced concrete bridge 8B are shown in Figure 46. As for the prestressed concrete bridges, the transient stresses fluctuated around an essentially constant stress level and the transient deflections fluctuated around a generally increasing level. The dead load strain in the tension reinforcing bars increased with time.

The dead load set at midspan of Bridge 8A showed seasonal fluctuation: a downward movement in March through June and an upward movement in October through December. Thus, the seasonal fluctuations in reinforced concrete bridges were in the opposite direction from those in prestressed concrete bridges but in the same direction as in the composite steel bridges. This suggests that the fluctuations were caused primarily by seasonal expansion and contraction of the slab, whereas in prestressed concrete bridges the seasonal changes in the length of the beams probably exceeded those of the slab. These stresses and deformations are typical of all reinforced concrete beams.

Table 41 summarizes the stresses and deformations caused by regular test traffic in prestressed concrete and reinforced concrete beams. Column 1 gives the means of the transient stresses computed from strains measured in the bottom layer of reinforcing steel at midspan. Individual values showed a normal distribution around the mean at all locations except in two beams of Bridge 6A, in which progressive development of cracks was observed, and in two reinforced concrete beams. The standard deviation (Col. 2) was particularly large for the cracked beams of prestressed concrete bridges 5A and 6A. The rebound factor, equal to the ratio of the sum of maximum stress and rebound stress to the maximum stress alone, was generally less than 1.1 for the prestressed concrete bridges; for reinforced concrete bridges it was usually more than 1.1.

Columns 4 and 5 give means of the maximum transient deflections at midspan, measured during the sampling periods at the beginning and at the end of test traffic. The mean transient deflections increased with time for every beam; they showed the same trends as the deflections obtained in reference tests (Table 33).

The values given for dead load strain represent the change from before the first regular test vehicles crossed the bridges until the end of test. With the exception of prestressed concrete bridges 5B and 6B, increases in tensile strains were observed in every bridge. Of particular interest are the strains for Bridges 7B and 8A. If added to the values given in Table 24, they indicate a reasonable agreement with the strains computed by the straightline theory for fully cracked sections.

The permanent set at midspan increased for every beam, even though the magnitude of the increase was small, particularly in Bridges 5B and 6B.

3.3.6 Cracking of Prestressed Concrete Beams

Tensile cracks formed during the first few trips of test vehicles in all three beams of Bridge 5A and in the exterior beam of Bridge 6A. Inspections of the bridges during the period of regular test traffic revealed tension cracking also in the remaining two beams of Bridge 6A, in all three beams of Bridge 6B and in two beams of Bridge 5B. Table 42 gives the number of vehicle trips at which the cracks were first detected either through strain measurements or by visual observations. In the interior beam of Bridge 5B, cracks were detected first during the accelerated fatigue tests.

Bridge 5A.—Strain measurements during the initial reference tests indicated that cracks developed in all three beams of the bridge. Visual observations after the initial tests confirmed the indications. Five cracks were found in each beam.

Additional cracks formed and the existing cracks widened during the course of regular traffic. Figure 47 shows the progress of the

TABLE 41

STEEL STRESSES AND DEFORMATIONS CAUSED IN CONCRETE BEAMS BY TEST TRAFFIC

Bridge	Beam	Transient Stress at Midspan (ksi)			Mean Trans. Defl. (in.)		End of Test	
		Stress	Std. Dev.	Rebound Factor	Beg. of Test	End of Test	Dead Load Strain [1] (10^{-6}in./in.)	Dead Load Set (in.)
		(1)	(2)	(3)	(4)	(5)	(6)	(7)
		(a) PRESTRESSED PRECAST BEAMS						
5A	Interior	22.2	3.43	1.02	0.46	0.86	312	0.30
	Center	19.8	3.21	1.02	0.46	0.81	559	0.29
	Exterior	25.4	4.73	1.03	0.45	0.98	911	0.29
5B	Interior	4.7	0.53	1.03	0.28	0.38	— 76	0.08
	Center	3.8	0.31	1.04	0.23	0.37	— 45	0.08
	Exterior	4.1	0.51	1.04	0.21	0.31	— 31	0.08
6A	Interior	2.5	0.34	1.05	0.17	0.27	106	0.13
	Center	4.8	2.09	1.03	0.16	0.26	80	0.13
	Exterior	6.8	1.66	1.03	0.14	0.23	166	0.16
6B	Interior	2.4	0.31	1.09	0.19	0.26	— 16	0.07
	Center	2.5	0.22	1.09	0.16	0.24	— 60	0.07
	Exterior	2.5	0.36	1.10	0.15	0.27	30	0.07
		(b) REINFORCED CONCRETE BEAMS						
7A	Interior	25.5	2.36	1.07	1.47	1.72	30	0.23
	Center	23.1	1.65	1.10	1.43	1.75	12	0.14
	Exterior	23.6	1.62	1.09	1.38	1.83	188	0.16
7B	Interior	22.0	2.65	1.16	1.40	1.74	91	0.30
	Center	22.0	2.44	1.16	1.32	1.64	117	0.22
	Exterior	22.7	2.05	1.16	1.21	1.58	154	0.20
8A	Interior	15.9	1.14	1.10	0.91	1.10	28	0.17
	Center	15.2	1.02	1.10	0.92	1.06	166	0.13
	Exterior	14.9	1.27	1.12	0.86	1.04	143	0.17
8B	Interior	15.2	1.27	1.13	0.90	1.09	50	0.18
	Center	14.8	1.52	1.15	0.84	1.08	105	0.17
	Exterior	15.7	1.39	1.14	0.86	1.06	43	0.17

[1] Negative sign indicates compressive strain.

crack formation; the number of cracks increased rapidly during the first 100,000 trips of vehicles. Some of the new cracks formed between the existing ones; others formed at locations nearer the supports. The increase in the number of cracks was accompanied by an increase in the average crack width.

The crack pattern in Bridge 5A was almost fully developed after the first 100,000 trips of load. The crack pattern on the exterior beam after 200,000 vehicle trips is shown in Figure 48. The cracks were distributed over a length of approximately 11 ft on each side of midspan, and most of them extended to the top flange. As only two additional cracks formed during the remainder of traffic, the wide spacing suggests that some loss of bond between the wires and the grout must have taken place between the cracks. The progressive development of

TABLE 42

TRIP COUNT AT TIME OF CRACKING OF PRESTRESSED CONCRETE BEAMS

Bridge	No. of Trips at Cracking of		
	Interior Beam	Center Beam	Exterior Beam
5A	1	1	1
5B	— [1]	144,000 [2]	144,000 [2]
6A	303,600	98,900	1
6B	556,800 [2]	556,800 [2]	303,600 [2]

[1] Cracks found during accelerated fatigue tests.
[2] Seen in epoxy coat only.

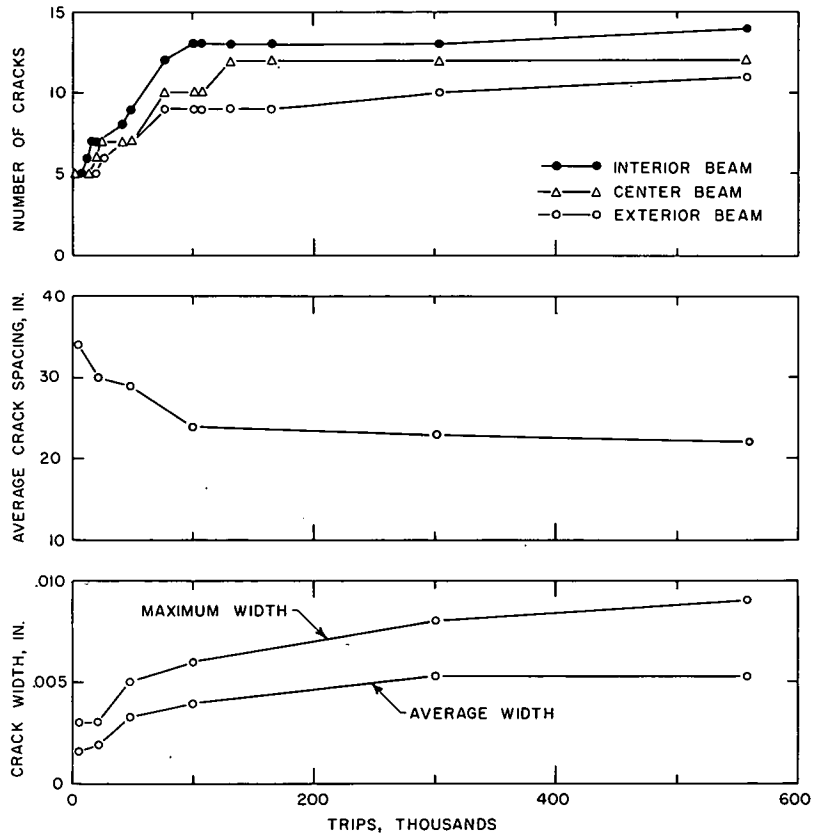

Figure 47. Tensile cracking of beams in Bridge 5A.

cracking explains the decrease of bridge stiffness evidenced by increased transient deflections (Tables 33 and 41).

The data in Figure 47 were taken when the bridges were unloaded. Crack widths in loaded bridges were measured in July 1959, April 1960, and January 1961 with a regular test vehicle standing in the position for maximum moment at midspan. These measurements indicated that the load caused the following average increases in crack width: 0.0075 in. in July 1959, 0.0051 in. in April 1960, and 0.0046 in. in January 1961. The progressive decrease in the incremental crack width suggests progressive loss of bond with traffic.

Bridge 6A.—Strain measurements during the initial reference tests indicated formation of a crack at midspan of the exterior beam of

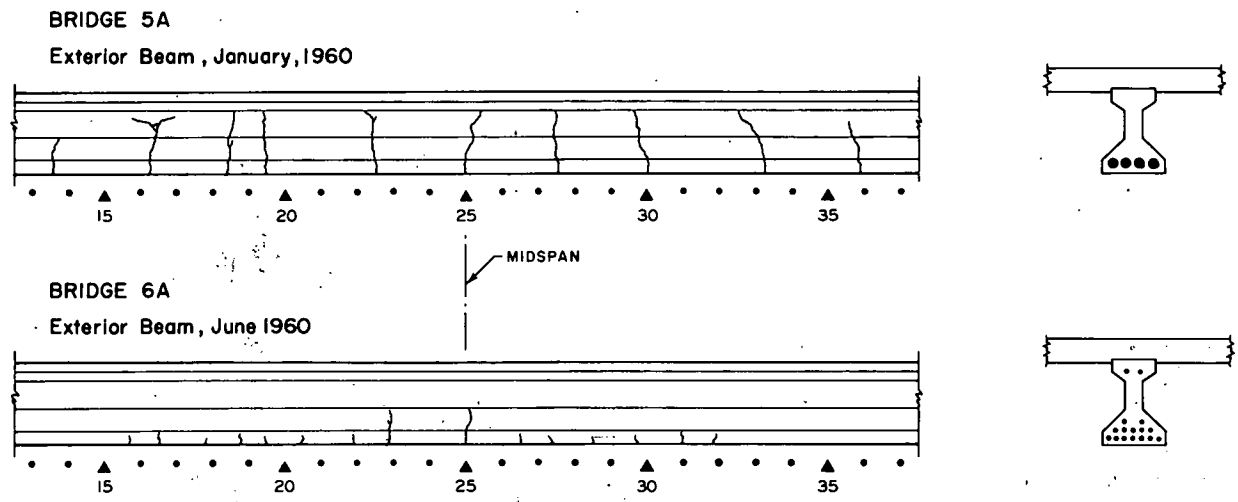

Figure 48. Crack patterns on prestressed concrete beams.

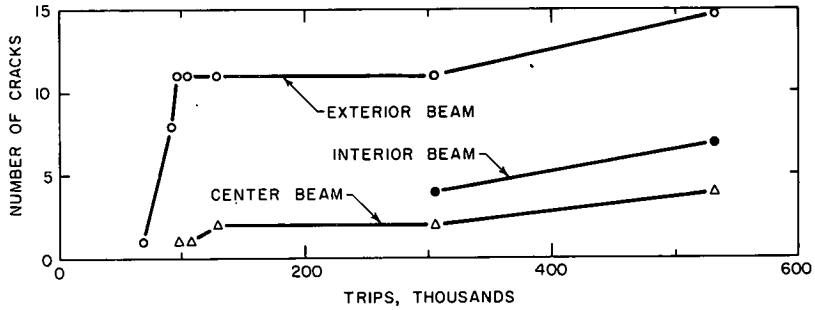

Figure 49. Tensile cracking of beams in Bridge 6A.

Bridge 6A. However, visual examinations did not succeed in detecting the crack. Strains measured at midspan of this beam during the regular traffic confirmed the results of the initial reference tests. As traffic continued, strains at the given location increased. Attempts to locate the crack visually were successful in June 1959 after 69,300 trips of regular test vehicles. Detection was aided by the use of a thin film of epoxy resin painted on the bottom surface of the exterior beam.

After this successful use of epoxy resin in detecting an elusive crack, the vertical side surfaces of the bottom flanges of all beams of Bridges 5B, 6A and 6B were coated with the resin. Additional cracks were soon discovered in the exterior beam of Bridge 6A. The progress of crack detection is shown in Figure 49, and the crack pattern on the exterior beam after 400,000 vehicle trips is shown in Figure 48. As in Bridge 5A, the cracking of the beams of Bridge 6A resulted in decreased stiffness of the bridge.

Cracks in Bridge 6A were mostly confined to the vertical surfaces of the bottom flange (Fig. 48). On the average, the cracks were spaced at 10 in. Crack width for the unloaded condition seldom exceeded 0.001 in. and the maximum observed width was 0.004 in.

When a regular test vehicle was placed on the bridge, crack width increased by approximately 0.001 in. Cracks in the center and interior beam were visible only in the coat of epoxy resin.

Bridges 5B and 6B.—Strain measurements throughout the period of regular test traffic indicated no cracking in any beam of Bridges 5B and 6B. However, observations aided by an epoxy resin film indicated the presence of a few hairline cracks in the center and exterior beams of Bridge 5B after 144,000 trips. Subsequent attempts to measure the width of these cracks, in both the unloaded and loaded conditions, were unsuccessful. Apparently, if the cracking was present at all, the width of the cracks was too small to be measured with a 40-power microscope.

Visual observations aided by the resin film indicated the presence of cracks in the exterior beam of Bridge 6B after 303,600 trips. In the other two beams, cracks were discovered at the conclusion of the test traffic. As on Bridge 5B, the width of the cracks in Bridge 6B could not be determined with a 40-power microscope.

None of the cracks in Bridges 5B and 6B could be seen on the uncoated vertical concrete surface above the epoxy resin coat.

3.3.7 Cracking of Reinforced Concrete Beams

Tension cracks were found in all beams of reinforced concrete bridges immediately after the removal of the forms. The first measurements of the cracks were made in May 1958 and the first set of photographs of the cracked beams was taken in September 1958. Crack patterns, copied from photographs of two typical beams, are shown in Figure 50.

The cracks extended along the beam length to within 7 ft of the supports before the traffic began. Cracks in the middle 30 ft generally extended to the fillet between the concrete stem and the slab. The regular test traffic caused a substantial increase in both the number and the extent of cracking. Most new cracks that formed in 1958 and early 1959 were vertical. In the spring of 1959, inclined cracks developed in all beams of Bridges 7A and 7B. When the second set of photographs was taken (June 1959) both vertical and inclined cracks were well developed (Fig. 50). Further traffic caused only minor changes in crack patterns, as shown by crack patterns copied from photographs taken in January 1961.

The number and width of cracks associated with 10-ft segments of each beam were determined by sampling within the segments (Fig. 23). In the three segments nearest to midspan the cracking was about the same; cracks were mostly vertical and essentially equally spaced. On the other hand, in the outer 10-ft segments cracks were either inclined (Bridges 7A and 7B) or slightly bent toward midspan (Bridges 8A and 8B) and the spacing was generally larger than in the three center segments. There was no consistent variation in cracking from beam to beam of the same bridge and appreciable differences existed between the bridges with high and low stresses. The most extensive

cracking was usually found in Bridge 7B and the least extensive in Bridge 8B. Bridge 7A generally showed more extensive cracking than Bridge 8A. Cracking was reasonably symmetrical about midspan of any one beam, and was more pronounced near the bottom of the beam than in the top portion of the stem.

Based on these observations, a quantitative summary of the test data for unloaded bridges is shown in Figure 51. The data included were obtained from the lower sampling regions (Fig. 23) located on the side surfaces of the beams. The data were averaged for all such regions located within the center 30 ft and for all such regions located in the outer 10-ft portions of the beams. Further averaging was done for the three beams of the same bridge, for Bridges 7A and 7B and for Bridges 8A and 8B.

Figure 51 shows the means of the observed number of cracks per 10-ft length of beam, sample crack width and maximum crack width as functions of the number of trips of regular test vehicles (see Section 2.4.1). The number of cracks, the sample crack width and the maximum crack width increased with the increase in the number of vehicle trips. The increases were particularly pronounced early in the test traffic period. With the exception of the sample crack width in the outer 10 ft of the beams, the quantities presented were larger for Bridges 7A and 7B than for Bridges 8A and 8B.

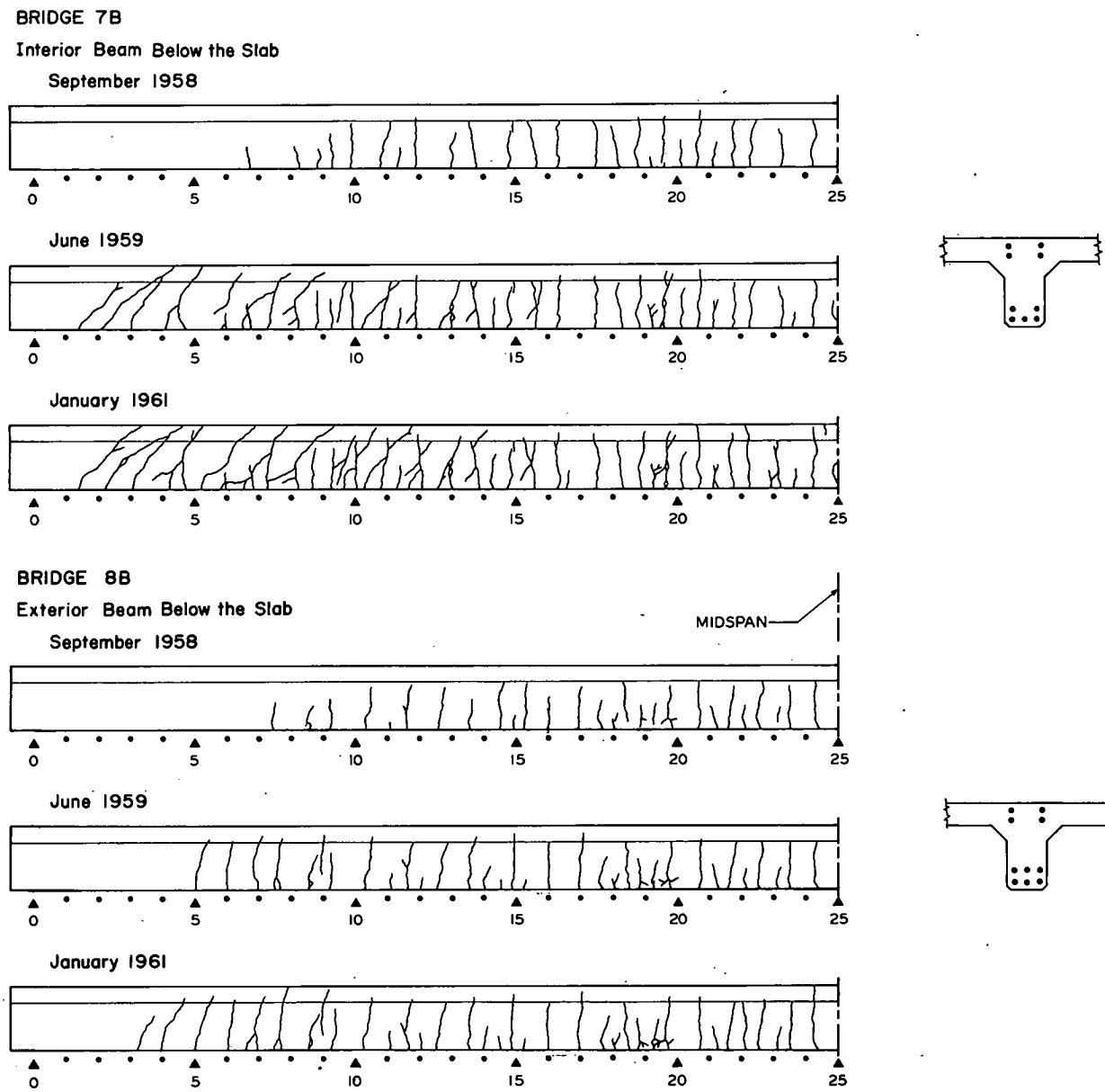

Figure 50. Crack patterns on reinforced concrete beams.

The increase of cracking with traffic resulted in a decrease of bridge stiffness and in an increase of transient deflections (Tables 33 and 41).

The maximum crack width exceeded 0.01 in. in all four bridges. The increase in the number of cracks was, of course, accompanied by a decrease in the crack spacing. However, throughout most of the experiment the average spacing was between 6 and 8 in. (The average spacing of cracks for the center portions of beams is obtained by dividing 120 in. by the number of cracks shown in Fig. 51.)

In addition to the measurement of cracking on unloaded bridges, observations were made during three sampling periods while a regular test vehicle was standing on the bridge in the position for maximum moment at midspan. The

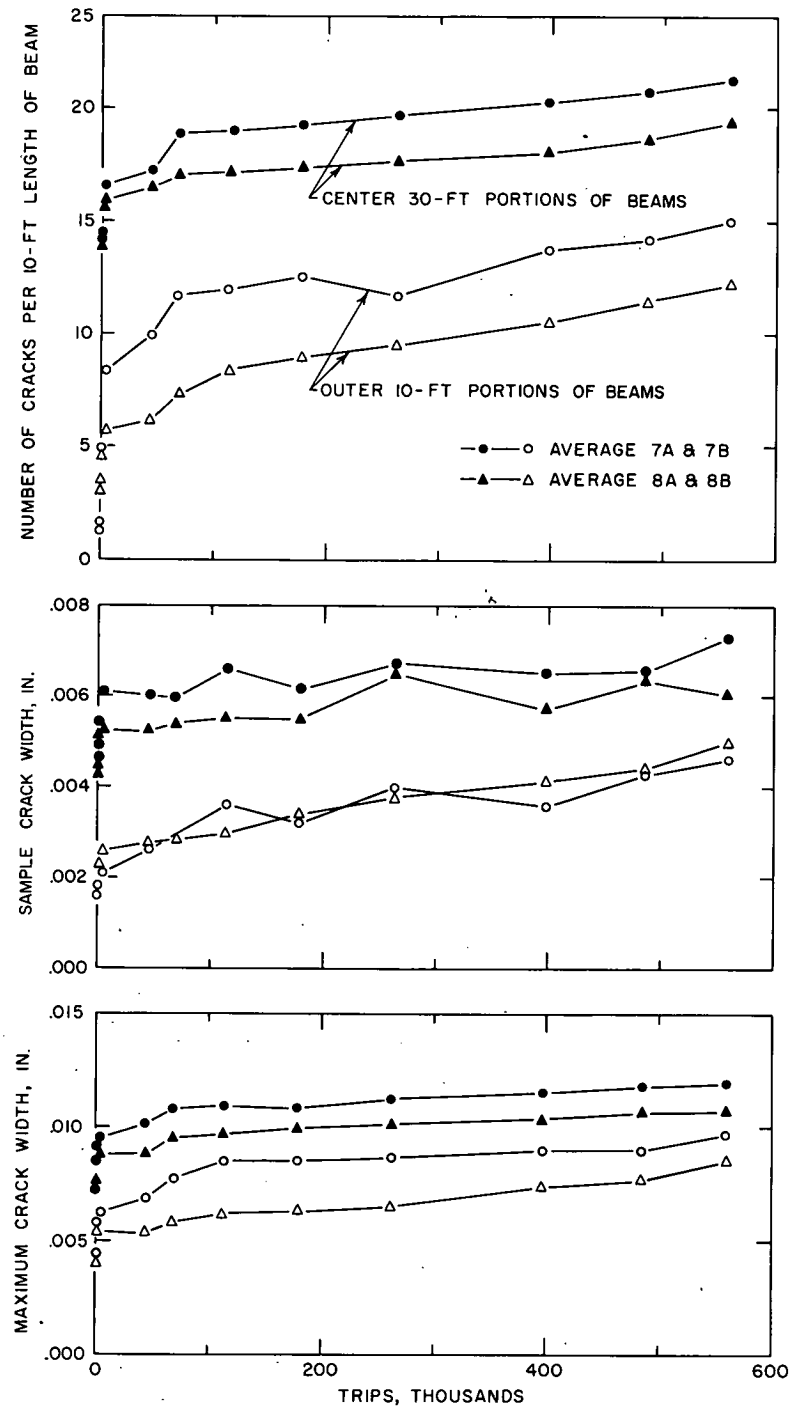

Figure 51. Tensile cracking of reinforced concrete beams.

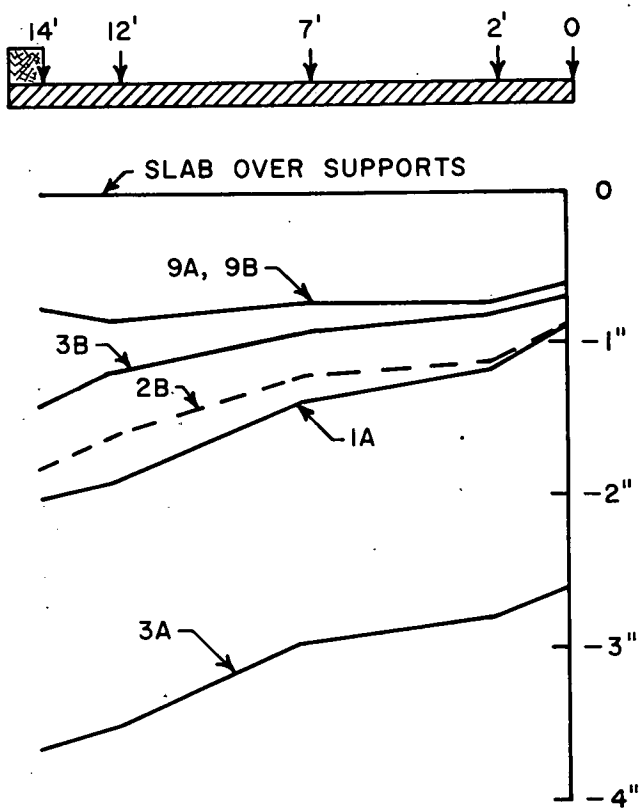

Figure 52. Transverse profiles at midspan at conclusion of traffic, steel bridges.

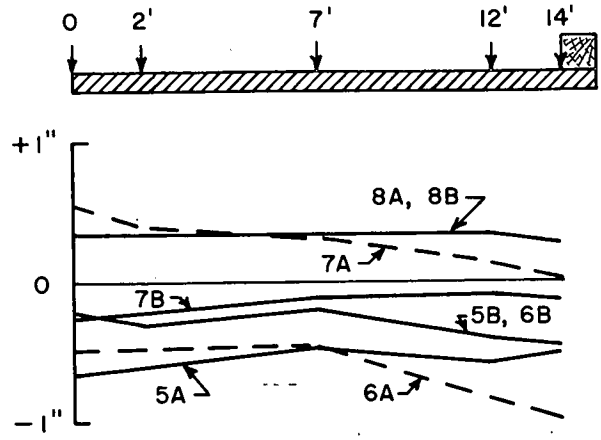

Figure 53. Transverse profiles at midspan at conclusion of traffic, concrete bridges.

truck load increased the crack width and the increase was nearly the same for all three periods. The maximum crack width increased 0.002 in. in the middle 30-ft portions of the beams and 0.001 in. in the end 10-ft portions of the beams. The sample crack width increased less than 0.001 in. Data on the distribution of crack widths and on relationships between various types of measurements of the crack width are reported in Section 5.4.

3.3.8 Behavior of Bridge Slabs and Supporting Members

Most of the measurements and observations on the test bridges were confined to the beams, since these were of primary interest in the experiment. However, the slabs and the supporting structures were examined during weekly inspections and noticeable changes in their condition were recorded. The observations were made partly because of their bearing on the over-all bridge behavior and partly to determine the need for maintenance of the structures during the test traffic.

Measurements on slabs included transverse and longitudinal profiles and temperature. Data on profiles are discussed in this section. A study of the temperature variations and of their effect on strains is discussed in Section 5.5.

Slab Profiles.—Transverse profiles at midspan at the conclusion of traffic are shown in Figure 52 for steel bridges. (Data for Bridges 3A and 1A are based on the last set of readings before the accidents that occurred in June and October 1960, Section 3.3.4) and in Figure 53 for concrete bridges. A comparison with the corresponding profiles after construction (Fig. 13) and just before the beginning of traffic (Fig. 32) shows that changes consisted almost entirely of vertical displacements.

Table 43 gives the ranges of average vertical displacements for the various types of bridges, and includes displacements that developed during the period of test traffic, and that occurred between the time of first measurements after construction and the end of traffic. The values suggest that although the displacements in noncomposite steel bridges occurred almost entirely as a result of traffic, the time effects were responsible for at least a considerable portion of the displacements of the midspan profile of the other bridges.

In connection with Figure 53, it is of interest that the camber of Bridge 7B was completely lost by the end of the test.

TABLE 43
VERTICAL DISPLACEMENT OF SLABS AT MIDSPAN DURING TEST TRAFFIC

Type of Bridge	Vertical Displacement[1] (in.)	
	During Traffic	Total
Noncomposite steel	0.43 to 3.28	0.43 to 3.54
Composite steel	0.32 to 0.64	0.62 to 0.82
Post-tensioned prestressed concrete	0.29 to 0.34	0.36 to 0.63
Pretensioned prestressed concrete	0.07 to 0.23	−0.02 to 0.17
Reinforced concrete	0.17 to 0.53	0.72 to 0.97

[1]Range of average values for individual bridges; negative sign represents upward movement.

Except for local irregularities, the longitudinal profiles remained essentially symmetrical about midspan with the maximum deviation from the plane connecting the abutments occurring at midspan. The local irregularities remained practically the same as they were at the beginning of the traffic.

Cracking of Slabs.—One of the more significant developments on the bridge slabs was that of cracking. All slabs were free of cracks up to the beginning of the test traffic. A few months after traffic operations began, cracks were discovered on the top surfaces of the slabs of steel bridges, prestressed concrete bridges and reinforced concrete bridge 7B. The cracks were located at the corners of the overhanging portions, starting over the interior or exterior beam at the ends of the spans and extending diagonally toward the longitudinal edge of the slab. The cracks were apparently confined by the slab reinforcement and did not penetrate to the bottom surface of the slab.

Immediately after a few trips of the regular test vehicles, transverse tension cracks formed on the bottom surfaces of the slabs of the noncomposite steel bridges. In Bridges 1A and 3A some of these cracks extended to the top surface of the slab in the early spring of 1959, and subsequently the cracks extended the full width of the slab. In Bridges 9A and 9B the first transverse cracks extending the full depth of the slab were found approximately one month after the traffic started. In the composite steel bridges 2B and 3B the first transverse cracks in the slab were discovered in August 1959.

The number of transverse cracks on the top surface increased with time. Figure 54 shows the progression of the crack formation for noncomposite bridge 1A and for composite bridge 2B. The number of cracks increased throughout the period of test traffic and was much larger in the noncomposite bridge. The relationships were typical of the two types of structures.

The transverse cracks in noncomposite bridges represented lines of progressive deterioration. A few months after their formation, these cracks were wide enough to permit free flow of water. The top edges of the cracks spalled with continued traffic, and toward the end of traffic pieces of concrete started falling out from the bottom surface of the slabs of Bridges 9A and 9B.

On composite bridges the cracks were limited in number and remained tight throughout the entire period of test traffic. Although, in the last year, water was able to seep through some of them, no deterioration was evident at these cracks.

The marked difference in the appearance of the slabs of composite and noncomposite bridges is shown in Figure 55, noncomposite bridge 9B in the left foreground and composite bridge 3B on the right. The photograph, taken after the conclusion of the test traffic, shows the transverse cracks on Bridge 9B; the short dark spots on Bridge 3B are tire marks.

Cracking of slabs caused decreases in the stiffness of steel bridges. The consequent increase of transient deflections (Tables 33 and 38) showed that this effect was larger on noncomposite than on composite bridges.

No transverse cracking was found in the slabs of concrete bridges. This and the timing of first cracking in the slabs of steel bridges suggest that shrinkage was an important factor in the development of transverse cracks.

Shrinkage took place primarily in the spring; the first transverse cracks were found in the spring and early summer of 1959 (Fig. 54).

In composite steel bridges shrinking of the slab is restrained by the beams so that tensile stresses develop in the slab. In concrete bridges shrinkage occurs not only in the slab but also

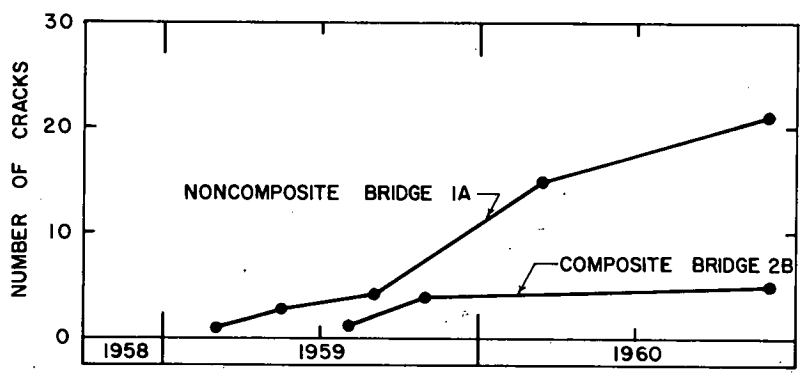

Figure 54. Formation of transverse cracks in bridge slabs.

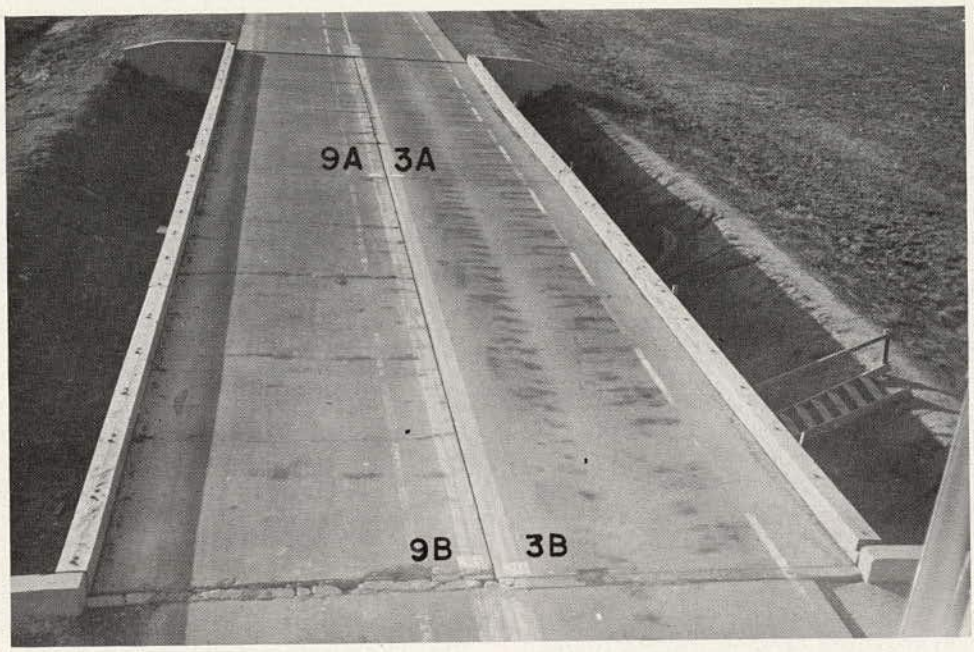

Figure 55. Bridge slabs on west end of Loop 6 at end of test traffic.

in the beams so that differential tensile stresses in the slab either do not develop at all or tend to be small. In noncomposite steel bridges, shrinkage of the slab cracked in tension is restrained by the longitudinal reinforcement and by friction between the slab and the beam.

Other Observations on Slabs.—The bridges were built with 1-in. spaces between the abutments and the slabs, and between adjacent slabs. After the beginning of the test traffic the slabs of the noncomposite bridges started moving in the direction of the test traffic, closing up the spaces at the exit abutment and between the two slabs located in tandem. To prevent damage to the slabs and the abutments, wooden blocks were inserted between the two vertical concrete surfaces in each gap, except that the opening at the approach end was left free to accommodate expansion.

At the exit end of Bridge 9B, the slab came in contact with the parapet wall. Progressive breakup of the end of the slab and of the parapet wall followed (Fig. 55).

The slabs of the steel bridges were thickened over the end diaphragms to be in contact with the top surface of the channel (Fig. 5). During the test traffic, a small gap formed between the bottom of the concrete and the top of the steel channel. In several instances this was followed by vertical cracking and later by crushing of the concrete. The crushing over the steel diaphragm was most extensive in Bridges 1A, 2B and 3B.

Supporting Members.—The rockers of the expansion bearings moved out of vertical position in all bridges shortly after the beginning of test traffic. The deviation increased with continuation of the traffic so that adjustments of the rockers were necessary several times during the period of traffic. The only bridges that required no rocker adjustments were the prestressed concrete bridges 6A and 6B. These bridges had the smallest transient deflections.

Before the beginning of test traffic, cracks were found in the parapet walls of the abutments. In general, these cracks caused no distress. However, in the spring of 1961 the parapet walls of the bridges located next to the rigid tangent pavement showed signs of breaking away from the wingwalls of the abutments and during the summer broke off completely at two locations. The manner of formation of the cracks suggested that this phenomenon was probably caused by expansion of the concrete pavement abutting the bridges.

3.3.9 Maintenance

Routine bridge maintenance included snow and ice removal, occasional adjustments of rocker bearings, dewatering of the excavations under the superstructures and painting of traffic guide lines. In addition, the cracking of the slabs and abutments necessitated minor repairs involving sealing with asphalt the cracks on Bridges 3A, 9A and 9B and filling in space above the parapet walls with cold asphaltic mix.

As a safety provision, timber cribs (Fig. 56) were erected under the test bridges at two intermediate points between the abutment and the pier. Sufficient space was left between the bottom of beams and the tops of the cribs to avoid contact while a test vehicle was on the

bridge. Whenever a bridge was eliminated from further tests, the cribs were brought up against the underside of the beams.

3.4 ACCELERATED FATIGUE TESTS

After the conclusion of the regular test traffic in December 1960, 7 out of the 13 surviving bridges were subjected to accelerated fatigue tests. The bridges were excited with a mechanical oscillator to such an amplitude that the maximum stress and the range of fluctuating stress at the critical section approximated the average condition observed during the test traffic. The vibration was continued at this amplitude until failure or until the total number of stress cycles reached 1,500,000 (including the cycles accumulated during the test traffic—each trip of a regular test vehicle was counted as one cycle of stress).

Bridges 2B, 5B, 6A, 6B, 7A, 7B and 8A were tested in accelerated fatigue. The available oscillators were incapable of properly exciting Bridges 1A, 5A, 9A and 9B. Bridges 3B and 8B were reserved for the tests to failure with increasing loads.

The accelerated fatigue tests were in all essential details equivalent to usual laboratory fatigue tests and thus differed in several respects from the tests under regular test traffic. (The differences between laboratory fatigue tests and the tests under regular test traffic are discussed in Section 3.5.) However, most of these differences were believed to be either susceptible to analytical interpretations or of relatively minor consequence. As it turned out, for those bridges that showed fatigue distress the number of stress cycles applied in the accelerated fatigue tests was small in relation to the number of vehicle trips, thus minimizing the effect of the over-all findings of the differences in the two types of tests.

3.4.1 Test to Failure of Bridge 2B

Bridge 2B sustained 558,400 trips of the assigned regular test vehicles. At the end of the test traffic, fatigue cracks were visible at five locations (Table 40). Three cracks were confined to the area of the toe of the weld. The crack at the south weld at the exit end of the cover plate on the center beam extended from the weld to the near edge of the flange. The crack at the south weld on the approach end of the cover plate on the interior beam extended the full depth of the bottom flange from the edge to the web.

At the beginning of the accelerated fatigue test, weights were placed on the bridge to compensate for the upward deflections caused by the oscillator. The resulting stresses at the ends of the cover plates are given in Table 44. The added dead load stresses measured during these tests were 7.0 ksi or higher except at the location of the large fatigue crack (approach end of interior beam).

The response of the bridge during the accelerated fatigue tests went through three distinct phases. The first phase included 25,800 cycles; the second phase, the period from 25,800 through 47,500 cycles; and the third phase, the remainder of the test.

During the first phase, the stresses were applied at a mean frequency of 3.10 cps. The bridge responded to the excitation extremely

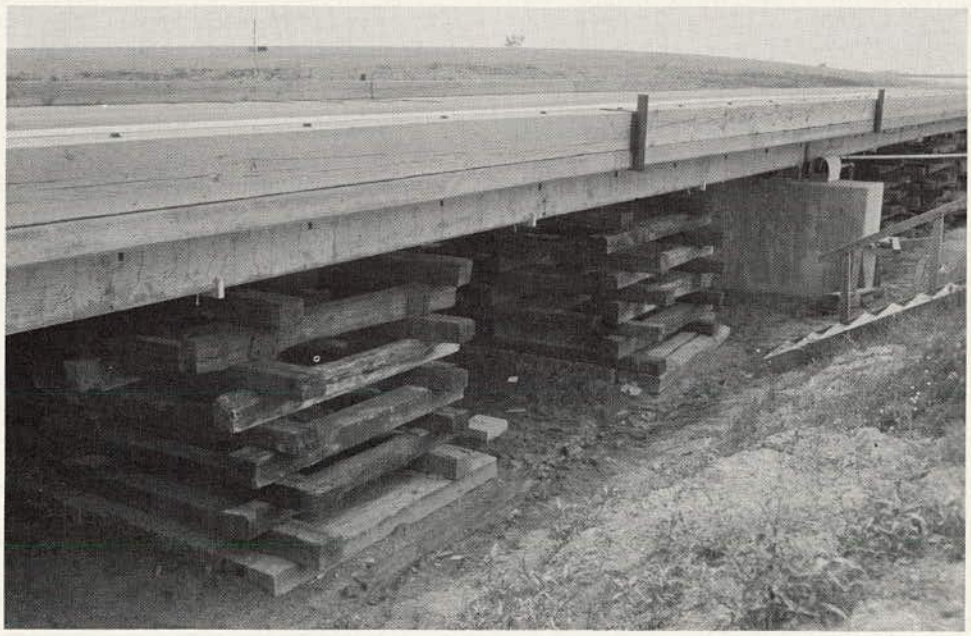

Figure 56. Safety cribs under Bridge 7B.

TABLE 44
ACCELERATED FATIGUE TEST DATA FOR BRIDGE 2B

Critical Section	Beam	Added Dead Load Stress (ksi)	Mean LL Stress (ksi)		Std. Dev., Mean LL Stress (ksi)		No. Cycles in Accel. Tests to		
							Fatigue Cracking		Complete Fracture Bottom Flange
			First Phase	Second Phase	First Phase	Second Phase	North Weld	South Weld	
Approach end	Interior	6.2	10.8	—	1.061	—	20,000	—[1]	25,800
	Center	7.6	15.0	21.6	1.390	2.833	—[1]	—[1]	47,200
	Exterior	7.5	15.6	14.9	0.823	0.889	47,500	47,500	
Exit end	Interior	7.1	11.2	10.9	0.584	0.632	—[2]	—[2]	
	Center	7.4	11.9	14.4	0.635	0.882	—[1]	—[1]	
	Exterior	7.0	12.6	14.1	0.706	0.740	—[2]	—[2]	

[1] Cracking present prior to accelerated tests.
[2] No fatigue cracks found.

well so that only infrequent adjustments of the operating frequency were required. The deviations from the mean frequency were very small; the standard deviation was 0.010 cps.

The additional cycles of stress caused growth of cracks primarily at the approach end of the cover plate on the inside beam. The large crack, originating at the south weld, extended slowly up the fillet between the bottom flange and the web. At 17,100 post-traffic cycles, the crack became visible on the north face of the web; at 20,000 cycles, a small crack was found at the north weld; and at 24,500 cycles, the two cracks joined. At 25,800 cycles, the flange fractured completely, and the crack extended 6.1 in. up the web.

Throughout the first phase, the live load stresses in the bottom flange held at a reasonably constant level, except for the approach end of the interior beam where some progressive decrease in stress was noted. The deflections were also stable. The means and standard deviations of the observed live load stresses are given in Table 44.

After the bottom flange of the interior beam broke at 25,800 post-traffic cycles, the operating frequency had to be lowered to 2.84 cps. During the next 21,700 cycles, the frequency had to be decreased very gradually; it was 2.76 cps by the time 47,200 were reached. During this second phase, the crack in the interior beam extended up the web, cracks on the center beam showed a substantial growth, and a crack became visible at the toe of each weld at the approach end of the cover plate on the exterior beam.

The crack on the interior beam opened up and moved rapidly up the web. At 26,700 post-traffic cycles, signs of spalling of concrete were noted on the bottom face of the slab near the crack in the beam, indicating that the slab was unable to follow the large concentrated rotations at the crack and tended to separate from the beam. The separation was resisted by shear connectors anchored in the concrete. At 27,800 cycles, the fatigue crack reached the bottom of the top flange and from then on extended progressively in both directions toward the edges of the top flange.

The north crack at the approach end of the plate on the center beam grew slowly toward the north edge of the flange, up the flange and toward the web. It reached the web at 44,200 post-traffic cycles and suddenly extended the full width and depth of the bottom flange and 6 in. up into the web.

The south crack at the exit end of the plate on the center beam extended slowly up the edge and along the top surface of the bottom flange. Its maximum visible length on the top of the flange was 1.5 in.

All other cracks remained confined to their respective weld regions.

The stresses at the ends of the cover plates were higher than during the first phase of the test, except in the interior beam (Table 44). The deflections were higher than in the first phase, particularly in the interior beam.

After 47,500 post-traffic cycles, the test was stopped for observations. On restarting the oscillator, it was impossible to excite the bridge to the desired amplitude. The response of the bridge was erratic. The count of revolutions of the oscillator, although continued, became meaningless because the bridge often failed to respond.

During the third phase, the large crack in the center beam extended to the bottom of the top flange, spalling of concrete occurred on the bottom of the slab in the vicinity of the fatigue crack in the center of the beam, and the fracture of the interior beam became complete. The fractured beam is shown in Figure 57; the separation of the beam from the slab and the failure on the bottom of the slab are visible.

Four times during the test, the oscillator and the weights were removed from the bridge, and a regular test vehicle assigned to Bridge 2B

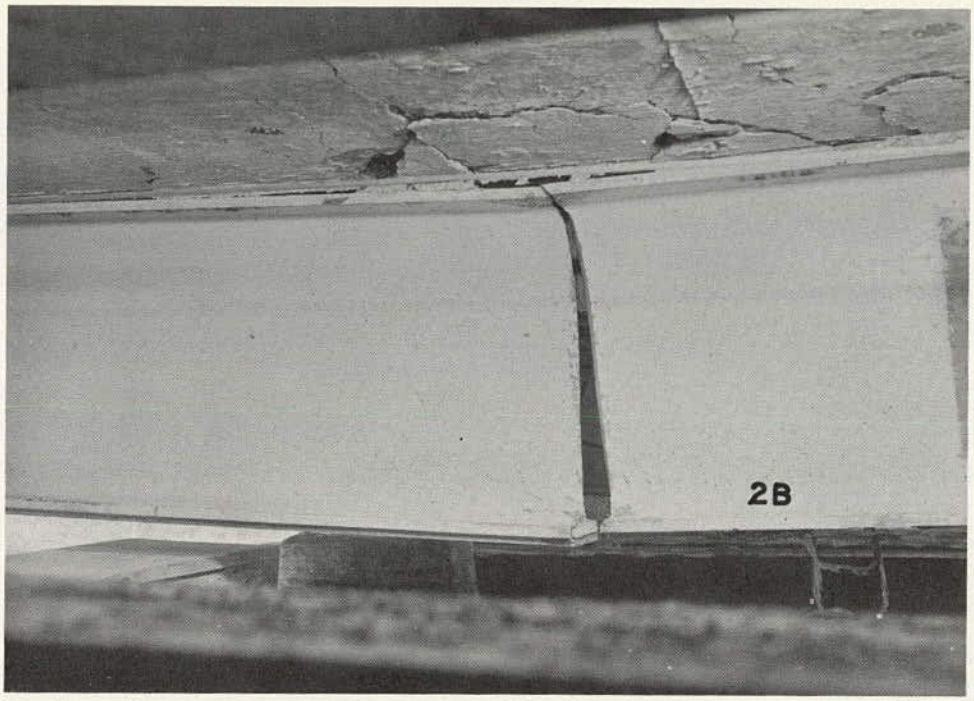

Figure 57. Fatigue failure of Bridge 2B.

made several trips over the bridge: 20 trips at 20,000 post-traffic cycles, 40 at 25,300 cycles, 30 at 25,800 and 3 at the end of the test. The first three sets of trips caused only very minor increases in the length of the larger cracks. On the other hand, the last three trips caused yielding of the exterior beam and rupture of the center beam. During the last trip, the large crack in the center beam extended through the top flange completing the break. After the rupture of the center beam, the exterior beam touched the safety crib before the vehicle could clear the bridge.

3.4.2 Tests to Failure of Bridges 7A and 7B

Accelerated fatigue tests of Bridges 7A and 7B were similar in all respects. The added weights increased the dead load stresses at midspan by about 10 ksi, and the oscillator caused live load stresses of approximately 25 ksi (Table 45). The mean frequency of transient bridge deformations was 2.47 cps on Bridge 7A, and 2.38 cps on Bridge 7B. There was no systematic variation of the frequency. The standard deviations were 0.039 and 0.024 cps.

The tests proceeded smoothly for more than 170,000 post-traffic cycles. At 172,600 cycles, the strain gages at midspan of the exterior beam on Bridge 7B began to drift. A few minutes later, before the cause of drift could be established, the gages stopped functioning, and the response of the other gages decreased appreciably. The testing was stopped at 174,000 post-traffic cycles.

An inspection of the beams showed that the concrete cover on the exterior beam fell off at both sides of midspan, and the north and center bars in the bottom layer were fractured (Fig. 58). The north bar fractured at midspan, and the center bar at 10 in. west of the break of the north bar. Both fractures passed through the corners of the diamonds formed by deformations (indicated by arrows, Fig. 59).

The south bar in the same beam was not broken, but several incipient cracks were found in the corners of the deformation diamonds. Five such cracks are shown in Figure 59.

In the test of Bridge 7A, bar fracture was signaled by a loud noise at 172,200 post-traffic cycles. The oscillator was stopped before the concrete cover could break off the beam. An inspection revealed a fatigue fracture in the center bar 10 in. away from midspan. The break was visible through the access hole for mechanical strain readings but did not go through the gage hole in the bar. A second fatigue fracture was discovered after the removal of concrete cover. It was located in the north bar 6 in. east of the fracture in the center bar. Incipient cracks were found in the south bar. All fractures and cracks passed through corners of the deformation diamonds.

An inspection of the bars in the two other beams of both bridges did not reveal any fatigue cracks.

3.4.3 Tests of Bridges 5B, 6A, 6B and 8A

The accelerated fatigue tests of prestressed concrete bridges 5B, 6A and 6B, and of rein-

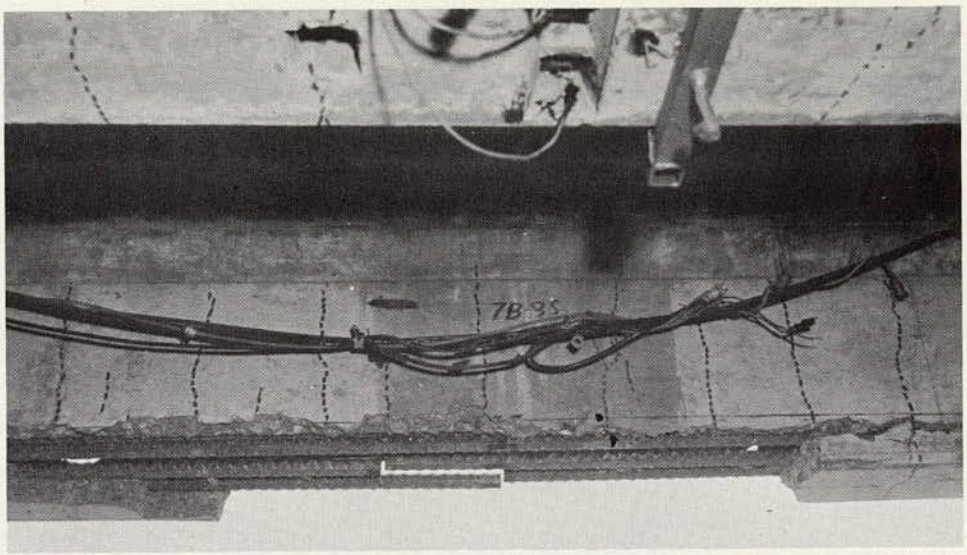

Figure 58. Fatigue failure of bars in Bridge 7B.

forced concrete bridge 8A, produced no substantial changes in the bridge appearance and behavior. The testing proceeded smoothly; the frequency of transient bridge deformations, the stresses and the deflections fluctuated around the means given in Table 45. Each of the three bridges was subjected to a total of approximately 1,500,000 cycles of live load stress with-

TABLE 45

ACCELERATED FATIGUE TEST DATA FOR CONCRETE BRIDGES

Bridge	Beam	Added Dead Load Stress (ksi)	Frequency of Bridge Deformations (cps)		Live Load Stress at Midspan (ksi)		Live Load Defl. at Midspan (in.)		No. of Cycles Applied
			Mean	Std. Dev.	Mean	Std. Dev.	Mean	Std. Dev.	
(a) PRESTRESSED CONCRETE									
5B	Interior	2.2	4.91	0.094	4.3	0.67	0.36	0.06	949,000
	Center	2.1			4.3	0.64	0.39	0.06	
	Exterior	2.4			4.5	0.73	0.37	0.07	
6A	Interior	1.8	4.62	0.107	2.5	0.23	0.28	0.04	943,400
	Center	2.1			13.4	2.00	0.25	0.03	
	Exterior	2.4			11.1	1.68	0.34	0.05	
6B	Interior	2.0	5.01	0.173	2.3	0.47	0.23	0.05	942,100
	Center	2.1			2.6	0.52	0.21	0.04	
	Exterior	1.9			2.6	0.50	0.25	0.07	
(b) REINFORCED CONCRETE									
7A	Interior	10.2	2.47	0.039	26.1	0.79	1.69	0.06	172,200 [1]
	Center	10.0			25.1	0.88	1.58	0.05	
	Exterior	10.7			25.8	0.86	1.67	0.05	
7B	Interior	9.8	2.38	0.024	23.1	1.88	1.54	0.12	174,100 [1]
	Center	10.7			24.5	1.49	1.48	0.11	
	Exterior	10.1			26.6	0.63	1.42	0.11	
8A	Interior	6.7	2.70	0.016	15.5	1.40	0.93	0.08	941,600
	Center	6.7			15.9	1.45	0.93	0.09	
	Exterior	7.1			16.1	1.42	0.98	0.10	

[1] Two No. 11 bars in the exterior beam fractured.

out failure. The numbers of stress cycles, applied during the accelerated fatigue test period, are given in Table 45.

No cracks were found on Bridge 5B during the inspection prior to the accelerated fatigue test. The cracks in the center and exterior beam which had been found during the period of test traffic (Section 3.3.6) could not be found at this time. A few hairline cracks were found after 600,000 cycles and, at the end of the test, on to four hairline cracks were noted on the side faces of all three beams. The width of the cracks was of the order of 0.001 in. All cracks were detected with the aid of the epoxy resin coat and were confied to the vertical faces of the bottom flanges. No connection could be traced on the bottom face between the cracks on opposite sides of the same beam.

All three beams of Bridge 6A were cracked before the beginning of the test. However, the stress indicated that no crack crossed the gages at midspan of the interior beam (Table 45). The results of the crack measurements after the test were essentially the same as those before the test.

Bridge 6B had one or more hairline cracks in each beam before the accelerated fatigue testing began. The fatigue tests resulted in one additional crack in the center beam. As in the test of Bridge 5B, this crack was found with the aid of epoxy resin. All cracks were confined to the vertical surfaces of the bottom flanges, and no connection could be traced between the cracks on opposite surfaces of the same beam. The crack widths were of the order of 0.001 in.

The accelerated fatigue test of Bridge 8A caused a small increase in the number and width of cracks. No other changes were detected in this bridge.

3.5 ANALYSIS OF FATIGUE STRENGTH OF BEAMS

Fatigue cracking of steel beams with partial length cover plates (Sections 3.3.3 and 3.4.1), cracking of prestressed concrete beams during the regular test traffic and accelerated fatigue tests (Sections 3.3.6 and 3.4.3), and fatigue failures of reinforcing bars (Section 3.4.2) furnished data for quantitative comparisons with the results of simpler laboratory tests. Although less effective, comparative data were provided by those bridges that survived a large number of repetitions of stress without any visible fatigue damage.

The laboratory tests, used in the comparisons presented in this section, were made on specimens closely approximating essential details of corresponding bridge beams. Specimens were subjected to repeated loading fluctuating between a minimum and a maximum level until fatigue cracking or failure developed. During any one test, both the minimum and the maximum stress were kept constant. The results were expressed in the form of equations relating the number of cycles causing cracking or failure to the test stresses. Fatigue strength of steel members (Section 2.2.1) was expressed in terms of the maximum stress and the stress range (*i.e.*, the difference between the maximum and minimum stresses). The probability of survival of concrete without cracking was expressed in terms of the tensile stress range (Section 2.2.2).

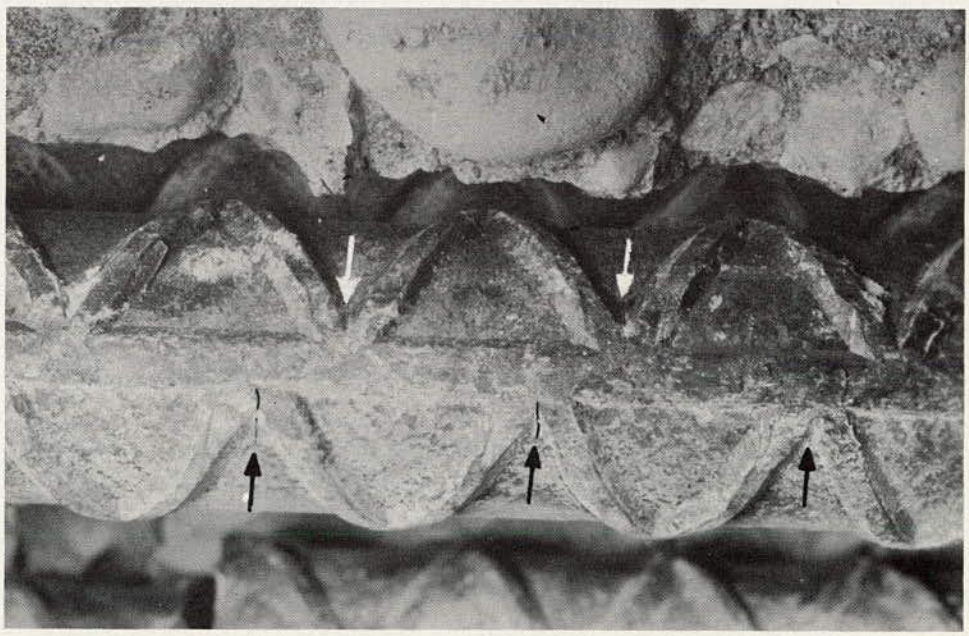

Figure 59. Incipient fatigue cracks in reinforcing bars.

The test bridges were also subjected to stresses fluctuating between minimum and maximum levels. However, unlike in the laboratory tests, neither the minimum stress nor the stress range remained constant through the duration of the test. Furthermore, although in the laboratory tests the stress fluctuations followed a simple sine wave, in the bridge tests the shape of the time-stress curves was irregular including major stress waves caused by the weight of the moving vehicles, minor stress waves caused by vibrations of the bridge and rest periods corresponding to the intervals between the trucks and to breaks in the test traffic. Finally, in the laboratory tests the duration of one stress cycle was of the order of 1 sec or less, whereas in the bridges tests the intervals of the major stress cycles, corresponding to vehicle trips, were of the order of 40 sec or more. Thus the stress histories of the bridge tests differed considerably from those of the laboratory tests. To be meaningful, the comparisons between the two types of tests had to account for at least the major differences in these stress histories.

Minimum Stress and Stress Range in Bridge Tests.—The minimum stress and the stress range represent two principal characteristics of the stress histories. They were evaluated for each critical bridge section from dead load, live load and rebound stresses observed during the regular test traffic and from the ranges of stress observed in the accelerated fatigue tests. The minimum stress was obtained as the difference between the dead load stress and the rebound stress. The stress range for the regular test traffic was obtained as the sum of the maximum live load stress and the rebound stress.

TABLE 46

COMPARISON OF FATIGUE STRENGTH OF STEEL BRIDGES WITH LABORATORY DATA

Bridge	Beam	Critical Section	Bridge Tests				$\frac{n_1}{N_1'}$	Miner's Hypothesis, $\Sigma(n_r/N_r')$
			Min. Stress (ksi)	Stress Range (ksi)		Cycles to Cracking[1]		
				Mean	Std. Dev.			
(1)	(2)	(3)	(4)	(5)	(6)	(7)	(8)	(9)
1A	Interior	Approach	10.7	13.3	1.20	556,900	0.53	0.54
	Center	Approach	13.8	13.6	0.92	536,000	0.57	0.59
	Exterior	Approach	16.5	12.8	0.94	536,000	0.53	0.56
	Interior	Exit	10.5	15.5	1.17	557,300	0.77	0.79
	Center	Exit	13.6	15.7	0.98	536,000	0.82	0.84
	Exterior	Exit	16.1	15.1	1.04	536,000	0.79	0.81
2B	Interior	Approach	14.0	15.9	1.75	531,500	0.84	0.87
	Center	Approach	18.0	15.8	1.74	531,500	0.90	0.95
	Exterior	Approach	21.1	15.2	1.80	606,000	1.00	1.07
	Interior	Exit	14.2	16.2	1.25	(608,500)	(0.97)	(1.03)
	Center	Exit	18.0	15.4	1.39	531,500	0.84	0.87
	Exterior	Exit	21.2	15.1	1.45	(608,500)	(0.99)	(1.04)
3B	Interior	Approach	12.2	13.7	1.60	(557,800)	(0.58)	(0.61)
	Center	Approach	15.0	14.0	2.08	535,500	0.62	0.67
	Exterior	Approach	17.9	13.3	1.63	(557,800)	(0.62)	(0.65)
	Interior	Exit	12.2	13.5	1.66	(557,800)	(0.56)	(0.58)
	Center	Exit	15.1	13.4	1.31	(557,800)	(0.59)	(0.61)
	Exterior	Exit	17.9	13.4	1.59	557,800	0.63	0.70
9A	Interior	Approach	6.2	17.8	1.47	(477,900)	(0.89)	(0.89)
	Center	Approach	7.8	17.3	0.82	(477,900)	(0.86)	(0.85)
	Exterior	Approach	9.4	16.1	1.44	477,900	0.72	0.74
	Interior	Exit	6.1	17.8	1.24	(477,900)	(0.89)	(0.88)
	Center	Exit	7.8	17.1	1.03	(477,900)	(0.83)	(0.83)
	Exterior	Exit	9.2	16.4	1.21	477,900	0.76	0.77
9B	Interior	Approach	5.7	17.7	1.64	(477,900)	(0.87)	(0.89)
	Center	Approach	6.7	17.6	1.40	477,900	0.81	0.90
	Exterior	Approach	8.6	17.1	1.60	(477,900)	(0.85)	(0.87)
	Interior	Exit	5.8	17.9	1.61	(477,900)	(0.90)	(0.91)
	Center	Exit	6.6	17.6	1.48	(477,900)	(0.88)	(0.89)
	Exterior	Exit	8.5	16.9	1.90	(477,900)	(0.82)	(0.85)
Over-all mean							*0.774*	*0.794*

[1] Number of cycles given in parentheses for specimens in which no cracks were found during either regular test traffic or accelerated fatigue tests.

TABLE 47

STRESS RANGE AND FATIGUE LIMIT FOR BRIDGES WITHOUT FATIGUE FAILURE

Bridge	Total No. of Cycles	Minimum Stress (ksi)	Mean Range of Steel Stress (ksi)			Stress Range at Endurance (ksi)
			Interior Beam	Center Beam	Exterior Beam	
3A	392,400	12.7	19.1	18.9	21.0	28.0 [1]
5A	556,700	146.3	22.6	20.2	26.2	49.0 [2]
5B	1,505,700	151.4	4.8	4.0	4.3	48.0 [2]
6A	1,500,200	165.1	2.6	5.0	7.1	35.0
6B	1,498,900	170.9	2.6	2.7	2.8	35.0
8A	1,500,000	18.3	17.7	16.9	16.6	24.0
8B	558,400	18.0	17.2	16.7	17.7	24.0

[1] Estimated fatigue strength at 2,000,000 cycles—computed as $(31.2 - 0.25 \times 12.6)$ ksi.

[2] Function of minimum stress level; the value given is the lowest for the three beams of the bridge.

The minimum stress at any particular critical section was considered constant. It was computed from the values of dead load stresses given in Tables 29, 30 and 31 and from rebound stresses computed from mean live load stresses and the rebound factors given in Tables 38 and 41.

The stress range was considered variable. It was evaluated from the samples of live load and rebound stress obtained during the regular test traffic and from the samples of the stress range obtained during the accelerated fatigue tests. For any particular critical section of a beam, the distribution of the stress range was assumed equal to the composite distribution of individual samples around the means for each sampling period. On the basis of this distribution and the known number of trips of vehicles during every sampling period, it was possible to determine the number of trips corresponding to each selected interval of stress range. A summation of the number of trips in each interval for all sampling periods resulted in the histogram of stress range for the period of regular test traffic.

The distribution of the stress range during the accelerated fatigue tests was assumed normal. The known total number of cycles, the mean stress range and the standard deviation permitted construction of a histogram with the same intervals as those used for the regular tests. The two histograms, one for the regular test traffic and the other for accelerated fatigue tests, were combined to give the final histograms of the stress ranges to which the critical section was considered to have been subjected. For most of the sections, it would have been equally accurate to assume normal distribution also for the stresses caused by regular test traffic (Tables 38 and 41).

For almost all critical sections, the final histograms of the stress range showed normal distribution. The means and standard deviations of the final histograms for critical sections of bridges with fatigue cracks (or failure) in steel are given in Tables 46 and 49. There was a considerable variation in the magnitude of the stress range: for example, mean stress range at the critical section off the approach end of the cover plate on the interior beam of Bridge 1A was 13.3 ksi, but the smallest stress range was less than 10.9 ksi and the largest stress range was more than 15.7 ksi. Nevertheless, the variations in the stress range were smaller than one could expect to find under mixed traffic on bridges in the highway system.

The minimum stresses and mean stress ranges for bridges without visible fatigue distress in steel are given in Table 47.

Comparisons Between Bridge and Laboratory Tests.—In comparing quantitatively the results of the bridge tests with laboratory data, the only characteristics of the stress histories considered were the minimum stress and the stress range. The effects of the speed of loading, rest periods and vibrations were disregarded primarily because of lack of methods which would permit their inclusion in the analysis.

For bridges that showed no sings of fatigue distress, the mean stress range to which the critical bridge section was subjected was compared with the endurance limit. The endurance limit was estimated on the basis of laboratory tests and the minimum stress observed in the bridge tests. More refined methods of comparison were considered unnecessary because in all cases the endurance limit was substantially higher than the observed mean stress range (Sections 3.5.1, 3.5.3 and 3.5.4).

For prestressed concrete bridges that showed fatigue cracking of concrete, comparisons with laboratory tests were based primarily on the probability of survival (Section 3.5.3).

For bridges that showed signs of fatigue distress in steel, the comparisons were based on fatigue strength Eqs. 1 and 8. Two methods were used: one comparing the total observed number of stress cycles with that computed for mean stress range and another utilizing the hypothesis of cumulative damage proposed by Miner.* The two methods, presented in detail in Section 3.5.2 were used for comparisons included in Sections 3.5.2 and 3.5.4.

3.5.1 Steel Beams Without Cover Plates

The 392,400 trips of regular test vehicles over Bridge 3A caused no fatigue cracking. Wilson * has shown by laboratory tests that a rolled beam of A-7 steel tested from zero stress to a tension of 31,200 psi has a fatigue life of about 2,000,000 cycles.

Table 47 gives the minimum stress for the three beams and the mean range of stress for each beam of Bridge 3A. Assuming that an increase in minimum stress decreases fatigue strength, the stress range expected to cause fatigue cracking in Bridge 3A after 2,000,000 cycles was estimated as 28 ksi. It is apparent that fatigue cracking should not have developed in any beam of Bridge 3A in 392,400 cycles. As none had developed, the test of Bridge 3A was in agreement with Wilson's finding.

3.5.2 Steel Beams with Cover Plates

Mean Stress Range.—According to the laboratory tests, fatigue cracking in a steel beam with partial-length cover plates, of the type used in the test bridges, may be expected to occur when the number of cycles of stress is equal to or larger than that given by

$$\log N_1 = 7.136 - 0.0742\,S_r - 0.0102\,S_{min} \pm 0.257 \qquad (1)$$

in which

S_{min} = minimum stress, ksi; and

S_r = stress range, ksi.

The values of the minimum stress, S_{min}, are given in Table 46 for the five steel bridges in which fatigue cracks were found. The values of the stress range are given in terms of the mean (Col. 5) and the standard deviation (Col. 6). As long as the standard deviation is small, the stress range is essentially constant and the mean stress range may be used for S_r in Eq. 1.

With S_{min} and S_r known, the number of cycles to first cracking, N_1, may be computed from Eq. 1. However, two values of N_1 are obtained: they represent the limits of the laboratory data. When the observed number of cycles to first cracking n_1 falls within these limits, the test may be said to be within the estimate indicated by laboratory tests.

The need for computation and tabulation of two values of N_1 may be avoided by rewriting Eq. 1 as follows: Designating the mean estimate of the number of cycles to cracking as N'_1, Eq. 1 becomes

$$N_1 = N'_1\,10^{\pm 0.257} \qquad (15)$$

Substitution of the observed number of cycles n_1 for the estimated number of cycles N_1 and rearrangement shows that the result of the bridge test is in agreement with the laboratory data as long as

$$\frac{n_1}{N'_1} = 10^{\pm 0.257} \qquad (16)$$

The ratios n_1/N'_1 are listed in Column 8 of Table 46. The limits of variability of the laboratory data, given by the right side of Eq. 16, are 0.55 and 1.83.

Miner's Hypothesis.—It has been pointed out that the use of the mean stress range in place of S_r is justified if the variations in the stress range are small. The standard deviations (Col. 6, Table 46) show that, although not extreme, the variations in the stress range were substantial. It is possible, then, that the analysis based on the mean stress range is too crude and a more refined method, accounting for the variations in the stress range, may be required.

The effect of the variations in the range of the fluctuating stress may be accounted for with the aid of Miner's hypothesis. Accordingly, at fatigue failure the sum of the ratios of the actual number of cycles at each particular stress to the number of cycles required to cause failure at the same stress is equal to unity.

$$\sum_{x=1}^{x=m} \frac{n_x}{N_x} = 1.0 \qquad (17)$$

in which

n_x = actual number of cycles of stress S_x;

N_x = number of cycles of stress S_x that would be required to cause failure by stress S_x alone;

x = 1, 2, . . ., m—a number denoting the intervals of stress in the histogram of the fluctuating stress;

m = total number of stress intervals in the histogram; and

S_x = mean stress of interval x.

* Miner, M. A., "Cumulative Damage in Fatigue." *Jour. of Applied Mechanics*, pp. A-159—A-164 (Sept. 1945).

* Wilson, W. M., "Flexural Fatigue Strength of Steel Beams." Univ. of Illinois, Eng. Exp. Sta., Bull. 377 (1948).

The values of n_x and N_x in Eq. 17 may be obtained from the known minimum stress, histogram of the stress range and Eq. 1.

If the stress axis of the histogram of the stress range is divided into small enough increments, the stress of each increment may be represented accurately by the mean S_{rx}. (As the test data were evaluated in terms of the stress range, the symbol S_{rx} is used instead of the general notation S_x.) The number of stress repetitions n_x falling into each interval is given by the histogram. The number of cycles N_x required to cause failure under the known minimum stress S_{min} and the stress range S_{rx} may be computed from Eq. 1.

$$\log N_x = 7.136 - 0.0742\, S_{rx} - 0.0102\, S_{min} \pm 0.257 \qquad (18)$$

Using the notation N'_x to designate the estimate of the mean number of cycles to failure, the equation becomes

$$N_x = N'_x\, 10^{\pm 0.257}$$

and Eq. 17 may be expressed in the following form:*

$$\sum_{x=1}^{x=m} \frac{n_x}{N'_x} = 10^{\pm 0.257} \qquad (19)$$

in which N'_x is the mean number of cycles to failure for stress S_{min} and stress range S_{rx}. As long as the summation of ratios n_x/N'_x falls within the range $10^{\pm 0.257}$, the test may be said to be within the estimate indicated by the laboratory data.

The left side of Eq. 19 was evaluated for all critical sections of Bridges 1A, 2B, 3B, 9A and 9B on the basis of histograms of stress range having intervals of 0.3 ksi for Bridge 1A and 0.5 ksi for the other bridges. The resulting sums of ratios are listed in Column 9 (Table 46). The limits of variability of the laboratory data, given by the right side of Eq. 19, are 0.55 and 1.83.

Generally, the sums of ratios in Column 9 are higher than the ratios in Column 8, based on mean stress range. But the differences are small so that the two methods may be considered equally suitable for the conditions encountered in the steel test bridges.

Discussion of Results.—All but three ratios in Columns 8 and 9 (Table 46) are within the range 0.55 to 1.83 representing the variability of the test data; therefore, the analyses indicate that the fatigue strength of steel bridges with partial-length cover plates was in agreement with the results of laboratory tests. However, almost all ratios are less than 1.0. Although these low ratios may be explained in part by the fact that the tests were discontinued before the development of visible cracks at half of the sections considered (values in parentheses), several other factors could have contributed to this result.

With few exceptions, the ratios for Bridges 1A and 3B were lower than the ratios for the other bridges. Bridges 1A and 3B were located in the inside lanes and were crossed a few times by the heavier vehicles from the adjacent lane. The last passage of such vehicles preceded the first discovery of the fatigue cracks by 10,000 trips on Bridge 1A and by 75,000 trips on Bridge 3B. It is possible that this overstressing, particularly on Bridge 1A, helped to make the fatigue cracks visible earlier than would have been the case otherwise.

The mean stress range on the approach end of Bridge 1A and on both ends of Bridge 3B never exceeded 14 ksi. At all other locations it was always equal to or more than 15 ksi. The lower mean was consistently accompanied by the lower ratios, suggesting that the effect of the stress range was either slightly different from that observed in the laboratory or it was not considered properly in the analysis.

Several known differences between the laboratory and bridge tests were not included in the analyses, such as speed of loading, secondary stress cycles caused by vibrations and rest periods. Although information available in the literature suggests that the individual effects of these differences were probably small, their cumulative effect could well have caused observable differences between the results of the bridge and laboratory tests.

3.5.3 Prestressed Concrete Beams

Table 47 gives the minimum stress in the tension steel and the mean range of the steel stress for all prestressed concrete beams, as well as the stress range corresponding to the endurance limit (Section 2.2.1). According to the laboratory tests, no fatigue failure should have occurred in the prestressing steel. No failures occurred during either the regular test traffic or the accelerated repeated load tests.

At the beginning of the regular test traffic, tension cracks in concrete were found to form only in three beams of Bridge 5A and one beam of Bridge 6A. However, by the conclusion of the accelerated fatigue tests several tensile cracks were present in all beams. All cracks in Bridges 5B and 6B, as well as most of the cracks in Bridge 6A, appeared to be of a very limited extent, and none could be detected without special aids.

Several attempts were made to correlate the number of stress cycles at which the cracks

* The limits of variability ± 0.257 were assumed independent of x. A more rigorous error analysis involves the probability distribution of individual variation and the moments of distribution. It turns out, however, that the right side of Eq. 19 represents a suitable approximation for the corresponding interval developed from the more rigorous analysis.

TABLE 48
CRACKING OF PRESTRESSED CONCRETE BEAMS

Bridge	Beam	Stress (psi)		Cycles to Cracking
		Minimum	Maximum	
5B	Interior	−859	141	1,156,700
	Center	−643	289	144,000
	Exterior	−321	663	144,000
6A	Interior	5	545	303,600
	Center	129	681	98,900
	Exterior	473	1,370	69,000
6B	Interior	−470	95	556,800
	Center	−374	214	556,800
	Exterior	9	600	303,600

were first noted in the concrete of the individual bridge beams with available laboratory data for fatigue strength of plain concrete beams. Because of large dispersion in the laboratory data and the probabilistic nature of the problem, principal attempts at correlation were made with the aid of Eq. 11. No satisfactory correlation was found. Other studies, involving data reported by Murdock and Kesler,* were also unsuccessful.

The minimum stress level, the maximum stress level and the number of cycles at which the cracks in concrete were discovered are given in Table 48. It is apparent that no consistent correlation was present between the number of cycles and the stress levels. This lack of correlation explains the lack of success in applying the results of laboratory tests to the results of the bridge study.

3.5.4 Reinforced Concrete Beams

Two No. 11 bars in the exterior beam of Bridge 7A and in the exterior beam of Bridge 7B fractured during the accelerated fatigue tests. The numbers of cycles at failure of the bars were examined with the aid of the two methods described in detail in Section 3.5.2 and Eq. 8 obtained from laboratory tests.

Mean Stress Range.—The final equation used in the comparisons of the results of tests of reinforced concrete bridges with laboratory data was

$$\frac{n_5}{N'_5} = 10^{\pm 0.182} \qquad (20)$$

in which

n_5 = observed number of cycles to failure (Table 49, Col. 6) ; and
N'_5 = mean estimate of the number of cycles to failure computed from Eq. 8 and the mean stress range (Table 49, Col. 4).

The ratios are listed in Column 7 of Table 49.

Miner's Hyopthesis.—For reinforced concrete bridges, the final equation based on Miner's hypothesis was written as follows:

$$\sum_{x=1}^{x=m} \frac{n_x}{N'_x} = 10^{\pm 0.182} \qquad (21)$$

* Murdock, J. W., and Kesler, C. E., "Effect of Range of Stress on Fatigue Strength of Plain Concrete Beams." *Jour. of A.C.I.*, pp. 221-231 (August 1958).

TABLE 49
COMPARISON OF FATIGUE STRENGTH OF REINFORCED CONCRETE BRIDGES WITH LABORATORY DATA

Bridge	Beam	Bridge Tests				$\frac{n_5}{N_5'}$	Miner's Hypothesis, $\Sigma(n_x/N_x')$
		Minimum Stress (ksi)	Stress Range (ksi)		Cycles to Failure [1]		
			Mean	Std. Dev.			
(1)	(2)	(3)	(4)	(5)	(6)	(7)	(8)
7A	Interior	15.7	27.5	2.61	(728,300)	(0.66)	(0.71)
	Center	16.1	25.5	2.61	(728,300)	(0.54)	(0.53)
	Exterior	19.5	25.8	2.50	728,300	0.57	0.60
7B	Interior	14.7	25.0	3.36	(730,200)	(0.52)	(0.57)
	Center	15.1	25.1	3.17	(730,200)	(0.53)	(0.57)
	Exterior	18.1	26.4	2.97	730,200	0.63	0.66
Over-all mean						*0.575*	*0.650*

[1] Cycles in parentheses for specimens in which no failure occurred during either regular test traffic or accelerated fatigue tests.

Figure 60. Special vehicle with extra heavy load during test to failure with increasing loads.

in which

n_x = actual number of cycles of stress S_{rx};
$\log N'_x = 7.432 - 0.0515\, S_{rx}$; and
S_{rx} = mean stress of interval x.

In computing the left side of Eq. 21, 1-ksi stress intervals were used. The resulting sums of ratios are listed in Column 8.

Discussion of Results.—A comparison of Columns 7 and 8 shows that, as for steel beams with partial-length cover plates, the differences between the two methods were small. On the other hand, except for the interior beam of Bridge 7A and for the exterior beam of Bridge 7B, the ratios were outside the range of laboratory tests equal to 0.66 through 1.52. However, only the values for exterior beams relate to failure conditions; the results for both of these beams were on the lower edge of the band representing laboratory tests. Failure of the other four beams would have required further additional cycles of stress leading to higher ratios than those shown.

For Bridges 8A and 8B, the laboratory tests indicated a 24-ksi endurance limit, well above the actual mean stress ranges shown in Table 47. No fatigue failures occurred in either of the two bridges even though one, Bridge 8B, was subjected to 1,500,000 cycles of stress.

3.6 TESTS TO FAILURE WITH INCREASING LOADS

Steel bridges 1A, 3B, 9A and 9B, prestressed concrete bridges 5A, 5B, 6A and 6B, and reinforced concrete bridges 8A and 8B were tested to failure with vehicles loaded with successively heavier loads (Fig. 60). These tests were conducted in order to study the response of the bridges to loads approaching their ultimate capacity, to determine the manner of failure under moving loads, and to provide approximate test data for checking ultimate strength theories.

Each selected load usually crossed the bridge 30 times. The test was discontinued when the concrete of the slab was crushed, the tension steel fractured, or when an already extreme permanent set at midspan continued to increase at an increasing rate with each successive trip of the vehicle.

The results of tests to failure with increasing loads are presented in the form of moment-deflection diagrams and set-trip diagrams. The two plots describe in detail the history of one test.

The moment-deflection diagram (Fig. 61) is a plot of the maximum static moment, caused at midspan by the test vehicle, as a function of the mean deflection at midspan. The static moment is computed from the known axle weights and spacings. The deflection is the mean of the deflections measured on the three beams. It includes both the elastic deformation and the permanent sets accumulated from the beginning of tests with increasing loads.

The first few loads, producing no permanent changes in the structure or in its response, are shown as dots. The heavier loads, producing permanent changes in the structure or in its response, are shown as horizontal lines. The maximum deflection on the first trip of a particular load corresponds to the left end of the horizontal line; the deflection on the last trip of the same load corresponds to the right end of the same horizontal line. The permanent set is shown cumulatively on the line of zero moment.

An additional scale is shown at the right of each moment-deflection diagram. The scale expresses the total external moment, M (in-

cluding maximum static moment and dead load moment), at midspan in terms of the moment corresponding to the design stress currently allowed by bridge specifications. The magnitude of this allowable stress is indicated by the subscript; for example, M_{18} represents moment corresponding to a design stress of 18 ksi.

Each dot or shaded block area represents all trips of one load. Generally, 30 trips were made. When other than 30, the actual number of trips is indicated on the diagram; for example, 13 trips were made with the heaviest load on Bridge 1A.

The set-trip diagram (Fig. 61) is a plot of the permanent set at midspan as a function of the number of trips of the test vehicle. Both the permanent set and the number of trips are plotted cumulatively. The diagram also includes consecutive load numbers and approximate speeds of the vehicle.

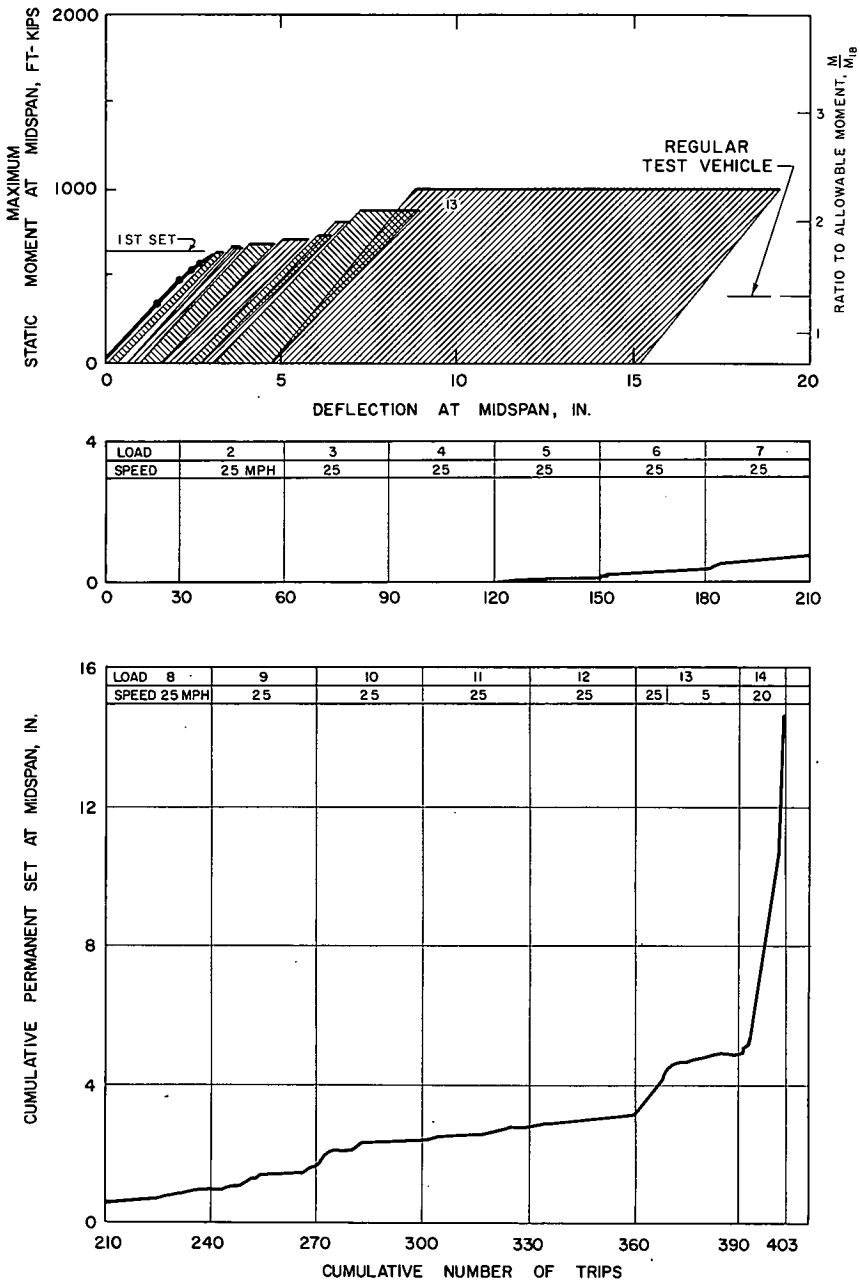

Figure 61. Test to failure of Bridge 1A.

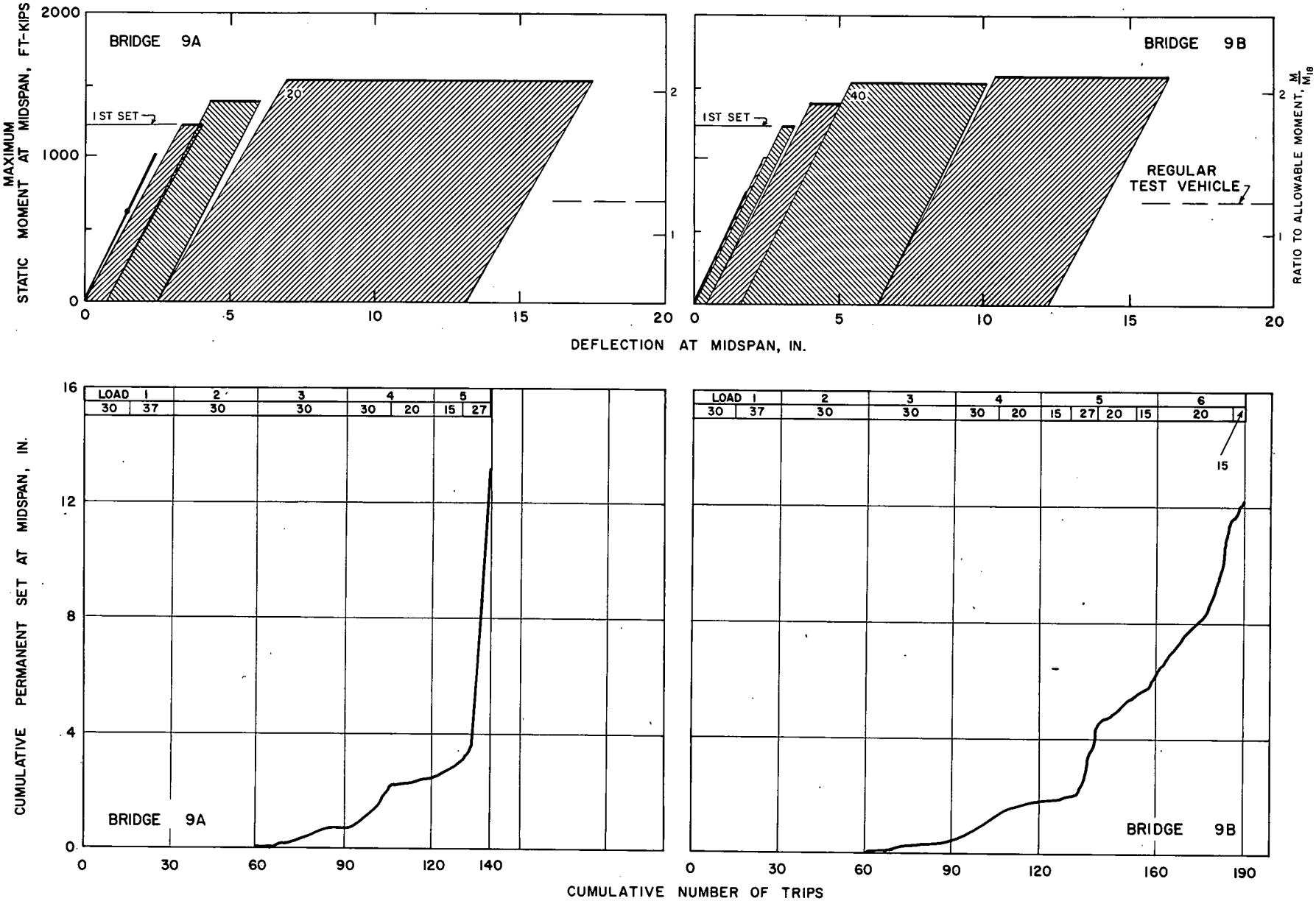

Figure 62. Tests to failure of Bridges 9A and 9B.

3.6:1 Noncomposite Steel Bridges 1A, 9A and 9B

The beams of the noncomposite steel bridges 1A, 9A and 9B were permanently deformed (Section 3.3.2) prior to tests to failure with successively heavier loaded vehicles. Visible fatigue cracks were observed at the welds near the ends of the cover plates on several beams (Section 3.3.3), and the slabs were cracked transversely at several locations (Section 3.3.8). The permanent deformations of beams were particularly large on Bridge 1A, and the slab deterioration was in a very advanced stage on Bridges 9A and 9B. The fatigue cracks were confined to the bottom surface of the flange and caused no change in the stiffness of the bridge.

The test to failure of Bridge 1A was carried out with 14 increments of load applied by three different vehicles. The first seven loads were applied with tandem axle vehicle 62 from Loop 6 (Table 19); the next six loads were applied with vehicle 96 (Fig. 28); vehicle 97 was used for the heaviest load (Fig. 28). Bridges 9A and 9B were tested with vehicle 97 using five and six increments of load, respectively.

The vehicles traveled at approximately 25 mph over Bridge 1A and 30 mph over Bridges 9A and 9B except that during the last few increments of load the speed was decreased to prevent damage to the vehicle. The vehicles traveled in the same direction as during regular test traffic and were centered on the 14-ft roadway. Bridges 9A and 9B were tested as a pair.

Bridge Response.—The results of the tests are shown in Figures 61 and 62. Practically no permanent deformation occurred during the first five loadings on Bridge 1A and during the first two loadings on Bridges 9A and 9B.

Starting with the sixth loading on Bridge 1A and with the third loading on the other two bridges, permanent deformations occurred during almost every trip of the vehicle. As long as the speed remained constant, the first few trips usually produced larger permanent deformations than the later trips of the same load, except at maximum loads. Whenever the speed was decreased, the permanent deformation per trip also decreased. On the other hand, an increase in speed resulted in an increased rate of permanent deformations with successive trips.

The permanent deformations accumulated rapidly with each increment of load after the load increment causing the first large permanent set. Yield lines indicated the formation of plastic hinges at both ends of the cover plates on Bridge 1A and at the approach end of cover plates on Bridges 9A and 9B. Tensile yielding in the cover-plated portions of the beams was noted only at higher load increments and was generally confined to the cover plate. On Bridge 1A, heavy yielding of the top flange was observed in the middle 30 ft of the beam.

During the fifth load increment, the rate of permanent deformation of Bridge 9A started increasing from trip to trip. Very large increments after the twelfth trip indicated that yielding penetrated the full depth of beams at the approach end of cover plates. The test of Bridge 9A was discontinued after the 20th trip

TABLE 50

VEHICLE LOADS CAUSING FIRST SET OR DECREASE OF STIFFNESS

Bridge	Vehicle [1]	Axle Weight (kips)							
		Axle 1 [2]	Axle 2	Axle 3	Axle 4	Axle 5	Axle 6	Axle 7	Axle 8
				(*a*) STEEL BRIDGES					
1A	62	11.4	23.8	23.3	23.6	24.2	—	—	—
3B	99	17.0	21.9	21.9	27.5	27.9	32.9	32.3	32.3
9A	97	14.1	13.8	19.6	20.7	35.8	36.6	38.9	—
9B	97	14.1	14.2	16.9	17.0	21.8	23.2	23.0	—
				(*b*) PRESTRESSED CONCRETE BRIDGES					
5B	97	13.5	14.0	27.6	26.0	37.1	38.6	41.6	—
6A	97	14.5	13.4	18.4	19.7	28.3	30.0	32.5	—
6B	97	13.5	14.0	27.6	26.0	37.1	38.9	41.6	—
				(*c*) REINFORCED CONCRETE BRIDGES					
8A	97	13.6	13.7	24.2	24.7	37.5	41.2	47.8	—
8B	97	13.6	13.7	24.2	24.7	37.5	41.2	47.8	—

[1] See Table 19, Figures 25 and 28 for type and dimensions.
[2] Front axle; remaining axles numbered consecutively from front to back.

of the fifth load increment. The last trip caused almost 2 in. of permanent set at midspan.

The permanent deformations of Bridge 9B increased less rapidly than those of Bridge 9A. The test of Bridge 9B was continued after shoring up Bridge 9A. Large increases of permanent set from trip to trip occurred in Bridge 9B with the sixth increment of load. Twenty-six trips in the direction of regular traffic were followed by four trips in the opposite direction in an attempt to develop plastic hinges at the opposite end of the cover plates. However, the test was stopped short of that goal because the permanent deformation of the bridge was considered too great for safe operation of the vehicle.

The eleventh and twelfth loadings on Bridge 1A caused smaller permanent sets than either of the preceding two loads. At this stage, the yielding outside the cover plated regions was very heavy both on the tension and the compression side. Yield lines, extending practically the full depth of the beams, indicated that plastic hinges formed at both ends of cover plates in all three beams. This condition and the relatively small set on the eleventh and twelfth loadings suggest that strain hardening may have developed off the ends of the cover plates.

Further increase of load on Bridge 1A caused the appearance of yield lines on the cover plates of all three beams. On the fourteenth loading the rate of permanent deformation increased with each trip, and the test was discontinued

TABLE 51
MAXIMUM VEHICLE[1] LOADS

Bridge	Axle Weight (kips)						
	Axle 1[2]	Axle 2	Axle 3	Axle 4	Axle 5	Axle 6	Axle 7
(a) STEEL BRIDGES							
1A	14.1	14.2	16.7	18.3	28.4	29.8	31.8
3B	13.8	13.9	31.5	30.6	72.3	73.5	82.3
9A	13.8	13.8	28.8	29.0	42.8	45.4	50.2
9B	14.2	14.4	29.3	30.7	44.8	46.5	51.2
(b) PRESTRESSED CONCRETE BRIDGES							
5A	13.5	14.0	27.6	26.0	37.1	38.9	41.6
5B	13.8	13.9	31.5	30.6	72.3	73.5	82.3
6A	14.2	14.0	24.4	23.5	41.7	45.0	49.1
6B	13.8	13.9	31.5	30.6	72.3	73.5	82.3
(c) REINFORCED CONCRETE BRIDGES							
8A	14.5	14.0	30.9	30.3	43.0	44.9	52.8
8B	14.5	14.0	30.9	30.3	43.0	44.9	52.8

[1] Vehicle 97 (Fig. 28) used in all tests.
[2] Front axle; remaining axles numbered consecutively from front to back.

TABLE 52
SUMMARY OF DATA AT FIRST SET OR DECREASE OF STIFFNESS

Bridge	Load Causing First Set or Decrease of Stiffness								Total No. of Trips[2]	Total Perm. Set[2] (in.)	Mode of Bridge Tests
	Load No.	No. of Trips	Speed (mph)	Max. Static Moment (ft-kips)		Est. Impact[1] (%)	Live Load Defl. (in.)	Perm. Set (in.)			
				Midspan	End Plate						
(a) STEEL BRIDGES											
1A	6	30	25	635	633	21	3.0	0.3	180	0.4	Yielding of steel
3B	3	30	30	1,060	920	13	1.3	0.3	69	0.4	Yielding of steel
9A	3	30	30	1,230	1,160	13	3.3	0.7	90	0.8	Yielding of steel
9B	3	30	30	1,230	1,160	9	2.9	0.4	90	0.5	Yielding of steel
(b) PRESTRESSED CONCRETE BRIDGES											
5B	3	35	30	1,315	—	12	0.7	0	95	0	Cracking of conc.
6A	3	30	30	1,000	—	20	0.7	0	90	0	Cracking of conc.
6B	5	30	30	1,300	—	10	0.8	0	150	0	Cracking of conc.
(c) REINFORCED CONCRETE BRIDGES											
8A	4	30	30	1,390	—	11	1.7	10.7	120	10.9	Yielding of steel
8B	4	30	30	1,390	—	13	1.7	5.9	120	6.1	Yielding of steel

[1] Based on strains.
[2] From beginning of tests with increasing loads.

Figure 63. Bridge 1A at end of test.

after 15 trips. The last trip caused heavy yielding of the webs near midspan and a permanent set in excess of 2 in.

The fatigue cracks noted in the bridges before the test became wider during the test but did not increase in length. Although no fatigue cracks were found before the test at the toes of several cover plate welds, typical fatigue cracks became visible at all such locations during the progress of the tests with successively heavier loads.

Summaries of Test Data.—The axle loads for the loadings causing the first substantial permanent set are given in Table 50 and those for the maximum loading are given in Table 51. The test results for these two loadings are given in Tables 52 and 53.

The data in Tables 52 and 53 include estimates of impact. These were computed from elastic deformations measured during the regular speed runs and during the occasional creep speed runs. Strains at the bottom flange at midspan or, when strain data were not available, midspan deflections were used for this purpose. When the tests were discontinued, all three noncomposite steel bridges had a total permanent set at midspan in excess of 12 in. (Table 53). A large portion of this set occurred at the maximum load. Figures 63 and 64 show all three bridges after failure. The large permanent deformations are apparent.

3.6.2 Composite Steel Bridge 3B

At the end of the regular test traffic, Bridge 3B had a small permanent set (Section 3.3.2), two visible fatigue cracks (Section 3.3.3) and a few transverse cracks in the slab (Section 3.3.8). One of the two fatigue cracks extended through the full thickness of the flange and was approximately 1.5 in. long (Fig. 65). The bridge appeared to be in good condition. Deformation measurements toward the end of the test traffic indicated no effect of fatigue cracking on the stiffness of the bridge; a small decrease of stiffness during the period of test traffic was attributed to the cracking of the slab.

During the first six increments of loading with successively heavier loads, the fatigue crack did not increase in length, although it increased appreciably in width. During the seventh loading, the length of the crack in-

creased to 2 in. To prevent further spreading, the crack was repaired with a butt weld prior to the eighth loading.

Bridge 3B was tested with nine increments of load. Load increments 1 and 4 were applied with vehicle 98, increments 2 and 3 with vehicle 99, and all others with vehicle 97 (Fig. 28). Load increments 2, 3 and 4 produced essentially the same static moment at midspan. During the first six load increments, the vehicle traveled at 30 mph in the direction of regular test traffic. For the seventh increment of loading, the speed was reduced to 17 mph. The eighth and ninth loadings were applied at 3 mph with the vehicle facing in the direction of the regular test traffic but moving alternately forward and backward across the bridge.

The moment-deflection and set-trip diagrams for the test of Bridge 3B are shown in Figure 66. The first appreciable permanent set was measured during the third loading. With this and the loadings that followed, the largest permanent deformations occurred during the first few trips. A decrease in the rate of the permanent set increase with successive trips is apparent in the set-trip diagram.

Yield lines began to appear on the bottom flange during the fifth loading, first near the approach end and later near the exit end of the cover plates. They appeared all along the bottom flange, except near the ends of the spans, and on the bottom of the cover plate during the sixth loading and in the web during the seventh loading. On the eighth loading, heavy yielding in the web was observed, particularly near both ends of the cover plates. Tension cracks appeared in the bottom of the slab reaching about halfway into the deck at sections near the ends of the cover plates.

On the first trip of the last loading, yielding was noticed to spread upward to the top flange at the section near the approach end of the cover plates and, by the fifth run, scattered yield lines could be found all along the top

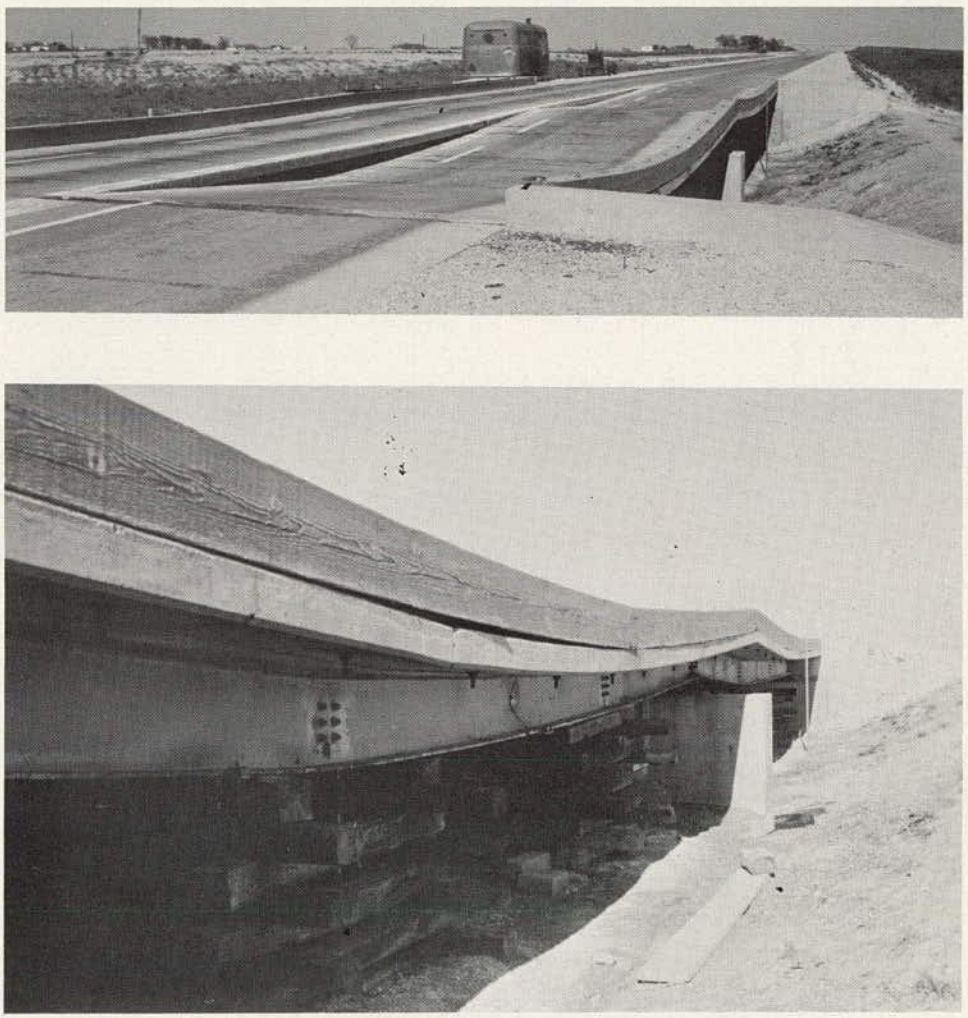

Figure 64. Bridges 9A and 9B at end of test.

TABLE 53
SUMMARY OF DATA AT MAXIMUM TEST LOAD

Bridge	Maximum Load							Total No. of Trips [1]	Total Perm. Set [1] (in.)	Mode of Failure
	No. of Trips	Nominal Speed (mph)	Max. Static Moment (ft-kips)		Estimated Impact (%)	Live Load Deflection (in.)	Perm. Set (in.)			
			Midspan	End Plate						
					(a) STEEL BRIDGES					
1A	13	20	1,000	900	15 [2]	3.9	10.4	403	15.4	Permanent set
3B	14	Creep	2,520	2,330	0	3.2	5.5	214	14.1	Permanent set
9A	20	20	1,535	1,490	28 [2]	4.4	10.6	140	13.2	Permanent set
9B	30	20	1,580	1,520	14 [3]	4.0	5.9	190	12.3	Permanent set
					(b) PRESTRESSED CONCRETE BRIDGES					
5A	35	30	1,315	—	—	7.8	10.8	95	10.9	Concrete crushing
5B	70	Creep	2,520	—	0	8.5	7.3	285	8.1	Steel fracture
6A	18	20	1,500	—	20 [2]	7.9	1.5	198	7.6	Steel fracture
6B	45	Creep	2,520	—	0	8.0	4.8	365	6.4	Steel fracture
					(c) REINFORCED CONCRETE BRIDGES					
8A	2	30	1,550	—	18 [2]	3.2	4.3	122	15.2	Concrete crushing
8B	7	30	1,550	—	16 [2]	3.0	8.4	127	14.5	Concrete crushing

[1] During tests with increasing loads.
[2] Based on deflections.
[3] Based on strains.

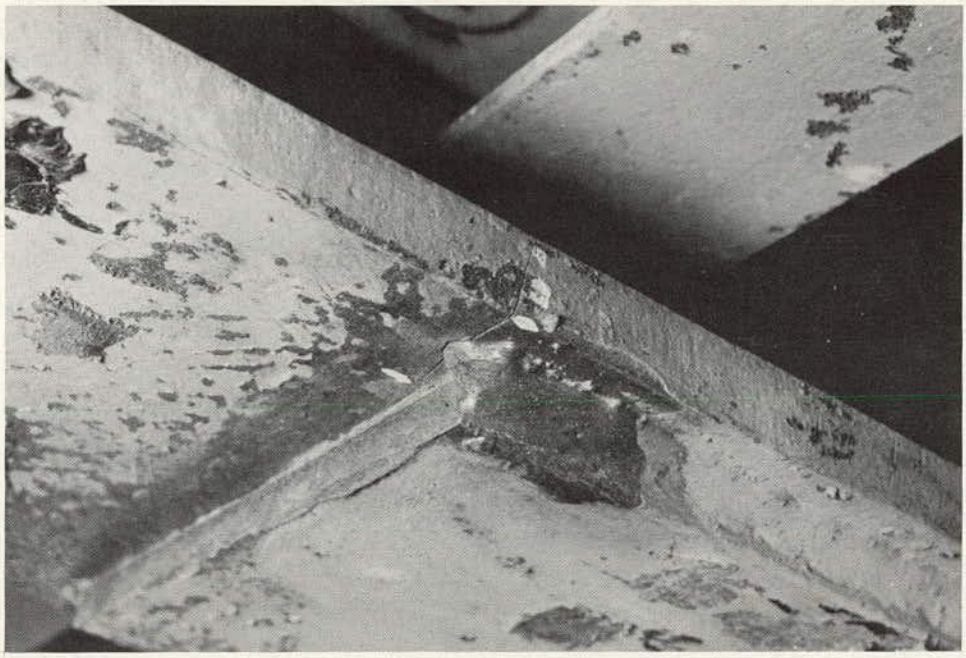

Figure 65. Fatigue cracking on Bridge 3B.

flange except near the ends of the spans. The tension cracks in the slab extended above mid-depth. The first run of the ninth loading caused a permanent set at midspan of 1.12 in. However, the increase in the permanent set decreased rapidly during the successive trips and after ten trips it was only of the order of 0.2 in. per run, indicating that failure under this loading was unlikely. As the total permanent set at midspan, accumulated during the tests with increasing loads, was in excess of 13 in. and further loading of the vehicle was undesirable, the test was discontinued.

Bridge 3B after failure is shown in the upper photograph of Figure 67. By the end of the test, yield lines on the surfaces of the beams indicated tensile yielding through the full depth of the steel section outside both ends of the cover plates. The yield lines on the exterior beam, near the approach end of the cover plate, are shown in the lower photograph (Fig. 67). At midspan, tensile yield lines reached the underside of the top flange. The tension cracking in the slab extended to within 2 in. of the top surface, but no signs of crushing appeared on the top surface.

Table 50 gives the axle loads of the test vehicle at third loading, and Table 51 gives those for the last loading. Summaries of the more important data obtained with the two loadings are given in Tables 52 and 53.

A comparison between the composite steel bridge 3B and the noncomposite steel bridges is of particular interest. All four bridges had beams of the same depth, but the weight of the steel sections was 55 lb per ft in Bridge 1A, 60 lb per ft in Bridge 3B and 96 lb per ft in Bridges 9A and 9B. The last two bridges had cover plates on both the top and the bottom flange, whereas the other two had them only on the bottom flange. The strengthening and stiffening effects of the composite action are apparent. The stiffening effect can be seen best on the moment-deflection diagrams; for example, for the moment at midspan of 500 ft-kips the deflections at midspan were as follows: noncomposite bridge 1A, 2.2 in.; composite bridge 3B, 0.6 in.; and noncomposite bridges 9A and 9B, 1.2 in.

The strengthening effect of composite action is well illustrated by the values of the maximum static moment at midspan: noncomposite bridge 1A, 1,000 ft-kips; composite bridge 3B, 2,500 ft-kips; noncomposite bridge 9A, 1,535 ft-kips; and noncomposite bridge 9B, 1,580 ft-kips.

It is apparent that the differences in beam sizes, impact factors and properties of materials cannot account for the substantially higher stiffness and ultimate moment resistance of the composite bridge 3B.

Another characteristic of composite bridges that was demonstrated by the test of Bridge 3B is the shape of the moment-deflection diagram past yielding. The transition from elastic deformations to the maximum load was very gradual so that even relatively large increases of load beyond that causing first yielding resulted in only small permanent deformations (Fig. 66). This was in marked contrast to

noncomposite bridges (Figs. 61 and 62) in which large permanent deformations occurred at loads not greatly in excess of the yield load. In other words, for a composite bridge the magnitude of the yield load is a less critical quantity than for a noncomposite bridge.

3.6.3 Prestressed Concrete Bridges 5A, 5B, 6A and 6B

Prior to the tests with increasing loads, Bridge 5A had been subjected to the regular test traffic only; Bridges 5B, 6A and 6B had been subjected to the accelerated fatigue tests in addition to the regular test traffic. By the end of the regular test traffic, each of the four bridges had assumed a small permanent set at midspan. All three beams of Bridge 5A had a large number of widely spaced cracks (Section 3.3.6) extending into the top flange of the beams. Several cracks were visible also on the exterior beam of Bridge 6A. In the other two beams of Bridge 6A, and all the beams of Bridges 5B and 6B, only a few cracks had been found, and these were detectable only with special aids.

Bridge 5A was tested with 3 increments of load, Bridge 5B with 8 increments, Bridge 6A with 7 increments and Bridge 6B with 12 incre-

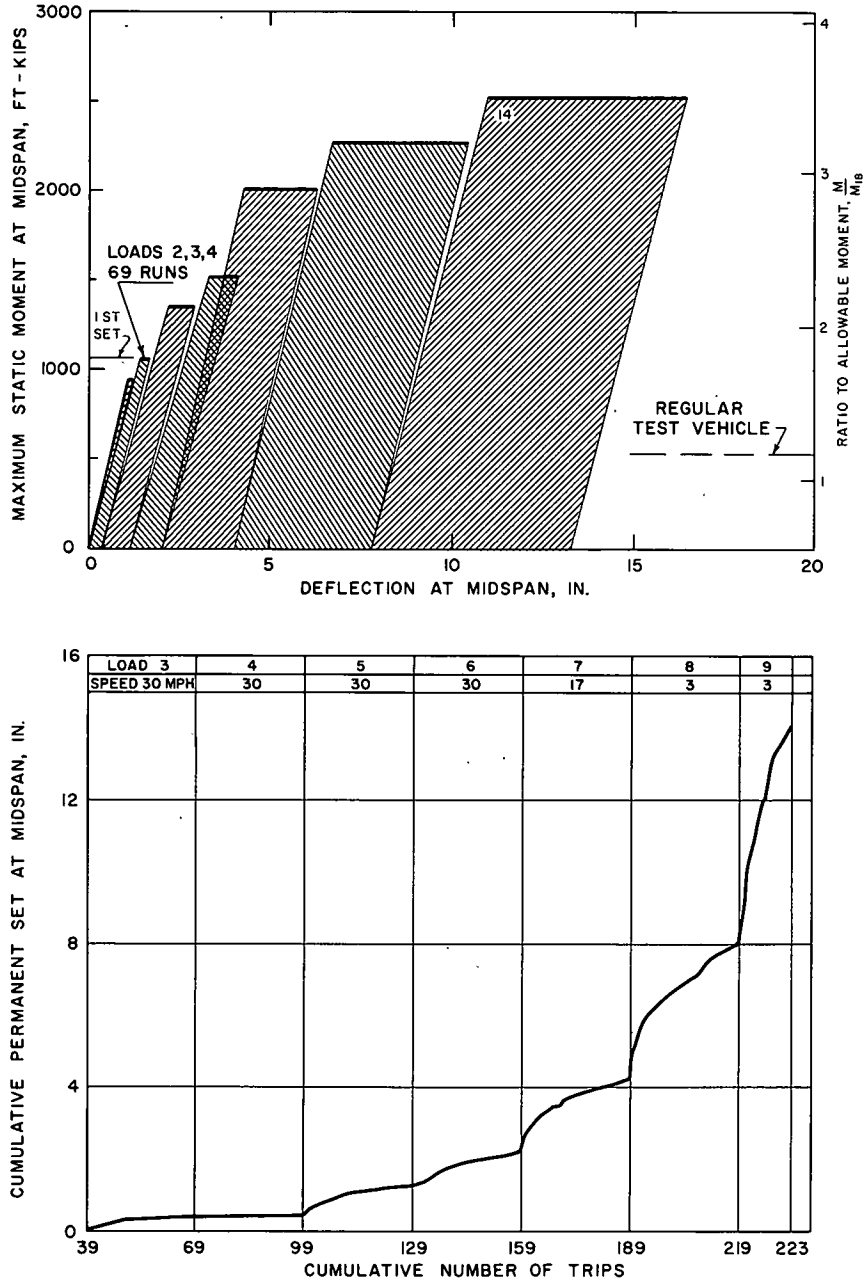

Figure 66. Test to failure of Bridge 3B.

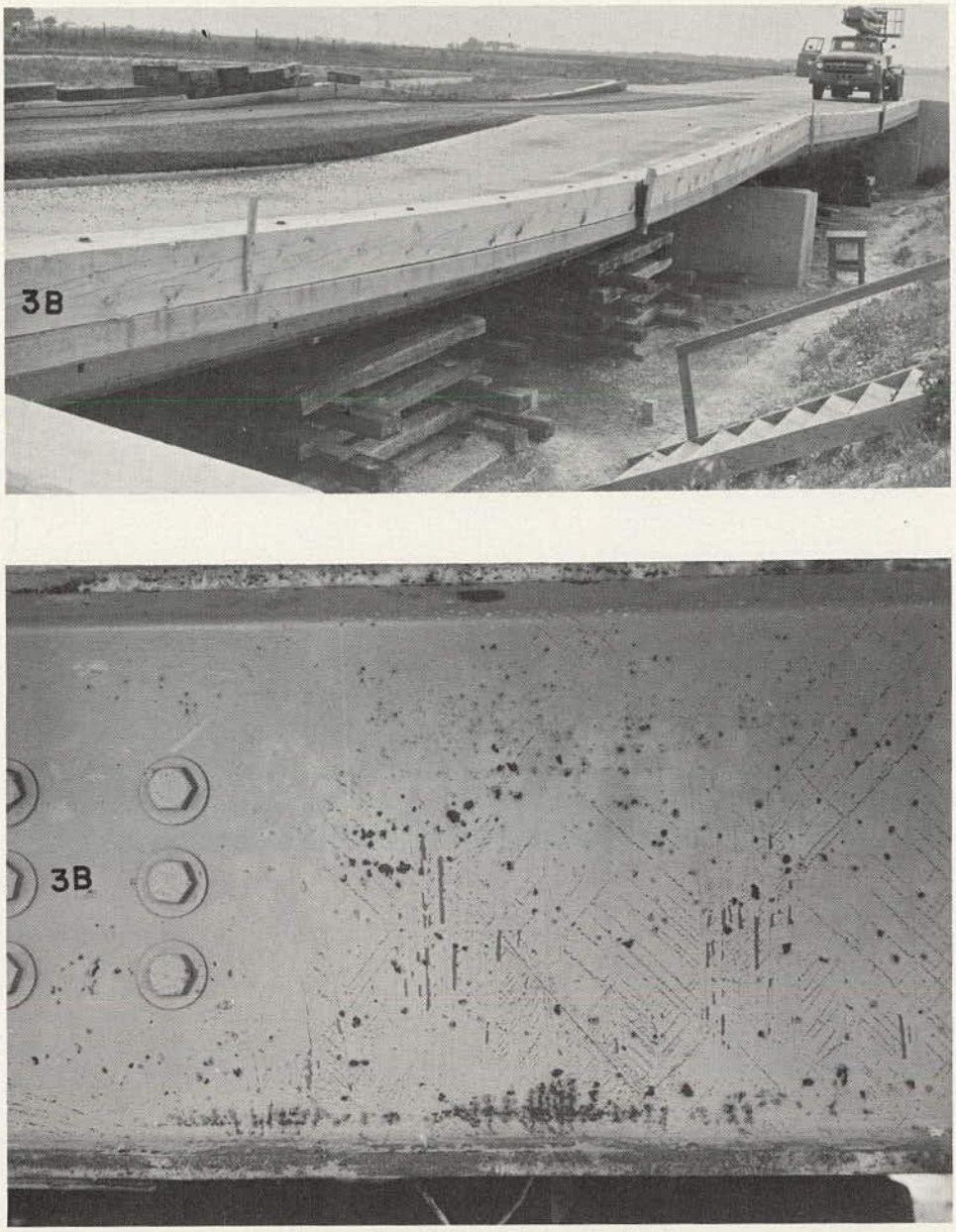

Figure 67. Bridge 3B at end of test.

ments. The loads were applied with vehicle 97 traveling, except for the last three loadings on Bridges 5B and 6B, in the direction of the regular test traffic. Until failure of Bridge 5A, Bridges 5A and 5B were tested as a pair. Similarly, until failure of Bridge 6A, Bridges 6A and 6B were tested as a pair. During the last three loadings on Bridges 6B and 5B, the vehicle was moved forward and backward across the bridge, facing in the direction of the regular test traffic.

The first 3 loadings on Bridges 5A and 5B, and the first 5 loadings on Bridges 6A and 6B, were made with the vehicle traveling at 30 mph. During the next few loadings, the speed was varied between 15 and 30 mph, and the speed was 3 mph when the vehicle was moving back and forth.

General Behavior.—The moment-deflection and set-trip diagrams for the prestressed concrete bridges are shown in Figures 68 and 69. The moment-deflection curves for all four bridges show that beyond a certain load the stiffness of the bridge decreased during the repeated trips with the same load. The decrease in stiffness is indicated by the change of the slope of the lines at the beginning and at the end of the same loading block. Apparently,

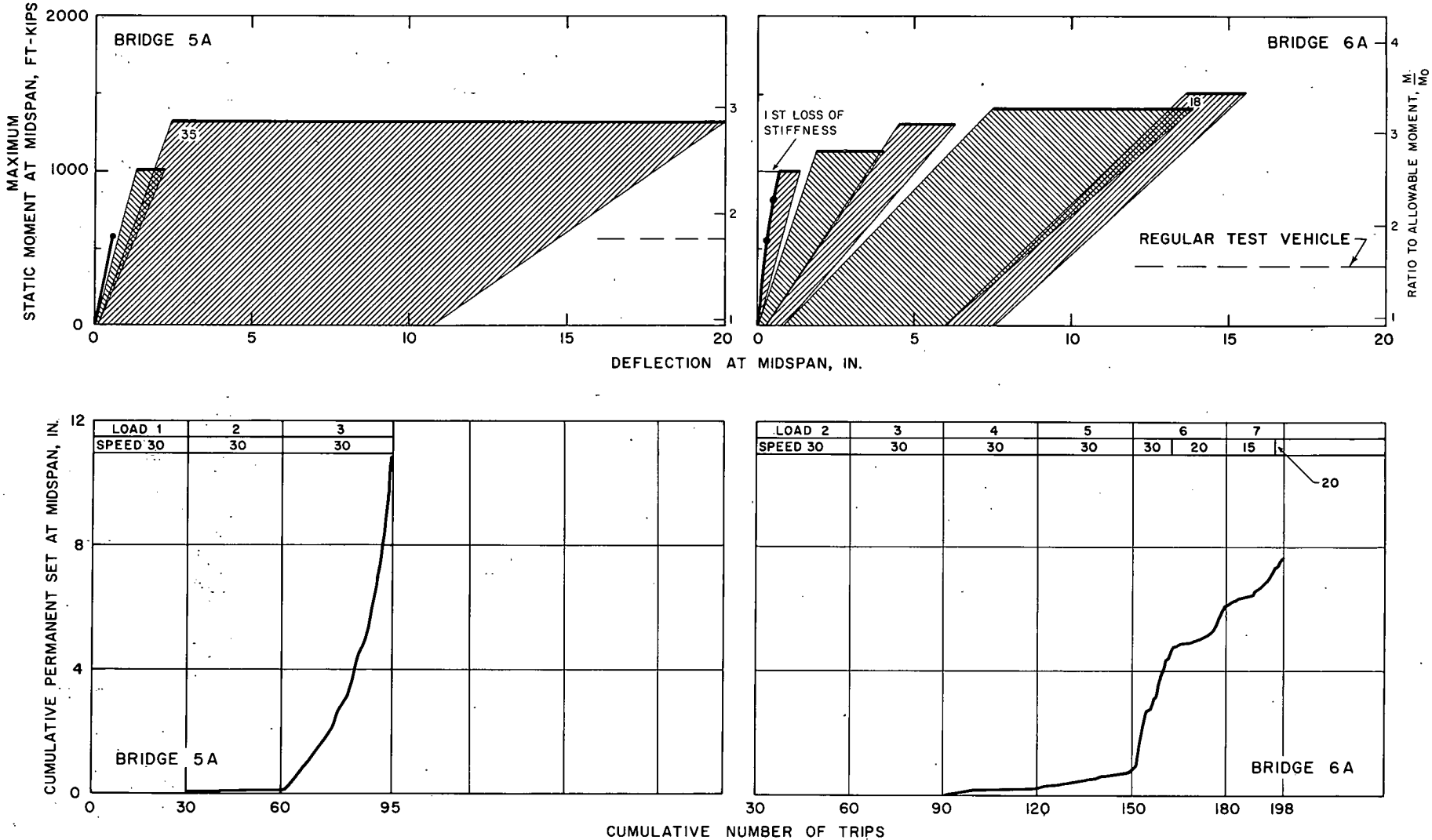

Figure 68. Tests to failure of Bridges 5A and 6A.

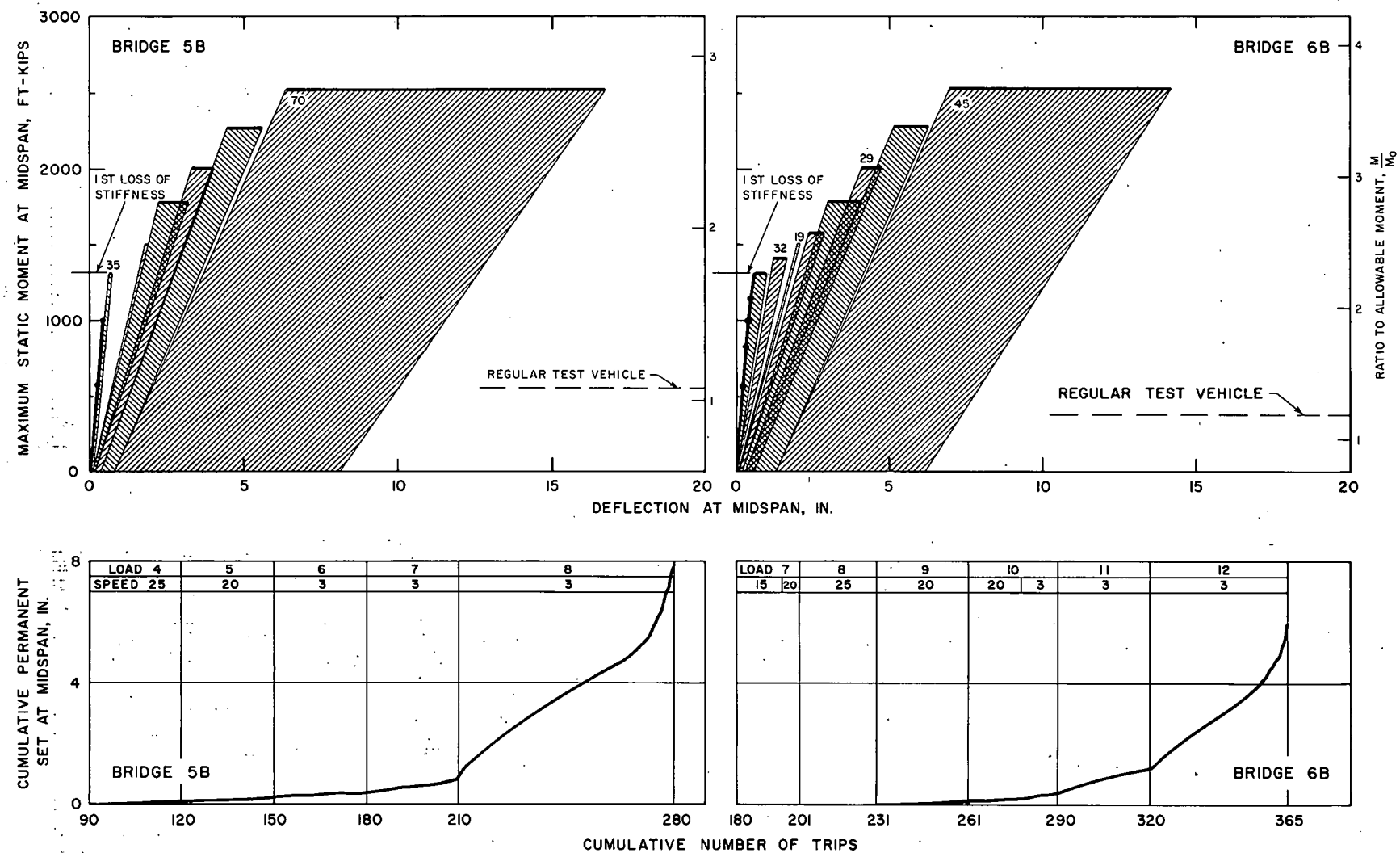

Figure 69. Tests to failure of Bridges 5B and 6B.

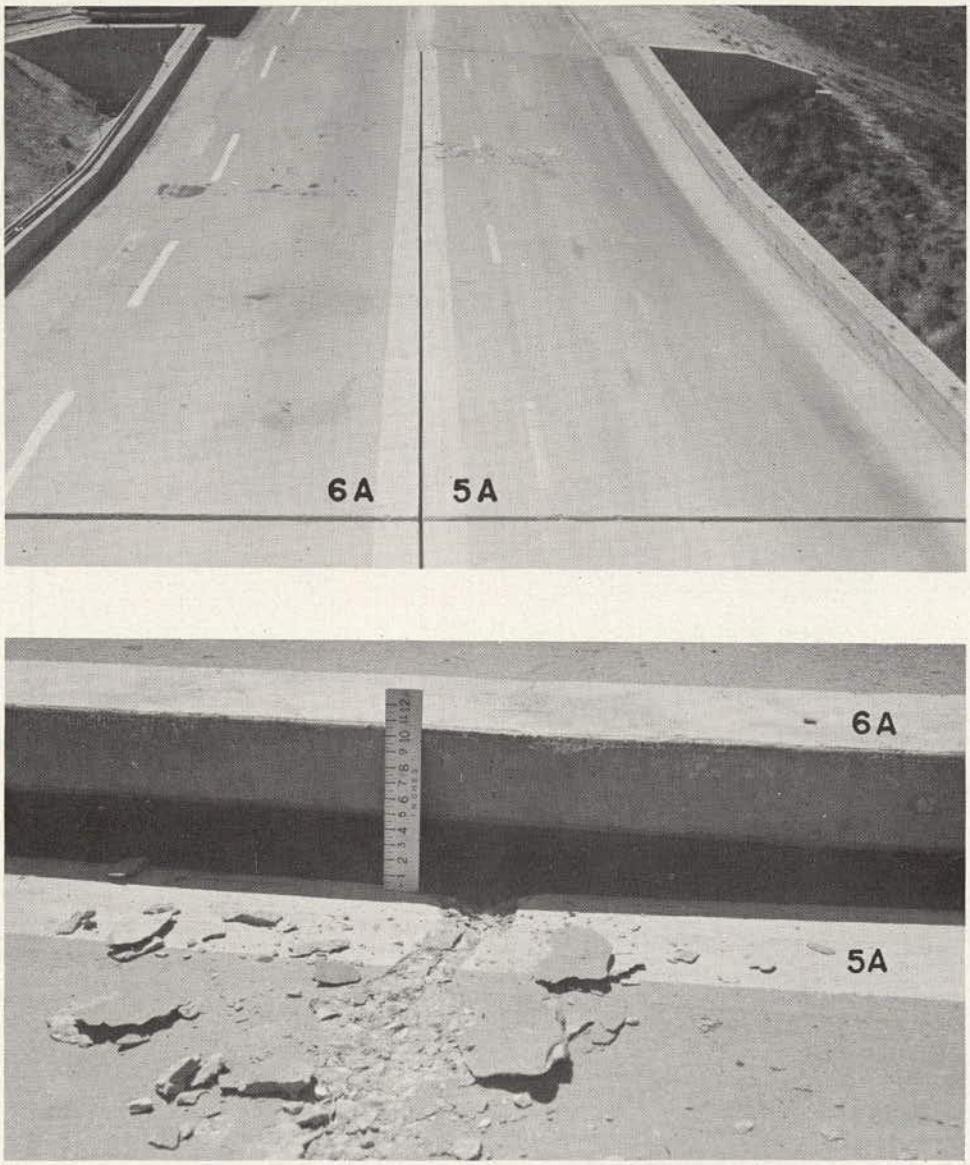

Figure 70. Slabs of Bridges 5A and 6A after failure.

there was a progressive increase of tension cracking.

At first, the decrease in stiffness was not accompanied by any appreciable permanent set. However, as the ultimate load was approached, permanent set was observed in addition to the decrease in stiffness. Strain measurements indicated that the permanent set was caused primarily by inelastic deformations of the prestressing steel.

Tension cracks became visible on Bridge 5B during the third loading, on Bridge 6B during the fourth loading, and on the center and interior beams of Bridge 6A during the third loading. With further increments of load new cracks formed, and the old cracks extended upward. The cracks were closely spaced, in contrast with the relatively large spacing of cracks in Bridge 5A.

Behavior of Bridges 5A and 6A at High Loads.—During the last few trips of the second loading, tensile stresses in the prestressing steel of the interior beam of Bridge 5A began to decrease. During the third increment of load, strains decreased in all three beams and several cracks opened very wide, indicating a bond failure. The permanent deformations increased at a rate increasing from trip to trip of the third loading. During the 36th trip the slab failed in compression by crushing of concrete. Figures 70 and 71 show Bridges 5A and 6A after failure; the crushing of the slab and wide opening of a tension crack of Bridge 5A are clearly visible.

To check on the loss of bond, a 6-ft length of cable was recovered near midspan, and a 2-ft length was recovered from an uncracked portion of the beam near the support. The grout inside the metal sheathing was crumbled in the sample from midspan but was solid in the other sample. Furthermore, the grout in the sample from midspan did not adhere to the wires, whereas that from the other sample adhered to the wires to such an extent that it was difficult to break it away. No voids in the grout were discovered in either sample, and

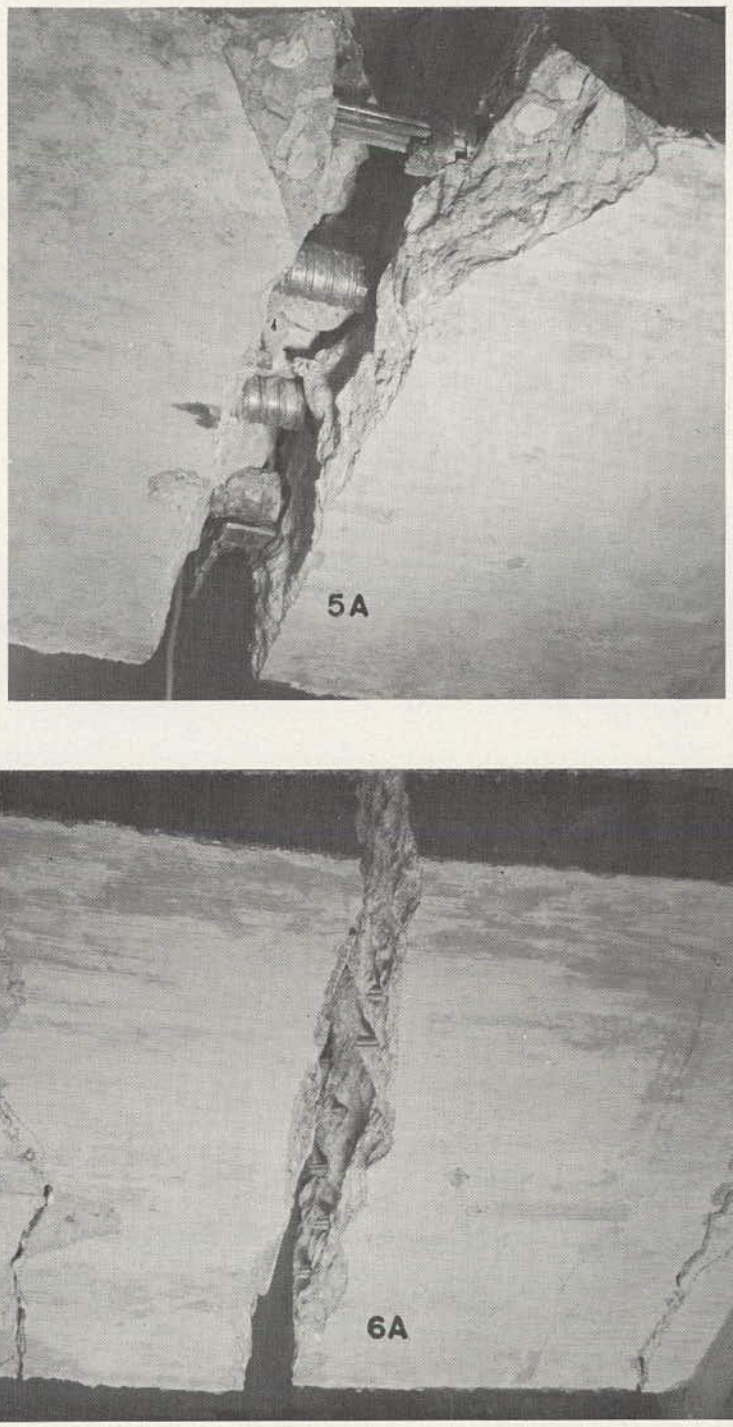

Figure 71. Beams of Bridges 5A and 6A after failure.

there were no bare spots on the wires. Thus, a thorough compaction of the grout was indicated.

The increase of permanent deformations in Bridge 6A was somewhat erratic, as shown in the set trip diagram. On the seventh loading the increase of the deformation was still relatively slow and not too easily noticeable by eye. During the nineteenth trip the wires in the exterior and center beam suddenly ruptured with a loud noise, and the bridge settled on the safety cribs. Subsequent inspection indicated that all wires in the two beams were broken, but the strands in the interior beam appeared to be unbroken. Only minor crushing, in one small area, occurred on the top of the slab. Breaks in the strands are clearly visible in Figure 71.

An interesting phenomenon observed on Bridge 6A was an extremely violent rebound after the passage of the vehicle. Toward the end of the fifth loading and at the beginning of the sixth loading, the recovery of the elastic deflection was so sudden and violent that the bridge jumped off its bearings on each recovery. When the speed of the vehicle was reduced to 20 mph after the eleventh trip of the sixth loading, the violent rebound was eliminated. Similar rebound, although less violent, was observed on Bridges 5B and 6B after the development of appreciable tensile cracking.

Behavior of Bridges 5B and 6B at High Loads.—During the seventh loading, large shear cracks appeared near the third-points on beams of Bridge 5B, and the slab began pulling away from the beams. The resulting horizontal crack started at the top of the shear cracks and advanced toward midspan. In Bridge 6B, similar shear cracks were observed to form during the eleventh loading, and a sign of separation of the slab, less severe than on Bridge 5B, appeared during the twelfth loading.

During the first few trips of the last load increment, the permanent deformations of both bridges increased at an almost constant rate. However, after 35 trips on Bridge 6B and 50 trips on Bridge 5B, the rate of permanent deformations started increasing. After the forty-fourth trip on Bridge 6B and sixty-ninth trip on Bridge 5B, light crushing was noted on the top of the slabs at midspan. A subsequent backward crossing caused no visible distress, but during the forward trip that followed each bridge collapsed on the cribbing. The

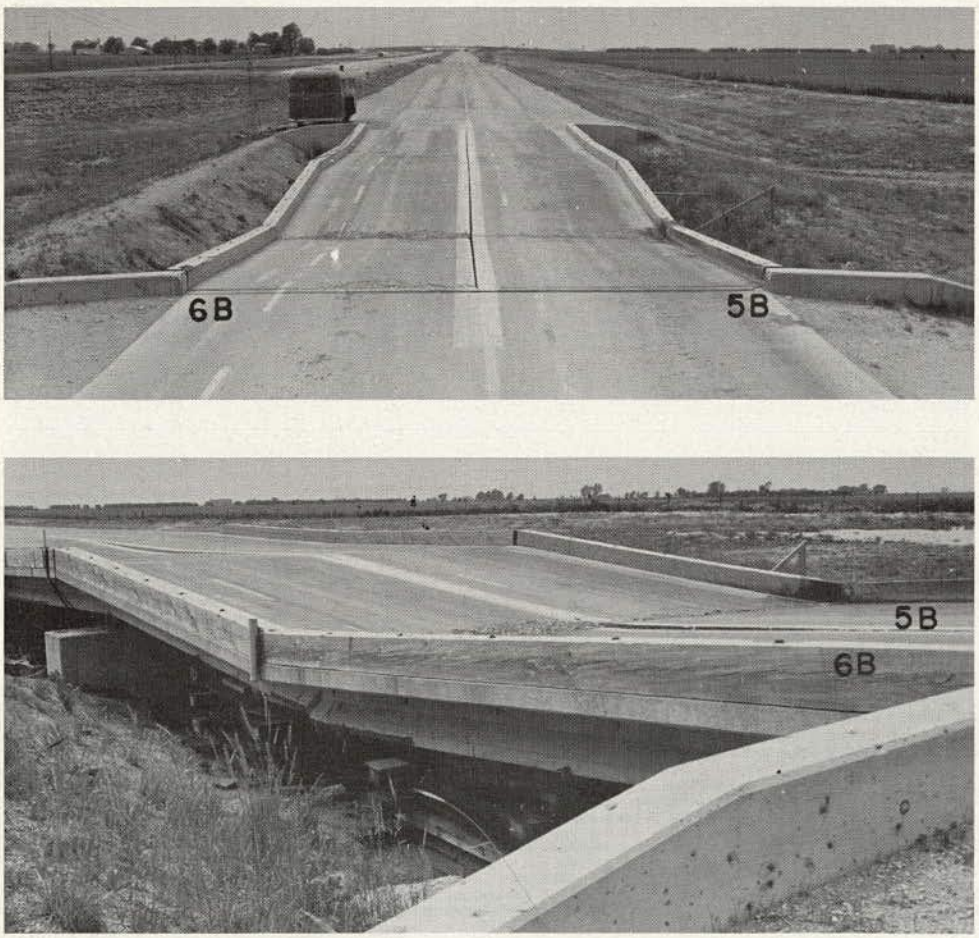

Figure 72. Bridges 5B and 6B after failure.

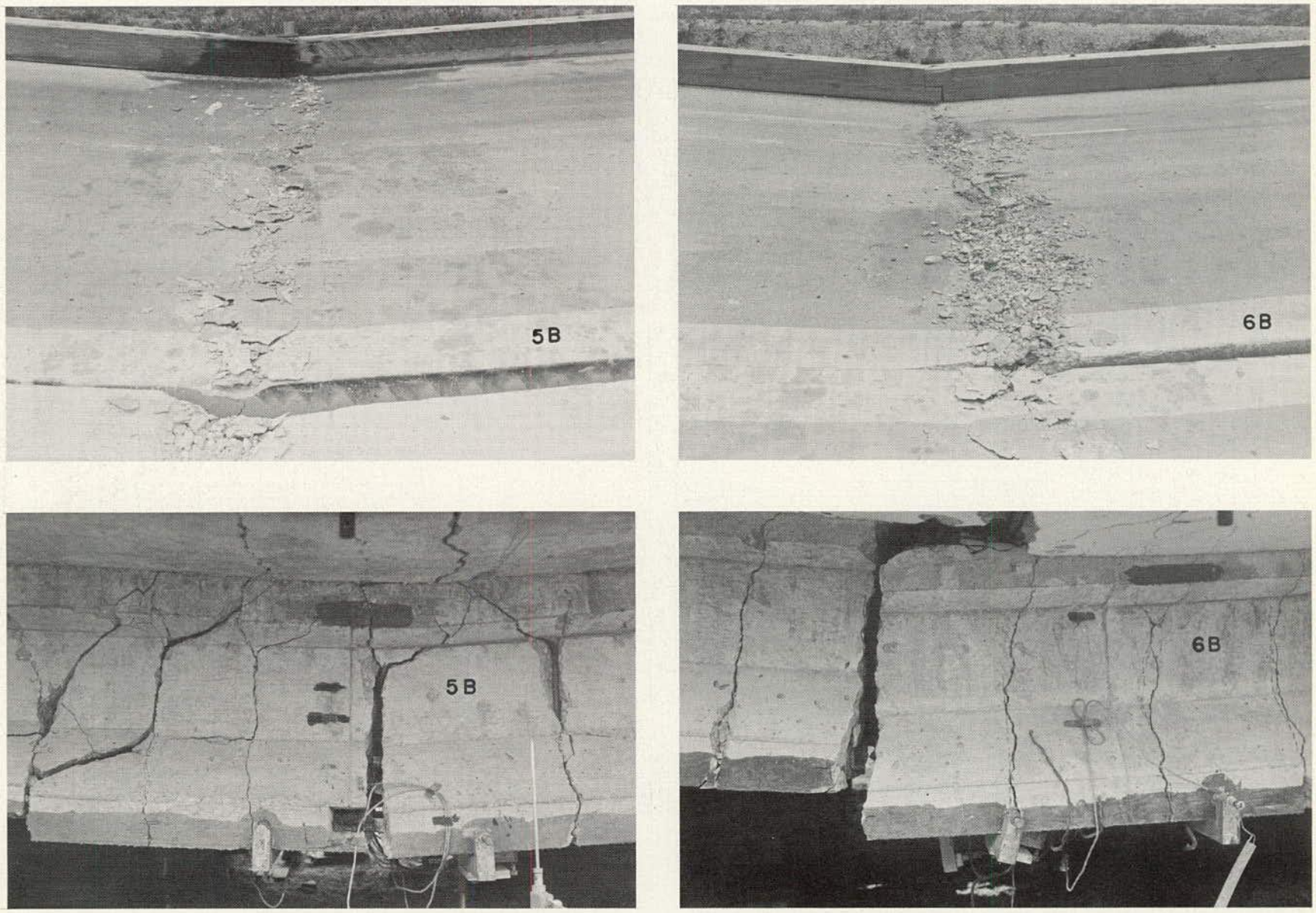

Figure 73. Details of Bridges 5B and 6B after failure.

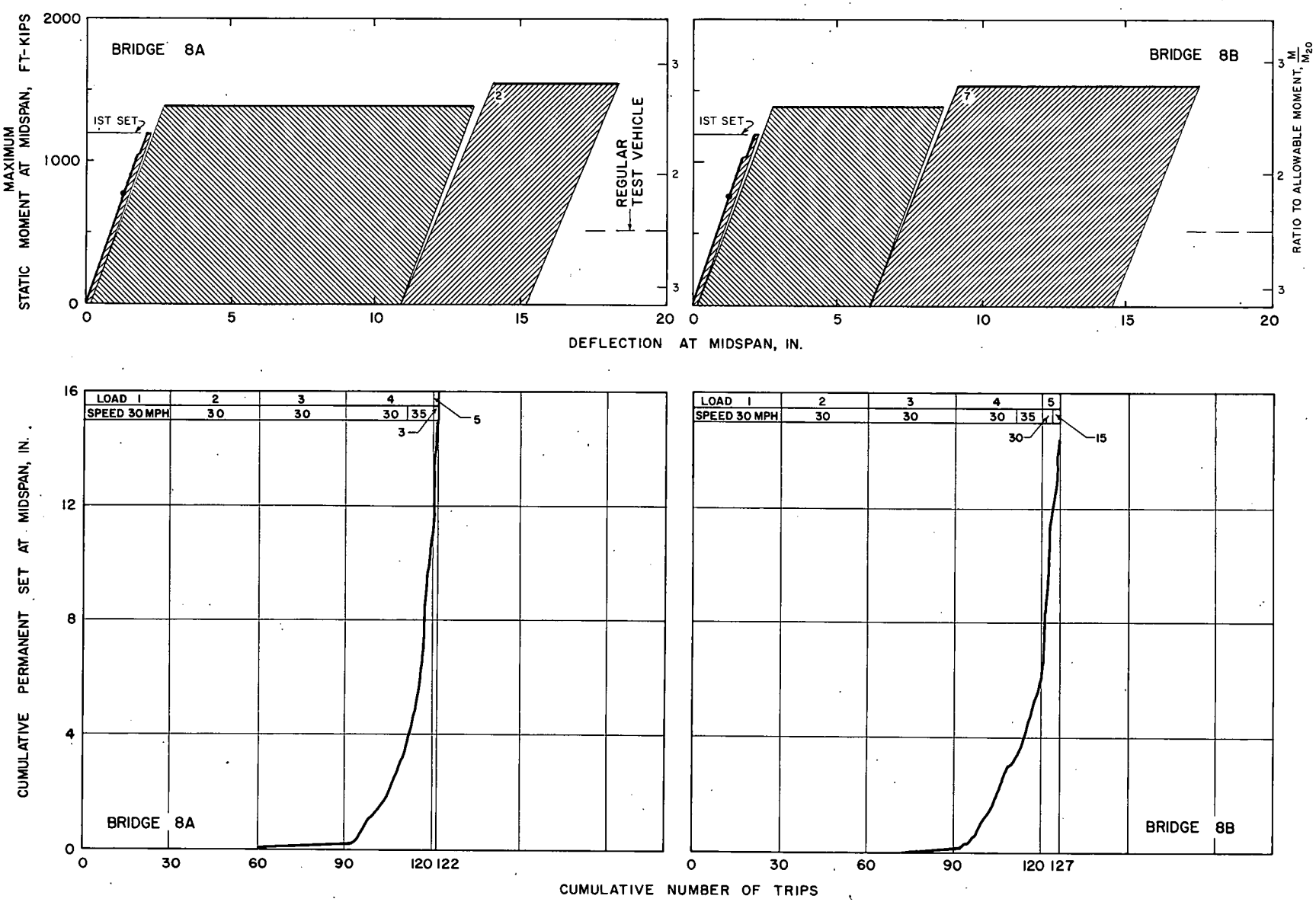

Figure 74. Tests to failure of Bridges 8A and 8B.

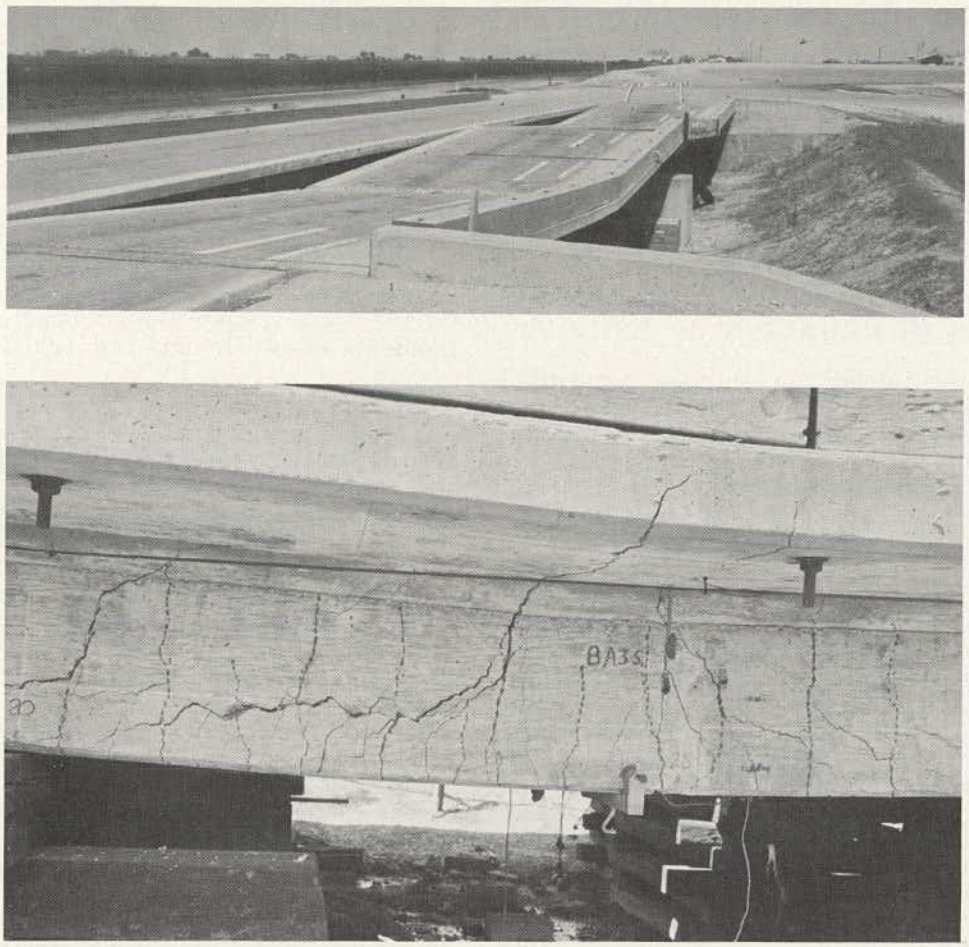

Figure 75. Bridges 8A and 8B after failure.

collapse was accompanied by heavy crushing of the slab. An inspection after the failures revealed that prestressing elements were broken in all beams of both bridges. Figure 72 shows over-all views of Bridges 6A and 6B after failure; Figure 73 shows details of the slab and beam failures.

Tabular Data.—The weights of the axles of vehicles causing first appreciable decrease of stiffness and failure are given in Tables 50 and 51. Summaries of the most important test data pertaining to these loads are given in Tables 52 and 53.

3.6.4 Reinforced Concrete Bridges 8A and 8B

Bridges 8A and 8B were replicates in that they were built to the same specifications and were located in the same traffic lane. Prior to the tests with increasing loads, Bridge 8A was subjected to the regular test traffic and to the accelerated fatigue tests; Bridge 8B was subjected to the regular test traffic only. Both bridges assumed some permanent set during the regular test traffic and were cracked extensively in tension. Only a few isolated inclined cracks were found. The cracking was somewhat more extensive in Bridge 8A than in Bridge 8B, but the differences were small.

Bridges 8A and 8B were tested with five increments of load applied by vehicle 97. The vehicle traveled at 30 mph in the direction of regular test traffic. The response of the two bridges to vehicle trips was very similar. Practically no changes, except for increases in elastic deflections and stresses, were noted during the first three increment of load (Fig. 74). The fourth loading produced yielding and inclined cracking in all beams. The cracks near midspan widened noticeably, and extended almost to the top surface of the slab. Permanent deformations increased at an increasing rate as shown in the set-trip curves. The principal difference between the response of Bridges 8A and 8B during this load increment was the higher rate of increase of the permanent set in Bridge 8A. The second trip of the fifth loading produced crushing of the concrete slab of Bridge 8A. After the second trip, Bridge 8A

was supported on cribs. Similar crushing occurred in the slab of Bridge 8B during the seventh trip.

Figure 75 shows Bridges 8A and 8B after failure. The loads causing first yielding and failure are given in Tables 50 and 51, respectively, and the more important test data taken at these loads are summarized in Tables 52 and 53. The total permanent sets at midspan exceeded 14 in. when the failures occurred.

3.7 LOAD CAPACITY AT SIGNIFICANT CHANGES IN BEHAVIOR OF BRIDGES

The moment-deflection curves previously presented have shown that the load-deformation characteristics of the test bridges may be approximated by three straight lines: (1) a steep sloping line representing the initial elastic behavior; (2) a second line, less steep than the first one, representing the post-yielding or post-cracking range of behavior; and (3) a horizontal line representing the ultimate load.

The slope of the first line is an essentially fixed quantity that can readily be determined from the elastic properties of the structure. The slope of the second line is indeterminate because it is a function of loading, speed and number of trips of the vehicle. For ordinary purposes, the slope of the second line is unimportant so that the load-deflection characteristics may be estimated if the loads corresponding to the end of the elastic line and to failure can be determined.

Methods for estimating both loads are available for static loading. The purpose of this section is to compare such methods with the data obtained for the test bridges.

The static capacity of any cross-section of the test bridges at first yielding, cracking or failure may readily be determined, assuming that the bridge responded as a beam. This assumption is justified by the generally uniform response to transient loads of all three beams of the same bridge.

The external force was composed of the weight of the bridge and of the forces exerted by the test vehicle. Because of uncertainties concerning the actual values of impact, all comparisons presented in this section are based on the static rather than the actual dynamic moments caused by the test vehicles.

3.7.1 Yield Strength

The yield strength M_y of the steel and reinforced concrete bridges was computed from the ordinary elastic theory of flexure, assuming that the stress on the bottom face of the steel beam or in the bottom layer of reinforcing bars was equal to the static yield point of the steel and that the concrete had no tensile strength. (The static yield point of the reinforcing bars was assumed equal to that listed in Table 9.) Complete interaction between the beams and the slab was assumed for composite steel and reinforced concrete bridges. For noncomposite steel bridges, the slab was assumed to be independent of the beams.

The external moments at first set in the steel and reinforced concrete bridges, obtained from the tests to failure with increasing loads, are compared in Table 54 with the computed yield strengths. For all but one bridge the calculated yield strength was 10 to 20 percent lower than the external moment at first large permanent set. The only exception was the

TABLE 54

YIELD STRENGTH OF TEST BRIDGES

Bridge	Type	Moment (ft-kips)			Ratio, Observed to Calculated
		Regular Test Traffic,[1] $M_{LL} + M_{DL}$	Observed Yield Strength,[1] $M_{LL} + M_{DL}$	Calculated Yield Strength,[2] M_y	
1A	Noncomposite steel	744	1,025	844	1.21
3B	Composite steel	866	1,329	1,427	0.93
9A	Noncomposite steel	1,127	1,621	1,382	1.17
9B	Noncomposite steel	1,118	1,612	1,388	1.16
8A	Reinforced concrete	1,156	2,043	1,824	1.12
8B	Reinforced concrete	1,156	2,043	1,824	1.12

[1] M_{LL} = static moment at critical section caused by test vehicle; M_{DL} = moment at critical section caused by weight of bridge.

[2] M_y = moment based on static yield point.

composite steel bridge 3B in which substantial increases of load caused relatively small increases of permanent deformations (Fig. 66) so that the selection of the load causing the "first" set in this bridge was subject of the largest error.

The bridges had acquired varying amounts of permanent set during the regular test traffic. The total external static moments caused by the weight of the bridge and of the regular test vehicle (Table 54) were always smaller than the calculated yield strength. Apparently, the first permanent set took place before the yield strength of the bridge was reached. Residual stresses in rolled steel sections, and creep and cracking of concrete were indicated in the preceding sections as the probable causes of permanent deformations at relatively low stresses.

It may be well to emphasize at this point that several factors could be approximated only roughly or had to be neglected altogether in the comparisons presented in this section. For example, whereas the calculated yield strength pertains to first yielding in extreme fibers at one cross-section of the bridge only, the observed yield strength was determined by measurements of permanent deformations which obviously could accumulate only after fairly extensively yielding. All observations were made for moving loads; the calculations were based on static yield point. The impact was disregarded in all computations. The distribution of load to the individual axles may have been different from that determined by static weighing, particularly after large deformations of the bridge. In view of these and other possible uncertainties, the calculated values should be considered only as approximations of the observed moments.

3.7.2 *Cracking Strength*

The cracking moment for the prestressed concrete bridges was computed from the ordinary elastic theory of flexure, assuming that at cracking the stress on the bottom face of the beams was equal to the difference between the modulus of rupture and the stress that existed in the unloaded bridge. The modulus of rupture at the beginning of test traffic was used in computations for Bridge 5A, and that at the end of the test traffic was used for all other bridges.

The computed cracking moments are compared (Table 55) with the static moments caused at midspan by the test vehicle. Truck moments are given for (1) the regular test vehicle, (2) the vehicle causing first visible cracks, and (3) the vehicle causing first loss of stiffness. The computed cracking moment was reasonably close to the moment at the observed loss of stiffness.

TABLE 55
LOSS OF STIFFNESS OF PRESTRESSED CONCRETE BRIDGES

Bridge	Truck Moment[1] (ft-kips)			Computed Cracking Moment[2] (ft-kips)
	Regular Test	At Visible Cracks	At Observed Loss of Stiffness	
5A	562	562[3]	—	495
5B	562	1,315	1,315	1,368
6A	382	1,000[4]	1,000	720
6B	382	1,130	1,300	1,090

[1] Static moment at midspan caused by test vehicle.
[2] Based on modulus of rupture at beginning of test traffic for 5A, at end of test traffic for all other bridges.
[3] All three beams had large visible cracks shortly after beginning of test traffic.
[4] Visible cracking found in one beam during regular test traffic.

3.7.3 *Ultimate Strength*

Reinforced Concrete Bridges.—The ultimate strength of reinforced concrete bridges was computed from

$$M_u = \left(1 - c_1 \frac{\Sigma F}{b\bar{d}f'_c}\right) \Sigma(Fd) \qquad (22)$$

in which

M_u = ultimate moment resistance;
F = force in one layer of tension reinforcement;
d = distance from a layer of tension reinforcement to the top surface of the slab;
$\bar{d} = \Sigma(Fd)/\Sigma F$;
b = width of slab;
f'_c = compressive strength of concrete; and
c_1 = empirical coefficient.

The force F in each layer of tension reinforcement was assumed equal to the product of the yield point and the area of the bars. The empirical coefficient c_1 was taken as 0.59 in conformity with laboratory test data.*

Prestressed Concrete Bridges.—The ultimate strength of prestressed concrete bridges was computed from Eq. 22 using $c_1 = 0.6$.** The forces F were computed as the product of the stress at failure and the area of steel. The stress in prestressing steel was computed from

* "Report of ASCE-ACI Joint Committee on Ultimate Strength Design." Amer. Soc. of Civil Engineers, *Proceedings*, Paper 806 (October 1955).

** "Tentative Recommendations for Prestressed Concrete." ACI-ASCE Joint Committee 323, *Jour. of the ACI* (January 1958) pp. 545-578.

an assumed strain, and the stress-strain diagram for the steel. The stress in non-prestressed reinforcing bars in tension was taken as equal to the yield point.

The total strain in any layer of prestressing steel was assumed to be made up of two components: ε_p caused by prestressing and ε_{LL} caused by the total applied load. Whereas ε_p was known for each layer, ε_{LL} was assumed to be linearly distributed through the depth of the cross-section. Thus, it was necessary to assume the value of ε_{LL} only for one layer.

Except for the case of unbonded reinforcement,* the prestressing steel in the bottom layer was assumed to be stressed to its ultimate strength. For the unbonded condition, assumed for Bridge 5A, strain ε_{LL} was computed from

$$\varepsilon_{LL} = 0.0005 \left(\frac{c_2 f'_c bd}{\Sigma F} - 1 \right) \qquad (23)$$

in which

$$1/c_2 = 0.8 + 0.0001\, f'_c.$$

Steel Bridges.—The ultimate strength of steel bridges was evaluated assuming fully plastic stress distribution in the steel and using the static yield point for the wide-flange sections and cover plates.

Full interaction between the slab and the beams was assumed for the composite bridges; as the neutral axis was found to be near the top of the slab, the bottom layer of the longitudinal slab reinforcement was assumed to be stressed to its yield point. The compressive stresses in the slab were taken as equal to $0.85\, f'_c$ and the concrete was assumed to have no tensile strength.

Independent action of the beams and the slab was assumed for the noncomposite bridges. The contribution of the slab was computed from Eq. 22.

Comparisons with Test Data.—The computed ultimate strengths are compared with the test data in Table 56, which includes all bridges except 2B, 3A, 7A and 7B for which test data on ultimate strength were not available; and

* For more detailed discussion of the theory of the strength of unbonded prestressed concrete beams, see Warwaruk, J., Sozen, M. A., and Siess, C. P., "Investigation of Prestressed Reinforced Concrete for Highway Bridges, Part III; Strength and Behavior in Flexure of Prestressed Concrete Beams." Univ. of Illinois, Eng. Exp. Sta. Bull. 464 (1962).

TABLE 56
ULTIMATE STRENGTH OF TEST BRIDGES

Bridge	Dead Load Moment, M_{DL} (ft-kips)		Maximum Truck Moment,[1] M_{LL} (ft-kips)		Computed Ultimate Strength, M_u (ft-kips)		Ratio, $\frac{M_{LL} + M_{DL}}{M_u}$	
	Midspan	End Plate	Midspan	End Plate	Midspan	End Plate	Midspan	End Plate
				(*a*) STEEL BRIDGES				
1A	471	392	1,000	900	1,158	978	(1.27)	1.32
3B	476	409	2,520	2,330	2,733	2,194	(1.10)	1.25
9A	521	461	1,535	1,490	2,008	1,580	(1.02)	1.23
9B	511	452	1,580	1,520	2,007	1,579	(1.04)	1.25
1B	494	—	562[2]	—	968	—	1.09	—
2A	458	—	562	—	976	—	1.05	—
4A	473	405	696	649	1,226	1,040	(0.95)	1.01
4B	475	406	696	649	1,226	1,040	(0.96)	1.01
				(*b*) PRESTRESSED CONCRETE BRIDGES				
5A	654	—	1,315	—	2,215[3]	—	0.89	—
					2,041[4]	—	0.96	—
5B	652	—	2,520	—	3,043	—	1.04	—
6A	646	—	1,500	—	2,109	—	1.02	—
6B	653	—	2,520	—	2,731	—	1.16	—
				(*c*) REINFORCED CONCRETE BRIDGES				
8A	653	—	1,550	—	2,122	—	1.04	—
8B	653	—	1,550	—	2,110	—	1.04	—

[1] Static moment caused by test vehicle.
[2] Two vehicles causing static moment of 562 ft-kips at midspan crossed the bridge; all other vehicles crossing the bridge caused static moment of 382 ft-kips or less.
[3] Assuming full bond between prestressing steel and concrete.
[4] Assuming no bond between prestressing steel and concrete.

which gives moments at midspan and at the end of cover plates for dead load and for the heaviest vehicle that crossed the bridge. The sum of the moments caused by the two external loads is compared with the computed ultimate strength in the last two columns. For every bridge except 5A the ratio was larger than unity.

Steel bridges 3B, 9A and 9B were 23 to 25 percent stronger than their computed static fully-plastic capacity. This high resistance was developed at the ends of the cover plates; the observed strength at midspan (ratios in parentheses) was only 2 to 10 percent in excess of the computed strength. The corresponding figures for Bridge 1A were 32 and 27 percent.

The high strengths, large amounts of yielding and the shapes of the diagrams of maximum moments suggest that some strain hardening took place outside the cover plates.

The ratios for steel bridges 1B, 2A, 4A and 4B, which failed during the initial reference tests, were lower than for the other four steel bridges. The tests were stopped when the permanent set at midspan was between 3 and 4 in. Further increase of load would have been needed, particularly for Bridges 4A and 4B, to reach permanent set of the magnitude observed in tests of the other four steel bridges.

The observed strength of the prestressed concrete bridges 5B and 6A, and of the reinforced concrete bridges 8A and 8B, was 2 to 4 percent in excess of the computed ultimate strength. On the other hand, Bridge 5A, which showed signs of bond failure, developed only 89 percent of the strength computed on the assumption of a fully-bonded condition. When absence of bond was assumed, the strength ratio for Bridge 5A became 0.95.

Bridges 1A and 6B developed substantially higher strength ratios than other comparable test structures, but no factors were found that would explain satisfactorily these large capacities.

Chapter 4

Dynamic Load Tests

This chapter contains descriptions and summarizations of data on the dynamic load tests conducted by the University of Illinois under contract with the Highway Research Board.* It describes the characteristics of the bridges and vehicles and the bridge-vehicle behavior. It gives the results of regular and special dynamic tests, and compares the test data with analytical solutions.

4.1 MEASURED BRIDGE AND VEHICLE CHARACTERISTICS

In addition to the bridge and vehicle characteristics discussed in Chapters 2 and 3, the studies of dynamic effects of moving vehicles on bridges required the knowledge of the natural fequencies and damping characteristics of the bridges, the longitudinal profiles of the approaches and the bridge slabs, and the natural frequencies of the axles of the vehicles. These properties, determined by independent measurements, are reported in this section. Also included are the results of tests with vehicles running over smooth and rough pavements intended to study the dynamic characteristics of the vehicles.

4.1.1 Dynamic Properties of Bridges

Frequencies of Unloaded Bridges.—Bridge frequencies were determined from the free vibration portions of the dynamic records. The average frequency of a bridge was computed over 5 cycles of oscillations immediately after the passage of the test vehicle. This procedure was repeated for at least four records from every subseries and the results were averaged. The averages for the five series of tests, conducted between September 1958 and October 1960 are listed in Columns 1 through 5 (Table 57). The deviation of individual values from the averages was generally of the order of a few percent.

For seven of the bridges the frequencies were determined for four or five series. The measured frequencies decreased gradually with time for the noncomposite steel bridges and reinforced concrete bridges, but remained essentially unchanged for the composite steel bridges and prestressed concrete bridges.

Natural frequencies of the test bridges computed from the measured dimensions and properties of materials were given in Section 2.2.5. They are reproduced in Column 6 for comparison with the measured frequencies.

Before the test traffic began, measured frequencies of noncomposite steel and reinforced concrete bridges were higher than the computed frequencies, but at the end of the traffic period measured frequencies were only slightly in excess of the computed values. For composite steel and prestressed concrete bridges, measured frequencies were in excellent agreement with the computed values.

The computed frequencies of noncomposite steel bridges were based on the assumption of no interaction between the slab and the beam. The frequencies computed for the same bridges on the assumption of composite action between the slab and the steel beams were 4.5 cps for Bridges 4A and 4B, and 4.1 cps for Bridges 9A and 9B. A comparison of these values with the observed frequencies suggests that before the beginning of regular test traffic these bridges had practically complete composite action in the free vibration era. However, this interaction was almost completely lost by the end of traffic. Loss of friction between the slab and the beams and cracking of the slab probably were responsible for this change in the characteristics of noncomposite steel bridges.

The gradual decrease in the frequencies of the reinforced concrete bridges, approaching the computed frequency, indicated progressive cracking of the beams. The discussion (Section 3.3.7) established conclusively that all reinforced concrete test bridges cracked progressively with test traffic.

Frequencies of Loaded Bridges.—Natural frequencies of unloaded bridges were determined from free vibration records corresponding to deformations much smaller than those to which the bridges were subjected during the passage of a vehicle. The magnitude of the deformations may influence the characteristics of bridge response. For example, it is known that the stiffness of a cracked prestressed concrete bridge decreases with increasing load.

The frequency of bridges corresponding to

* The entire report on the dynamic studies is available as "Dynamic Studies of Bridges on the AASHO Test Road." Civil Engineering Studies, Structural Research Series No. 227, Univ. of Illinois (1961).

their loaded condition was evaluated by two methods. The first method was based on the relative stiffness of the loaded and unloaded bridge; the frequency was computed from

$$f_L = f_u \sqrt{\frac{(EI)_L}{(EI)_u}} \quad (24)$$

in which

f_L = natural frequency of a loaded bridge, not considering the mass of the vehicle;
f_u = natural frequency of an unloaded bridge determined from test records for the free vibration era (Col. 3, Table 57);
$(EI)_L$ = stiffness of a loaded bridge computed from deflections measured during January-June 1960; and
$(EI)_u$ = stiffness of an unloaded bridge computed from f_u.

The second method was a direct experimental approach through frequency-response tests with a mechanical oscillator. These tests were made in February 1961. The resulting values of natural frequencies are given in Columns 7 and 8 (Table 57).

Weight of the vehicle did not enter the computations of frequencies listed in Column 7, but the values in Column 8 included the effect of the weight of the mechanical oscillator. However, the weight of the oscillator was very small relative to the weight of the bridge. Thus, any differences between frequencies of loaded bridges and corresponding frequencies of unloaded bridges were essentially due to changes in the properties of the bridge.

For the noncomposite steel bridges, the frequencies of the loaded bridges (Col. 7) were lower than those of the unloaded bridges (Col. 3) and very close to the computed natural frequencies based on no interaction between the slab and the beam (Col. 6). This is in agreement with the observation (Section 3.2.4) that there was no composite action in the noncomposite steel bridges. Apparently, as a vehicle entered the bridge the friction between the slab

TABLE 57

MEASURED FREQUENCIES OF TEST BRIDGES

Bridge	Measured Frequency (cps)							
	Unloaded Bridges					Computed Natural Frequency	Loaded Bridges	
	Sept.-Oct. 1958	June-Nov. 1959	Jan.-June 1960	July-Sept. 1960	Oct. 1960		Jan.-June 1960	Feb.[1] 1961
	(1)	(2)	(3)	(4)	(5)	(6)	(7)	(8)
				(a) NONCOMPOSITE STEEL BRIDGES				
4A	4.15	—	—	—	—	2.64	—	—
4B	4.46	—	—	—	—	2.66	—	—
9A	—	4.50	4.15	3.83	3.67	3.21	3.12	2.9
9B	—	4.51	4.00	3.84	3.38	3.23	3.12	—
				(b) COMPOSITE STEEL BRIDGES				
2B	4.60	4.43	4.17	—	4.39	4.26	4.25	—
3B	—	—	4.39	—	—	4.52	—	4.1
				(c) PRESTRESSED CONCRETE BRIDGES				
5A	7.03	6.81	6.67	—	6.81	7.00	5.84	—
6A	6.94	—	—	—	—	6.80	—	—
5B	6.75	6.89	6.89	—	6.89	6.91	6.38	—
6B	6.78	—	—	—	—	6.75	—	5.3
				(d) REINFORCED CONCRETE BRIDGES				
7A	3.77	3.34	3.43	3.15	3.15	3.08	3.01	—
7B	3.64	3.21	3.21	3.08	3.12	3.10	2.97	—
8A	—	—	3.48	—	—	3.16	—	3.1
8B	—	—	3.59	—	—	3.19	—	—

[1] Obtained from frequency-response tests.

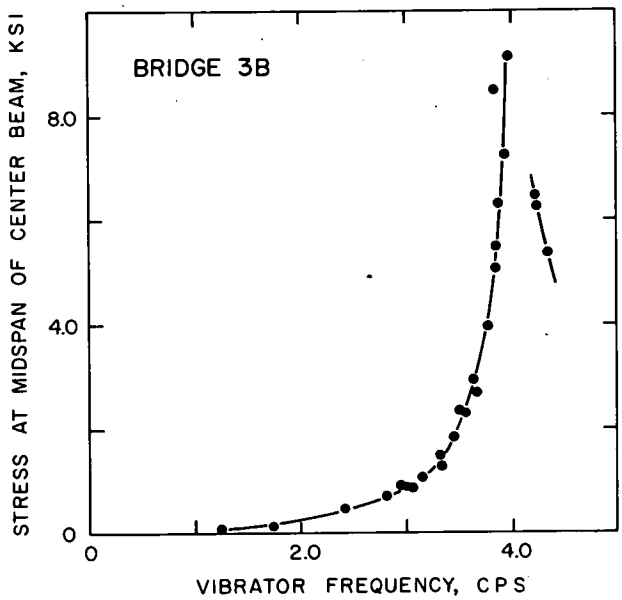

Figure 76. Frequency response curve.

and the beams was overcome so that the bridge responded essentially as a noncomposite structure. On the other hand, as soon as the vehicle left the bridge the frictional force restored an appreciable degree of composite action.

For composite steel bridge 2B, the measured frequencies were essentially the same for the unloaded and loaded conditions.

For prestressed concrete Bridge 5A, the loaded frequency was substantially below the unloaded frequency. Apparently the cracking of the beams decreased both the stiffness and the natural frequency. A smaller decrease of frequency was observed for prestressed concrete Bridge 5B. Although it is known that a few microcracks were present in the beams of Bridge 5B, it appears unlikely that these could have decreased the frequency by the amount indicated in Table 57.

Column 7 frequencies of loaded reinforced concrete bridges 7A and 7B were below those given in Columns 3 and 6. Although small, the decrease was consistent, indicating that the stiffness of the reinforced concrete bridges was also a function of the load.

The frequency-response tests produced records of the type shown in Figure 76. It is apparent that the amplitude of bridge response near the resonant frequency was of the same order of magnitude as that caused by the passage of a test vehicle. Thus, the characteristics of the bridges, determined from the frequency-response tests, may be considered comparable to those of loaded bridges. The natural frequency of Bridge 3B was between 4 and 4.2 cycles per second. Data from this frequency response test were insufficient to determine accurately the natural frequencies. The value of 4.1 cps (Col. 8, Table 57) represents the best estimate based on the available data. Similar uncertainties existed in the resonant frequencies of other bridges for which values are also given in Column 8.

Bridge Damping.—The damping of the bridge was determined from the free vibration portions of the dynamic records and from the frequency-response tests. The interpretation of the free vibration records was complicated by the presence of minor low-frequency oscillations superimposed on the main oscillations. To eliminate the low-frequency oscillations, the records were "smoothed out" before determination of the damping characteristics.

The damping of the bridges was neither purely of the viscous nor purely of the frictional type, but some combination of both. Nevertheless, logarithmic decrements were computed on the assumption of viscous damping to provide some measure of the damping characteristics of the bridges.

For the records used in the determination of natural frequencies, logarithmic decrements were computed on the basis of 5 cycles of oscillation immediately after the passage of the test vehicle. The average values are given in Table 58. Although there was considerable scatter between the individual values making up the

TABLE 58
DAMPING OF TEST BRIDGES

Bridge	Unloaded Bridge		Oscillator, Percent of Critical
	Logarithmic Decrement	Percent of Critical	
(*a*) NONCOMPOSITE STEEL BRIDGES			
4A	0.23	3.6	—
4B	0.29	4.6	—
9A	0.21	3.3	6.0
9B	0.19	3.0	—
(*b*) COMPOSITE STEEL BRIDGES			
2B	0.07	1.1	—
3B	0.05	0.8	3.5
(*c*) PRESTRESSED CONCRETE BRIDGES			
5A	0.11	1.7	—
6A	0.11	1.7	—
5B	0.08	1.2	—
6B	0.04	0.6	—
(*d*) REINFORCED CONCRETE BRIDGES			
7A	0.09	1.4	—
7B	0.10	1.6	—
8A	0.13	2.0	3.9
8B	0.12	1.9	—

averages for different bridges, the averages show consistent trends. The logarithmic decrement was the lowest for the composite steel bridges and for the uncracked prestressed concrete bridges 5B and 6B (0.04 to 0.08); these were followed by the cracked prestressed concrete bridges and reinforced concrete bridges (0.09 to 0.13); and by the noncomposite steel bridges (0.10 to 0.29). Table 58 also gives the logarithmic decrements as well as the damping coefficients expressed as percentage of critical damping.

The high damping in the noncomposite steel bridges may have been caused by the previously discussed mobilization of the frictional force between the slab and the beams. Large scatter in the damping factors observed for these bridges suggested that the change from noncomposite to composite behavior took place in an unpredictable manner.

The relatively small damping in the reinforced concrete bridges, coupled with their low frequency, accounted for the persistence of visible vibrations for a long time after the passage of the test vehicle, a phenomenon observed by many visitors to the test site.

A limited number of studies of additional records suggested that there was no significant change in the magnitude of the logarithmic decrement during the period of regular test traffic.

The damping coefficients, evaluated from the frequency-response tests with the mechanical oscillator, are given in the last column of Table 58. For the cases considered, they were consistently higher than the damping coefficients determined from the free-vibration records. In the frequency-response tests, the amplitude of the oscillations was large enough to mobilize frictional forces in bridge bearings, usually the principal source of bridge damping, whereas in the free vibration era there must have been practically no movements of bearings. Furthermore, in frequency tests the live load stresses fluctuated around the dead load stress, whereas in the tests with vehicles the live load stresses were added to the dead load stresses; this could have changed damping in cracked slabs. These differences in behavior could account for the differences in the damping coefficients. Thus, the damping in loaded bridges was probably higher than is indicated by the logarithmic decrements obtained from the free vibration records.

4.1.2 Profiles of Approaches and Bridges

The shapes and relative elevations of the transverse bridge profiles at midspan were discussed in Sections 2.2.4, 3.1.3 and 3.3.8. The discussions also included general references to the shape of the longitudinal bridge profiles. However, in the dynamic studies, not only the general characteristics but also local irregularities in the profiles of the bridges and of the approaches were important. Therefore, the shapes of the longitudinal profiles are discussed in considerable detail in this section.

Profiles of Approaches.—The longitudinal profiles of the approach pavement to Bridges 2B, 3B, 5A and 7A are shown in Figure 77. For each bridge, the profile of an 80-ft approach pavement is given for two periods: (1) before the test traffic and (2) immediately after the test traffic. Elevations were measured at 1-ft intervals along two wheelpaths concentric in relation to the center beam; averages of the two paths are shown. The differences between elevations in the two individual wheelpaths were usually less than $\frac{3}{8}$ in.

The four profiles pertain to one bridge at each of the four locations. The approaches to the adjacent bridges were similar to those shown. The ordinates represent the deviations of the actual profile from the design grade (0.2 percent slope) passing through a point on the intersection of the outside pavement edge and the bridge abutment.

The approaches for Bridges 2B and 3B were considerably smoother than those for Bridges 5A and 7A. Although changes occurred with time on all four approaches, the major irregularities were reproduced from one day to another. In most cases, the major irregularities became more pronounced with time. The largest change in individual profiles was a sharp rise between 40 and 70 ft from the abutment caused by placement of overlays.

To assess the importance of the effects of various profile irregularities on the response of the vehicle, it must be kept in mind that the response depends not only on the length and amplitude of the different irregularities, but also on the speed and natural period of the vehicle. For a particular configuration of irregularity, the response of an axle is a function of the ratio t_r/T_v, in which t_r is the time of transit of an axle over the irregularity and T_v is the natural period of the axle. For a single wave of practically any shape, the effects are maximum when t_r/T_v is of the order of 0.5 to 1.0. The effect of the irregularity on the response of the vehicle may be negligible for values less than 0.1 or greater than 3.0.

The natural periods of axles T_v ranged approximately from 0.25 to 0.5 sec (Section 4.1.3). Therefore, for speeds in the range of 30 to 40 mph, the length of the wave corresponding to the critical values of t_r/T_v was from 6 to 30 ft. Irregularities within these lengths could be expected to have significant influence on the response of the vehicle.

The lengths of the irregularities fell within the significant range on the approaches (Fig. 77). Therefore, except for the approaches to

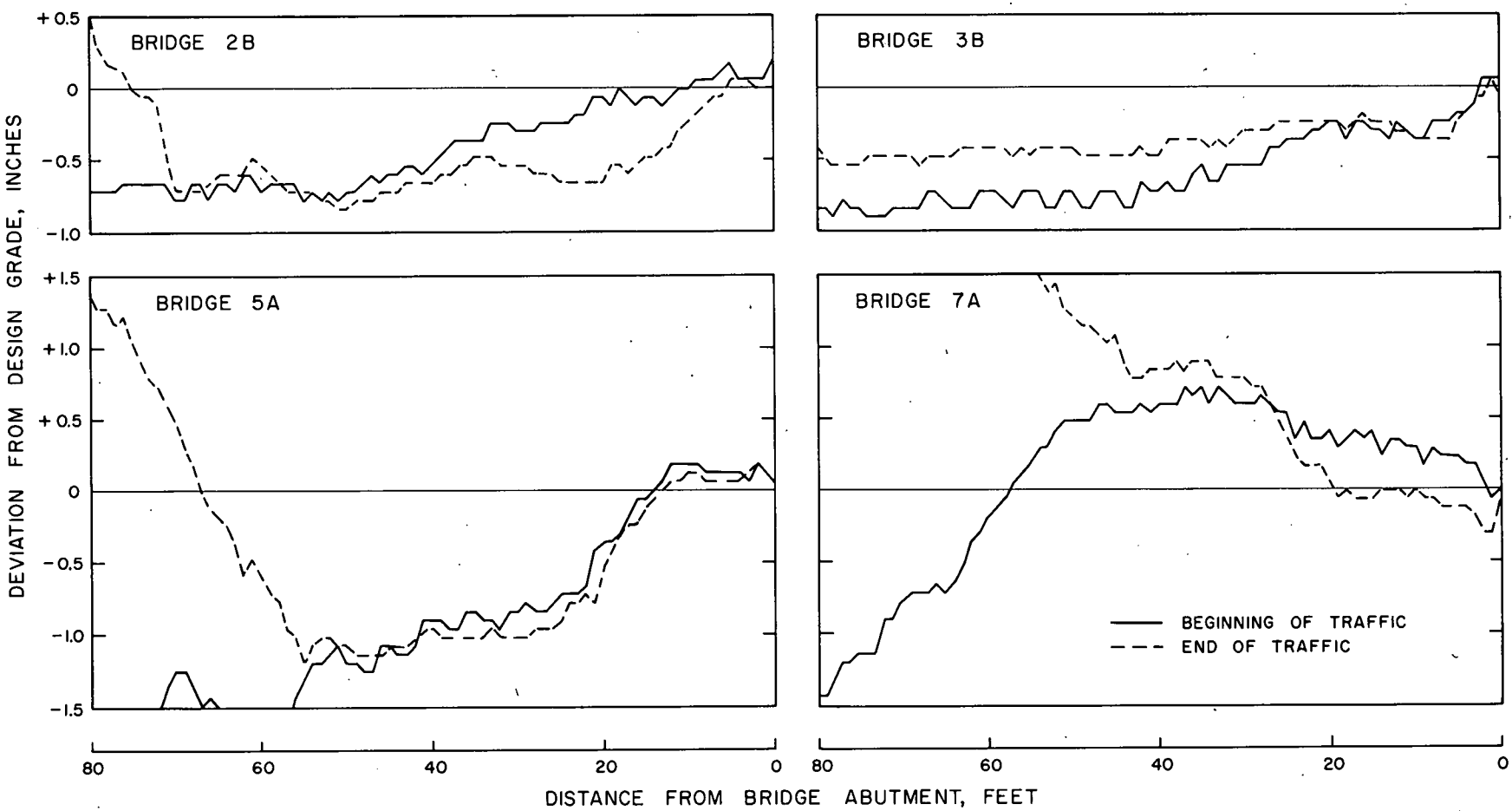

Figure 77. Longitudinal profile of approach pavements.

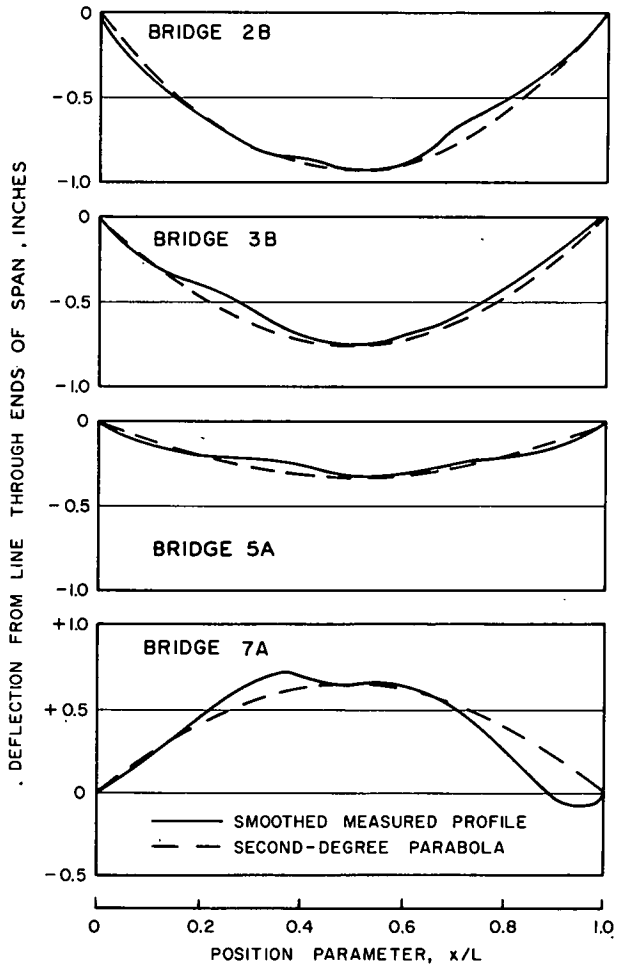

Figure 78. Longitudinal bridge profiles in March 1960.

Bridges 2B and 3B in the early tests, all approaches had to be considered irregular. The dynamic condition of the vehicle at the entrance to the bridge was highly uncertain, particularly for Bridges 5A and 7A.

The closer an irregularity was to the bridge the more important was its effect on bridge response. At 30 mph the test vehicles underwent approximately 4 to 8 oscillations while traveling 80 ft. The friction in the vehicle suspension system acted to reduce oscillations to a very small fraction of their original value in a few cycles (Section 4.1.5). Thus, the portions of the approach profile (Fig. 77) represented lengths sufficient for evaluation of the effect of irregularities on the behavior of the bridge-vehicle systems.

Bridge Profiles.—The longitudinal bridge profiles were determined in the same manner as the profiles of the approaches. Figure 78 shows smoothed-out average curves for one period of measurements for Bridges 2B, 3B, 5A and 7A and parabolas drawn through the ordinate of the profile at midspan and through the abutments.

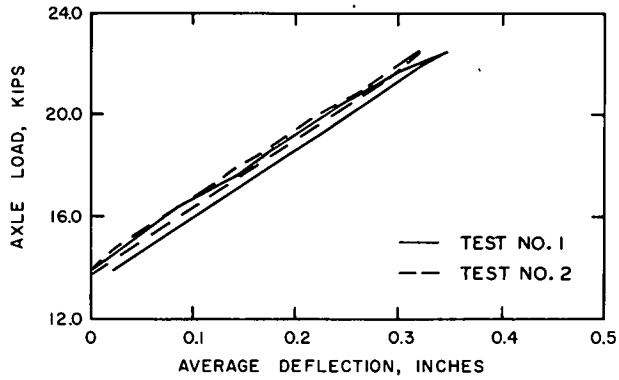

Figure 79. Load-deflection curves for vehicle tires; drive axle, vehicle 415.

Some major irregularities, of the order of 10 to 20 ft, were present in the profiles of all bridges. Thus, the irregularities of the bridge deck itself could have contributed significantly to the response of the bridge-vehicle system. The irregularities were most pronounced on Bridge 7A.

All bridges moved downward with time (Section 3.3.8). However, the major irregularities remained practically unchanged. The transverse profiles at midspan of Bridges 5A, 5B, 7B, 8A, 8B, 9A and 9B were essentially horizontal; in all other bridges they sloped steeply toward the exterior beam (Section 3.1.3 and 3.3.8). The slope of the transverse profiles remained essentially the same throughout the test even though the elevation of midspan changed.

4.1.3 Load-Deflection Characteristics of Tires and Springs

Tires.—Two typical load-deflection curves for a set of tires on an axle, obtained by loading and unloading of the axle, are shown in Figure 79. The abscissas represent the average deflection of the two sets of tires on the axle measured from the equilibrium position at the beginning of the loading test. Thus, the axle load recorded at zero deflection is that of the unloaded vehicle. The ordinates represent the total axle load. The dashed line represents a replicate test.

The slopes of the ascending and descending lines, corresponding to loading and unloading of the tire, differed by small amounts. The difference is believed to have been caused by the friction between the tire surface and the surface of the pavement.

These diagrams (Fig. 79) are typical of all 43 tire loading tests. The spread between the loading and unloading portions was always noticeable. The reproducibility of the load-deflection curves for tires was excellent. In several instances the differences in the slope of

the duplicate diagrams were of the same order of magnitude as those determined from the loading and unloading portions of the diagram for one test. In view of this, no distinction was made between the two portions of the load-deflection curves, and the tires were considered to behave as linearly elastic springs.

The spring constants were determined as the average slope of the load-deflection diagrams at the level of the static load. Under dynamic conditions, with the tire rolling over the pavement, the spread between the loading and unloading portions of the load-deflection curves can be expected to be smaller than under static conditions.

Average spring constants for the tires studied are given in Table 59 in kips of axle load per inch of average deflection of the tire. There were two tires on each front axle and four tires on each drive and rear axle. Thus, the grand average values of the spring constant per individual tire were 5.1 kips per in. for the front axle tires and 6.1 kips per in. for the drive and rear axle tires. The ratio of the axle load to the corresponding spring constant for the tire is designated as the static deflection. As the initial portion of the load-deflection curve may not be linear, the static deflection serves only as a measure of the tire stiffness.

Suspension Springs.—Two typical load-deflection diagrams for the spring of the drive axle of a test vehicle are shown in the lower half of Figure 80. The deflection is the average for the measurements at the two springs of the same axle, and the load is the total axle load. The loading was accomplished in steps. The axle weight was 13.8 kips at the time the loading was started. The springs did not deflect during the first few increments of load. The increments after 16.2 kips caused deflections of the springs increasing at an approximately constant rate up to the maximum test load of 22.6 kips. Unloading to about 17 kips produced practically no change in the spring deflections. Further unloading caused decreases in spring deflection at an approximately constant rate but slightly lower than that observed during loading. When the initial load of 13.8 kips was reached, the springs had a residual deflection of about 0.2 in.

The response of the leaf-type vehicle spring may be represented by the idealized model

TABLE 59

LOAD-DEFLECTION CHARACTERISTICS OF VEHICLES

Vehicle	Axle	Static Axle Load (kips)	Spring Constants (kips/in.)		Deflection at Static Load (in.)		Coeff. of Interleaf Friction (%)
			Tires	Springs	Tires	Springs	
			(*a*) TWO-AXLE VEHICLES				
91	Front	6.3	10.3	4.0	0.6	1.6	8
	Drive	15.0	21.0	15.8	0.7	0.9	11
94 [1]	Front	6.6	13.5	9.4	0.5	0.7	8
	Drive	15.0	29.0	16.7	0.5	0.9	11
94 [2]	Front	6.6	9.5	5.8	0.7	1.1	—
	Drive	15.0	19.6	8.7	0.8	1.7	11
A	Front	5.1	8.9	3.6	0.6	1.4	—
	Drive	15.1	27.0	7.7	0.6	2.0	17
			(*b*) THREE-AXLE VEHICLES				
B	Front	4.5	8.9	3.6	0.5	1.7	—
	Drive	15.8	27.0	7.7	0.6	2.1	16
	Rear	14.1	26.1	15.8	0.5	0.9	20
C	Front	4.6	8.9	3.6	0.5	1.8	—
	Drive	20.1	24.7	8.3	0.8	2.4	17
	Rear	20.5	25.7	15.3	0.8	1.3	19
315	Front	—	—	—	—	—	—
	Drive	12.3	20.9	8.6	0.6	1.4	11
	Rear	12.2	19.9	12.3	0.6	1.0	18
415	Front	5.8	12.2	31.7	0.5	0.2	4
	Drive	18.4	26.8	7.6	0.7	2.4	13
	Rear	18.7	26.2	16.2	0.7	1.2	19
513	Front	4.7	9.8	1.6	0.5	2.9	11
	Drive	22.4	21.2	14.0	1.1	1.6	13
	Rear	22.6	26.1	24.0	0.9	0.9	—

[1] Test made in July 1959.
[2] Tests made in June 1960.

(Fig. 80). The model consists of a linear spring of stiffness k_s and a parallel frictional damper. Denoting by P the total load on the suspension system and by P_s the component of the load carried by the spring, the maximum or limiting frictional force may be expressed as $F = \mu P_s$. The coefficient of interleaf friction, μ, is considered constant, but the limiting frictional force F increases with P_s

In an actual test, the loading starts from some initial value P_o corresponding to a deflection y_o as shown in Figure 80. In this case, the frictional force may have any value between $\pm \mu P_s$ and, as the load is increased, no deflection is produced until the frictional force reaches its limiting value and the springs engage.

The response of the model corresponds closely to the observed behavior of the interleaf springs. The model, with one modification, was used in the analytical solutions presented in Section 4.5. The limiting frictional force in the suspension system of the vehicle was assumed to have a constant value of $F = \mu P_{st}$, in which P_{st} is the static axle load. This is equivalent to assuming that the loading and unloading portions of the load-deflection diagram were parallel and were $2F = 2\,\mu P_{st}$ apart vertically. This assumption is justified because the variation of the dynamic loads from the static load was usually so small that the true value of the limiting frictional force varied little from the assumed constant value.

The spring constant of the vehicle spring k_s was evaluated from the load deflection records as the average of the slopes of the loading and unloading portions of the diagram at the static load level. The coefficient of interleaf friction was determined as one-half the vertical distance between the loading and unloading portions, measured at the point where the horizontal line representing the static axle load bisected the distance between the loading and unloading portions of the load-deflection diagram.

Figure 80 pertains to the springs of a drive axle of a three-axle vehicle. All other tests on drive axles exhibited similar general characteristics. Although the results of duplicate tests on the same drive axle were in reasonable agreement, differences in duplicate tests were found especially when partial unloading and reloading was used.

The front axles had coil springs. The loading tests on the front axles showed a behavior similar to that described for the leaf springs of the drive axles, but the amount of friction in the coil springs was considerably smaller. Reproducibility was again reasonable.

The rear axles of the semitrailers had leaf springs. The load-deflection diagrams for these springs exhibited general characteristics similar to the leaf springs of the drive axles. However, in most tests there was a gradual transition between the vertical and sloping portions of the diagram, and in many cases no distinct spring constant could be obtained. The replication of the tests was consistently poor.

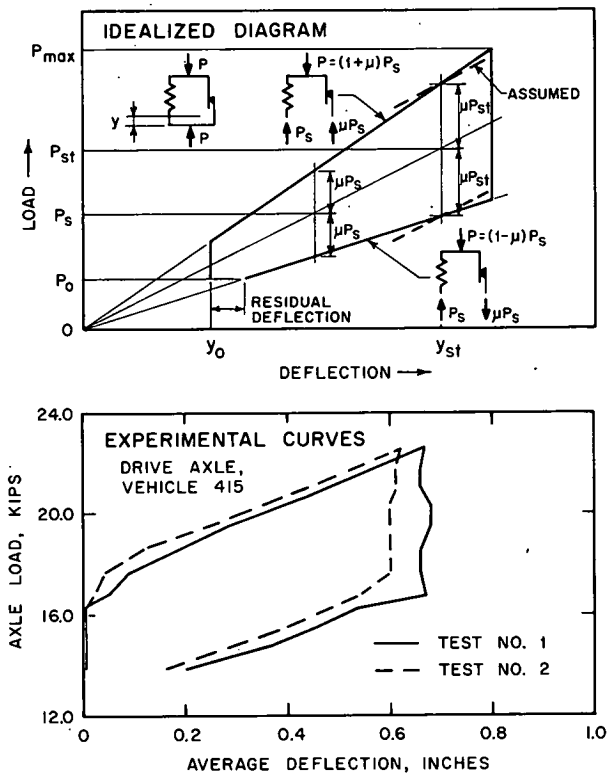

Figure 80. Load-deflection curves for vehicle springs.

The average values of the spring stiffness for all vehicles tested are summarized in Table 59. In general, two to four loadings were performed on each axle. The differences between individual tests and the averages recorded in the table were of the order of 5 to 10 percent for the front and drive axles, but up to 50 percent for the rear axles of the semitrailers. An exception was vehicle 94 for which two sets of values are given. The values, obtained one year apart, showed a decrease in spring stiffness of about 50 percent for both axles.

The spring constants ranged from 7.6 to 16.7 kips per in. for the drive-axle springs, and from 12.3 to 24.0 kips per in. for the rear-axle springs.

Table 59 also gives the static deflections of the springs, computed as the ratio of the axle load to the corresponding spring constant, and the coefficients of interleaf friction, μ, expressed in percent of the static load. The average values of the coefficients of interleaf friction ranged from 4 to 11 percent for the front axle, from 11 to 17 percent for the drive axle and from 18 to 20 percent for the rear axle of the semitrailer. The frictional force at the begin-

ning of the loading tests ranged from 6 to 25 percent of the static load or 0.4 to 1.5 times the coefficient of interleaf friction.

Computed Frequencies of Axles.—The tires and the springs of an axle may be represented by a single-degree of freedom system characterized by three quantities: the axle frequency for the springs blocked, the axle frequency for the springs free and the limting frictional force. The axle frequencies are defined by

$$\bar{f} = \frac{1}{2\pi}\sqrt{\frac{k_e g}{W}} \qquad (25)$$

in which

$\bar{f}$ = natural frequency of vibration;
k_e = effective spring constant;
g = acceleration due to gravity; and
W = weight on the axle.

For the case of blocked springs, the effective stiffness, k_e, was taken equal to the stiffness of the tires k_t. For the case of springs free, the springs were assumed to be acting in series with the tires, and the effective stiffness of the system was taken as

$$k_e = \frac{1}{\frac{1}{k_t} + \frac{1}{k_s}} \qquad (26)$$

Values obtained from Eq. 26 are given in Table 60.

The two assumptions concerning the action of the springs represent two extreme possibilities of the behavior of the test vehicle. In any time period during which the dynamic axle load varies by less than twice the limiting frictional force ($2\mu P_{st}$), the springs remain locked and there is no change in the force carried by the suspension springs. Whenever the frictional force is exceeded, the springs engage, the effective stiffness is reduced, and the change in the force carried by the suspension springs is equal to the variation in the axle load. If the direction of movement is reversed, the vehicle springs become locked until the frictional force is again exceeded. Thus, the actual frequency of the vehicle is a continuously varying quantity which depends on the change in the axle load.

4.1.4 Frequencies of Vehicles

Although the axle frequency (Section 4.1.3) is a convenient measure of the dynamic characteristics of an individual axle, the frequencies of the vehicles are useful in studies of experimental data.

Natural Frequencies of 2-Axle Vehicles.—A two-axle vehicle is characterized by two natural frequencies—the bounce frequency and the pitch frequency. The bounce frequency repre-

TABLE 60

COMPUTED NATURAL FREQUENCIES OF AXLES AND VEHICLES

Vehicle	Condition of Springs	Axle Frequency (cps)			Vehicle Frequency (cps)	
		Front	Drive	Rear	Bounce	Pitch
		(*a*) TWO-AXLE VEHICLES				
91	Blocked	4.0	3.7	—	3.8	4.4
	Free	2.1	2.4	—	2.3	2.6
94 [1]	Blocked	4.5	4.4	—	4.4	5.6
	Free	2.9	2.6	—	2.7	3.5
94 [2]	Blocked	3.8	3.6	—	3.6	4.2
	Free	2.3	2.5	—	2.4	2.7
A	Blocked	4.1	4.2	—	4.2	4.6
	Free	2.2	2.0	—	2.0	2.4
		(*b*) THREE-AXLE VEHICLES				
B	Blocked	4.4	4.1	4.3	4.1	4.5
	Free	2.4	1.9	2.6	2.0	2.4
C	Blocked	4.4	3.5	3.5	3.3	4.7
	Free	2.3	1.7	2.1	1.8	2.4
315	Blocked	—	4.1	4.0	—	—
	Free	—	2.2	2.5	—	—
415	Blocked	4.5	3.8	3.7	3.8	4.9
	Free	3.9	1.8	2.1	1.8	4.0
513	Blocked	4.6	3.0	3.4	3.1	4.6
	Free	1.7	1.9	2.3	1.7	2.0

[1] Tests made in July 1959.
[2] Tests made in June 1960.

sents the vertical motion, and the pitch frequency represents the rotary motion in the longitudinal direction.

The two natural frequencies of a two-axle vehicle can be related to the axle frequencies $\bar{f}_1$ and $\bar{f}_2$ as follows

$$(f_{1,2})^2 = \frac{1}{2}\left(C_1 \pm \sqrt{C_1^2 - 4C_2}\right) \quad (27)$$

in which

$$C_1 = \bar{f}_1^2 + \bar{f}_2^2 + \frac{1-i}{i}\left(\frac{a_1}{s}\bar{f}_1^2 + \frac{a_2}{s}\bar{f}_2^2\right);$$

$$C_2 = \frac{\bar{f}_1^2\bar{f}_2^2}{i};$$

s = wheel base;
a_1 = horizontal distance from front axle to center of gravity of the sprung mass;
$a_2 = s - a_1$; and
i = dynamic index.

The lower value of f represents the bounce frequency and the larger value represents the pitch frequency. The dynamic index is a measure of the longitudinal distribution of the vehicle mass. It is given by

$$i = \frac{r^2}{a_1 a_2} \quad (28)$$

in which r is the radius of gyration of the sprung mass. In the computation of i, the distances a_1 and a_2 could be found by statics from the axle loads; however, the values of the radii of gyration of the test vehicles were not known. This quantity is extremely difficult to evaluate, and no attempt was made to measure it in the field. Based on published data pertaining to vehicles similar in size and weight to the test vehicles, a value of $i=0.8$ was assumed for all two-axle vehicles and for tractors of the tractor-semitrailer combinations.*

Natural Frequencies of 3-Axle Vehicles.—The natural frequencies of a three-axle tractor-semitrailer combination depend on the dynamic indices of both the tractor and the semitrailer as well as on the position of the junction between the tractor and semitrailer (the fifth-wheel support).

Expressions for computing the three natural frequencies of a three-axle vehicle were presented by Huang and Veletsos.** The equations were based on the assumption that there were no horizontal components of inertia forces due to angular rotations transmitted at the fifth wheel.

On the trailers used in these tests, the loading consisted essentially of two large masses placed directly over the fifth wheel and the rear axle. For this type of loading, it can be assumed that $i=1.0$, and this value was used in the computations. It can be shown that, for $i=1.0$, the motion of the rear axle is independent of the tractor, and the frequency of the rear axle is a true natural frequency for the system. In this case the modal shapes associated with the vibration of a three-axle vehicle correspond to the bounce and pitch motions of the tractor while the rear axle remains stationary, and the vertical motion of the rear axle with the tractor in a stationary position.

The last two columns of Table 60 give the computed natural bounce and pitch frequencies of the two-axle vehicles and of the tractors of three-axle vehicles. The bounce frequencies of all vehicles were remarkably uniform, ranging from 3.1 to 4.2 cps when the suspension springs were considered blocked, and from 1.7 to 2.7 cps when the springs were considered to act in series with the tires. The natural frequency of the drive axle was very close to the bounce frequency of the vehicle, the two quantities actually being identical for 9 out of the 18 sets of values given. The pitch frequencies of all vehicles were from 30 to 40 percent higher than the corresponding bounce frequencies.

Tire-Hop Frequency.—Another natural frequency is of interest for comparisons with experimental data—the tire-hop frequency of the axle which corresponds essentially to the frequency of the chassis vibrating between the roadway and the body of the vehicle. It is given by

$$f_h = \frac{1}{2\pi}\sqrt{\frac{(k_t + k_s)\,g}{w}} \quad (29)$$

in which w is the unsprung weight of the axle. (The term "unsprung" mass or weight is used to designate the portions of the vehicle supported on the tires only.)

For vehicle 91 the computed tire-hop frequencies of the front and rear axles were 12.5 and 13.2 cps. If there is any play in the spring-suspension system, the unsprung mass may be found to vibrate on the tires only without engaging the springs. For such a case, the computed tire-hop frequency of vehicle 91 was approximately 10 cps for both axles.

4.1.5 Response of Vehicles in Tests on Pavements

The frequencies and damping characteristics of vehicles (Sections 4.1.3 and 4.1.4) were based on static loading tests. Similar characteristics could be determined dynamically with an oscillator or by dropping the vehicle from

* Janeway, R. N., "A Better Truck Ride for Driver and Cargo." Special Report No. 154, Soc. of Automotive Engrs., pp. 1-5 (1958).

** Huang, T., and Veletsos, A. S., "Dynamic Response of Three-Span Continuous Highway Bridges." Civil Engineering Studies, Structural Research Series No. 190, Univ. of Illinois (1960).

a ramp and recording the free vibrations of the stationary vehicle after the drop. Inasmuch as the necessary equipment for such tests was not available, the dynamic response of the test vehicles was studied by dynamic runs on pavements and the results were compared with the properties based on static loading tests.

The quantities of interest in the tests of vehicles on pavements were the observed frequencies of the vehicles, the damping characteristics of the tires and the suspension system, and the magnitude of the variation of the interaction force.

Each test vehicle was a complex dynamic system charactrized by either two or three degrees of freedom associated with the sprung mass and by additional degrees of freedom due to the unsprung masses. This complex system was excited by irregularities of the pavement surface. Only the predominant components of response could be distinguished in the records obtained in such tests; and the natural frequencies, amplitudes and damping characteristics associated with the predominant components of response could only be inferred from the records.

All experimental data showed variations in tire or spring forces with respect to a base value of unknown magnitude. The tire pressure measurements gave variations with respect to the ambient tire pressure at the instant the recording was started. Because the vehicle was in motion at that instant, the actual pressure and corresponding wheel loads were unknown. Similarly, the spring records showed the deformation of the springs from the equilibrium position at the beginning of the particular test run.

Additional uncertainties in the measurements were associated with the scatter in the calibration curves, with drifting of records due to loss of air pressure in the tire pressure equipment, and with inaccuracies of the time scales on the records. Thus, quantative evaluations of the tire and spring deflection records had to be considered as approximate only.

Tests over the pavements included two- and three-axle vehicles both with regular suspensions and with blocked springs. They were conducted over smooth pavements provided with a ramp to produce a sharp drop and over smooth and rough pavements without such an obstruction. Results are presented separately for the drop tests and the tests without obstruction. The results are presented concurrently for the tests of vehicles with blocked springs (on the three-axle vehicles only the drive and rear-axle springs were blocked) and vehicles with normal suspension systems, since comparisons between the two types of tests illustrated clearly the function of the springs (Figs. 81-85).

Tire pressure measurements are shown as plots of the variation of the interaction force with time elapsed from the beginning of the test. The interaction force between the pavement surface and the tire was expressed in terms of the static axle load. The base line corresponding to the static load on the axle was selected to bisect approximately the amplitude of the response.

The results of the spring-deflection measurements are shown as plots of the variation of the force in the springs with time elapsed from the beginning of the test. The force in the springs was expressed in terms of the static axle load. The equilibrium position of the spring was taken as the baseline for the spring records, and the value of 1.0 P_{st} was assigned to it although the actual force in the springs could be anywhere within the limits of P_{st} $(1 \pm \mu)$ as in Section 4.1.3.

Drop Tests on Pavements.—The results of the drop tests with a two-axle vehicle are shown in Figure 81. As an axle entered the ramp the interaction force increased both in the vehicle with blocked springs and in the vehicle with normal suspensions. In the vehicle with normal suspensions the tire-hop motion was at first predominant in the response of both axles but was rapidly damped out. The springs on both axles were compressed immediately upon entrance on the ramp and remained engaged while the vehicle was on the ramp.

The interaction force in both vehicles and the force in the springs in the vehicle with normal suspensions increased as the axle left the ramp. The motion of the two axles of the vehicle with blocked springs was essentially in phase, but the rate of decay was rapid in the front axle and gradual in the drive axle. The difference in the rate of decay for the two axles was probably caused by the interference of the rear axle; the center of oscillation for the pitching mode was located close to the rear axle, so that the effect of any component of the pitching mode was more pronounced on the front axle response than on the rear axle response.

In the vehicle with normal suspensions, the springs of the front and rear axles returned to their equilibrium position in about ½ and 1½ cycles, respectively.

The magnitude of the double amplitude of force variation for the first cycle was approximately 2.0 P_{st} for blocked springs and 1.1 P_{st} for normal suspensions. The measured frequency of the vehicle with blocked springs was of the order of 3.1 cps, or approximately 82 percent of the value determined on the basis of static measurements. In view of the inaccuracies in the measurements of tire pressure, it is impossible to say whether this difference was real or resulted only from an error in measurements. However, because differences

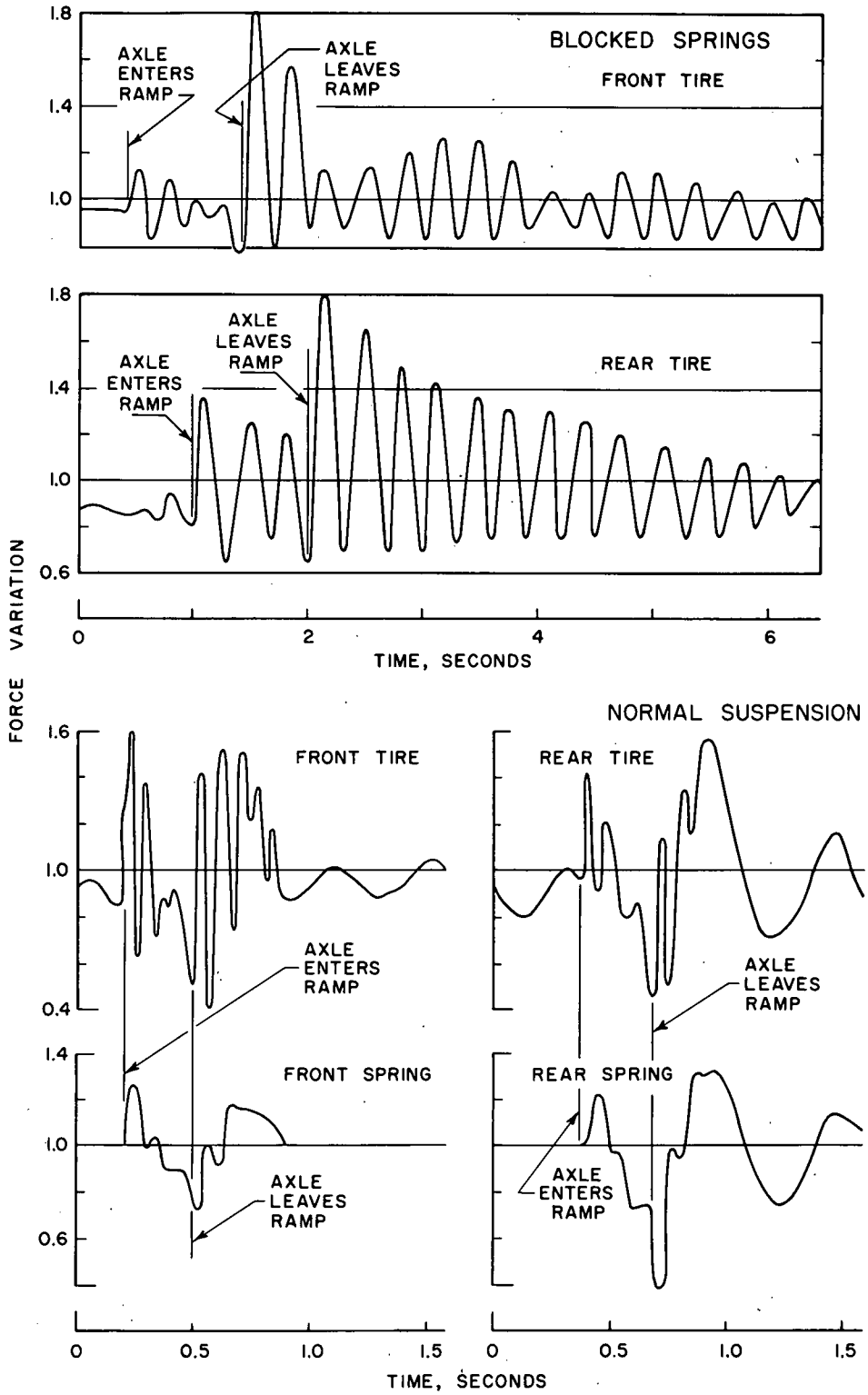

Figure 81. Drop tests on pavements with two-axle vehicle.

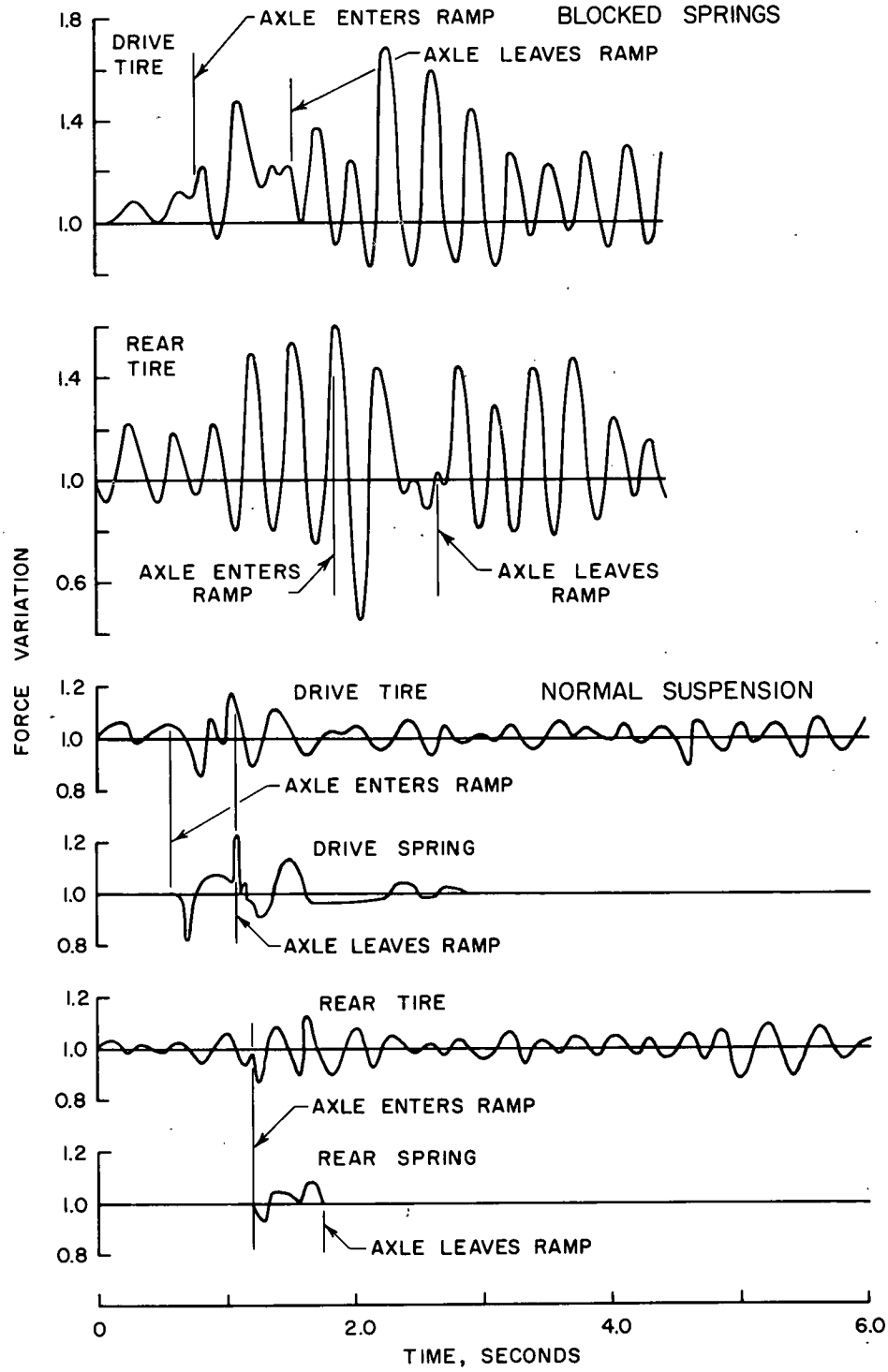

Figure 82. Drop tests on pavements with three-axle vehicle.

of the same order of magnitude were observed also in bridge tests, it appears that the frequency based on static measurements may be somewhat higher than the true frequency of the vehicle in motion.

The damping characteristics of the tire were evaluated from the records for the vehicle with blocked springs. The observed decay for the rear axles corresponded to an equivalent viscous damping coefficient of the order of 0.8 percent of critical. The damping coefficient for the front axle, based on the first cycle of oscillation, was comparable.

The frictional force in the springs was determined by comparing the amplitudes of the tire pressure and spring displacement records. On the basis of the idealized model (Section 4.1.3) the response measured from the spring record must be $(1-2\mu)\Delta P$ whenever the double amplitude of force variation on the tire pressure record is ΔP. When this relationship was applied to successive half-cycles of the rear axle response (Fig. 81) the following values of μ were obtained:

first half cycle $\mu = 0.10$
second half cycle $\mu = 0.08$
third half cycle $\mu = 0.05$
succeeding cycles $\mu > 0.10$ (*i.e.*, no spring response)

The value of μ measured in the static tests was 0.11.

Thus, the coefficient of interleaf friction μ was not a constant quantity but appeared to decrease with each oscillation. This phenomenon was observed on several records of tests with normal suspensions. It is possible that there was a certain amount of play between the leaves of the springs; as the excitation built up, the normal force between the spring leaves was reduced, and the friction force decreased in proportion. When the severity of the excitation was reduced, the coefficient of friction seems to have returned essentially to its static value.

Figure 82 shows the response of the drive and rear axle both with blocked springs and with normal suspensions for the drop tests with a three-axle vehicle. The records for the front axle of the vehicle with the drive- and rear-axle springs blocked (springs on the front axle of the three-axle vehicle always remained unblocked) showed distinctly the tire-hop response after its exit from the ramp. The measured resonant frequency of the tire-hop motion was 13 cps.

The responses of the drive and the rear axles were in phase. Furthermore, the record for the vehicle with blocked springs showed an increase in the motion of the rear axle when the drive axle was on the ramp, and the response of the drive axle showed a buildup coincident with the entry of the rear axle on the ramp. Apparently, there was a coupling between the two axles in addition to that assumed in the

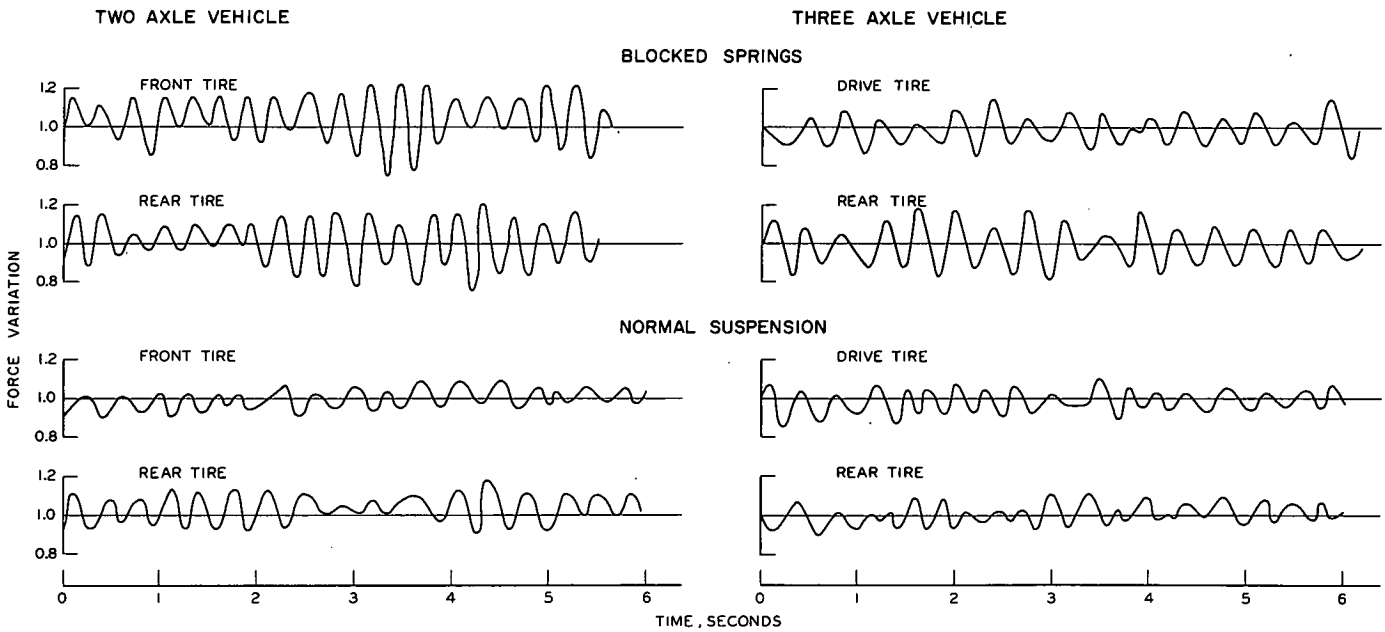

Figure 83. Tests on smooth pavements.

computations of the vehicle frequencies (Section 4.1.4). However, the effect of this coupling was small, as the data (Fig. 82) for the vehicle with blocked springs indicated a frequency of 3.4 cps, a value in reasonable agreement with the computed bounce frequency of 3.1 cps and the computed trailer-axle frequency of 3.4 cps.

Curves of force variation in the springs of the vehicle with normal suspension suggested that the coefficient of friction in the drive-axle springs was reduced to zero on the ramp and immediately after the drop; that is, the vehicle was oscillating continuously on the combined springs and tires while on the ramp. During the later portions of the run the springs remained blocked as long as the variation in the interaction force was less than the frictional force. This latter behavior was in agreement with the bilinear model for leaf springs (Section 4.1.3).

The maximum double-amplitude of force variation on the rear axle was 1.2 P_{st} with blocked springs and of the order of 0.3 P_{st} with normal suspension.

Tests on Smooth Pavements.—Figure 83 shows typical responses on a smooth pavement for both the two- and three-axle vehicles. The double amplitudes of oscillations were low, of the order 0.4 to 0.5 P_{st} for vehicles with blocked springs and of the order of 0.2 P_{st} for vehicles with normal suspensions. The spring records showed no discernible displacements and are not presented. Apparently the springs provided some damping in spite of the absence of any discernible displacements. Small changes in the spring displacements may have occurred, but were too small to be noticeable on the records.

All vehicles performed essentially a bounce motion, but the response was influenced by the

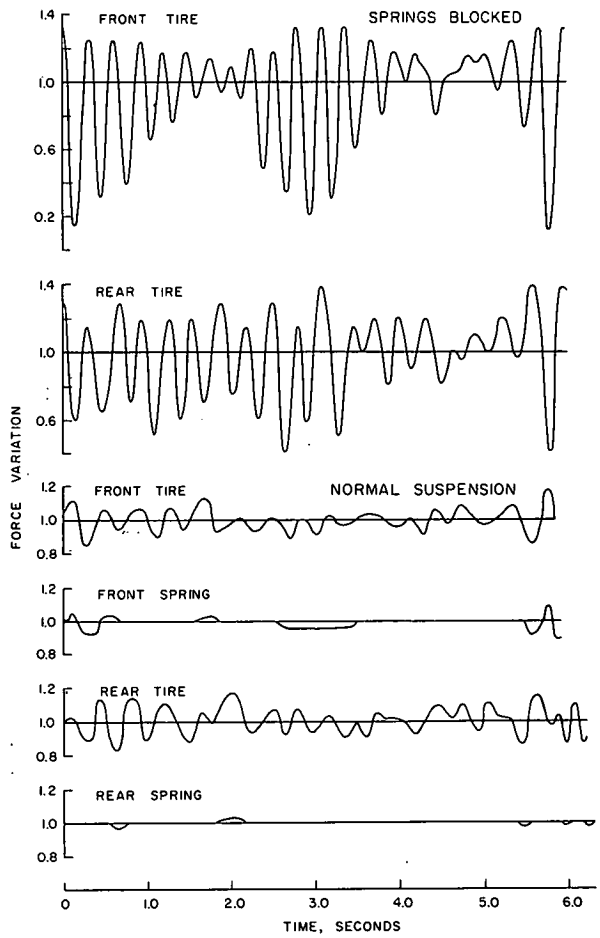

Figure 84. Tests on rough pavement with two-axle vehicle.

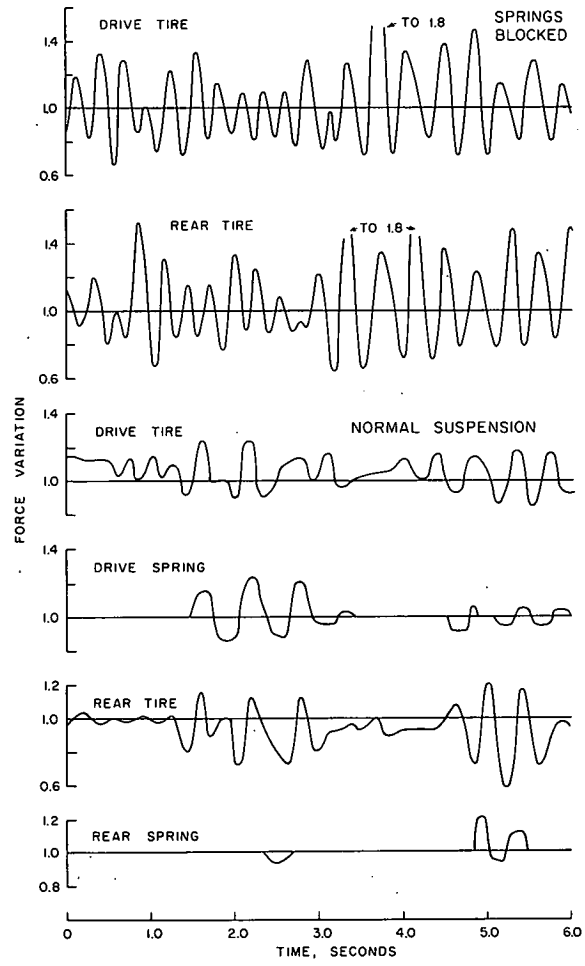

Figure 85. Tests on rough pavement with three-axle vehicle.

details of the irregularities of the pavements. The measured frequencies were essentially the same for the vehicles with blocked springs and with normal suspension, as would be expected from the observation that no discernible spring deflections were recorded in the vehicles with normal springs.

Tests on Rough Pavements.—The response curves for the two-axle vehicle on a rough pavement are shown in Figure 84. The double amplitude of force variation for the vehicle with blocked springs was of the order of 1.2 P_{st}, considerably larger than that observed on smooth pavement and approaching those recorded for the drop tests. Considerable beating effect was noticeable, particularly on the front axle.

The excitation of the vehicle with normal suspension was not continuous, but consisted of occasional impulses strong enough to produce changes in the spring deflections. The springs returned to their original position in a time corresponding to from one-half to several cycles of oscillations. The values of the coefficient of friction μ measured on the records, ranged from 10 to 12 percent for the front-axle springs and 13 to 15 percent for the rear-axle springs. The values computed from static measurements (Table 59) were 8 to 11 and 11 to 20 percent, respectively.

The response of the three-axle vehicle with blocked springs (Fig. 85) was similar to that discussed for the two-axle vehicle. The response of the drive and rear axles was generally in phase, indicating the existence of coupling between the axles. However, in certain parts of the records, the two responses were out of phase and showed higher frequencies and lower amplitudes than in former parts. Thus, some interference was probably created between the response of the two axles.

In the three-axle vehicle with normal suspensions, spring excitations lasted for several cycles of oscillation. The coefficients of interleaf friction obtained for a rear spring were between 16 and 18 percent. On the drive axle, however, the apparent friction gradually reduced to zero and then built up again.

Double amplitudes of force variation for both vehicles with normal suspension ranged up to 0.4 P_{st}, or approximately one-third of the values observed for the blocked springs. Larger amplitudes of force were always accompanied by deflection of springs.

4.2 BRIDGE-VEHICLE BEHAVIOR

4.2.1 Evaluation of Static Bridge Response

Throughout this chapter, the dynamic effects produced in the bridges under the influence of moving vehicles are expressed in terms of the corresponding effects produced at creep speed. A typical crawl curve, representing a test at crawl speed, is shown in Figure 86. Small dynamic effects amounting to several percent of the maximum response are clearly visible even at this low speed of the vehicle. Because of the presence of these small disturbances in reducing the crawl curves, a mean curve was drawn through the actual records and the mean curve was taken to represent the crawl effects.

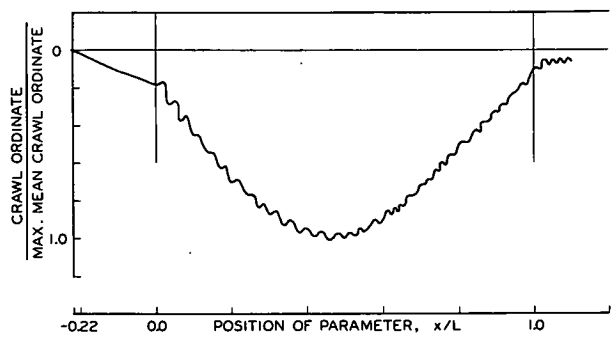

Figure 86. Crawl test; midspan deflection of center beam, Bridge 3B, vehicle 91.

In the early stages of the program, a study was made to determine whether the maximum ordinate of the mean-crawl curve was a reliable measure of the maximum static effect. Several crawl-speed records were studied, and these were correlated with the effects produced by vehicles standing on the bridge. The following quantities were compared:

1. The maximum ordinates of the mean-crawl curves;
2. The maximum crawl ordinates including minor vibrations;
3. The static response; and
4. The ordinates of the mean-crawl curve measured at the instant when the vehicle was in the same position as in the static tests.

The maximum ordinates of the mean-crawl curves were the most reproducible and were in reasonable agreement with the maximum static response.

To check the conclusions concerning the representation of the static bridge response, a separate statistical investigation was carried out involving tests on one noncomposite steel bridge, one composite steel bridge, one prestressed concrete bridge and one reinforced concrete bridge. Static and crawl measurements were obtained for each bridge as described in Section 2.4.3. The quantities were then subjected to a statistical analysis aimed at determining significant relationships. Three major conclusions were reached from this study:

1. The run-to-run variations in the measured deformations were very small and of about the same magnitude in both the crawl-speed and static tests.

2. The maximum ordinates of the mean-crawl curves were found to give the best overall approximation of the maximum static response both for strains and for deflections.

3. The differences between the maximum ordinates of the mean-crawl curves and the maximum static response were always small; in more than 50 percent of the cases the differences were less than 1.0 percent. The differences were not statistically significant for steel bridges, but even though small were usually statistically significant at the 5 percent level for concrete bridges.

In the remainder of this chapter the terms maximum crawl values or crawl values refer to the maximum ordinate of the mean-crawl curve and all crawl curves, except in Figure 86, are the mean curves drawn through the actual record.

4.2.2 Curves of Dynamic Response of Bridges and Vehicles

The response of the vehicle and the bridge is presented in terms of history curves and spectrum curves. A history curve is a plot of the variation of a quantity—such as an interaction force, deflection or moment—as a function of time. A spectrum curve represents a plot of the maximum dynamic values of a selected response as a function of the vehicle speed. Thus, for each dynamic test run there is one history curve for each measured quantity, but only the maximum response from this run is plotted on the spectrum curve.

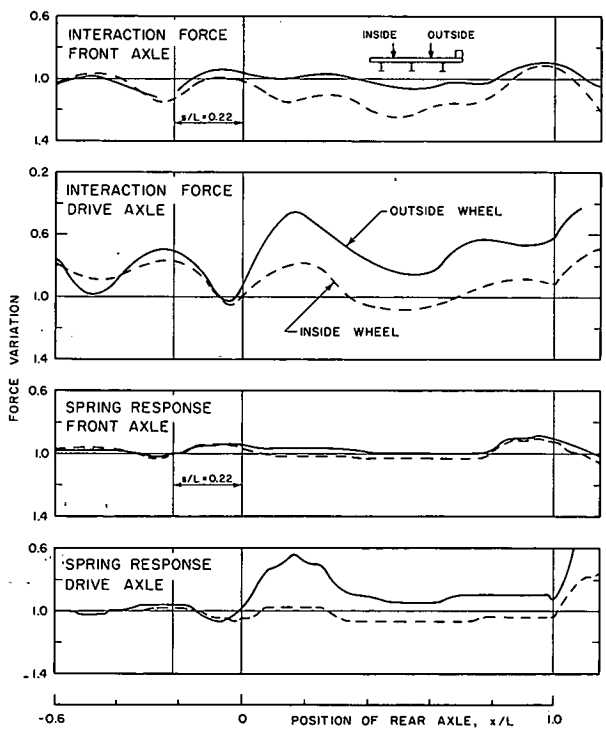

Figure 87. History curves for a regular test vehicle response, Bridge 3B, two-axle vehicle.

In this section history and spectrum curves are presented to illustrate important characteristics of the response of one test bridge under the passage of a two-axle vehicle and of the response of the vehicle itself.

History Curves.—The various types of history curves, representing the response of the vehicle and the bridge during the passage of the vehicle over the bridge, are illustrated by the results of a regular test on Bridge 3B with two-axle vehicle 91. There were no induced initial oscillations in the vehicle, and the vehicle was centered over the middle beam of the bridge producing a concentric loading.

History curves for the response of the vehicle are shown in Figure 87. The abscissas of all history curves are given in terms of the ratio x/L, in which x is the distance between the entrance to the bridge and the position of the rear axle of the vehicle and L is the span length. Thus,

$$\frac{x}{L} = \frac{vt}{L} = \frac{t}{t'} \qquad (30)$$

in which

v = speed of vehicle;
t = elapsed time measured from the instant of entry of the rear axle on the bridge; and
t' = time of transit.

The abscissas of history curves may be interpreted as position coordinates or as time coordinates. Negative values of x/L are times prior to the entrance of the rear axle on the bridge. Of particular interest is the point of entry of the front axle which occurs at $x/L = -s/L$, where s is the axle spacing. Values of x/L greater than 1.0 correspond to the free bridge vibration era following the exit of the vehicle.

The upper curves (Fig. 87) are history curves of the interaction force for all four wheels. The dynamic interaction forces, plotted as ordinates, are given in terms of their static value as in Section 4.1.5 in presenting the response of the vehicles on pavements. However, in contrast to curves for pavement tests, the increase in force variation is plotted downward to conform with the direction of increased bridge deformations.

Both axles had a vertical component of motion prior to entering the bridge. This was observed on all records. Although the motion of the front axle was small, the double amplitude of oscillation of the rear axle was of the

order of 0.3 P_{st}, somewhat higher than the results obtained from tests on smooth pavements.

The variation of the interaction forces while the vehicle was on the bridge was generally small for the front axle. For the rear axle, however, there was a large reduction in the interaction forces immediately after the entrance, caused partially by the sudden change in the curvature of the profile at that point and to some extent by the deflection of the bridge itself. The ensuing motion of the rear axle had a frequency of the order of 2.2 cps. At the exit, forces were again reduced as the axle passed to Bridge 3A.

Response of the vehicle springs is shown in the lower curves. As for tests on pavements (Section 4.1.5) the ordinates give the dynamic forces in the springs in terms of the static load. It is apparent that the springs engaged only for a small fraction of the time of transit so that, generally the vehicle vibrated on its tires only.

The history curves for the dynamic response of the bridge are shown in Figure 88, including amplification factors and dynamic increments of deflection and moment. Curves for the amplification factors also include the corresponding crawl curves shown as dashed lines. The amplification factors are the ratios of the measured instantaneous dynamic response to the maximum crawl response. The dynamic increment is the instantaneous difference between the dynamic response and the corresponding crawl ordinate, expressed in terms of the maximum crawl response. (The dynamic effects designated in this chapter as pertaining to moment were computed as ratios of strains measured at the bottom of the bridge beam; usually at midspan of the center beam.

The charactristics of the dynamic behavior can best be observed on the dynamic increment curves. It is of particular interest that the frequency of oscillation throughout the test run was essentially the natural frequency of the bridge. Oscillations corresponding to the frequency of the interaction force can not be distinguished on the curves.

The history curves of amplification factors for deflection and moment show that the total dynamic responses for these two quantities at midspan of the center beam were different. This was primarily due to the differences in the shapes of the corresponding crawl curves. However, when the history curves of dynamic increments for the two responses are compared, the experimental data confirm the

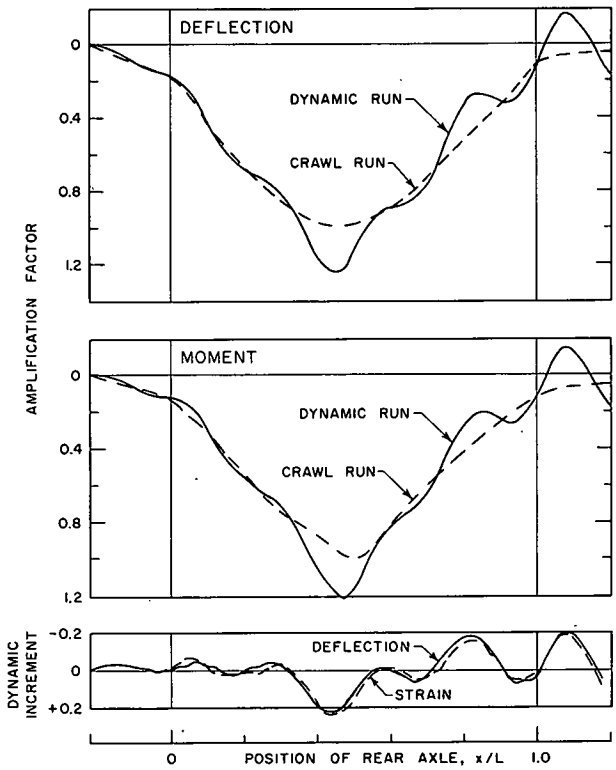

Figure 88. History curves for a regular test bridge response, midspan of center beam.

theoretical predictions * that the two curves are practically identical, even though the amplitude of the dynamic increment curves for deflection was generally somewhat larger than that for moment. Thus, knowing the dynamic increment for one response, the corresponding value for the other can be estimated.

Longitudinal and Lateral Distribution of Dynamic Effects.—Figure 89 shows the history curves of the response of strain gages at the third points and at midspan of the center beam of Bridge 3B. The amplification factors were obtained by dividing the history curve ordinates by the maximum crawl value at the section considered. A comparison of the total response (amplification factor) curves and dynamic increment curves shows that differences in the total response were caused by differences in the shapes of the crawl curves and that the dynamic increments were essentially equal in both phase and magnitude. The dynamic increment curves showed a response only in the first mode of vibration; the contribution of the second mode was negligible even at the third points.

The dynamic increment curves for deflection and moment at midspan of the center beam are

* Huang, T., and Veletsos, A. S., "Dynamic Response of Three-Span Continuous Highway Bridges." Civil Eng. Studies, Structural Research Series No. 190, Univ. of Illinois, pp. 66-70 (1960). See also Oran, C., and Veletsos, A. S., "Analysis of Static and Dynamic Response of Simple-Span, Multigirder Highway Bridges." Civil Eng. Studies, Structural Research Series No. 221, Univ. of Illinois, p. 77 (1961).

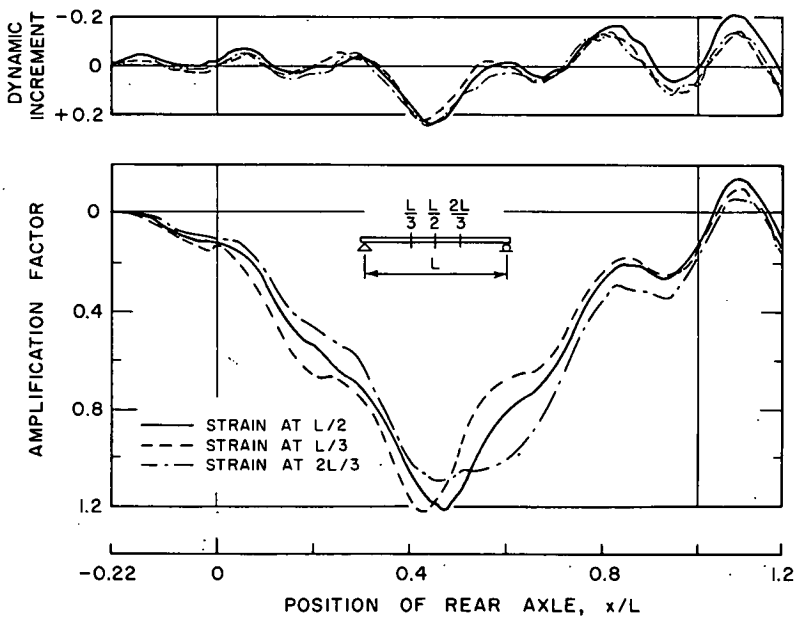

Figure 89. Third-point response of center beam.

compared with the corresponding curves for the edge beams in Figure 90. The dynamic increment curve for each gage location has been normalized with respect to the maximum crawl value at the location considered. The bridge behaved essentially as a beam, as the three dynamic increment curves were similar. However, if the dynamic increments were proportional to the static effects, the curves for the three beams would coincide. It is apparent that this condition was not satisfied exactly; although the response of the three beams was in phase, there were slight differences in magnitude.

History curves of dynamic increments of moment at midspan of all three beams of Bridge 3B, and at the third points and midspan of the center beam of Bridge 3B, are shown in Figure 91 for a run with induced initial oscillations of the vehicle. The curves are practically the same for the three beams for strain at midspan. In contrast to the regular runs, the dynamic increment curves reflect the contribution of the variation of the interaction

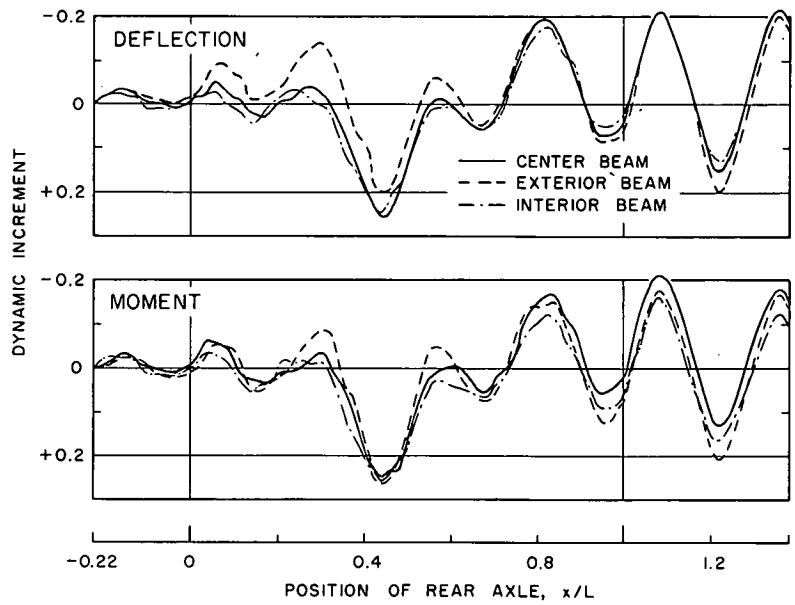

Figure 90. Midspan response of three beams.

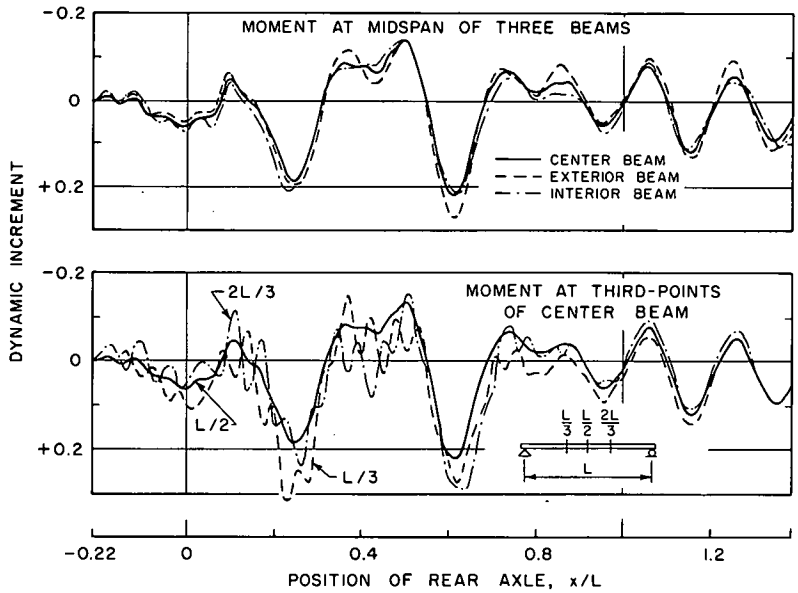

Figure 91. Run with induced vehicle oscillations; bridge response.

force in addition to the contribution of the inertia of the bridge. The records also show that the curves for the edge beams oscillated about the curve for the center beam, indicating the presence of a slight contribution of the torsional mode of vibration.

History curves for dynamic increments for moment at the third points and midspan of the center beam, for the run with induced initial oscillations, are shown in the lower part of Figure 91. The high frequency oscillations observed at the third points corresponded to the second natural frequency of the bridge. (The third-point responses are 180 deg out of phase and have a frequency approximately 4 times the natural frequency of the bridge.) This contribution of the second mode was always most pronounced in the early stages of the response and tended to decrease at later stages. This was to be expected since damping in the bridge tended to decrease the high frequency oscillations faster than those of lower frequencies.

In comparison with the regular tests (Fig. 90) the contribution of the second mode (Fig. 91) was more pronounced because of the greater initial disturbance applied to the bridge. However, in all records studied, the contribution of the second mode was only of the order of 10 percent or less of the maximum static response. It is apparent that the high frequency oscillations contributed a relatively small amount to the total bridge response.

The data (Figs. 89-91) illustrate that the response of a single gage, expressed as a history curve of dynamic increments in the form presented, reflects the dynamic behavior of the entire bridge with sufficient accuracy. In the following portions of this chapter emphasis is placed primarily on the dynamic effects at midspan of the center beam.

Spectrum Curves.—Although history curves for individual runs give the most complete picture of the bridge-vehicle behavior, the large volume of data obtained precluded the study and presentation of dynamic effects in terms of history curves alone. From a design point of view, the maximum value of a given response is of primary interest; consequently, most of the data are presented in the form of spectrum curves.

Two typical sets of spectrum curves are shown in Figure 92, pertaining to tests of Bridge 3B with vehicle 91. The curves in the upper section correspond to runs with no induced initial oscillations, and the curves in the lower section are for tests with initial vehicle oscillations. The ordinates are maximum amplification factors for moment or deflection. The abscissas are given in terms of the speed parameter α defined as

$$\alpha = \frac{vT_b}{2L} \qquad (31)$$

in which T_b is the fundamental natural period of the bridge.

Spectrum curves include amplification factors for moment and deflection at midspan of the center beam. Spectrum plots show all experimental points obtained in one subseries and a curve drawn through the points to emphasize the trend. Although the scatter in the data prevents a clear definition of the shape of the curve, a difference in the magnitude in the spectrum curves for deflection and moment is evident. The difference is related primarily to

the shape of the crawl curves for the loading considered. It may be noted in Figure 88 that in the region of the maximum response, the crawl curve for moment is peaked while the crawl curve for deflection is relatively flat. If the maximum dynamic increment occurs anywhere in this relatively flat region, the total response will be essentially the same. On the other hand, the maximum moment response is sensitive to variations in the position of the maximum dynamic increment. Thus the amplification factor depends both on the position and magnitude of the "critical" dynamic increment, *i.e.*, that peak dynamic increment which produces the maximum amplification factor when combined with the crawl curve.

Spectrum curves for the dynamic tests with initial vehicle oscillations have two features noticeably different from those for regular tests. First, the scatter of the individual test points is substantially smaller for the tests with initial vehicle oscillations. This was observed in all tests in which the initial oscillations of either the vehicle or the bridge were controlled. Apparently, the uncontrolled variation in the initial conditions occurring in the normal runs affected both the magnitude and phase of the dynamic increments and thus the maximum amplification factors. Second, the amplification factors were considerably more sensitive to variations in speed than for the regular runs. In tests with initial oscillations of the vehicle there were two components of the response, one due to inertia of the bridge, and the other due to variation in the interaction force. Both could change the magnitude and position of the critical dynamic increment and thus increase sensitivity to speed.

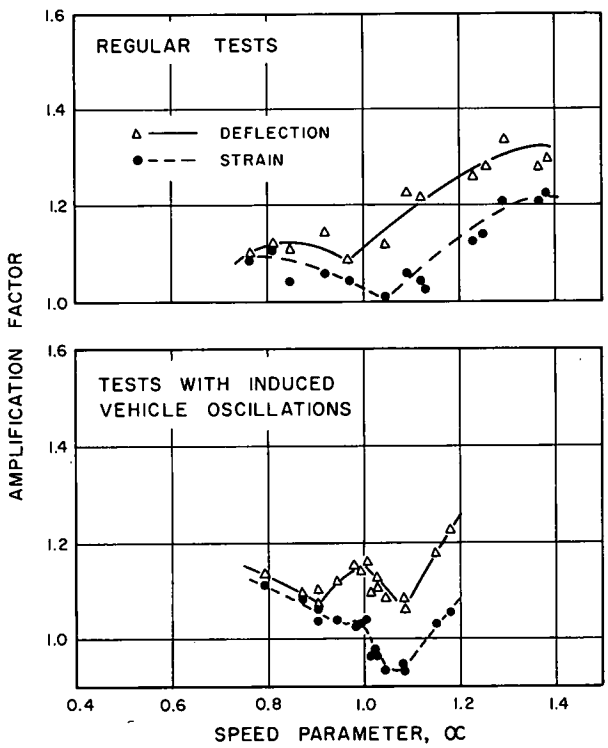

Figure 92. Representative spectrum curves at midspan of center beam Bridge 3B, vehicle 91.

4.2.3 Bridge-Vehicle Parameters

The dynamic response of the bridge-vehicle system depends on the vehicle speed and the combination of several pertinent bridge and vehicle parameters. The bridge parameters include weight, frequency and permanent deflection. The vehicle parameters include axle spacing, total weight, weight distribution to the axles, axle freqencies, limiting frictional forces in the springs and the dynamic index. These parameters enter the analysis as dimensionless ratios.

The speed parameter, weight ratio, frequency ratio and profile variation parameter are discussed in the following. Other parameters either were known to be of minor importance or were essentially constant in this study. The axle spacing ratio s/L belonged in the latter category.

Speed Parameter.—The speed parameter α is defined by Eq. 31. It follows from the definition of α that the bridge undergoes approximately $\frac{1}{2}\ \alpha$ cycles of oscillation during the passage of an axle over the span. This relationship is only approximate because the period of the bridge-vehicle system is a function of the position of the vehicle on the bridge. It is apparent from Section 4.2.2 that the frequency of the dynamic increments is important in determining what ordinate of the crawl curve combines with a peak dynamic increment to produce the maximum total response. Thus, the parameter α is obviously a more significant measure of the effect of speed than the vehicle speed alone.

Weight Ratio.—The weight ratio is defined as

$$R = \frac{\text{gross weight of vehicle}}{\text{total weight of bridge}} \qquad (32)$$

The total weights of the vehicles are given in Table 20, and the total weights of the bridges, in Table 18.

Frequency Ratio.—Associated with each axle of the vehicle is a frequency ratio defined as

$$\phi = \frac{\text{frequency of axle}}{\text{natural frequency of bridge}} \qquad (33)$$

The axle frequency is the natural frequency of a single-degree freedom system. The mass of the system corresponds to the axle load, and its stiffness is equal to the effective spring stiffness of the axle. In the discussion of the test data, the term "axle frequency" refers to the frequency of the drive axle of the vehicle, because

it corresponded closely to the computed natural frequency of the vehicle.

Two subscripts are used in conjunction with the frequency ratio ϕ. Subscript t refers to blocked springs, and subscript ts refers to normal suspension.

Profile Variation Parameter.—Also associated with each axle is the ratio denoted by Δ which is defined as:

$$\Delta = \frac{\text{deflection of unloaded bridge at midspan}}{\text{static deflection of axle}} \tag{34}$$

The numerator of this ratio may be positive or negative, depending on whether the deflection is downward (sag) or upward (camber). Thus, the sign of Δ is the sign of bridge deflection. The static deflection of the axle used in computing Δ is taken to be that of the drive axle of the vehicle, assuming blocked springs.

The deflection of the unloaded bridge was taken as that at midspan of the center beam measured from a straight line connecting the supports. It was obtained from plots relating the midspan deflections with time. The static deflection of the axle is given in Table 59.

The profile variation parameter has a simple physical meaning. It represents the change in the interaction force due to a vertical movement equal to the deflection of the unloaded bridge at midspan. The interaction force is expressed in terms of the static axle load, and the springs are assumed to be blocked.

Ranges of Parameters.—Table 61 gives the ranges of the principal bridge-vehicle parameters for various bridge-vehicle combinations used in regular dynamic tests. The speed parameter α_{max} is the maximum value of speed parameter α for any particular subseries of tests.

The values of α ranged up to 0.22. For regular highway bridges of the same span, this value of α corresponds to higher vehicle speeds than those used in this program. The test bridges were designed for high stress levels and therefore their natural periods were higher than those of bridges designed for conventional allowable stresses.

Parameters R, ϕ_t and ϕ_{ts} varied approximately by a factor of 2. The maximum values of the weight ratio, $R = 0.66$, and of the frequency ratios, $\phi_t = 1.23$ and $\phi_{ts} = 0.76$, are high for 50-ft simple-span bridges, but the ranges of these parameters are representative of regular highway bridges.

The bridges were not specifically designed for dynamic tests, and the test vehicles were trucks available at the project. The significant parameters could not be varied continuously and independently of each other throughout their respective ranges. Therefore, complete isolation of the effects of the individual parameters was not possible.

4.2.4 Initial Oscillations

In addition to the parameters described in the preceding section, the behavior of the bridge-vehicle system depends on the state of oscillation of the bridge and the vehicle at the instant the vehicle enters the span. The bridge was initially at rest in all regular tests. The vehicle, however, generally was in vertical motion on its suspension system prior to its entrance on the bridge. The magnitude and phase of this oscillation were uncontrolled.

Initial vehicle oscillations were caused by the unevenness of the approach pavement, including the discontinuity between the approach pavement and the bridge deck. For the majority of the regular tests the nature and magnitude of the initial vehicle oscillations were unknown. However, in one series of tests tire pressure measurements provided information for a detailed study of the initial vehicle oscillations.

Typical curves of the variation of the interaction force on approach pavements are shown in Figure 93. The variations in the interaction force are given in terms of the static load, plotted against time, with time 0.0 correspond-

TABLE 61
RANGE OF PARAMETERS FOR REGULAR TESTS

Bridge Type	Max. Value of Speed Parameter α_{max}	Weight Ratio, R		Frequency Ratio				Profile Variation Parameter,[1] Δ	
				Springs Blocked, ϕ_t		Springs Acting, ϕ_{ts}			
		2-Axle Veh.	3-Axle Veh.	2-Axle Veh.	3-Axle Veh.	2-Axle Veh.	3-Axle Veh.	2-Axle Veh.	3-Axle Veh.
Composite steel	0.18	0.28	0.38–0.66	0.78–0.91	0.64–0.91	0.48–0.51	0.37–0.47	1.3	0.6–1.7
Noncomp. steel	0.19	0.26	0.32–0.61	0.97	0.84–1.04	0.63	0.24–0.54	0.9	0.6–1.0
Prestressed concrete	0.11	0.21	0.28–0.44	0.56	0.56–0.78	0.36	0.26–0.38	0.7	0.0–0.7
Reinforced concrete	0.22	0.21	0.28–0.48	1.18	0.90–1.23	0.76	0.45–0.63	(−0.6)	(−0.4)–(−1.3)

[1] Negative sign indicates camber.

ing to the entrance of the axle on the bridge. The force-time curves are given for four bridges; two runs of two-axle vehicle 91 at different speeds are given for each bridge. Only the response of one rear wheel is given for each set of conditions.

The curves show clearly the vertical motion of the vehicle at approximately the natural frequency of the vehicle with springs blocked, and the tire-hop motion caused by the sudden discontinuity between the approach slab and the bridge deck. (Occasionally tire-hop motion was recorded also while the vehicle was on the approach pavement; the corresponding high-frequency oscillations were eliminated from Figure 93 in order to indicate clearly the predominant frequency of the vehicle oscillations.) It is also apparent that the initial motion of the vehicle at the entrance varied from run to run. In general, the initial condition varied from an almost true smooth rolling condition to high values of initial variation in the interaction force and in vertical velocity.

TABLE 62
MEAN AMPLITUDES OF FORCE VARIATIONS ON APPROACHES

Bridge	Mean Amplitude of Rear Axle [1]	
	Vehicle 91	Vehicle 513
3B	0.14	0.16
7A	0.16	0.16
9B	0.08	0.08
6A	0.09	—

[1] In terms of static load.

Data on the magnitude of the initial oscillations from seven subseries were studied. Four bridges with two-axle vehicle 91 (Fig. 94) and three-axle vehicle 513 were included. For each bridge the amplitude of oscillation, for the cycle immediately preceding the entrance of the axle on the bridge, is plotted as a function of vehicle speed. The amplitude is given in terms

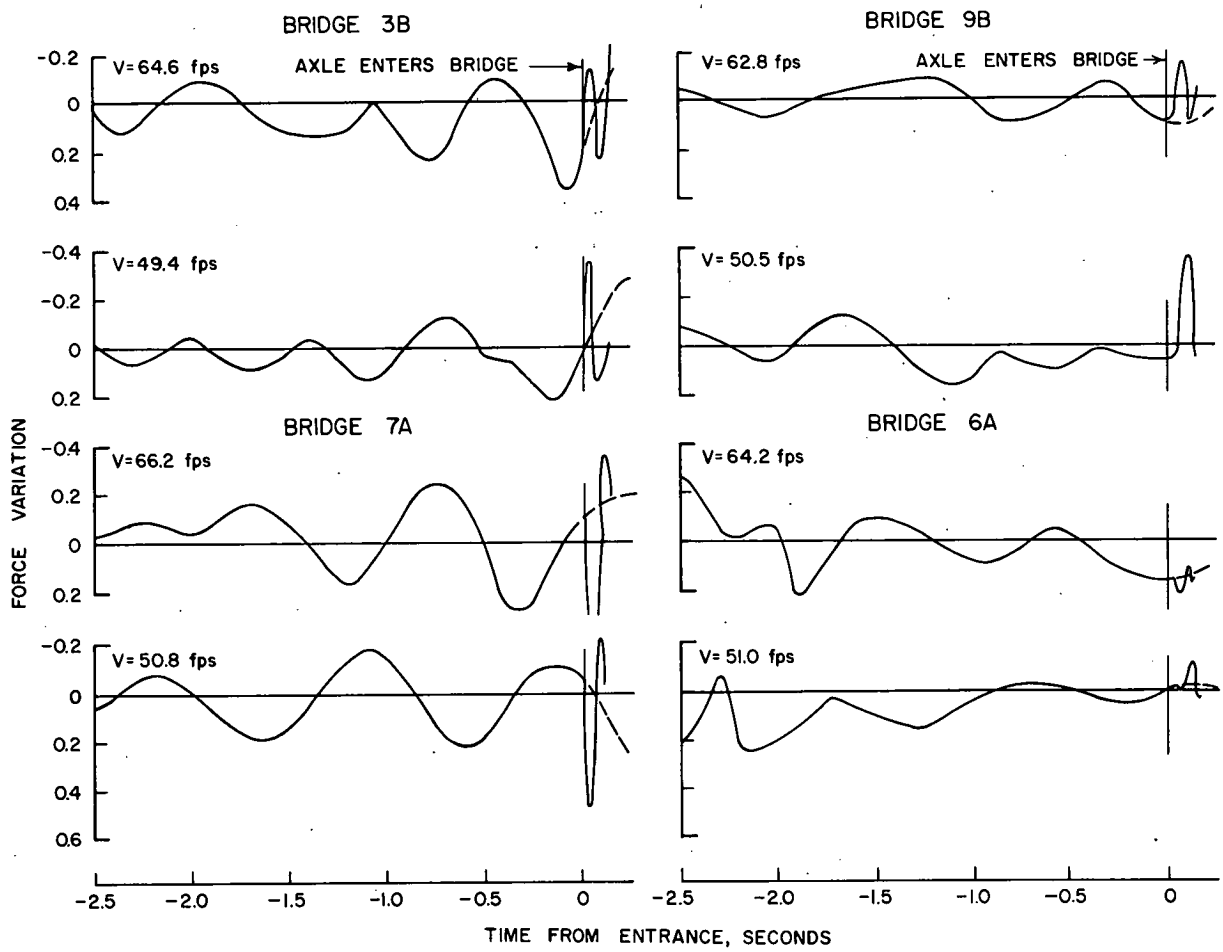

Figure 93. Typical variations of forces on approach pavements, vehicle 91, rear wheel.

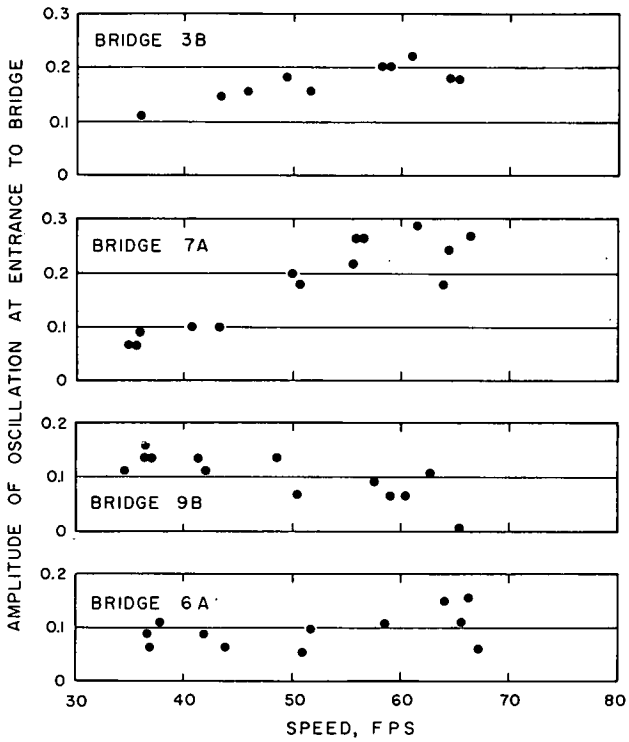

Figure 94. Variation of magnitude of initial oscillations with speed, vehicle 91.

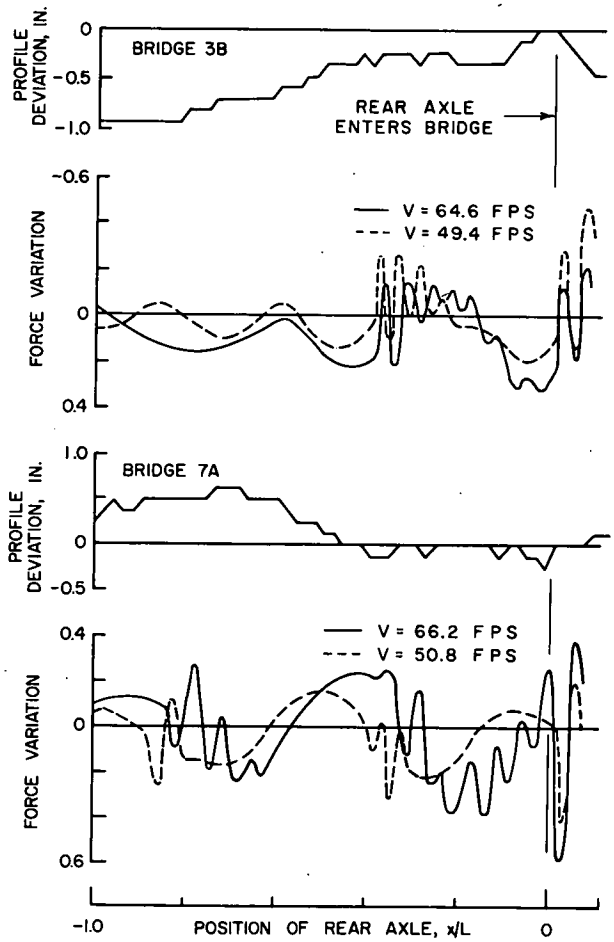

Figure 95. Relationship between approach profile and vehicle oscillations.

of the static axle load. It varied between 0.0 and 0.3, and with the exception of Bridge 9B, generally increased with speed. The largest amplitude of initial oscillation occurred on the approaches to Bridges 3B and 7A, and the smallest on Bridges 9B and 6A. The scatter of the points in Figure 94 was not particularly large.

Table 62 gives mean amplitudes of force variation in terms of static load in the seven subseries considered. The ranges of speed covered by the two different vehicles were about the same as was the mean amplitude of oscillations for the two-axle and the three-axle vehicles on the same approach.

The variation in the interaction force for two runs on Bridge 3B and two runs on Bridge 7A are also plotted in Figure 95 containing the profiles of the approaches in addition to the force-variation curves. The runs selected are the same as those shown in Figure 93, but the tire-hop oscillations were not smoothed out. The beginning of the high frequency tire-hop oscillations and of some lower frequency components were generally related to the profile variations. Of particular interest is the sharp rise in the profile starting approximately at $x/L = -0.1$, or 5 ft from the entrance to Bridge 3B. This rise seemed to have induced a rather large upward velocity in the axle. Tire pressure records for all test runs on this bridge showed essentially the same phase angle when the axle entered the bridge. In contrast to Bridge 3B, the phase angle of the interaction-force curves at the instant of entry was arbitrary for all other bridges.

Studies of the relationship between the magnitude of the initial vehicle oscillations and the characteristics of the approaches were based on measured longitudinal profiles such as those shown in Figure 95 and on the present serviceability index.* The dynamic amplitudes computed on the basis of simple approximations of the measured longitudinal profile were in reasonable agreement with the measured values. On the other hand, no correlation was found between the force variation and the present serviceability index.

4.2.5 Reproducibility of Test Results

Experimental Scatter.—The extent of experimental scatter was studied with three subseries of tests on Bridge 3B carried out on July 6, 9 and 10, 1960. The three subseries were made with vehicle 415, and each included at

* The present serviceability index (PSI) is described in Road Test Report No. 5.

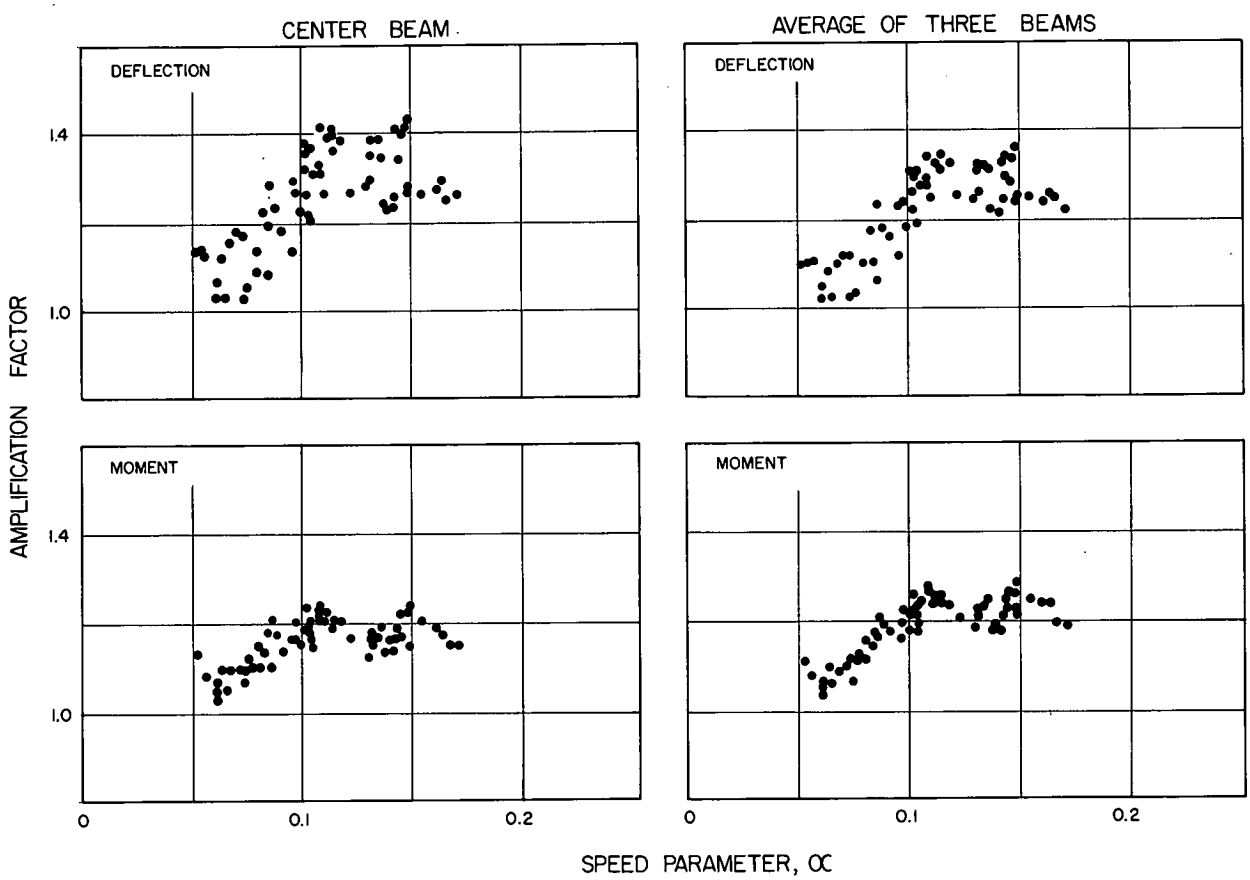

Figure 96. Spectrum curves for regular tests on Bridge 3B, vehicle 415.

least 49 dynamic runs with speed varying roughly from 20 to 50 mph. Two comparisons are of prime interest: (1) a comparison of the results of individual replicate runs within one subseries and (2) a comparison of the trends in behavior in replicate subseries.

The spectrum curves (Fig. 96) for the first subseries are for both deflection and moment. Data for the response of the center beam at midspan are shown on the left and the average response of the three beams at midspan is shown on the right. The width of the scatter band for the center beam was approximately 20 percent of the maximum static response for the deflection and 10 percent for the moment. The scatter was reduced by averaging the responses of the three beams, but the trends of the data were the same for the average of the three beams as for the center beam.

The larger scatter for deflection than for moment was related to the shapes of the crawl-response curves. For the three-axle vehicles, the crawl curve for deflection at midspan showed more change in the vicinity of maximum static response than the crawl curve for strain. (For two-axle vehicles the relative shapes of crawl curves were just reversed, see Section 4.2.2.) Thus, the deflection was more sensitive to the location of the maximum dynamic increment in relation to the maximum crawl response.

History curves of dynamic increments of deflection at midspan of the center beam are shown in Figure 97 for two different values of α—two runs for the higher value of α and three for the lower value.

For the two replicate runs corresponding to the higer value of α the bridge behavior was identical for all practical purposes, except for a consistent difference in the magnitude of the dynamic increments. For the slower speed, however, the agreement was reasonably good only up to the value of $x/L = 0.3$; at higher values of x/L the records showed a superimposed wave of high frequency.

The value of $x/L = 0.3$ corresponded approximately to the entrance of the drive axle on the span, suggesting that discrepancies were primarily due to different initial oscillations of the vehicle. No tire pressure measurements were available to substantiate this explanation; however, it was corroborated by the fact that better duplication of results was usually obtained in the earlier subseries conducted while the approach pavements were relatively smooth.

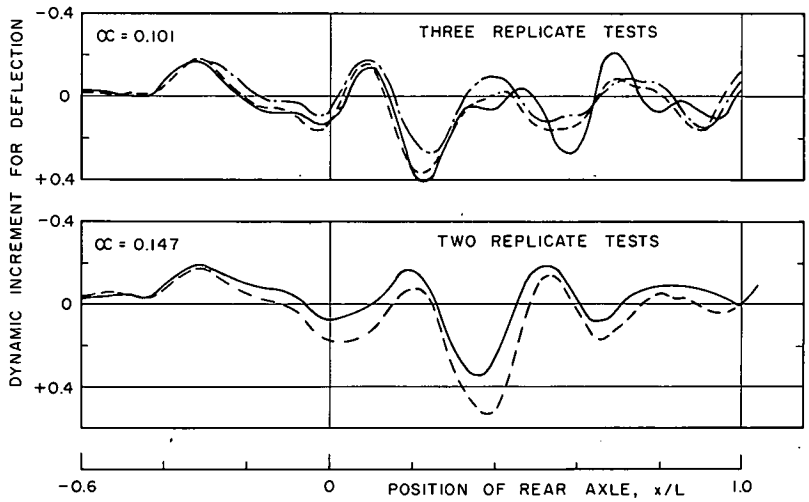

Figure 97. Dynamic increment curves for replicate tests, Bridge 3B, vehicle 415.

The spectrum curves for the other two subseries are plotted in Figure 98. A comparison between the three subseries (Figs. 96 and 98) shows day-to-day variations in spectrum curves. The shape of the spectrum curves agreed very well for all three subseries, even though the magnitude of the average results for the three days varied somewhat. Interestingly the experimental scatter for the first subseries was larger than the over-all scatter for the second and third series combined. The data show that a single point on a spectrum curve has little meaning because of the experimental scatter introduced by uncontrolled test conditions and by errors in recording and reduction of the data. However, the aggregate of the points described adequately the general trends in the maximum dynamic response.

Replicate Bridges.—Three pairs of bridges, built to the same specifications, afforded an opportunity to study the duplication of the response from bridge to bridge. As the two bridges of each pair were located in tandem in the same lane, the response of both bridges was recorded during the same vehicle runs so that vehicle characteristics and time were eliminated as variables. The only apparent differences between the tests on the two bridges of a pair were associated with the uncontrolled initial oscillations of the vehicle (The vehicle entered the second bridge after oscillations had been imparted to it by the motion of the first bridge.) and with the irregularities of the bridge profiles.

In the top section of Figure 99, the response of Bridge 9B (first in line of travel) and 9A (second in line of travel) is compared for one subseries of tests. The responses of the two bridges were essentially the same. An examination of the amplitudes of the interaction forces indicated that the oscillations on the approach pavement and on Bridge 9A (acting as the approach to Bridge 9B) had essentially the same amplitude, averaging 7 to 8 percent of the static load. For such small amplitudes, the phase of the initial motion of the vehicle was unimportant.

The lower section of Figure 99 similarly compares Bridges 7A (first) and 7B (second). The spectrum curves for the two bridges are

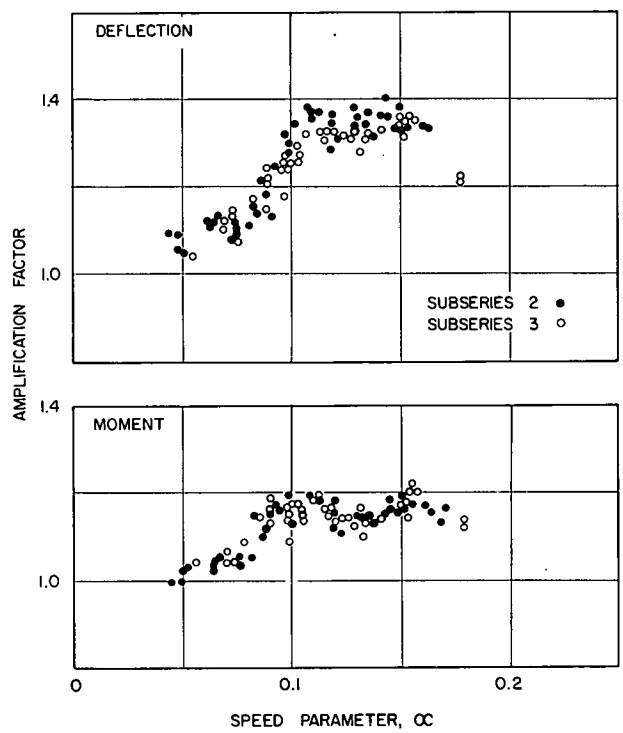

Figure 98. Duplication of spectrum curves, Bridge 3B, vehicle 415.

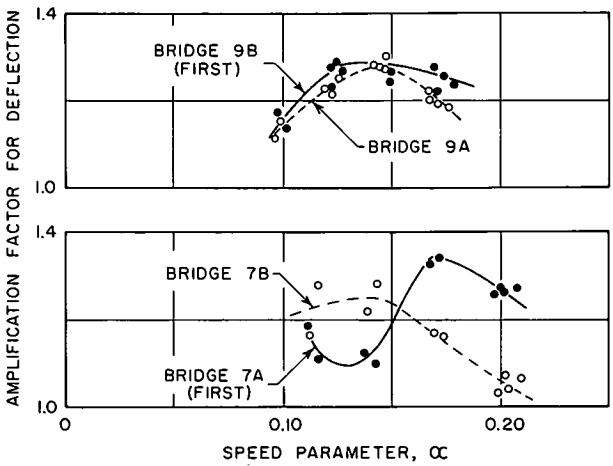

Figure 99. Comparison of responses of first and second bridges, vehicle 513.

radically different. The amplitude of the initial oscillation of the vehicle prior to entrance on Bridge 7A was of the order of 18 percent of the static load. By the time of exit from the first bridge, the amplitude was generally reduced to approximately 10 percent of the static load. However, this reduction in the amplitude of initial oscillation alone could not account for the differences. It is indicated in Section 4.5.3 that large irregularities in the profile of Bridge 7A contributed substantially to the large amplification factor at $\alpha = 0.2$.

4.3 RESULTS OF REGULAR TESTS

4.3.1 Summary of Maximum Amplification Factors

A summary is given in this section of all test results for the regular tests except those shown in Figures 96 and 98. The results are presented in the form of spectrum curves for both deflection and moment based on the response at midspan of the center beam.

Major Trends.—Spectrum curves for three-axle vehicles are shown for steel bridges (Fig. 100) and for concrete bridges (Fig. 101). On the left are the spectrum curves for deflection and on the right are those for moment. A separate plot is included for each bridge. Various symbols distinguish individual subseries of tests.

Spectrum curves for deflection show that the dynamic effects increased with increasing speed parameter α. This increase was apparent both for the upper and lower bounds of the data even though other bridge-vehicle parameters varied within wide limits for every bridge.

The only exception was the plot showing the results for Bridge 3B. For the subseries, the experimental points generally followed a broad curve with maximum values occurring between $\alpha = 0.10$ and 0.14. The subseries shown covered a relatively narrow range of α; a broader range of the speed parameter was covered in the tests shown in Figures 96 and 98. For the broader range, a general increase was apparent in the amplification factors with increasing values of α.

The spectrum curves for moment followed the same general pattern as those for deflection, but the amplification factors were lower. A very large scatter was obtained for moment amplification factors of Bridge 5A (Fig. 101). This large scatter is believed to have been associated with cracking of the prestressed concrete beams.

The largest amplification factors observed were those for Bridge 7A corresponding to the largest values of α. However, a consistent pattern of differences is apparent among the spectrum curves for the various bridges. For example, for the same values of α, the lowest recorded amplification factors for Bridge 5A were consistently higher than the highest values obtained for Bridge 7A. The amplification factors for Bridges 2B and 9B generally fell between these two extremes. It is apparent that although α was an important parameter, the cumulative effects of parameters other than α caused major differences in the response of different bridges.

The spectrum curves for all regular tests with two-axle vehicles are shown in Figure 102. The trends discussed for the three-axle vehicles are apparent also for the deflections under the two-axle vehicles; *i.e.*, there was a general increase in amplification factors with α and consistent differences were present in the magnitude of the responses of the different bridges. The amplification factors for moment were smaller than those for deflection and showed only a slight increase with the speed parameter.

Summary of Data.—Figures 103 and 104 show histograms and cumulative distribution curves of the amplification factors for all 533 regular test runs with three-axle vehicles. The amplification factors for deflections were higher than 1.40 for only 5 percent of the test runs; whereas, 88 percent of the runs fell between 1.10 and 1.40. The maximum single amplification factor for deflection was 1.63.

The maximum amplification for moment was 1.41, with only 3 percent of the runs exceeding 1.30. For 90 percent of the runs the amplification factors were between 1.05 and 1.30.

A heavy line on the graph of cumulative distributions (Fig. 104) indicates the impact factor formula given by the AASHO Specifications.* The value of the impact factor for all test bridges was 28.6 percent, corresponding to an amplification factor of 1.286. Of the 533 tests reported only 24 tests, or 4.4 percent of the total, gave amplification factors for moment that exceeded this value.

* AASHO, "Standard Specifications for Highway Bridges." 7th Ed., Washington, D .C. (1957).

Because of the large experimental scatter and the effects of the bridge-vehicle parameters, it is not possible to draw a meaningful curve of maximum amplification factors as a function of the speed parameter α. Instead, all amplification factors for deflection exceeding 1.30 and all amplification factors for moment exceeding 1.20 are shown in Figure 105. The majority of the points pertain to composite steel bridges 2B and 3B on which 64 percent of all regular tests were made. The data for other bridges suggest, however, that if a similar number of tests were run on the other bridges, a proportionately larger number of points with high amplification factors would have been obtained.

The data suggest that the maximum single effects do not increase noticeably with the speed parameter and that for values of α up to approximately 0.18, amplification factors of 1.4 for deflection and 1.3 for moment could be considered reasonable absolute maximum values. Figure 105 includes all tests with three-axle vehicles, and reflects the effects of all additional parameters discussed in the following section.

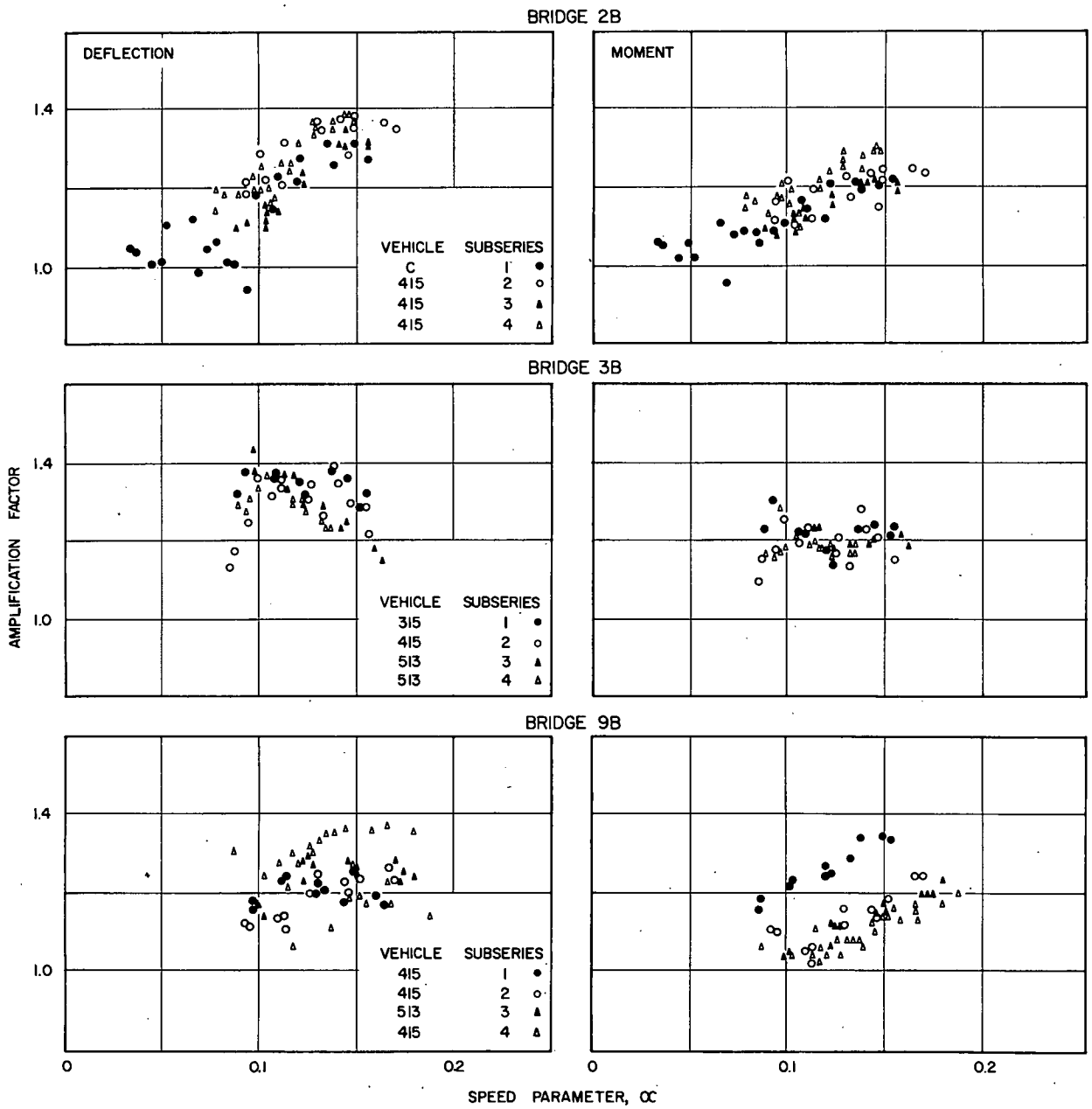

Figure 100. Spectrum curves for regular tests on steel bridges with three-axle vehicles.

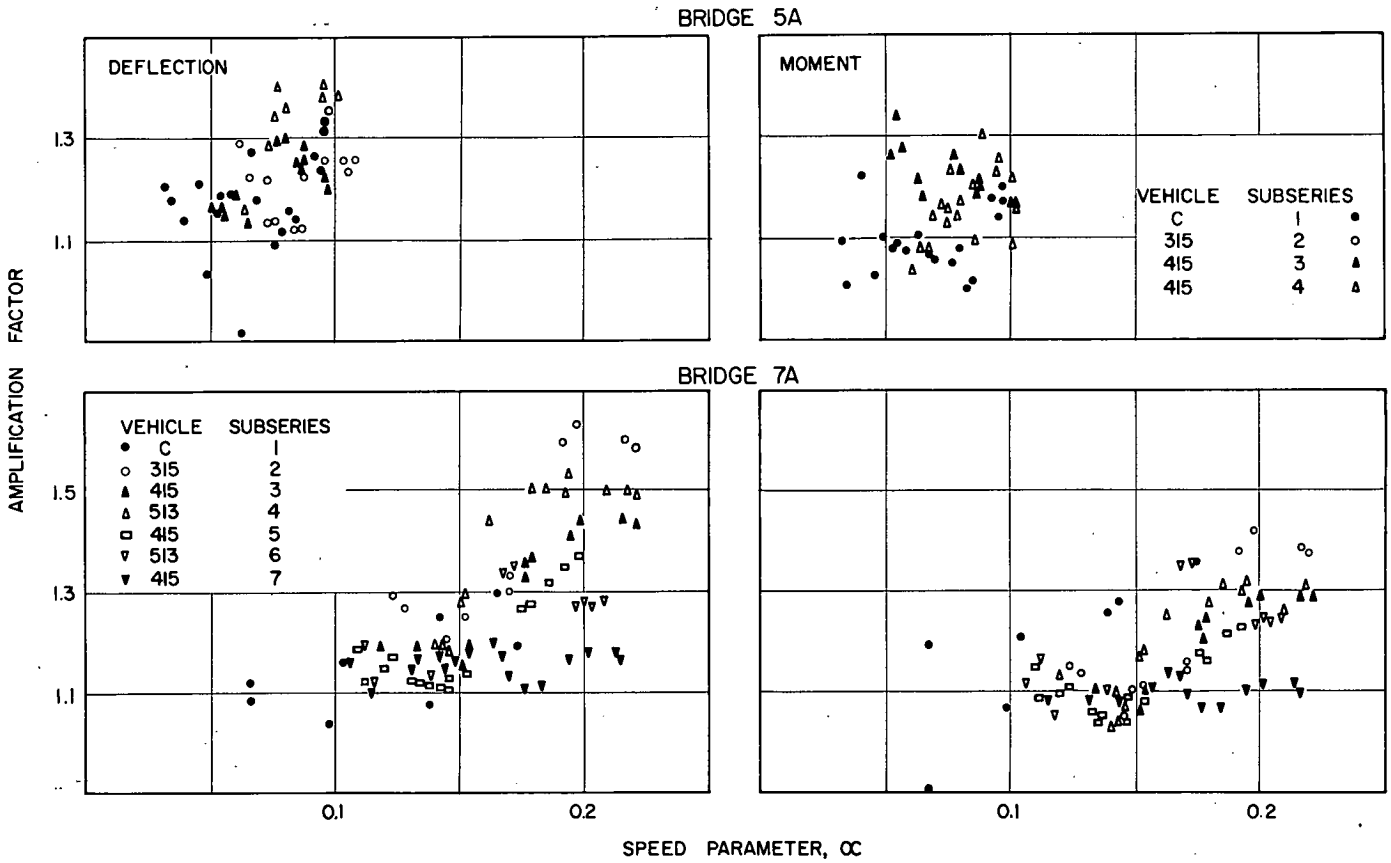

Figure 101. Spectrum curves for regular tests on concrete bridges with three-axle vehicles.

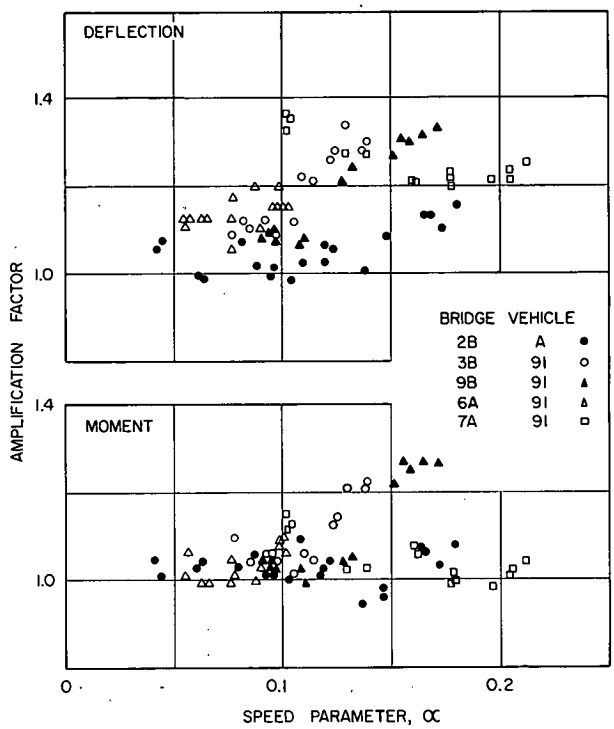

Figure 102. Spectrum curves for regular tests with two-axle vehicles.

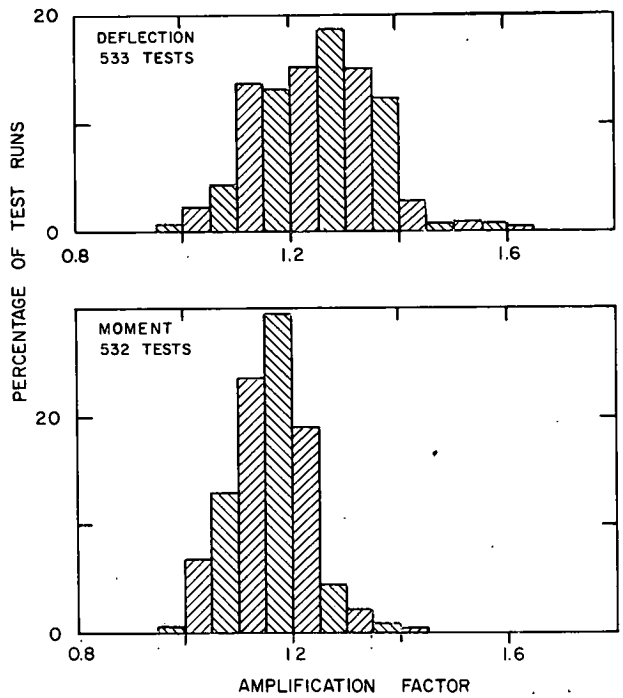

Figure 103. Distribution of amplification factors, regular tests, three-axle vehicles.

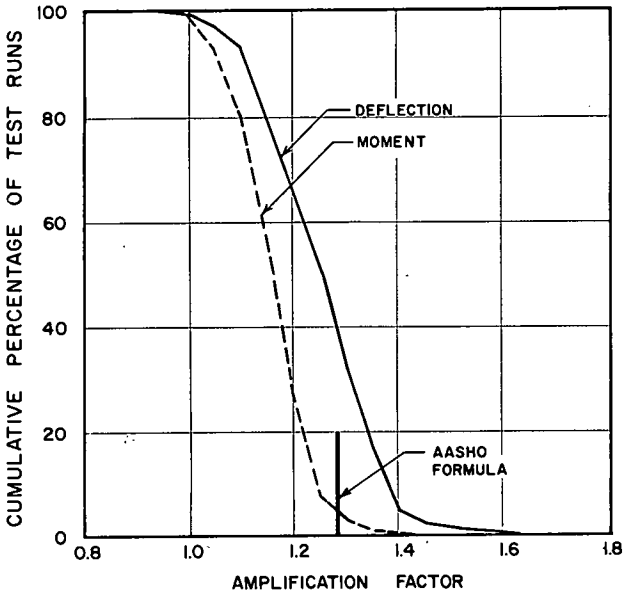

Figure 104. Cumulative distribution of amplification factors, regular tests, three-axle vehicles.

4.3.2 Effects of Bridge-Vehicle Parameters

The effects of various bridge-vehicle parameters were investigated by comparing spectrum curves for which all but one of the dimensionless parameters given in Section 4.2.3 were nearly identical. Data available for such comparisons were limited and contaminated by unknown, uncontrolled initial oscillations of the vehicle. These comparisons presented are limited to composite steel bridges 2B and 3B and the noncomposite steel bridge 9B.

Speed Parameter α.—The effect of the speed parameter is illustrated with spectrum curves for four subseries of tests involving three bridges and three vehicles (Fig. 106). The values of parameters R, ϕ_t and Δ for the four subseries were as follows:

Bridge	Vehicle	R	ϕ_t	Δ
2B	C	0.62	0.76	0.9
3B	415	0.56	0.81	1.0
3B	513	0.66	0.66	0.8
9B	415	0.52	0.84	0.7

Therefore, all major parameters, except the speed parameter α and possibly the unknown initial oscillations, were almost constant.

An over-all increase in the peak amplification factors with α is evident. The peak values of the two spectrum curves for deflection of Bridge 3B were essentially the same, whereas there was a spread of approximately 15 percent between the peak values of spectrum curves for vehicle 415 on Bridges 3B and 9B. This spread was of the order of that observed for a single subseries (Section 4.2.5). Thus, the difference between the spectrum curves could have been caused by uncontrolled factors such as initial

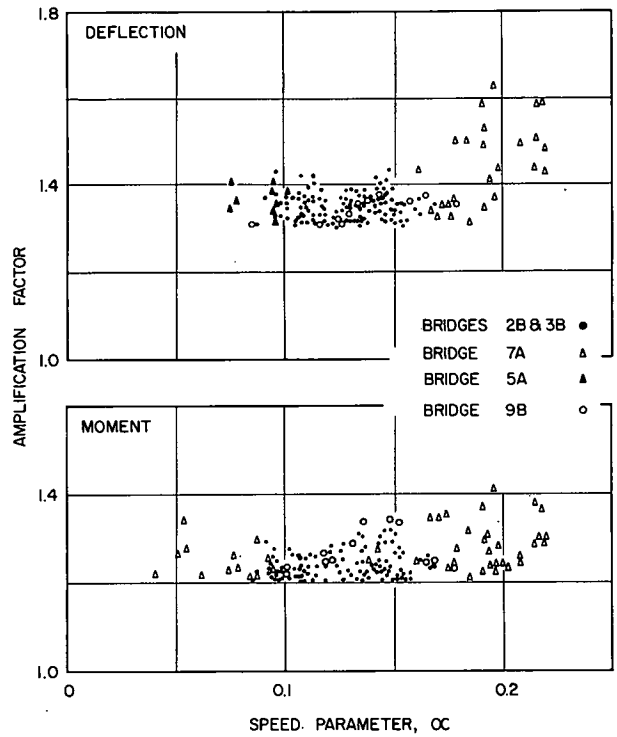

Figure 105. Maximum amplification factors, regular tests, three-axle vehicles.

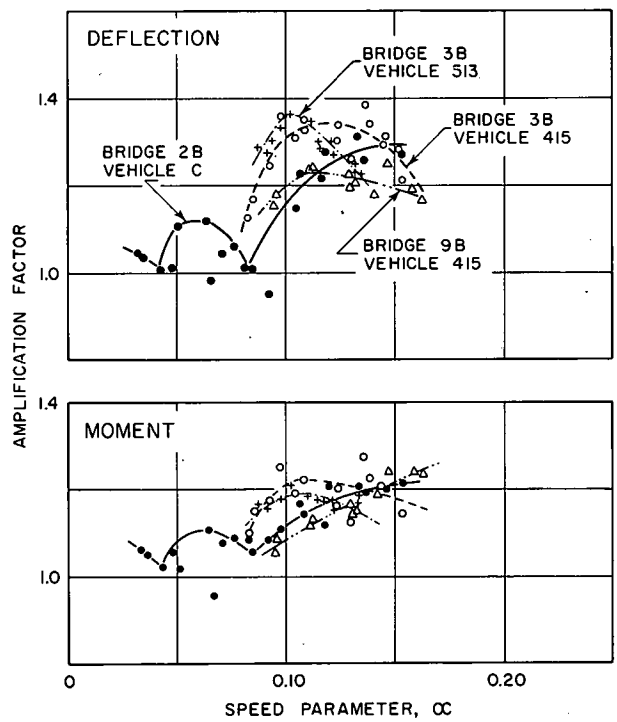

Figure 106. Effect of speed parameter.

oscillations. It is noteworthy in this connection that the initial oscillations observed on Bridge 9B were smaller than those observed on Bridge 3B, and that the approach pavement to Bridge 2B was relatively smooth at the time of conduct of the tests.

The scatter in the amplification factors for moment was smaller than that for deflection. This is consistent with the findings discussed in Section 4.2.5.

Parameters R, ϕ *and* Δ.—Spectrum curves for deflections involving large variations in the weight ratio R are shown in Figure 107. The characteristics of the subseries were as follows:

Bridge	R	Vehicle	ϕ_t	Δ
3B	0.56	415	0.81	1.0
3B	0.28	91	0.78	1.3
9B	0.52	415	0.95	0.9
9B	0.26	91	0.97	0.9

The ratio R varied by a factor of two in each bridge, but parameters ϕ_t and Δ were about the same for both subseries of any one bridge.

The effect of the frequency ratio was difficult to isolate. For the only data for which parameter ϕ varied independently of R (Bridges 3B and 9B) the change was of the order of 25 percent. Possible effects of this change, if any, were completely obscured by the differences in the initial state of oscillations of the vehicles and by an unusually large scatter in the data for Bridge 9B.

The effect of the profile parameter is indicated by spectrum curves for two subseries for which the variation of Δ was the largest and the initial oscillations were expected or known to be small (Fig. 108). Both subseries were run with vehicle 415; parameters R were 0.59 and 0.52, and parameters ϕ_t were 0.86 and 0.84 for Bridges 2B and 9B, respectively.

Even the doubling of parameters R (Fig. 107) and Δ (Fig. 108) had only small effect on the peak values of amplification factors. The largest effect was that of the profile parameter on the amplification factor for deflection: the doubling of Δ caused a 15 percent increase of the amplification factor in terms of the static deflection.

The spectrum curves for Bridge 9B (Fig. 107) and for moment (Fig. 108) showed no definite trends with the changes in the respective parameters.

4.3.3 Effects of Controlled Test Vehicles

The type of comparisons presented in Section 4.3.2 cannot be extended to other subseries because the ranges of most of the parameters for different bridges did not overlap. To present comparisons for all tests, the dimensionless parameters R, ϕ_t, and Δ must be allowed to vary simultaneously.

The only variables in the regular tests were the speed of the vehicle, the vehicle, and the bridge. The comparisons in this section are made always over a range of speeds either keeping the bridge constant and varying the vehicle or keeping the vehicle constant and varying the bridge.

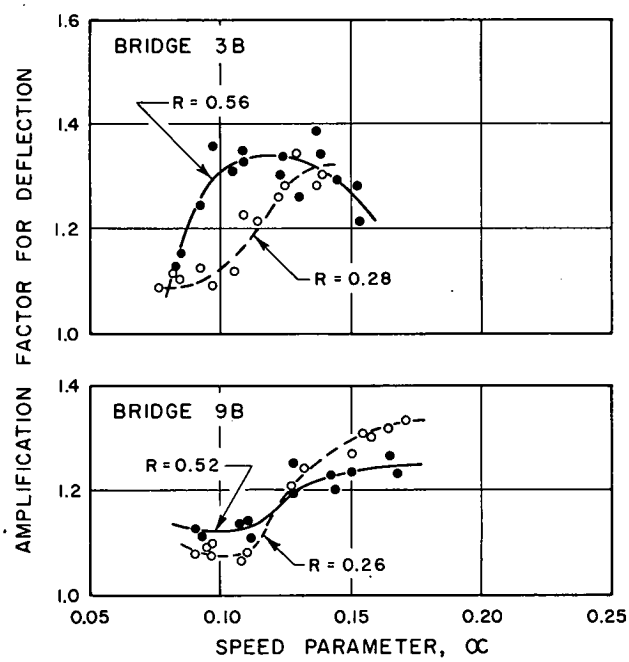

Figure 107. Effect of weight ratio.

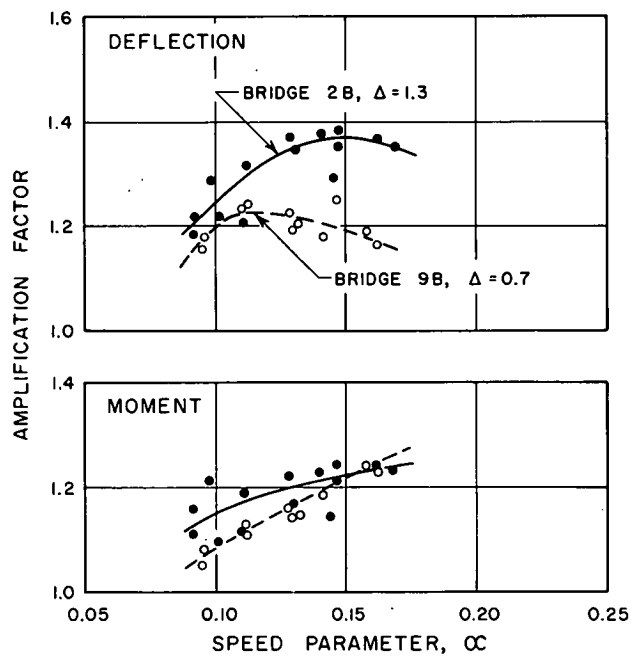

Figure 108. Effect of profile parameter.

Effect of Variation in Vehicle Types.—The effects of three different vehicles were investigated separately for Bridge 3B and for Bridge 7A. On both bridges the tests were made with three-axle vehicles 315, 415, and 513. All tests were made within a short space of time. The values of the dimensionless parameters for both bridges were as follows:

Bridge	Vehicle	R	ϕ_1	Δ
3B	315	0.38	0.87	1.2
	415	0.56	0.81	1.0
	513	0.66	0.64	0.6
7A	315	0.28	1.23	−1.3
	415	0.42	1.15	−1.0
	513	0.49	0.90	−0.7

The results for Bridge 3B are shown in Figure 109. The peak amplification factors for the three vehicles were about the same. It appears that the effect of the larger profile parameter, Δ, was counterbalanced by that of the smaller weight ratio R.

For Bridge 7A (Fig. 109), the effects of the same vehicles were much larger than on Bridge 3B; the maximum amplification factor was 1.63 for Bridge 7A, 1.43 for Bridge 3B. The three spectrum curves were similar in shape, but there was a difference of about 20 percent between the peak amplification factors caused by vehicles 315 and 415.

Figure 110 shows dynamic increment curves for Bridge 7A caused by the three vehicles at $\alpha = 0.19$. The three curves are in phase. The critical dynamic increments occurred almost exactly at the value of x/L for which the crawl curve was a maximum and were much larger than any of the other peak ordinates.

There were no tire pressure measurements available for this particular subseries, but spring records showed the first change in deformation approximately 30 ft from the entrance. A pronounced irregularity in the bridge profile ended at this location (Fig. 78). It appears that the variation in the interaction force caused by this irregularity, in combination with frequency ratios close to unity, could account for the large increase in the critical dynamic increments because it occurred at the point of maximum static moment.

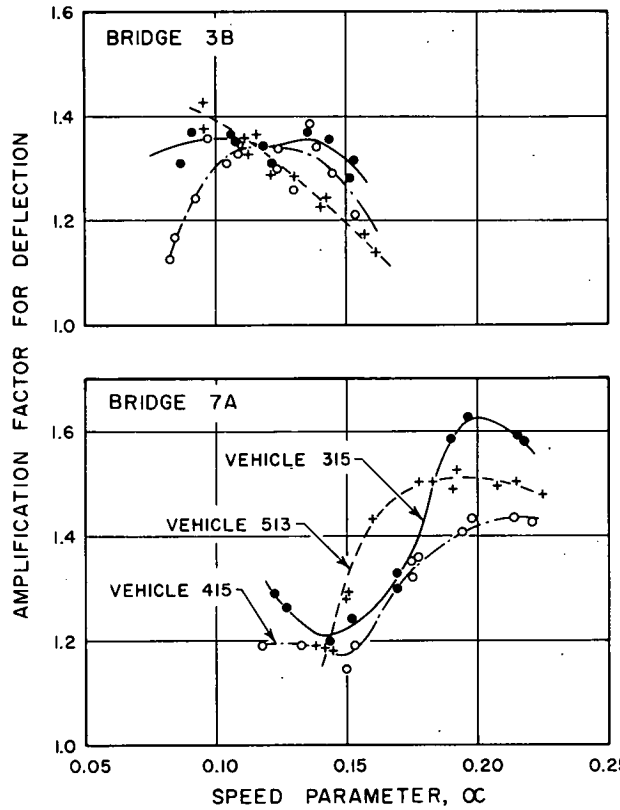

Figure 109. Effect of vehicle characteristics.

Effects of Variation in the Bridge Types.—In Figure 111, four plots of spectrum curves are shown, each pertaining to one vehicle. Three or four bridges are included in each plot. The bridge-vehicle combinations are characterized by the following values of dimensionless parameters:

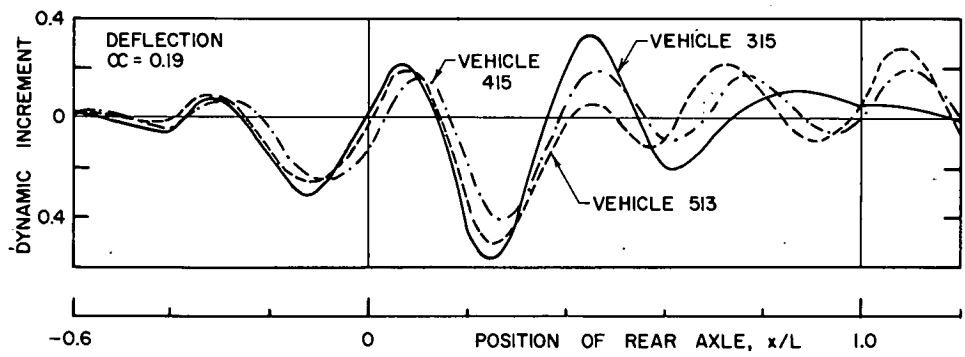

Figure 110. Dynamic increments for three different vehicles, Bridge 7A.

Vehicle	Bridge	R	ϕ_1	Δ
315	3B	0.38	0.87	1.2
	5A	0.28	0.60	0.2
	7A	0.28	1.27	−1.2
415	2B	0.59	0.85	1.3
	3B	0.56	0.81	1.0
	9B	0.52	0.84	0.7
	7A	0.42	1.15	−1.0
513	3B	0.66	0.66	0.8
	9B	0.61	0.84	0.6
	7A	0.49	0.98	−0.4
91	3B	0.28	0.78	1.3
	9B	0.26	0.97	0.9
	6A	0.21	0.56	0.7
	7A	0.21	0.56	−0.6

The ranges of the weight and frequency ratios for each vehicle were of the same order as those in earlier comparisons; the variation in the profile parameter was much larger than before because of the negative Δ of Bridge 7A. The approach pavements of all bridges compared were different so that the effect of initial vehicle oscillations could be expected to be different for each bridge. The top speed of the vehicles was essentially the same in all tests, but the maximum values of α were different because of the large range in bridge frequencies.

In general, there is no agreement between the spectrum curves for the different bridges in any one of the plots (Fig. 111). The results for Bridge 7A differ from those for the other bridges. It is believed that this was caused partly by the difference in the profile parameter Δ and partly by the irregularity of the bridge deck. With the exception of Bridge 7A, the general effect of the variations in the bridge parameters and in the initial vehicle oscillations was to shift the position of the peak ordinates of the spectrum curves.

4.3.4 Effect of Time and Traffic

One of the objectives of the test program was to determine the effect of time and traffic on the dynamic response of the test bridges. Four of the bridges were tested in three identical subseries approximately eight months apart (2B, 9B, 5A and 7A). Vehicle 415 was used in all tests. The number of trips of regular test vehicles prior to each of these tests is given for each bridge in Table 63.

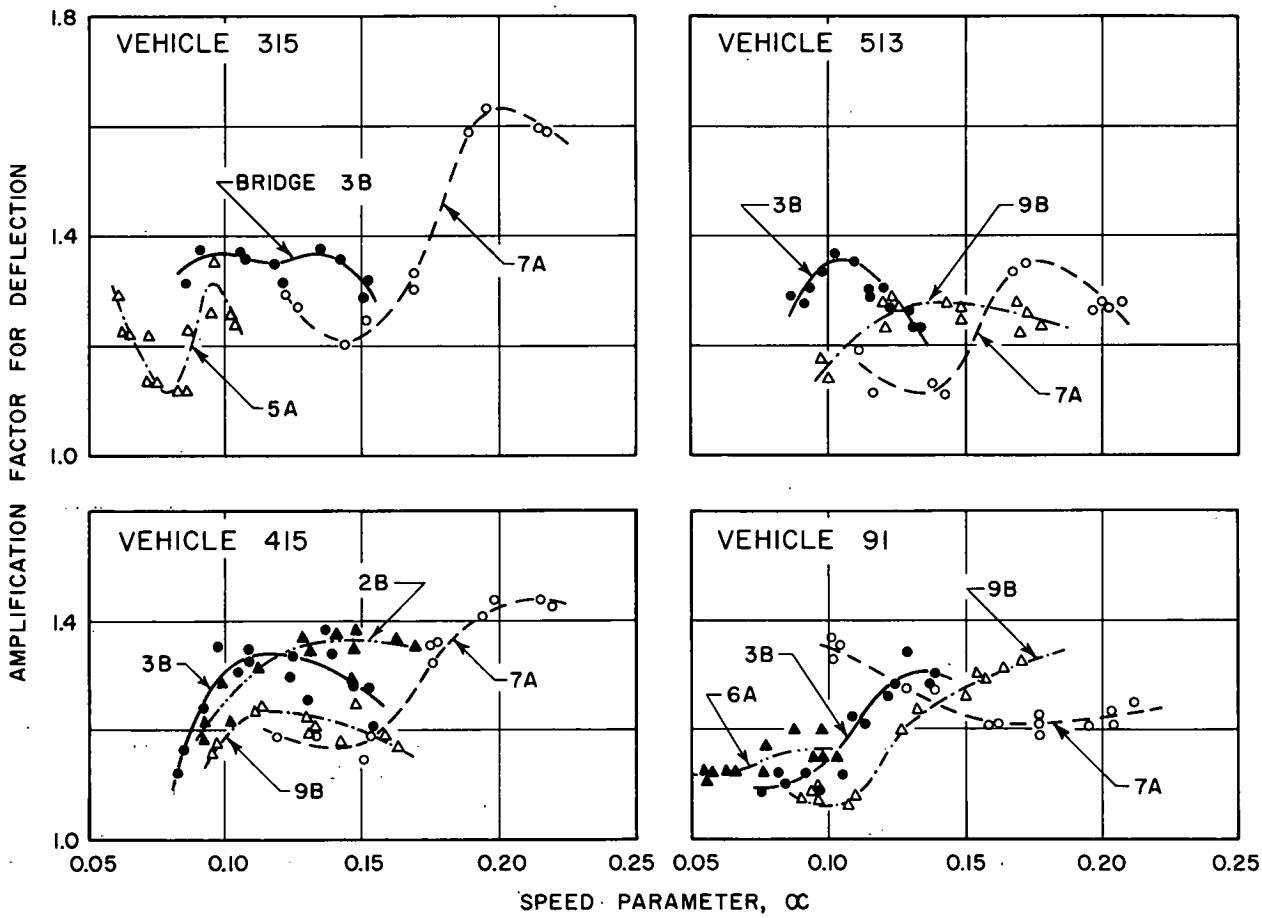

Figure 111. Effect of bridge characteristics.

The primary changes that occurred in the bridges between the successive tests were (a) a progressive decrease in stiffness indicated by a reduction in the bridge frequencies; (b) a consistent increase in the permanent set or, in the case of Bridge 7A, a decrease in camber; and (c) an increase in the magnitude of the unevenness of the approach pavements evidenced by profile measurements.

The changes in the bridge frequencies and in the dead load sets at midspan corresponded to changes in the frequency ratios and profile parameters evident in the following:

Bridge	June-July 1959		February 1960		October 1960	
	ϕ_i	Δ	ϕ_i	Δ	ϕ_i	Δ
2B	0.86	1.3	0.91	1.4	0.87	1.7
9B	0.84	0.7	0.95	0.9	1.00	1.0
5A	—	—	0.42	0.4	0.42	0.7
7A	1.15	−1.1	1.10	−0.8	1.21	−0.6

The dimensionless parameters were computed on the basis of constant values of properties of the test vehicles. The available data were insufficient to determine whether changes occurred in the properties of the vehicles during the test period.

TABLE 63
TRAFFIC COUNT AT TIME OF DYNAMIC TESTS OF TIME SERIES

Time of Test	Number of Vehicle Passages			
	Bridge 2B	Bridge 9B	Bridge 5A	Bridge 7A
June-July 1959	75,000	7,900	85,500	77,300
February 1960	230,900	150,200	239,700	242,000
October 1960	525,200	441,500	523,500	518,400

Spectrum curves for the midspan deflection of the center beam of the four bridges are shown in Figure 112. Changes in the response of Bridge 2B with time were small and inconsistent. The approach pavement of this bridge remained relatively smooth, and both the frequency and the permanent set at midspan changed very little during the period. Thus, the lack of change in spectrum curves appears reasonable.

The change in the bridge-vehicle parameters for Bridge 9B was of the same order as for Bridge 2B. The spectrum curves showed essentially no change in the response between the

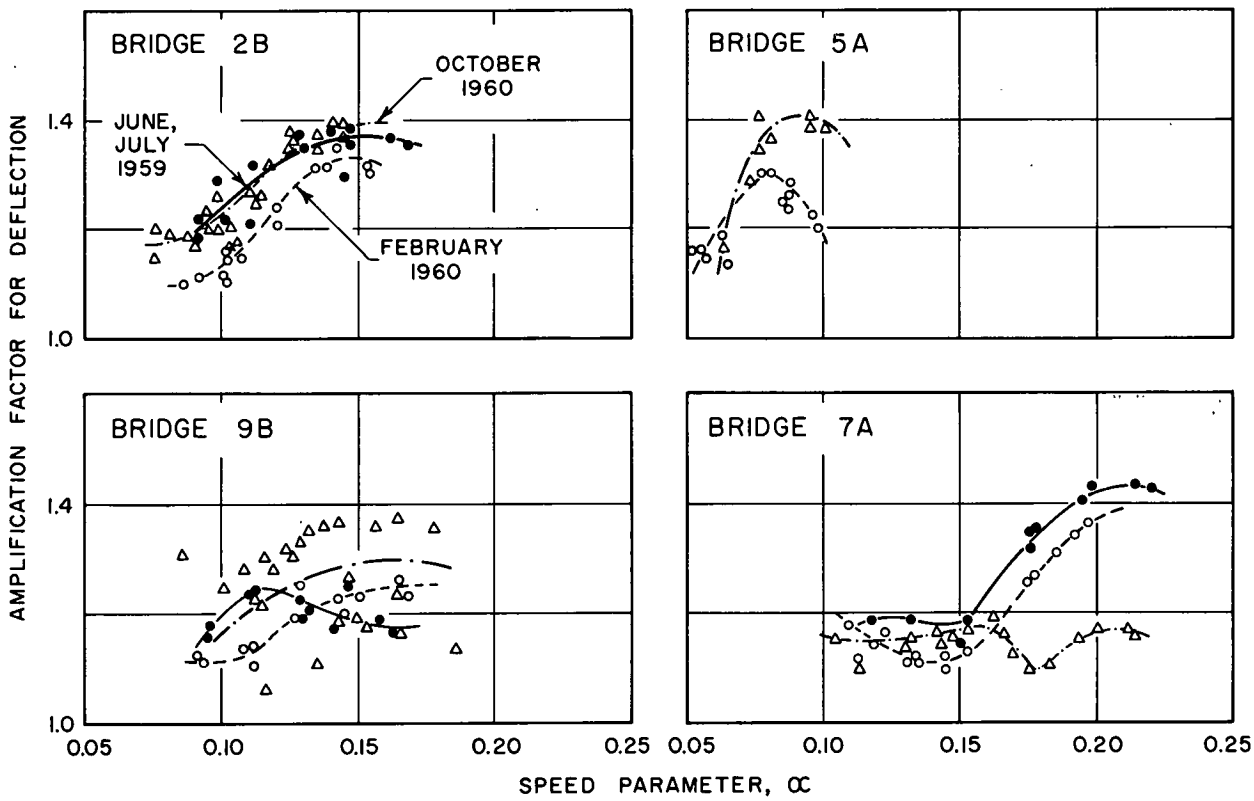

Figure 112. Effect of time and traffic, vehicle 415.

TABLE 64
MAXIMUM AMPLIFICATION FACTOR IN STATISTICAL STUDY OF DYNAMIC EFFECTS

Bridge	Maximum Speed Parameter	Maximum Amplification Factor for	
		Deflection	Moment
3B	0.16	1.39	1.28
6A	0.12	1.44	1.27
6B	0.12	1.36	1.28
8A	0.25	1.42	1.38
8B	0.25	1.28	1.23

first and second series of tests. The results for the third series showed extreme variations. Several points fell into the range of data from the first two series, but the majority of the results showed higher amplification factors. By the time of the third series of tests, the slab of Bridge 9B was extensively cracked and wedged between the parapet wall of the abutment and the slab of Bridge 9A. It is possible that the erratic behavior in this series was related to this condition.

For the two series of tests of Bridge 5A there was a difference in the peak amplification factors of about 10 percent. The difference could have been caused either by the change in the profile parameter or by changes in the condition of cracking of the prestressed concrete beams.

The profile parameter for Bridge 7A decreased by a factor of two within the time considered. Furthermore, the profile of the approach pavement was changed radically between the times of the second and third series of tests; placement of an asphaltic overlay on the approach pavement eliminated the largest irregularity in the profile. The major irregularity on the bridge deck also appeared to have become less pronounced. The spectrum curves showed very little change between the first and second series, but the curve for the third series had both different shape and a substantially reduced peak amplification factor. These differences can be attributed to the combined effects of the changes in the initial oscillations, the bridge camber, and the irregularities of the bridge profile, all of which influenced the location of the critical dynamic increment.

4.3.5 Statistical Study of Amplification Factors

An extensive series of tests was carried out on Bridges 3B, 6A, 6B, 8A and 8B. The purposes of these tests were to determine the order of magnitude of the dynamic effects in the bridges considered, to insure that no condition producing major effects was overlooked in the test program, and to secure data on the effects of different types of moving vehicles that would be susceptible to statistical evaluation. All tests were made with three-axle tractor-semitrailer combinations: two single-axle vehicles from Loop 4, two single-axle vehicles from Loop 5 and three tandem-axle vehicles from Loop 3. The different vehicles from the same loop had essentially the same dimensions and weights but were of different manufacture.

The test runs were made at vehicle speeds of 25 to 45 mph, divided into four 5-mph intervals, and at creep speed. The variables were arranged into a complete factorial experiment with replication for every test so that each bridge was tested twice with each vehicle at each of the four dynamic speed intervals. The conduct of the tests and the bridge instrumentation were the same as for regular tests, but the vehicles were not instrumented. All of the tests were performed within approximately 2 months.

Table 64 gives the largest observed amplification factors for each bridge. Because of the large increments of speed, these amplification factors may not represent absolute maximum effects within the range of speeds considered. However, it is unlikely that any major effects have been overlooked in this comparison.

The maximum values of the amplification factors for Bridge 3B fall within the experimental scatter observed in other tests (Fig. 96) and the results for Bridge 6A are essentially in agreement with those for prestressed concrete bridge 5A (Fig. 101). On the other hand, the results for Bridge 8A were somewhat lower than the corresponding values for Bridge 7A (Fig. 101), even though the maximum value of α obtained for Bridge 8A was larger than that for Bridge 7A. It is believed that this difference in amplification factors was caused by the presence of pronounced surface irregularities in the slab of Bridge 7A; no such irregularity existed on Bridge 8A. The maximum amplification factors for tandem Bridges 6B and 8B, placed second in the line of travel, were consistently lower than the corresponding values for the first bridges (6A and 8A).

The statistical evaluation of the effects of test variables was based on the amplification factors for deflection and moment at midspan of the three beams corresponding to vehicle speeds of 30, 35 and 40 mph. The more important conclusions of the study are as follows:

1. The deflection amplification factors for the three beams of the same bridge generally did not differ significantly. ("Significant" indicates that the hypothesis of no effect was rejected at the 5 percent level.) On the other hand, the moment amplification factors for the center beam were generally lower than for the interior and exterior beams, even though these differences were generally small.

2. The difference between the amplification factors for the same group of vehicles (Each group included three vehicles: one tandem-axle vehicle from Loop 3, one single-axle vehicle from Loop 4 and one single-axle vehicle from Loop 5.) run at different times was generally significant. This finding was consistent for all bridges for both moment and deflection.

3. The difference between the amplification factors for two groups of the same types of vehicles was usually significant for both deflection and moment.

4. Tandem-axle vehicles usually gave lower or equal amplification factors, for both deflection and moment, than did either of the single-axle vehicles. A further comparison of vehicle types indicated that the difference between the effects of a single-axle vehicle at different times was as great as the difference between the effects of two single-axle vehicles of different types.

5. The effect of speed was generally found to be significant for the three levels studied. The same general trend with regard to speed was noted for both moment and deflection.

Except for the finding concerning tandem-axle vehicles, for which no other data were obtained, the conclusions of the statistical studies substantiated the discussions of the data presented in previous sections. In particular, they confirmed that different results may be obtained under seemingly identical conditions, that the amplification factors are not sensitive to variations in vehicle parameters within the range considered and that speed is an important parameter.

4.4 RESULTS OF SPECIAL TESTS

The objective of the special tests was to place the regular tests in proper perspective. This was accomplished through the study of the effects of certain parameters over a range of values wider than that possible in the regular tests. A secondary objective was to obtain quantative information on the effect of certain unusual conditions of bridge-vehicle behavior. The tests included two subseries with blocked vehicle springs, nine subseries with induced vehicle oscillations and two subseries with simulated continuous traffic; one subseries with sudden braking on the bridge and five subseries with vehicles placed eccentrically on the bridge.

It was anticipated that the effect of braking would be to increase the force on the front axle, producing increased dynamic effects on the bridge. The tests proved inconclusive because the braking applied to the vehicle was too small to produce discernible effects. Therefore, data on braking tests are not presented in this report.

4.4.1 Blocked Vehicle Springs

The objective of these tests was to study the effect of large variations in the interaction force resulting from the absence of damping in the vehicle suspension. The tests were made on Bridge 3B with two-axle vehicle 91 and with three-axle vehicle 513. Springs were blocked on both axles of the two-axle vehicle and on the drive and rear axles of the three-axle vehicle.

Additional tests with blocked springs were performed on Bridges 3B, 7A, 7B, 9A and 9B. These tests are discussed in Section 4.4.2, because they also included induced initial oscillations.

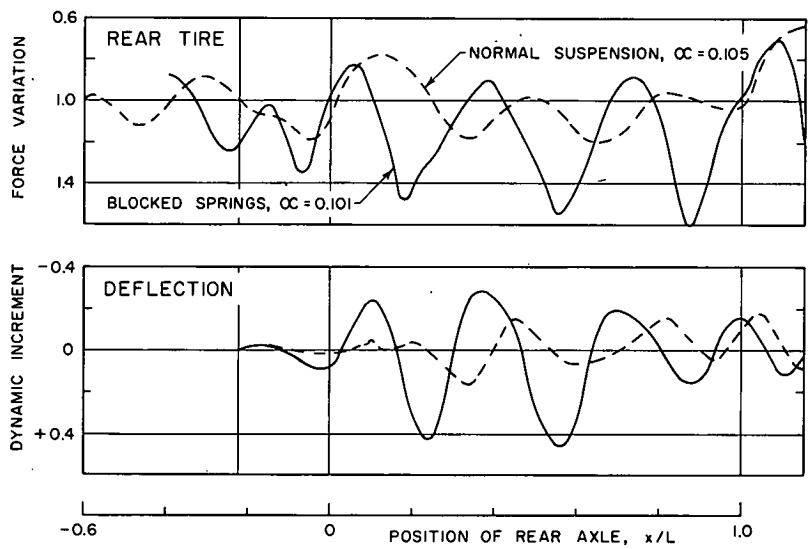

Figure 113. Tests with blocked springs, two-axle vehicle, Bridge 3B, vehicle 91.

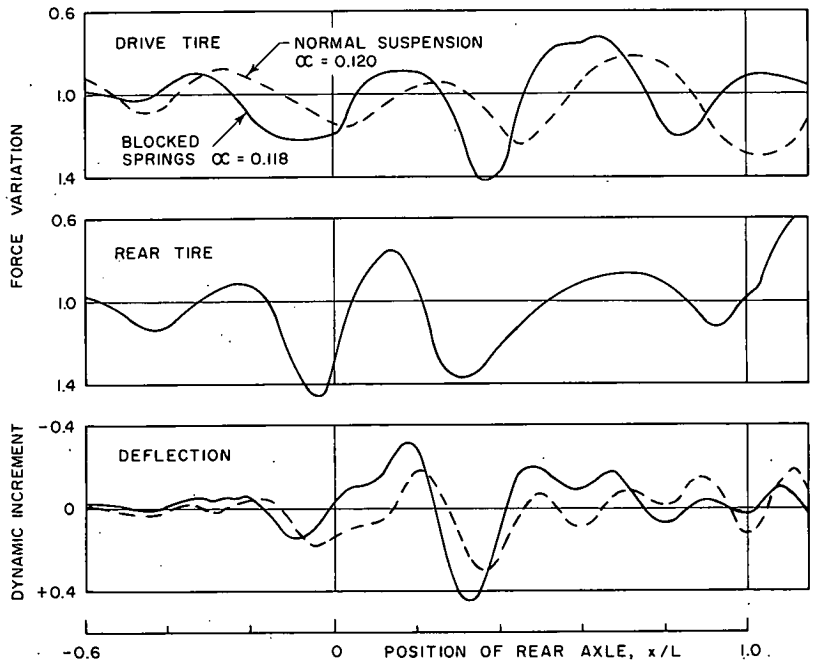

Figure 114. Tests with blocked springs, three-axle vehicle, Bridge 3B, vehicle 513.

Typical vehicle and bridge-response curves are shown as solid lines (Fig. 113) for the tests with the two-axle vehicle (Fig. 113) and the three-axle vehicle (Fig. 114). The vehicle response is in terms of the interaction force curves, and the bridge response is in terms of dynamic increment curves for deflection at midspan of the center beam.

Behavior of the vehicle was characterized by large variations in the interaction force clearly indicating that the damping of the vehicle was very small. With the suspension springs blocked, the only damping mechanism in the vehicle was that in the tires.

The severity of the variation in the interaction forces made the bridge respond predominantly at the frequency of this variation. For the two-axle vehicle the bridge response reflected almost exclusively the frequency of the force variation in the rear axle. For the three-axle vehicle, for which the amplitude of variation of interaction forces was smaller, the major component of the bridge response was still at the frequency of the interaction forces. However, the bridge frequency also was noticeable throughout the record (Fig. 114).

The frequency of the interaction-force variation of the two-axle vehicle was about 3.0 cps (Fig. 113). This was only 80 percent of the computed value of the natural frequency of the vehicle. The reason for this discrepancy was discussed in Section 4.1.5.

The typical history curves for vehicles with blocked springs are compared with corresponding curves (dashed lines) obtained from regular tests at comparable values of speed parameter α. For the runs in Figure 113, the peak dynamic increments for deflection were increased from 0.16 for the vehicle with normal suspension to 0.48 for the vehicle with blocked springs. The corresponding increase in the amplification factor was from 1.12 to 1.45, showing that the peak dynamic increments for both cases occurred in the region of the maximum crawl response. For the three-axle vehicle (Fig. 114) the increase in the peak dynamic increment was only from 0.31 to 0.50. This corresponded to an increase in the amplification factor from 1.27 to 1.49.

In the two subseries, amplitudes of initial oscillation of the vehicle were found to vary over a wide range. The double amplitude of force variation at the entrance ranged from almost 0.0 to 1.5 P_{st} for the rear axle of vehicle 91 and from 0.2 to 1.0 P_{st} for the drive and rear axles of vehicle 513. The corresponding values for vehicles with normal suspension were between 0.2 and 0.4 P_{st} for vehicle 91 and between 0.2 to 0.5 P_{st} for vehicle 513.

Spectrum curves for tests with blocked springs are shown in Figure 115 as solid lines; results with regular suspension are shown as dashed lines. The blocking of springs changed considerably the characteristics of the curves, particularly the values of α corresponding to the peak amplification factors. The shift reflected a change in the position of the critical dynamic increments. There was also noticeable increase in the magnitude of the peak amplification factors. For the two-axle vehicle the increase was approximately 20 percent of the maximum static value for both moment and

deflection; for the three-axle vehicle the increase was approximately 15 percent for deflection and 25 percent for moment.

In summary, blocking of vehicle springs increased the variation in the interaction forces and the resulting dynamic effects on the bridge. The magnitude of the peak dynamic increments was approximately twice that produced by the same vehicle with normal suspension. Of the tests considered, the maximum amplification factor for deflection was 1.54 as compared to 1.37 for the corresponding vehicle with normal suspension.

4.4.2 Induced Initial Vehicle Oscillations

The objective of this study was to determine the effect of controlled initial oscillations of the test vehicles with both normal suspensions and blocked springs. Two groups of tests were performed: (1) in two subseries an attempt was made to obtain maximum dynamic effect at midspan, and (2) in seven subseries the vehicle oscillations were induced at the bridge entrance. The tests were made on Bridges 3B, 5A, 5B, 7A, 7B, 9A and 9B. Two-axle vehicles 91 and 94 and three-axle vehicle 513 were used in all tests. In some tests on Bridges 3B, 7A, 7B, 9A and 9B the springs of the vehicle were blocked.

Initial oscillations in the vehicle were induced by allowing the vehicle to drop from a ramp. The ramp consisted of two boards, one placed in each wheelpath. The boards were 1 in. high and 18 ft long, and the initial 1 ft of each board was planed down to provide gradual transition from the pavement to the ramp.

In the two series aimed at obtaining maximum dynamic effects at midspan the position of the ramp was varied for different speeds of vehicle. In the remaining subseries the exit end of the ramp was placed directly over the bridge abutment approximately 10 in. ahead of the bridge bearings. Except for the presence of the ramp, the tests were executed in the same manner as the regular tests. The crawl runs were performed without the ramps.

Vehicle Response.—Typical history curves of the interaction force variation are shown for the tests with initial oscillations as solid lines in Figure 116. The top two curves pertain to the rear axle of vehicle 91 for tests on Bridges 3B and 7A; the third curve pertains to vehicle 91 with blocked springs; and the fourth curve shows the response of the rear axle of vehicle 513.

The largest variations in the interaction forces occurred for the vehicle with blocked springs, and the smallest variations occurred for the three-axle vehicle with regular suspension.

Except for the presence of high frequency oscillations at the beginning of the record, the response curves for vehicle 91 on Bridges 3B and 7A were of similar shape, but the amplitudes were three times as large for Bridge 7A as for Bridge 3B. This difference reflected different states of oscillation of the vehicle prior to the entrance on the ramp. It is ap-

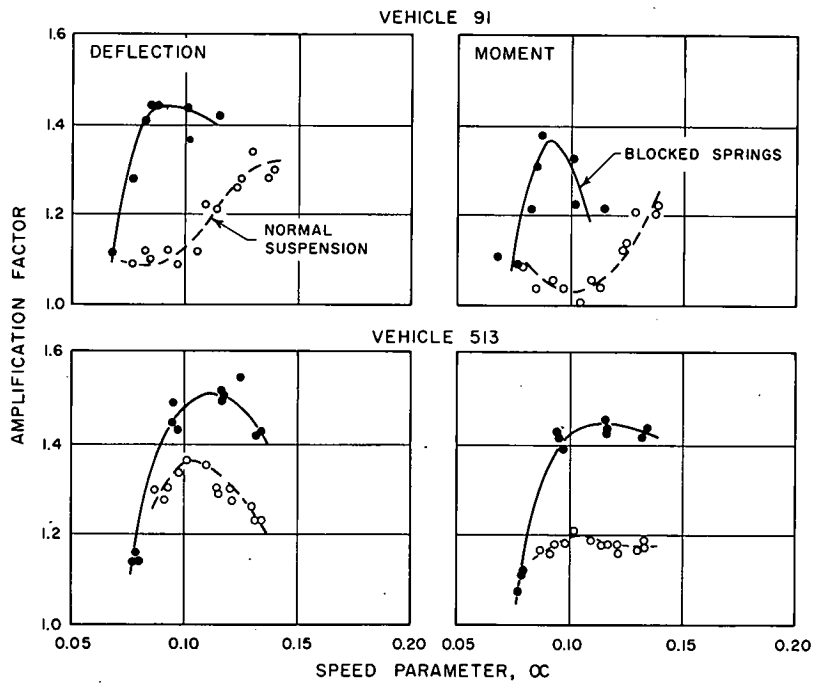

Figure 115. Spectrum curves for tests with blocked springs, Bridge 3B.

parent from the curves of interaction forces that the ramp was not sufficiently long to block out the effects of the vehicle oscillation prior to entrance on the ramp. The major irregularity on the approach to Bridge 7A terminated approximately 20 ft ahead of the bridge and was in front of the ramp. On the other hand, the most pronounced discontinuity on the approach to Bridge 3B was located immediately ahead of the entrance and was, therefore, covered by the ramp.

The vehicle response was essentially independent of the bridge response. This is substantiated by comparing the results of the bridge tests with those obtained from the tests with ramps on rigid pavement (dashed lines in Fig. 116). The excellent agreement between the solid and dashed curves for the test run on Bridge 7A is noteworthy. For the run on Bridge 3B, the agreement was good in phase but there were differences in amplitude, undoubtedly caused by the different initial conditions of the vehicle prior to the entrance on the ramp.

Based on the records for all series considered, the following two major conclusions were drawn regarding the vehicle behavior in the tests with initial oscillations: (1) the vehicle behavior on the bridge was essentially the same as that on rigid pavements, and (2) the inter-

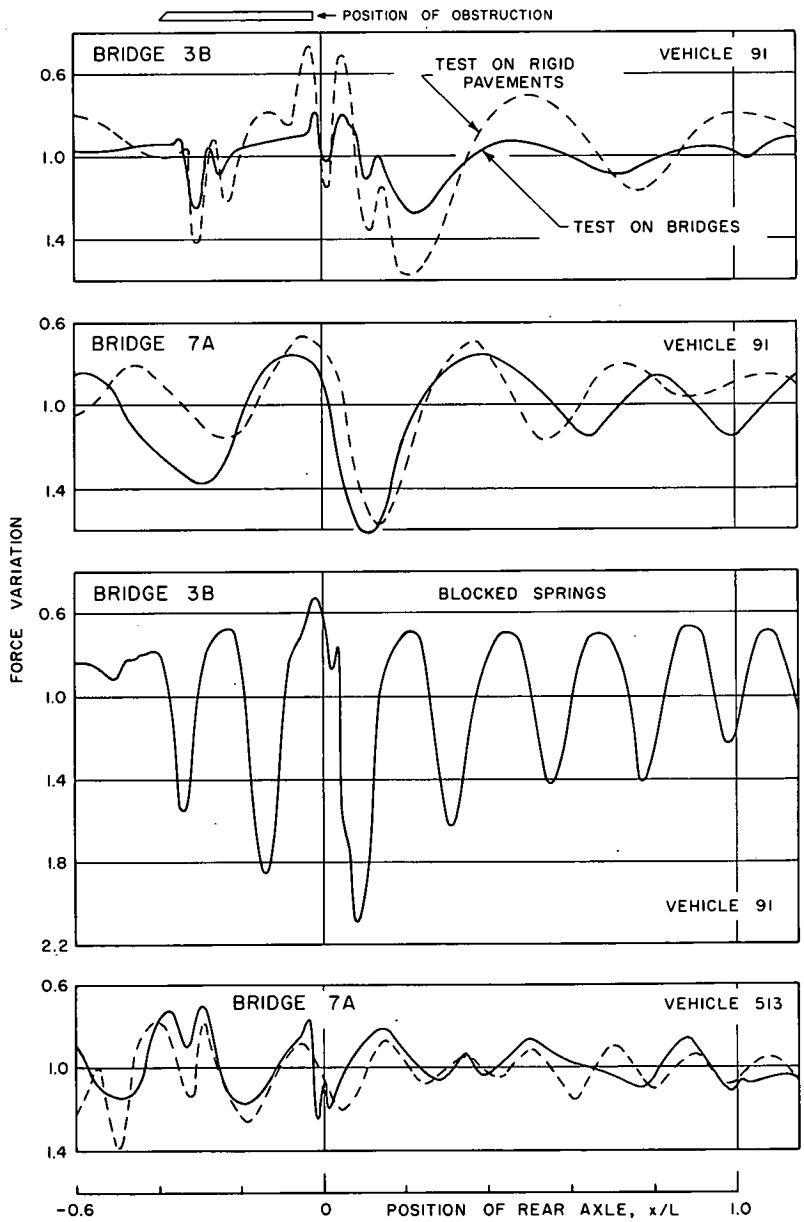

Figure 116. Response of rear wheel in tests with induced initial oscillations.

action force variation for the three-axle vehicle was small. The first conclusion is in agreement with theoretical studies by Nieto,* who has shown that for low frequency ratios and large initial oscillations the vehicle behavior on the bridge may be predicted reliably by an analysis assuming a rigid surface.

Bridge Response.—The dynamic increment curves for deflection at midspan of the center beam for three tests with vehicle 91 are shown as solid lines in Figure 117. The dynamic increment curves were obtained from the same tests as the interaction-force curves (Fig. 116). The dashed lines represent the corresponding response in regular tests for comparable values of α.

In the tests with normal suspension, the induced vehicle oscillations produced increased dynamic increments. In the early portions of the record, the predominant frequency of the dynamic increment curves was that of the interaction force. However, because of large damping in the suspension system, only the first bottoming of the vehicle produced a large variation in the interaction force, and thus, a large dynamic increment. The first bottoming of the vehicle occurred early during the passage over the bridge so that the large dynamic increment was always associated with a low crawl ordinate. The critical dynamic increment often corresponded to the second bottoming of the vehicle which was associated with the change in the interaction force of the same order of magnitude as in the regular tests. Consequently, the maximum effects at midspan were not much larger than those obtained in the regular tests.

The history curve of dynamic increments for deflection in the tests with blocked vehicle springs showed very large variations in the interaction force throughout the test run. The dynamic increments were in phase with the interaction force for the entire record. The extremely large ordinates, varying from —1.36 to 1.10, were more than twice as large as those for comparable runs without induced initial oscillations (Fig. 113).

Spectrum curves for amplification factors at midspan of the center beams are shown in Figures 118, 119, and 120. The data for tests with induced vehicle oscillations are shown as dots, and the trends of the data are indicated by solid lines. Data are also included for corresponding regular tests indicated as circles and dashed lines.

The curves for the tests with induced oscillations are distinguished from the curves for regular tests by more sharply defined peaks and

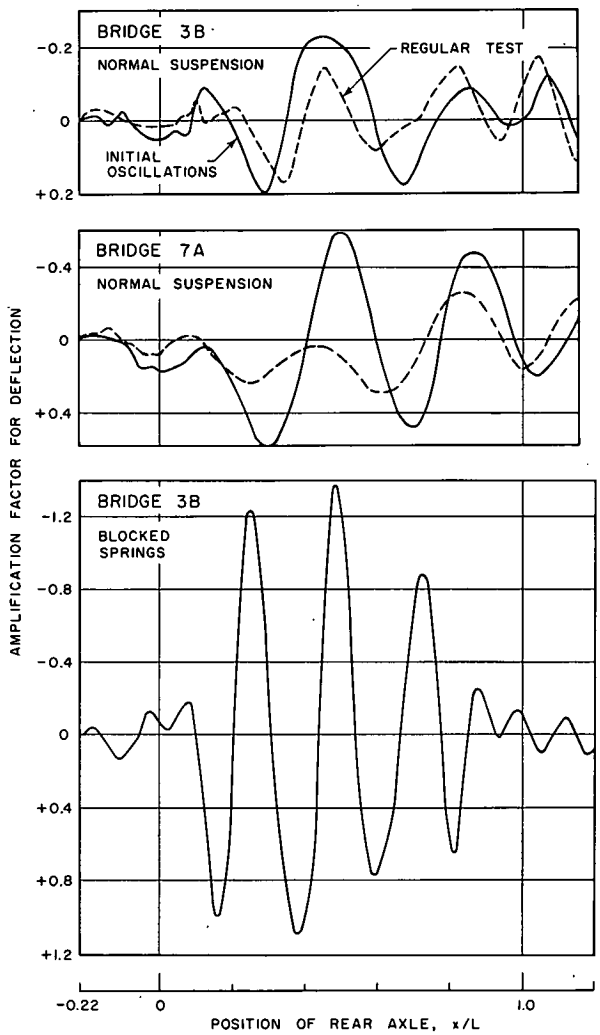

Figure 117. Bridge deflection in tests with induced initial oscillations.

valleys, especially for the two-axle vehicle. Furthermore, the experimental scatter for the tests with induced initial oscillations was smaller than in the regular tests. The major cause of the experimental scatter in the regular tests was the initial oscillation of the vehicle; the obstruction tended to control the initial state of vehicle oscillation and thus tended to reduce the influence of the major cause of scatter.

The amplification factors were particularly large in the tests with blocked springs as shown in Figure 120 for the test on Bridge 3B and in Table 65 for several additional tests. The table includes maximum amplification factors obtained in the tests with induced initial vehicle oscillations and the corresponding values for the tests without induced oscillations. The largest amplification factors oc-

* Nieto, J. A., "A Study of Effect of Interleaf Vehicle Friction on the Dynamic Response of Simple Span Highway Bridges." Tenth Progress Report, Highway Bridge Impact Investigation, Part C, Univ. of Illinois (1960).

curred on Bridges 5A and 7A. The factors were particularly large in the tests with induced oscillations and blocked springs in which several amplification factors exceeded a value of 2.0.

4.4.3 Initial Bridge Oscillations

One subseries of tests on Bridge 3B and one subseries of tests on Bridge 7A were conducted with two trucks following one another over the bridge within a short time. Vehicle 417 crossed the bridge first and was followed by vehicle 415 which entered the bridge while it was still vibrating. Vehicle speed varied from 19 to 31 mph and the distance from the rear axle of the first vehicle to the front axle of the second vehicle varied from 51 to 143 ft. The two vehicles had the same weights and dimensions. Although no detailed measurements were made on

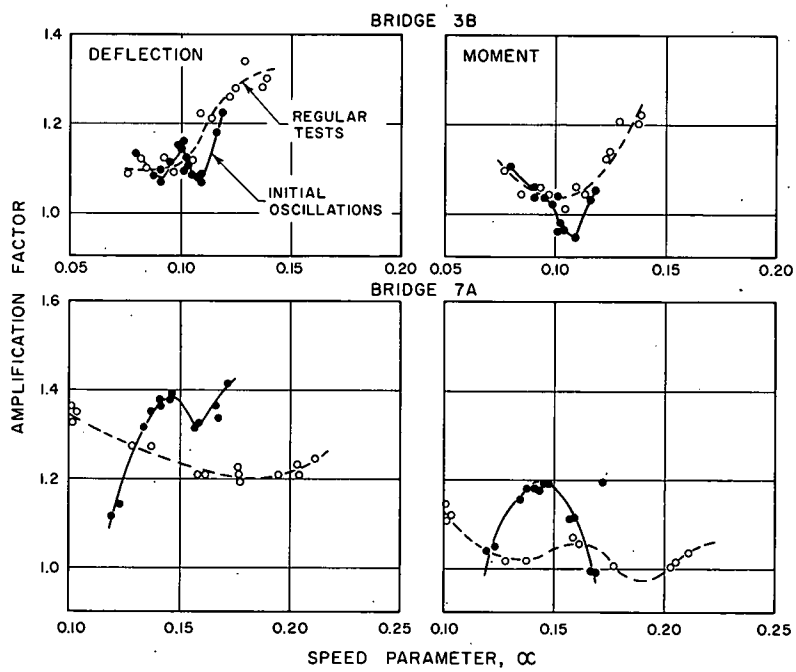

Figure 118. Spectrum curves for tests with initial oscillations, two-axle vehicle, vehicle 91.

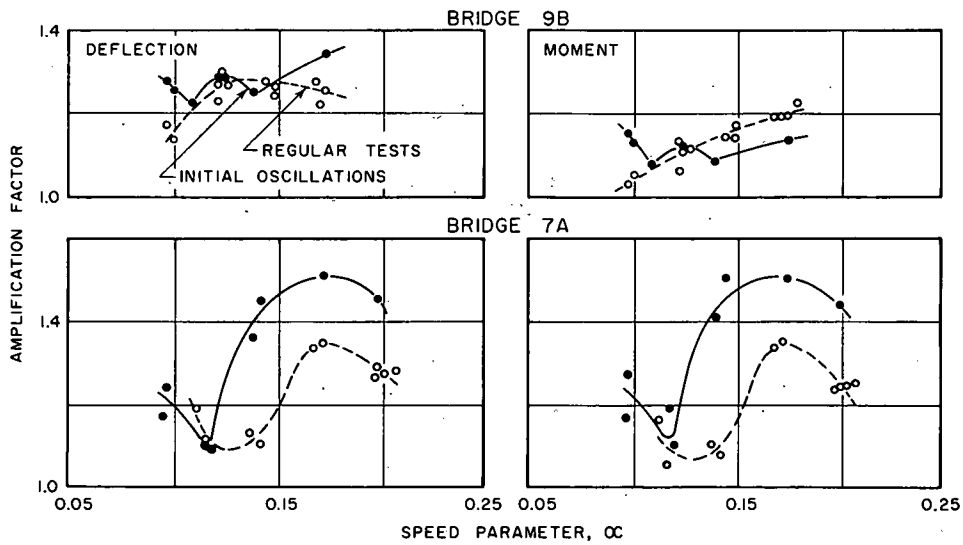

Figure 119. Spectrum curves for tests with initial oscillations, three-axle vehicle, vehicle 513.

vehicle 417, the two vehicles could be considered essentially the same.

The following discussion is based on the results for Bridge 3B only, because the response of Bridge 7A was complicated by the presence of profile irregularities discussed previously.

The dynamic increment curves for two typical runs are shown in Figure 121 as solid lines. The curves show only those portions of the records that were of interest in this study; that is, from the time the rear axle of the first vehicle left the bridge until the second vehicle was part of the way across the bridge. The dashed line represents a dynamic increment curve for a regular test with vehicle 415.

The data show that after the entrance of the rear axle of the second truck, the bridge behavior was essentially the same in all three tests. In general, the amplitudes of free vibration, the number of cycles of free vibration between the exit of the first vehicle and the entrance of the second vehicle, and the phase angle of the bridge motion at the instant the second vehicle entered the bridge influenced the bridge response under the second vehicle only up to the time the rear axle of the second vehicle entered. After this time the bridge behavior was essentially the same for records that were examined. Because the critical dynamic increment and the maximum total effect occurred after the entrance of the rear axle, the initial bridge oscillations were found to have no appreciable effect on the maximum bridge response.

The ranges of amplification factors for deflection caused by the second vehicle are compared in Table 66 with the ranges of ampilfication factors obtained in regular tests with the same vehicle. The values for the tests with initial bridge oscillations fell within the limits of the regular tests.

Comparing the bridge response, the amplification factors due to the first vehicle were generally somewhat higher than those due to the second vehicle. The difference was of the order of 10 percent of the maximum static value, which is of the same order as for the same two vehicles in regular tests described in Section 4.3.5. Finally, the amplification factors for the first vehicle showed a larger scatter than those for the second vehicle.

TABLE 65

MAXIMUM AMPLIFICATION FACTORS IN TESTS WITH INDUCED INITIAL VEHICLE OSCILLATIONS

Bridge	Vehicle	Maximum Amplification Factor			
		Tests with Induced Oscillations		Tests without Induced Oscillations	
		Deflection	Moment	Deflection	Moment
		(*a*) VEHICLES WITH NORMAL SUSPENSION			
3B	91	1.23	1.11	1.34	1.22
	94	1.37	1.15	—	—
5A	94	1.63	1.53	—	—
7A	91	1.42	1.19	1.36	1.15
	513	1.51	1.50	1 35	1.35
9B	513	1.35	1.14	1.29	1.23
		(*b*) VEHICLES WITH BLOCKED SPRINGS			
3B	91	2.10	1.89	1.44	1.38
7A	513	2.24	2,27	—	—
9B	513	1.57	1.43	—	—

4.4.4 Eccentric Loading

Six subseries of tests were made with one line of wheels passing over the interior beam. Two positions of the test vehicle were used, positions 3 and 4 (Fig. 141). The centerline of the load applied to the bridge under test was approximately 24 in. (or 20 in.) from the center beam in the first case and 60 in. (or 56 in.) from the center beam in the second case. (Values in parentheses apply to concrete bridges; the exact distance for position 3 varied slightly from vehicle to vehicle.)

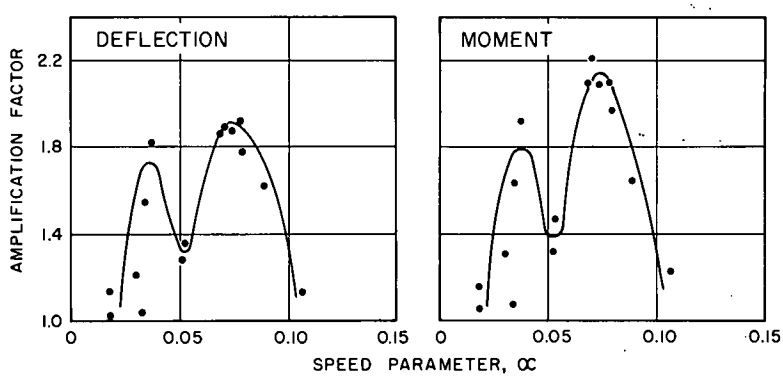

Figure 120. Spectrum curves for tests with initial oscillations of vehicle with blocked springs, Bridge 3B, vehicle 91.

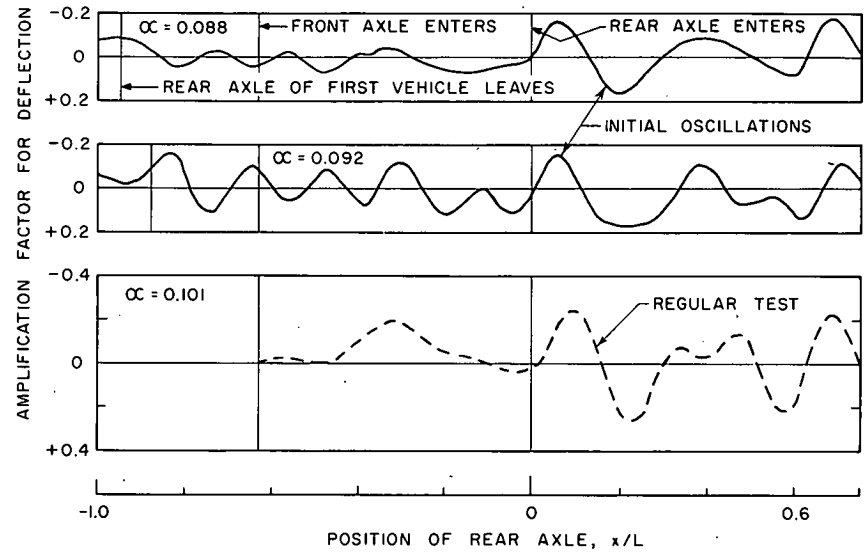

Figure 121. Effect of initial bridge oscillations, Bridge 3B, vehicle 415.

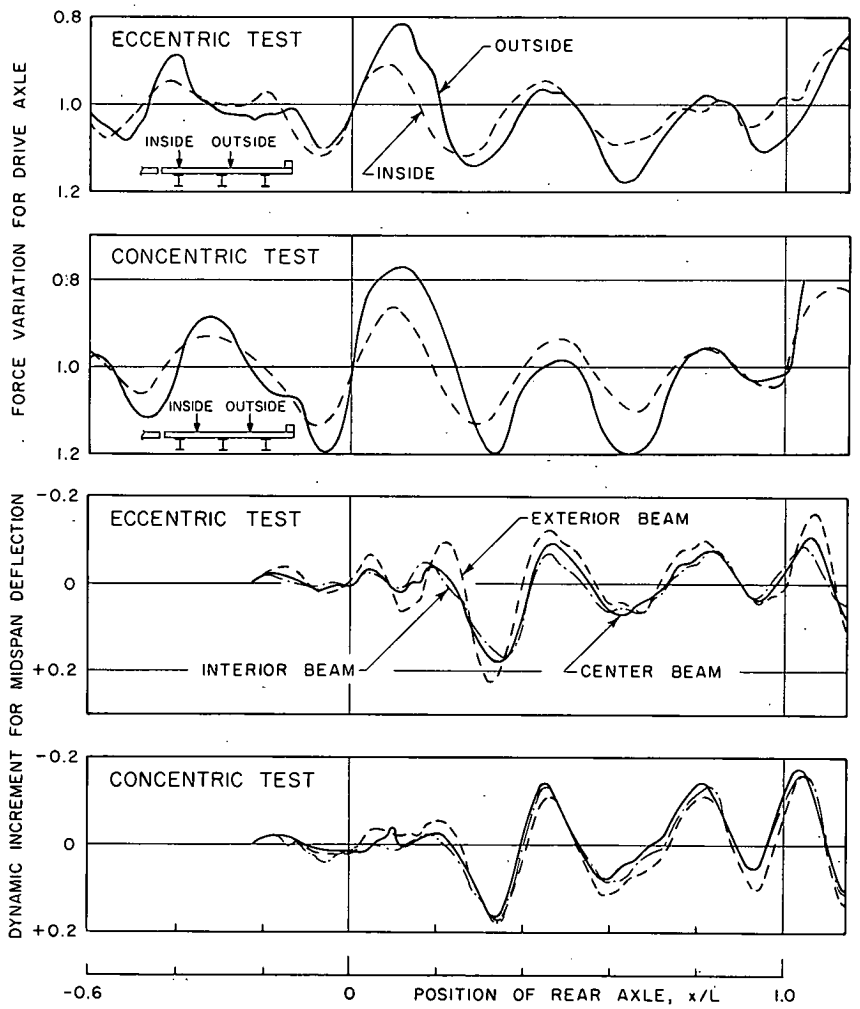

Figure 122. Comparison of response in eccentric and concentric tests, two-axle vehicle, Bridge 3B, vehicle 91, $\alpha = 0.105$.

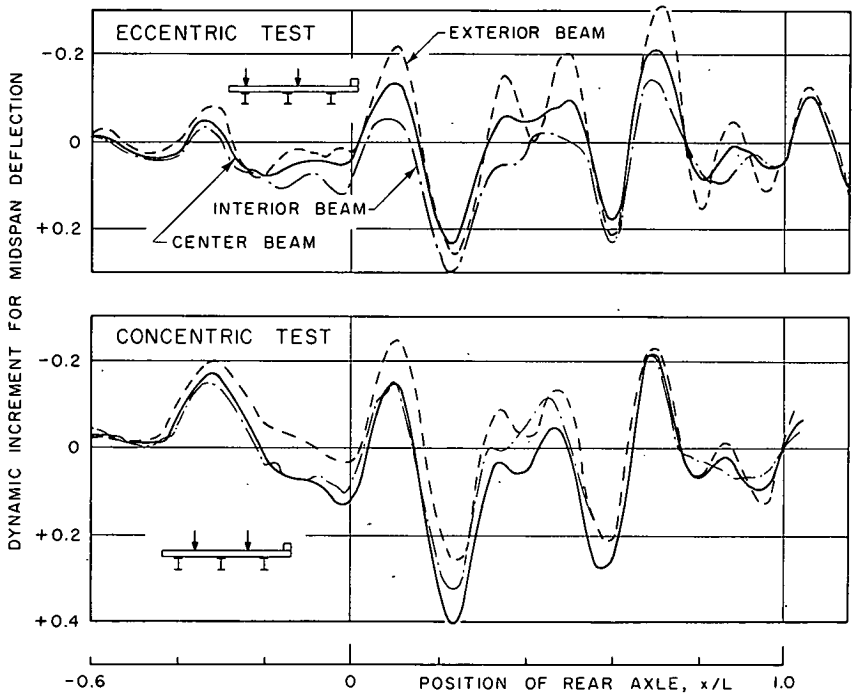

Figure 123. Comparison of response in eccentric and concentric tests, three-axle vehicle, Bridge 3B, vehicle 415, $\alpha = 0.10$.

The tests were made with vehicle C, 94, 91 and 415 on Bridges 4B, 3B, 5A, 5B, 7A and 7B. The crawl tests were made with the same lateral position of the vehicle as the dynamic tests. Except for the vehicle position, the conduct of the tests was identical to that for regular tests.

Typical history curves of vehicle and bridge response for eccentric tests with a two-axle vehicle are shown in Figure 122 and of bridge response to a three-axle vehicle in Figure 123. The results of corresponding tests with concentric loading are also shown.

The dynamic response of the vehicles as well as the three bridge beams in the eccentric tests was essentially the same as in the corresponding concentric tests, when the bridge response was expressed in terms of dynamic increment for the individual beams. Particularly, dynamic increments for the interior beam, in which the 24-in. eccentric loading produced the maximum total effects, were essentially the same as those for the center beam in the tests with concentric loading.

Results for a test run with only one line of wheels on the bridge are shown in Figure 124. Although the critical dynamic increments (at $x/L = 0.4$), expressed in terms of respective maximum crawl values of the three beams, were essentially the same for all three beams there was a major difference in the response of the bridge as compared to tests with 24-in. eccentricity. A shift in the location of the peaks for the three beams indicated a pronounced contribution of the torsional mode of vibration of the bridge. The very large dynamic incre-

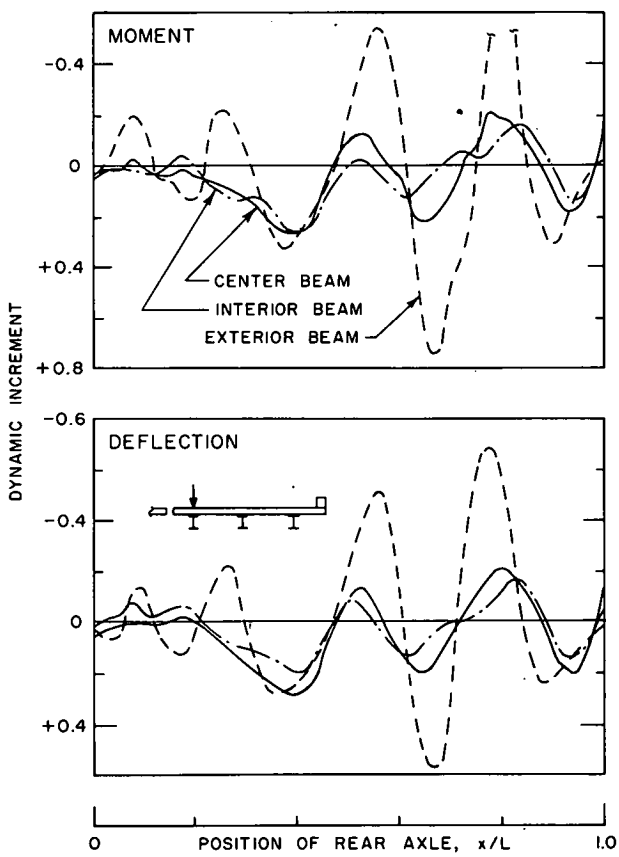

Figure 124. Bridge response for test with 60-in. eccentricity, Bridge 3B, vehicle 94, $\alpha = 0.130$.

TABLE 66
AMPLIFICATION FACTORS IN TESTS WITH INITIAL BRIDGE OSCILLATIONS

Speed (mph)	α	Range of Amplification Factor [1]	
		Tests with Initial Oscillations	Regular Tests
20	0.064	1.05–1.06	1.04–1.16
26	0 085	1.09–1.14	1.09–1.28
30	0.096	1.17–1.18	1.14–1.32

[1] For deflection at midspan of center beam of Bridge 3B.

TABLE 67
MAXIMUM AMPLIFICATION FACTORS IN TESTS WITH ECCENTRIC LOADS

Bridge	Vehicle	Maximum Amplification Factor			
		Interior Beam, Eccentric Tests		Center Beam, Concentric Tests	
		Deflection	Moment	Deflection	Moment
3B	91	1.24	1.22	1.34	1.22
3B	415	1.34	1.23	1.39	1.28
7A	415	1.36	1.22	1.44	1.29

ments of the exterior beam were of no practical significance, inasmuch as the maximum crawl values for both deflection and moment of the exterior beam were equal to only 54 and 58 percent of the corresponding values for the interior beam.

From the standpoint of design, only the maximum effect in the loaded beam is of interest. Spectrum curves for the total response at midspan of the interior beam for 24-in. eccentricity are shown as solid lines; corresponding curves for the center beam in the concentric tests, as dashed lines (Fig. 125). Peak amplification factors for the two sets of tests are summarized in Table 67. The spectrum curves and the maximum amplification factors show that results for the 24-in. eccentric tests were substantially in agreement with the results of the concentric tests throughout the range of speeds considered. The maximum effects in the interior beam caused by eccentric loading were consistently from 5 to 10 percent lower than the corresponding values for the center beam caused by concentric loading. This difference was less than the observed experimental scatter for the concentric tests.

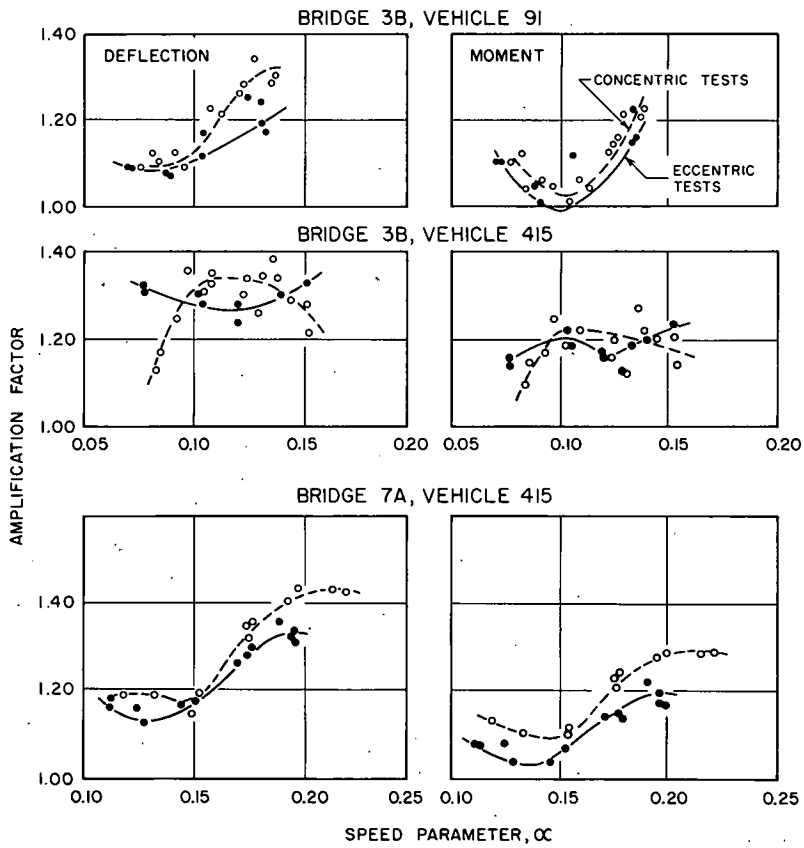

Figure 125. Spectrum curves for eccentric tests.

4.5 COMPARISON OF TEST DATA WITH ANALYTICAL SOLUTIONS

In this section the experimental results are compared with curves obtained by analytical solutions. Comparisons are presented for ten subseries involving four bridges and five test vehicles. The subseries selected were primarily those for which tire pressure measurements were available. Bridges 3B, 2B, 5A and 7A were studied; most of the comparisons pertained to composite steel bridges, the properties of which were least uncertain.

The principal objectives of the comparisons between the experimental and analytical curves were (1) to investigate the adequacy of the available method of analysis, and (2) to account for differences that may exist between the observed and the predicted behavior. The success in meeting these objectives depended in large measure on the reliability of the experimental results and on the ability to incorporate the conditions of the tests in the analysis.

The experimental uncertainties involved both the bridge-vehicle parameters and the experimental data characterizing the response of the bridge-vehicle system. The frequencies and damping characteristics of the bridges used in most analyses were those determined from the free-vibration records; they were not necessarily representative of the true properties for the loaded bridges. The profiles, although known, were only approximated in the analysis. The speed of the vehicle was generally not exactly uniform throughout its passage over the bridge. The frequencies and coefficients of interleaf friction of the vehicle suspension system used in most analyses were those computed on the basis of static measurements; they were generally higher than those determined by dynamic tests. At the instant of its entry on the bridge, the initial condition of the vehicle was uncertain. In the majority of the dynamic tests no measure of the initial conditions was available. Where tire pressure measurements were available, only a rough order of magnitude of the initial condition could be ascertained because of the limitations of the test equipment.

Concerning the uncertainties connected with measurements of the response of the bridge-vehicle system, the replication errors and the unavoidable errors in data processing had to be considered. The errors were particularly large in history curves of dynamic increments, since the dynamic increments were obtained as the difference between two experimental records of the same order of magnitude (one for the dynamic run and one for the corresponding crawl run).

In considering the validity of the theory used for the analytical solutions, a distinction has to be made between the general method of analysis and its specific application embodied in the available computer programs. The method of analysis is general; *i.e.*, it permits inclusion of most or all factors that are known to enter the problem. The computer programs, however, are necessarily less general. Therefore, differences between the measured and computed responses do not necessarily reflect shortcomings of the general theory, but possibly reflect the limitations of the computer programs used.

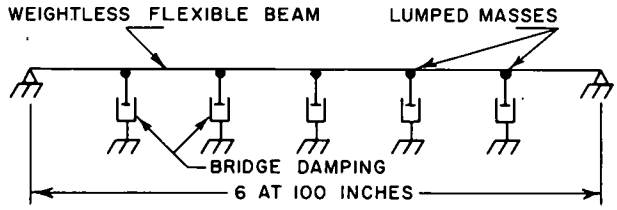

Figure 126. Model of test bridges.

Comparisons were made on the level of both history curves and spectrum curves. The history curves afforded a better basis for comparisons since discrepancies could readily be detected and the effects of uncertainties studied.

4.5.1 Method of Analysis

The analytical solutions were obtained by the method presented by Huang and Veletsos.* The analysis is based on the ordinary beam theory which neglects the effects of shearing deformations and axial forces. The beam, which in reality has an infinite number of degrees of freedom, is replaced by a discrete system having a finite number of degrees of freedom. This simplification is effected by concentrating the distributed mass of the beam into a series of point masses; the stiffness of the beam is assumed to be distributed as in the actual system. The vehicle is represented by one or two masses supported by two or three axles. Each axle is represented by two springs in series, and a frictional mechanism in parallel with one of the springs. The vehicle is assumed to remain in contact with the bridge at all times. The equations of the system are obtained by writing one equation for each concentrated mass and one for each axle of the vehicle. Resulting differential equations are integrated numerically.

The idealized model of the test bridges used in the analysis consisted of a simply supported beam with five equally spaced concentrated masses (Fig. 126). The damping was neglected in most solutions. The idealized models of the test vehicles are shown schematically in Figure 127. The masses included all components of the loaded vehicle, and were supported on the previously described suspension system.

The solutions were obtained on ILLIAC, the high speed computer at the University of Illi-

* Huang, T., and Veletsos, A. S., "Dynamic Response of Three Span Continuous Highway Bridges." Civil Engineering Studies, Structural Research Series No. 190, Univ. of Illinois (1960).

nois. The program for the computer was a slight modification of that described by Huang and Veletsos in that the bridge model considered was a simple-span beam.

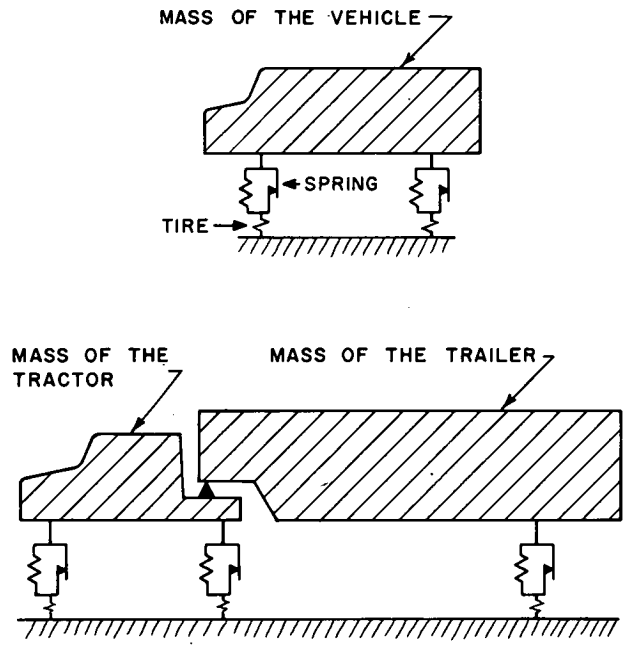

Figure 127. Models of test vehicles.

The principal dimensionless bridge-vehicle parameters entering the analysis were defined in Section 4.2.3, and the magnitudes of the component characteristics were given in Sections 2.2.5, 2.4.3, 4.1.2 and 4.1.3. The values of the dimensionless parameters computed from these characteristics and used in the analytical solutions are given in Table 68. Included are the natural frequency of the bridge f_b, the weight ratio R and the profile parameter Δ, the speed parameter α, the frequency ratios ϕ_t and ϕ_{ts} and the coefficient of interleaf friction μ.

One analytical solution for each selected test run was based on the values of the parameters and the assumption of smoothly rolling load. When tire pressure measurements were available, at least one additional solution was made attempting to reproduce the state of oscillation of the vehicle at the time of entry on the bridge.

In the version of the computer program used in this study, initial oscillations could be specified only at the beginning of the problem, *i.e.*, when the front axle entered the span. The initial oscillations were specified in terms of the interaction force, vertical velocity and frictional force for each axle. In cases where an attempt was made to reproduce the initial conditions of the drive and rear axles, a set of frictional conditions was specified at the beginning of the problem.

TABLE 68

PARAMETERS USED IN ANALYTICAL SOLUTIONS

Bridge	Vehicle	f_b (cps)	R	Δ	ϕ_t[1]	ϕ_{ts}[1]	μ[1]	Range of α
3B	91	4.37	0.277	1.79	0.868 0.762			0.091–0.106
3B	513	4.44	0.652	1.79	0.975 0.636 0.721			0.118–0.138
3B[2]	91	4.72	0.277	1.79	0.868 0.762	0.448 0.487	0.08 0.12	0.077–0.138
3B	513	4.56	0.652	1.79	0.975 0.636 0.721	0.360 0.403 0.488	0.11 0.13 0.19	0.087–0.146
3B	415	4.46	0.563	1.19	1.116 0.846 0.820	0.864 0.433 0.496	0.04 0.09 0.18	0.040–0.180
2B	A	4.67	0.277	1.20	0.882 0.885	0.474 0.444	0.02 0.18	0.040–0.205
2B	C	4.67	0.621	1.20	0.932 0.729 0.741	0.501 0.451 0.410	0.02 0.18 0.18	0.030–0.203
2B	B	4.67	0.473	1.20	0.940 0.851 0.917	0.505 0.452 0.462	0.02 0.18 0.18	0.030–0.203
6A	91	6.67	0.206	1.72	0.600 0.553	0.315 0.360	0.08 0.12	0.096–0.102
7A	91	3.14	0.206	−0.40	1.272 1.177	0.668 0.763	0.08 0.12	0.114–0.204

[1] Values listed in order: front, drive and rear axle.

[2] Effects of variations of ϕ_t and ϕ_{ts} were studied on this problem.

The values of several of the parameters (Table 68) were known to be only rough estimates; therefore, for several test runs the effect of varying the parameters within reasonable limits was studied analytically. Such studies included the speed parameter, the frequency ratio of the drive axle, the profile parameter, the coefficient of interleaf friction, the damping characteristics of the bridge and the dynamic index of the vehicle.

The analytical curves included in the comparisons that follow are the best solutions obtained for the particular run presented.

4.5.2 Composite Steel Bridges 2B and 3B

The comparisons between analytical and experimental history and spectrum curves for Bridges 2B and 3B are presented for runs with three- and two-axle vehicles, both with normal suspension system and with blocked springs.

History Curves for Two-Axle Vehicles.— Figures 128 through 131 show history curves for tests with two-axle vehicles. The experimental curves are solid lines; the analytical curves, dashed lines. The analytical solutions for Bridge 3B (Figs. 128 and 129) included

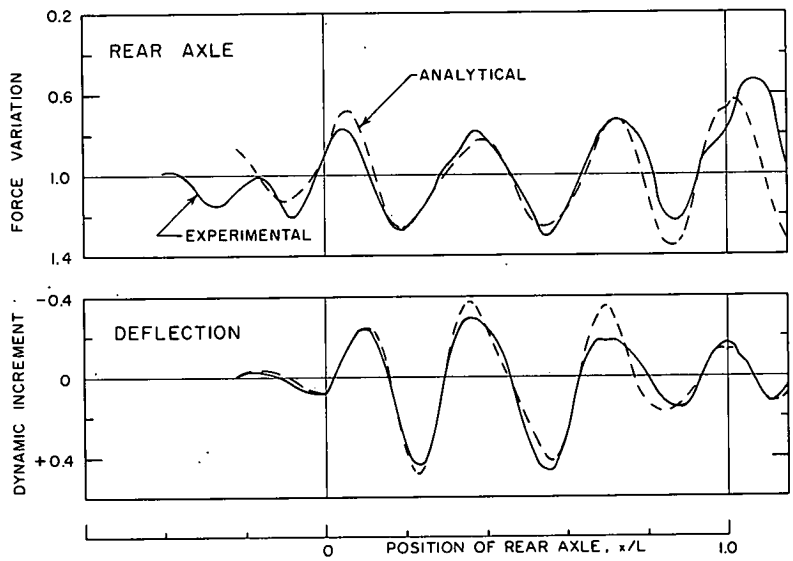

Figure 128. Effects of two-axle vehicle with blocked springs, Bridge 3B, vehicle 91, $\alpha = 0.101$.

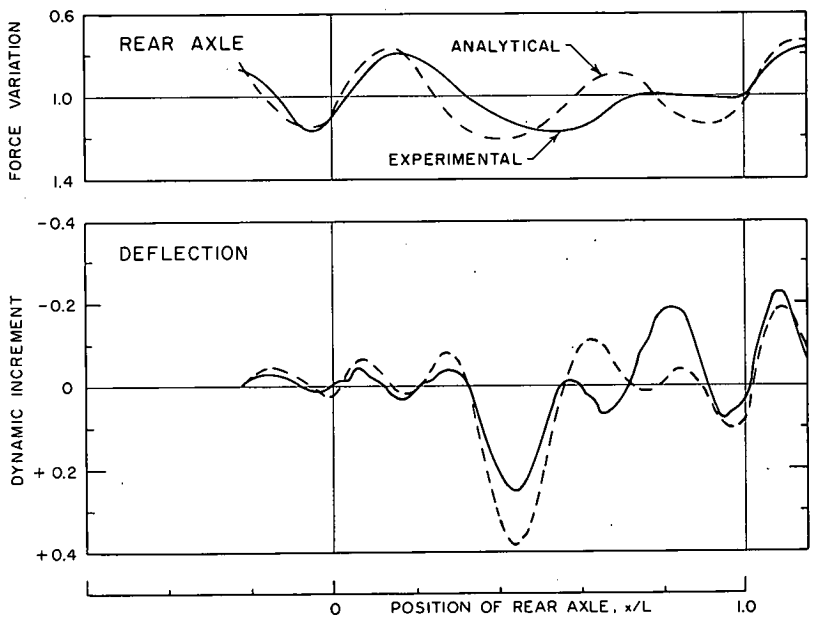

Figure 129. Effects of two-axle vehicle with normal suspension, Bridge 3B, vehicle 91, $\alpha = 0.138$.

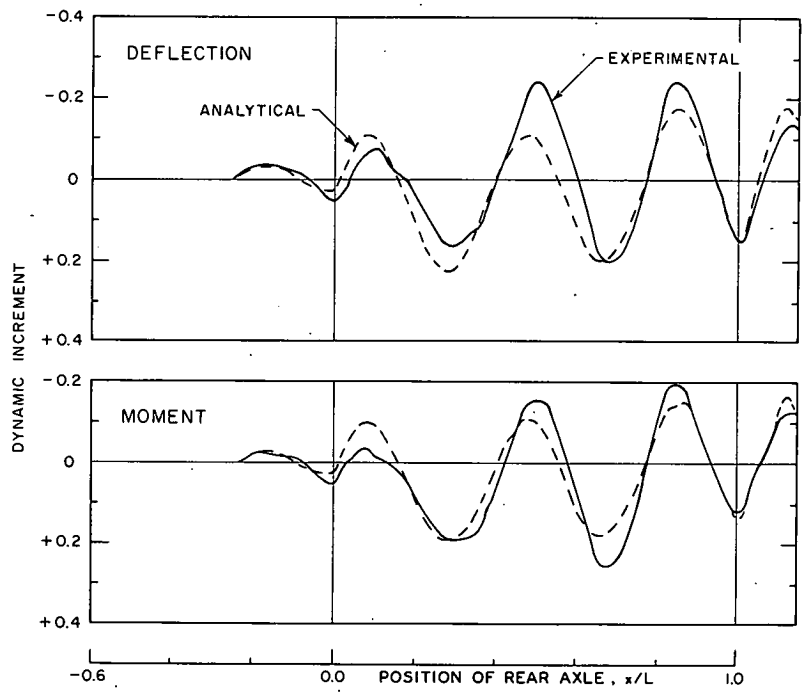

Figure 130. Effects of two-axle vehicle with normal suspension, Bridge 2B, vehicle A, $\alpha = 0.146$.

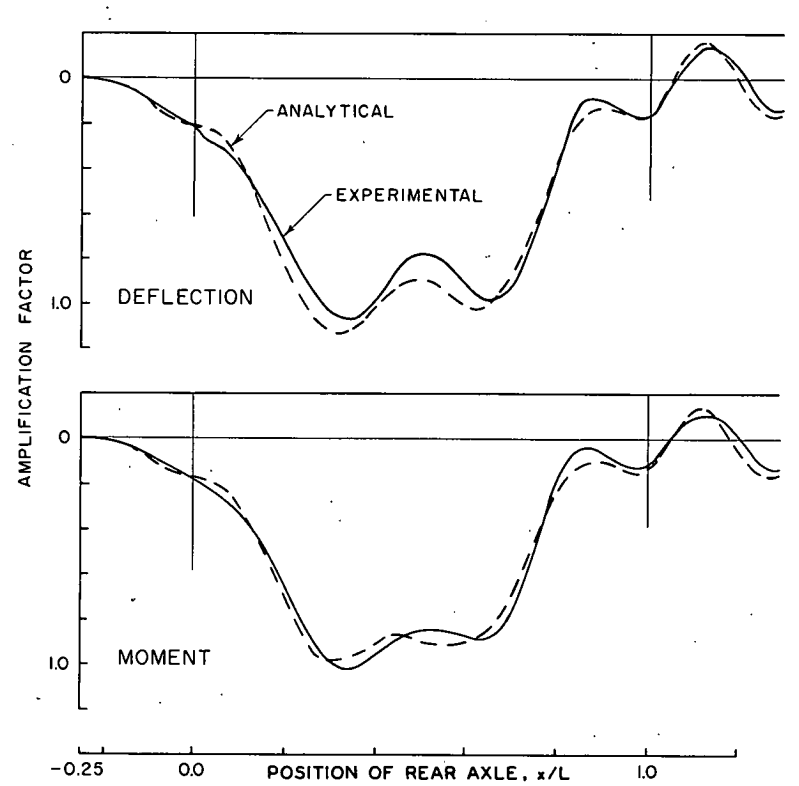

Figure 131. History curves for amplification factors, Bridge 2B, vehicle A, $\alpha = 0.146$.

initial oscillations; those for Bridge 2B (Figs. 130 and 131) were based on the assumption of smoothly rolling loads entering the bridge. The effects of initial oscillations could not be included in the solutions for Bridge 2B because no measurements of the variations in the interaction force were available for this bridge. For Bridge 3B and two-axle vehicle 91, the analytical solution is considered to be in excellent agreement with the results of the experiment (Fig. 128).

The curves in Figure 129 represent a test with a two-axle vehicle 91 with regular suspension. The analytical solutions, based on a natural frequency for the drive axle reduced by 20 percent from the value determined on the basis of static tests, reproduced the general shape of the experimental curves, although there were differences in the magnitude of the response. In this solution the initial magnitude and slope of the interaction force were properly matched, but the assumed initial interleaf friction might have been in error.

The dynamic increment curves for a test of Bridge 2B with two-axle vehicle A are shown in Figure 130 and the amplification factors for the same tests are shown in Figure 131. The analytical solution for smoothly rolling loads, was based on slightly different coefficients of interleaf friction than the values determined from the static loading tests. The agreement between the analytical and experimental records was excellent, particularly for moment. For this run, a solution was also made by neglecting the effect of interleaf friction in the suspension springs of the vehicle. No agreement could be obtained in this manner, indicating the importance of including the effect of interleaf friction in the theoretical solution.

History Curves for Three-Axle Vehicle.—History curves for tests with three-axle vehicle 513 are shown in Figures 132 and 133 for the springs on the drive and rear axles blocked and for normal suspensions. In the analytical solutions for both figures an attempt was made to account for the initial oscillations of the vehicle.

For the tests with blocked springs, the agreement between the analysis and the experiment was reasonably good for the variation of the interaction force of the drive axle, but was poor for the rear axle. The observed frequency of the rear axle was lower than the computed one so that the computed phase angle at the instant of entry of the rear axle on the bridge was in error.

In spite of the differences in the vehicle response, the agreement in the bridge response was satisfactory up to about $x/L = 0.5$. The computed peak dynamic increment closely approximated the measured value. After the rear axle passed midspan and the drive axle left the bridge ($x/L = 0.59$), the measured and computed responses were not comparable. It was assumed in the analysis that the dynamic index for the trailer was $i = 1.0$; that is, the motion of the rear axle was unaffected by the oscillations of the tractor. Furthermore, it was assumed in the analysis that after leaving the bridge, the vehicle continued on a smooth, level surface, whereas actually the vehicle traversed the second bridge in the line of travel.

The history curves for the three-axle vehicle with normal suspension passing over Bridge 3B show a reasonable agreement between the experiment and the analysis, except for the magnitude of the variation in the interaction force of the rear axle and for the second half of bridge response pertaining to the period after the exit of the drive axle from the bridge.

Spectrum Curves.—Comparisons between the theory and the experiment were made for spectrum curves for three subseries of tests (Figs. 134, 135 and 136). The test data are shown as dots and the analytical solution for the smoothly rolling load as a solid line; furthermore, dashed lines (Fig. 134) represent the analytical solution considering an initial oscillation. Amplification factors for both deflection and moment are also shown.

There is a satisfactory agreement between the experimental data and the analytical curves. Particularly interesting is the bracketing of the test data by the two analytical curves in Figure 134. The curves show that the smoothly rolling condition does not necessarily imply a lower bound of the response. The actual interaction force and frictional force may have any value at the entry on the bridge, and the vertical movement may be in either direction. Thus, it is possible for these effects to combine in such a manner as to produce smaller or larger response than a smoothly rolling vehicle with no frictional force at the instant of entry.

Data in Figure 135 were chosen for the comparison with the analytical solution because of the extensive coverage both as to the number of tests and the range of parameter α.

The analytical curve in Figure 136 shows large variations at low values of the speed parameter. It is noteworthy that the test data showed more scatter in this range than at higher values of α.

4.5.3 Concrete Bridges 6A and 7A

The comparisons presented in the previous sections dealt with the composite steel bridges, the properties of which were subject only to relatively small uncertainties. This section presents the results for prestressed concrete and reinforced concrete bridges, the properties of which were most uncertain.

Bridge 6A.—The dynamic increment curves for two runs with two-axle vehicle 91 over the prestressed concrete bridge 6A are shown in

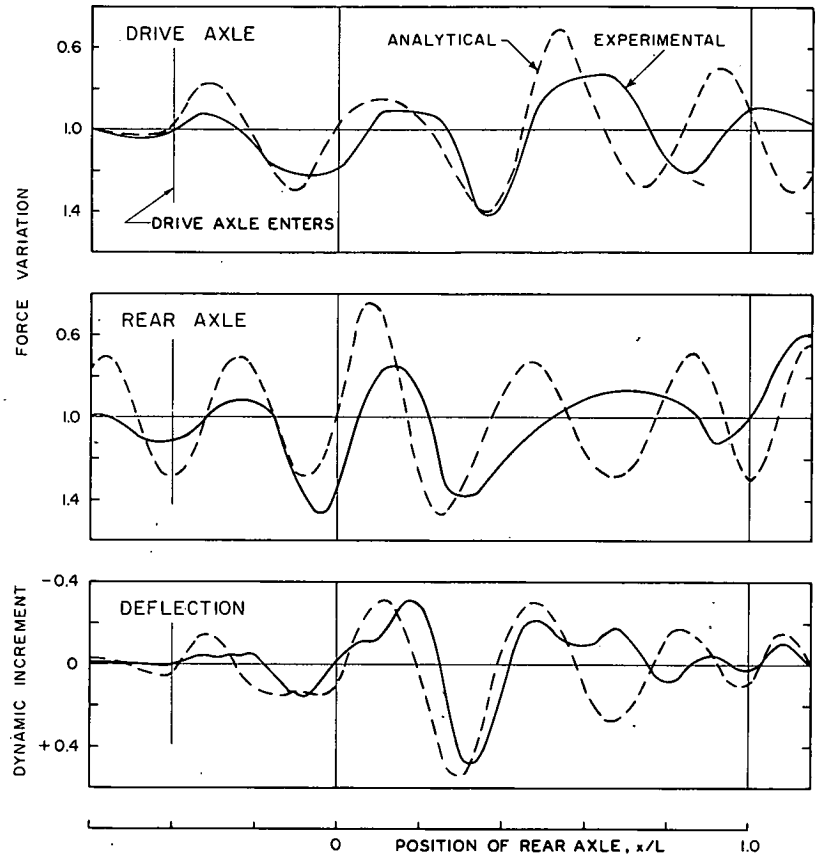

Figure 132. Effects of three-axle vehicle with blocked springs, Bridge 3B, vehicle 513, α = 0.118.

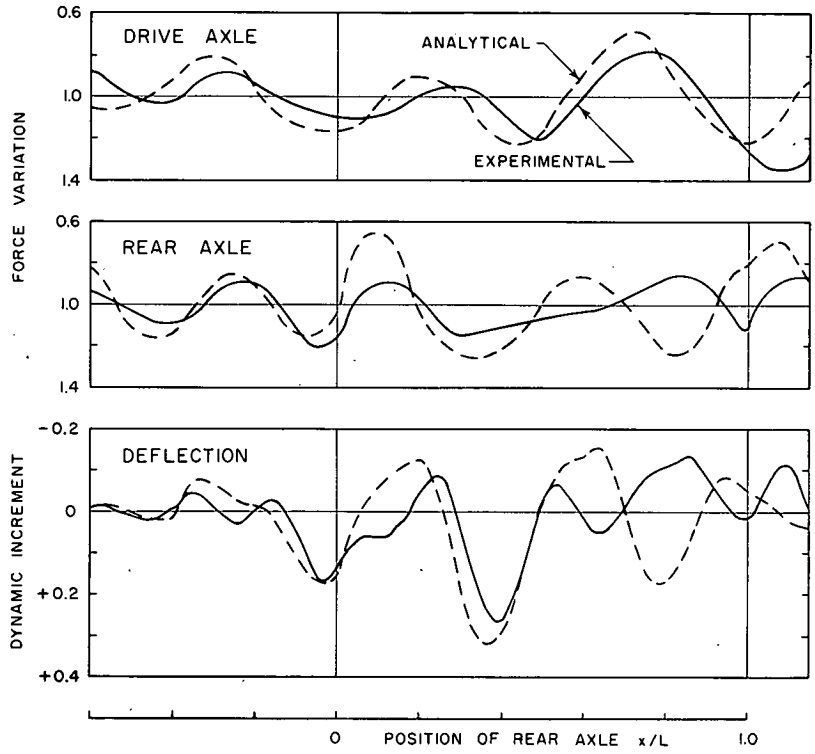

Figure 133. Effects of three-axle vehicle with normal suspension, Bridge 3B, vehicle 513, α = 0.130.

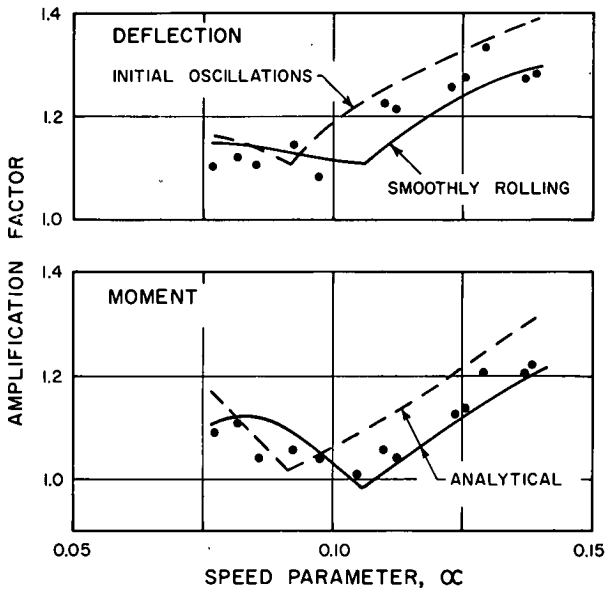

Figure 134. Spectrum curves for Bridge 3B and vehicle 91.

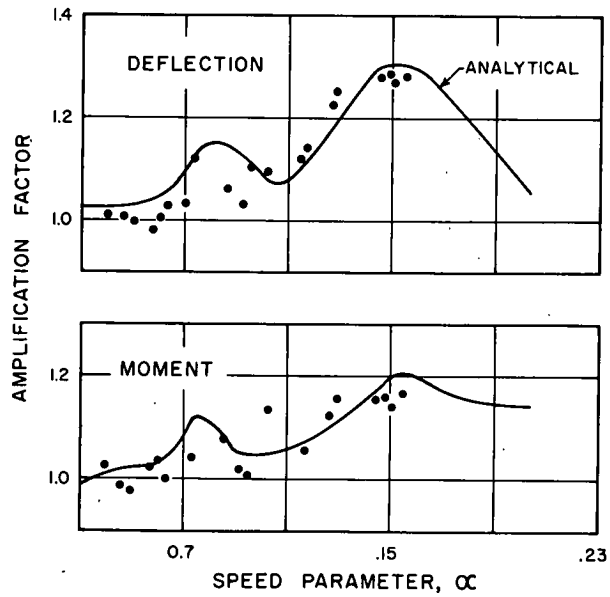

Figure 136. Spectrum curves for Bridge 2B and vehicle B.

Figure 137. The measured natural frequency of the bridge, determined from the vibration records and used in computing the analytical curves, was 6.67 cps or 98 percent of the computed frequency based on an uncracked cross-section. However, at the time of the tests the beams of the bridge had been cracked on both sides of midspan, particularly in the exterior beam; therefore, the measured frequency may not be representative of the loaded bridge.

The experimental interaction force records were not usable because the times of entrance and exit on the bridge were not properly recorded. However, the amplitude of the variation of the interaction forces on the approach pavement was only of the order of 0.08 P_{st}, suggesting that the assumption of a smoothly rolling vehicle should be realistic. The computed curves of dynamic increments pertain to a smoothly rolling condition.

There was reasonable agreement between the measured and computed response only when the load was at a considerable distance from midspan. There was no agreement between the theory and the analysis when the heavy axle of the vehicle was near midspan. In this region the experimental records showed high-frequency components observed only on

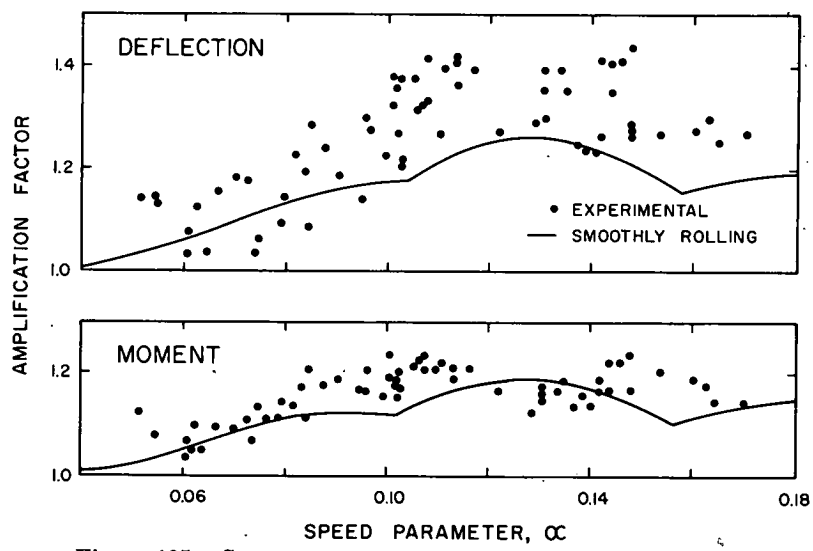

Figure 135. Spectrum curves for Bridge 3B and vehicle 415.

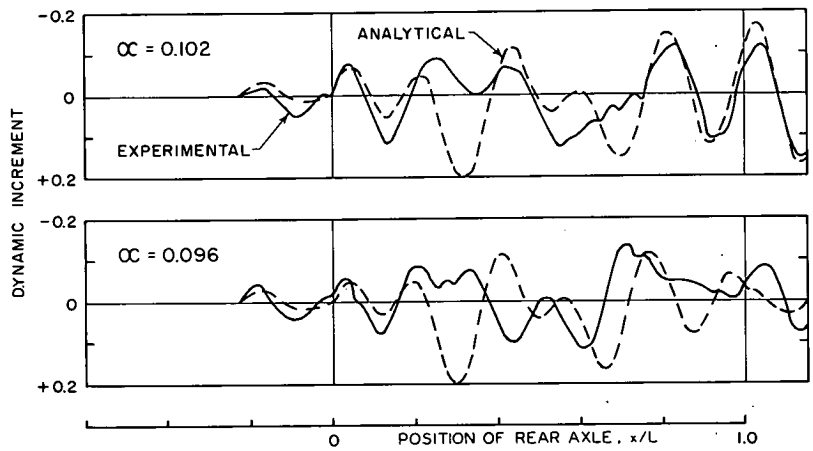

Figure 137. Dynamic increment curves for deflections of Bridge 6A, vehicle 91.

the records of this bridge and of prestressed concrete bridge 5A.

It is suspected that the discrepancy between the theoretical and analytical curves was caused by the change in the bridge characteristics due to opening of tensile cracks on loading. The amount of opening of the cracks was related to the magnitude of the applied moment and, thus, to the position of the vehicle on the span. In other words, the frequency of the bridge depended on the position of the load. The largest differences between the experimentally and analytically determined behavior can be expected to occur when the difference between the actual frequency and the free vibration frequency was the largest, that is, when the heavy axle of the vehicle was near midspan. Although further studies would be necessary to explain the discrepancies, it appears that no satisfactory agreement can be obtained with a theoretical solution which assumes that the properties of the structures are constant.

For the two tests considered, the maximum measured amplification factors were 1.15, and

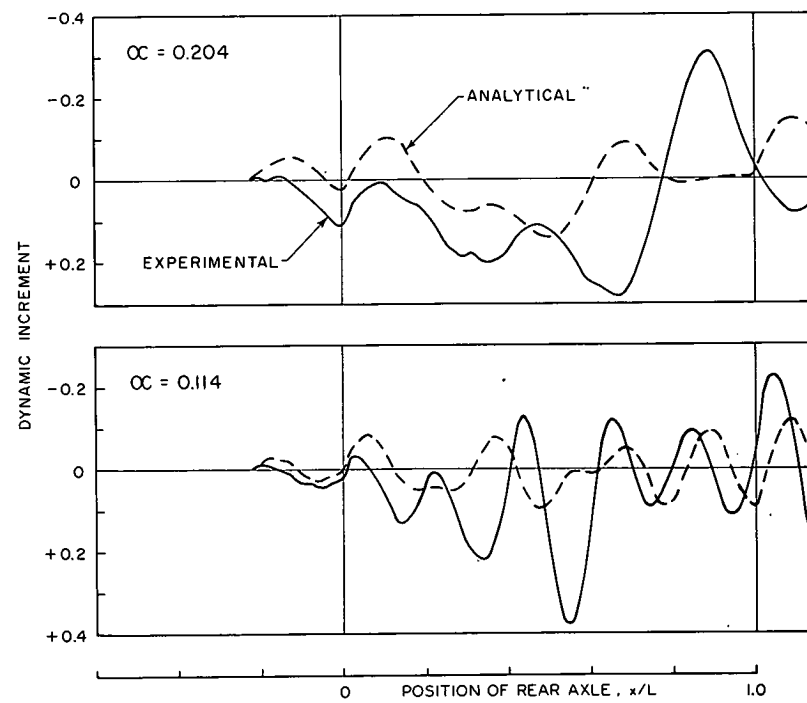

Figure 138. Dynamic increment curves for deflections of Bridge 7A, vehicle 91.

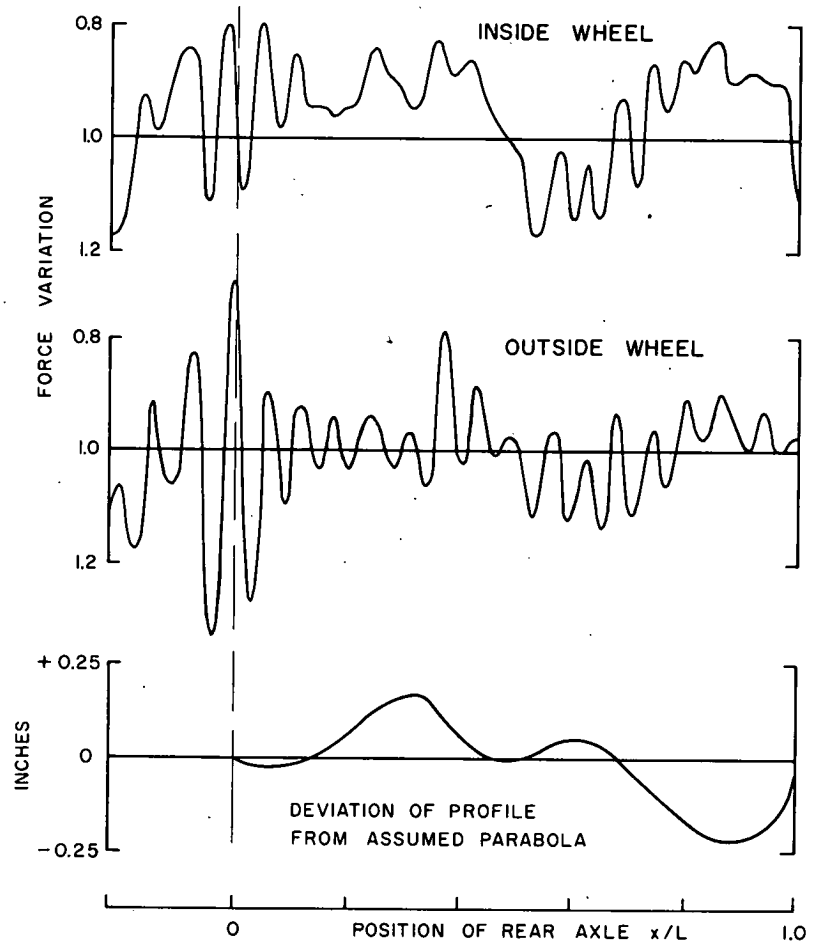

Figure 139. Effect of surface irregularities on variation of interaction force, Bridge 7A, vehicle 91.

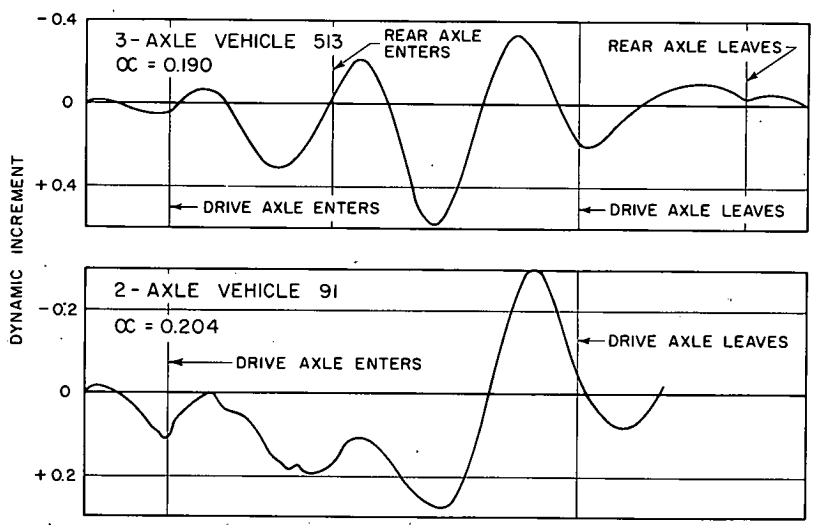

Figure 140. Effect of number of axles on dynamic increment curves for deflection of Bridge 7A.

the maximum computed amplification factors were 1.12 for the lower speed and 1.14 for the higher speed. This apparent agreement points out that, in order to understand the true behavior, the comparisons must be made at the level of history curves.

Bridge 7A.—The solid lines in Figure 138 show measured dynamic increments for deflection for two test runs involving reinforced concrete bridge 7A and two-axle vehicle 91; the dashed lines, analytical solutions assuming a smoothly rolling vehicle. The bridge profile was assumed in the analytical solution to be a second-degree parabola with a midspan ordinate equal to that of the actual bridge profile. There was no agreement between the measured and the computed responses.

Experimental interaction force curves for the two rear-axle wheels are shown for the faster run (Fig. 139). Pronounced high-frequency tire-hop oscillations are evident throughout the record. These oscillations are typical for all test runs on this bridge and are considerably more pronounced than those observed on other test bridges.

The presence of high-frequency oscillations in the records of variation of the interaction force for runs over Bridge 7A indicates a high degree of roughness of the bridge pavement. The deviations of the bridge profile from the parabola used in the analytical solution (Fig. 139) show two pronounced bumps—one near the third point and the other near the end of the bridge. Although the latter cannot be expected to have large effects on the bridge-vehicle response, the first bump may have accounted for the large dynamic effect observed on this bridge.

The measured dynamic increments (Fig. 138) increased drastically in amplitude starting approximately at $x/L = 0.4$. This corresponded to the end of the bump. For the higher speed, the peak dynamic increment caused by the bump occurred at $x/L = 0.85$, producing a low total effect. However, for the slower speed the peak dynamic increment occurred when the axle was still near midspan and the resulting total amplification factor was very large.

Because of the limitations of the available computer program it was not possible to consider the effect of the profile irregularities in the analytical solutions. The profile irregularities seemed to explain the differences between the spectrum curves for tests with two-axle and three-axle vehicles, supporting the assumption that the discrepancy between the analytical and experimental curves (Fig. 138) was also caused by profile irregularities.

For the two-axle vehicles the spectrum curve ordinates for higher speeds were lower than those for lower speeds (Fig. 102). For the lower speeds the critical dynamic increment occurred near midspan causing large amplification factors. As the speed increased, and the time of transit decreased with respect to the bridge period, the critical dynamic increments occurred at larger values x/L, and, consequently, combined with lower crawl ordinates.

On the other hand, the spectrum curves for the three-axle vehicle showed very high amplification factors. For the three-axle vehicles used, the spacing of the two heavy axles was approximately 0.41. When the rear axle entered the bridge, the drive axle encountered the previously described bump. Consequently, the high oscillation produced by the excitation of the drive axle occurred when the rear axle was close to midspan, that is, when the static effect was near the maximum.

The high dynamic increments for tests with the three-axle vehicles are shown in Figure 140 which compares the measured dynamic increments for two- and three-axle vehicles. The points of entry of the drive axles of both vehicles are lined up. The two responses were in phase until the drive axle left the span and the critical dynamic increments occurred for the same position of the drive axle.

Chapter 5

Miscellaneous Tests and Studies

This chapter contains descriptions and summaries of data from several independent studies carried out in connection with the primary research on bridges.

5.1 TRANSVERSE DISTRIBUTION OF MOMENTS AND DEFLECTIONS

The external moment caused by a vehicle on a bridge is resisted by the slab and the beams. The proportion resisted by any one element depends on the transverse location of the vehicle on the bridge. As a result, the stresses and deflections in the various elements of the bridge vary with the transverse position of the vehicle.

The majority of the tests on bridges were made with a vehicle straddling the center beam. To obtain data for other transverse positions of vehicles, special tests were carried out. The results are compared with theoretical values computed from the elastic analysis that forms the basis for current specifications for the design of highway bridges.*

5.1.1 Details of Experiment

Every bridge was tested with two-axle vehicles (vehicles 91 and 94, Table 20) placed in six transverse positions. The dump truck was operated over the bridges in the direction of traffic at crawl speed or was placed in the positions for maximum moment at midspan or at the third points (always facing in the normal direction of traffic). Thus, test data were obtained for 18 static positions of the vehicle as well as from crawl tests in six different transverse positions.

The six transverse positions are shown in Figure 141. In position 1, the vehicle straddled the center beam so that the centerline of the vehicle coincided with the center beam. In positions 2 and 3, one line of wheels was directly over the exterior or interior beam, and the other line of wheels was located on the same bridge. In position 4, one line of wheels was located over the interior beam while the other line of wheels was on the adjacent bridge. In positions 5 and 6, the centerline of the truck was located 12 in. away from the center beam toward the interior or exterior beam.

The center-to-center spacing was 69 in. for the rear wheels and 64 in. for the front wheels of the truck. The rear wheels had dual tires; the front wheels, single tires. The axles were spaced at 132 in. The axle loads are given in Table 69. First tests were made before the beginning of the test traffic. However, because of experimental difficulties, the tests had to be repeated at later dates. Bridges 1B, 2A, 4A and 4B are not included because they were tested only before the beginning of test traffic and the data obtained were not considered reliable.

The measurements included bottom strains on all three beams at midspan, at the third points and at the ends of cover plates; and deflections at midspan of all three beams. Additional strain measurements were made on the top flanges of the steel beams at midspan. Each test was replicated at least three times. The order of all tests on any bridge was randomized.

5.1.2 Theoretical Analysis

Theoretical moment and deflection influence surfaces for each bridge were computed by the method of finite differences described elsewhere.* This method is based on the assumptions, and approximates closely the results, of a more rigorous method of analysis** forming the basis of current design specifications.

The method is based on the ordinary elastic theory of medium-thick plates.† In addition to those usually embodied in plate theory, its assumptions are:

1. The beams exert only vertical forces on the slab; there is no shear between the beams and the slab.
2. The effect of diaphragms is neglected.
3. The reaction of the beam acts on the slab along a line, and is not distributed over a finite width.
4. A beam and the slab directly over it deflect alike.

* AASHO, "Standard Specifications for Highway Bridges." Washington, D. C. (1957).

* Chen, T. Y., Siess, C. P., and Newmark, N. M., "Studies of Slab and Beam Highway Bridges, Part IV —Moments in Simply Supported Skew I-Beam Bridges." Univ. of Illinois Engg. Exp. Sta., Bull. 439 (1957).

** Newmark, N. M., "A Distribution Procedure for the Analysis of Slabs Continuous Over Flexible Supports." Univ. of Illinois Engg. Exp. Sta., Bull. 304 (1938).

† See, for example, Timoshenko, S., "Theory of Plates and Shells." New York, McGraw-Hill (1940).

TABLE 69

TRANSVERSE LOAD DISTRIBUTION TESTS

Date of Tests	Axle Weights (kips)		Bridges Tested
	Front	Rear	
27 Jan 59–5 Feb 59	6.8	14.3	2B, 3A, 3B, 7A
25 Aug 59	6.1	14.1	6A, 6B
1 Jan 59–23 Sept. 59	6.4	14.6	1A, 5A, 5B, 8A, 8B, 9A, 9B
22 Mar 60	6.5	14.7	7B

5. The edge beams on each side of the bridge are located at the edge of the slab.

6. Both the slab and the beams are simply supported at the ends of the span.

7. The torsional resistance of the beams is neglected.

For the purposes of the analysis, the bridge was replaced by a network of nodal points shown in Figure 142. Influence ordinates were obtained at each nodal point of all bridges for beam moments at midspan, for beam moments at the third points, and for beam deflections at midspan.

In addition to the dimensions of the network, the determination of the influence surfaces involved the relative stiffness H (Section 3.2.4) of individual beams and, for cover-plated beams, the ratio of the moment of inertia of the cover-plated section to the moment of inertia of the section without cover plates. Both quantities were computed from the measured dimensions and moduli of elasticity of the materials. For concrete, the computations used the value of the modulus of elasticity determined at the beginning of the test traffic. Poisson's ratio for concrete, also required in the analysis, was assumed equal to zero.

In view of the first assumption, the analysis is directly applicable only to noncomposite bridges. However, it was applied to all other bridges, using H computed on the basis of the transformed T-beam sections.

For any particular position of the truck, the influence ordinates were obtained for each wheel. For locations other than the nodal points, a parabolic interpolation and extrapolation procedure was programed for com-

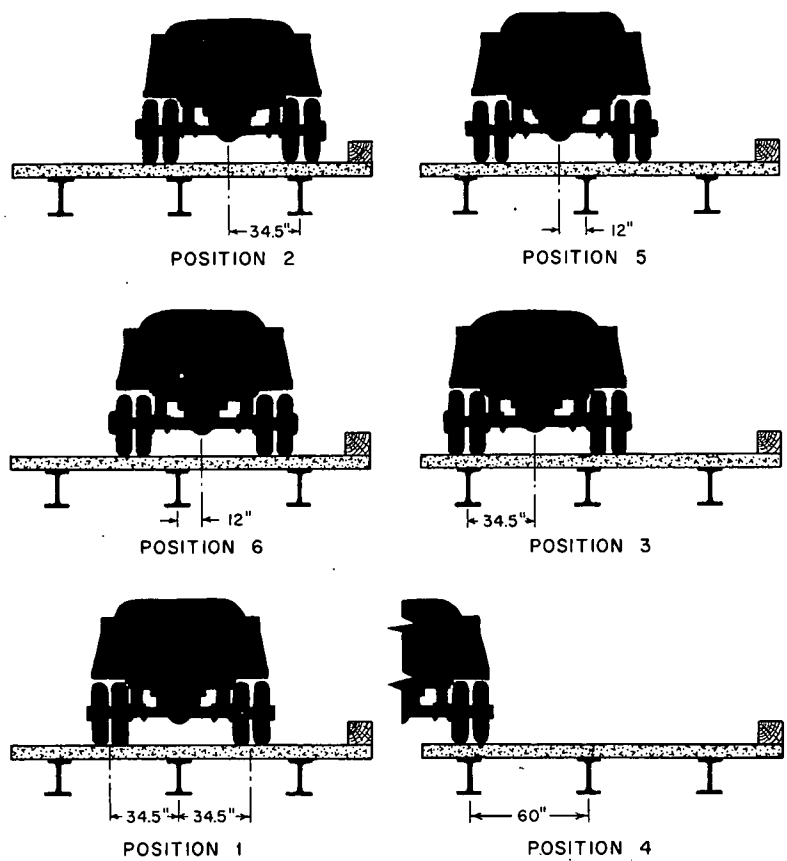

Figure 141. Vehicle positions in load distribution tests.

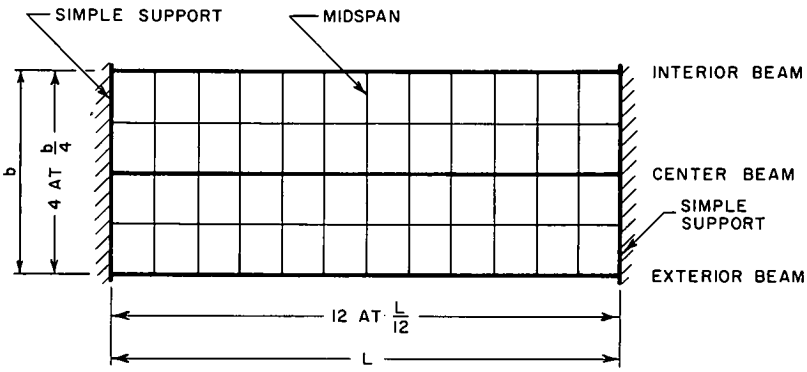

Figure 142. Network for difference analysis.

puter solution.* For moments, the influence ordinates were multiplied by the magnitude of the wheel load P and by the span length L. For deflections, the multiplication factor for the influence ordinates was $PL^3(EI)_{beam}$, where $(EI)_{beam}$ was the beam stiffness at the point considered.

5.1.3 Results of Study

For comparative purposes, the measured strains and the computed moments were converted into stresses. Since all strains were measured on steel, the computation of stresses from measured strains involved only the modulus of elasticity for the particular type of steel (structural steel, prestressing steel, or reinforcing bars). The computed moments were divided by the section modulus of the particular beam section under consideration; properties of concrete at the beginning of test traffic were used for this purpose.

Comparisons between test results and theory are shown in Figure 143. Data are included for two reinforced concrete bridges (7A and 7B), two noncomposite steel bridges (9A and 9B), and two prestressed concrete bridges (5B and 6B). The pairs of steel and reinforced concrete bridges were replicates; the prestressed concrete bridges were not exact replicates, but their properties were such that the theoretical deflections for both bridges were represented by the same line. The beams of reinforced concrete bridges were thoroughly cracked, whereas those of Bridges 5B and 6B were essentially uncracked, thus fulfilling the assumptions made in computing the theoretical stresses and deflections.

Figure 143 includes stresses and deflections of the interior, center and exterior beam at midspan, given as a function of the position of the truck expressed as the distance of the centerline of the truck from the center beam. The test data are shown as dots or circles connected by dashed lines, and the theoretical values are shown as heavy lines. The test data are in closest agreement with the theory for the noncomposite steel bridges (9A and 9B). The correlation is not as good for the prestressed concrete bridges, and is worse for the reinforced concrete bridges. The data are typical of the three types of bridges tested—steel, prestressed concrete and reinforced concrete.

Tables 70 and 71 give the ratios of the measured and the computed stress or deflection for vehicle positions 1 and 4 (Fig. 141) for groups of bridges having the same value of the relative stiffness H. The tables include means for noncomposite steel bridges with $H = 0.5$ (Bridges 1A and 3A), noncomposite steel bridges with $H = 0.8$ (Bridges 9A and 9B), reinforced concrete bridges with $H = 1.0$ (Bridges 7A, 7B, 8A and 8B), composite steel bridges with $H = 1.7$ (Bridges 2B and 3B), and prestressed concrete bridges with $H = 4.5$ (Bridges 5B and 6B).

With the exception of the noncomposite bridges with low H, all ratios for the center beam were close to unity. Furthermore, for the concentric truck position 1, the ratios for the exterior and interior beams were also close to unity. The center beam was insensitive to the position of load (Fig. 143); and for the concentric truck position, the bridges behaved essentially as beams. Thus, the good agreement between the theory and the test data for these cases merely indicated that correct bridge properties were entered in the analysis.

For the eccentric truck position 4, the ratios for the interior (loaded) beams were close to unity for steel bridges, but consistently less than unity for the concrete bridges. For the exterior beam, subjected to very small deformations, there was a considerable scatter in the ratios, and those for reinforced concrete bridges were consistently greater than unity.

Thus, the data indicate that the analysis predicted reasonably well the transverse distribution of both moments and deflections for steel bridges, but indicated less than the actual

* The computer programs for influence ordinates and for interpolation were prepared by S. J. Fenves.

TABLE 70
RESULTS OF STUDY OF TRANSVERSE DISTRIBUTION OF MOMENTS AT MIDSPAN

Type of Bridge	H [1]	Mean Ratio of Measured to Computed Stress			Ratio, Σ Measured to Σ Computed
		Interior Beam	Center Beam	Exterior Beam	
(a) TRUCK POSITION 1, REAR AXLE AT MIDSPAN					
Noncomposite steel	0.5	0.91	0.91	1.01	0.94
Noncomposite steel	0.8	1.01	0.94	0.99	0.97
Reinforced concrete	1.0	1.06	1.02	1.04	1.03
Composite steel	1.7	0.97	0.93	1.02	0.98
Prestressed concrete	4.5	1.02	1.02	1.07	1.03
(b) TRUCK POSITION 4, REAR AXLE AT MIDSPAN					
Noncomposite steel	0.5	0.86	0.83	0.85	0.85
Noncomposite steel	0.8	1.01	0.97	0.85	0.97
Reinforced concrete	1.0	0.81	1.01	1.60	0.98
Composite steel	1.7	0.91	0.94	1.10	0.94
Prestressed concrete	4.5	0.94	1.04	—[2]	1.05

[1] $H = \frac{(EI)_{beam}}{L(EI)_{slab}}$ = relative stiffness of beam to slab.

[2] Mean ratio unrealistic, resulting from a small positive value for measured moment and a small negative value for computed moment.

TABLE 71
RESULTS OF STUDY OF TRANSVERSE DISTRIBUTION OF DEFLECTION AT MIDSPAN

Type of Bridge	H [1]	Mean Ratio of Measured to Computed Deflection		
		Interior Beam	Center Beam	Exterior Beam
(a) TRUCK POSITION 1, REAR AXLE AT MIDSPAN				
Noncomposite steel	0.5	0.97	0.97	0.95
Noncomposite steel	0.8	1.06	0.96	1.05
Reinforced concrete	1.0	1.06	1.02	0.99
Composite steel	1.7	1.05	0.88	1.00
Prestressed concrete	4.5	0.97	0.98	1.01
(b) TRUCK POSITION 4, REAR AXLE AT MIDSPAN				
Noncomposite steel	0.5	0.93	0.88	0.64
Noncomposite steel	0.8	1.09	0.92	0.72
Reinforced concrete	1.0	0.78	0.99	1.54
Composite steel	1.7	1.01	0.96	1.23
Prestressed concrete	4.5	0.80	1.03	—[2]

[1] $H = \frac{(EI)_{beam}}{L(EI)_{slab}}$ = relative stiffness of beam to slab.

[2] Mean ratio unrealistic, resulting from small values for both measured and computed deflections.

distribution for the reinforced concrete bridges. The prestressed concrete bridges appeared to fall between these two extremes. It is believed that these differences were caused primarily by the neglect of torsional stiffness of the beams in the analysis.

The last column in Table 70 contains ratios of the total measured stress to the total computed stress, indicating the degree of agreement between the computed and observed proportions of the total external moment resisted by the beams. The agreement is excellent even for the eccentric location of the truck. The proportion of the total external moment resisted by the beams was found to be essentially the same as that reported for the reference test data (Section 3.2.4).

5.2 LOAD-DEFORMATION STUDY

A special study of the behavior of pavements on Loop 6 required the use of trucks from all loops. The vehicles were operated over Bridges 7A, 7B, 9A and 9B thus affording an opportunity to determine experimentally the moment-strain relationships for the beams of the two pairs of replicate bridges.

5.2.1 Conduct of Tests

The tests were made in three series: two on Bridges 7A and 7B and one on Bridges 9A and 9B. In each series at least one of each of the following types of vehicles was used: single-axle vehicles 22, 31, 41, 51, 61 and tandem-axle vehicles 32, 42, 52, and 62. Two

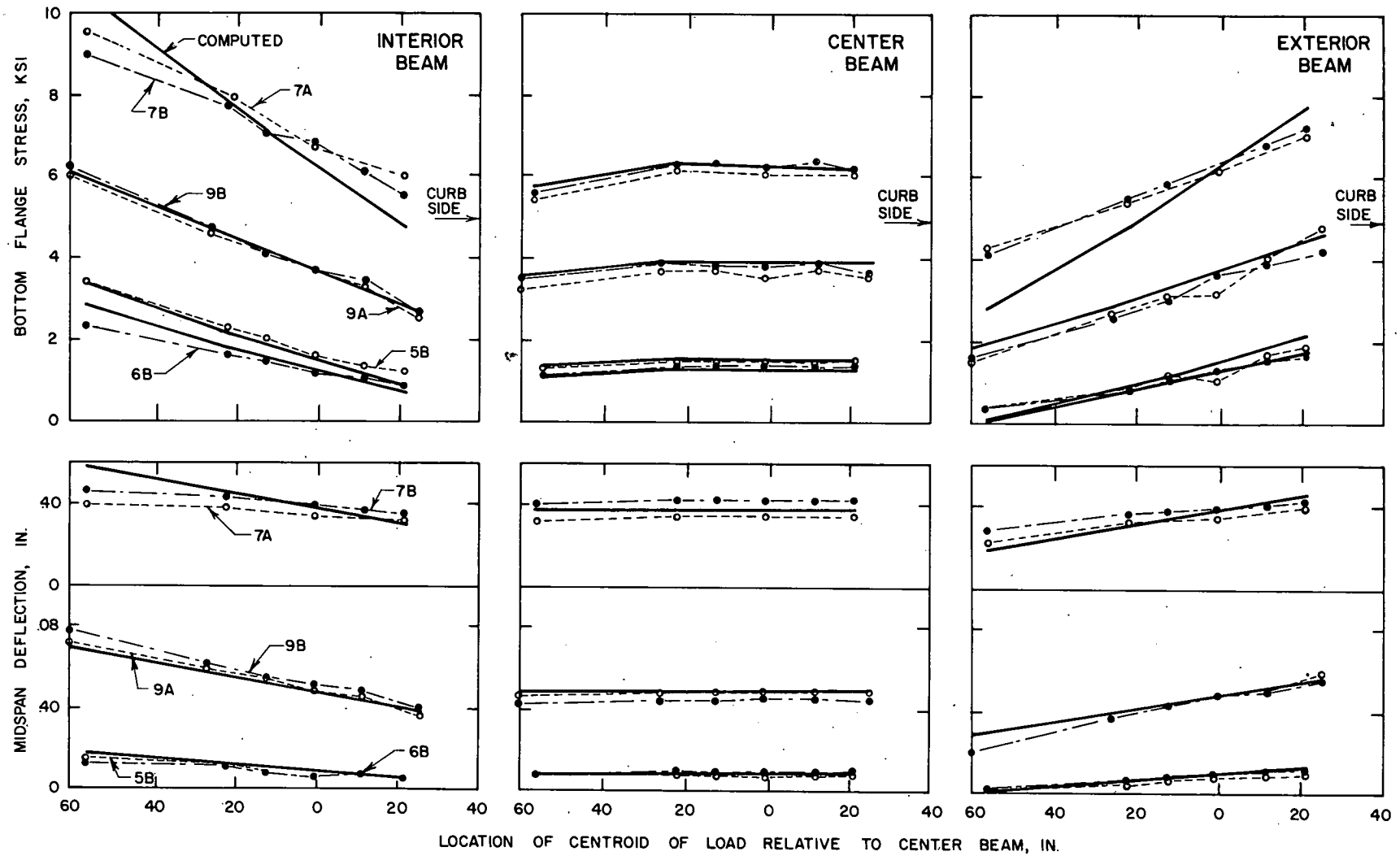

Figure 143. Comparison of theoretical and measured transverse distributions.

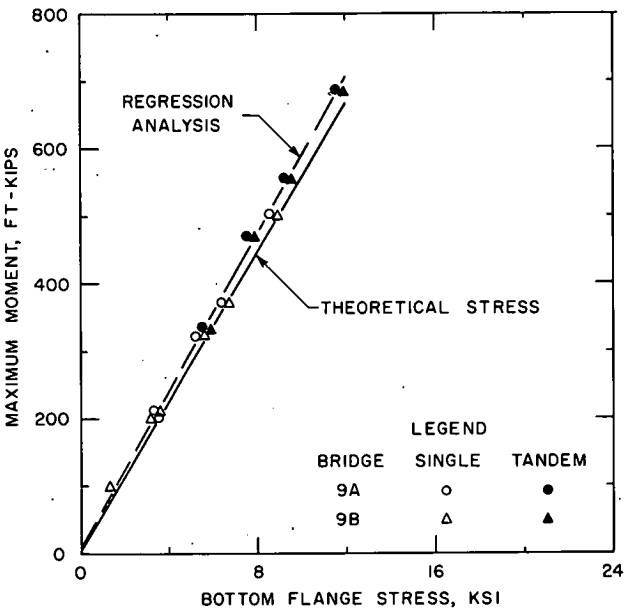

Figure 144. Moment-stress relationship for Bridges 9A and 9B at midspan.

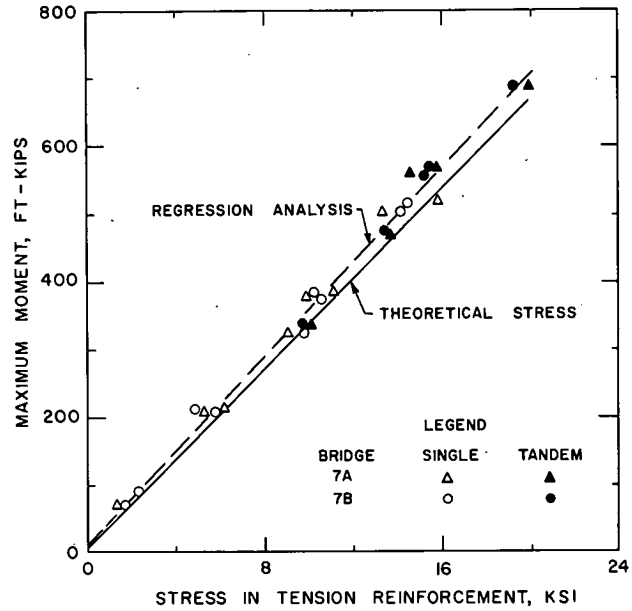

Figure 145. Moment-stress relationship for Bridges 7A and 7B at midspan.

vehicles of types 31, 32 and 52 were used at times to provide replication.

The mean dimensions and nominal axle weights of the vehicles are given in Table 19. The axle weights, determined during the conduct of the test, were close to the specified values.

The vehicles traveled over the bridges at creep speed in the direction of regular test traffic. They were centered on the bridge lane.

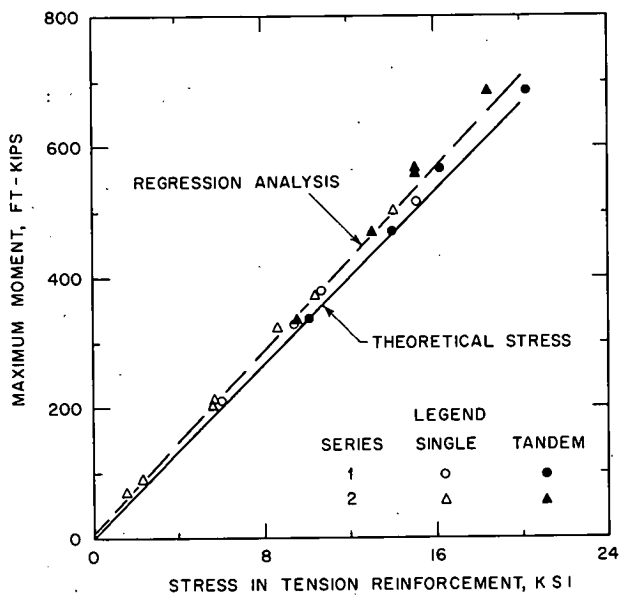

Figure 146. Day-to-day variation in moment-stress relationship at midspan for Bridges 7A and 7B.

Every vehicle made three runs within each series. The order of runs was randomized within groups, each group containing all vehicles.

The measurements included deflections and bottom steel strains at midspan on all three beams for all runs. In the test of Bridges 9A and 9B and one series of tests of Bridges 7A and 7B, bottom steel strains were measured also at the third points of all beams; and in the test of Bridges 9A and 9B strains were measured also at the critical sections near the ends of the cover plates.

5.2.2 Results of Study

Typical results obtained in the load deformation tests are shown in Figures 144, 145 and 146 in which the maximum moment caused by the vehicle at midspan is plotted as a function of stress obtained from strains measured at midspan. The test data, shown as circles and triangles, are averages for all trips made with the same vehicle and for measurements on all three beams.

Comparisons between the two replicate bridges of each pair are shown in Figures 144 and 145. The test data for Bridges 9A and 9B are shown in Figure 144; they contain only one set of measurements. Small but consistent differences were found between the two replicate bridges and also between the two types of vehicles.

A similar finding was observed in the first series of tests on Bridges 7A and 7B. However, in the second series the differences were opposite to those observed in the first series. The averages of both series of tests, shown

in Figure 145 by bridge and type of vehicle, reveal no consistent differences from bridge to bridge nor from vehicle type to vehicle type.

The data for Bridges 7A and 7B are shown (Fig. 146) by series rather than by bridges. Each symbol represents the average for the two replicate bridges. It will be noted, by comparison with Figure 145, that the variation between series was at least equal to the variation between replicate bridges.

In addition to the test data, Figures 144-146 include regression equations (obtained by the method of least squares assuming linear correlation) shown as dashed lines and theoretical moment stress relationships shown as full lines. The regression lines were computed from all data included in any particular figure. In each case the regression line almost passes through the origin of the coordinate system; furthermore, each regression line is located to the left of line of the theoretical stress.

The lines of theoretical stress were computed from the total external moment and the moment of inertia of the whole bridge cross-section considering the bridge as a beam. The measured stresses, represented by the regression lines, were 5 to 6 percent lower than those computed by the ordinary theory of flexure. The portion of the external moment corresponding to this difference was resisted by the slab, *i.e.*, the slab effected a longitudinal distribution of load not accounted for in the computations. This contribution of the slab was observed also in the reference tests (Section 3.2.4) and in the study of the transverse distribution of moments and deflections (Section 5.1.3).

5.3 STRESSES AT END OF COVER PLATE

For the steel beams with partial length cover plates, the critical section was located at the end of the plates. Strain gages were cemented to the bottom flange outside the cover plate cutoff for measurement of actual strains caused by test traffic. The gages were placed 6 in. away from the cutoff. A special study was carried out to determine the stress variation in this region. Measurements made on both sides of the cover plate cutoff were included.

5.3.1 Scope of Study

The length of cover plates varied from 14 to 20.5 ft. Thus, gage lines 3 and 7 (Fig. 14) were at several different distances from the cutoff since they were placed at a fixed distance of 100 in. from midspan. Gage lines 1 and 9 were located 6 in. off the cover plate, and gage lines 2 and 8 (with gages only on the center beams) were 6 in. on the plate. Thus, measurements with the regular gages on the center beam provided data at 6 and 16 in. off the cover plate and at 2 to 23 in. on the plate.

Additional gages were placed 1 in. away from the cover plate cutoff to provide strain measurements at points located close to the welds. Special tests were carried out specifically for the purpose of determining the stress gradient close to the cover plates.

Although the special experiment was limited to Bridge 2B, the study also included measurements made on all other bridges with partial length cover plates, except Bridge 4B, which was not included because all available data were obtained prior to the test traffic, and these were too limited and erratic to be considered reliable. The data for Bridges 1A, 2B, 3B, 4A, 9A and 9B, in addition to those obtained in the special test, were obtained in the reference tests.

All data included in this study were strains measured while a regular test vehicle was standing on the bridge in the position for maximum moment at the cover plate cutoff on the exit end. The vehicle was facing in the direction of regular test traffic. All data pertain to the center beam.

5.3.2 Results of Study

All strains measured on the same strain gage line of one beam were averaged, and the average was divided by theoretical strain. The theoretical strain was computed from

$$\varepsilon = \frac{M_b c}{E_s I_b} \qquad (35)$$

in which

M_b = external beam moment at the section considered;
c = distance from the neutral axis to the location of the gage;
E_s = modulus of elasticity of steel; and
I_b = moment of inertia of the beam at the section considered.

The external beam moment was computed as the product of the truck moment and the appropriate distribution factor given in Table 34.

The results of the study show (Fig. 147) that strains measured 6 in. off the cover plate were in excellent agreement with the values computed from Eq. 35. Apparently, the strains at this location were unaffected by the stress concentrations present at the ends of the cover plates. On the other hand, strains measured on the cover plates showed that the cover plate was fully developed only beyond about 1 ft away from the cutoff point.

5.4 DISTRIBUTION OF TENSILE CRACK WIDTH

The sampling procedure for determination of the width of cracks in reinforced concrete beams (Section 2.4.1) was based on the maxi-

mum width of three cracks selected at random within the sampling region. Two special series of measurements were made in April and July 1960 to provide data on the distribution of this sample crack width and on the relationships between the sample crack width, the crack width at the level of the tension reinforcement and the maximum crack width.

5.4.1 Scope of Study

The study included all four reinforced concrete bridges but only four sampling regions per beam—those located at midspan on the bottom face and in the lower half of the two side faces (Fig. 86). Ten cracks were selected at random in each region. For each selected crack, the point of maximum crack width was selected visually, and the crack width was measured at this point. This reading corresponded to the "sample crack width" of the regular studies. Then the width of the crack was measured near the edges of the sampling region and in the middle of the sampling regions. The average of these three readings for any particular crack was designated as the "average crack width."

In addition to the sample crack width and the average crack width, in the two regions located on the side surfaces of the beam, the width of each randomly selected crack was measured at the level of the center of gravity of the tension reinforcement. Furthermore, in the second series, the point of the maximum crack width within the whole region was selected visually and the crack width was measured at this point. This measurement corresponded to the "maximum crack width" of the regular crack studies.

All measurements were made on unloaded bridges following the procedures used in the regular crack studies with the previously described exceptions.

5.4.2 Results of Special Crack Studies

The results of the two series or special crack studies are shown in the form of distribution and cumulative distribution curves for the sample crack width, the average crack width and the crack width at the level of the tension reinforcement (Figs. 148-150). The distribution of the maximum crack width is shown in the form of histograms (Fig. 151). Miscellaneous characteristics and comparisons of crack widths are given in Table 72.

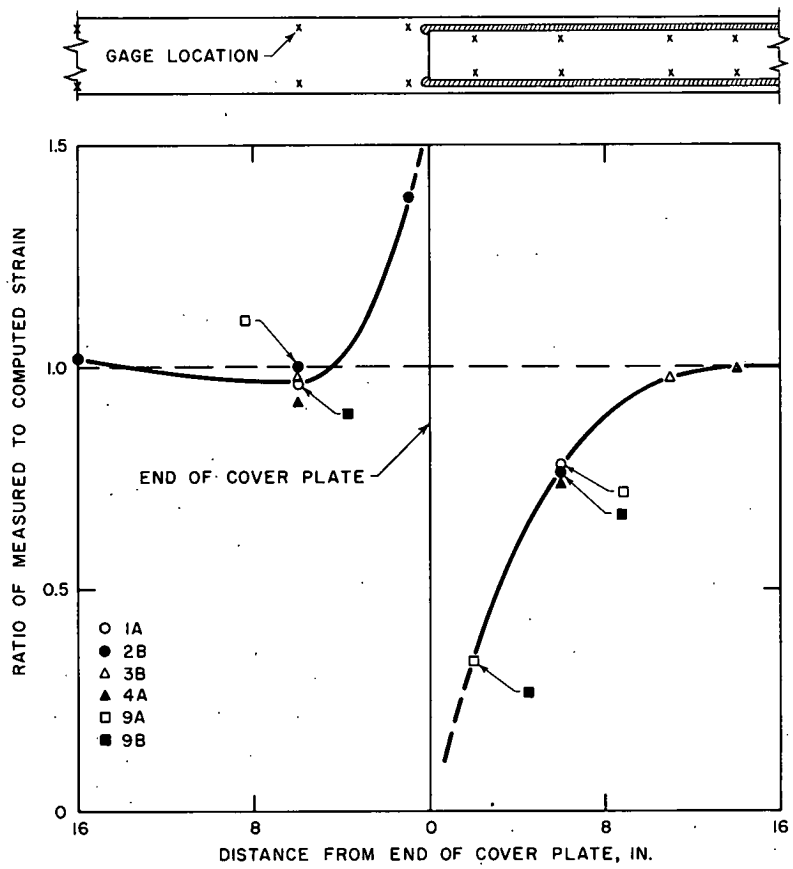

Figure 147. Stress distribution at cover plate cutoff.

The data are shown by series and separately for the pairs of Bridges 7A, 7B and 8A, 8B. All distribution curves were found to be normal. The means (Table 72) for Bridges 8A and 8B were consistently lower than for Bridges 7A and 7B, but the standard deviations were homogeneous for all bridges and types of measurements. The differences between the means of the two pairs of bridges were significant at the 1 percent level.

The sample crack width was found to be consistently larger than both the average crack width and the crack width at the level of steel. The ratios of the means were found to be different for Bridges 7A and 7B than for Bridges 8A and 8B, but essentially the same for both series of measurements. The width of the cracks at the level of steel was approximately 0.9 times the sample crack width for Bridges 7A and 7B and approximately 0.85 times the sample crack width for Bridges 8A and 8B. The sample crack width was approximately 1.06 times the average crack width for Bridges 7A and 7B, and approximately 1.10 times the average crack width for Bridges 8A and 8B.

A comparison between the means in Table 72 and the data in Figure 151 indicates that the maximum crack width was almost twice as large as the mean of the sample crack widths. For both sets of bridges the maximum crack width was 0.012 in. However, this width occurred more frequently in Bridges 7A and 7B than in Bridges 8A and 8B.

5.5 TEMPERATURE STRAINS

Strain readings on unloaded bridges for determination of cumulative effects of time and traffic were taken only when the differential temperature in the bridge was less than 5 F. A special study was conducted from May through September 1960 to check whether this procedure was appropriate and to study the effect of temperature differentials on strains in the bridge beams.

5.5.1 Details of Experiment

The study involved measurements of strains and temperature. The strains were measured with the Whittemore strain gage at midspan on the bottom of all three beams. The temperature of the air under the bridge and the temperature of the bridge were recorded. The record of bridge temperature included all thermocouples except those located in the slab between the beams (Fig. 22) ; for bridges with no thermocouples, the bridge temperature was assumed to be the same as in the adjacent bridge with thermocouples.

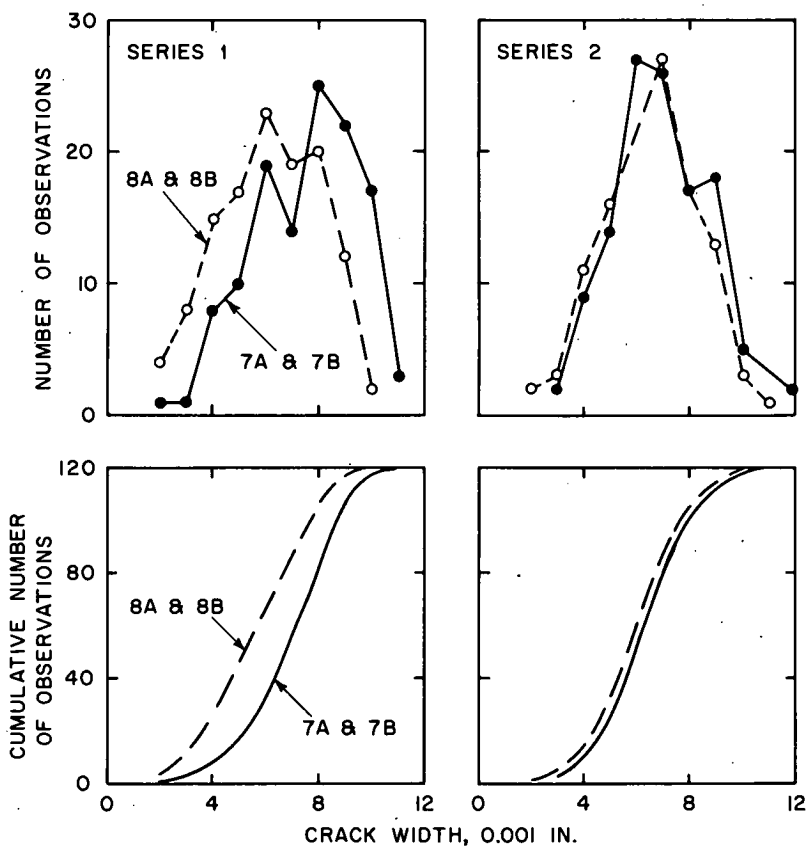

Figure 148. Distribution of sample crack width.

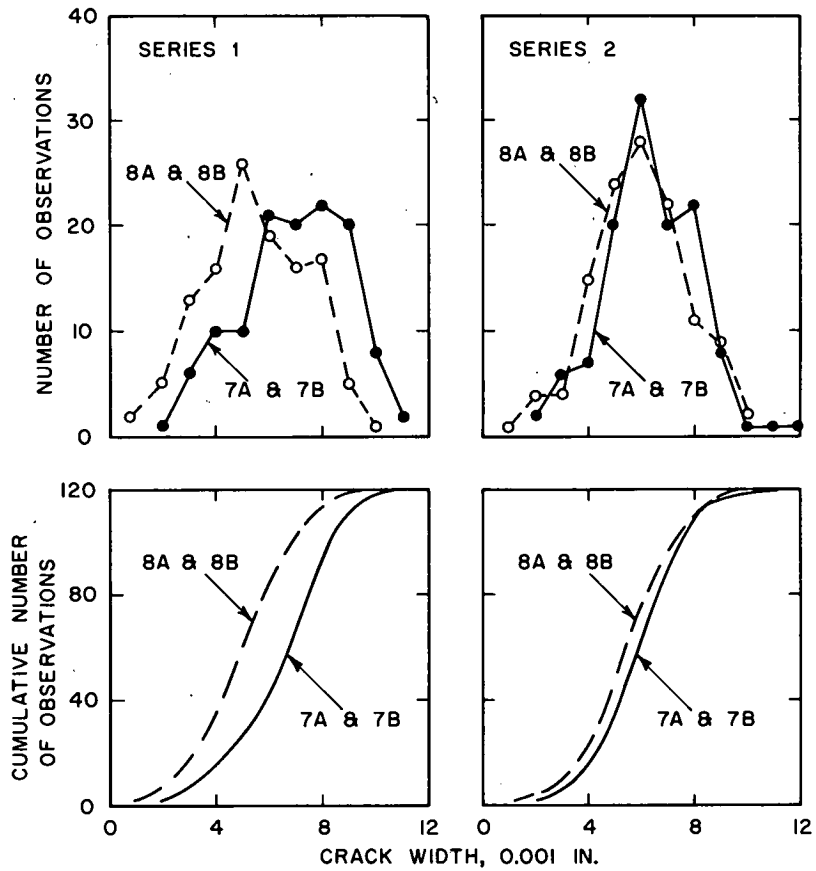

Figure 149. Distribution of average crack width.

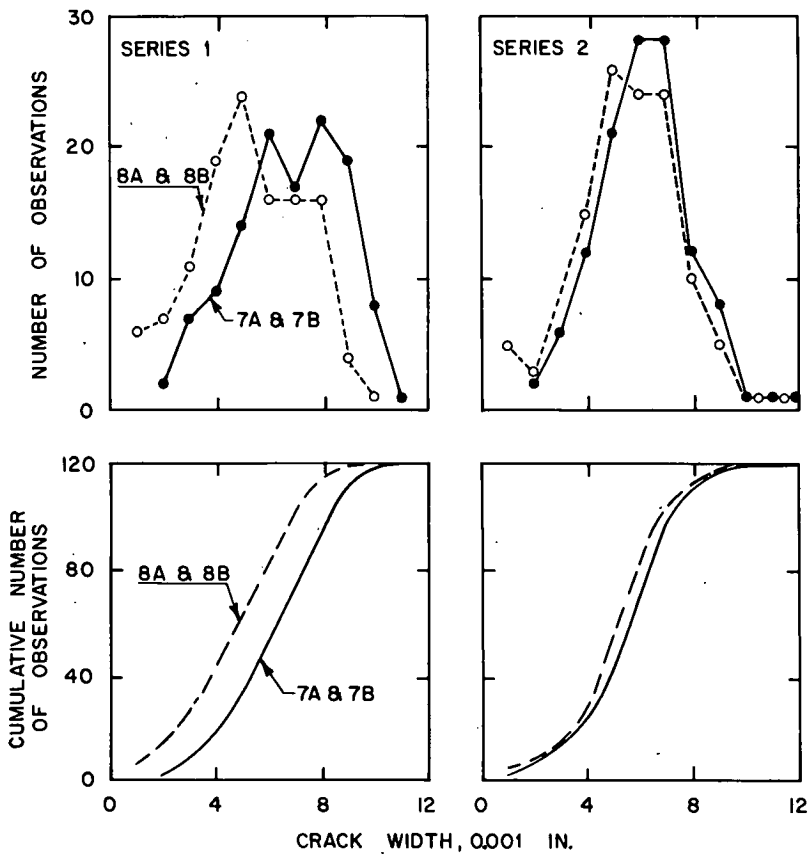

Figure 150. Distribution of crack width at the level of tension reinforcement.

The study was divided into 24-hr periods. During each period, the temperatures were recorded every half hour; strain readings were taken every four hours; and a record was kept of the weather conditions.

Observations were made on all bridges except 1B, 2A, 4A and 4B. They were made during three 24-hr periods on steel Bridges 3B and 9B, prestressed concrete bridges 5A and 6B and reinforced concrete bridges 7A and 8A. All of these bridges were equipped with thermocouples. On other bridges, one or two sets of readings were obtained. The data were collected in various types of weather, including sunny, partly cloudy, cloudy and rainy days.

5.5.2 Results of Observations

For Bridges 3B, 6A and 7A, Figures 152, 153 and 154 show data for two 24-hr periods—for a sunny or a partly-cloudy day on the right, and for a cloudy or a rainy day on the left. Six curves are included for each period: the air temperature, the slab temperature measured near the top, the slab temperature measured near the bottom, the beam temperature measured near the top, the beam temperature measured near the bottom, and strain measured at midspan. All six curves are plotted as functions of time.

Each of the curves of bridge temperature represents the average of all thermocouples for the given location. For example, there were nine thermocouples located near the top of the slab, three at midspan and three at each end of the bridge. Thus, every point for the temperature on the top of the slab represents the average of nine readings. The individual temperature readings did not vary from the given averages by more than ±2 F.

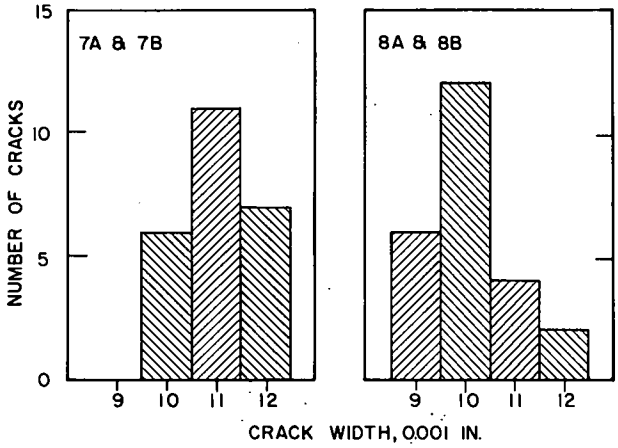

Figure 151. Distribution of maximum crack width.

The strains are the averages of all strain readings at midspan. One or two gage lines per beam were involved (Fig. 18) so that the averages pertain to three or six gage lines.

On cloudy or rainy days the temperature differential for the 24-hr period did not exceed 10 F; whereas, on sunny or partly-cloudy days,

TABLE 72

RESULTS OF SPECIAL CRACK STUDY

Bridge	Average Crack Width (in.)		Crack Width at Level of Steel (in.)		Sample Crack Width (in.)		Ratio	
							(1)	(3)
	Mean	Std. Dev.	Mean	Std. Dev.	Mean	Std. Dev.	(5)	(5)
	(1)	(2)	(3)	(4)	(5)	(6)		
				(a) PERIOD 1				
7A	0.0070	—	0.0069	—	0.0076	—	0.92	0.91
7B	0.0069	—	0.0067	—	0.0073	—	0.94	0.92
7A,7B	*0.0070*	*0.0021*	*0.0068*	*0.0020*	*0.0075*	*0.0021*	*0.93*	*0.91*
8A	0.0055	—	0.0053	—	0.0062	—	0.89	0.85
8B	0.0055	—	0.0053	—	0.0060	—	0.92	0.88
8A,8B	*0.0055*	*0.0021*	*0.0053*	*0.0021*	*0.0061*	*0.0021*	*0.90*	*0.87*
				(b) PERIOD 2				
7A	0.0063	—	0.0062	—	0.0068	—	0.93	0.91
7B	0.0064	—	0.0062	—	0.0070	—	0.93	0.89
7A,7B	*0.0064*	*0.0021*	*0.0062*	*0.0018*	*0.0069*	*0.0021*	*0.93*	*0.90*
8A	0.0060	—	0.0057	—	0.0065	—	0.93	0.88
8B	0.0059	—	0.0055	—	0.0066	—	0.89	0.83
8A,8B	*0.0059*	*0.0021*	*0.0056*	*0.0017*	*0.0065*	*0.0021*	*0.91*	*0.86*

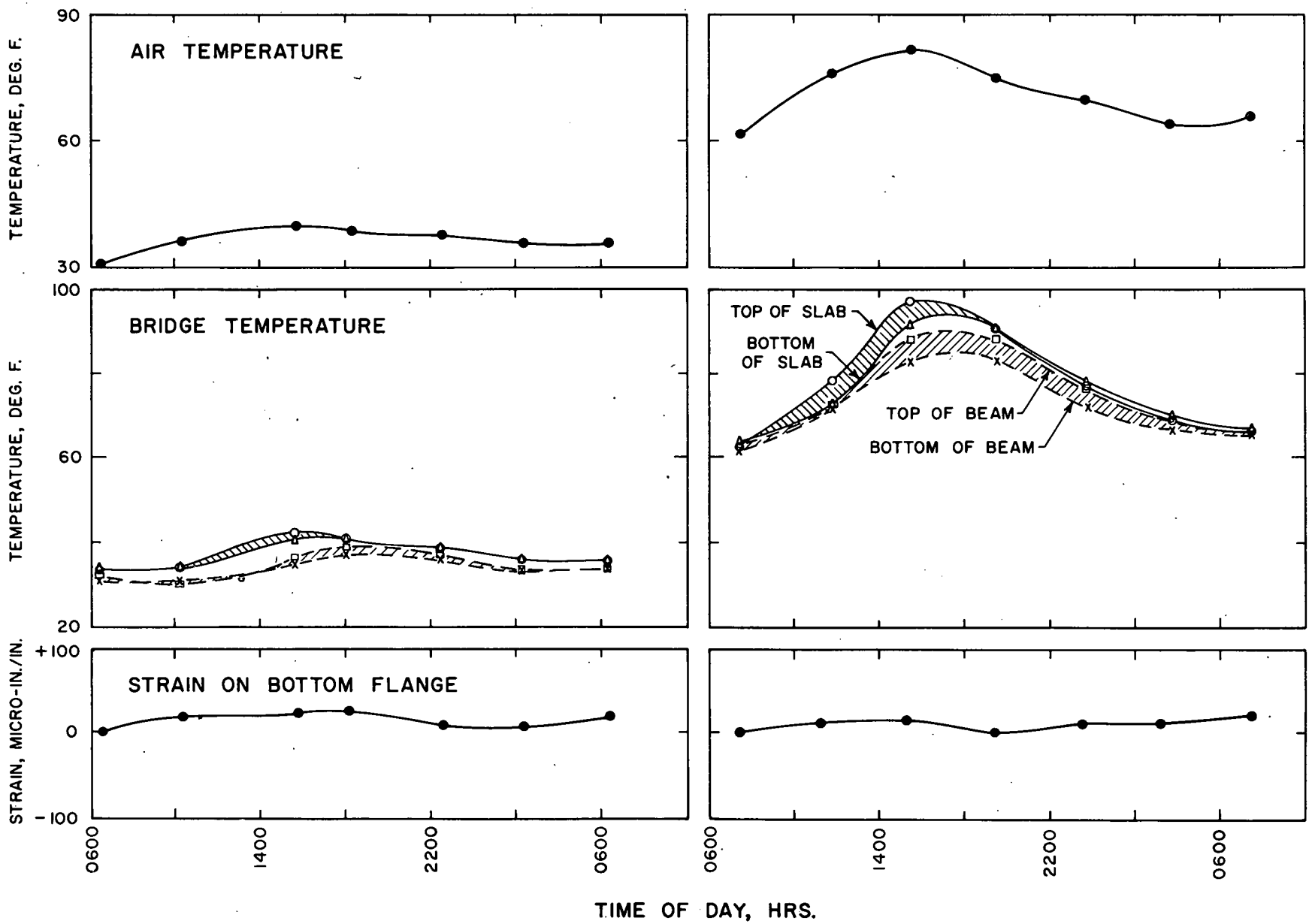

Figure 152. Daily temperature and strain variations in Bridge 3B.

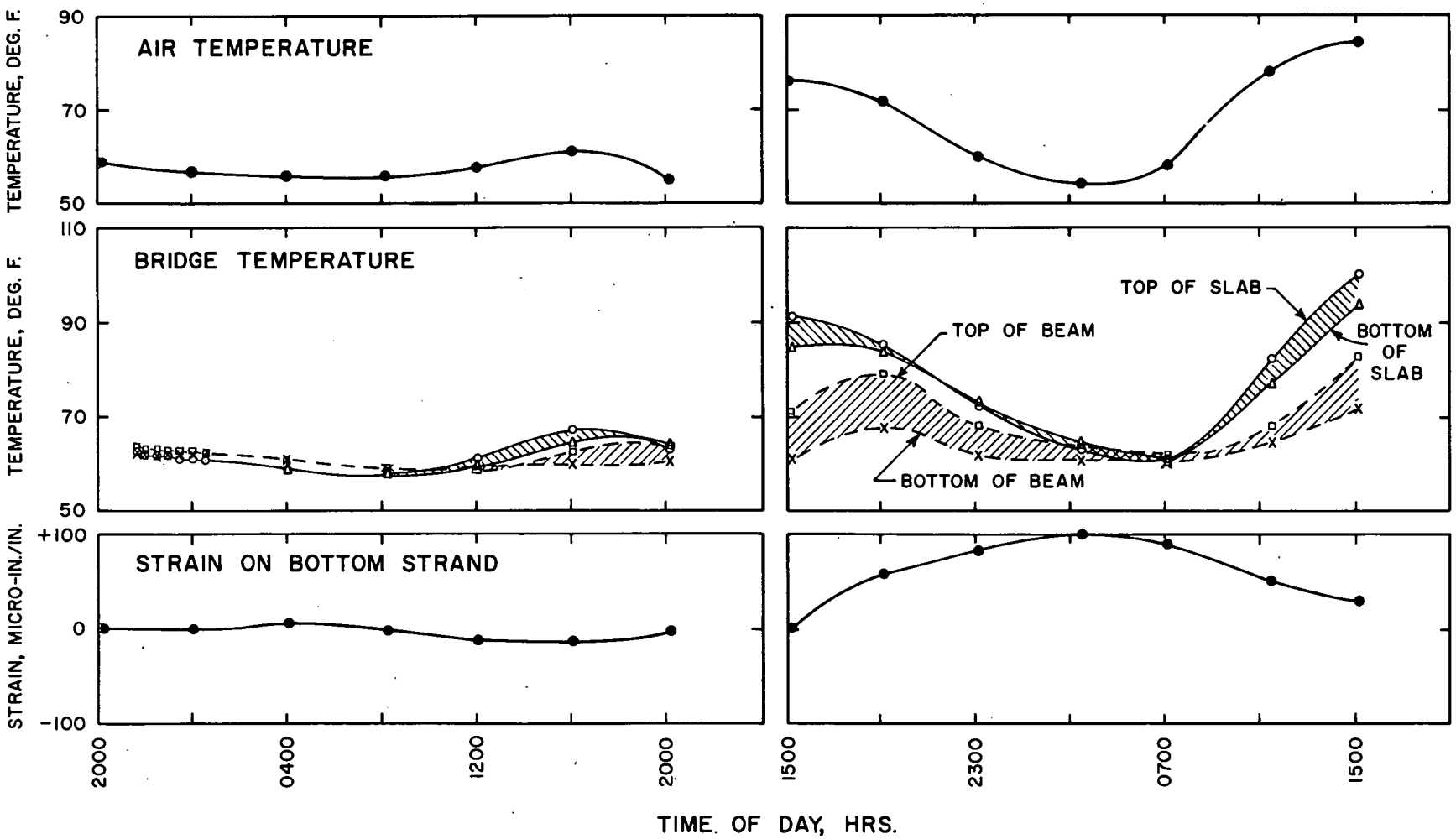

Figure 153. Daily temperature and strain variations in Bridge 6A.

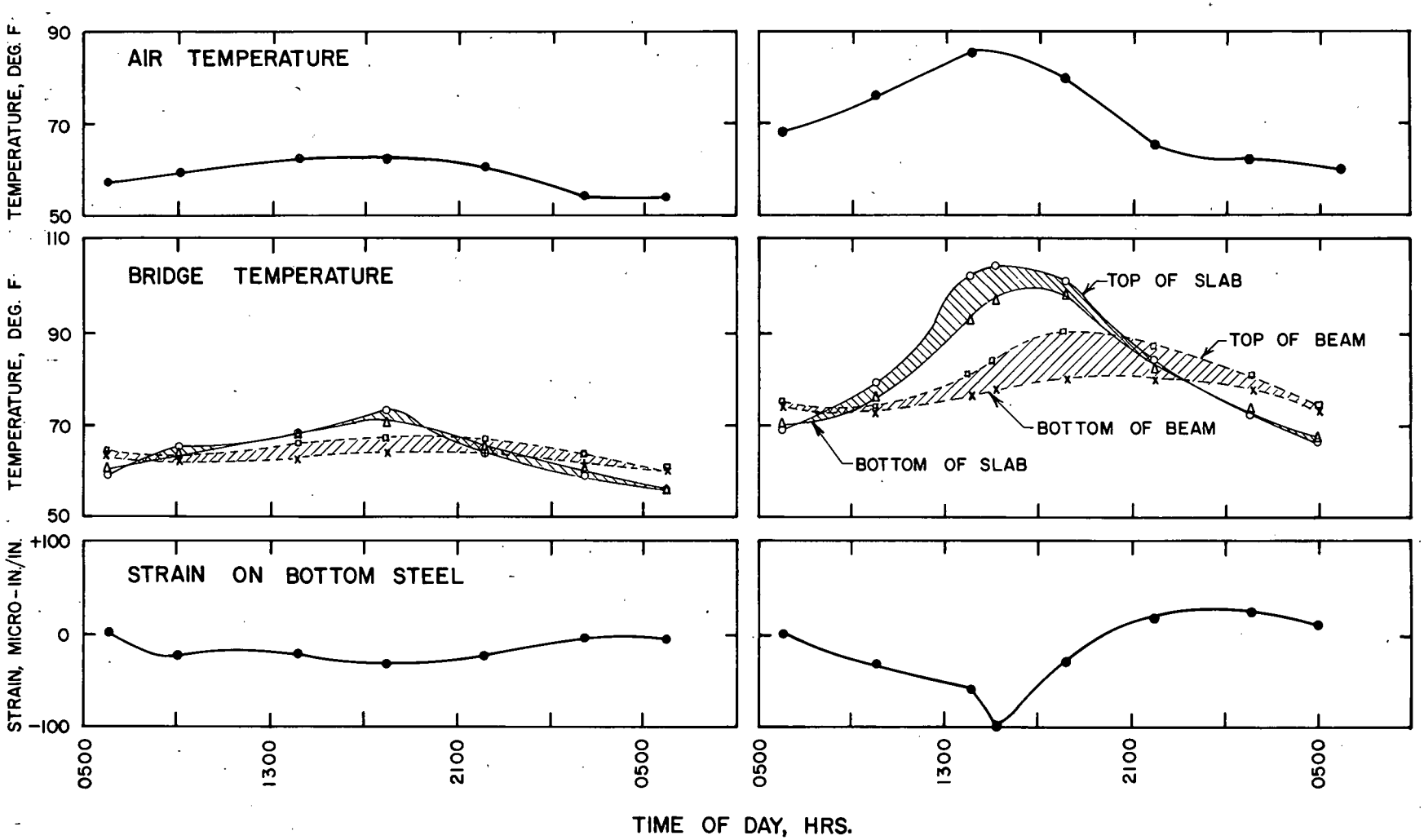

Figure 154. Daily temperature and strain variations in Bridge 7A.

the air temperature changed by at least 20 F. For all bridges the effects of the change of the air temperature were more pronounced in the slab than in the beams. The change in the air temperature caused a temperature gradient through the depth of the bridge. The temperature gradient was particularly pronounced on sunny days. During most of the day, the temperature of the slab was higher than that of the beam. At night, however, either the slab and the beam attained equal temperature or the slab became cooler than the beams. During the night, the temperature differentials were always less than 10 F.

The strain readings were corrected with the aid of readings of a standard bar placed at or near the bottom flange of the beam. The strain measurements in the steel bridges showed no consistent fluctuation with either the air temperature or the temperature differential in the bridge. The differences in strain were of the order of 0.000025 which was well within the range of accuracy of the strain gage. It appears that the compensation for temperature changes with the aid of the standard gage successfully eliminated all temperature effects on strains on steel beams.

In the prestressed and reinforced concrete bridges strains increased as the temperature differential of the bridge decreased. The magnitude of the strain differential during rainy and cloudy days was relatively small, of the order of 0.000025. On sunny days substantial strain differentials, of the order of 0.000100, were recorded. It is apparent that the compensation for temperature strains was not entirely satisfactory for the concrete bridges. Thus the accuracy of strain measurements on unloaded concrete bridges must be considered particularly low.

5.6 CABLE FRICTION LOSSES

The cables in the post-tensioned beams for Bridges 5A and 5B were curved so that it was necessary to determine the friction losses during tensioning of the cables. The data for the 30 cables provided an opportunity to check the equation for friction losses given in the AASHO Specifications.*

5.6.1 Measurement of Friction Losses

The cables of the post-tensioned beams were prestressed with two double-acting Freyssinet jacks, one placed at each end of the beam. The load was measured by a calibrated pressure gage and the elongation with a scale.

The friction between the conduits and the wires was determined for each tendon by a trial procedure with the aid of the following:

$$F_t = 2\left(F_1 - \frac{ae_1E}{d}\right) \qquad (36)$$

in which

F_t = loss in prestressing force caused by friction;

F_1 = observed tensile force at the jack;

a = cross-section area of the prestressing element;

e_1 = observed elongation of the element at the jack when the force in the jack is F_1;

E = secant modulus of elasticity of the element for the stress F_1/a as determined from the stress-strain diagram of the element (28.6 psi); and

d = distance from the jack to midspan of the beam.

An initial 500-psi force on the page was applied to each end of a tendon and reference marks were established for measuring the elongation in 50 ft 8 in. The force was increased to a total force F_1 computed on the basis of an assumed friction loss. The elongation was measured next, and the friction loss was computed from Eq. 36. The friction loss was taken as the basis for recomputation of the force F_1. The recomputed force was applied next, and the process was repeated until the assumed and computed friction losses were identical. The first estimate of loss was made purposely low in order to approach the final prestress with successively higher forces F_1.

The results of the friction loss measurements are given in Table 73 for all cables in order of decreasing α (the total angular change of prestressing cable from jacking end to midspan). The friction loss for cable d of the interior beam of Bridge 5B and the loss for cable c of the exterior beam of Bridge 5A were much lower than other losses. In stressing these two cables, the final prestressing force was accidentally approached from above rather than with successively higher forces F_1.

5.6.2 Equation for Friction Losses

From consideration of the forces exerted by the prestressing steel on the duct, the following equation may be written for friction losses:*

$$T_0 = T_x e^{(KL + \mu\alpha)} \qquad (37)$$

in which

T_0 = steel stress at jacking end;

T_x = steel stress at midspan;

e = base of natural logarithm;

K = friction wobble coefficient;

* AASHO, "Standard Specifications for Highway Bridges." 8th Edition, Washington, D.C. (1961).

* For a derivation of Eq. 37 see, for example, Lin, T. Y., "Design of Prestressed Concrete Structures." John Wiley and Sons, Inc., New York (1955).

L = length of prestressing steel element from jacking end to midspan;

μ = friction curvature coefficient; and

α = total angular change of prestressing steel element in radians from jack to midspan.

For small values of KL and $\mu\alpha$ the following approximate equation may be used:

$$e^{(KL+\mu\alpha)} \cong 1+KL+\mu\alpha \qquad (38)$$

As long as the quantity $(KL + \mu\alpha)$ does not exceed 0.15, the error caused by the use of the right side of Eq. 38 does not exceed 1.0 percent.

Substitution from Eq. 38 into Eq. 37 and rearrangement leads to the following:

$$\frac{T_0 - T_x}{T_x} = KL + \mu\alpha \qquad (39)$$

With the quantities T_0, T_x, L and α known, the coefficients K and μ may be evaluated with the aid of regression analysis in which an error term added to the right side of Eq. 39 is minimized.

The test data given in Table 73 are plotted in Figure 155. The individual test points are shown as dots; the point for cable *d* of the interior beam of Bridge 5B was omitted as an extreme value, both from Figure 155 and from the regression analysis. The means for each value of α are shown as circled dots. The regression analysis, made on these means, gave the following values of coefficients for Eq. 39: $K = 0.004$ and $\mu = 0.258$.

Tests showed the value of coefficient K to be significant at the 1 percent level, but the value of coefficient μ was not significant even at the 10 percent level. In other words, for the small range of α encountered in this study the test results could be described just as accurately by an arithmetic mean as by Eq. 39.

Eq. 39, with the coefficients given by the regression analysis, and the mean of the test data are plotted in Figure 155. Also included is a line corresponding to the values of coefficients $K = 0.002$ and $\mu = 0.30$ suggested by the AASHO Specifications for the conditions met in the tests. With the exception of one value, α, the mean measured friction losses were considerably higher than those suggested by the design specifications, indicating that the value of K given in the Specifications is too low.

5.7 SPECIAL POST-TRAFFIC TESTS

After the completion of regular test traffic and accelerated fatigue tests, an extensive group of special tests was carried out on pavements and bridges at the request of and in close cooperation with the Department of Defense. The tests were conducted and reported by the Special Assignments Branch of the AASHO Road Test. They are presented in detail in AASHO Road Test Report 6.

5.7.1 Objective and Scope

The tests on bridges were conducted to study the effects on bridge response of the following: (1) tire pressure-tire design, (2) commercial construction equipment, (3) special suspension systems, and (4) military vehicles. Concurrent tests with regular test vehicles furnished comparative data.

The study of tire pressure and tire design included 18 vehicles divided evenly between single-axle and tandem-axle loads. Wire and nylon cord tires were used. The inflation pres-

TABLE 73

MEASURED FRICTION LOSSES

Bridge	Designation of Cable [1]	Angular Change, α (radians)	Friction loss [2] (ksi)					
			Interior Beam		Center Beam		Exterior Beam	
			T_0	T_0–T_x	T_0	T_0–T_x	T_0	T_0–T_x
5A	a	0.103	175.4	16.4	176.5	18.4	178.8	23.2
5B	a	0.086	183.6	21.2	182.2	18.4	182.6	19.1
5B	b	0.068	177.1	8.2	183.6	15.7	183.6	13.0
5A	b	0.063	173.4	17.7	176.1	23.2	176.8	19.1
5B	c	0.050	185.3	19.1	190.1	22.5	194.9	26.6
5B	d	0.012	174.7	3.4	187.0	22.5	186.0	20.5
5A	c	0.007	172.7	16.4	172.7	16.4	165.5	8.9
5A	d	0.007	171.7	15.0	167.3	11.6	171.7	19.8
5B	e	0.007	181.9	18.4	176.5	13.0	177.1	14.3
5B	f	0.007	181.6	23.2	174.1	13.7	176.8	13.7

[1] Locations of individual cables may be found in AASHO Road Test Report 2, Section 7.3.2.
[2] T_0 is initial stress in cable at anchorage; T_0–T_x is friction loss between anchorage and midspan.

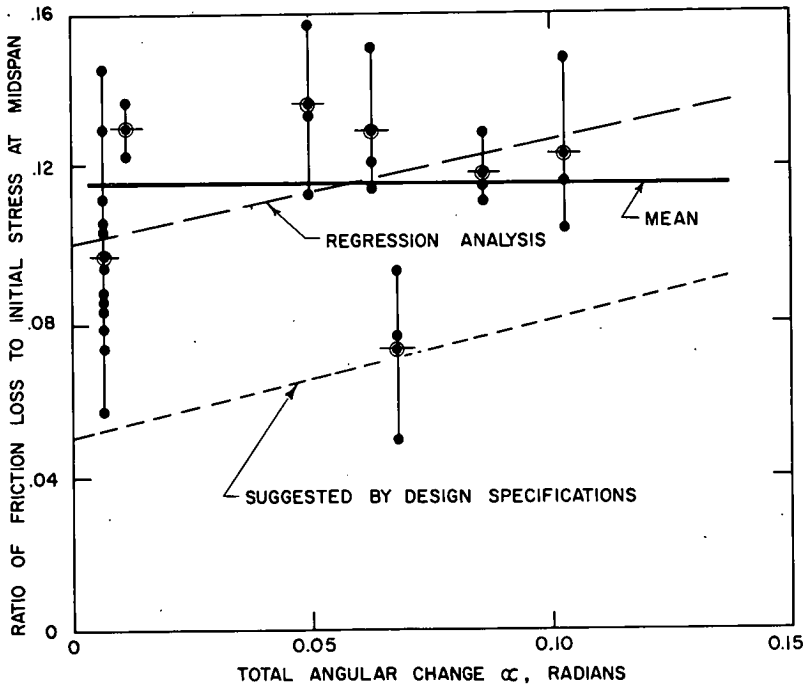

Figure 155. Correlation of data on friction losses.

sures varied between 60 and 130 psi (actual pressures at the time of test).

One medium and one small two-axle tractor-scraper unit, with struck capacity of 21 and 14 cu yds, were selected for the study with construction equipment. The tire pressure was 30 to 45 psi for both vehicles.

Five special systems were included in the study of the effects of suspensions: (1) a combination fluid and air suspension, (2) a staggered wheel suspension, (3) a variable single leaf spring suspension, (4) walking beam suspension with rubber load cushions, and (5) walking beam suspension with steel leaf springs. In addition, one regular test vehicle was equipped with low pressure low silhouette (LPLS) tires inflated to 35 psi. The tire pressure was kept at 75 to 80 psi except as noted.

The study with military equipment included tandem-axle tractor-semitrailers with LPLS and conventional tires, a heavy-duty tank transporter, two units of off-road train cargo trailers and one unit of rolling fluid transporter trailer.

The studies of tire pressure and with construction equipment were conducted on Bridges 3A, 8A, 8B, 9A and 9B; those of suspension systems and with military equipment were conducted on Bridges 3A, 8A and 8B. At least three tests were made with each vehicle at crawl speed, at 15 mph, and at 30 mph; for the construction and most of the military equipment the 30-mph runs were omitted.

In each test, deflections and bottom strains were measured at midspan of every beam. In a few tests with military vehicles transverse strains in the bottom layer of slab reinforcement were recorded at all three-quarter points of the span half-way between the exterior and center beam.

In addition to the outlined four studies, a pilot study of the effect of maximum braking effort was attempted on Bridge 6A. Bridge deformation records failed to indicate any effects of the forces caused by the sudden braking.

5.7.2 Summary of Findings

The results of all special post-traffic tests were studied in terms of amplification factors computed from the measured strains and deflections as the ratio of the quantity measured in the speed run to that measured in the corresponding crawl run. Most of the amplification factors were greater than 1.0 and less than 1.2.

The principal findings were as follows:

1. No consistent trend of the amplification factors with respect to changes in the tire pressure or the tire design was noted.
2. The over-all mean amplification factors for both scraper units were lower than those for the single-axle but greater than those for the tandem-axle regular test vehicles. However, this relationship did not hold for all individual bridges.

3. The amplification factors varied from one suspension system to another, but the variations were not consistent from bridge to bridge. At 30 mph the mean strain amplification factors were found to be appreciably higher for the vehicles with special suspensions than for the conventional tandem units. The mean amplification factors for the special vehicles for deflection at 15 and 30 mph and for strains at 15 mph were similar to those for the conventional tandem units.

4. The rolling fluid transporter caused consistently higher amplification factors than any of the conventional vehicles tested.

5. The amplification factors for slab strains were generally small.

6. The effects of vehicle speed and type (single-axle vs tandem-axle) were found in agreement with the results reported in Chapter 4; *i.e.*, an increase in speed was associated with larger amplification factors and the amplification factors for the single-axle vehicles were generally greater than those for the tandem-axle vehicles.

Chapter 6

Summary of Findings

6.1 OUTLINE OF STRUCTURES AND EXPERIMENTS

The bridge research at the AASHO Road Test was planned as a series of case studies expected to yield information on the behavior, under vehicular traffic causing overstress, of structures of the types included in this investigation. The study was concerned mainly with the flexural behavior of beams.

Detailed objectives of the study were formulated by the Advisory Panel on Bridges and approved by the National Advisory Committee. The first objective—to determine the behavior of certain short-span highway bridges under repeated applications of overstress—was concerned with the fatigue life of structures subjected to repeated high stresses and the manner in which distress is caused by repeated high stresses.

The second objective—to determine the dynamic effects of moving vehicles on these short-span highway bridges—was concerned with the behavior of individual test bridges under a range of loads. It involved the correlation of observed dynamic effects with those predicted by theoretical computations.

Eighteen test bridges were included in the study. Each bridge was a simple span structure consisting of three beams and a reinforced concrete slab. The beams were supported on 50-ft spans. The slabs were 15 ft wide and 6½ in. thick; they provided one 14-ft lane for the test traffic.

Beams in eight bridges were fabricated from wide-flange rolled-steel sections and were independent of the slabs. A treatment of the top surface of the top flanges inhibited formation of natural bond between the slab and the steel beams. In two bridges the wide-flange steel beams were connected to the slab with channel connectors. All steel beams were rolled of ASTM Designation A7 steel and, except for one bridge, were 18 in. deep. The exception was a noncomposite bridge which had beams 21 in. deep. Beams of five bridges had welded partial-length cover plates on the bottom flange only. Beams of two bridges had welded partial-length cover plates on both the top and bottom flanges. Beams of three bridges had no cover plates.

Four bridges were built with precast prestressed beams made of high-strength concrete. All beams had unsymmetrical I sections 25 in. deep. Beams for two bridges were post-tensioned with cables made of ten parallel wires. Beams for the other two bridges were pretensioned with 7-wire strands. Both the cables and the wires were of high carbon steel and were cold drawn and stress relieved. The beams were connected to the cast-in-place slabs through bond, shear keys, and extensions of stirrups.

Four reinforced concrete bridges were of cast-in-place T-beam construction. They were made of medium strength concrete and deformed reinforcing bars of intermediate grade. The stems of the beams were 20 in. deep.

The construction of the bridges started in the fall of 1956 and the testing began in August 1958. All tests were completed by the middle of June 1961.

Five types of tests were conducted. The principal tests were concerned with the behavior and life of the bridges under repeated high overstress, with the ultimate strength of the bridges, and with dynamic effects of moving vehicles.

The bridges were subjected to repeated trips of tractor-semitrailers loaded to specified axle weights. The weights of the drive and rear axle varied from bridge to bridge, covering a range from 22,400 lb to 48,000 lb. Both single- and tandem-axle vehicles were included.

The bridges were designed for the following maximum tensile stresses in the beams under the passage of the assigned test vehicles:

1. 27,000 psi and 35,000 psi for the steel beams;
2. 300 psi and 800 psi for the concrete of the prestressed concrete beams; and
3. 30,000 psi and 40,000 psi for the reinforcing bars of reinforced concrete beams.

The choice of the stress levels was dictated by the objective of the bridge research concerned with the effects of repeated overstress. In steel bridges the primary interest was in the fatigue strength of rolled beams with partial-length cover plates and the progression of yielding. In prestressed concrete bridges the attention was focused on the fatigue cracking of concrete subjected to tensile stresses and on the fatigue behavior of the prestressing steel in cracked beams. In reinforced concrete beams the studies were concerned with the fatigue behavior of deformed bars and the effect of repeated stressing on the width and spacing of tensile cracks.

To obtain the above stresses in the tests, the designs of beams were based on moments com-

puted by an elastic analysis rather than on moments obtained by conventional design methods. On the other hand, the slabs, web reinforcement and miscellaneous details were designed by conventional methods and for conventional allowable stresses.

Because of the differences in the design criteria for the various types of bridges, *direct comparisons between the steel, prestressed concrete and reinforced concrete test structures could not be made on the basis of their response to the repeated applications of overstress.*

The signs of fatigue distress at the conclusion of the regular test traffic were limited. Since the maximum number of stress repetitions caused by trips of test vehicles was only 558,400 (laboratory fatigue tests are usually made to 1 million or more cycles of stress), the number of stress repetitions was augmented in several bridges by oscillation at frequencies close to the natural frequencies of the bridges. The critical sections of the bridges were subjected to stress fluctuations similar to those observed during the regular test traffic. Bridges that survived these tests were subjected to a total of about 1,500,000 cycles of high overstress, including the passages of the test vehicles and the cycles of stress in the accelerated fatigue tests.

Bridges that survived the tests with repeated high overstress were utilized in a study of the flexural bridge capacity. A special test vehicle with increasingly heavier axle loads crossed the bridges 30 times at each load increment until the bridge was considered failed or until further loading of the test vehicle was considered undesirable.

The dynamic effects of moving vehicles on the response of test bridges were studied through special tests conducted at irregular intervals. Test vehicles, including two-axle trucks and three-axle tractor-semitrailer combinations, made approximately 1,900 trips over 15 test bridges at speeds varying between 20 and 50 mph. The tests were conducted under rigorously controlled conditions. The primary emphasis was placed on determining accurately the pertinent properties and the dynamic response of the briges and of the vehicles.

TABLE 74
SUMMARY OF INITIAL STRESSES IN STEEL BRIDGES

Bridge	Design Stress (ksi)		Actual Stress (ksi)		
	Center Beam	Exterior Beam	Interior Beam	Center Beam	Exterior Beam
(*a*) NONCOMPOSITE BRIDGES					
1A	27.0	—	25.3	27.7	30.1
1B	34.8	—	32.5	35.4	40.5
2A	35.0	—	35.0	39.4	41.1
3A	27.3	—	28.6	30.9	35.4
4A	34.7	—	35.9	38.9	41.1
4B	34.7	—	39.1	42.1	42.3
9A	—	27.0	22.9	24.7	25.5
9B	—	27.0	24.0	24.6	26.0
(*b*) COMPOSITE BRIDGES					
2B	35.0	—	30.2	33.8	35.8
3B	26.9	—	26.0	28.8	31.0

6.2 SUMMARY OF STUDIES WITH REPEATED STRESSES

6.2.1 Steel Bridges

Stresses.—The maximum stresses occurred at or near midspan in the steel beams without cover plates and just off the ends of the plates in the steel beams with cover plates. The tensile dead load stresses at these critical sections varied from a low of 8.3 ksi to a high of 25.6 ksi. In any one bridge, the exterior beam had the highest dead load stresses, and the interior beam had the lowest dead load stresses. During the period of casting the slab, but before the beginning of the tests, the dead load stresses remained essentially unchanged.

There was no interaction between the slab and the beams in the noncomposite bridges under dynamic loading. (The top surfaces of the steel beams were treated with graphite, a condition not encountered in bridges on the highway system.) On the other hand, the composite bridges had full interaction between the slab and the beams. The slabs resisted 8 to 22 percent of the truck moment, with the percentage increasing with decreasing stiffness of the beams. The portion of the truck moment resisted by the beams was distributed equally to the three beams.

The tensile live load stresses caused at the critical section by regular test vehicles moving at 30 mph and centered over the center beam of the bridge ranged from 12.1 to 26.8 ksi in the initial tests. These stresses were essentially the same in all three beams of the same bridge.

The sums of the initial dead load and live load stresses are compared with the design stresses in Table 74. The design stresses compared favorably with the actual stresses in those beams for which the design was made, except that in noncomposite bridges 2A, 3A, 4A and 4B the actual stresses exceeded the design values by more than 10 percent. However, the maximum total stress occurred in the exterior beam whereas the design was made for the center beam (except Bridges 9A and 9B). Thus the maximum total stress exceeded the design stress in every steel bridge except 9A and 9B.

The excess of actual stresses over the design stresses was caused primarily by two factors: (1) the dead load, including the timber curb,

TABLE 75
SUMMARY OF TESTS WITH REPEATED STRESSES ON STEEL BRIDGES

Bridge	No. of Vehicle Passages		Mean Transient Stress (ksi)			Mean Trans. Defl. (in.)		Tests to Failure		Mode of Failure
	To First Cracking	Total	Interior Beam	Center Beam	Exterior Beam	Beg. of Test	End of Test	Max. Applied Moment (ft - kips)	Total Perm. Set (in.)	
(a) NONCOMPOSITE BRIDGES										
1A	536,000	557,400	13.7	14.0	13.2	1.64	1.83	1,000	15.4	Yielding
1B	—	235	—	—	—	—	—	—	—	Yielding
2A	—	26	—	—	—	—	—	—	—	Yielding
3A	—	392,400	16.9	16.7	18.2	1.94	2.06	—	—	Accident
4A	—	106	—	—	—	—	—	—	—	Yielding
4B	—	106	—	—	—	—	—	—	—	Yielding
9A	477,900	477,900	15.5	14.8	13.5	1.82	1.99	1,535	13.2	Yielding
9B	477,900	477,900	15.1	14.8	14.0	1.88	2.01	1,580	12.3	Yielding
(b) COMPOSITE BRIDGES										
2B	531,500	558,400	15.4	14.6	14.2	0.90	1.02	—	—	Fatigue fracture
3B	535,500	557,800	12.8	13.0	12.3	0.79	0.84	2,520	14.1	Yielding

had been assumed in the design to be evenly distributed to the three beams, but in reality the exterior beam supported substantially more than one-third of the total; and (2) in the noncomposite bridges a 10 percent interaction between the slab and the beams had been assumed in the design although, in reality, no interaction existed.

Effects of Repeated Stresses.—During the early tests with vehicles, beams of steel bridges yielded and deformed permanently to a varying degree. The most extensive yielding occurred in noncomposite bridges 2A, 4A and 4B in which the $(DL + LL)$ strains were in excess of the yield point strain of the material in all three beams. The least yielding and the smallest permanent set occurred in noncomposite bridges 9A, 9B and in composite bridge 3B. Bridges 9A and 9B were subjected to the lowest total stresses. Bridge 3B was the lower stressed composite bridge but was stressed higher than three of the noncomposite bridges.

Tests of Bridges 1B, 2A, 4A and 4B were discontinued after a small number of trips of the regular test vehicles because of large permanent deformations. In all other bridges, the permanent set increased rapidly during the initial phases of the regular test traffic, but the bridges became almost stable after a few hundred trips. The only exception was noncomposite bridge 3A which continued to deform at a moderately rapid rate throughout the first 50,000 trips of vehicles. In composite bridges seasonal fluctuations in permanent set were observed; the midspan moved up in winter and down in summer (Section 3.3.2).

The mean live load stresses caused by regular test traffic remained essentially constant throughout the period of regular test traffic even though individual samples showed substantial variation about the mean. The mean values of live load stresses are summarized in Table 75. Most of the individual stresses were within approximately 1.3 to 3.2 ksi of the mean.

The live load deflections increased with time; the average values at the beginning and end of the traffic are shown in Table 75. A small decrease in stiffness between the beginning and the end of the test traffic period was evident.

The total numbers of vehicle trips over individual bridges are also summarized in Table 75. Bridges 1B, 2A, 4A and 4B failed by progressive yielding. The $(DL + LL)$ strains exceeded the yield point strain in all three beams of Bridges 2A, 4A and 4B, but in Bridge 1B the yield point strain was exceeded only in the exterior beam. However, Bridge 1B was the fourth highest stressed bridge, its beams had no cover plates, and very large residual tensile stresses were found in the flanges of the rolled sections. Furthermore, Bridge 1B was crossed accidentally by two vehicles heavier than the assigned regular test vehicles, causing strains well in excess of the yield point strain in all three beams. At the time these four bridges were declared out of test, the permanent set exceeded 3 in. at midspan of every bridge beam.

Bridge 3A sustained 392,000 trips of the test vehicles; it was eliminated from further testing by an accident causing severe permanent deformations of all three beams. Although at the time of the accident the set at midspan of this

bridge was already approximately 3 in., the test history (Section 3.3.2) indicated that the bridge probably would have survived the period of test traffic if the accident had not taken place.

Noncomposite bridges 1A, 9A, 9B and composite bridges 2B and 3B survived the period of test traffic amounting to between 477,900 and 558,400 repetitions of stress. By the end of traffic the permanent deformation of composite bridge 3B was only 0.33 in.; that of composite bridge 2B and noncomposite bridges 9A and 9B was about twice as large. The $(DL + LL)$ strains in the beams of composite bridge 2B were often in excess of the yield point strain of the material.

By the end of the regular test traffic one or more fatigue cracks were found in all steel bridges that survived the test traffic. All of them had partial-length cover plates. The fatigue cracks first appeared in the bottom surface of the rolled section at the toe of the welds connecting the plates. They were found toward the end of the test traffic; except for one crack on Bridge 2B, the cracks changed either very little or not at all during the 26,900 or fewer trips accumulated during the remainder of the traffic. The crack on Bridge 2B spread through one-half of the bottom flange in 26,900 trips.

Although the regular test traffic caused yielding in the rolled sections of all steel bridges, practically no yield lines were found on the cover plates nor on the lengths of the beam flanges covered by cover plates. This restraining effect of the cover plates on the extent of yielding was indicated also by the relative magnitudes of permanent deflections.

Transverse cracks were found in the slabs of all steel bridges. They were first noted on the bottom side of the slabs of noncomposite bridges after the first few passages of the regular test vehicles. (Although designed for conventional allowable stresses, the slabs had to conform to large live-load deflections of beams.) In the late spring following the beginning of traffic, these cracks extended through the full depth of the slab and a number of them reached the top surface. The number of the transverse cracks extending the full depth of the slab increased with continued traffic. The transverse cracks in noncomposite bridges represented lines of progressive deterioration of the slabs. A few transverse cracks extending the full depth of the slab formed also in the decks of composite bridges but these caused no observable deterioration nor any substantial changes in the response of the bridges to loading.

In the accelerated fatigue test conducted on Bridge 2B, an additional 47,500 cycles of fluctuating stress resulted in rupture of the interior and center beams. The total number of stress cycles to failure, including the regular test traffic and the accelerated tests, was 605,900.

In the tests with increasingly heavier loads, noncomposite bridges 1A, 9A and 9B were tested until the permanent deformations increased at an increasing rate with each successive passage of the same load. At this stage yielding spread through the full depth of the beams, at least at one end of the cover plates, with both the tensile and the compressive yield lines reaching the neutral axis. The total permanent set at midspan exceeded 12 in. in all three bridges at the time the overload tests were discontinued.

In the tests with increasingly heavier loads of composite bridge 3B the tensile yielding reached into the top flange of the steel beams at both ends of the cover plates and near midspan. Tensile cracking extended to within approximately 1½ in. of the top surface of the slab. However, the test had to be discontinued before crushing of the concrete slab occurred, because of limitations on the capacity of the test vehicle. The total permanent set at midspan exceeded 14 in. at the conclusion of the test. The maximum test load for Bridge 3B was extremely large in relation to those causing failure of the noncomposite bridges.

Strength Calculations.—The tests of steel bridges brought out quantitative information on the limits of four stages of behavior of particular importance in relation to design. The four limits were:

1. Loads corresponding to the effective yield stress; when these loads were exceeded, particularly in noncomposite bridges without cover plates, large permanent set accumulated after relatively few trips of test vehicles.

2. Loads corresponding to the yield point of steel; when these loads were exceeded, large permanent set occurred in all bridges.

3. Ultimate flexural strength; when the applied moment exceeded the ultimate moment resistance of the bridge, the permanent deformations of the bridge per vehicle trip increased with each successive trip of the same load.

4. Loads that caused fatigue cracking; large number of cycles of transient stresses caused by vehicle trips resulted in formation of fatigue cracks at the toes of the welds connecting the cover plates to the rolled sections.

Studies of the test data indicated that these four loads may be estimated on the basis of existing methods of analysis.

In estimating the practical limit of the elastic behavior it was necessary to make an allowance for the residual stresses in the rolled beams. The limit was obtained as the effective yield stress equal to the difference between the yield point of the steel and the average residual

stress in the flanges of the rolled section. The permanent set was found to increase with increasing ratio of the applied stress to the effective yield stress and was smaller for composite bridges than for noncomposite bridges.

Loads corresponding to the yield point of steel were computed using elastic theory and yield point of the flanges of rolled sections. For all but one bridge the calculated yield strength was 10 to 20 percent lower than the external moment at first observed large set. In composite bridge 3B the first large set occurred at an external moment 7 percent lower than the calculated yield strength.

The ultimate strength of those bridges that failed by yielding was estimated on the basis of the fully plastic stress distribution and the static yield point of the steel. This computed capacity was compared with the maximum external moment caused by dead loads and by the heaviest test vehicle, but neglecting impact. The external moment exceeded the computed capacity by amounts varying from 1 to 32 percent.

The fatigue strength of the test bridges was compared with laboratory data obtained for specimens having the same details as those present in the test bridges. As the test bridges were subject to a varying range of live load stresses, the comparisons were based on not only the mean stress range but also on Miner's hypothesis of cumulative damage. The comparisons showed that nearly all results of the bridge tests fell within the range of the laboratory data. However, the comparisons suggested also that the bridges tended to fail at a lower number of cycles than the laboratory specimens. It is not known whether this suggested difference in strength was caused by the differences in the manner of loading, by the differences in the specimens, by the shortcomings of the analysis or whether it was simply the result of an experimental scatter.

Comparison Between Composite and Noncomposite Steel Bridges.—Although the design of the bridge experiment was such that in no two bridges was the composite action the only variable, the tests have demonstrated clearly that the composite bridges were superior to the noncomposite bridges. The composite bridges were stiffer than the noncomposite ones. For example, the transient deflection caused at midspan by the same vehicles was 2.2 times as great in noncomposite bridge 3A as in composite bridge 3B (Table 32) even though the moment of inertia of the steel sections was about 10 percent higher for Bridge 3A.

Composite action increased both the yield and ultimate strength. Tests with increasing loads to failure of Bridges 1A and 3B illustrated this point. Even though the steel beams of composite bridge 3B had less than 10 percent larger area than the steel beams of noncomposite bridge 1A, Bridge 3B carried a 50 percent higher moment at first large set and 150 percent higher moment at ultimate load (Tables 52 and 53).

The performance of composite bridges during the period of test traffic was strikingly superior to that of noncomposite bridges. Even though one of the two composite bridges was stressed, on average, to 88 percent of the yield point of the steel beams, it survived the test traffic in good condition. The permanent deformations of beams (Table 38) observed in the composite bridges varied between 0.19 and 0.80 in.; those of noncomposite bridges varied between 0.50 and 3.52 in. (The value of 3.52 in. does not include permanent set caused by an accident.) The transient deflections increased during the period of test traffic in all bridges; but although the increase for the composite bridges was only of the order of 5 percent, for noncomposite bridges it was of the order of about 15 percent (Table 33).

It appears that the decrease in stiffness, indicated by the increased transient deflections, was caused by transverse cracking of slabs. The cracks in composite bridges were fewer in number and remained tight through the duration of the traffic. The cracks in the slabs of noncomposite bridges opened up a few months after formation and led to progressive deterioration of the slabs by spalling of edges and seepage of water. At the conclusion of the test traffic, the slabs of composite bridges were in excellent condition while those of noncomposite bridges were in a moderate to advanced state of deterioration.

It should be noted, however, that the noncomposite test bridges had no interaction between the slab and the beams. Formation of natural bond was prevented by a treatment of the top surfaces of the steel beams prior to casting of the slabs. This artificial condition is not encountered in bridges on the highway system.

6.2.2 Prestressed Concrete Bridges

Stresses.—The dead load stresses on the bottom of prestressed concrete beams, just before beginning of tests with vehicles, varied between a compression of 859 psi and a tension of 473 psi. The smallest compressive stresses and the largest tensile stresses occurred in the exterior beams. The time dependent losses during the period between release of prestress and the first tests with vehicles were of the order of 10 percent of the stresses in concrete on the bottom at midspan caused by initial prestress and by beam weight.

First passages of regular test vehicles over the prestressed concrete bridges resulted in tensile cracking in all three beams of Bridge 5A and in the exterior beam of Bridge 6A. The

tensile live load stresses on the bottom of uncracked beams at midspan, caused by regular test vehicles moving at 30 mph and centered over the center beam of the bridge, ranged from 468 to 1,020 psi.

The dead load stresses in the bottom layer of prestressing steel at midspan varied between 145 and 172 ksi. The corresponding live load stresses were equal to between 18.4 and 26.1 ksi in the wires of Bridge 5A and between 2.3 and 4.5 ksi in the prestressing steel of the remaining bridges.

The beams of the uncracked bridges 5B and 6B shared roughly equal proportions of the external moment; between them, they resisted over 90 percent of the total external moment. On the other hand, in Bridges 5A and 6A the external beam resisted less than one-third of the total resisted by the three beams; the moment resistance of the exterior beam of Bridge 6A was particularly low in relation to the other two beams.

The sums of the initial dead and live load stresses are compared in Table 76 with the design values. For post-tensioned bridges 5A and 5B the design stresses compared favorably with the actual stresses in the center beam; on the other hand, for the center beams of pretensioned bridges 6A and 6B the actual stresses in concrete were lower and in steel were higher than the design values. The total stresses in the exterior beams of all bridges were higher than in the center beam; they were in excess of the design values.

The principal reason for the excess of the actual maximum stresses over the design stresses was the uneven distribution of the weight of the bridge. The difference in the stresses in the center beams of pretensioned bridges was caused by the time dependent losses being lower than those assumed in the design.

Effects of Repeated Stresses.—In the three beams of Bridge 5A and in the exterior beam of Bridge 6A, which cracked during the first few trips of test vehicles, additional cracks formed and the existing cracks widened during the first 100,000 trips of vehicles. Further traffic caused only minor increases in the number of cracks but the maximum crack width in Bridge 5A continued to increase throughout the period of regular test traffic. When the traffic was completed, the maximum crack width in unloaded bridges was close to 0.010 in. in Bridge 5A and 0.004 in. in Bridge 6A. The average crack spacing was 22 in. in Bridge 5A but only 10 in. in the exterior beam of Bridge 6A.

TABLE 76
SUMMARY OF INITIAL STRESSES IN PRESTRESSED CONCRETE BRIDGES

Bridge	Beam	Stress in Concrete (psi)		Stress in Steel (ksi)	
		Design	Actual	Design	Actual
5A	Interior	—	—	—	168 3
	Center	820	—	150.6	163.4
	Exterior	—	—	—	176.6
5B	Interior	—	160	—	157.3
	Center	346	377	152.2	153.6
	Exterior	—	647	—	157.2
6A	Interior	—	535	—	167.2
	Center	828	699	148.1	166.3
	Exterior	—	—	—	172.4
6B	Interior	—	−1	—	172.4
	Center	310	115	150.0	173.5
	Exterior	—	558	—	175.0

Cracks were found in all bridge beams during the period of test traffic or during the accelerated fatigue tests. However, most of those in Bridges 5B and 6B and in the center and interior beams of Bridge 6A were discovered only with special aids and their width was not measurable with a 40-power microscope.

The dead load sets and strains at midspan showed seasonal fluctuations caused probably by differential seasonal shrinkage between the slab and the beam. In addition to the seasonal fluctuation, the beams of Bridge 5A exhibited a pronounced increase of permanent set and strain with time and traffic; some over-all increase in permanent set was observed also in the other bridges, but the dead load strains in bridges other than Bridge 5A remained essentially constant.

The tensile live load stresses in Bridge 5A showed a substantial decrease during the very early stage of the tests; in Bridge 6A an increase of the steel stresses accompanied the progressive cracking at midspan of the exterior beam and later also of the center beam. The mean values of the steel stresses are summarized in Table 77. Most of the individual stresses were approximately within 0.44 and 1.06 ksi of the mean in the essentially uncracked beams, and within 3.3 and 9.5 ksi of the mean in the cracked beams.

The live load deflections increased with time; average values at the beginning and at the end of traffic are shown in Table 77. Although some decrease in stiffness was evident in all beams, the largest decrease was associated with the cracked beams of Bridge 5A.

All four prestressed concrete bridges survived the period of test traffic during which about 557,000 trips of regular test vehicles were made over each bridge. Only negligible permanent set at midspan was accumulated by the end of the test traffic: the largest, observed in Bridge 5A, was of the order of 0.3 in.

Accelerated fatigue tests were conducted on Bridges 5B, 6A and 6B. The number of stress cycles was raised by these tests to a total of 1,500,000 including both the trips of the regular

TABLE 77

SUMMARY OF TESTS WITH REPEATED STRESSES ON PRESTRESSED CONCRETE BRIDGES

Bridge	No. of Stress Cycles		Mean Transient Steel Stress (ksi)			Mean Trans. Defl. (in.)		Tests to Failure		Mode of Failure
	Regular Traffic	Accel. Fatigue Tests	Interior Beam	Center Beam	Exterior Beam	Beg. of Test	End of Test	Max. Appl. Moment (ft—kips)	Total Perm. Set (in.)	
5A	556,700	—	22.2	19.8	25.4	0.46	0.88	1,315	10.9	Concrete crushing
6A	556,800	943,400	2.5	4.8	6.8	0.16	0.25	1,500	8.1	Steel fracture
5B	556,700	949,000	4.7	3.8	4.1	0.24	0.35	2,520	7.6	Steel fracture
6B	556,800	942,100	2.4	2.5	2.5	0.17	0.26	2,520	6.4	Steel fracture

test vehicles and the number of stress cycles in the accelerated fatigue tests. No change of importance was noted on any of the three prestressed concrete bridges during the accelerated fatigue tests.

All four prestresed concrete bridges were tested to failure with increasingly heavier loads. With the exception of the beams of Bridge 5A, which were already thoroughly cracked, the increasing loads produced visible, general cracking accompanied by progressive decrease of stiffness. Only at loads approaching the ultimate was the decrease in stiffness accompanied by appreciable permanent deformations.

As ultimate loads of the bridges were approached, the cracks opened very wide on each trip of the vehicle. Tension cracks extended into the upper half of the slab; progressive bond failure occurred in Bridge 5A; heavy inclined cracks developed near both quarter points of the spans of Bridges 5B and 6B, and horizontal cracks formed at the junction of the slab and the beams progressing from the heavy inclined cracks toward midspan. At ultimate load, Bridge 5A failed by crushing of the concrete slab at or near midspan after an apparent bond failure occurred between the wires and the grout; the other three bridges failed by fracture of the prestressing steel. In Bridges 5B and 6B all prestressing steel was fractured in all three beams and the bridges collapsed on the safety cribs.

Strength Calculations.—The tests of prestressed concrete bridges brought out quantitative information on two stages of behavior of particular importance in relation to design—loads beyond which large losses of stiffness were observed, and the failure loads. The information obtained on the fatigue strength of prestressing steel, although helpful, was less valuable because no fatigue failure of prestressing steel occurred. Finally, quantitative information was also obtained on fatigue cracking of concrete (Bridges 5B, 6A and 6B); however, this cracking caused no significant changes in the behavior of the bridges.

Appreciable loss of stiffness was observed only after the tensile cracks were well developed. A lower limit for loads causing such cracking was estimated reasonably well as the cracking moment based on the static modulus of rupture.

The ultimate strength of all four prestressed concrete bridges was estimated from commonly accepted formulas developed on the basis of laboratory beam tests, assuming fully bonded condition for Bridges 5B, 6A and 6B and fully unbonded condition for Bridge 5A. This computed capacity was compared with the maximum static moment caused by the heaviest vehicle. The ratio of the maximum static moment caused by the test vehicle to the com-

puted capacity was 0.96 for the unbonded case (Bridge 5A) and from 1.02 to 1.16 for the bridges in which bond was preserved.

Laboratory data on the fatigue strength of the prestressing steel indicated that the ranges of stress, caused by the test traffic in the steel of prestressed concrete bridges, were well below the endurance limit. Accordingly, no fatigue failure of prestressing steel could be expected and none had occurred.

Finally, no correlation was found between the fatigue strength of concrete determined by laboratory tests of plain concrete beams and the fatigue cracking of the bridge beams.

Comparison Between Pretensioned and Post-Tensioned Beams.—The experiment was designed so that in two prestressed concrete bridges (5B, 6B) the stresses were well below the modulus of rupture and in two (5A, 6A) they were above it. In both pairs one bridge was pretensioned (6A, 6B) and one was post-tensioned (5A, 5B) thus permitting direct comparisons between these two types of construction.

Bridges 5B and 6B, which remained essentially uncracked through most of the tests, responded to the test traffic in the same manner. No difference was found in the behavior of the pretensioned and post-tensioned uncracked beams that could not be accounted for by the differences in loading.

Three beams in the post-tensioned bridge 5A and one in the pretensioned bridge 6A were stressed well above the modulus of rupture of concrete and cracked at the beginning of the tests with regular test vehicles. As the traffic continued, some cracking developed also in the other two beams of Bridge 6A. The pretensioned and post-tensioned cracked beams showed a markedly different behavior.

The cracks in the post-tensioned beams (5A) formed far apart and extended rapidly high into the web. On every trip of the test vehicle, the cracks opened wide so that the total opening of the crack under load exceeded 0.01 in. The cracks in the pretensioned cracked beam of Bridge 6A formed closed together and were confined mostly to the bottom flange of the I-section; the cracks were too narrow to be found by unaided eye. The cracking of the post-tensioned beams was accompanied by an appreciable decrease in stiffness; a comparison of the deflections of Bridges 5A and 5B indicates that cracking increased the transient deflections at midspan by about 90 percent (Table 41). On the other hand, the cracking of pretensioned beams appeared to have no immediate effect on the stiffness of the bridge.

The test traffic resulted in formation of new cracks and in growth of old ones but the differences between the crack patterns and effects on stiffness persisted. In the post-tensioned beams the dead load crack width increased but the total crack width on a loaded bridge remained practically unchanged. In the pretensioned beams some of the cracks became visible, with the maximum crack width observed on a loaded bridge equal to 0.005 in. However, even at the end of the traffic period the transient deflections of Bridge 6A with cracked beams were essentially the same as those of Bridge 6B which was essentially uncracked.

In addition to the effect on stiffness, the differences in cracking of the pretensioned and post-tensioned beams had a pronounced influence on the permanent set, substantially greater in the post-tensioned beams (Table 41), and on the ultimate strength. The cracked post-tensioned bridge 5A failed by crushing of concrete, after failure of bond between the wires and the grout, at the applied moment of 1,315 ft-kips. The pretensioned bridge 6A failed by breaking of wires at the moment of 1,500 ft-kips. The two bridges that remained essentially uncracked during the period of regular test traffic, failed by fracture of the prestressing steel. Thus bond failure occurred only in the post-tensioned beam thoroughly cracked by the test traffic.

It should be noted that in addition to the differences in the method of tensioning, Bridges 5A and 5B differed from Bridges 6A and 6B in several other features. Probably the most important among them were the differences in the type of prestressing steel. The post-tensioned beams were stressed with smooth wires and were grouted; the pretensioned beams were stressed with 7-wire strand. The test results indicate strongly that the bond provided by the strand was greatly superior to that provided by the smooth wires embedded in grout.

6.2.3 Reinforced Concrete Bridges

Stresses.—Before traffic began, dead load stresses in the bottom bars at midspan of reinforced concrete beams were lower than those computed by the straightline cracked section theory. During the period after casting the slab but before the beginning of testing the dead load stresses remained essentially unchanged. After the traffic began there was a rapid growth of cracking in the reinforced concrete bridges, resulting in a progressive increase of dead load stresses to the values given by the straightline theory. The computed dead load stresses in the bottom layer of the tension reinforcement at midspan of the reinforced concrete beams varied from 16.4 to 21.8 ksi.

In addition to their contribution as the top flanges of the T-beams, the slabs resisted 2 to 13 percent of the external moment caused by the vehicle; in other words, the slabs effected a longitudinal distribution of the load. The total beam moment was distributed evenly among the three beams. The live load stresses

TABLE 78
SUMMARY OF INITIAL STRESSES IN REINFORCED CONCRETE BRIDGES

Bridge	Design Stress in Center Beams (ksi)	Actual Stress (ksi)		
		Interior Beam	Center Beam	Exterior Beam
7A	40.0	41.2	40.0	44.4
7B	40.0	40.1	40.0	44.4
8A	30.9	32.9	31.7	34.7
8B	30.9	30.0	31.9	35.4

in the tension reinforcement at midspan caused by regular test vehicles moving at 30 mph and centered over the center beam varied from 13.5 to 23.5 ksi. The differences in these stresses from beam to beam of the same bridge were small. There was also good agreement between the two bridges of each pair of duplicate bridges (7A and 7B, 8A and 8B).

The sums of the initial dead load and live load stresses are compared with the design stresses in Table 78. The design stresses were in excellent agreement with the actual stresses in the center beam for which the design was made. However, the maximum total stresses occurred in the exterior beam carrying the largest proportion of the weight of the bridge. Thus, the maximum total stress exceeded the design stress in every reinforced concrete bridge.

Effects of Repeated Stresses.—The test traffic increased substantially the extent of tension cracking in all reinforced concrete bridge beams. In Bridges 8A and 8B, subjected to the lower stresses, the increase consisted primarily of formation of new vertical cracks and of extensions of the cracks in existence before the beginning of traffic. In Bridges 7A and 7B, subjected to the higher stresses, numerous inclined cracks formed in the outer 15-ft segments of the beams and a considerable amount of irregular cracking occurred near the level of the tension reinforcement.

Both the number of cracks and their width were increasing throughout the full period of test traffic. At the end of the traffic, in unloaded bridges the maximum crack width exceeded 0.01 in. in all four bridges, while the average crack width in midspan segments of the beams was in excess of 0.006 in. in Bridges 7A, 7B and less than 0.006 in. in Bridges 8A, 8B. The regular test vehicles increased the crack width only by 0.001 to 0.002 in.

The mean transient live load stresses caused in the bottom bars at midspan by regular test traffic remained essentially constant throughout the period of test traffic even though individual samples indicated a substantial variation around the mean. The mean values are given in Table 79. Most of the individual stresses were within 2.0 to 5.3 ksi of the mean.

The live load deflection increased with time. Average values at the beginning and at the end of test traffic are also given in Table 79. The decrease in stiffness between the beginning and the end of the traffic is evident.

The dead load strains in the tension reinforcing bars increased with time and indicated that dead load stresses approached the values computed by the cracked-section theory. The dead load set at midspan showed seasonal fluctuations similar to those observed in composite steel bridges. Apparently seasonal shrinkage and expansion of the slab were responsible for these fluctuations.

All four reinforced concrete bridges survived the period of regular test traffic during which over 556,000 trips of regular test vehicles were made over each bridge (Table 77). The maximum total set accumulated during the period of test traffic was 0.3 in. However, the total permanent set including the period before the beginning of traffic was substantial. For example, Bridge 7B had no camber left when the test traffic had ended; the original camber at midspan of this bridge was approximately 1 in.

Accelerated fatigue tests were conducted on Bridges 7A, 7B and 8A. The tests proceeded without changes in the response or general appearance of the bridges until fracture of bars or until the test was discontinued. In Bridges 7A and 7B, stressed to the higher stress level, two bars broke in the exterior beam after a total of approximately 730,000 stress cycles, including both the stresses caused by trips of regular test vehicles and the stress cycles accumulated during the accelerated tests. In Bridge 8A a total of 1,500,000 stress cycles was reached without failure; the 941,600 cycles in the accelerated tests caused only a small increase in the number and width of cracks.

Bridges 8A and 8B were tested to failure with increasingly heavier loads. Both bridges failed by yielding of the tension reinforcement followed by crushing of the slab. The permanent set at failure exceeded 14 in. in both structures.

Strength Calculations.—The tests of reinforced concrete bridges produced quantitative information on three stages of behavior of particular importance in relation to design: (1) loads below which the bridge response was essentially elastic; (2) ultimate flexural strength; and (3) loads causing fatigue failure of bars. Studies of the test data indicated that these loads may be estimated on the basis of existing methods of analysis.

For estimating the limit of elastic behavior, the moment at first yielding of the reinforcement, computed from the ordinary straightline cracked-section theory and from the yield point of the reinforcing bars, was found satisfactory.

TABLE 79
SUMMARY OF TESTS WITH REPEATED STRESSES ON REINFORCED CONCRETE BRIDGES

Bridge	No. of Stress Cycles		Mean Transient Steel Stress (ksi)			Mean Trans. Defl. (in.)		Tests to Failure		Mode of Failure
	Regular Traffic	Accel. Fatigue Tests	Interior Beam	Center Beam	Exterior Beam	Beg. of Test	End of Test	Max. Applied Moment (ft-kips)	Total Perm. Set (in.)	
7A	556,100	172,200	25.5	23.1	23.6	1.43	1.77	—	—	Fatigue fracture
7B	556,100	174,100	22.0	22.0	22.7	1.31	1.65	—	—	Fatigue fracture
8A	558,400	941,600	15.9	15.2	14.9	0.90	1.07	1,550	15.2	Concrete crushing
8B	558,400	—	15.2	14.8	15.7	0.87	1.08	1,550	14.5	Concrete crushing

The ultimate strength of the bridges was computed from the commonly accepted formulas developed on the basis of laboratory beam tests. This computed capacity was compared with the maximum static moment caused by the heaviest vehicle. The maximum static moment caused by the vehicle exceeded the computed strength by 4 percent.

The fatigue strength of the test bridges was compared with laboratory fatigue data obtained from samples of reinforcing bars used in the test bridges. As the bridges were subjected to a varying range of live load stresses, the comparisons were based not only on mean stress range but also on Miner's hypothesis of cumulative damage. The comparisons suggested that the bars in the test bridges were slightly weaker in fatigue than indicated by the lower limit of the laboratory data.

6.3 SUMMARY OF STUDY OF DYNAMIC EFFECTS

6.3.1 Experimental Observations

Properties of Bridges and Vehicles.—For concentric loads, each test bridge acted essentially as a single simply-supported beam. The differences between the magnitudes of the static response among the three beams were generally negligible. Both magnitudes of the measured deflections and stresses and the shapes of the crawl history curves agreed with the corresponding values computed on the basis of a simply-supported prismatic beam.

For the noncomposite steel, prestressed concrete, and reinforced concrete bridges the frequencies determined from the free vibration era were not representative of the stiffness of the bridges while the vehicle was on the span. This difference was due to the different degrees of composite action or extent of opening of cracks under the two conditions. There appeared to be a corresponding difference in the damping characteristics of loaded and unloaded bridges.

The static load-deflection characteristics of the vehicles could be represented acceptably by a linear spring for the tires and a bilinear model for the springs, which included the effect of frictional damping in the suspension system. However, large differences were observed between the results of replicate loading tests.

Although there were uncertainties in the time scales of the experimental records, the frequencies of the vehicles under dynamic conditions appeared to be lower than predicted by the static measurements, reflecting the presence of additional flexibility provided by the vehicle frame. The damping in the tires could be approximated on the basis of a viscous damping coefficient of the order of 1.0 percent. Under certain conditions of severe excitation of the vehicle the frictional force in the suspension

system was found to be less than the value obtained from the static tests and occasionally it disappeared entirely.

Blocking of vehicle springs was found to increase the amplitude of the interaction force variation by as much as a factor of 3.0. The maximum observed double amplitudes of variation in the interaction force in dynamic tests on rigid pavements were as follows:

Drop tests using a 1-in. obstruction:

Two-axle vehicle, spring blocked	2.0 P_{st}
Two-axle vehicle, springs normal	1.1 P_{st}
Three-axle vehicle, springs blocked	1.2 P_{st}
Three-axle vehicle, springs normal	0.3 P_{st}

Tests on smooth pavements:

Two- and three-axle vehicles, spring blocked	0.5 P_{st}
Two- and three-axle vehicles, springs normal	0.2 P_{st}

P_{st} is the static axle load. For both blocked springs and normal suspension the variation in the interaction force was found to be less for the three-axle vehicles than for the two-axle vehicles, due to the dynamic coupling between the tractor and semitrailer.

Bridge Response.—History curves of dynamic increments provided the best measure of the dynamic behavior of the bridges. Comparisons of history curves of bridge response confirmed the theoretical predictions that the dynamic increments for moment and deflection at one cross-section as well as those for the effects at a different cross-section of the same beam are essentially identical. Furthermore, for the bridges considered, the dynamic increments at midspan of the three beams were also found to be comparable so that the midspan response of the center beam, expressed in terms of dynamic increments, depicted with sufficient accuracy the dynamic behavior of the entire bridge.

Initial vertical oscillations of the vehicle were present in practically all tests and introduced a large uncertainty in the dynamic response of the bridges. A qualitative measure of the trend in the amplitude of the vehicle oscillations at the entrance of the bridge was obtained on the basis of simple approximations of the major surface irregularities of the approach pavements immediately preceding the bridge.

Under seemingly identical conditions, the dispersion in the measured amplification factors was of the order of 20 percent for deflections and 10 percent for strains. The dispersion was caused by the differences in the initial conditions of the vehicles, the variation in the characteristics of the vehicle, and the unavoidable errors in recording and reduction.

In comparing the results of the regular tests of bridges, the maximum amplification factors generally increased with the speed parameter α. The differences in the amplification factors of the same bridge for different vehicles at different times as well as between the responses of the different bridges were generally larger than the experimental dispersion of the data. The largest amplification factor for deflection was 1.63; however, only 5 percent of measured amplification factors for deflection exceeded 1.40. The largest amplification factor for moment was 1.41 and only approximately 5 percent of the amplification factors for moment exceeded the value of 1.286 specified by the impact formula of the AASHO Standard Specifications for Highway Bridges. The largest effects were observed on a reinforced concrete bridge, but these results appeared to be influenced by a pronounced irregularity on the bridge surface.

Where the effects of individual bridge-vehicle parameters could be isolated, the observed trends in these effects were in a general agreement with theoretical considerations. Doubling the weight ratio R had little effect on the peak value of the amplification factors, and the effect of doubling the profile parameter Δ was to increase slightly the amplification factors for deflection, primarily due to a shift in the position of the critical dynamic increments. The presence of vehicle oscillations produced by irregularities both on the approach pavements and on the bridge itself made difficult the comparisons of the effects of individual bridge-vehicle parameters. In general, different vehicles on the same bridge produced comparable effects whereas the same vehicle on different bridges produced markedly different effects. The large differences of dynamic effects between bridges were caused by relatively large differences in the pertinent parameters and in the profiles of the approaches and bridges.

The increase in the number of vehicle trips during regular test traffic resulted in increased amplification factors only for those bridges for which the permanent set and the approach profile roughness increased with time. In bridges in which there was a decrease in camber and the approach profile was smoothed by patching there was a decrease in dynamic effects.

Blocking of vehicle springs resulted in approximately doubling the dynamic increments on bridges and in imparting to the bridge response a noticeable component proportional to the variation in the interaction force.

In the tests with induced vehicle oscillations, the vehicle behavior on the bridge was found to be essentially the same as on a rigid pavement.

For vehicles with normal suspension, only the first bottoming of the vehicle produced large changes in the interaction force because of the large amount of frictional damping. By the time the vehicle reached midspan, the variation in the interaction force was reduced to values comparable to those for regular tests. Consequently, maximum amplification factors at midspan were generally only slightly larger than those produced without induced oscillations. However, the effects away from midspan were larger than those observed for the regular tests. On the other hand, initial bridge oscillations, similar to those produced by continuous traffic, were found to have no noticeable effects.

Vehicle eccentricity of 24 in. was found to have no significant effect on the bridge behavior but a single-wheel loading at an eccentricity of 60 in. excited a large component of the torsional mode of vibration of the bridge.

6.3.2 Analysis vs *Experiments*

Comparisons between experimental and theoretical results were based on a small portion of the available test data. The comparisons were intended primarily as a study of the reliability of the theoretical method used. For those cases where there was little uncertainty about the properties of the bridges and vehicles, the theoretical solutions were found to be in excellent agreement with the experimental data. These cases comprised all tests with blocked vehicle springs and almost all of the results studied for the regular tests on composite steel bridges. The comparisons with the test data have shown that the interleaf friction is an extremely significant quantity which must be taken into account in the theoretical analysis.

In the prestressed concrete bridge examined, the cracking of beams appeared to have changed significantly the properties of the bridge while the vehicle was on the span. Because of this, no agreement could be obtained using a theoretical method in which it was assumed that the properties of the bridge were independent of the position of the load.

In general, the agreement between the theory and experiment was hampered by a large number of uncertainties involved in the experimentally determined parameters, by experimental uncertainties concerning the data forming the basis of comparisons, and by certain limitations of the computer program used to obtain the theoretical solutions.

Of the items not considered in detail in the analysis but significantly affecting the bridge-vehicle behavior were the state of oscillation of the individual vehicle axles at the time of their entry on the bridge, the irregularities of the bridge surface, and the horizontal forces transmitted between the tractor and semitrailer of the three-axle vehicles.

6.4 PRINCIPAL FINDINGS

The tests of the bridges at the AASHO Road Test furnished an over-all description of the behavior of beam and slab bridges under repeated high stresses and a detailed insight into the problem of the dynamic effects of moving vehicles on the response of bridges. In applying the results of these tests to design problems, it must always be kept in mind that these were not typical highway bridges, and that the stress levels at which the tests were conducted were above the stresses normally experienced in the actual service life of a highway bridge.

Of the numerous specific findings obtained in this investigation and summarized in the preceding sections, the following items deserve special emphasis:

1. Fatigue cracking in varying amounts occurred in all five steel bridges with partial-length cover plates, welded to the tension flanges of the rolled sections, after they were subjected to between 477,900 and 536,000 trips of test vehicles. The mean stress ranges, caused by the test vehicles at the end of cover plates of these bridges, were 12.8 to 17.8 ksi. The minimum stresses, caused primarily by dead loads, were 5.7 to 21.2 ksi. The total dead load and mean live load stresses were 24.1 to 35.9 ksi.

2. Fatigue failures of reinforcing bars occurred in both reinforced concrete bridges in which the mean stress range was 26 ksi and the minimum stress was 19 ksi. These failures occurred after approximately 730,000 cycles of stress including 556,100 trips of test vehicles; the balance of the stress cycles was applied by vibration of the bridges.

3. Fatigue distress observed in the beams with partial-length cover plates of the steel bridges and in the reinforcing bars of the reinforced concrete bridges occurred in the same manner as that observed in laboratory tests. The number of cycles to fatigue distress in these bridge members agreed reasonably well with the number of cycles computed from equations developed from simpler laboratory tests of beams. Thus, where a reasonable estimate of the magnitude and number of repetitions of stress can be made, laboratory fatigue data for the material can forecast the life to fatigue failure within reasonable limits.

4. The steel bridge without cover plates subjected to 392,400 trips of test vehicles withstood the repeated stressing without fatigue cracking. The mean stress ranges at midspan of the steel beams were 18.9 to 21.0 ksi and the minimum stress was 12.7 ksi. According to laboratory data these beams could have resisted approximately 2,000,000 repetitions of 28-ksi stress range superimposed on the actual minimum stress. Thus the laboratory data in-

dicated that a fatigue failure under the conditions existing in the test bridge was improbable.

5. In the most highly stressed prestressed concrete bridge, the prestressing steel withstood 556,700 cycles of stress without failure. The mean stress ranges in the prestressing steel were 20.2 to 26.2 ksi and the minimum stress was 146 ksi. Laboratory fatigue tests have established an endurance limit of 49 ksi on the stress range. Thus the laboratory data indicated that a fatigue failure in the prestressing steel was improbable.

6. Fatigue cracking of concrete was detected in prestressed concrete beams subjected to tensile stresses lower than the modulus of rupture of concrete. The cracking was detected only with special aids and had no readily observable effects on the behavior of the bridge. No correlation was found between the number of cycles of stress at which the fatigue cracks were found and the fatigue strength of plain concrete determined from laboratory tests of beams.

7. The behavior of composite steel bridges was clearly superior to that of the noncomposite steel bridges. The superiority was manifested not only by higher stiffness and strength but also by substantially smaller permanent set at stresses approaching yield point of the material and by lack of deterioration of the slab. However, it should be noted that in the noncomposite test bridges there was practically no interaction between the concrete slab and the steel beams.

8. There was a marked difference between the cracking of the prestressed concrete beams post-tensioned with parallel wire cables and those pretensioned with 7-wire strands. In the beams stressed with parallel wire cables severe cracking changed radically the response of the beams to loading. The stiffness of the beams was decreased substantially by cracking, progressive loss of bond was indicated and the ultimate flexural capacity of the bridge was decreased because of bond failure. On the other hand, the cracking of the beams with 7-wire strand caused practically no change in the response of the beams to loading. Deflections during the period of test traffic were essentially the same as those of an uncracked bridge, and excellent bond was preserved at all stages of tests up to the ultimate load.

9. The pattern of tension cracking of reinforced concrete beams was substantially different in the bridges with reinforcement stressed to about 33,000 psi than in those with reinforcement stressed to about 42,000 psi. In both types of bridges the maximum crack width exceeded 0.01 in. in the unloaded condition and the test vehicles caused a maximum additional opening of 0.002 in., but the incidence of the largest cracks was greater in the higher stressed beams. The cracking of the lower stressed beams consisted essentially of only vertical cracks, with only a few inclined cracks in the outer 10-ft lengths of the spans near the supports. The inclined cracking of the beams with the higher stresses was extremely severe, particularly in the outer 15 ft of each span. In addition to the vertical and inclined cracks a number of small irregular cracks formed near the level of the tension reinforcement in the higher stressed beams.

10. The results of the dynamic tests on the bridges were found to be in satisfactory agreement with those obtained from the theory used in this study. This agreement was obtained only by including in the analyses all pertinent characteristics of the bridges and the vehicles, some of which were shown to be significant for the first time in these tests. For example, it was found that the interleaf friction in the suspension system of the trucks had an extremely important effect on the dynamic response of the bridge.

11. Because of the special conditions of the bridge tests, the relative magnitudes of the dynamic effects for the different bridge types are not indicative of those which would be obtained under more typical conditions. The theoretical analyses referred to under item 10 can be used to study the relative dynamic effects for various types of bridges after sufficient information regarding the pertinent properties of bridges and vehicles will have been obtained from dynamic field tests on the highway system.

12. The observed effects of irregularities in the bridge decks and in the approach pavements re-emphasized the importance of smooth deck and pavement surfaces. The advantage of limiting vehicular speeds to about 15 mph or less for loads considerably in excess of the design assumptions was indicated.

Appendix A

DATA SYSTEMS

The principal data collected as a part of the bridge research are stored on IBM punch cards. The data may be obtained from the Highway Research Board at the cost of reproduction either in the form of printouts or of IBM cards. The titles and brief descriptions of the data systems pertaining to bridge research are given below. Design caluclations, construction drawing and construction specifications are on file with the Highway Research Board. Data systems associated with pavement research are listed in Appendix I, AASHO Road Test Report 5.

Data System Number	Number of IBM Cards	Number of Printout Pages	Title	Description
1400	18	1	Bridge Experiment Design, Summary	Designation, location and principal design features of all 18 test bridges.
2410	223	9	Tension Tests of Coupons from Wide Flange Beams	Location, dimensions, yield point, ultimate strength, reduction of area, ultimate elongation and modulus of elasticity for individual test coupons.
2411	54	1	Tension Tests of Coupons from Cover Plates	Location, dimensions, yield point, ultimate strength, reduction of area, ultimate elongation and modulus of elasticity for individual test coupons.
2412	156	10	Tension Tests of Reinforcing Bars	Source, dimensions, yield point, ultimate strength, reduction of area, ultimate elongation and modulus of elasticity of individual test coupons.
2413	123	5	Tension Tests of Prestressing Steel	Area, yield strength, ultimate strength, ultimate elongation, reduction in area and modulus of elasticity of individual test coupons.
2414	1197	32	Relaxation Tests of Prestressing Steel	10 samples of prestressing wire and 12 samples of prestressing strand; minimum duration 1,000 hr, maximum duration 12,000 hr.
2415	124	4	Fatigue Tests of Reinforcing Bars and Prestressing Steel	Minimum and maximum stress levels and number of applied cycles of stress on 18 reinforcing bars, 82 prestressing wires and 24 prestressing strands.
2416	12	1	Chemical Analysis of Prestressing Steel	6 samples of wire and 6 samples of prestressing strand.
2417	22	1	Residual Stresses in Wide Flange Beams	16 samples of rolled steel sections.
2420	176	4	Compression Tests of Concrete Cylinders	At time of release of prestress, at 28 days, at beginning and at end of test traffic. Compressive strength and modulus of elasticity for individual cylinders.
2421	24	1	Flexural Beam Tests of Concrete	Modulus of rupture of individual beams at time of release of prestress, at age of 28 days, at beginning and end of test traffic.
2422	16	1	Coefficient of Thermal Expansion of Concrete	16 concrete specimens; temperature range, 37 to 100 F.
2423	304	8	Bridges—Shrinkage Measurements	8 concrete cylinders kept outdoors for 1,300 days.
2424	8	1	Bridges, Creep; Initial Elastic Strains (Electric)	Measurements with SR–4 strain gages on cylinders used in creep experiment (see DS 2425 for creep measurements).

Data System Number	Number of IBM Cards	Number of Printout Pages	Title	Description
2425	364	8	Bridges, Creep Measurements	16 concrete cylinders kept under load in outdoor exposure for 1,300 days.
2430	22	1	Compressive Strength of Concrete, Summary	Summary of DS 2420, including average strengths for individual bridges; averages and standard deviations.
2431	22	1	Modulus of Elasticity of Concrete, Summary	Summary of DS 2420, including average for individual bridges; averages and standard deviations.
2432	4	1	Modulus of Rupture of Concrete, Summary	Summary of data from DS 2421; average modulus of rupture and standard deviations for individual bridges.
2440	15	2	Tension Tests of Coupons from Wide Flange Beams, Summary	Summary of DS 2410; averages and standard deviations for individual bridges.
2441	7	1	Tension Tests of Coupons from Coverplates, Summary	Summary of data from DS 2411; averages and standard deviations for individual bridges.
2442	10	1	Tension Tests of Reinforcing Bars, Summary	Summary of data from DS 2412; averages and standard deviations for individual bar sizes from same heat.
2443	4	1	Tension Tests of Prestressing Steel, Summary	Summary of data from DS 2413; means and standard deviations for individual bridges.
2450	40	1	Dimensions of Steel Bridges	Measured dimension of rolled steel beams with and without cover plates; mean values for each beam and each bridge.
2451	16	2	Dimensions of Prestressed Concrete Bridges	Average measured dimensions; means for individual beams and bridges.
2452	16	1	Dimensions of Reinforced Concrete Bridges	Measured dimensions; means for individual beams and bridges.
2460	56	2	Section Properties of Steel Bridges	Area, moment of inertia and position of neutral axis computed from measured dimensions of steel beams with and without cover plates; properties for steel section alone and for composite section including slab.
2461	48	3	Section Properties of Prestressed Concrete Bridges	Area, moment of inertia and position of neutral axis computed from measured dimensions of the cross-section for prestressed concrete beams alone and for composite section including slab; uncracked section assumed.
2462	48	3	Section Properties of Reinforced Concrete Bridges	Moment of inertia and position of neutral axis for reinforced concrete beams, computed from measured dimensions assuming cracked section.
2470	1782	64	Influence Surfaces for Moment and Deflection	Computed for each bridge as described in Section 5.1.2.
4400	559	20	Permanent Dead Load Deflections	Measurement of elevation of bottom of beams at quarter points and at midspan relative to straightline connecting supports; measurements at least once per month starting just before beginning of test traffic, all for unloaded bridges.
4410	762	22	Cumulative Dead Load Strains	Measurements of strains on bottom of beams at midspan for unloaded bridges; measurements started either before or shortly after casting slab and made at least once per month.
4411	336	42	24-Hour Study of Strains and Temperatures	Temperatures at various points of slab and beams, and changes in strain at midspan in bottom of beams every 4 hr during 24-hr periods on selected bridges.

Data System Number	Number of IBM Cards	Number of Printout Pages	Title	Description
4412	46	1	Monfore Readings, Bridge 9B	Comparative measurements of strains at midspan of Bridge 9B made with Monfore and Whittemore gages.
4420	4410	123	Crack Study, Dead Load, Original Data	Measurements of number of cracks and crack width on all reinforced concrete bridges taken approximately every 3 months; unloaded bridges.
4421	432	24	Summary Card, Crack Study	Summary of data from DS 4420.
4422	1323	49	Crack Study, Dead Load, Average Data	Averages of data from DS 4420.
4423	216	6	Crack Study, Dead Load, Summary	Summary of data from DS 4422.
4440	848	51	Longitudinal Profiles	The approach pavements and bridges in the two wheelpaths taken every foot; measurements at four different times.
4441	300	10	Transverse Profiles	Bridge slabs at midspan and at quarter points relative to abutments; measurements taken at approximately 6-month intervals.
5400	867	44	Transverse Load Distribution Study	Strains in beams, at midspan and at other locations, caused by vehicle placed in six different transverse and three different longitudinal positions.
5405	670	24	Transverse Load Distribution, Tests vs Analysis	Average data from DS 5400 and corresponding values computed from the influence surfaces in DS 2470.
5410 to 5414	1822+284	73+10	Repeated Load Reference Data and Summary, Stresses	Stresses caused by regular test vehicles moving at 30 mph or creep speeds or standing on the bridge in concentric transverse position; strain measurements on all gages at five different times.
5415 to 5419	1822+284	73+10	Repeated Load Reference Data and Summary, Midspan Stress and Deflections	Stresses at midspan and midspan deflections caused by regular test vehicles moving at 30 mph or 3 mph, or caused by standing vehicles centered on the bridge; data taken at five different times.
5420 to 5440	6943+1320	212+42	Repeated Load Deformations and Summary	Stresses at midspan and at the ends of cover plates, and deflections at midspan caused by regular test traffic.
5444	157	8	Repeated Load Deformations, After Traffic Series	Supplemental data for DS 5440 taken after the completion of the regular test traffic.
5445	1015	133	Repeated Load Deformations, Stress Range Data	Stress range during regular test traffic.
5450 to 5454	2505	139	Dynamic Load Effects	Stresses and deflections caused by moving vehicles during studies of dynamic effects of vehicles on response of test bridges.
5470 to 5471	192	8	Load-Deformations	Stresses and deflections obtained in load-deformation studies.
5480	1080	30	Live Load Cracking of Reinforced Concrete Beams	Number of cracks and crack width measured on loaded reinforced concrete bridges; bridges loaded with standing regular test vehicles.
5481	108	6	Cracking Summary	Summary from DS 5480.
5482	324	14	Crack Study, Live Load, Average Data	Averages from DS 5480.
5483	54	2	Crack Study, Live Load, Summary	Summary of DS 5482.
5490	468	12	Accelerated Fatigue Test Data	Complete data from accelerated fatigue tests.
5491	557	17	Overload Tests, Stresses	Strain measurements during tests to failure with increasing loads.

Data System Number	Number of IBM Cards	Number of Printout Pages	Title	Description
5492	2157	75	Overload Tests, Deflections	Permanent and transient deflections during tests to failure with increasing loads.
5493	74	2	Overload Tests, Axle Weights and Axle Spacings	Axle loads of vehicles used in tests to failure with increasing loads.
6400	10941		Count of Vehicle Trips on Bridges	Day-to-day count on individual bridges; AASHO calendar.
6410	282	6	Transverse Vehicle Placement on Bridges	Sampling during regular test traffic.
6420	390	11	History of Events for Test Bridges	Dates of significant construction and test events for individual bridges.

NOTE: Most of the printouts require 11- by 14-in. sheets.

Appendix B

HISTORY OF EVENTS

Dates of miscellaneous events in the construction and tests of bridges are listed in Tables 1-B and 2-B. The dates are given in AASHO Road Test calendar numbering days consecutively from July 1, 1956, with the following correspondency:

July 1, 1956 = 0
July 1, 1957 = 365
July 1, 1958 = 730
July 1, 1959 = 1095
July 1, 1960 = 1461

Januray 1, 1957 = 184
January 1, 1958 = 549
January 1, 1959 = 914
January 1, 1960 = 1279
January 1, 1961 = 1645

TABLE 1-B

STEEL BRIDGES

Event	AASHO Date									
	Bridge 1A	Bridge 1B	Bridge 2A	Bridge 2B	Bridge 3A	Bridge 3B	Bridge 4A	Bridge 4B	Bridge 9A	Bridge 9B
First pour of foundations	96	96	96	96	108	108	108	108		
Erection of beams	337	337	337	337	346	346	346	346	1041	1041
Slab concrete cast	396	410	410	396	402	408	408	402	1059	1059
End of wet curing	404	417	417	404	409					
Slab forms removed	411			416	418	422	422	421	1065	1065
Bridge moved in place									1083	1083
End adjacent pavement construction	722	722	722	722	729	729	729	729		
End loop pavement construction	786	786	786	786	800	800	800	800		
First recorded vehicle crossing bridge	802	802	802	802	794	794	789	789	1085	1085
First regular test vehicle crossing bridge	834	834	834	834	833	833	833	833	1085	1085
Beginning of regular test traffic	856			856	856	856			1085	1085
1,000 trips completed	859			859	860	860			1087	1087
10,000 trips completed	897			898	897	897			1105	1105
100,000 trips completed	1127			1123	1124	1124			1255	1255
200,000 trips completed	1288			1288	1288	1288			1359	1359
300,000 trips completed	1374			1375	1374	1374			1444	1444
400,000 trips completed	1458			1456		1457			1539	1539
500,000 trips completed	1550			1552		1550				
End of regular test traffic	1606			1608	1450	1613			1616	1616
Beginning of accelerated fatigue tests				1620						
End of accelerated fatigue tests				1623						
Beginning of tests with increasing loads	1730					1782			1773	1773
End of tests with increasing loads	1767					1808			1775	1776
Testing completed	1767	836	834	1623	1450	1808	833	833	1775	1776

TABLE 2-B

CONCRETE BRIDGES

Event	AASHO Date							
	Bridge 5A	Bridge 5B	Bridge 6A	Bridge 6B	Bridge 7A	Bridge 7B	Bridge 8A	Bridge 8B
First pour of foundations	303	309	303	309	327	331	327	331
Interior beam cast	509	391	454	460	397	432	432	397
Center beam cast	480	496	472	466	397	432	432	397
Exterior beam cast	508	496	454	460	397	432	432	397
Interior beam stressed	512	488	457	463				
Center beam stressed	491	495	539	470				
Exterior beam stressed	512	500	457	463				
Beams grouted	513	502						
Erection of beams	516	507	485	485				
Slab concrete cast	654	654	514	514	397	432	432	397
End of wet curing	663	663	526	526	404			404
Slab forms removed	668	668	528	528	411	449	450	414
End of adjacent pavement construction	786	786	786	786	800	800	800	800
End of loop pavement construction	786	786	786	786	800	800	800	800
First recorded vehicle crossing bridge	814	814	814	814	801	801	801	801
First regular test vehicle crossing bridge	834	834	834	834	833	833	832	832
Beginning of regular test traffic	856	856	856	856	856	856	856	856
1,000 trips completed	859	859	859	859	860	860	860	860
10,000 trips completed	897	897	897	897	898	898	896	896
100,000 trips completed	1123	1123	1127	1127	1128	1128	1124	1124
200,000 trips completed	1288	1288	1288	1288	1289	1289	1288	1288
300,000 trips completed	1375	1375	1374	1374	1379	1379	1374	1374
400,000 trips completed	1456	1456	1458	1458	1466	1466	1456	1456
500,000 trips completed	1553	1553	1550	1550	1559	1559	1550	1550
End of regular test traffic	1606	1606	1608	1608	1616	1616	1613	1613
Beginning of accelerated fatigue tests		1626	1643	1656	1664	1661	1674	
End of accelerated fatigue tests		1643	1655	1692	1667	1663	1684	
Beginning of tests with increasing loads	1761	1761	1762	1762			1796	1796
End of tests with increasing loads	1766	1808	1767	1808			1797	1797
Testing completed	1766	1808	1767	1808	1667	1663	1797	1797

Appendix C

NOMENCLATURE

The following symbols, used throughout this report, are defined where they first appear and are gathered here for ready reference.

C_1, C_2 = Parameters for evaluation of natural frequencies of a two-axle vehicle.

D = Span length plus distance between front and rear axle.

E = Secant modulus of elasticity of the element for stress F_1/a as determined from the stress-strain diagram of the element.

EI = Stiffness of bridge cross-section.

$(EI)_{beam}$ = Average beam stiffness at midspan of a bridge.

$(EI)_L$ = Stiffness of a loaded bridge inferred from measured deflections.

$(EI)_{slab}$ = Stiffness of a 1-ft wide strip of slab.

$(EI)_u$ = Stiffness of an unloaded bridge inferred from f_u.

E_c = Modulus of elasticity of slab concrete.

E_s = Modulus of elasticity of steel.

F = Force in one layer of tension reinforcement.

F_t = Loss in prestressing force caused by friction.

F_1 = Observed tensile force at the jack.

H = Ratio of longitudinal beam stiffness to transverse slab stiffness.

I_b = Moment of inertia of the beam at the section considered.

K = Friction wobble coefficient.

L = Span length; also length of prestressing steel element from jacking end to midspan (Section 5.6).

M_b = External beam moment at the section considered.

M_{DL} = Moment caused by weight of the bridge.

M_{LL} = Static moment caused by the test vehicle.

M_u = Ultimate moment resistance.

M_y = Moment resistance based on the static yield point.

N_x = Number of cycles of stress S_x to failure.

N'_x = Mean number of cycles to failure for stress S_{min} and stress range S_{rx}.

N_1, N_5 = Number of cycles to failure.

N'_1, N'_5 = Mean estimate of the number of cycles to cracking or failure.

P = Total load on the axle suspension system.

P_s = Load carried by vehicle spring.

P_{st} = Static axle load.

R = Ratio of gross vehicle weight to weight of the bridge.

S = Mean live and dead load stress.

S_{min} = Minimum stress.

S_r = Stress range.

S_x = Stress of interval x.

T_b = Fundamental natural period of bridge.

T_v = Natural period of vehicle axle.

T_x = Steel stress at midspan.

T_0 = Steel stress at jacking end.

W = Out-to-out width of test vehicle.

Y_b = Distance from neutral axis to bottom face of beam or to bottom layer of reinforcing bars.

a = Cross-section area of a prestressing element.

a_1 = Horizontal distance from front axle to center of gravity of the sprung mass.

a_2 = Horizontal distance from rear axle to center of gravity of the sprung mass.

b = Total width of slab.

c = Distance from neutral axis to location of gage.

c_1 = Empirical coefficient.

c_2 = Empirical parameter.

d = Distance from a layer of tension reinforcement to top surface of slab; also distance from jack to midspan of beam (Section 5.6).

$\bar{d}$ = Distance from centroid of multilayered tension reinforcement to top surface of slab.

e = Base of natural logarithm.

e_1 = Observed elongation of a prestressing element at the jack when force in the jack is F_1.

$\bar{f}$ = Natural frequency of vibration of an axle.

$\bar{f}_1, \bar{f}_2$ = Natural frequencies of the axles of a two-axle vehicle.

f_1, f_2 = Natural frequencies of a two-axle vehicle; smaller value is bounce frequency, larger value is pitch frequency.
f_b = Natural frequency of a bridge.
f_c = Load per unit area of concrete.
f'_c = Compressive strength of concrete.
f'_{ci} = Strength of concrete at time of loading.
f_e = Effective yield strength.
f_i = Initial stress.
f_L = Natural frequency of a loaded bridge, not considering mass of vehicle.
f_r = Ratio of applied stress to modulus of rupture of concrete.
f'_s = Ultimate strength of steel.
f_u = Natural frequency of an unloaded bridge determined from test records for the free vibration era.
g = Acceleration due to gravity.
i = Dynamic index.
k_e = Effective spring constant.
k_s = Spring constant of a vehicle spring.
k_t = Spring constant of a set of tires.
m = Total number of stress intervals in the histogram.
n, n_1, n_5 = Observed number of cycles of applied stress.
n_x = Actual number of cycles of stress S_x.
p = Probability of survival at n cycles of stress.
r = Radius of gyration of the sprung mass.
s = Wheelbase.
s_1, s_2, s_3, s_4 = Axle spacings.
t, t' = Time.
t_r = Time of transit of an axle over an irregularity.
t_s = Average thickness of slab.
v = Speed of vehicle.
w = Weight of an axle.
w_b = Weight of bridge per unit length.
x = 1, 2, . . . m; a number denoting the intervals of stress in the histogram of the fluctuating stress.
α = Speed parameter; also total angular change of prestressing element, in radians, from jack to midspan (Section 5.6).
α_{max} = Maximum value of speed parameter.
ε = Strain.
ε_{LL} = Strain in a layer of prestressing steel caused by total applied load.
ε_{max} = Maximum strain on passage of vehicle.
ε_0 = Maximum strain within the center portion of a bridge beam.
ε_p = Strain in a layer of prestressing steel caused by prestressing.
Δ = Profile variation parameter equal to ratio of midspan deflection of an unloaded bridge to static deflection of vehicle axle.
Δ_c = Creep strain at time t.
Δ_r = Relaxation stress loss at time t.
Δ_s = Shrinkage strain at time t.
μ = Coefficient of interleaf friction; also friction curvature coefficient (Section 5.6).
ν = Poisson's ratio.
ϕ = Ratio of axle frequency to natural frequency of bridge.
ϕ_t = Frequency ratio for axle with blocked spring.
ϕ_{ts} = Frequency ratio for axle having normal suspension.

Appendix D

RESIDUAL STRESSES AND STATIC YIELD POINT OF STRUCTURAL STEEL FOR TEST BRIDGES *

Residual Stresses

Residual stresses were determined for 16 wide-flange beams by the method of sectioning. Measurements were made on a 10-in. gage length at locations shown in Figure 1-D on six 9-ft beams and ten 2-ft beams. The 9-ft beams had a 2-ft section cut out of the center which was then cut into strips ½ in. wide and 11 in. long. Readings were taken before cutting, after the 2-ft section was cut out, and again after the 2-ft section was cut into strips. The 2-ft beams were sectioned into ½ x 11-in. strips after the initial readings were taken; a second set of readings was taken on the strips.

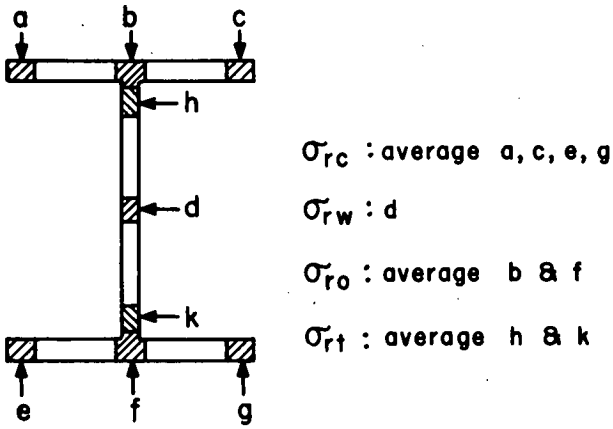

Figure 1–D. Location of residual stress measurements.

Table 1-D gives all specimens by heat and shape and the measured residual stresses. The residual stresses for 9-ft beams are the difference in measurements made on these beams and those made after the beams were cut into strips. The residual stresses listed for 2-ft beams are the difference between measurements made before and after the 2-ft beams were cut into strips. The meaning of symbols σ_{rc}, σ_{ro}, σ_{rw} and σ_{rt} is explained in Figure 1-D.

The residual stresses obtained from the 9-ft 18WF96 beams may be compared to those reported by Beedle and Tall.** The ratio of the depth of section to its flange width, d/b, for the 18WF96 beam is 1.55, making it a borderline case in terms of the classification suggested by

* This material may also be found in a discussion by Fisher and Viest published in *Proc. ASCE*, Vol. 87, No. ST2, pp. 53–57 (Feb. 1961).

**Beedle, Lynn S. and Tall, Lambert, "Basic Column Strength." *Proc. ASCE*, Vol. 86, No. ST7, pp. 139–173 (July 1960).

TABLE 1-D

RESIDUAL STRESSES (SUMMARY OF DS 2417)

Test No.	Heat	Shape	Residual Stress (ksi)							
			9-Ft. Beams				2-Ft. Beams			
			σ_{rc}	σ_{ro}	σ_{rw}	σ_{rt}	σ_{rc}	σ_{ro}	σ_{rw}	σ_{rt}
9A1	36	18WF96	− 6.3	−9.5	15.8	8.5	− 1.7	− 7.6	0.9	5.8
9A2	36	18WF96	− 9.5	−6.4	18.4	12.4	− 4.4	− 4.1	1.5	9.5
9A3	36	18WF96	− 9.1	0.2	2.2	6.8	− 7.9	0.7	− 1.5	5.5
9B1	36	18WF96	−11.1	−2.9	6.8	10.7	− 7.3	− 1.4	0.8	9.2
9B2	36	18WF96	−13.5	−7.9	19.0	9.6	− 8.7	− 5.4	4.1	6.9
9B3	36	18WF96	−13.3	−7.0	19.5	13.5	− 7.4	− 5.2	2.4	8.5
1A1	74	18WF55					− 5.4	16.9	−16.1	− 7.3
1A2	74	18WF55					− 6.8	16.5	−17.2	− 5.5
1B1	90	18WF50					− 9.8	11.9	−13.6	− 6.8
2B1	90	18WF50					− 7.2	17.8	−10.8	−14.1
3A1	93	21WF62					− 7.6	13.7	− 7.3	− 9.5
3A2	83	21WF62					−11.4	17.5	− 8.9	− 3.1
3A3	83	21WF62					− 8.1	15.3	− 8.3	− 5.5
3B3	42	18WF60					− 9.4	14.7	−13.0	− 9.4
4A2	42	18WF60					− 2.4	7.2	− 9.2	− 6.4
4B1	86	18WF60					− 1.7	0.9	−15.4	− 0.7

Beedle and Tall. Table 2-D gives the suggested maximum, minimum and average values of the residual stresses as well as those found in the 18WF96 shapes. The average residual stress at the center of the flange (σ_{ro}) and at the center of the web (σ_{rw}) fall outside, but the residual stress at the flange edge (σ_{rc}) falls inside the limits suggested by Beedle and Tall.

An analysis of variance was made for the residual stress in the flange edge (σ_{rc}) of the 9-ft beams to determine the variation between specimens within a beam and between beams within a heat. This analysis showed that the variation in residual stress from beams of the same heat was significant, at the 1 percent level, when compared to the variation within a beam.

An analysis of variance was made also to determine the variation within a beam, between beams within a heat, and between heats (The comparison between heats is confounded by beam size.) for the residual stress at the flange tips (σ_{rc}) of the 2-ft beams. The variation between beams and between heats was found significant, at the 1 percent level, compared to the variation within a beam.

The results obtained from the 2-ft specimens are smaller than those in longer beams. This is evident from the data for heat 36 in Table 1-D. The ratios of mean residual stresses observed on 9-ft beams to those on 2-ft beams are 1.9, 1.5, 5.8 and 1.4 for σ_{rc}, σ_{ro}, σ_{rw} and σ_{rt}, respectively.

Beedle and Tall reported that ". . . cooling residual stresses are constant along the member except for a distance approximately equal to the larger cross-sectional dimension at the ends." They also reported data on the effect of beam length on the magnitude of ratios σ_{rc} and σ_{ro}. Their data are in general agreement with the values reported herein when compared on the basis of equal values of l/d (l = beam length, d = the larger cross-sectional dimension of the shape). This suggests that the residual stresses σ_{rc} and σ_{ro} in long beams 18 in. deep may be estimated from the values obtained from short beams by multiplication with the ratios obtained for heat 36.

Static Yield Point

The results of 98 static tension tests concerning the yield stress level are given in Table 3-D. The tests were carried out in a 100,000-lb capacity screw-type mechanical testing machine. The data cover six different heats, five sizes of rolled wide-flange beams and one thickness of plate material.

The order of testing the coupons was randomized with respect to heat and thickness. The load was applied at a rate of 140 μ in. per in. per sec up to the yielding of the steel. The yield point was determined by the drop-of-beam of the testing machine. This same rate of straining was continued in the plastic region up to the point of strain hardening; however, in the plastic region the testing machine was stopped three times and a few minutes were allowed to elapse to enable the load to decrease to the minimum value and thus to determine the value of the static yield point. (The mean of the three minimum values was taken as the static yield point.) Deformations were observed on each specimen with an 8-in. extensometer up to strain hardening to insure that the static level was approached through increasing rather than decreasing strain.

The large number of corresponding data on the static yield point and the drop-of-beam yield point made possible a statistical analysis of the effect of heat, thickness and yield stress level on the ratio of the dynamic yield stress to the static yield stress for the strain rate of 140 μ in. per in. per sec. Tests at the 5 percent significance level indicated no effect of heat, thickness, or yield stress level on the ratio of dynamic yield stress to the static yield stress. Hence, the mean value of the ratio, 1.08, represents all tests reported herein regardless of the source.

The mean ratio of dynamic to static yield

TABLE 2-D

RESIDUAL STRESSES IN WIDE-FLANGE SHAPES DUE TO COOLING

Item	Residual Stress (ksi)								
	Flange Edge, σ_{rc}			Flange Center, σ_{ro}			Web Center, σ_{rw}		
	Max.	Avg.	Min.	Max.	Avg.	Min.	Max.	Avg.	Min.
Author's columns $d/b \leqq 1.5$	−7.7	−12.8	−18.7	+16.5	+ 4.7	−4.1	−18.2	+ 8.0	−15.5
18WF96 $d/b = 1.55$	−6.3	−10.5	−13.5	+ 0.2	− 5.6	−9.5	+19.5	+13.6	− 2.2
Author's beams $d/b > 1.5$	−4.1	− 7.5	−10.8	+24.2	+15.1	+8.3	− 8.8	−21.8	−41.0

TABLE 3-D

YIELD POINT OF COUPONS FROM WIDE FLANGE BEAMS AND COVER PLATES

(Summary of DS 2410 and 2411)

Heat	Beam Size	Number of Beams or Plates	Static Yield Point			Drop-of-Beam Yield Point			Mill Test
			No. Spec.	σ_{ys} (ksi)	s [1] (ksi)	No. Spec.	σ_y (ksi)	s [1] (ksi)	σ_y (ksi)
				(a) FLANGE SPECIMENS					
90	18WF50	3	6	35.9	2.00	6	38.8	2.24	
74	18WF55	3	6	31.5	1.22	6	34.4	1.15	
83	21WF62	2	4	31.9	0.92	4	34.6	1.43	
42	18WF60	5	10	32.8	1.70	10	35.5	1.79	
36	18WF96	6	24	29.9	1.04	24	32.5	1.21	
				(b) WEB SPECIMENS					
90	18WF50	3	3	36.8	4.17	3	39.8	4.22	38.2
74	18WF55	3	3	36.6	1.30	3	39.5	1.22	40.3
83	21WF62	2	2	37.5	0.42	2	40.6	0.35	41.3
42	18WF60	5	5	36.9	1.98	5	39.6	1.77	39.9
36	18WF96	6	10	33.2	1.27	10	36.1	1.25	37.9
				(c) PLATE					
85	$\frac{7}{16} \times 6$	12	24	34.8	1.02	24	37.5	1.04	36.1

[1] Standard deviation.

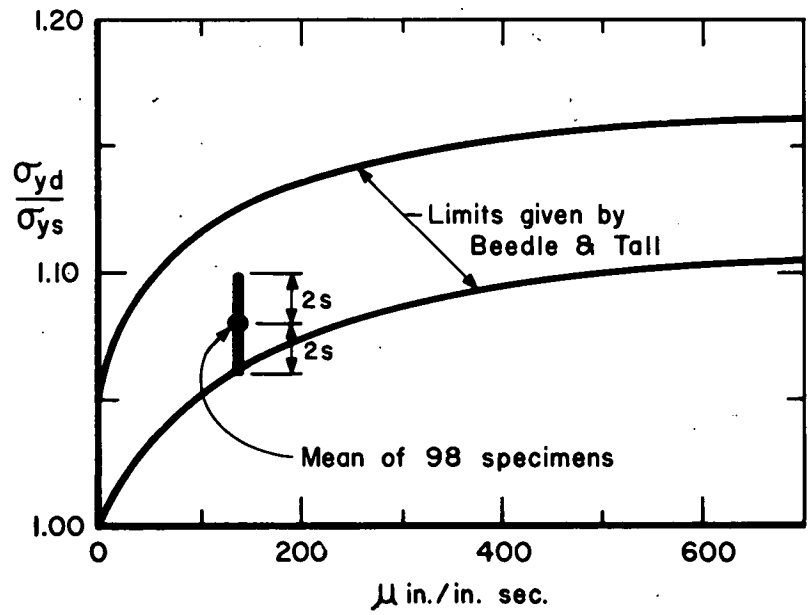

Figure 2-D. Influence of strain rate on yield stress level.

stress is compared in Figure 2-D with the limits suggested by Beedle and Tall. The spread of the data is indicated by the 95 percent confidence limits. (Ninety-five percent confidence limits correspond to $\pm 2s$ around the mean.) The mean falls within the suggested limits but is located closer to the lower than to the upper limit.

The tension tests of structural steel from test bridges given in Table 5 were made at the speed of 0.104 in. per min up to yielding corresponding to the strain rate of about 140 μ in. per in. per sec. Thus the static yield point for any wide-flange beam or coverplate is equal to 92.5 percent of the yield point given in Table 5. The dynamic yield point corresponding to any given strain rate may be estimated from the static yield point with the aid of Figure 2-D.

Appendix E

REGIONAL ADVISORY COMMITTEES

These committees were appointed by the Highway Research Board to maintain liaison between the state highway departments and the research project, through the National Advisory Committee. Three members of each Regional Committee were appointed to the National Advisory Committee.

Region 1

F. M. Auer, Planning and Economics Engineer, New Hampshire Department of Public Works and Highways

E. B. Bly, Engineering Assistant to Commissioner, Vermont Department of Highways

T. V. Bohner, Special Assistant, Engineering Department, D. C. Department of Highways and Traffic

W. M. Creamer, Chief, Highway Staff Services, Connecticut State Highway Department

F. W. Hauck, Supervising Civil Engineer (Road Designing), Rhode Island Department of Public Works

C. D. Jensen, Director of Research and Testing, Pennsylvania Department of Highways

G. W. McAlpin, Assistant Deputy Chief Engineer (Research), New York State Department of Public Works

J. F. McGovern, Structures Maintenance Engineer, Massachusetts Department of Public Works

L. W. Novinger, Contract and Design Engineer, Delaware State Highway Department

V. A. Savage, Engineer of Primary Highways, Maine State Highway Commission

W. Van Breemen, Research Engineer, New Jersey State Highway Department

The following were members of the Region 1 Advisory Committee during the years indicated:

H. F. Clemmer, formerly *Chairman;* Consultant, D. C. Department of Highways and Traffic (1956-1960)

R. A. Farley, formerly Deputy Secretary, Engineering, Pennsylvania Department of Highways (1956-1958)

W. C. Hopkins, Deputy Chief Engineer, Maryland State Roads Commission (1956-1961)

F. S. Poorman, Deputy Secretary, Engineering, Pennsylvania Department of Highways (1959)

L. K. Murphy, formerly Construction Engineer, Primary Highways, Maine State Highway Commission (1955-1959)

Region 2

T. E. Shelburne, *Chairman,* Director of Research, Virginia Department of Highways

W. F. Abercrombie, Engineer of Materials and Tests, Georgia State Highway Department

T. L. Bransford, Engineer of Research and In-Service Training, Florida State Road Department

L. D. Hicks, Chief Soils Engineer, North Carolina State Highway and Public Works Commission

G. W. McAlpin, Director, Program Office, and Assistant Chief Engineer, West Virginia State Road Commission

J. D. McMahan, Construction Engineer, South Carolina State Highway Department

A. O. Neiser, Assistant State Highway Engineer, Kentucky Department of Highways

T. W. Parish, Assistant Chief Engineer (Construction), Louisiana Department of Highways

R. S. Patton, Engineer of Surveys and Designs, Tennessee Department of Highways and Public Works

Angel (2) Silva, Director, Puerto Rico Department of Public Works

H. O. Thompson, Testing Engineer, Mississippi State Highway Department

J. F. Tribble, Materials and Research Engineer, Alabama State Highway Department

E. L. Wales, Engineer of Materials and Tests, Arkansas State Highway Commission

The following was a member of the Region 2 Advisory Committee during the years indicated:

J. L. Land, formerly Chief Engineer, Bureau of Materials and Tests, Alabama State Highway Department (1956)

Region 3

W. E. Chastain, Sr., *Chairman,* Engineer of Physical Research, Illinois Division of Highways

J. G. Butter, Consultant, Iowa State Highway Commission

E. A. Finney, Director, Research Laboratory, Michigan State Highway Department

R. A. Helmer, Research Engineer, Oklahoma State Highway Department

J. W. Hossack, State Engineer, Nebraska Department of Roads

C. P. Jorgensen, Manager, Research and Planning, South Dakota State Highway Commission

H. E. Marshall, Research Engineer, Ohio Department of Highways

R. L. Peyton; Assistant State Highway Engineer, State Highway Commission of Kansas

J. S. Piltz, Engineer of Design, Wisconsin State Highway Commission

C. K. Preus, Materials and Research Engineer, Minnesota Department of Highways

F. V. Reagel, Engineer of Special Assignments, Missouri State Highway Commission

W. T. Spencer, Soils Engineer, Indiana State Highway Department

W. A. Wise, Director, Field Division, North Dakota State Highway Department

The following were members of the Region 3 Advisory Committee during the years indicated:

L. N. Ress, formerly State Engineer, Nebraska Department of Roads (1956-1958)

H. G. Schlitt, formerly Deputy State Engineer, Nebraska Department of Roads (1959)

C. W. Allen, formerly Research Engineer, Ohio Department of Highways (1956-1958)

J. H. Swanberg, Chief Engineer, Minnesota Department of Highways (1956-1958)

Region 4

R. E. Livingston, *Chairman,* Planning and Research Engineer, Colorado Department of Highways

J. R. Bromley, Superintendent and Chief Engineer, Wyoming State Highway Department

L. F. Erickson, Assistant Construction Engineer, Idaho Department of Highways

L. B. Fox, Construction Engineer, Montana State Highway Commission

T. S. Huff, Chief Engineer of Highway Design, Texas State Highway Department

F. N. Hveem, Materials and Research Engineer, California Division of Highways

C. W. Johnson, Materials and Testing Engineer, New Mexico State Highway Commission

D. F. Larsen, Chief Materials Engineer, Utah State Road Commission

C. E. Minor, Materials and Research Engineer, Washington Department of Highways

W. G. O'Harra, Materials Engineer, Arizona Highway Department

W. M. Wachter, Highway Engineer, Hawaii Division of Highways

W. O. Wright, State Highway Engineer, Nevada Department of Highways

The following were members of the Region 4 Advisory Committee during the years indicated:

W. T. Holcomb, formerly Assistant State Highway Engineer, Nevada Department of Highways (1956-1959)

I. B. Miller, Operations Engineer, New Mexico State Highway Commission (1956-1958)

B. E. Nutter, formerly Territorial Highway Engineer, Hawaii Territorial Highway Department (1956-1958)

S. B. Sanders, formerly District Engineer, Montana State Highway Commission (1956-1958)

W. C. Williams, State Highway Engineer, Oregon State Highway Commission (1956-1961) (deceased)

SUBCOMMITTEE ON BRIDGES

Working Committee of ASSHO Committee on Highway Transport

This subcommittee functioned during the period 1952-1955. It selected the design variables and the criteria for the design of the test bridges, and reviewed the designs.

G. M. Foster, *Chairman,* Chief Deputy Commissioner, Michigan State Highway Department

E. L. Erickson, Chief, Bridge Division, Bureau of Public Roads

C. P. Siess, Professor of Civil Engineering, University of Illinois

J. J. Hogan, Regional Structural Engineer, Portland Cement Association

ADVISORY PANEL ON BRIDGES

This panel was appointed by the Highway Research Board to advise on the bridge research. It examined the experiment design and advised on the conduct of tests and interpretation of results.

G. S. Paxson, *Chairman,* Deputy State Highway Engineer, Oregon State Highway Department

J. M. Biggs, Associate Professor of Structural Engineering, Massachusetts Institute of Technology

E. L. Erickson, Chief, Bridge Division, Bureau of Public Roads

A. E. LaBonte, Chief, Bridge Division, Minnesota Department of Highways

C. P. Siess, Professor of Civil Engineering, University of Illinois

G. S. Vincent, Chief, Bridge Research Branch, Bureau of Public Roads

The following were members of this panel during the years indicated:

O. L. Kipp, formerly Assistant Commissioner and Chief Engineer, Minnesota Department of Highways (1957-1958)

Bruno Thurlimann, formerly Professor of Civil Engineering, Lehigh University (resigned 1960)

W. C. Hopkins, Deputy Chief Engineer, Maryland State Roads Commission (1957-1961)

SPECIAL COMMITTEE ON DYNAMIC BEHAVIOR OF TEST BRIDGES

This committee was appointed by the Highway Research Board as an advisory group for the cooperative investigation of dynamic behavior conducted at the University of Illinois. It planned the dynamic tests and advised on the interpretation and reporting of the results.

G. S. Paxson, *Chairman,* Deputy State Highway Engineer, Oregon State Highway Department

W. N. Carey, Jr., Chief Engineer for Research, AASHO Road Test, Highway Research Board

C. P. Siess, Professor of Civil Engineering, University of Illinois

A. S. Veletsos, Professor of Civil Engineering, University of Illinois

I. M. Viest, Bridge Research Engineer, AASHO Road Test, Highway Research Board

SPECIAL PUBLICATION SUBCOMMITTEE FOR AASHO ROAD TEST REPORT 4 ON BRIDGE RESEARCH

This subcommittee, appointed by the Highway Research Board, advised the staff on the preparation of AASHO Road Test Report 4, "Bridge Research," and recommended approval of the report for publication.

G. S. Paxson, *Chairman,* Deputy State Highway Engineer, Oregon State Highway Department

D. K. Chacey, Director of Transportation Engineering, Office of the Chief of Transportation, Department of the Army

E. L. Erickson, Chief, Bridge Division, Bureau of Public Roads

M. T. Hayes, Assistant Truck Engineer, Truck and Coach Division, General Motors Corporation

C. P. Siess, Professor of Civil Engineering, University of Illinois

G. S. Vincent, Chief, Bridge Research Branch, Bureau of Public Roads

The following also was a member of this subcommittee:

W. C. Hopkins, Deputy Chief Engineer, Maryland State Roads Commission (resigned October 1961)

PROJECT PERSONNEL

Project Staff

W. B. McKendrick, Jr., Project Director

W. N. Carey, Jr., Chief Engineer for Research

Peter Talovich, Business Administrator
L. A. Ptak, Accountant
R. S. Semple, Purchasing Assistant

A. C. Tosetti, Assistant to the Project Director
W. R. Milligan, Assistant Operations Manager
D. L. Thorp, Shop Superintendent

A. C. Benkelman, Flexible Pavement Research Engineer
L. E. Dixon, Assistant Flexible Pavement Research Engineer
H. M. Schmitt, Assistant Flexible Pavement Research Engineer

F. H. Scrivner, Rigid Pavement Research Engineer
W. R. Hudson, Assistant Rigid Pavement Research Engineer
R. J. Little, Assistant Rigid Pavement Research Engineer

I. M. Viest, Bridge Research Engineer
J. W. Fisher, Assistant Bridge Research Engineer

P. E. Irick, Chief, Data Processing and Analysis
R. C. Hain, Assistant Chief, Data Processing and Analysis

J. F. Shook, Materials Engineer

D. R. Schwartz, Engineer of Reports
H. R. Hubbell, Assistant Engineer of Reports

H. H. Boswell, Maintenance Engineer
James Gardner, Maintenance Superintendent
Allen Bartelson, Maintenance Supervisor

R. C. Leathers, Engineer of Special Assignments

H. C. Huckins, Supervisor, Instrument Laboratory

W. J. Schmidt, Chief, Public Information

The following were members of the Project Staff during the years indicated:

H. H. Cole, Shop Superintendent (1958)

L. Q. Mettes, Materials Engineer (1956)

Moreland Herrin, Assistant Materials Engineer (1958)

Temporary Engineering Personnel
Bridge Branch

The following engineers were assigned to the Bridge Branch for periods of several months. The resident staff consultants and observers carried out specific studies. The junior engineers, assigned to the project by the Bureau of Public Roads for periods of about six months as a part of their training program, performed miscellaneous engineering tasks involving instrumentation, testing, data reduction, and data analyses. After completion of this training program, C. F. Galambos, Bridge Engineer, was assigned to the project for periods of several weeks to conduct and assist in the interpretation of the tests to failure with increasing loads. Similarly, J. H. Hatton, Assistant Regional Bridge Engineer, assisted in the interpretation of the results of bridge research.

Resident Staff Consultants and Observers

B. E. Colley, Portland Cement Association
S. M. King, American Trucking Associations
R. I. Kingham, Canadian Good Roads Association

Junior Engineers

J. W. Schmidt	G. W. Million	D. J. Philbrick
G. N. Lind	L. R. Cayes	K. D. Jaeger
V. Buchele	J. L. Budwig	J. H. Hatton
D. C. Briggs	C. F. Galambos	N. W. Loeffler
G. C. Hoxie	N. C. Mueller	R. E. Stanford

R. A. Richter
W. T. Medley

Photography

Still photography was done by Frank W. Bazzoni of the staff. His work was augmented and all motion picture photography and the production of motion pictures relating to the project were done by Bureau of Public Roads photographers Roy B. Dame, T. Welby Kines, George Crum, and Charles Ritter.

Illinois Division of Highways
Permanent Task Force During Research Phase

The Illinois Division of Highways established a permanent task force for the project in 1955. The first function of this group was to prepare plans and specifications for construction. Later the group assumed responsibility for construction inspection and direction. With the exception of W. E. Chastain, Sr., the members of the Task Force were absorbed by the research units during the research phase. They resumed their identity as an agency of the Illinois Division of Highways in 1961 when detailed planning for the rehabilitation of the test site was undertaken.

W. E. Chastain, Sr., Engineer of Physical Research
A. C. Tosetti, Assistant to the Project Director
D. R. Schwartz, Assigned to the Research Staff
H. R. Hubbell, Assigned to the Research Staff
R. J. Little, Assigned to the Research Staff
A. J. Wright, Assigned to the Research Staff

U. S. Army Transportation Corps Road Test Support Activity (AASHO)

The Transportation Corps Road Test Support Group furnished truck drivers for all of the test vehicles for the entire traffic phase and during the special studies period following the main traffic test.

Commanding Officer
Col. A. A. Wilson (1958-59)
Lt. Col. R. J. Lombard (1959-61)

Deputy Commander
Maj. W. A. Duncan (1958-60)
Capt. R. G. Farwell (1960-61)

Company Commander
Capt. R. D. Smith (1958-59)

Personnel of the Cooperative Investigation at the University of Illinois

The University of Illinois undertook the analysis and interpretation of the dynamic studies reported in Chapter 4 of this report. The investigation was conducted under a cooperative agreement between the National Academy of Sciences, acting in behalf of the Highway Research Board, and the University. The studies were carried out in the Department of Civil Engineering under the general direction of C. P. Siess and A. S. Veletsos, Professors of Civil Engineering. Immediate supervision was the responsibility of R. K. L. Wen, formerly Assistant Professor of Civil Engineering, from February 1958 to February 1959, and of S. J. Fenves, Assistant Professor of Civil Engineering, since that date. The project personnel consisted of E. G. Endebrock, N. L. Hickerson, A. Korn, W. P. Moore and R. L. Rolf, Research Assistants in Civil Engineering. The computer program used to obtain analytical solutions was developed by Tseng Huang, formerly Assistant Professor of Civil Engineering.

THE NATIONAL ACADEMY OF SCIENCES—NATIONAL RESEARCH COUNCIL is a private, nonprofit organization of scientists, dedicated to the furtherance of science and to its use for the general welfare. The ACADEMY itself was established in 1863 under a congressional charter signed by President Lincoln. Empowered to provide for all activities appropriate to academies of science, it was also required by its charter to act as an adviser to the federal government in scientific matters. This provision accounts for the close ties that have always existed between the ACADEMY and the government, although the ACADEMY is not a governmental agency.

The NATIONAL RESEARCH COUNCIL was established by the ACADEMY in 1916, at the request of President Wilson, to enable scientists generally to associate their efforts with those of the limited membership of the ACADEMY in service to the nation, to society, and to science at home and abroad. Members of the NATIONAL RESEARCH COUNCIL receive their appointments from the president of the ACADEMY. They include representatives nominated by the major scientific and technical societies, representatives of the federal government, and a number of members at large. In addition, several thousand scientists and engineers take part in the activities of the research council through membership on its various boards and committees.

Receiving funds from both public and private sources, by contribution, grant, or contract, the ACADEMY and its RESEARCH COUNCIL thus work to stimulate research and its applications, to survey the broad possibilities of science, to promote effective utilization of the scientific and technical resources of the country, to serve the government, and to further the general interests of science.

The HIGHWAY RESEARCH BOARD was organized November 11, 1920, as an agency of the Division of Engineering and Industrial Research, one of the eight functional divisions of the NATIONAL RESEARCH COUNCIL. The BOARD is a cooperative organization of the highway technologists of America operating under the auspices of the ACADEMY-COUNCIL and with the support of the several highway departments, the Bureau of Public Roads, and many other organizations interested in the development of highway transportation. The purposes of the BOARD are to encourage research and to provide a national clearinghouse and correlation service for research activities and information on highway administration and technology.